frontiers | Research Topics

Women in cardiovascular therapeutics

Edited by
Hong S. Lu, Liya Yin, Xiaochun Long, Hongyu Qiu, Ze Zheng and Ting Zhou

Published in
Frontiers in Cardiovascular Medicine

ISSN 1664-8714
ISBN 978-2-8325-2539-5
DOI 10.3389/978-2-8325-2539-5

About Frontiers

Frontiers is more than just an open access publisher of scholarly articles: it is a pioneering approach to the world of academia, radically improving the way scholarly research is managed. The grand vision of Frontiers is a world where all people have an equal opportunity to seek, share and generate knowledge. Frontiers provides immediate and permanent online open access to all its publications, but this alone is not enough to realize our grand goals.

Frontiers journal series

The Frontiers journal series is a multi-tier and interdisciplinary set of open-access, online journals, promising a paradigm shift from the current review, selection and dissemination processes in academic publishing. All Frontiers journals are driven by researchers for researchers; therefore, they constitute a service to the scholarly community. At the same time, the *Frontiers journal series* operates on a revolutionary invention, the tiered publishing system, initially addressing specific communities of scholars, and gradually climbing up to broader public understanding, thus serving the interests of the lay society, too.

Dedication to quality

Each Frontiers article is a landmark of the highest quality, thanks to genuinely collaborative interactions between authors and review editors, who include some of the world's best academicians. Research must be certified by peers before entering a stream of knowledge that may eventually reach the public - and shape society; therefore, Frontiers only applies the most rigorous and unbiased reviews. Frontiers revolutionizes research publishing by freely delivering the most outstanding research, evaluated with no bias from both the academic and social point of view. By applying the most advanced information technologies, Frontiers is catapulting scholarly publishing into a new generation.

What are Frontiers Research Topics?

Frontiers Research Topics are very popular trademarks of the *Frontiers journals series*: they are collections of at least ten articles, all centered on a particular subject. With their unique mix of varied contributions from Original Research to Review Articles, Frontiers Research Topics unify the most influential researchers, the latest key findings and historical advances in a hot research area.

Find out more on how to host your own Frontiers Research Topic or contribute to one as an author by contacting the Frontiers editorial office: frontiersin.org/about/contact

Women in cardiovascular therapeutics

Topic editors

Hong S. Lu — University of Kentucky, United States
Liya Yin — Northeast Ohio Medical University, United States
Xiaochun Long — Augusta University, United States
Hongyu Qiu — Georgia State University, United States
Ze Zheng — Medical College of Wisconsin, United States
Ting Zhou — University of Wisconsin-Madison, United States

Citation

Lu, H. S., Yin, L., Long, X., Qiu, H., Zheng, Z., Zhou, T., eds. (2023). *Women in cardiovascular therapeutics*. Lausanne: Frontiers Media SA.
doi: 10.3389/978-2-8325-2539-5

Table of contents

frontiers | Frontiers in Cardiovascular Medicine

TYPE Editorial
PUBLISHED 10 May 2023
DOI 10.3389/fcvm.2023.1183427

OPEN ACCESS

EDITED AND REVIEWED BY
Hendrik Tevaearai Stahel,
University Hospital of Bern, Switzerland

*CORRESPONDENCE
Liya Yin
lyin@neomed.edu
Hong S. Lu
hong.lu@uky.edu

RECEIVED 10 March 2023
ACCEPTED 27 April 2023
PUBLISHED 10 May 2023

CITATION
Yin L, Zhou T, Zheng Z, Long X, Qiu H and Lu HS (2023) Editorial: Women in cardiovascular therapeutics.
Front. Cardiovasc. Med. 10:1183427.
doi: 10.3389/fcvm.2023.1183427

Editorial: Women in cardiovascular therapeutics

Liya Yin[1]*, Ting Zhou[2], Ze Zheng[3,4], Xiaochun Long[5], Hongyu Qiu[6] and Hong S. Lu[7]*

[1]Department of Integrative Medical Sciences, North Ohio Medical University, Rootstown, OH, United States, [2]Department of Surgery, School of Medicine and Public Health, University of Wisconsin-Madison, Madison, WI, United States, [3]Department of Medicine, Medical College of Wisconsin, Milwaukee, WI, United States, [4]Versiti Blood Research Institute, Milwaukee, WI, United States, [5]Vascular Biology Center, Medical College of Georgia at Augusta University, Augusta, GA, United States, [6]Translational Cardiovascular Research Center, Department of Internal Medicine, College of Medicine at Phoenix, University of Arizona, Phoenix, AZ, United States, [7]Department of Physiology, Saha Cardiovascular Research Center and Saha Aortic Center, College of Medicine, University of Kentucky, Lexington, KY, United States

KEYWORDS

editorial, cardiovascular function, treatment, pathogenesis, women

Editorial on the Research Topic
Women in cardiovascular therapeutics

The special issue of "Women in Cardiovascular Therapeutics" of Frontiers in Cardiovascular Medicine aims to highlight the cardiovascular research work of female scientists. For this purpose, this special issue required that the first and/or last author must be a woman. Also, the 6 editors are female scientists in the cardiovascular research field: 2 are senior scientists, 2 are in their middle career stage, and 2 are early career investigators. We are grateful that we received 18 submissions for this purpose, and successfully published 15 articles with either or both the first and corresponding authors being female. These articles include 2 brief reviews, 1 case report, and 12 original research articles in many areas of cardiovascular research, including cardiac disorders, atherosclerosis, metabolic disorders, and aortic aneurysms and dissection. Some articles also discussed sex differences in cardiovascular diseases.

In addition to the first and/or last author, the published articles include many female scientists as co-authors. Consistent with the goal of this special issue to promote women scientists, this special issue published one article by 7 female scientists in Japan (Atsuko Nakayama et al.). The authors conducted a study on the leadership role of Japanese women scientists. They report the awareness and feasibility of women chairing cardiology sessions in scientific meetings through a nationwide survey by the Circulation Society. They found female cardiologists were less likely to accept chairing sessions compared with male cardiologists, and the presence of female cardiovascular specialists positively influenced chair acceptance. To encourage more female cardiologists to take on leadership roles, the Japanese Circulation Society–Josei Junkanki subcommittee was formed to increase the proportion of female cardiologists for chairing sessions in annual academic meetings. Moreover, a policy is recommended to improve the work environment, research support, and leadership opportunities for women in the field. The editors agree that the recommended improvement is essential in order to promote female scientists and acknowledge their contributions to the research community.

Collectively, this special issue features articles from female scientists who work on cardiovascular research from zebrafish and mouse models to human data, providing a comprehensive understanding of the mechanisms, pathogenesis, and clinical relevance of cardiovascular diseases. All manuscripts were peer-reviewed. Unfortunately, we do not have the information to determine whether male vs. female reviewers have different influences on manuscript evaluations. This special issue is only a first step in encouraging women to attain better positions in the cardiovascular research field. There is still more that needs to be done. In addition to promoting publications in the field, we encourage more women to be involved in the manuscript review process and other opportunities such as presenting at international conferences.

We would like to thank the outstanding women scientists and wish they continuously publish their solid and innovative research. We would also like to thank the reviewers, irrespective of male or female scientists, for providing constructive comments to help improve each article.

Below we briefly introduce each article published in this special issue to guide readers.

Cardiac disorders

Heart failure is a major cause of morbidity and mortality in the world. There are significant sex differences in the etiology, pathophysiology, and prognosis of heart failure. Men have a greater prevalence of heart failure with reduced ejection fraction, while women have heart failure with preserved ejection fraction more commonly Wang et al. (1). Jones-Ungerleide et al. provided an insightful review of sex-based considerations for implementing ventricular assist device therapy.

Sleep apnea is one of the most frequent comorbidities in patients with heart failure of reduced ejection fraction (HFrEF), enhancing HF morbidity and mortality (2). Current therapies for sleep apnea have limited benefits for heart failure. Pelaia et al. evaluated the effects of sacubitril-valsartan on patients with sleep apnea and HFrEF.

Chronic Chagas cardiomyopathy caused by infection with the protozoan Trypanosoma cruzi is a life-threatening clinical condition. Despite its unique pathophysiological mechanism, no specific treatment is available for this disease. Macedo and Larocca as co-first authors and their colleagues reported a phase II double-blind, randomized, placebo-controlled clinical trial with Granulocyte-Colony Stimulating Factor (G-CSF) to treat chronic Chagas cardiomyopathy in Salvador, Brazil (www.ClinicalTrials.gov, NCT02154269).

Dual-antiplatelet therapy, including aspirin and P2Y12 inhibitors, reduces thrombotic risk after percutaneous coronary intervention (PCI), but increases bleeding risk. In a two-year follow-up study by Doomun et al. the bleeding risk was assessed in a single-center, all-comers registry of 1,080 patients post-PCI.

Atherosclerosis

Atherosclerotic cardiovascular disease is a significant cause of mortality and morbidity worldwide. Atherosclerotic plaques accumulate on the arterial wall, reducing blood flow to organs and limiting nutrients to be delivered to the rest of the body. Progressive atherosclerotic plaques lead to myocardial infarction, ischemic stroke, and peripheral arterial disease. Clearance of dying cells by efferocytosis is essential to maintaining cardiovascular hemostasis and myocardial repair after myocardial infarction (3, 4). A mini-review by the Chen group discussed the signaling and regulation of efferocytosis in atherosclerosis.

Vascular smooth muscle cell phenotypic changes play an essential role in neointimal formation and remodeling after vascular injury (5). Shan and colleagues reported that anemoside B4, a unique saponin, attenuated neointima formation in a mouse model with femoral artery endothelium denudation.

Inflammation plays a critical role in cardiovascular diseases. Winnicki and colleagues reported an interesting aortic stenosis phenotype of endothelial-specific C-X-C motif chemokine receptor 4 (CXCR4) knockouts with Tie2-*Cre*. Huang et al. discovered an important role of ferroptosis, a newly identified form of regulated cell death in septic cardiac dysfunction (SCD).

Metabolic complications

Diabetes is a chronic disease that has many cardiovascular complications. Tu et al. reported that a sodium-glucose cotransporter 2 (SGLT2) inhibitor empagliflozin improved coronary and its microvessel functions in a diabetic mouse model. Gupta et al. examined the differences in the development of atherosclerosis between male and female mice with metabolic syndrome.

Aortic aneurysms

Aortic aneurysms and dissection are critical pathological conditions that can lead to uncontrolled bleeding and death without predictive signs (6). Wang et al. used Global Health Data Exchange to analyze aortic aneurysm data from 1990 to 2019 (7). In addition to human data, many animal studies also provide mechanistic insights. The renin-angiotensin system plays a critical role in developing aortic aneurysms and dissection (8). Bramel and colleagues reported contributions of global vs. second heart field-specific deletion of angiotensin II type 1a (AT1a) receptor to aortic pathology in a mouse model of Loeys-Dietz syndrome.

SMAD Family Member 3 (SMAD3) is a component in the transforming growth factor beta (TGF-β) signaling pathway. Its variants are one cause of familial aortic disease. Sheppard and colleagues found a novel SMAD3 variant, V244F, in a patient with aortic root dilation and abdominal aortic aneurysms. The

authors demonstrated that this variant could induce aortic pathology in a zebrafish embryo model.

Bronchial artery aneurysm

Bronchial artery aneurysm is not a common disease but can be fatal. Lin et al. retrospectively compared endovascular embolization treatment and imaging characteristics of one patient with true bronchial artery aneurysm and another patient with a pseudobronchial aneurysm.

Author contributions

Editorial draft: every author. Editorial editing: every author. All authors contributed to the article and approved the submitted version.

Funding

The authors' research work was supported by the National Institutes of Health, American Heart Association (AHA), and other research foundations: R56HL165207 and AHA 970663 to LY; AHA 20CDA35350009 to TZ; R01HL163516, AHA CSA952422, and National Hemophilia Foundation CDA to ZZ; R01HL142291, HL115195 and HL137962 to HQ, R01HL122686 and HL139794 to XL, and R01HL139748 to HL. The content in this editorial is solely the responsibility of the authors and does not necessarily represent the official views of the National Institutes of Health.

Conflict of interest

The authors declare that the research was conducted in the absence of any commercial or financial relationships that could be construed as a potential conflict of interest.

Publisher's note

All claims expressed in this article are solely those of the authors and do not necessarily represent those of their affiliated organizations, or those of the publisher, the editors and the reviewers. Any product that may be evaluated in this article, or claim that may be made by its manufacturer, is not guaranteed or endorsed by the publisher.

References

1. Wang N, Evans J, Sawant S, Sindone J, Lal S. Sex-specific differences in the efficacy of heart failure therapies: a meta-analysis of 84,818 patients. *Heart Fail Rev.* (2023). doi: 10.1007/s10741-022-10275-1

2. Javaheri S, Javaheri S. Obstructive sleep apnea in heart failure: current knowledge and future directions. *J Clin Med.* (2022) 11:3458. doi: 10.3390/jcm11123458

3. Glinton KE, Ma W, Lantz C, Grigoryeva LS, DeBerge M, Liu X, et al. Macrophage-produced VEGFC is induced by efferocytosis to ameliorate cardiac injury and inflammation. *J Clin Invest.* (2022) 132:e140685. doi: 10.1172/JCI140685

4. D'Amore PA, Alcaide P. Macrophage efferocytosis with VEGFC and lymphangiogenesis: rescuing the broken heart. *J Clin Invest.* (2022) 132:e158703. doi: 10.1172/JCI158703

5. Tang HY, Chen AQ, Zhang H, Gao XF, Kong XQ, Zhang JJ. Vascular smooth muscle cells phenotypic switching in cardiovascular diseases. *Cells.* (2022) 11:4060. doi: 10.3390/cells11244060

6. Shen YH, LeMaire SA, Webb NR, Cassis LA, Daugherty A, Lu HS. Aortic aneurysms and dissections series. *Arterioscler Thromb Vasc Biol.* (2020) 40:e37–e46. doi: 10.1161/ATVBAHA.120.313991

7. Roth GA, Mensah GA, Johnson CO, Addolorato G, Ammirati E, Baddour LM, et al. Global burden of cardiovascular diseases and risk factors, 1990–2019: update from the GBD 2019 study. *J Am Coll Cardiol.* (2020) 76:2982–3021. doi: 10.1016/j.jacc.2020.11.010

8. Sawada H, Lu HS, Cassis LA, Daugherty A. Twenty years of studying AngII (angiotensin II)-induced abdominal aortic pathologies in mice: continuing questions and challenges to provide insight into the human disease. *Arterioscler Thromb Vasc Biol.* (2022) 42:277–88. doi: 10.1161/ATVBAHA.122.317712

frontiers in Cardiovascular Medicine

ORIGINAL RESEARCH
published: 02 December 2021
doi: 10.3389/fcvm.2021.620354

Ischemic and Bleeding Outcomes According to the Academic Research Consortium High Bleeding Risk Criteria in All Comers Treated by Percutaneous Coronary Interventions

Daphné Doomun†, Ianis Doomun†, Sara Schukraft, Diego Arroyo, Selma Cook, Tibor Huwyler, Peter Wenaweser, Jean-Christophe Stauffer, Jean-Jacques Goy, Mario Togni, Serban Puricel and Stéphane Cook*

Department of Cardiology, University and Hospital Fribourg, Fribourg, Switzerland

OPEN ACCESS

Edited by:
Alfonso Ielasi, Istituto Clinico Sant'Ambrogio, Italy

Reviewed by:
Tommaso Gori, Johannes Gutenberg University Mainz, Germany
Philip Urban, Centre Européen de Recherche Cardiovasculaire (CERC), France

***Correspondence:**
Sara Schukraft
sara.schukraft@yahoo.com

† These authors have contributed equally to this work

Specialty section:
This article was submitted to Cardiovascular Therapeutics, a section of the journal Frontiers in Cardiovascular Medicine

Received: *23 December 2020*
Accepted: *08 November 2021*
Published: *02 December 2021*

Citation:
Doomun D, Doomun I, Schukraft S, Arroyo D, Cook S, Huwyler T, Wenaweser P, Stauffer J-C, Goy J-J, Togni M, Puricel S and Cook S (2021) Ischemic and Bleeding Outcomes According to the Academic Research Consortium High Bleeding Risk Criteria in All Comers Treated by Percutaneous Coronary Interventions. Front. Cardiovasc. Med. 8:620354. doi: 10.3389/fcvm.2021.620354

Background: The Academic Research Consortium have identified a set of major and minor risk factors in order to standardize the definition of a High Bleeding Risk (ACR-HBR).

Aims: The aim of this study is to stratify the bleeding risk in patients included in the Cardio-Fribourg registry, according to the Academic Research Consortium for High Bleeding Risk (ACR-HBR) definition, and to report ischemic and hemorrhagic events at 2-year of clinical follow-up.

Methods: Between 2015 and 2017, consecutive patients undergoing percutaneous coronary intervention were prospectively included in the Cardio-Fribourg registry. Patients were considered high (HBR) or low (LBR) bleeding risk depending on the ARC-HBR definition. Primary endpoints were hierarchical major bleeding events as defined by the Bleeding Academic Research Consortium (BARC) grade 3–5, and ARC patient-oriented major adverse cardiac events (POCE) at 2-year follow-up.

Results: Follow-up was complete in 1,080 patients. There were 354 patients in the HBR group (32.7%) and 726 patients in the low-bleeding risk (LBR) group (67.2%). At 2-year follow-up, cumulative BARC 3–5 bleedings were higher in HBR (10.5%) compared to LBR patients (1.5%, $p < 0.01$) and the impact of HBR risk factors was incremental. At 2-year follow-up, POCE were more frequent in HBR (27.4%) compared to LBR group (18.2%, <0.01). Overall mortality was higher in HBR (14.0%) vs. LBR (2.9%, $p < 0.01$).

Conclusions: ARC-HBR criteria appropriately identified a population at a higher risk of bleeding after percutaneous coronary intervention. An increased risk of bleeding is also associated with an increased risk of ischemic events at 2-year follow-up.

Keywords: high bleeding risk, ACR-HBR criteria, percutaneous coronary intervention, antithrombotic therapy, major criteria, minor criteria

INTRODUCTION

Dual-antiplatelet therapy (DAPT) is mandatory after percutaneous coronary intervention (PCI) but increases the risk of bleeding (1, 2). The type and duration of DAPT are balanced according to the thrombotic and bleeding risks (3). Patients at high thrombotic and low hemorrhagic risk benefit from extended DAPT, whereas patients at high bleeding but low ischemic risk do better with shorter DAPT durations (4, 5). Over the years, patient and procedural factors that increase the thrombotic risk have been identified, amongst which: diabetes mellitus, renal failure, acute coronary syndromes, heavily calcified lesions, bifurcation, extensive stent length, small stent diameter, presence of incomplete stent expansion or apposition (6–8).

Recently, the Academic Research Consortium for High Bleeding Risk (ACR-HBR) identified key factors associated with bleeding risk post PCI (9). The ARC-HBR definition is dichotomous and defines HBR as a Bleeding Academic Research Consortium (BARC) 3 or 5 bleeding risk of > 4% and/or risk of intracranial hemorrhage > 1% within 1 year after PCI. These key factors are stratified into major criteria and minor criteria (9, 10). There is emerging evidence on the discriminatory capacity and predictability of this new definition (11–13). However, the prognostic value of ARC-HBR criteria for bleeding events beyond 1 year is poorly described.

Therefore, we planned to report (a) the bleeding outcomes at 2-years of patients enrolled in the all-comers Cardio-Fribourg registry based on presence or absence of ARC-HBR major and minor risk factors, and (b) the ischemic outcomes, as HBR has to be balanced with the thrombotic risk.

METHODS

Study Population and Data Collection

The Cardio-FR is a single-center, all-comers registry. All patients who underwent PCI at our institution between June 2015 and July 2017 and gave informed consent were included. The only exclusion criterion was the inability to sign the informed consent and/or unwillingness to participate in clinical follow-up. The indication for PCI was based on established European guidelines (14). There were no limitations on the type, number or length of the lesions treated. Treatment modalities and antithrombotic management were at the physician's discretion and according to the local standard of care at the time of intervention. Clinical follow-up was scheduled at 1, 2, 5 and 10 years. The Cardio-FR registry complied with the Helsinki Declaration and was approved by the local ethics committee (003-REP-CER-FR). All patients provided written informed consent.

Abbreviations: BARC, Bleeding Academic Research Consortium; CKD, chronic kidney disease; DAPT, dual antiplatelet therapy; HBR, high bleeding risk; ARC-HBR, Academic Research Consortium High Bleeding Risk; LBR, low bleeding risk; MACE, major adverse cardiac events; MI, myocardial infarction; PCI, percutaneous coronary intervention; POCE, patient-oriented composite endpoints; TAT, triple antithrombotic therapy.

Definition of High-Bleeding Risk

Patients were considered high (HBR) or low (LBR) bleeding risk depending on the definition of ARC-HBR. The definition being dichotomous, if the patient did not meet the criteria to be classified as HBR, he fell into the LBR classification. So, in fact, the LBR group does not only correspond to patients at low risk of bleeding but also to patients at medium risk of bleeding. The ARC-HBR definition considered HBR as a risk of major (BARC 3 to 5) bleeding of $\geq$4% or risk of intracranial hemorrhage of $\geq$1% at 1 year. The major and minor criteria were described by Urban et al. (9) and are summarized in **Table 1**. Patients are at HBR if at least 1 major or 2 minor criteria are met. The bleeding risk was assessed at time of PCI.

Clinical Endpoints

Clinical endpoints were reported at 2-year follow-up. Bleeding was defined as per BARC definition, with type 3 and 5 considered "major bleeding" (15). Ischemic outcomes were defined as a patient-oriented composite endpoint (POCE): all-cause mortality, any myocardial infarction, any coronary revascularization. In-hospital events were directly reported to the database, while post-discharge events were recorded by research nurses by iterative telephone calls during follow-up. These events were finally adjudicated by a clinical event committee for the present analysis.

Statistical Analysis

Categorical variables are reported as counts and percentages; continuous variables are reported as mean and SD. Normality was assessed by visual inspection of histograms and the computation of Q-Q plots. Continuous variables are analyzed using the Student *t*-test or the Wilcoxon rank-sum test per distribution. Categorical variables were compared using chi-square or Fisher exact test as appropriate. Survival free from the occurrence of clinical endpoints was assessed by computation of Kaplan-Meier curves. Survival was compared using the log-rank test. Furthermore, clinical outcome was reported as Kaplan-Meier failure estimations. Hazard ratios are derived from univariate Cox regression.

To better illustrate the incremental risk of bleeding conditioned by an increasing number of ACR-HBR criteria per patient, we performed subgroup analysis dividing patients into groups according to the number of HBR criteria. Every subgroup was then univariately compared to the reference group consisting of patients without any ACR-HBR criteria using Cox Regression. Hazard ratios reflect the incremental risk for patients according to the number of ACR-HBR criteria compared to the reference group (i.e., patients without any criteria).

As a supplementary analysis we performed multivariate Cox Regression to identify which individual components of the HBR-Score were most strongly associated with the occurrence of bleeding in our sample. We performed backward stepwise selection separately for major and minor criteria initially saturating the model with all relevant variables. The removal criterion for the final model was $p > 0.10$.

TABLE 1 | Distribution of HBR-ARC criteria.

	All N= 1,080	HBR N= 354	LBR N= 726	*p*-value
Major HBR criteria				
Long-term OAC, n (%)	130 (12.0)	130 (36.7)	0 (0)	<0.01
eGFR <30 ml/min, n (%)	24 (2.2)	24 (6.8)	0 (0)	<0.01
Hemoglobin < 11 g/dL, n (%)	55 (5.1)	55 (15.5)	0 (0)	<0.01
Recent or recurrent major bleeding, n (%)	1 (0.1)	1 (0.3)	0 (0)	0.33
Platelet count <100 G/L, n (%)	12 (1.1)	12 (3.4)	0 (0)	<0.01
Chronic bleeding diathesis, n (%)	0 (0)	0 (0)	0 (0)	na
Liver cirrhosis with portal hypertension, n (%)	4 (0.4)	4 (1.1)	0 (0)	<0.01
Active malignancy < 12 months, n (%)	19 (1.8)	19 (5.4)	0 (0)	<0.01
Previous spontaneous ICH (any time), previous traumatic ICH <12 months, presence of bAVM, major ICH <6 months, n (%)	5 (0.5)	5 (1.4)	0 (0)	<0.01
Non-deferrable major surgery on DAPT, n (%)	6 (0.6)	6 (1.7)	0 (0)	<0.01
Recent major surgery or major trauma <30 days before PCI, n (%)	0 (0)	0 (0)	0 (0)	na
Minor HBR criteria				
Age ≥ 75 years, n (%)	282 (26.1)	211 (60.0)	71 (9.8)	<0.01
eGFR 30–59mL/min, n (%)	213 (19.7)	183 (51.7)	30 (4.1)	<0.01
Hemoglobin 11–12.9 g/dL for men and 11–11.9 g/dL for women, n (%)	150 (13.9)	108 (30.5)	42 (5.8)	<0.01
Spontaneous major bleeding not meeting the major criterion, n (%)	0 (0)	0 (0)	0 (0)	na
Long-term use of oral NSAIDs or steroids, n (%)	60 (5.6)	41 (11.6)	19 (2.6)	<0.01
Any ischemic stroke > 6 months, n (%)	45 (4.2)	31 (8.8)	14 (1.9)	<0.01

bAVM, brain arteriovenous malformation; DAPT, dual antiplatelet therapy; eGFR, eGFR, estimated glomerular filtration rate; HBR, high bleeding risk; LBR, low bleeding risk, ICH, intracerebral hemorrhage; NSAIDs, Non-steroidal anti-inflammatory drugs; OAC, oral anticoagulation. eGFR: the closest plasma creatinine value before the procedure was taken, excluding values that may be consistent with acute renal failure; Hemoglobin: same reasoning as for eGFR; Platelet count: same reasoning as for eGFR and Hb; Non-deferrable major surgery on DAPT: we considered that any patient who had surgery that was done under DAPT was assigned this major criterion.

All statistical analyses were performed using dedicated software (StataCorp LP, College Station, Texas) at a 2-tailed significance level of alpha = 0.05.

RESULTS

Baseline Characteristics

Of the 1,080 patients enrolled in the registry, 354 (32.7%) fulfilled the HBR definition and the remaining 726 (67.2%) were considered LBR (**Supplementary Figure 1**). HBR criteria and distribution are summarized in **Table 1,** and baseline characteristics are found in **Table 2**. The most frequent major HBR criterion was oral anticoagulation (OAC) (36.7%). Patients in the HBR group were older (76 [70–82] vs. 63 [56–70], $p < 0.01$), with more women (29.7% vs. 20.8%, $p < 0.01$), a higher incidence of arterial hypertension (72.0 vs. 56.3%, $p < 0.01$) but a lower incidence of positive family history for cardiovascular events (15.6 vs. 23.8%, $p < 0.01$) and less current smoker (17.8 vs. 33.3%, $p < 0.01$).

The LBR group had a higher proportion of NSTEMI and STEMI. HAS-BLED, HEMMORR2HAGE and PARIS bleeding score were significantly higher in the HBR group.

In the whole patient population, at least 1 minor criterion was present in 456 patients (42.2%), while in the LBR group at least 1 minor criterion was found in 176 patients (24.4%). The most frequent minor HBR criterion was age >75 years (26.1%).

Antithrombotic Regimens

The antithrombotic regimens were collected at hospital discharge and are summarized in **Table 3.** A DAPT therapy was initiated in 87.7%, of which aspirin + prasugrel was the most frequent combination (54.4%). As expected, there are significant differences between HBR and LBR groups with less DAPT (64.7 vs. 98.9%, $p < 0.01$), and half as much prasugrel use ($p < 0.01$) in the HBR (27.7%) compared to the LBR (67.4%) group. Triple antithrombotic therapy (TAT) was prescribed in 11.4% of patients. Interestingly, 1 (0.1%) LBR patient was given VKA after PCI. Since bleeding risk was assessed at time of PCI, even though the patient fulfilled a major HBR criteria at time of discharge, he was still considered in the LBR group.

Clinical Endpoints

Clinical endpoints are summarized in **Table 4**; **Figures 1**, **2**.

At 2-year follow-up, (17.5%) patients had a bleeding event, and (21.3%) an ischemic event. As anticipated, bleeding rates were higher in HBR compared to the LBR group with a 2.2-fold higher risk of any bleeding (26.6 vs. LBR 13.1%, $p < 0.01$) and a 7.5-fold higher risk of major

TABLE 2 | Baseline characteristics.

	All $N = 1,080$	HBR $N = 354$	LBR $N = 726$	*p*-value
Age, year [IQR]	67 [58–75]	76 [70–82]	63 [56–70]	<0.01
Male, n (%)	824 (76.3)	249 (70.3)	575 (79.2)	<0.01
Hypertension, n (%)	664 (61.5)	255 (72.0)	409 (56.3)	<0.01
Diabetes, n (%)	263 (24.4)	103 (29.1)	160 (22.0)	0.01
Insulin-dependent, n (%)	78 (7.2)	35 (9.9)	43 (5.9)	0.02
Smoking, n (%)	305 (28.2)	63 (17.8)	242 (33.3)	<0.01
Dyslipidemia, n (%)	501 (46.4)	155 (43.8)	346 (47.7)	0.24
BMI, kg/m^2 [IQR]	27.0 [24.2–29.8]	26.2 [23.6–29.4]	27.2 [24.7–29.9]	<0.01
eGFR, mL/min [IQR]	82.2 [62.3–107.2]	56.9 [43.1–77.6]	92.0 [75.1–113.3]	<0.01
Hemoglobin, g/dL [IQR]	14.2 [12.9–15.3]	12.9 [11.7–14.2]	14.6 [13.8–15.6]	<0.01
Thrombocytes, G/L [IQR]	232.0 [193.0–275.5]	228 [186–278]	233 [199–273]	0.31
Family History, n (%)	227 (21.0)	56 (15.8)	171 (23.6)	<0.01
Previous PCI, n (%)	319 (29.5)	109 (30.8)	210 (28.9)	0.57
Previous CABG, n (%)	115 (10.7)	46 (13.0)	69 (9.5)	0.09
Previous MI, n (%)	137 (12.7)	49 (13.8)	88 (12.1)	0.44
Clinical presentation				
Silent ischemia, n (%)	111 (10.3)	33 (9.3)	78 (10.7)	0.52
Stable angina, n (%)	222 (20.6)	76 (20.1)	146 (21.5)	0.63
Unstable angina, n (%)	114 (10.6)	29 (8.2)	85 (11.7)	0.09
NSTEMI, n (%)	259 (24.0)	71 (20.1)	188 (25.9)	0.04
STEMI, n (%)	245 (22.7)	67 (18.9)	178 (24.5)	0.04
Staged procedure, n (%)	20 (1.8)	10 (2.8)	10 (1.4)	0.15
Other, n (%)	109 (10.1)	68 (19.2)	41 (5.7)	<0.01
HAS-BLED score, mean ± SD	2.23 ± 0.97	2.92 ± 0.90	1.89 ± 0.79	<0.01
HEMMORR2HAGE score, mean ± SD	2.05 ± 1.37	3.12 ± 1.70	1.52 ± 0.76	<0.01
PARIS score, mean ± SD	4.44 ± 2.55	6.86 ± 2.45	3.26 ± 1.59	<0.01

Continuous variables are expressed as mean ± SD, median [interquartile range] or number (%).
BMI, body mass index; CABG, coronary artery bypass grafting; eGFR, estimated glomerular filtration rate; HBR, high bleeding risk; LBR, low bleeding risk; MI, myocardial infarction; PCI, percutaneous coronary intervention.

TABLE 3 | Antithrombotic regimen at hospital discharge.

	All $N = 1,080$	HBR $N = 354$	LBR $N = 726$	*p*-value
DAPT, n (%)	947 (87.7)	229 (64.7)	718 (98.9)	<0.01
aspirin-clopidogrel, n (%)	264 (24.4)	116 (32.8)	148 (20.4)	<0.01
aspirin-prasugrel, n (%)	587 (54.4)	98 (27.7)	489 (67.4)	<0.01
aspirin-ticagrelor, n (%)	96 (8.9)	15 (4.2)	81 (11.2)	<0.01
TAT, n (%)	123 (11.4)	122 (34.5)	1 (0.1)	<0.01
DAPT-VKA, n (%)	69 (6.4)	68 (19.2)	1 (0.1)	<0.01
DAPT-DOAC, n (%)	54 (5.0)	54 (15.2)	0 (0)	<0.01
SAPT, n (%)	6 (0.6)	0 (0)	6 (0.8)	0.2
OAC + SAPT, n (%)	3 (0.3)	3 (0.8)	0 (0)	0.04
Only OAC, n (%)	1 (0.1)	0 (0)	1 (0.1)	1

DAPT, dual antiplatelet therapy; DOAC, direct oral anticoagulant; HBR, high bleeding risk; LBR, low bleeding risk; TAT, triple antithrombotic therapy; VKA, vitamin K antagonist; SAPT, single antiplatelet therapy.

TABLE 4 | Clinical outcome at 2-year follow-up.

	All $N = 1,080$	HBR $N = 354$	LBR $N = 726$	*p*-value
Bleeding				
Any bleeding, n (%)	189 (17.5)	94 (26.6)	95 (13.1)	<0.01
Cumulative incidence, in % (95% CI)	17.9 (1.2–15.7)	27.7 (23.3–32.8)	13.3 (1.3–11.0)	
Major bleeding (BARC 3-5) at 1 year, n (%)	41 (3.8)	31 (8.8)	10 (1.4)	<0.01
Cumulative incidence, in % (95% CI)	3.9 (0.3–5.2)	9.0 (6.4–12.6)	1.4 (0.8–2.6)	
Major bleeding (BARC 3–5) at 2 years, n (%)	48 (4.4)	37 (10.5)	11 (1.5)	<0.01
Cumulative incidence, in % (95% CI)	4.6 (3.5–6.0)	11.0 (8.1–14.8)	1.6 (0.9–2.8)	
POCE				
Any POCE, n (%)	230 (21.3)	100 (27.4)	130 (18.2)	<0.01
Any death, n (%)	72 (6.7)	51 (14.0)	21 (2.9)	<0.01
MI, n (%)	54 (5.0)	28 (7.7)	26 (3.6)	<0.01
Repeat revascularization, n (%)	150 (13.9)	49 (13.4)	101 (14.1)	0.99

BARC, Bleeding Academic Research Consortium; CI, confidence interval; HBR, high bleeding risk; LBR, low bleeding risk; MI, myocardial infarction; POCE, patient-oriented composite endpoints.

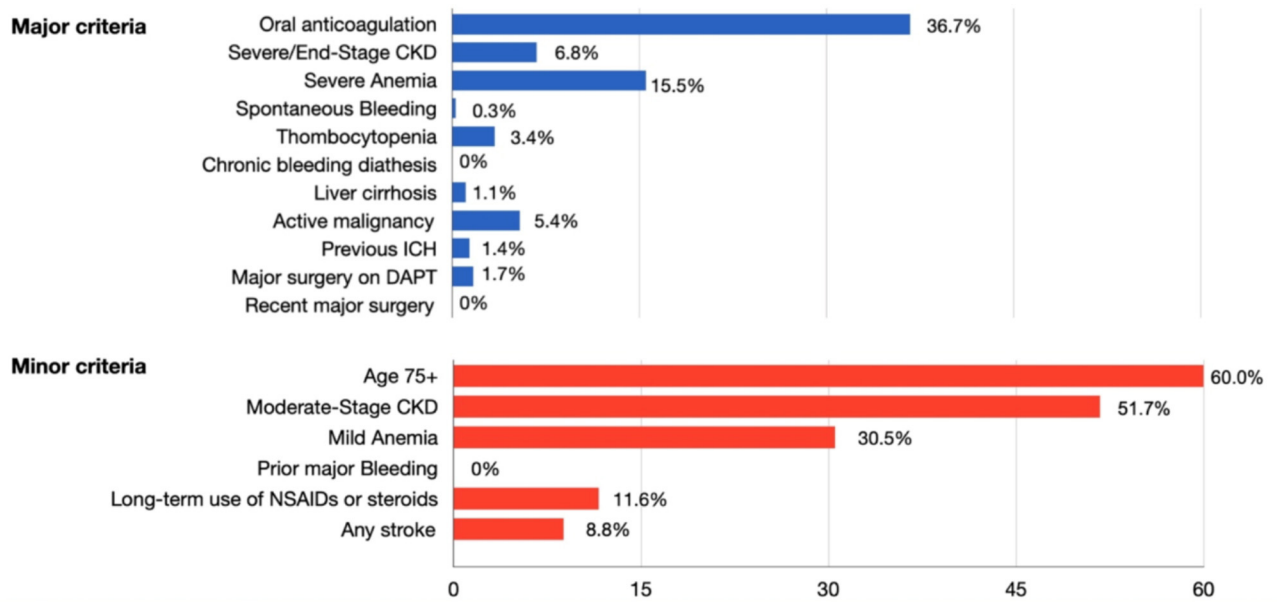

FIGURE 1 | Prevalence of the ARC-HBR criteria in the HBR group. ARC, Academic Research Consortium; CKD, chronic kidney disease; DAPT, dual antiplatelet therapy; HBR, high bleeding risk; ICH, intracerebral hemorrhage; NSAIDs, non-steroidal anti-inflammatory drugs.

bleeding (10.5 vs. LBR 1.5%, $p < 0.01$). Interestingly, one-third of major bleedings occurred during the first month after PCI.

Multivariate Analysis of ARC-HBR Criteria

When included in the multivariable analysis, the major criteria mostly associated with BARC 3–5 major bleeding were moderate to severe anemia (HR 10.20 [5.39–19.30]; $p < 0.01$) and recent or recurrent major bleeding (HR 10.30 [1.30–82.19]; $p = 0.03$). With regards to minor criteria, major bleeding was mostly associated with age ≥75 year (HR 2.36 [1.19–4.70]; $p = 0.01$) and moderate renal failure (HR 2.36 [1.19–4.68]; $p = 0.01$). Overall, moderate to severe anemia was the ARC-HBR criterion associated with the highest risk of major bleeding complications at 2 years (**Supplementary Table 1**).

Subgroup Analysis

Among patients with multiple ARC-HBR criteria, major bleeding risk increases incrementally (one ARC-HBR criterion: 2.8-fold higher risk of bleeding; two ARC-HBR criteria: 3.2-fold higher risk of bleeding; three ARC-HBR criteria: 8.1-fold higher risk of bleeding, four ARC-HBR criteria: 14.9-fold higher risk of bleeding) (**Figure 3**).

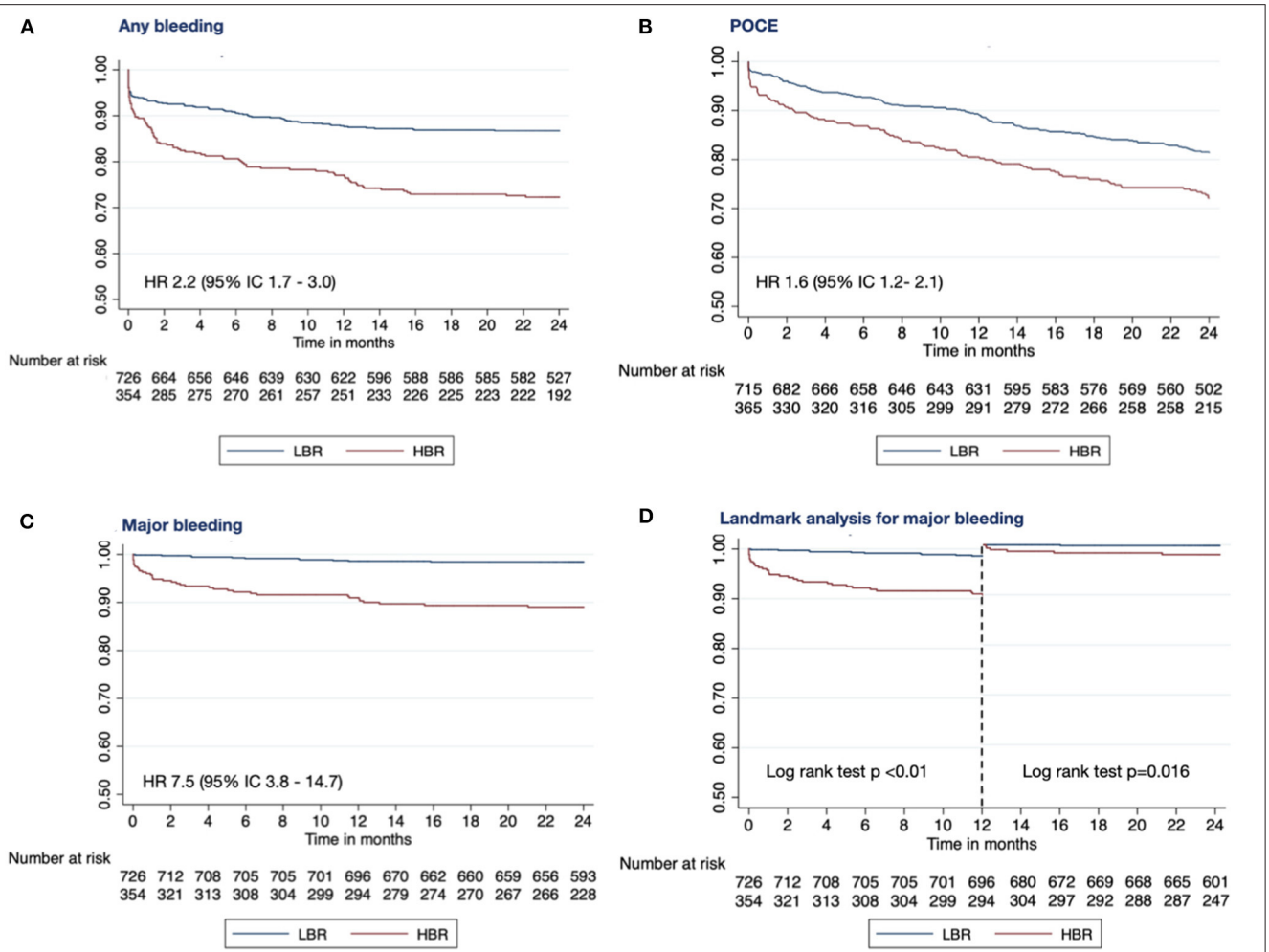

FIGURE 2 | Kaplan-Meier survival curves showing any bleeding **(A)**, POCE [composite of all-cause death, any myocardial infarction and any repeat revascularization; **(B)**] and major bleeding **(C)** survival free at 2 years of follow-up. Landmark analysis **(D)** in patients with low-(LBR) and high-(HBR) bleeding risk. HBR, high bleeding risk; LBR, low bleeding risk; POCE, patient oriented composite endpoint.

DISCUSSION

The main results of this study are: (1) patients defined as HBR by the ARC-HBR definition are frequent in an unselected European population undergoing PCI; (2) the criteria defined by ARC-HBR accurately predict bleeding risk; (3) the impact of HBR risk factors is incremental; (4) one-third of major bleeding occurs during the first month after PCI; (5) the increased risk of bleeding is associated with an increased risk of ischemic events during a 2-year clinical follow-up.

Although a significant proportion of patients undergoing PCI are at high bleeding risk, they are often unrecognized and have also been excluded from many clinical trials (16). In a Japanese registry including 13,018 patients, Natsuaki et al. have observed that 43% fulfilled the ARC-HBR definition (17). The risk of bleeding at one year was 10.4% for HBR vs. 3.4% for the non-HBR group. They also demonstrated an incremental increase in GUSTO moderate to severe bleeding events according to the presence or absence of major and minor criteria. The risk of bleeding was 6.6% in patients without HBR-criteria, 14.7% with two minor HBR-criteria, 18.5% with one major HBR-criteria, 30.6% with two majors HBR-criteria, and 49.9% in patients with $\geq$3 major HBR-criteria. However, the use of GUSTO definition to define major bleedings, with a follow-up at one year, limits direct comparison with other registers.

Recently, Cao et al. (12) applied the ARC-HBR definition in a large cohort of 9,623 patients. The rate of primary bleeding endpoint at 1 year was 9.1% in HBR patients compared with 3.2% in non-HBR patients ($p < 0.001$). Not all the 20 ARC-HBR criteria were present in the analysis and reported severe bleeding events only partially overlapped with the BARC type 3 to 5 criteria.

We observed a similar rate of 32.8% of patients fulfilling the ARC-HBR definition. Our bleeding rates differ slightly with 8.8% of HBR patients presenting a major bleeding event vs. 1.4% in the LBR group. This may be in part explained by the inherent

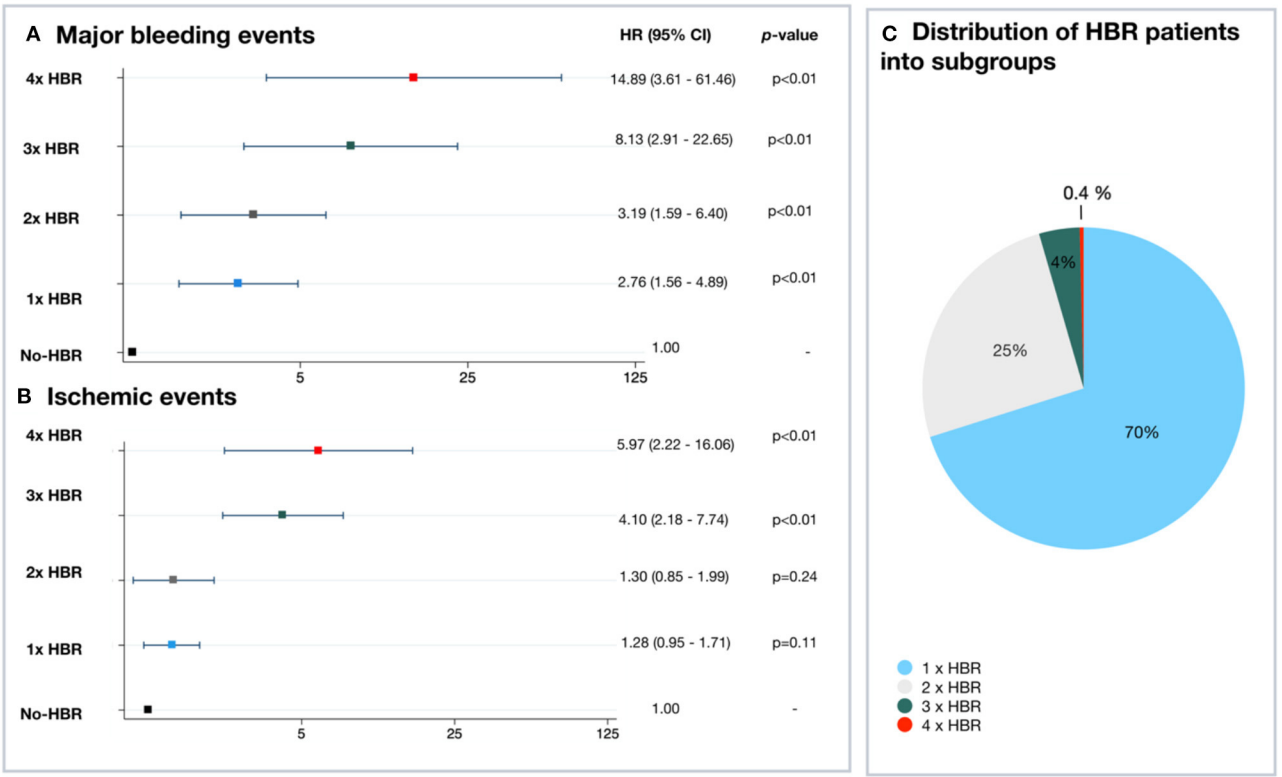

FIGURE 3 | Incremental risk of major bleeding and ischemic endpoints according to the number of ARC-HBR criteria. **(A,B)** Risk of major bleeding and ischemic endpoints at 2 years for each HBR subgroup. **(C)** Distribution of HBR patients into subgroups. ARC, Academic Research Consortium; CI, confidence interval; HBR, high bleeding risk; HR, hazard ratio; LBR, low bleeding risk.

differences in baseline characteristics, DAPT strategies, bleeding definitions, and also the fact that not all major and minor criteria identified by the consortium were taken into consideration in the Japanese cohort.

In line with previous studies, we have observed a higher rate of POCE in HBR patients compared to LBR (18, 19). Overall, ACR-HBR patients may be at increased ischemic risk, as some risk factors present in the ARC-HBR definition are also global ischemic factors (20).

When considering DAPT duration strategies, it seems, that the bleeding risk may outweigh the ischemic risk in HBR patients, favoring shorter DAPT strategies (21). Eikelboom et al. have observed that 53% of bleeding in HBR and LBR patients occurred within the first month after PCI for acute coronary syndromes (22). Some patients will have a switch of DAPT therapy or anticoagulation which increases the risk of bleeding. Moreover, even short DAPT strategies recommend a minimum of 1-month DAPT. This vulnerable period may warrant a more specific and closer follow-up in HBR patients. We observed that one-third of patients bleed during the first month, which still implies that the majority of patients bleed after this critical period and underscores the importance of de-escalation of antiplatelet and antithrombotic therapies where appropriate.

Finally, we have observed an increased overall mortality in HBR patients compared to LBR patients. This observation may, in part, be driven by the fact that HBR patients have substantially more comorbidities than LBR patients. We did not observe any fatal bleeding events.

LIMITATIONS

Our study is limited in size and conclusions should be interpreted as hypothesis-generating. This is was not a prospective assessment of the ARC-HBR definition, and the retrospective nature of the study raises the issue of unmeasured bias as well as incomplete data collection. However, patients with incomplete records were excluded from the study. One should be cautious in extrapolating the current results as this was a single-center study with homogenous practices amongst operators, a preponderant use of the femoral approach, and a majority of prasugrel as P2Y12 inhibitor for DAPT. We did not have data on DAPT adherence after discharge, and future research is important to understand how these factor influence bleeding rates in HBR patients. Another limitation is that some criteria are binary for simplification purposes, while the risk of bleeding and ischemic events is a continuum.

CONCLUSION

The new ARC-HBR definition appropriately identified a population of patients at higher risk of bleeding after percutaneous coronary intervention. This increased risk of bleeding is associated with an increased risk of ischemic events during a 2-year clinical follow-up.

DATA AVAILABILITY STATEMENT

The raw data supporting the conclusions of this article will be made available by the authors, without undue reservation.

ETHICS STATEMENT

The studies involving human participants were reviewed and approved by CER-VD (Lausanne). The patients/participants provided their written informed consent to participate in this study.

AUTHOR CONTRIBUTIONS

DD, ID, SS, DA, SeC, TH, PW, J-CS, J-JG, MT, SP, and StC have made substantial contributions to conception and design of the study, data acquisition, data analysis and interpretation, writing of the paper, and critical review for important intellectual content. All authors contributed to the article and approved the submitted version.

FUNDING

The trial was an investigator-initiated study supported by an unrestricted grant from the Fonds Scientifique Cardiovasculaire (Fribourg, Switzerland).

ACKNOWLEDGMENTS

The authors would like to acknowledge research nurses Estelle Boute and Yannick Faucherre for their dedication and contribution to the patients' follow-up and database record.

SUPPLEMENTARY MATERIAL

The Supplementary Material for this article can be found online at: https://www.frontiersin.org/articles/10.3389/fcvm.2021.620354/full#supplementary-material

REFERENCES

1. Mauri L, Kereiakes DJ, Yeh RW, Driscoll-Shempp P, Cutlip DE, Steg PG, et al. Twelve or 30 months of dual antiplatelet therapy after drug-eluting stents. *N Engl J Med.* (2014) 371:2155–66. doi: 10.1056/NEJMoa1409312
2. Yeh RW, Kereiakes DJ, Steg PG, Windecker S, Rinaldi MJ, Gershlick AH, et al. Benefits and risks of extended duration dual antiplatelet therapy after PCI in patients with and without acute myocardial infarction. *J Am Coll Cardiol.* (2015) 65:2211–21. doi: 10.1016/j.jacc.2015.03.003
3. Garg P, Galper BZ, Cohen DJ, Yeh RW, Mauri L. Balancing the risks of bleeding and stent thrombosis: a decision analytic model to compare duration of dual antiplatelet therapy after drug-eluting stents. *Am Heart J.* (2015) 169:222–33. doi: 10.1016/j.ahj.2014.11.002
4. Valgimigli M, Bueno H, Byrne RA, Collet JP, Costa F, Jeppsson A, et al. 2017 ESC focused update on dual antiplatelet therapy in coronary artery disease developed in collaboration with EACTST. *Eur Heart J.* (2020) 39:213–60. doi: 10.1093/eurheartj/ehx419
5. Levine GN, Bates ER, Bittl JA, Brindis RG, Fihn SD, Fleisher LA, et al. 2016 ACC/AHA Guideline focused update on duration of dual antiplatelet therapy in patients with coronary artery disease: a report of the American College of Cardiology/American Heart Association Task Force on clinical practice guidelines. *J Am Coll Cardiol.* (2016) 134:192–4. doi: 10.1161/CIR.0000000000000453
6. Barber U, Mehran R, Giustino G, Cohen DJ, Henry TD, Sartori S et al. Coronary thrombosis and major bleeding after PCI with drug-eluting stents: risk scores from PARIS. *J Am Coll Cardiol.* (2016) 67:2224–34. doi: 10.1016/j.jacc.2016.02.064
7. Dangas GD, Claessen BE, Mehran R, Xu K, Fahy M, Parise H, et al. Development and validation of a stent thrombosis risk score in patients with acute coronary syndromes. *JACC Cardiovasc Interv.* (2012) 5:1097–105. doi: 10.1016/j.jcin.2012.07.012
8. Palmerini T, Genereux P, Caixeta A, Cristea E, Lansky A, Mehran R, et al. A new score for risk stratification of patients with acute coronary syndromes undergoing percutaneous coronary intervention: the ACUITY-PCI (Acute Catheterization and Urgent Intervention Triage Strategy-Percutaneous Coronary Intervention) risk score. *JACC Cardiovasc Interv.* (2012) 5:1108–16. doi: 10.1016/j.jcin.2012.07.011
9. Urban P, Mehran R, Colleran R, Angiolillo DJ, Byrne RA, Capodanno D, et al. Defining high bleeding risk in patients undergoing percutaneous coronary intervention: a consensus document from the Academic Research Consortium for High Bleeding Risk. *Eur Heart J.* (2019) 40:2632–53. doi: 10.1093/eurheartj/ehz372
10. Gage BF, Yan Y, Milligan PE, Waterman AD, Culverhouse R, Rich MW et al. Clinical classification schemes for predicting hemorrhage: results from the National Registry of Atrial Fibrillation (NRAF). *Am Heart J.* (2006) 151:713–9. doi: 10.1016/j.ahj.2005.04.017
11. Miura K, Shimada T, Ohya M, Murai R, Amano H, Kubo S, et al. Prevalence of the Academic Research Consortium for high bleeding risk criteria and prognostic value of a simplified definition. *Circ J.* (2020) 84:1560–7. doi: 10.1253/circj.CJ-20-0395
12. Cao D, Mehran R, Dangas G, Baber U, Sartori S, Chandiramani R, et al. Validation of the Academic Research Consortium high bleeding risk definition in contemporary PCI patients. *J Am Coll Cardiol.* (2020) 75:2711–22. doi: 10.1016/j.jacc.2020.03.070
13. Nakamura M, Kadota K, Nakao K, Nakagawa Y, Shite J, Yokoi H, et al. High bleeding risk and clinical outcomes in east asian patients undergoing percutaneous coronary intervention: the PENDULUM registry. *EuroIntervention.* (2020) 75:2711–22. doi: 10.4244/EIJ-D-20-00345
14. Neumann F-J, Sousa-Uva M, Ahlsson A, Alfonso F, Banning AP, Benedetto U, et al. 2018 ESC/EACTS guidelines on myocardial revascularization. *Eur Heart J.* (2020) 40:87–165. doi: 10.1093/eurheartj/ehy855
15. Mehran R, Rao SV, Bhatt DL, Gibson CM, Caixeta A, Eikelboom J, et al. Standardized bleeding definitions for cardiovascular clinical trials: a consensus report from the Bleeding Academic Research Consortium. *Circulation.* (2011) 123:2736–47. doi: 10.1161/CIRCULATIONAHA.110.009449
16. Mortensen J, Thygesen SS, Johnsen SP, Vinther PM, Kristensen SD, Refsgaard J. Incidence of bleeding in 'real-life' acute coronary syndrome patients treated with antithrombotic therapy. *Cardiology.* (2008) 111:41–6. doi: 10.1159/000113426

17. Natsuaki M, Morimoto T, Shiomi H, Yamaji K, Watanabe H, Shizuta S, et al. Application of the Academic Research Consortium high bleeding risk criteria in an all-comers registry of percutaneous coronary intervention. *Circ Cardiovasc Interv*. (2019) 12:e008307. doi: 10.1161/CIRCINTERVENTIONS.119.008307
18. Yeh RW, Secemsky EA, Kereiakes DJ, Normand SL, Gershlick AH, Cohen DJ, et al. Development and validation of a prediction rule for benefit and harm of dual antiplatelet therapy beyond 1 year after percutaneous coronary intervention. *JAMA*. (2016) 315:1735–49. doi: 10.1001/jama.2016.3775
19. Natsuaki M, Morimoto T, Yamaji K, Watanabe H, Yoshikawa Y, Shiomi H, et al. Prediction of thrombotic and bleeding events after percutaneous coronary intervention: CREDO-Kyoto thrombotic and bleeding risk scores. *J Am Heart Assoc*. (2018) 7:e008708. doi: 10.1161/JAHA.118.008708
20. Costa F, van Klaveren D, James S, Heg D, Räber L, Feres F, et al. Derivation and validation of the predicting bleeding complications in patients undergoing stent implantation and subsequent dual antiplatelet therapy (PRECISE-DAPT) score: a pooled analysis of individual-patient datasets from clinical trials. *Lancet*. (2017) 389:1025–34. doi: 10.1016/S0140-6736(17)30397-5
21. Costa F, Van Klaveren D, Feres F, James S, Räber L, Pilgrim T, et al. Dual antiplatelet therapy duration based on ischemic and bleeding risks after coronary stenting. *J Am Coll Cardiol*. (2019) 73:741–54. doi: 10.1016/j.jacc.2018.11.048
22. Eikelboom JW, Mehta SR, Anand SS, Xie C, Fox KA. and Yusuf S. Adverse impact of bleeding on prognosis in patients with acute coronary syndromes. *Circulation*. (2006) 114:774–82. doi: 10.1161/CIRCULATIONAHA.106.612812

Conflict of Interest: The authors declare that the research was conducted in the absence of any commercial or financial relationships that could be construed as a potential conflict of interest.

Publisher's Note: All claims expressed in this article are solely those of the authors and do not necessarily represent those of their affiliated organizations, or those of the publisher, the editors and the reviewers. Any product that may be evaluated in this article, or claim that may be made by its manufacturer, is not guaranteed or endorsed by the publisher.

frontiers in Cardiovascular Medicine

BRIEF RESEARCH REPORT
published: 09 March 2022
doi: 10.3389/fcvm.2022.856684

Rare Cases of Bronchial Aneurysm and Comparison of Interventional Embolization in the Treatment of True Bronchial Aneurysm and Pseudobronchial Aneurysm

Jia-Li Lin[1†], Yuan-Yuan Ji[1†], Ming-Zhe Zhang[1†], Yi Tang[1,2], Ruo-Li Wang[1], Dan-Dan Ruan[1], Yan-Feng Zhou[1,2], Shao-Jie Wu[1,2], Sen-Lin Cai[1,2], Jian-Hui Zhang[1], Xiao-Rong Meng[1], Jie-Wei Luo[1] and Zhu-Ting Fang[1,2]**

[1] Shengli Clinical Medical College of Fujian Medical University, Fuzhou, China, [2] Department of Interventional Radiology, Fujian Provincial Hospital, Fuzhou, China

OPEN ACCESS

Edited by:
Xiaofeng Yang,
Temple University, United States

Reviewed by:
Paul C. Tang,
University of Michigan, United States
Antonio Bozzani,
San Matteo Hospital Foundation (IRCCS), Italy

***Correspondence:**
Jie-Wei Luo
docluo0421@aliyun.com
Zhu-Ting Fang
470389481@qq.com

[†] These authors have contributed equally to this work

Specialty section:
This article was submitted to Cardiovascular Therapeutics, a section of the journal Frontiers in Cardiovascular Medicine

Received: 17 January 2022
Accepted: 17 February 2022
Published: 09 March 2022

Citation:
Lin J-L, Ji Y-Y, Zhang M-Z, Tang Y, Wang R-L, Ruan D-D, Zhou Y-F, Wu S-J, Cai S-L, Zhang J-H, Meng X-R, Luo J-W and Fang Z-T (2022) Rare Cases of Bronchial Aneurysm and Comparison of Interventional Embolization in the Treatment of True Bronchial Aneurysm and Pseudobronchial Aneurysm. Front. Cardiovasc. Med. 9:856684. doi: 10.3389/fcvm.2022.856684

Background: Bronchial artery aneurysm (BAA) is a rare disease. Rupture of BAA can lead to life-threatening hemoptysis, and once diagnosed, treatment is needed regardless of symptoms. Transcatheter artery embolization is the first choice of treatment because it is minimally invasive and effective. This study aimed to retrospectively compare the embolization treatment of a case of true BAA and that of a pseudobranchial aneurysm and explore the choice of embolization method for BAA with short neck or no neck.

Materials and Methods: Embolization treatment and imaging characteristics of one case of true BAA and one case of pseudobronchial aneurysm admitted to our hospital were analyzed retrospectively. Embolization methods and therapeutic effects of two cases of BAAs were compared.

Results: Case 1 was that of an intact true BAA inside the mediastinum located at the opening of the bronchial artery. The distal end of the aneurysm was embolized, and tumor cavity was occluded. No recurrence of BAA was found after the operation. Case 2 was that of a ruptured and hemorrhagic pseudobronchial aneurysm of the mediastinum. Coil embolization combined with covered stent graft exclusion of the thoracic aorta were performed, and the left bronchial artery and BAA were almost occluded. Nine months postoperatively, the mediastinal hematoma was almost completely absorbed.

Conclusion: Endovascular embolization has become the most commonly used for the treatment of BAA. Different methods should be selected according to the location and nature of the aneurysm.

Keywords: bronchial artery aneurysm, transcatheter artery embolization, pseudobronchial aneurysm, endovascular treatment, rare disease

Abbreviations: BAA, bronchial artery aneurysm; TAE, transcatheter artery embolization; CT, computed tomography; CTA, computed tomography angiography; DSA, digital subtraction angiography; Hb, hemoglobin.

INTRODUCTION

Bronchial artery aneurysm (BAA) is a rare disease, and less than 1% of all patients with selective bronchial arteriography have been found (1). Since the first report of BAA, approximately 60 cases have been reported (2). Rupture of BAA can lead to life-threatening hemoptysis (3), and once diagnosed, treatment is needed regardless of symptoms. Transcatheter artery embolization (TAE) is the first choice of treatment because it is minimally invasive and effective. However, due to its low incidence, there are fewer reports on TAE of BAA in China, we present the embolization methods of two patients with BAAs in our study.

CASE PRESENTATION

Case 1

In July 2020, a 63-year-old man presented with recurrent chronic productive cough for more than 40 years prior to admission, occasionally with blood in the sputum. The patient was asymptomatic for dyspnea, dysphagia, or hemoptysis, and denied previous thoracic trauma. Plain chest computed tomography (CT) scan was performed due to cough and shortness of breath with the following findings: bronchiectasis with infection in the middle lobe of the right lung, the lingual segment of the upper lobe, and the lower lobe of the left lung. The patient was examined by gastroscopy (**Figure 1a**) at the local hospital, which showed an "esophageal mass." Then, the patient visited our hospital, and ultrasonic gastroscopy showed an esophageal bulge, vascular compression, and suspected BAA (**Figures 1b,c**). A contrast-enhanced CT scan showed multiple tortuous and thickened vascular shadows, partial aneurysmal dilation (maximum width about 1.3 cm), vaguely connected with the thoracic aorta and left pulmonary vein, and adjacent esophageal compression. Partial bronchiectasis in both lungs with a small amount of inflammation (**Figures 1d–i**).

The patient was normal on physical examination. His laboratory results were generally non-significant, except *hemoglobin* (Hb) level was 119 g/L (normal value 120∼165 g/L) and D-Dimer was 2.43 mg/L (normal value 0–0.55 mg/L). The patient is a chronic HBV carrier and his laboratory tests revealed normal liver function.

The patient was then taken to interventional radiology suite for angiographic evaluation. Percutaneous right femoral artery catheterization was performed under local anesthesia. With digital subtraction angiography(DSA), a 5F catheter was used for thoracic aorta and left and right bronchial artery angiography. Bronchial artery angiography showed no obvious abnormality in ascending, arched and descending aorta; It was equivalent to an aneurysm at the opening of the bronchial artery, approximately 1.5 cm × 1.7 cm. The left and right bronchial arteries were thickened, and disorder vessels were seen in the lungs, especially in the lower left lung, with pulmonary artery branches visible. Embolization of the left bronchial artery was performed with gelatin sponge particles (350–560 um), and the blood flow of the left bronchial artery slowed down significantly after embolization. We decided to embolize the BAA and prepare a thoracic aortic stent implantation. Before the procedures he signed a written informed consent to an endoluminal stent of the thoracic aorta in accordance with our institutional guidelines. Percutaneous right femoral artery puncture and catheterization under local anesthesia were performed, and 5F catheters were used for the thoracic aorta, abdominal aorta, left and right iliac arteries, and left and right bronchial arteriography with DSA. The distal end of the aneurysm was embolized with 700–900 μm microspheres and NESTER coils, and the tumor cavity was occluded. To achieve satisfactory angiographic results, no thoracic aortic stent implantation (**Figure 2**) was performed. The postoperative course was uneventful and the patient was discharged home on postoperative day 6. On CT scan at 4 months, we confirmed satisfactory placement of the aortic stent graft with exclusion and thrombosis of the BAA. No recurrence of bronchial artery aneurysm was found at 10 months after operation.

Case 2

A 65-year-old male patient presented to the emergency department with a 1-day history of retrosternal pain, which was located behind the sternum and was diffuse in scope without fixed location and severe in degree, radiating to the xiphoid process, accompanied by shortness of breath and sweating, occasional cough and sputum. He denied any nausea, hematemesis, or hematochezia. His medical history was retinal detachment. Chest computed tomography angiography(CTA) revealed tortuous and thickened arteries in the posterior mediastinum, hilum of the lung, and left lower lung, which were considered abnormally enlarged and dilated bronchial arteries, accompanied by the formation of proximal aneurysms; therefore posterior mediastinal hematoma was likely (**Figures 3a–c,e,f**). The laboratory results were as follows: peripheral blood white blood cell (WBC) count was 13.8 × 10^9/L (normal value 4–10 × 10^9/L), C reactive protein (CRP) level was 43.70 mg/L (normal value 0.8–8 mg/L), Hb level was 110 g/L, and erythrocyte sedimentation rate (ESR) level was 85 mm in the 1st h. Troponins and D-dimer were negative. Serum tumor markers were negative. Liver and renal function tests were within normal limits. Coagulation profile was normal.

Thoracic surgery and cardiovascular surgery consultation: patients with bronchial pseudoaneurysm, the neck of the aneurysm is shorter, less than 5 mm, the risk of simple embolization is higher, and the patient is prepared for posterior mediastinal hematoma removal in thoracic surgery in the later stage, and the operation has the risk of rebleeding. Therefore, implantation of covered stent in thoracic aorta was proposed. Bronchial arteriography and coil embolization combined with covered stent graft exclusion of thoracic aorta (**Figures 3d,g–l**). The results showed that aneurysmal dilatation of the proximal end of the left bronchial artery with a diameter of approximately 2.6 cm; its branches were tortuous and thickened, and the left pulmonary artery branches could be seen; the right bronchial artery thickened and communicating branches were seen between the right and left bronchial arteries. Bronchial arteriography and coil embolization combined with covered stent graft exclusion of the thoracic aorta

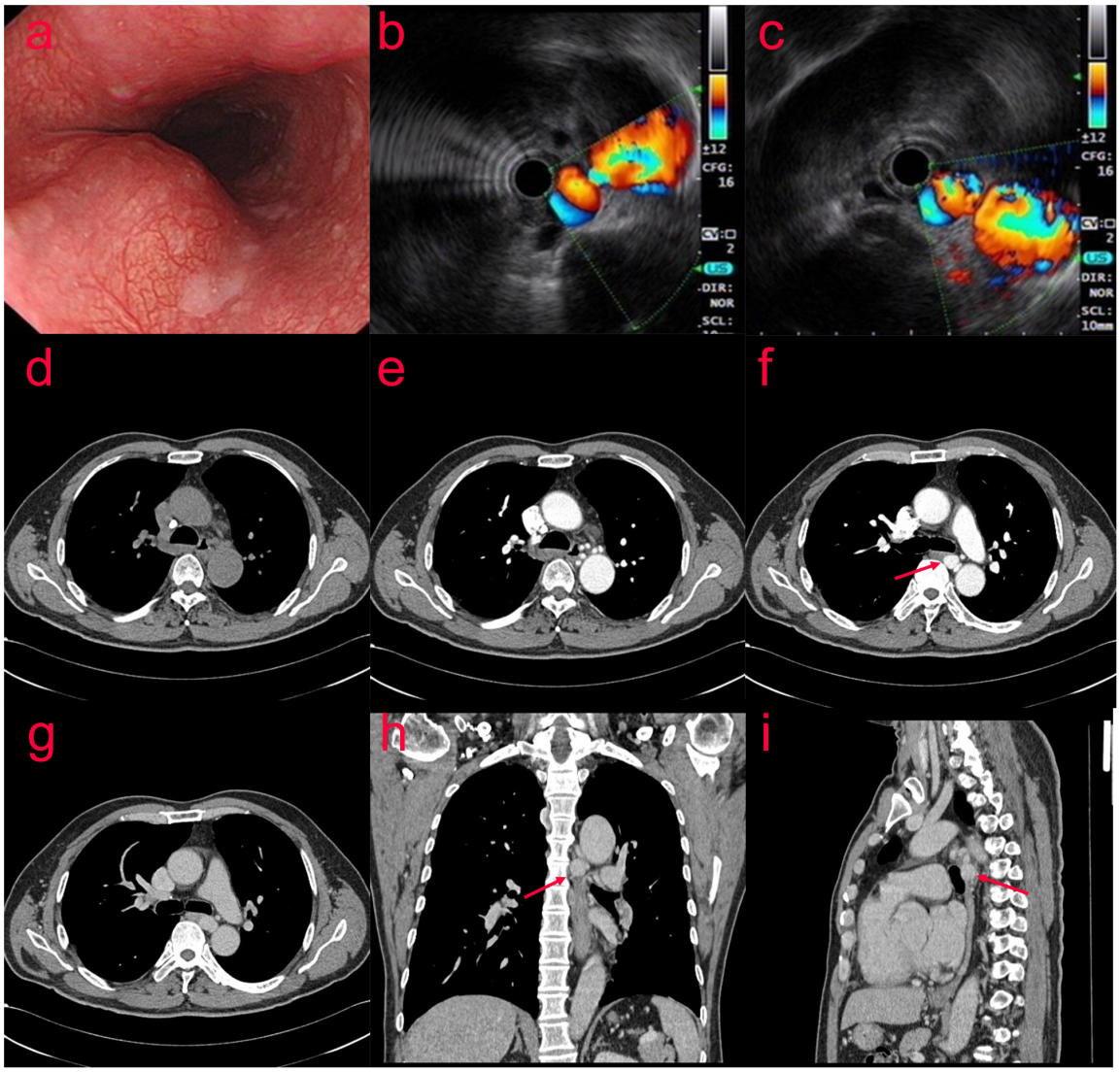

FIGURE 1 | (Case one) The patient with Bronchial artery aneurysm (BAA) was examined by gastroscopy **(a)** at the local hospital, which showed an "esophageal mass." After visiting our hospital, ultrasonic gastroscopy showed an esophageal bulge, vascular compression, and suspected BAA **(b,c)**. A contrast-enhanced CT scan showed multiple tortuous and thickened vascular shadows (maximum width about 1.3 cm) in the middle and posterior mediastinum and around the esophagus **(d–i)**.

was performed (**Figures 3d,g–l**). Microspheres were used for embolization (500–700 um) and coils for embolization were used to occlude the right bronchial artery. After embolizing the left bronchial artery with PVA particles, the left main bronchial trunk and proximal segment aneurysms were embolized with controllable coils. After embolization, the malformed vessels of the left bronchial artery decreased significantly, and the left bronchial artery and aneurysm were almost occluded. A 32/24 × 20 cm covered stent was implanted in the aortic arch and descending aorta. Repeated angiography did not reveal a left BAA. The patient was discharged after 3 days in good general condition.

CTA of thoracic aorta was reexamined 10 days after operation: after stenting of aortic arch and descending aorta, the shape and position of metal stents were good. It adhered to the wall well, and there was no displacement or internal leakage. The mediastinal hematoma was partially absorbed (**Figures 4a–f**). A CT scan performed after 2 months showed no endoleak, no stent migration and the mediastinal hematoma was further absorbed. (**Figures 4g,h**). Nine months after the operation, the mediastinal hematoma was almost completely absorbed (**Figures 4i–k**).

DISCUSSION

Bronchial artery aneurysm is a rare entity. However, it can cause life-threatening hemoptysis when it ruptures (3). There are currently no guidelines available in management of BAAs.

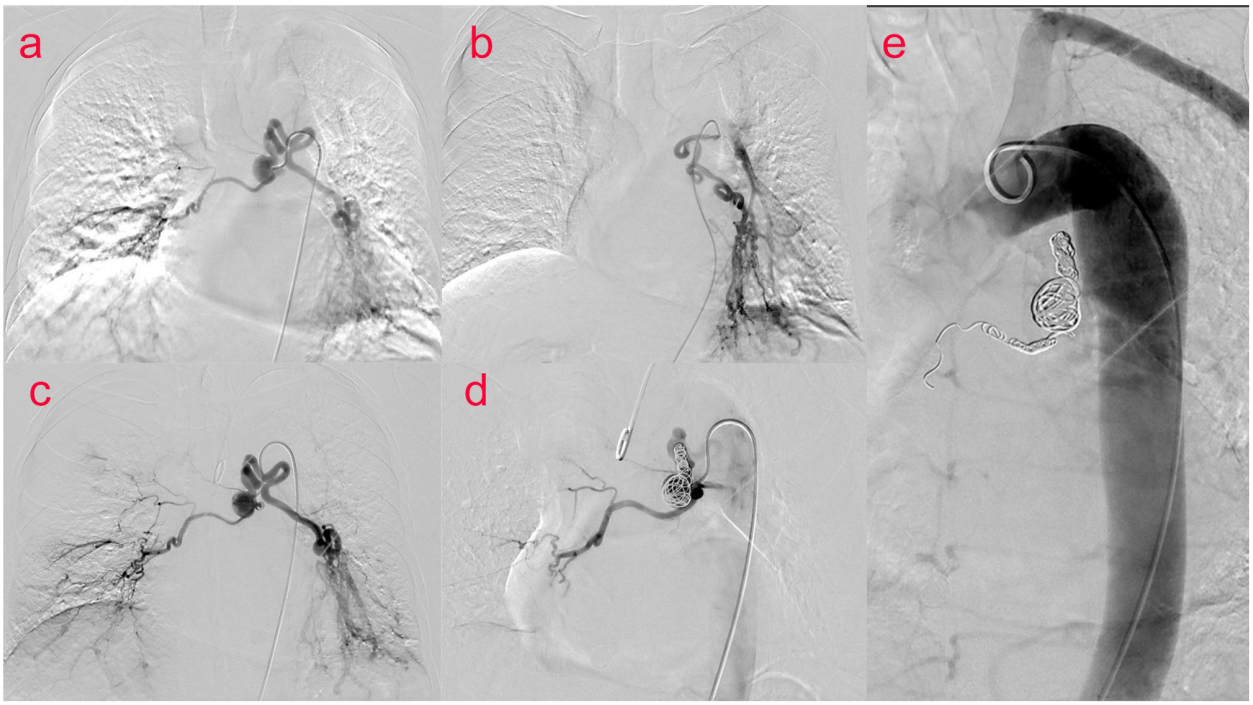

FIGURE 2 | (Case one) Bronchial arteriography **(a–c)** showed an aneurysm at the opening of the bronchial artery of about 1·5 cm × 1·7 cm. Left and right bronchial artery thickening, disordered vessels in the lung, most obviously in the left lower lung, and pulmonary artery branches were seen. BAA and left bronchial artery and pulmonary artery fistula were considered. Percutaneous catheterization of the right femoral artery thoracic aorta, abdominal aorta, left and right iliac arteries, and left and right bronchial arteries was performed. During digital subtraction angiography (DSA) **(d,e)**, the distal end of the aneurysm was embolized with 700–900 μm microspheres and NESTER coils, and the tumor cavity was occluded.

Due to the rarity and lack of animal models of BAA, information remains limited regarding its etiology. However, it is often associated with atherosclerosis, inflammatory lung disease, bronchiectasis, bronchitis, and systemic vascular abnormalities such as Osler-Weber-Rendu syndrome, which is considered to be caused by focal weakening of the blood vessel wall (4). Cheng (5) present a rare case of fatal hemoptysis due to bronchial aneurysm in a patient with active pulmonary tuberculosis. The patient in case 1 had a history of chronic pulmonary infection and bronchiectasis; however, many BAA patients, such as in case 2, do not have a pertinent history, which makes the diagnosis difficult. Pseudoaneurysm is a collection formed by a thrombus or fibrotic substance in its surrounding thrombus. Pseudoaneurysms may be caused by trauma, ruptured aneurysms, or postoperative anastomotic leakage (6).

For patients with BAA, the clinical manifestation depends on the location of the aneurysm and whether it is ruptured. BAA is located inside the mediastinum or inside the lungs. BAA in the mediastinum may show symptoms of compression, such as dysphagia (7, 8) or superior vena cava syndrome (9), or may enter adjacent structures causing ruptured aortic dissection (10). If the aneurysm is ruptured, the BAA inside the lung may cause hemoptysis or hematemesis. The most common symptom after aneurysm rupture is chest pain, followed by hemoptysis, back pain, epigastric pain, and shock. However, if the aneurysm remains intact, the BAA is usually incidentally found during a chest scan. In our hospital, there were two cases of BAA: one case which presented with hemoptysis secondary to bronchiectasis which was found on chest CT and the other case found after complaints of chest pain caused by a ruptured aneurysm. Bronchial arteriography revealed that the BAA in both cases was located inside the mediastinum.

Patients with true BAAs or pseudobronchial aneurysms can be treated with surgery or TAE. BAA resection, bronchial artery ligation, or total pneumonectomy can be performed *via* thoracotomy. Although the lesion can be completely resected, open surgery is more traumatic (11). Compared with surgical treatment, TAE is an effective minimally invasive treatment and is the first choice for BAA. The purpose of TAE is not only blocking the feeding vessels but also blocking the efferent branches to avoid retrograde filling of aneurysms. However, because the blood flow rate and coil transmission cannot be controlled, it is difficult to operate and may lead to embolism of other organs (11). Different methods such as direct embolization, combined film-coated stent isolation, and percutaneous puncture embolization should be selected according to the location and nature of the aneurysm.

If the proximal bronchial artery of the aneurysm is of sufficient length, endovascular coil embolization is preferred (7). However, the aneurysms in our two cases were mediastinal aneurysms, which were located at the opening and had a short neck, making it difficult to embolize the blood vessels.

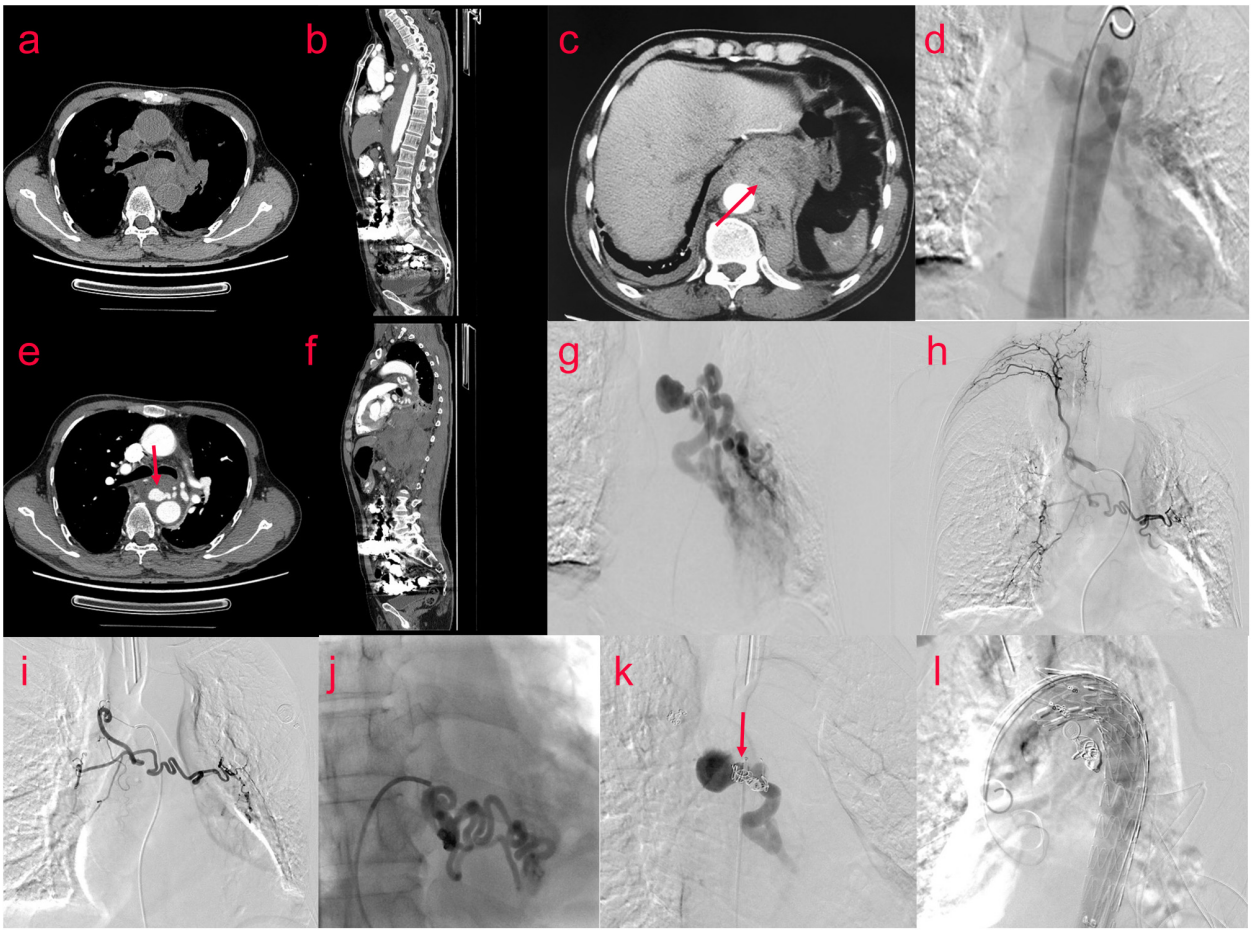

FIGURE 3 | (Case two) A 65-year-old male patient suffered from retrosternal pain for 1 day, the degree was severe, and the scope was diffused. Bronchial arteriography **(d,g,h)** was performed after examination of the chest CTA **(a–c,e,f)**. The aneurysmal dilatation of the proximal end of the left bronchial artery with a diameter of approximately 2.6 cm. Its branches were tortuous and thickened. The left pulmonary artery branches were seen. The right bronchial artery thickened, and the communicating branches were seen between the right bronchial artery and the left bronchial artery. The embolization operation and the thoracic aorta-covered stent implantation were performed. Percutaneous catheterization of left and right femoral artery under general anesthesia and local anesthesia, left and right bronchial artery, and thoracic aorta were performed. Digital subtraction angiography showed that the right bronchial artery was embolized by embolized microspheres (500–700 um) and coils, and the left bronchial artery was embolized by two branches of PVA particles (700 um) **(i,j)**. The left bronchial trunk and proximal segment aneurysms **(k)** were embolized with controllable coils, and a 32/24 × 20 cm covered stent **(l)** was implanted into the aortic arch and descending aorta through the left femoral artery.

When the neck between the BAA and the aorta is short, the operation may be accompanied by distal material migration or insufficient embolization of the aneurysm. In case 1, to maintain a complete true aneurysm, coil and microsphere embolization was used, and the tumor cavity was blocked. To achieve satisfactory angiographic results, a thoracic aorta stent was not implanted. Moreover, placing the stent at this time may be an overtreatment. An additional stent in the thoracic aorta also increases the risk of spinal cord ischemia. Goh believes that placement of a stent-graft may make it impossible for the patient to receive endovascular treatment in the future. A more cautious approach may be to follow-up the patient and place the stent when needed in the future (12). Fu reported that five cases of aneurysms near the opening of the bronchial artery were treated with TAE. Hemoptysis disappeared in all patients. No special or severe complications occurred, and no patient experienced a recurrence during the follow-up (2). In case 2, the body of the pseudoaneurysm was larger, the neck was shorter, the risk of simple embolization was higher, and the patient was prepared for thoracic surgery for posterior mediastinal hematoma removal in the later stage; however, the operation had a risk of rebleeding. Therefore, implantation of a covered stent in the thoracic aorta through coil embolization was proposed combined with covered stent graft exclusion of the thoracic aorta. The stent covered the opening of the bronchial artery and isolated the aortic blood flow. Concurrently, PVA and coils were used to embolize the aneurysm to prevent the aneurysm from refilling. In this case, we successfully isolated a large bronchial aneurysm from the circulation using a thoracic aortic stent graft to block the inflow branch and used coil

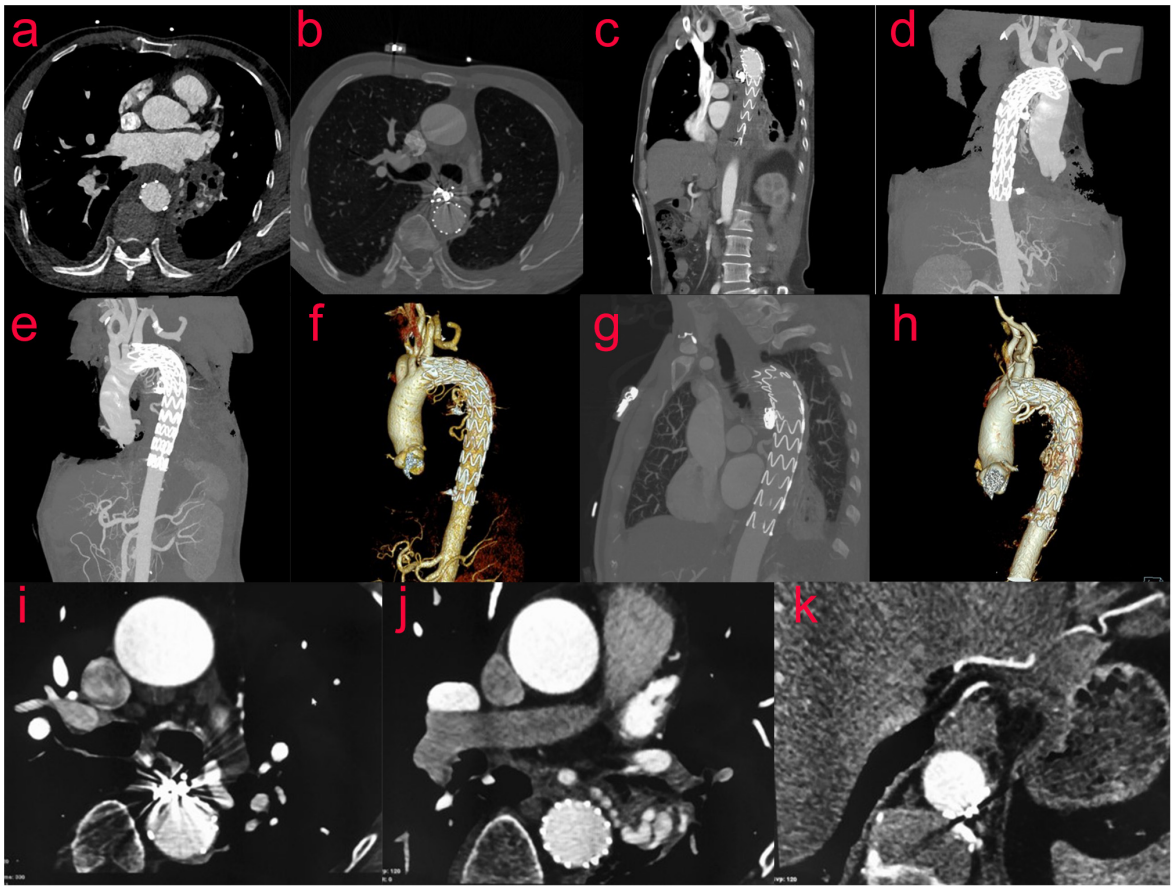

FIGURE 4 | (Case two) CTA of the thoracic aorta was reexamined 10 days after the operation **(a–f)**. After stenting of the aortic arch and descending aorta, the shape and position of the metal stents were evaluated to be good. It adhered to the wall well, and there was no displacement or internal leakage. The mediastinal hematoma was partially absorbed. After 2 months, the reexamination of the thoracic aorta by CTA showed that the mediastinal hematoma was further absorbed, and the stent was in good shape **(g,h)**. Nine months after the operation, the review of CT showed that the mediastinal hematoma was almost completely absorbed **(i–k)**.

to embolize the outflow branch. During follow-up 9 months post-surgery, the mediastinal hematoma was almost completely absorbed. Long-term follow-up of the case and further experience of similar cases are needed to prove the feasibility of this technique. Sakai also reported similar cases using TAE combined with stent implantation to resolve the problem of short neck aneurysms (11, 13–18). Wang (19) reported an aortic stent combined with arterial embolization for the treatment of multiple BAAs with a diffuse bronchial artery and pulmonary artery fistula. Compared with simple embolization, the advantages of embolization and stent implantation include blocking the blood supply to the aneurysm, preventing distal material migration, and blocking the blood flow of potential collateral arteries from the thoracic aorta.

According to the literature, aneurysms with a short neck or no neck can be embolized with detachable coils (20). Mediastinal BAAs with short inflow vessels can be successfully treated with occluders in the patent ductus arteriosus (21). One report pointed out that percutaneous embolization is an option for pseudobronchial aneurysms that cannot be achieved by angiography (22, 23).

CONCLUSION

Endovascular embolization has become the most commonly used and recommended technique, and different methods such as direct embolization, combined film-coated stent isolation, and percutaneous puncture embolization should be selected according to the location and nature of the aneurysm. The methods suitable for anatomical characteristics need to be selected according to the specific conditions of the lesion to achieve the ideal embolization effect, but it is also necessary to prevent over-treatment. Long-term follow-up and further experiences are necessary to evaluate the effectiveness of different treatments.

DATA AVAILABILITY STATEMENT

The original contributions presented in the study are included in the article/supplementary material, further inquiries can be directed to the corresponding authors.

ETHICS STATEMENT

The studies involving human participants were reviewed and approved by the Ethics Committee of Fujian Provincial Hospital. The patients/participants provided their written informed consent to participate in this study.

AUTHOR CONTRIBUTIONS

J-LL, J-HZ, YT, D-DR, and R-LW performed the acquisition, analysis, and interpretation of the clinical data. J-LL, M-ZZ, and Y-YJ drafted the manuscript. S-JW, Y-FZ, S-LC, and X-RM provided critical revision of the manuscript. J-WL and Z-TF designed and supervised the study. All authors read and approved the final manuscript.

FUNDING

This work was supported by the Fujian Province Natural Science Fund Project (2020J011096 and 2020J011064) and the Outstanding Youth Project of Fujian Provincial Hospital (2014YNQN31).

REFERENCES

1. Mizuguchi S, Inoue K, Kida A, Isota M, Hige K, Aoyama T, et al. Ruptured bronchial artery aneurysm associated with bronchiectasis: a case report. *Ann Thorac Cardiovasc Surg.* (2009) 15:115–8.
2. Le-Jun F, Sun Y, Fan Y, Jin S. The effect of transcatheter bronchial artery embolization in five patients with bronchial artery aneurysm. *Postepy Kardiol Interwencyjnej.* (2020) 16:330–5. doi: 10.5114/aic.2020.99269
3. Osada H, Kawada T, Ashida H, Sodemoto Y, Noguchi T. Bronchial artery aneurysm. *Ann Thorac Surg.* (1986) 41:440–2. doi: 10.1016/s0003-4975(10)62706-3
4. Tanaka K, Ihaya A, Horiuci T, Morioka K, Kimura T, Uesaka T, et al. Giant mediastinal bronchial artery aneurysm mimicking benign esophageal tumor: a case report and review of 26 cases from literature. *J Vasc Surg.* (2003) 38:1125–9. doi: 10.1016/s0741-5214(03)00707-9
5. Cheng YS, Lu ZW. Bronchial aneurysm secondary to tuberculosis presenting with fatal hemoptysis: a case report and review of the literature. *J Thorac Dis.* (2014) 6:E70–2. doi: 10.3978/j.issn.2072-1439.2014.04.07
6. Kaufman C, Kabutey NK, Sgroi M, Kim D. Bronchial artery pseudoaneurysm with symptomatic mediastinal hematoma. *Clin Imaging.* (2014) 38:536–9. doi: 10.1016/j.clinimag.2014.01.010
7. Sakuma K, Takase K, Saito H, Zuguchi M, Tabayashi K. Bronchial artery aneurysm treated with percutaneous transluminal coil embolization. *Jpn J Thorac Cardiovasc Surg.* (2001) 49:330–2. doi: 10.1007/bf02913144
8. Tringali S, Tiffet O, Berger JL, Cuilleret J. Bronchial artery aneurysm disguised as a leiomyoma of the esophagus. *Ann Thorac Surg.* (2002) 73:632–3. doi: 10.1016/s0003-4975(01)03121-6
9. Hoffmann V, Ysebaert D, De Schepper A, Colpaert C, Jorens P. Acute superior vena cava obstruction after rupture of a bronchial artery aneurysm. *Chest.* (1996) 110:1356–8. doi: 10.1378/chest.110.5.1356
10. Kalangos A, Khatchatourian G, Panos A, Faidutti B. Ruptured mediastinal bronchial artery aneurysm: a dilemma of diagnosis and therapeutic approach. *J Thorac Cardiovasc Surg.* (1997) 114:853–6. doi: 10.1016/s0022-5223(97)70094-1
11. Kano M, Nishibe T, Iwahashi T, Fujiyoshi T, Otaka J, Saguchi T, et al. Successful treatment of bronchial artery aneurysms associated with racemose hemangioma by combined therapy of transcatheter bronchial artery embolization and thoracic endovascular aortic repair. *Vasc Endovascular Surg.* (2020) 54:540–3. doi: 10.1177/1538574420927552
12. Goh Y, Rajendran PC, Loh SEK, Choong A, Ng SJK, Wee B. Transcatheter embolization of a large mediastinal bronchial artery aneurysm with short neck. *ANZ J Surg.* (2019) 89:597–9. doi: 10.1111/ans.14198
13. Sakai T, Razavi MK, Semba CP, Kee ST, Sze DY, Dake MD. Percutaneous treatment of bronchial artery aneurysm with use of transcatheter coil embolization and thoracic aortic stent-graft placement. *J Vasc Interv Radiol.* (1998) 9:1025–8. doi: 10.1016/s1051-0443(98)70445-2
14. Xu Z, Kong Y, Hu C, Huang S, Tan Y. Ruptured bronchial artery aneurysm treated with aortic stent graft and aneurysm embolization. *Curr Med Imaging Rev.* (2019) 15:74–7. doi: 10.2174/1573405613666170926164225
15. Di X, Ji DH, Chen Y, Liu CW, Liu B, Yang J. Endovascular treatment of ectopic bronchial artery aneurysm with brachiocephalic artery stent placement and coil embolization: a case report and literature review. *Medicine (Baltimore).* (2016) 95:e4461. doi: 10.1097/md.0000000000004461
16. Kim YK, Sung YM, Kim JH, Byun SS, Park YN, Lee SP. Aortic stent-graft for a giant bronchial artery aneurysm with ultrashort neck. *Ann Thorac Cardiovasc Surg.* (2014) 20(Suppl.):781–5. doi: 10.5761/atcs.cr.12.02117
17. Guzzardi G, Cerini P, Fossaceca R, Commodo M, Micalizzi E, Carriero A. Endovascular treatment of bronchial artery aneurysm with aortic stent-graft placement and coil embolization. *Ann Vasc Surg.* (2012) 26:1013.e5–8. doi: 10.1016/j.avsg.2012.02.021
18. Hu CX, Huang S, Xu ZW, Chen W, Huang JS, Fu Z. Combination of aortic stent-graft and arterial embolization for ruptured bronchial artery aneurysm. *Ann Thorac Surg.* (2011) 92:e19–21. doi: 10.1016/j.athoracsur.2011.02.082
19. Wang J, Zhou G, Liang B, Makamure J, Pan F, Zhao D, et al. Combination of aortic stent-graft and arterial embolization for multiple bronchial artery aneurysms associated with diffuse bronchial-pulmonary arterial fistulas. *J Vasc Interv Radiol.* (2018) 29:1283–5. doi: 10.1016/j.jvir.2017.12.017
20. Misselt AJ, Krowka MJ, Misra S. Successful coil embolization of mediastinal bronchial artery aneurysm. *J Vasc Interv Radiol.* (2010) 21:295–6. doi: 10.1016/j.jvir.2009.10.030
21. Patel NR, Sidiqi A, Qazi AA, Jaberi A, Forbes TL, Tan KT. Mediastinal bronchial artery aneurysm with short inflow segment successfully treated with a patent ductus arteriosus occluder device. *J Vasc Surg Cases Innov Tech.* (2020) 6:93–5. doi: 10.1016/j.jvscit.2019.12.005
22. Sridhar SK, Sadler D, McFadden SD, Ball CG, Kirkpatrick AW. Percutaneous embolization of an angiographically inaccessible pulmonary artery pseudoaneurysm after blunt chest trauma: a case report and review of the literature. *J Trauma.* (2010) 69:729. doi: 10.1097/TA.0b013e3181d0f69f
23. Urlings TAJ, Irani FG, Velaga J, Too CW. Ultrasound- and fluoroscopic-guided embolization of a bronchial artery pseudoaneurysm in a patient with lung cancer. *J Vasc Interv Radiol.* (2017) 28:1323–5. doi: 10.1016/j.jvir.2017.04.015

Conflict of Interest: The authors declare that the research was conducted in the absence of any commercial or financial relationships that could be construed as a potential conflict of interest.

Publisher's Note: All claims expressed in this article are solely those of the authors and do not necessarily represent those of their affiliated organizations, or those of the publisher, the editors and the reviewers. Any product that may be evaluated in this article, or claim that may be made by its manufacturer, is not guaranteed or endorsed by the publisher.

frontiers | Frontiers in Cardiovascular Medicine

ORIGINAL RESEARCH
published: 05 April 2022
doi: 10.3389/fcvm.2022.861663

Effects of Sacubitril-Valsartan on Clinical, Echocardiographic, and Polygraphic Parameters in Patients Affected by Heart Failure With Reduced Ejection Fraction and Sleep Apnea

Corrado Pelaia[1†], Giuseppe Armentaro[1†], Mara Volpentesta[1], Luana Mancuso[1], Sofia Miceli[1], Benedetto Caroleo[1], Maria Perticone[1], Raffaele Maio[1], Franco Arturi[1], Egidio Imbalzano[2], Francesco Andreozzi[1], Francesco Perticone[1], Giorgio Sesti[3] and Angela Sciacqua[1]*

[1] Department of Medical and Surgical Sciences, University Magna Græcia of Catanzaro, Catanzaro, Italy, [2] Department of Clinical and Experimental Medicine, University of Messina, Messina, Italy, [3] Department of Clinical and Molecular Medicine, Sapienza University of Rome, Rome, Italy

OPEN ACCESS

Edited by:
Atsushi Tanaka,
Saga University, Japan

Reviewed by:
Eiichi Watanabe,
Fujita Health University, Japan
Alberto Giannoni,
Sant'Anna School of Advanced Studies, Italy

***Correspondence:**
Angela Sciacqua
sciacqua@unicz.it

[†] These authors have contributed equally to this work

Specialty section:
This article was submitted to Cardiovascular Therapeutics, a section of the journal Frontiers in Cardiovascular Medicine

Received: 24 January 2022
Accepted: 11 March 2022
Published: 05 April 2022

Citation:
Pelaia C, Armentaro G, Volpentesta M, Mancuso L, Miceli S, Caroleo B, Perticone M, Maio R, Arturi F, Imbalzano E, Andreozzi F, Perticone F, Sesti G and Sciacqua A (2022) Effects of Sacubitril-Valsartan on Clinical, Echocardiographic, and Polygraphic Parameters in Patients Affected by Heart Failure With Reduced Ejection Fraction and Sleep Apnea. Front. Cardiovasc. Med. 9:861663. doi: 10.3389/fcvm.2022.861663

Background: Heart failure with reduced ejection fraction (HFrEF) is a clinical condition frequently diagnosed in clinical practice. In patients affected by HFrEF, sleep apnea (SA) can be detected among the most frequent comorbidities. Sacubitril–valsartan (sac/val) association has been proven to be effective in reducing disease progression and all-cause mortality in HFrEF patients. Sac/val treatment can potentially attenuate SA development *via* several pathophysiologic mechanisms, including improvement of global hemodynamics, reduction of extracellular fluid overload, and decrease of sympathetic neural activity.

Methods: We recruited 132 patients affected by HFrEF and SA, already under treatment with continuous positive airway pressure (CPAP), which was discontinued 24 h before the scheduled study timepoints. Physical examination, echocardiography, nocturnal cardio-respiratory monitoring, and laboratory tests were performed in each patient at baseline and after a 6-month treatment with sac/val.

Results: After 6 months, sac/val induced statistically significant changes in clinical, hemodynamic, biohumoral (NT-proBNP, serum electrolytes, creatinine, and uric acid), and echocardiographic parameters. In particular, cardiac index (CI), both atrial and ventricular volumes and global longitudinal strain (GLS) improved. Moreover, polysomnography, carried out during a temporary CPAP interruption, revealed a significant reduction in global apnea-hypopnea index (AHI) value ($p < 0.0001$), central AHI ($p < 0.0001$), obstructive AHI ($p < 0.0001$), oxygen desaturation index (ODI) ($p < 0.0001$), and percentage time of saturation below 90% (TC90) ($p < 0.0001$). The changes

of CI, estimated glomerular filtration rate (eGFR), NT-proBNP, and tricuspid annular plane excursion (TAPSE) contributed to 23.6, 7.6, 7.3, and 4.8% of AHI variability, respectively, and the whole model accounted for a 43.3% of AHI variation.

Conclusions: Our results suggest that treatment with sac/val is able to significantly improve the cardiorespiratory performance of patients with HFrEF and SA, integrating the positive impact of CPAP. Thus, both CPAP and sac/val therapy may synergistically contribute to lower the risks of both cardiac and pulmonary complications in HFrEF patients with SA.

Keywords: heart failure, sleep apnea, sacubitril-valsartan, echocardiography, apnea-hypopnea index

INTRODUCTION

Heart failure (HF) is a largely diffused clinical condition, being responsible for very high social and economic costs worldwide. In Western countries, about 1–2% of adult people are affected by HF, and the phenotype characterized by reduced ejection fraction (HFrEF) represents more than half of the cases (1). In spite of the relevant improvements recently achieved in pharmacological treatment of HF, prognosis remains quite poor, being characterized by high rates of hospitalization and death (2, 3). In more than 50% of patients with HF, central sleep apneas (CSA) and obstructive sleep apneas (OSA) can be detected among the most frequent comorbidities that significantly contribute to all-cause mortality (4–6). Many therapeutic strategies have been suggested to treat both CSA and OSA, but so far, no pharmacologic treatment is providing significant prognostic benefits for patients with HF (7–9). Although OSA can be regarded as an independent risk factor enhancing HF morbidity and mortality (10, 11), CSA seems to be an important indicator of HF severity, due to its association with a worse left ventricular function and an advanced New York Heart Association (NYHA) class (12). All sleep apnea (SA) phenotypes are characterized by an increased sympathetic activity, which represents a detrimental pathophysiologic condition for HF patients. In particular, an exaggerated function of the sympathetic neural pathway leads to an excessive activation of renin–angiotensin–aldosterone system (RAAS), responsible for high renal resorption of salt and water, associated with both increased heart rate (HR) and peripheral vasoconstriction (13, 14). Furthermore, hyperactivation of the adrenergic system directly causes vasoconstriction, as well as increases the overall arrhythmic risk. Therefore, SA is thought to be a potential target for therapeutic approaches which can improve the health status of HF patients (15). Whilst current evidence indicates that OSA treatment with continuous positive airway pressure (CPAP) decreases all-cause mortality in HF patients (16–18), the benefits of non-invasive ventilation (NIV) for CSA therapy are still debated (19–21), as suggested by the results of both SERVE-HF (22) and ADVENT-HF (23) randomized clinical trials.

Moreover, it is well-known that optimization of HFrEF therapy should represent the first line treatment of subjects affected by SA and HF (24, 25). In this scenario, sacubitril–valsartan (sac/val) association has been proven to be more effective than enalapril in reducing HF progression and all-cause mortality in HFrEF patients (26). This therapeutic combination inhibits neprilysin *via* LBQ657, the active metabolite of the prodrug sacubitril, and blocks the angiotensin II type-1 (AT1) receptor *via* valsartan. In a real-life setting, we have recently demonstrated that sac/val treatment is effective and safe, as shown by the long-lasting benefits including significant improvements in several clinical, hemodynamic, and echocardiographic parameters, observed in HFrEF outpatients monitored every 6 months up to 2-years (27). Indeed, sac/val is the gold-standard treatment of patients suffering from HFrEF, whose symptoms persist in spite of an optimized therapy including an angiotensin-converting enzyme inhibitor (ACE-I) or angiotensin receptor blockers (ARB), a beta-blocker, and a mineralocorticoid receptor antagonist (MRA) (26, 28, 29). Notably, sac/val treatment can potentially attenuate sleep apnea development *via* several mechanisms including improvement of global hemodynamics, decrease of extracellular fluid overload, and reduction of sympathetic neural activity (30).

To address this issue, we aimed to evaluate the effects of a 6-month therapy with sac/val on hemodynamic and metabolic parameters, as well as on apnea/hypopnea occurrence, and oxygen saturation in patients with HFrEF and SA, already under treatment with CPAP.

METHODS

Study Design and Endpoints

The study population consisted of 132 consecutive outpatients enrolled from March 2018 to January 2020, referring to both the Chronic Heart Failure Unit of the Geriatrics Division, located at the "Mater Domini" University Hospital of Catanzaro, Italy, and the Internal Medicine Unit—Center for the Prevention, Diagnosis, and Management of Cardiovascular Disease, located at the University Hospital of Messina, Italy.

The study included outpatients complaining of HFrEF and eligible for treatment with sac/val, because of symptom persistence despite an optimized therapy. They were recruited according to the indications of the previous European Society of Cardiology (ESC) guidelines for the diagnosis and treatment of acute and chronic HF (31), which have been later updated, after the completion of our study. The eligibility criteria included: written informed consent; age $\geq$ 18 years; left ventricular ejection

fraction (LVEF) ≤ 35%; NYHA class II–III; persistence of symptoms despite an optimized treatment with stable doses of ACE-Is or ARBs for at least 4 weeks; presence of SA under treatment with CPAP since at least 3 months. SA diagnosis was performed according to the current guidelines (32). No patient took drugs or other substances that could interfere with sleep. The exclusion criteria included: severe renal dysfunction (estimated glomerular filtrate-eGFR <30 mL/min/1.73 m^2); severe hepatic impairment (Child-Pugh Class C); history of angioedema or side effects induced by ACE inhibitors or ARBs; pregnancy or breastfeeding, systolic blood pressure (SBP) < 100 mmHg; serum potassium levels > 5.4 mmol/L; current treatment with sac/val; chronic obstructive pulmonary disease (COPD) and relevant valvular heart diseases (VHD); resynchronization therapy within 3 months before the enrolment.

Complete physical examination, including assessments of body mass index (BMI), body surface area (BSA), waist circumference (WC), NYHA functional class, and quality of life were evaluated in each patient. Moreover, 12-lead electrocardiogram (ECG), echocardiography and laboratory tests aimed to evaluate metabolic disorders were also carried out. The evaluation of NYHA functional class was performed as suggested by the ESC guidelines for the diagnosis and treatment of acute and chronic HF (31). Minnesota Living with Heart Failure Questionnaire (MLHFQ) (33) and Epworth Sleepiness Scale (34) were used to evaluate quality of life. Moreover, arterial blood pressure (BP) was also checked. The local Ethics Committee approved the study protocol, and informed consent was obtained from all participants. All investigations were carried out accordingly to the principles of Helsinki Declaration.

In addition to previous treatments, eligible patients for sac/val discontinued ACE-I (at least 36 h before) or ARB, and received initial dosages of 24/26 mg or 49/51 mg bid according to clinical conditions. Moreover, sac/val dosage was increased every 2–4 weeks up to the maximum tolerated dose, as recommended. All clinical, laboratory and instrumental evaluations, such as echocardiography and nocturnal cardio-respiratory monitoring (CRM), were performed at baseline and after a 6-month treatment with sac/val. All patients were under treatment with CPAP, which provided a satisfactory SA correction. In order to evaluate the direct effects of sac/val on SA, at both baseline and 6-month timepoints CRM was performed during a temporary CPAP interruption, lasting 24 h.

Polygraphic Parameters

All patients underwent nocturnal CRM, as previously described (35). In particular, our CRM device (Somtè, Compumedics, Australia) included five cables used to record electrocardiogram through two bipolar leads, a nasal cannula assessing the flow-meter trace, a microphone which was necessary to record snoring, two piezoelectric belts utilized to detect thoraco-abdominal movements, a digital pulse oximeter measuring peripheral arterial oxyhemoglobin saturation (SpO_2), and a gravity sensor able to localize patient's position. Heart rate (HR) values were also assessed. All recorded parameters were analyzed by the same operator, who was blinded to treatment protocol, and each event was judged to be either obstructive, central and/or mixed, apnoic and/or hypopnoic, according to the criteria of the American Academy of Sleep Medicine (32). The eventual presence of SA was checked, and patient population was stratified on the basis of baseline central/obstructive apnea-hypopnea index (AHI) values. Hypopneas were characterized according to a scoring system which established the threshold of 3% oxygen desaturation (32). On the basis of the presence or absence of respiratory effort, sleep apneas were classified as either obstructive or central, respectively (32). We diagnosed OSA when AHI was ≥5 events/h, and >50% of apneic events were obstructive, whilst we made a diagnosis of CSA when AHI was ≥5 events/h, and >50% of apneic events were central (32). Oxygen desaturation index (ODI) was defined as the number of desaturation episodes exceeding the percentage of 3% per hour of sleep. Moreover, we also recorded time below 90% (TC90), corresponding to the percentage time of saturation which resulted to be <90%.

Laboratory Parameters

All laboratory measurements were performed after at least 12 h of fasting. Blood levels of glucose, creatinine, uric acid (UA), total cholesterol, low-density lipoprotein (LDL) cholesterol, high-density lipoprotein (HDL) cholesterol, and triglycerides were measured. The estimation of glomerular filtration rate (eGFR) was based on the new CKD-EPI (Chronic Kidney Disease Epidemiology Collaboration) equation (36). The high sensitivity C-reactive protein (hs-CRP) and serum N-terminal pro-B-type natriuretic peptide (NT-proBNP) were also measured.

Echocardiographic Parameters

Standard left ventricular ultrasonography in both M-mode (motion mode) and B-mode (two-dimensional mode) was performed in all patients, according to the recommendations of the American Society of Echocardiography (37). Recordings were made using a VIVID E-95 ultrasound system (GE Technologies, Milwaukee, Wisconsin, USA) and a 2.5 MHz transducer. Echocardiographic parameters were detected by the same expert operator, in order to minimize measurement errors. However, the operator was not aware of patient's clinical data and the values represented the average of at least three measurements. Among the parameters of left ventricular global systolic function, LVEF, cardiac output (CO), and cardiac index (CI) were evaluated. Right ventricular systolic parameters were also measured, by estimating the systolic pulmonary arterial pressure (S-PAP). Diastolic dysfunction was detected by recording pulse-wave Doppler patterns at the mitral valve, in order to measure early (E) and late (A) diastolic filling velocities from the 4-chamber view. Assessment of the left ventricular global longitudinal strain (GLS) and multilayer parameters were obtained using a dedicated software (38).

Statistical Analysis

Continuous variables were expressed as mean ± standard deviation (SD) (normally distributed data) or as median with interquartile range (IQR) (non-normally distributed data), when appropriate. Categorical data were expressed as numbers and

percentages. Normally distributed data were analyzed by *t*-test for paired data, whereas non-normally distributed data were analyzed by Wilcoxon's test for paired data. Subsequently, because of the absence of binary outcomes, a simple linear regression model was constructed with delta (**Δ**) as the dependent variable, i.e., changes in AHI between follow-up and baseline, and deltas of different variables that differed in a statistically significant manner between follow-up and baseline as independent variables. Therefore, changes in the variables that correlated significantly with changes in the dependent variable were entered into a multivariate linear regression model. Statistical analysis was carried out using SPSS V20.0 program for Windows (SPSS Inc., Chicago, Illinois, USA).

RESULTS

The recruited subjects included 107 men (81.1%) and 25 women (18.9%), with an average age of 67 ± 9.8 years. **Table 1** shows the baseline characteristics of the entire study population. In details, 59 (44.7%) patients received a treatment with sac/val 24/26 mg, 45 (34.1%) subjects assumed a dose of 49/51 mg, and 28 (21.2%) individuals received a 97/103 mg dose. Moreover, 66 (50.0%) patients had an implantable cardioverter defibrillator (ICD), and 42 (31.8%) subjects had a cardiac resynchronization therapy (CRT). After a 6-months follow-up, 39 (29.5%) patients were taking the lowest dose of sac/val (24/26), 60 (45.5%) patients the intermediate dose (49/51), and 33 (25%) the highest dose (97/103). Comparative evaluation between baseline values and 6-months follow-up data showed significant improvements in clinical and hemodynamic parameters, including reductions in HR (76.2 ± 2.8 vs. 71.7 ± 7.5 bpm; $p < 0.0001$), respiratory rate (RR) (17.7 ± 2.8 vs. 16.0 ± 1.8 breaths/min; $p < 0.0001$), SBP (122.1 ± 11.7 vs. 119.1 ± 11.7 mmHg; $p < 0.0001$), diastolic blood pressure (DBP) (72.4 ± 7.6 vs. 69.9 ± 6.7 mmHg; $p < 0.0001$). Furthermore, there was a significant change in MLHFQ score (89.5 ± 3.4 vs. 84.4 ± 4.5; $p < 0.0001$), indicating a relevant improvement in clinical symptoms (**Table 2**). After 6 months of treatment with sac/val, we also noticed significant improvements in patient functional status, as shown by the significant reduction of individual with NYHA class III from 68.9 to 22.0%; $p < 0.0001$.

There were also statistically significant decreases of BMI (32.9 ± 4.6 vs. 31.1 ± 4.4 kg/m^2; $p < 0.0001$), hs-CRP (7.4 ± 0.4 vs. 6.6 ± 0.4 mg/L; $p < 0.0001$), serum uric acid (6.7 ± 0.8 vs. 5.9 ± 1.0 mg/dL; $p < 0.0001$), NT-proBNP levels [1,840 (886.0–3,378] pg/mL vs. 970.0 (571.3–2,870) pg/mL; $p < 0.0001$). Furthermore, there was a significant reduction of serum creatinine levels (1.1 ± 0.3 vs. 1.0 ± 0.2 mg/dL; $p < 0.0001$), associated with a significant increase in eGFR (67.2 ± 19.2 vs. 96.4 ± 31.0 mL/min/1.73 m^2; $p < 0.0001$). Additionally, a significant reduction in sodium (140.4 ± 2.1 vs. 139.7 ± 1.6 mmol/L; $p < 0.0001$) and potassium (4.4 ± 0.3 vs. 4.6 ± 0.3 mmol/L; $p < 0.0001$) serum levels were observed (**Table 2**).

Table 3 shows the echocardiographic characteristics of the study group. The echocardiographic analysis revealed an improvement of both left chambers diameters, as demonstrated by the reduction of LAVI, from 49.8 ± 13.7 to 46.1 ± 12.0 mL/m^2 ($p = 0.001$). Moreover, LVEDV/BSA decreased from 89.6 ± 9.8 to 87.8 ± 8.4 mL/m^2 ($p < 0.0001$), and LVESV/BSA from 61.0 ± 7.1 to 57.3 ± 5.9 mL/m^2 ($p < 0.0001$), respectively. We also found significant reductions of the right chambers diameters, as shown by the changes in right ventricular outflow tract (RVOT), which decreased from 2.6 ± 0.4 to 2.1 ± 0.4 cm ($p < 0.0001$), and in the area of the right atrium (RAA) which decreased from 20.5 ± 2.8 to 19.3 ± 2.3 cm^2 ($p < 0.0001$). A statistically significant reduction was found in left ventricular GLS, changing from −7.9 ± 1.7 to −9.0 ± 1.4% ($p < 0.0001$). Moreover, s-PAP changed from 44.5 ± 6.6 to 41.5 ± 6.6 mmHg ($p < 0.0001$) and E/e' decreased from 17.4 ± 3.5 to 15.9 ± 2.8 ($p < 0.0001$). In addition, we detected statistically significant improvement in LVEF, which increased from 31.9 ± 1.4 to 34.7 ± 1.6% ($p < 0.0001$), as well as in CI, which enhanced from 1,675.6 ± 199.9 to 1,856.6 ± 212.9 mL/min/m^2 ($p < 0.0001$); inferior vena cava (IVC) diameter decreased from 20.2 ± 1.3 to 19.1 ± 3.3 mm ($p < 0.0001$). Furthermore, we observed a statistically significant increase in tricuspid annular plane excursion (TAPSE), which enhanced from 16.3 ± 1.1 to 17.1 ± 1.7 mm ($p < 0.0001$). The TAPSE/S-PAP ratio improved from 0.37 ± 0.06 to 0.42 ± 0.08 mm/mmHg ($p < 0.0001$).

At baseline, OSA and CSA were diagnosed in 55 (41.7%) and 77 (58.3%) patients, respectively, and all patients were under treatment with CPAP. Assessment of polygraphic parameters, evaluated during a temporary CPAP interruption, revealed a significant reduction in global AHI value (26.5 ± 10.4 vs. 21.7 ± 8.3 e/h; $p < 0.0001$), ODI (18.0 ± 3.7 vs. 13.5 ± 4.9 e/h; $p < 0.0001$), and TC90 (14.1 ± 4.5 vs. 6.8 ± 3.9%; $p < 0.0001$), respectively. Moreover, significant elevations were detected in mean SpO_2, which increased from 91.3 ± 1.9 to 92.0 ± 2.0% ($p < 0.0001$) (**Table 4**). In addition, apnea severity improved, as indicated by the reduction of patients with severe apneas from 58 (43.9%) at baseline to 15 (11.4%) after 6 months of therapy

TABLE 1 | Baseline characteristics and comorbidities of enrolled patients.

Variables	Baseline ($n = 132$)
Age, years	67.0 ± 9.8
Gender, m/f	107/25
Ischemic heart disease, *n* (%)	96 (72.7)
Diabetes, *n* (%)	80 (60.6)
Atrial fibrillation, *n* (%)	45 (34.0)
Arterial hypertension, *n* (%)	114 (86.3)
Dyslipidemia, *n* (%)	112 (84.8)
NYHA functional class II, *n* (%)	41 (31.1)
NYHA functional class III, *n* (%)	91 (68.9)
Smokers, *n* (%)	28 (21.2)
Ex-smokers, *n* (%)	24 (18.2)
Hemoglobin, g/dl	12.0 ± 1.2
Implantable cardioverter defibrillator, *n* (%)	66 (50.0)
Cardiac resynchronization therapy, *n* (%)	42 (31.8)

NYHA, New York Heart Association.

TABLE 2 | Anthropometric, hemodynamic, and biohumoral characteristics at baseline and after 6 months of therapy with sac/val.

Variables	Baseline ($n = 132$)	Follow-up ($n = 132$)	Standardized mean difference (Hedges'g)	*p*
BMI, kg/m^2	32.0 ± 4.6	31.1 ± 4.4	0.19	<0.0001
SBP, mmHg	122.1 ± 11.7	119.1 ± 11.7	0.25	<0.0001
DBP, mmHg	72.4 ± 7.6	69.9 ± 6.7	0.35	<0.0001
HR, bpm	76.2 ± 2.8	71.7 ± 7.5	0.79	<0.0001
RR, breaths/min	17.7 ± 2.8	16.0 ± 1.8	0.72	<0.0001
MLHFQ, score	89.5 ± 3.4	84.4 ± 4.5	1.27	<0.0001
Serum sodium, mmol/L	140.4 ± 2.1	139.7 ± 1.6	0.37	<0.0001
Serum potassium, mmol/L	4.4 ± 0.3	4.6 ± 0.3	0.67	<0.0001
Serum creatinine, mg/dL	1.1 ± 0.3	1.0 ± 0.2	0.39	<0.0001
eGFR, mL/min/1.73m^2	67.2 ± 19.2	96.4 ± 31.0	1.13	<0.0001
Serum UA, mg/dL	6.7 ± 0.8	5.9 ± 1.0	0.88	<0.0001
hs-CRP, mg/dL	7.4 ± 0.4	6.6 ± 0.4	2	<0.0001
NT-proBNP, pg/mL	1840 (886.0–3,378)	970.0 (571.3–2,870)		<0.0001

BMI, body mass index; SBP, systolic blood pressure; DBP, diastolic blood pressure; HR, heart rate; RR, respiratory rate; MLHFQ, Minnesota Living with Heart Failure Questionnaire; eGFR, estimated glomerular filtration rate; UA, uric acid; hs-CRP, high-sensitivity C-reactive protein; NT-proBNP, N-terminal pro-B-type natriuretic peptide.

TABLE 3 | Echocardiographic parameters at baseline and after 6 months of therapy with sac/val.

Variables	Baseline ($n = 132$)	Follow-up ($n = 132$)	Standardized mean difference (Hedges'g)	*p*
LAVI, mL/m^2	49.8 ± 13.7	46.1 ± 12.0	0.27	0.001
LVEDV/BSA, mL/m^2	89.6 ± 9.8	87.8 ± 8.4	0.20	<0.0001
LVESV/BSA, mL/m^2	61.0 ± 7.1	57.3 ± 5.9	0.57	<0.0001
LVEF, %	31.9 ± 1.4	34.7 ± 1.6	1.86	<0.0001
CI, mL/min/m^2	1,675.6 ± 199.9	1,856.6 ± 212.9	0.87	<0.0001
E/e' ratio	17.4 ± 3.5	15.9 ± 2.8	0.47	<0.0001
GLS, %	−7.9 ± 1.7	−9.0 ± 1.4	0.71	<0.0001
RVOT, cm	2.6 ± 0.4	2.1 ± 0.4	1.25	<0.0001
RAA, cm^2	20.5 ± 2.8	19.3 ± 2.3	0.4	<0.0001
TAPSE, mm	16.3 ± 1.1	17.1 ± 1.7	0.56	<0.0001
S-PAP, mmHg	44.5 ± 6.6	41.5 ± 6.6	0.45	<0.0001
TAPSE/S-PAP, mm/mmHg	0.37 ± 0.06	0.42 ± 0.08	0.70	<0.0001
IVC, mm	20.2 ± 1.3	19.1 ± 3.3	0.44	<0.0001

LAVI, left atrium volume index; LVEDV, left ventricular end-diastolic volume; BSA, body surface area; LVESV, left ventricular end-systolic volume; LVEF, left ventricular ejection fraction; CI, cardiac index; GLS, left ventricular global longitudinal strain; RVOT, right ventricular outflow tract; RAA, right atrium area; TAPSE, tricuspid annular plane excursion; S-PAP, systolic pulmonary arterial pressure; IVC, inferior vena cava.

with sac/val ($p < 0.0001$). Significant improvements of AHI, ODI, mean SpO_2 and TC90 were also observed in both subgroups of patients with OSA (**Figure 1**) or CSA (**Figure 2**). The mean value of CPAP use time was 6.3 ± 0.17 h/night, remaining stable over time (6.3 ± 0.19 h/night, $p = 0.999$) thus reflecting the good patient compliance to device utilization.

Table 5 shows the differences occurring between the pharmacological treatments received at baseline and after 6 months of sac/val therapy, respectively. Notably, there was a significant reduction in diuretic drugs use.

Linear regression analysis using AHI variation (Δ AHI) as dependent variable revealed that AHI changes were significantly associated with variations of eGFR, CI, NT-proBNP, and TAPSE (**Table 6**). Moreover, variables significantly correlated to AHI changes were inserted in a multivariate linear regression model to determine the independent predictors of AHI changes. We found that the changes of CI, eGFR, NT-proBNP, and TAPSE contributed to 23.6, 7.6, 7.3, and 4.8% of AHI variability, respectively, and the whole model accounted for a 43.3% of AHI variation (**Table 7**).

Therapy with sac/val was well-tolerated, and no serious adverse reactions occurred throughout this real-life observational study.

DISCUSSION

The purpose of the present observational study was to evaluate the effects of sac/val on AHI, as well as on other clinical, functional and bio-humoral parameters patients affected by HFrEF and SA syndrome, under treatment with CPAP. In this regard, the ENTRESTO-SAS study has already shown that treatment with sac/val of patients with HFrEF and respiratory sleep disorders, induced significant AHI improvements after 3 months of therapy (39). Differently from the ENTRESTO-SAS study, our investigation was extended to 6 months, and was based not only on AHI evaluation, but also on polysomnography, as well as on the assessment of several other clinical, echocardiographic, and laboratory parameters. We observed significant improvements of AHI, ODI, TC90, mean SpO_2, LVEF, CI, S-PAP, MLHFQ score, NT-proBNP, and eGFR in patients treated with sac/val for 6 months. Because all enrolled patients were on treatment with CPAP throughout the entire study period with a good adherence to non-invasive ventilation, the observed effects were likely to be attributable to the pharmacological action of sac/val. Indeed, this drug association combines angiotensin receptor antagonism and neprilysin inhibition. As a consequence of this dual mechanism of action, the resulting effective vasodilation can lead to a decrease of peripheral, and pulmonary congestion (40–43). In fact, vasodilation arises from suppression of angiotensin-dependent vasomotor tone, as well as from inhibition of degradation of vasodilatory natriuretic peptides (NP). This powerful vasodilation is further potentiated by natriuresis, ensuing from NP increased levels, and also from RAAS inhibition. The natriuretic action of sac/val also contributes to enhance eGFR and to lower serum UA levels, which are well-known cardiovascular risk factors (44, 45). Furthermore, the improved renal function decreases pulmonary congestion, thus explaining why eGFR change is a significant contributor to AHI variation in the multivariate linear regression model. Taken together, these therapeutic effects amplify a virtuous feed-forward loop, leading to LVEF and CI increases,

TABLE 4 | Polygraphic parameters at baseline and after 6 months of therapy with sac/val.

Variables	Baseline ($n = 132$)	Follow-up ($n = 132$)	Standardized mean difference (Hedges'g)	p
AHI, e/h	26.5 ± 10.4	21.7 ± 8.3	0.51	<0.0001
ODI, e/h	18.0 ± 3.7	13.5 ± 4.9	1.03	<0.0001
Mean SpO_2, %	91.3 ± 1.9	92.0 ± 2.0	0.36	<0.0001
TC90, %	14.1 ± 4.5	6.8 ± 3.9	1.73	<0.0001

AHI, apnea hypopnea index; ODI, oxygen desaturation index; SpO_2, peripheral arterial oxyhemoglobin saturation; TC90, percentage time of saturation below 90%.

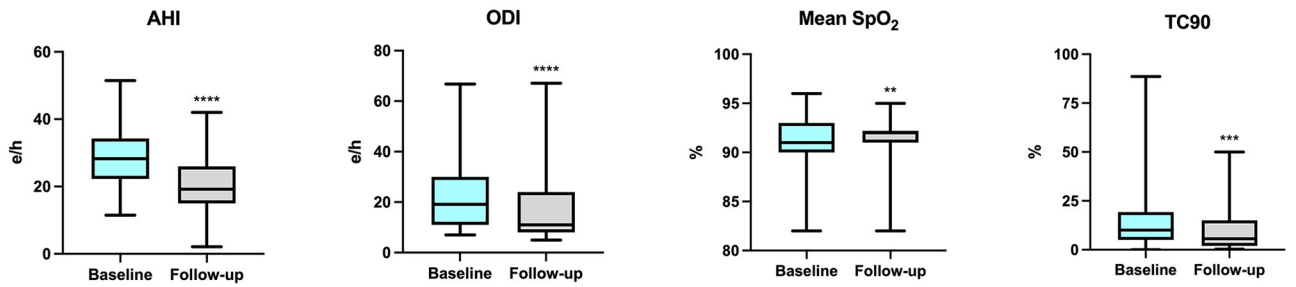

FIGURE 1 | Changes of AHI, ODI, mean SpO_2 and TC90 after 6 months of therapy with sac/val in the subgroup with OSA. AHI, apnea hypopnea index; ODI, oxygen desaturation index; SpO_2, peripheral arterial oxyhemoglobin saturation; TC90, percentage time of saturation below 90%; OSA, obstructive sleep apnea. $^{**}p < 0.01$; $^{***}p < 0.001$; $^{****}p < 0.0001$.

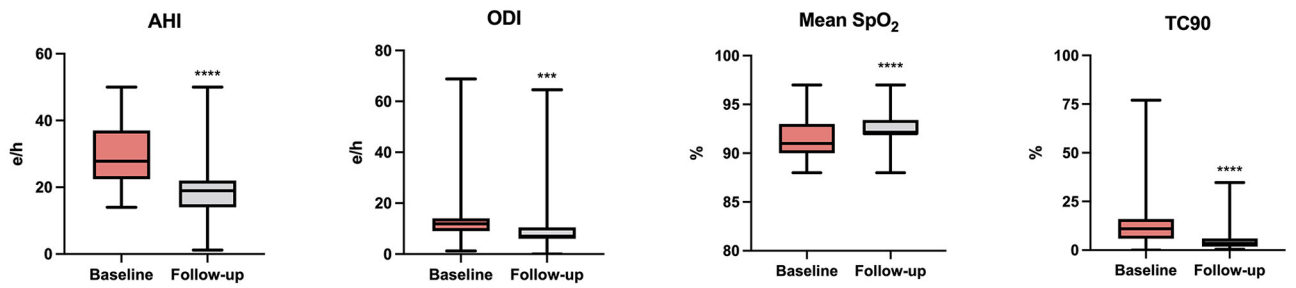

FIGURE 2 | Changes of AHI, ODI, mean SpO_2, and TC90 after 6 months of therapy with sac/val in the subgroup with CSA. AHI, apnea hypopnea index; ODI, oxygen desaturation index; SpO_2, peripheral arterial oxyhemoglobin saturation; TC90, percentage time of saturation below 90%; CSA, central sleep apnea. $^{***}p < 0.001$; $^{****}p < 0.0001$.

TABLE 5 | Pharmacological treatments at baseline and after 6 months of therapy with sac/val.

Variables	Baseline ($n = 132$)	Follow-up ($n = 132$)	*p*
ACE-I, *n* (%)	92 (69.7)	0 (0)	<0.0001
ARB, *n* (%)	40 (30.3)	0 (0)	<0.0001
MRA, *n* (%)	68 (51.5)	49 (37.1)	0.018
Loop diuretics, *n* (%)	131 (99.2)	115 (87.1)	<0.0001
Beta blockers, *n* (%)	131 (99.2)	131 (99.2)	0.999
Antiplatelet agents, *n* (%)	72 (54.5)	72 (54.5)	0.999
Oral antidiabetic drugs, *n* (%)	80 (60.6)	73 (55.3)	0.382
Oral anticoagulants, *n* (%)	44 (33.3)	44 (33.3)	0.999
Statins, *n* (%)	109 (82.6)	109 (82.6)	0.999

ACE-I, angiotensin-converting enzyme inhibitor; ARB, angiotensin receptor blockers; MRA, mineralocorticoid receptor antagonist.

TABLE 6 | Linear regression analysis focused on AHI variation (Δ AHI) as dependent variable.

Variables	*R*	*p*
Δ CI, mL/min/m^2	0.486	<0.0001
Δ TAPSE, mm	0.325	<0.0001
Δ NT-proBNP, pg/mL	−0.404	<0.0001
Δ IVC, mm	−0.048	0.293
Δ eGFR, mL/min/1.73m^2	0.405	<0.0001
Δ RAA, cm^2	−0.086	0.164
Δ MLHFQ, score	−0.066	0.228
Δ RVOT, cm	−0.104	0.218
Δ TAPSE/S-PAP, mm/mmHg	0.036	0.340
Δ E/e' ratio	−0.008	0.463
Δ LVEDV/BSA, mL/m^2	−0.022	0.401
Δ S-PAP, mmHg	−0.055	0.264

AHI, apnea hypopnea index; CI, cardiac index; TAPSE, tricuspid annular plane excursion; NT-proBNP, N-terminal pro-B-type natriuretic peptide; IVC, inferior vena cava; eGFR, estimated glomerular filtration rate; RAA, right atrium area; MLHFQ; Minnesota Living with Heart Failure Questionnaire; RVOT, right ventricular outflow tract; S-PAP, systolic pulmonary arterial pressure; LVEDV, left ventricular end-diastolic volume; BSA, body surface area.

as well as to partial reversal of cardiac remodeling (46, 47). Additionally, sac/val treatment leads to reduction in water content of lung interstitial spaces, thereby improving pulmonary congestion, ventilation dynamics, and gas exchange (48). Overall, these effects are also responsible for a decreased stimulation of lung stretch receptors, which positively impacts on respiratory mechanics (49). The increased cardiac output is paralleled by a decreased circulation time, associated with a reduced sensitiveness of the chemoreceptor reflex system to blood gas changes (50). Within the context of SA pathophysiology, the above pulmonary and cardiovascular improvements can contribute to dampen the hyperactivation of sympathetic neural pathways (51). Furthermore, sac/val treatment could reduce the cranial fluid influx occurring when patients like ours rest in supine position (52).

TABLE 7 | Stepwise multiple regression analysis focused on AHI variation (Δ AHI) as dependent variable.

Variables	Partial r^2 (%)	Total r^2 (%)	*p*
Δ CI, mL/min/m^2	23.6	23.6	<0.0001
Δ eGFR, mL/min/1.73 m^2	7.6	31.2	<0.0001
Δ NT-proBNP, pg/mL	7.3	38.5	<0.0001
Δ TAPSE, mm	4.8	43.3	0.001

AHI, apnea hypopnea index; CI, cardiac index; eGFR, estimated glomerular filtration rate; NT-proBNP, N-terminal pro-B-type natriuretic peptide; TAPSE, tricuspid annular plane excursion.

Similar to the characteristics of the PARADIGM-HF trial (26), also our patients experienced an overall very good response to sac/val. Moreover, our results are consistent with those of a very recent study carried out by Passino et al. (53), who showed that sac/val combination significantly improved the apnea burden due to CSA in patients with HFrEF; however, these authors did not detect significant changes in nighttime obstructive AHI referred to OSA patients. By contrast, we observed significant improvements in AHI which regarded both CSA and OSA in a quite larger number of enrolled patients. This discrepancy could be explained by the different baseline features of our patients, when compared with those enrolled by Passino et al., especially with regard to TC90 and AHI values. Additionally, despite the interruption of CPAP during the night of recording, some residual effects of mask treatment make explain the positive effects on OSA. Anyway, the two subgroups of patients (OSA and CSA), recruited in our study, do not appear to be characterized by relevant differences with regard to both body weight and BMI. In the AWAKE-HF study, the addition of sac/val therapy did not significantly improve sleep-disordered breathing or sleep duration in a cohort of patients with HFrEF, likely as a result of the short duration of the study (54). Overall, our patients responded quite well to sac/val in terms of SA improvement. However, 96 (72.7%) patients experienced the persistence of a residual AHI higher than 15, and 12 (9.1%) subjects were characterized by a residual AHI higher than 30. In particular, the persistence of about 20 events/h in both patient subgroups (OSA and CSA) suggests that the addition of further treatments should be tested, especially in regard to subjects with high loop gain OSA (e.g., acetazolamide and oxygen) (55). Acetazolamide, buspirone, and phrenic nerve stimulation could be useful for add-on treatment of CSA (56–60).

In conclusion, our results suggest that treatment with sac/val is able to significantly improve the cardiorespiratory performance of patients with HFrEF and SA. These findings are consistent with the recommendations of the current guidelines for the diagnosis and treatment of acute and chronic HF, that consider sac/val as a first-choice treatment in HFrEF (1). This real-life observation can be clinically relevant because cardiovascular diseases represent the main comorbidities of SA patients, negatively affecting both quality of life and survival. However, our study also presents some limitations. Firstly, similarly to all real-life experiences, the enrolled patients were not randomized,

and, therefore, bias selection cannot be excluded. Secondly, we used CRM instead of polysomnography equipped with electroencephalography channels, which may provide a more detailed characterization of sleep patterns. A further limitation arises from the night-to-night AHI variability, which can at least in part confound the effects of sac/val (61). Moreover, although some patients can experience central apneas even at daytime, while awake and in the upright position (62, 63), we chose to focus our attention only on nighttime registration, with the aim of increasing patient adherence. A further limitation refers to a possible misclassification of hypopneas; indeed, some residual respiratory efforts can be present even in central hypopneas. Nevertheless, the present results indicate that in patients with HFrEF and SA pharmacological treatment with sac/val can represent a valuable therapeutic option, integrating the positive impact of CPAP. Thus, both CPAP and sac/val therapy may synergistically contribute to improve the global performance of these patients, as well as to significantly lower the risks of both cardiac and pulmonary complications. Of course, it cannot be ruled out that alternative pharmacologic strategies to sac/val could be useful in different patients, characterized by heart failure with either preserved ejection fraction (HFpEF) or midrange ejection fraction (HFmrEF).

DATA AVAILABILITY STATEMENT

The raw data supporting the conclusions of this article will be made available by the authors, without undue reservation.

ETHICS STATEMENT

The studies involving human participants were reviewed and approved by Local Ethical Committee of Calabria Region. The patients/participants provided their written informed consent to participate in this study.

AUTHOR CONTRIBUTIONS

All authors listed have made a substantial, direct, and intellectual contribution to the work and approved it for publication.

REFERENCES

1. McDonagh TA, Metra M, Adamo M, Gardner RS, Baumbach A, Böhm M, et al. 2021 ESC Guidelines for the diagnosis and treatment of acute and chronic heart failure. *Eur Heart J.* (2021) 42:3599–726. doi: 10.1093/eurheartj/ehab368
2. Malik A, Gill GS, Lodhi FK, Tummala LS, Singh SN, Morgan CJ, et al. Prior heart failure hospitalization and outcomes in patients with heart failure with preserved and reduced ejection fraction. *Am J Med.* (2020) 133:84–94. doi: 10.1016/j.amjmed.2019.06.040
3. Wang H, Parker JD, Newton GE, Floras JS, Mak S, Chiu KL, et al. Influence of obstructive sleep apnea on mortality in patients with heart failure. *J Am Coll Cardiol.* (2007) 49:1625–31. doi: 10.1016/j.jacc.2006.12.046
4. Parati G, Lombardi C, Castagna F, Mattaliano P, Filardi PP, Agostoni P. Heart failure and sleep disorders. *Nat Rev Cardiol.* (2016) 13:389–403. doi: 10.1038/nrcardio.2016.71
5. Cowie MR, Gallagher AM. Sleep disordered breathing and heart failure: what does the future hold? *JACC Heart Fail.* (2017) 5:715–23. doi: 10.1016/j.jchf.2017.06.016
6. Luo Q, Zhang HL, Tao XC, Zhao ZH, Yang YJ, Liu ZH. Impact of untreated sleep apnea on prognosis of patients with congestive heart failure. *Int J Cardiol.* (2010) 144:420–2. doi: 10.1016/j.ijcard.2009.03.050
7. Emdin M, Passino C, Giannoni A. After the SERVE-HF trial, is there still a need for treatment of central apnea?. *J Card Fail.* (2015) 21:903–5. doi: 10.1016/j.cardfail.2015.09.005
8. Drager LF, McEvoy RD, Barbe F, Lorenzi-Filho G, Redline S; INCOSACT Initiative (International Collaboration of Sleep Apnea Cardiovascular Trialists). Sleep apnea and cardiovascular disease: lessons from recent trials and need for team science. *Circulation.* (2017) 136:1840–50. doi: 10.1161/CIRCULATIONAHA.117.029400
9. Selim BJ, Ramar K. Management of sleep apnea syndromes in heart failure. *Sleep Med Clin.* (2017) 12:107–21. doi: 10.1016/j.jsmc.2016.10.004
10. Gottlieb DJ, Yenokyan G, Newman AB, O'Connor GT, Punjabi NM, Quan SF, et al. Prospective study of obstructive sleep apnea and incident coronary heart disease and heart failure: the sleep heart health study. *Circulation.* (2010) 122:352–60. doi: 10.1161/CIRCULATIONAHA.109.901801
11. Khayat R, Jarjoura D, Porter K, Sow A, Wannemacher J, Dohar R, et al. Sleep disordered breathing and post-discharge mortality in patients with acute heart failure. *Eur Heart J.* (2015) 36:1463–9. doi: 10.1093/eurheartj/ehu522
12. Naughton MT. Heart failure and sleep-disordered breathing. The Chicken or the Egg?. *Am J Respir Crit Care Med.* (2016) 193:482–3. doi: 10.1164/rccm.201511-2176ED
13. Javaheri S, Barbe F, Campos-Rodriguez F, Dempsey JA, Khayat R, Javaheri S, et al. Sleep apnea: types, mechanisms, and clinical cardiovascular consequences. *J Am Coll Cardiol.* (2017) 69:841–58. doi: 10.1016/j.jacc.2016.11.069
14. Pearse SG, Cowie MR. Sleep-disordered breathing in heart failure. *Eur J Heart Fail.* (2016) 18:353–61. doi: 10.1002/ejhf.492
15. Piamjariyakul U, Shapiro AL, Wang K, Zulfikar R, Petitte T, Shafique S, et al. Impact of sleep apnea, daytime sleepiness, comorbidities, and depression on patients' heart failure health status. *Clin Nurs Res.* (2021) 30:1222–30. doi: 10.1177/10547738211015545
16. Javaheri S, Caref EB, Chen E, Tong KB, Abraham WT. Sleep apnea testing and outcomes in a large cohort of Medicare beneficiaries with newly diagnosed heart failure. *Am J Respir Crit Care Med.* (2011) 183:539–46. doi: 10.1164/rccm.201003-0406OC
17. Kasai T, Narui K, Dohi T, Yanagisawa N, Ishiwata S, Ohno M, et al. Prognosis of patients with heart failure and obstructive sleep apnea treated with continuous positive airway pressure. *Chest.* (2008) 133:690–6. doi: 10.1378/chest.07-1901
18. Damy T, Margarit L, Noroc A, Bodez D, Guendouz S, Boyer L, et al. Prognostic impact of sleep-disordered breathing and its treatment with nocturnal ventilation for chronic heart failure. *Eur J Heart Fail.* (2012) 14:1009–19. doi: 10.1093/eurjhf/hfs085
19. Holfinger S, Chan L, Donald R. All you need is sleep: the effects of sleep apnea and treatment benefits in the heart failure patient. *Curr Heart Fail Rep.* (2021) 18:144–52. doi: 10.1007/s11897-021-00506-1
20. Oates CP, Ananthram M, Gottlieb SS. Management of sleep disordered breathing in patients with heart failure. *Curr Heart Fail Rep.* (2018) 15:123–30. doi: 10.1007/s11897-018-0387-7
21. Naughton MT, Kee K. Sleep apnoea in heart failure: to treat or not to treat?. *Respirology.* (2017) 22:217–29. doi: 10.1111/resp.12964
22. Cowie MR, Woehrle H, Wegscheider K, Angermann C, d'Ortho MP, Erdmann E, et al. Adaptive servo-ventilation for central sleep apnea in systolic heart failure. *N Engl J Med.* (2015) 373:1095–105. doi: 10.1056/NEJMoa1506459
23. Lyons OD, Floras JS, Logan AG, Beanlands R, Cantolla JD, Fitzpatrick M, et al. Design of the effect of adaptive servo-ventilation on survival and cardiovascular hospital admissions in patients with heart failure and sleep apnoea: the ADVENT-HF trial. *Eur J Heart Fail.* (2017) 19:579–87. doi: 10.1002/ejhf.790
24. Javaheri S. Central sleep apnea in congestive heart failure: prevalence, mechanisms, impact, and therapeutic options. *Semin Respir Crit Care Med.* (2005) 26:44–55. doi: 10.1055/s-2005-864206

25. Maddox TM, Januzzi JL Jr, Allen LA, Breathett K, Butler J, Davis LL, et al. 2021 Update to the 2017 ACC expert consensus decision pathway for optimization of heart failure treatment: answers to 10 pivotal issues about heart failure with reduced ejection fraction: a report of the American College of Cardiology Solution Set Oversight Committee. *J Am Coll Cardiol.* (2021) 77:772–810. doi: 10.1016/j.jacc.2020.11.022
26. McMurray JJ, Packer M, Desai AS, Gong J, Lefkowitz MP, Rizkala AR, et al. Angiotensin-neprilysin inhibition versus enalapril in heart failure. *N Engl J Med.* (2014) 371:993–1004. doi: 10.1056/NEJMoa1409077
27. Armentaro G, D'Arrigo G, Magurno M, Toscani AF, Condoleo V, Miceli S, et al. Impact of sacubitril/valsartan on clinical and echocardiographic parameters in heart failure patients with reduced ejection fraction: data from a real life 2-year follow-up study. *Front Pharmacol.* (2021) 12:733475. doi: 10.3389/fphar.2021.733475
28. Mentz RJ, Xu H, O'Brien EC, Thomas L, Alexy T, Gupta B, et al. PROVIDE-HF primary results: patient-reported outcomes investigation following initiation of drug therapy with entresto (sacubitril/valsartan) in heart failure. *Am Heart J.* (2020) 230:35–43. doi: 10.1016/j.ahj.2020.09.012
29. Khariton Y, Fonarow GC, Arnold SV, Hellkamp A, Nassif ME, Sharma PP, et al. Association between sacubitril/valsartan initiation and health status outcomes in heart failure with reduced ejection fraction. *JACC Heart Fail.* (2019) 7:933–41. doi: 10.1016/j.jchf.2019.05.016
30. Jaffuel D, Molinari N, Berdague P, Pathak A, Galinier M, Dupuis M, et al. Impact of sacubitril-valsartan combination in patients with chronic heart failure and sleep apnoea syndrome: the ENTRESTO-SAS study design. *ESC Heart Fail.* (2018) 5:222–30. doi: 10.1002/ehf2.12270
31. Ponikowski P, Voors AA, Anker SD, Bueno H, Cleland JG, Coats AJ, et al. 2016 ESC Guidelines for the diagnosis treatment of acute chronic heart failure: the Task Force for the diagnosis treatment of acute chronic heart failure of the European Society of Cardiology (ESC). Developed with the special contribution of the Heart Failure Association (HFA) of the ESC. *Eur J Heart Fail.* (2016) 18:891–975. doi: 10.1002/ejhf.592
32. Berry RB, Budhiraja R, Gottlieb DJ, Gozal D, Iber C, Kapur VK, et al. Rules for scoring respiratory events in sleep: update of the 2007 AASM Manual for the Scoring of Sleep and Associated Events. Deliberations of the Sleep Apnea Definitions Task Force of the American Academy of Sleep Medicine. *J Clin Sleep Med.* (2012) 8:597–619. doi: 10.5664/jcsm.2172
33. Kularatna S, Senanayake S, Chen G, Parsonage W. Mapping the Minnesota living with heart failure questionnaire (MLHFQ) to EQ-5D-5L in patients with heart failure. *Health Qual Life Outcomes.* (2020) 18:115. doi: 10.1186/s12955-020-01368-2
34. Walker NA, Sunderram J, Zhang P, Lu SE, Scharf MT. Clinical utility of the Epworth sleepiness scale. *Sleep Breath.* (2020) 24:1759–65. doi: 10.1007/s11325-020-02015-2
35. Pelaia C, Armentaro G, Miceli S, Perticone M, Toscani AF, Condoleo V, et al. Association between sleep apnea and valvular heart diseases. *Front Med (Lausanne).* (2021) 8:667522. doi: 10.3389/fmed.2021.667522
36. Levey AS, Stevens LA, Schmid CH, Zhang YL, Castro AF 3rd, Feldman HI, et al. A new equation to estimate glomerular filtration rate. *Ann Intern Med.* (2009) 150:604–12. doi: 10.7326/0003-4819-150-9-200905050-00006
37. Lang RM, Badano LP, Mor-Avi V, Afilalo J, Armstrong A, Ernande L, et al. Recommendations for cardiac chamber quantification by echocardiography in adults: an update from the American Society of Echocardiography and the European Association of Cardiovascular Imaging. *Eur Heart J Cardiovasc Imaging.* (2015) 16:233–70. doi: 10.1093/ehjci/jev014
38. Kalam K, Otahal P, Marwick TH. Prognostic implications of global LV dysfunction: a systematic review and meta-analysis of global longitudinal strain and ejection fraction. *Heart.* (2014) 100:1673–80. doi: 10.1136/heartjnl-2014-305538
39. Jaffuel D, Nogue E, Berdague P, Galinier M, Fournier P, Dupuis M, et al. Sacubitril-valsartan initiation in chronic heart failure patients impacts sleep apnea: the ENTRESTO-SAS study. *ESC Heart Fail.* (2021) 8:2513–26. doi: 10.1002/ehf2.13455
40. Selvaraj S, Claggett B, Pozzi A, McMurray JJV, Jhund PS, Packer M, et al. Prognostic implications of congestion on physical examination among contemporary patients with heart failure and reduced ejection fraction: PARADIGM-HF. *Circulation.* (2019) 140:1369–79. doi: 10.1161/CIRCULATIONAHA.119.039920
41. Myhre PL, Vaduganathan M, Claggett B, Packer M, Desai AS, Rouleau JL, et al. B-type natriuretic peptide during treatment with sacubitril/valsartan: the PARADIGM-HF trial. *J Am Coll Cardiol.* (2019) 73:1264–72. doi: 10.1016/j.jacc.2019.01.018
42. Nougué H, Pezel T, Picard F, Sadoune M, Arrigo M, Beauvais F, et al. Effects of sacubitril/valsartan on neprilysin targets and the metabolism of natriuretic peptides in chronic heart failure: a mechanistic clinical study. *Eur J Heart Fail.* (2019) 21:598–605. doi: 10.1002/ejhf.1342
43. Sciacqua A, Succurro E, Armentaro G, Miceli S, Pastori D, Rengo G, et al. Pharmacological treatment of type 2 diabetes in elderly patients with heart failure: randomized trials and beyond. *Heart Fail Rev.* (2021). doi: 10.1007/s10741-021-10182-x. [Epub ahead of print].
44. Cassano V, Crescibene D, Hribal ML, Pelaia C, Armentaro G, Magurno M, et al. Uric Acid and vascular damage in essential hypertension: role of insulin resistance. *Nutrients.* (2020) 12:2509. doi: 10.3390/nu12092509
45. Pelaia C, Pastori D, Armentaro G, Miceli S, Cassano V, Barbara K, et al. Predictors of renal function worsening in patients with chronic obstructive pulmonary disease (COPD): a multicenter observational study. *Nutrients.* (2021) 13:2811. doi: 10.3390/nu13082811
46. Bayard G, Da Costa A, Pierrard R, Roméyer-Bouchard C, Guichard JB, Isaaz K. Impact of sacubitril/valsartan on echo parameters in heart failure patients with reduced ejection fraction a prospective evaluation. *Int J Cardiol Heart Vasc.* (2019) 25:100418. doi: 10.1016/j.ijcha.2019.100418
47. Romano G, Vitale G, Ajello L, Agnese V, Bellavia D, Caccamo G, et al. The effects of sacubitril/valsartan on clinical, biochemical and echocardiographic parameters in patients with heart failure with reduced ejection fraction: the "Hemodynamic Recovery". *J Clin Med.* (2019) 8:2165. doi: 10.3390/jcm8122165
48. Giannoni A, Gentile F, Navari A, Borrelli C, Mirizzi G, Catapano G, et al. Contribution of the lung to the genesis of cheyne-stokes respiration in heart failure: plant gain beyond chemoreflex gain and circulation time. *J Am Heart Assoc.* (2019) 8:e012419. doi: 10.1161/JAHA.119.012419
49. Gunawardena S, Ravi K, Longhurst JC, Kaufman MP, Ma A, Bravo M, et al. Responses of C fiber afferents of the rabbit airways and lungs to changes in extra-vascular fluid volume. *Respir Physiol Neurobiol.* (2002) 132:239–1. doi: 10.1016/S1569-9048(02)00114-3
50. Mansukhani MP, Wang S, Somers VK. Chemoreflex physiology and implications for sleep apnoea: insights from studies in humans. *Exp Physiol.* (2015) 100:130–5. doi: 10.1113/expphysiol.2014.082826
51. Sascău R, Zota IM, Stătescu C, Boiăteanu D, Roca M, Maștaleru A, et al. Review of echocardiographic findings in patients with obstructive sleep apnea. *Can Respir J.* (2018) 2018:1206217. doi: 10.1155/2018/1206217
52. White LH, Bradley TD. Role of nocturnal rostral fluid shift in the pathogenesis of obstructive and central sleep apnoea. *J Physiol.* (2013) 591:1179–93. doi: 10.1113/jphysiol.2012.245159
53. Passino C, Sciarrone P, Vergaro G, Borrelli C, Spiesshoefer J, Gentile F, et al. Sacubitril-valsartan treatment is associated with decrease in central apneas in patients with heart failure with reduced ejection fraction. *Int J Cardiol.* (2021) 330:112–9. doi: 10.1016/j.ijcard.2021.02.012
54. Owens RL, Birkeland K, Heywood JT, Steinhubl SR, Dorn J, Grant D, et al. Sleep outcomes from AWAKE-HF: a randomized clinical trial of sacubitril/valsartan vs enalapril in patients with heart failure and reduced ejection fraction. *J Card Fail.* (2021) 27:1466–71. doi: 10.1016/j.cardfail.2021.07.021
55. White DP. Pharmacologic approaches to the treatment of obstructive sleep apnea. *Sleep Med Clin.* (2016) 11:203–12. doi: 10.1016/j.jsmc.2016.01.007
56. Javaheri S. Acetazolamide improves central sleep apnea in heart failure: a double-blind, prospective study. *Am J Respir Crit Care Med.* (2006) 173:234–7. doi: 10.1164/rccm.200507-1035OC
57. Ni YN, Yang H, Thomas RJ. The role of acetazolamide in sleep apnea at sea level: a systematic review and meta-analysis. *J Clin Sleep Med.* (2021) 17:1295–304. doi: 10.5664/jcsm.9116
58. Giannoni A, Borrelli C, Mirizzi G, Richerson GB, Emdin M, Passino C. Benefit of buspirone on chemoreflex and central apnoeas in heart failure: a randomized controlled crossover trial. *Eur J Heart Fail.* (2021) 23:312–20. doi: 10.1002/ejhf.1854
59. Costanzo MR, Ponikowski P, Javaheri S, Augostini R, Goldberg L, Holcomb R, et al. Transvenous neurostimulation for central

sleep apnoea: a randomised controlled trial. *Lancet.* (2016) 388:974–82. doi: 10.1016/S0140-6736(16)30961-8
60. Fox H, Oldenburg O, Javaheri S, Ponikowski P, Augostini R, Goldberg LR, et al. Long-term efficacy and safety of phrenic nerve stimulation for the treatment of central sleep apnea. *Sleep.* (2019) 42:zsz158. doi: 10.1093/sleep/zsz158
61. Hayano J, Yuda E. Night-to-night variability of sleep apnea detected by cyclic variation of heart rate during long-term continuous ECG monitoring. *Ann Noninvasive Electrocardiol.* (2021) 27:e12901. doi: 10.1111/anec.12901
62. Emdin M, Mirizzi G, Giannoni A, Poletti R, Iudice G, Bramanti F, et al. Prognostic significance of central apneas throughout a 24-hour period in patients with heart failure. *J Am Coll Cardiol.* (2017) 70:1351–64. doi: 10.1016/j.jacc.2017.07.740
63. Giannoni A, Gentile F, Sciarrone P, Borrelli C, Pasero G, Mirizzi G, et al. Upright cheyne-stokes respiration in patients with heart failure. *J Am Coll Cardiol.* (2020) 75:2934–46. doi: 10.1016/j.jacc.2020.04.033

Conflict of Interest: The authors declare that the research was conducted in the absence of any commercial or financial relationships that could be construed as a potential conflict of interest.

frontiers | Frontiers in Cardiovascular Medicine

ORIGINAL RESEARCH
published: 10 May 2022
doi: 10.3389/fcvm.2022.907490

Anemoside B4 Inhibits Vascular Smooth Muscle Cell Proliferation, Migration, and Neointimal Hyperplasia

*Dan Shan[1,2,3], Ping Qu[2], Chao Zhong[1,2], Luling He[1], Qingshan Zhang[3], Guoyue Zhong[4], Wenhui Hu[2], Yulin Feng[5], Shilin Yang[5], Xiao-feng Yang[2] and Jun Yu[2]**

[1] Center for Translational Medicine, Jiangxi University of Traditional Chinese Medicine, Nanchang, China, [2] Department of Cardiovascular Sciences and Center for Metabolic Disease Research, Lewis Katz School of Medicine, Temple University, Philadelphia, PA, United States, [3] Department of Internal Medicine, Affiliated Hospital of Inner Mongolia University for the Nationalities, Tongliao, China, [4] Research Center of Natural Resources of Chinese Medicinal Materials and Ethnic Medicine, Jiangxi University of Traditional Chinese Medicine, Nanchang, China, [5] The National Pharmaceutical Engineering Center for Solid Preparation in Chinese Herbal Medicine, Nanchang, China

Vascular smooth muscle cell (VSMC) phenotypic transformation, proliferation, and migration play a pivotal role in developing neointimal hyperplasia after vascular injury, including percutaneous transluminal angioplasty and other cardiovascular interventions. Anemoside B4 (B4) is a unique saponin identified from the Pulsatilla chinensis (Bge.) Regel, which has known anti-inflammatory activities. However, its role in modulating VSMC functions and neointima formation has not been evaluated. Herein, we demonstrate that B4 administration had a potent therapeutic effect in reducing neointima formation in a preclinical mouse femoral artery endothelium denudation model. Bromodeoxyuridine incorporation study showed that B4 attenuated neointimal VSMC proliferation *in vivo*. Consistent with the *in vivo* findings, B4 attenuated PDGF-BB-induced mouse VSMC proliferation and migration *in vitro*. Moreover, quantitative RT-PCR and Western blot analysis demonstrated that B4 suppressed PDGF-BB-induced reduction of SM22α, SMA, and Calponin, suggesting that B4 inhibited the transformation of VSMCs from contractile to the synthetic phenotype. Mechanistically, our data showed B4 dose-dependently inhibited the activation of the phosphatidylinositol 3-kinase (PI3K)/AKT and p38 mitogen-activated protein kinase MAPK signaling pathways. Subsequently, we determined that B4 attenuated VSMC proliferation and migration in a p38 MAPK and AKT dependent manner using pharmacological inhibitors. Taken together, this study identified, for the first time, Anemoside B4 as a potential therapeutic agent in regulating VSMC plasticity and combating restenosis after the vascular intervention.

Keywords: Anemoside B4, vascular smooth muscle cell, proliferation, migration, neointimal hyperplasia

OPEN ACCESS

Edited by:
Hong S. Lu,
University of Kentucky, United States

Reviewed by:
Shiyou Chen,
University of Missouri, United States
Mei-Zhen Cui,
University of Texas of the Permian Basin, United States

***Correspondence:**
Jun Yu
jun.yu@temple.edu

Specialty section:
This article was submitted to Cardiovascular Therapeutics, a section of the journal Frontiers in Cardiovascular Medicine

Received: *29 March 2022*
Accepted: *19 April 2022*
Published: *10 May 2022*

Citation:
Shan D, Qu P, Zhong C, He L, Zhang Q, Zhong G, Hu W, Feng Y, Yang S, Yang X-f and Yu J (2022) Anemoside B4 Inhibits Vascular Smooth Muscle Cell Proliferation, Migration, and Neointimal Hyperplasia. Front. Cardiovasc. Med. 9:907490. doi: 10.3389/fcvm.2022.907490

INTRODUCTION

Vascular smooth muscle cell (VSMC) is the major cell type in arteries. Unlike terminally differentiated cardiac or skeletal myocytes, VSMCs retain remarkable plasticity (1). VSMCs can be modulated from a quiescent status to a hyperproliferative phenotype that contributes to vascular remodeling and neointima formation in response to environmental cues such as

vascular injury or inflammatory stimuli. Abnormal proliferation and migration of VSMCs is a hallmark of many occlusive vascular diseases, such as atherosclerosis, intimal hyperplasia and/or restenosis following percutaneous transluminal angioplasty (PTA), bypass surgery, and arterial-venous fistular (2–5). VSMCs exhibit differentiated and contractile phenotype in mature blood vessels, typically proliferating at an extremely low rate and having shallow synthetic activity (6). However, differentiated VSMCs can reversibly switch to a dedifferentiated state in response to mechanical insults, such as angioplasty, stenting, or bypass surgery (7). This phenotypic modulation is characterized by an increased rate of proliferation and migration, which contributes to intimal hyperplasia (8, 9). Therefore, finding therapies to effectively inhibit VSMCs proliferation, migration, and phenotype switching is a primary focus for preventing post-intervention complications in coronary and peripheral arterial diseases, along with endothelium protection and anti-thrombotic therapy.

It has been well documented that vascular injury induces the release of cytokines and growth factors to stimulate VSMCs proliferation and migration. The increased production of growth factors like PDGF-BB stimulates VSMCs proliferation, and migration (10) and modulates differentiated to dedifferentiated phenotype switching (11, 12) in response to vascular injury *via* initiating downstream signaling pathways. PDGF-BB, as a natural ligand of PDGFR-β (13), activates downstream signaling mitogen-activated protein kinases (MAPKs) and phosphatidylinositol 3-kinase (PI3K)/protein kinase B (AKT), which have been demonstrated to affect cell proliferation and migration (14–16). Moreover, previous studies have shown that PDGF-BB significantly inhibited the expression of VSMC differentiation markers, including α-SMA, SM22α, and calponin (17–19), through mechanisms including upregulation Kruppel-like factor 4 (KLF4). PDGF-PDGFR-MAPK-PI3K/AKT and KLF-myocardin pathways have attracted great interest as therapeutic targets for modulating VSMC pathophysiology and managing neointimal hyperplasia.

Pulsatilla chinensis (Bge.) Regel is a well-known and widely used herbal medicine in Asian countries attributed to its antimicrobial and anti-inflammatory properties (20, 21). Previous studies have shown that Pulsatilla chinensis saponins have a wide range of pharmacological effects, including anti-inflammatory, antioxidant, immunomodulatory, and cognitive enhancement (22). Saponins are the major ingredients in Pulsatilla. Among those, Anemoside B4 (B4) is one of the most abundant saponin compounds identified from the Pulsatilla chinensis (23). While most of the research has focused on the separation, extraction, pharmacokinetics, and pharmacodynamics of B4, a recent study reported that B4 could inhibit the phosphorylation of AKT and mTOR and induce apoptosis and autophagy of hepatocellular carcinoma (24). Another study has shown that Anemoside B4 prevents acute ulcerative colitis by inhibiting the TLR4/NF-κB/MAPK signaling pathway (25).

However, the role of B4 in modulating neointima hyperplasia and VSMC function is unknown. In the current study, we aimed to determine the effect of B4 on VSMC proliferation and migration and its ability to attenuate restenosis *in vivo*. Our data point to a model wherein B4 inhibits PDGF-BB-induced VSMC proliferation and migration, prevents the transformation of VSMCs from contractile to the synthetic phenotype, and attenuates neointima formation in a mouse acute femoral artery injury model through PI3K/Akt and p38 MAPK signaling. For the first time, our results reveal that B4 is a promising saponin to ameliorate occlusive vascular disease.

MATERIALS AND METHODS

Reagents

Anemoside B4 (B4, chemical structure $C_59H_96O_{26}$, molecular weight = 1,221.38, purity >98%) was purchased from the Chinese National Institute for the Control of Pharmaceutical and Biological Products. PDGF-BB was purchased from PEPROTECH. The small molecule inhibitors LY294002 (PI3K/Akt inhibitor), SD98059 (ERK inhibitor), SB203580 (p38 MAPK inhibitor), and SP600125 (JNK inhibitor) were obtained from Sigma-Aldrich (St. Louis, MO). Primary antibodies against Akt/phospho-Akt, ERK/phospho-ERK, p38 MAPK/ phospho-p38 MAPK, and JNK/phospho-JNK were from Cell Signaling Technology (Massachusetts, USA). Antibodies against α-SMA, Calponin, SM22-α, and BrdU were obtained from Abcam (Cambridge, UK). TUNEL staining kit was obtained from Roche. 5-Bromo-3′-deoxyuridine (BrdU) was purchased from Sigma-Aldrich (St. Louis, MO). See **Supplementary Tables 1, 2** for detailed information.

Animal and Mouse Femoral Artery Wire Injury

Six-week-old male C57BL/6J mice were purchased from the Jackson Laboratory. All experiments were performed in accordance with the guidelines/regulations and were approved by the Institutional Animal Care and Use Committee (IACUC) of Temple University. Mice were anesthetized with an intraperitoneal (IP) injection of ketamine (100 mg/kg) and xylazine (10 mg/kg). As previously described, the wire-induced left femoral artery injury was performed (26, 27). Mice were injected with B4 (20 mg/kg or 40 mg/kg) or equal volum of vehicle control (saline) daily intraperitoneally (IP) for 3 weeks. Mice were injected with BrdU subcutaneously (25 mg/kg) daily for 3 days and IP (30 mg/kg) 12 h before sacrifice. Femoral arteries were collected at the experimental endpoint and cryopreserved for histological staining. Cryosections (5 μm) were obtained for H&E, EVG, and BrdU staining. Morphometric analyses were performed as previously described (26, 28). Ten cross-sections were stained with H&E or EVG and used for lumen, neointimal, medial, and vessel area quantification. Each section was collected 100 μm apart to cover the whole injured vessel. Values were then averaged for each animal, and the mean was calculated from 5 to 6 animals per treatment.

Primary VSMC Isolation and Culture

Primary mouse VSMCs (MVSMCs) were separated from the thoracic arteries of 6-week-old male C57BL/6J mice using collagenase, as previously described (28). In brief, mouse vessels

were minced with a sterile blade and digested in a digestion mix (175 U/ml collagenase II, 1.25 U/ml elastase in 2.5 ml HBSS) by shaking at 500 rpm at 37°C for 30 min. The cell suspension was centrifuged at 920 rpm for 5 min, washed once with DMEM supplemented with 20% FBS, penicillin G (100 units/ml), and streptomycin sulfate (100 μg/ml). Plated cells on desired dishes in the same media. Cells were sub-cultured 1: 3 once confluent. Cells in passages 4–9 were used for all the experiments. The cells were starved with starvation media (0.3% FBS) for 24 h before experimental treatments.

Histological Staining and BrdU Incorporation

Mice were anesthetized with an intraperitoneal injection of ketamine (100 mg/kg) and xylazine (10 mg/kg), then systemically perfused with PBS *via* the left ventricle. Isolated femoral arteries were fixed with 2%PFA in PBS for 24 h at 4°C, then kept in 30% sucrose in PBS until the next day at 4°C. Finally, tissues were embedded in OCT and kept at −80°C. Serial 5 μm sections were cut using a cryostat, and several morphometric and histological analyses were performed as previously described (29). H&E and EVG stained images were captured using inverted Olympus IX71microscopes and a digital camera. A BrdU incorporation assay measured the frozen mouse femoral arteries (3). Artery sections were washed with PBS, fixed with 2% PFA for 10 min, and incubated with 0.1% Triton-X100 for 20 min to permeabilize the cell membrane. Samples were neutralized by incubation in phosphate/citric acid buffer (pH 7.4) for 10 min at room temperature. Samples were then blocked with blocking buffer (5% normal goat serum, 0.5% BSA, 0.1% Triton-X100 in PBS) for 1 h. A primary anti-BrdU antibody was used at a 1:40 dilution. A FITC-labeled

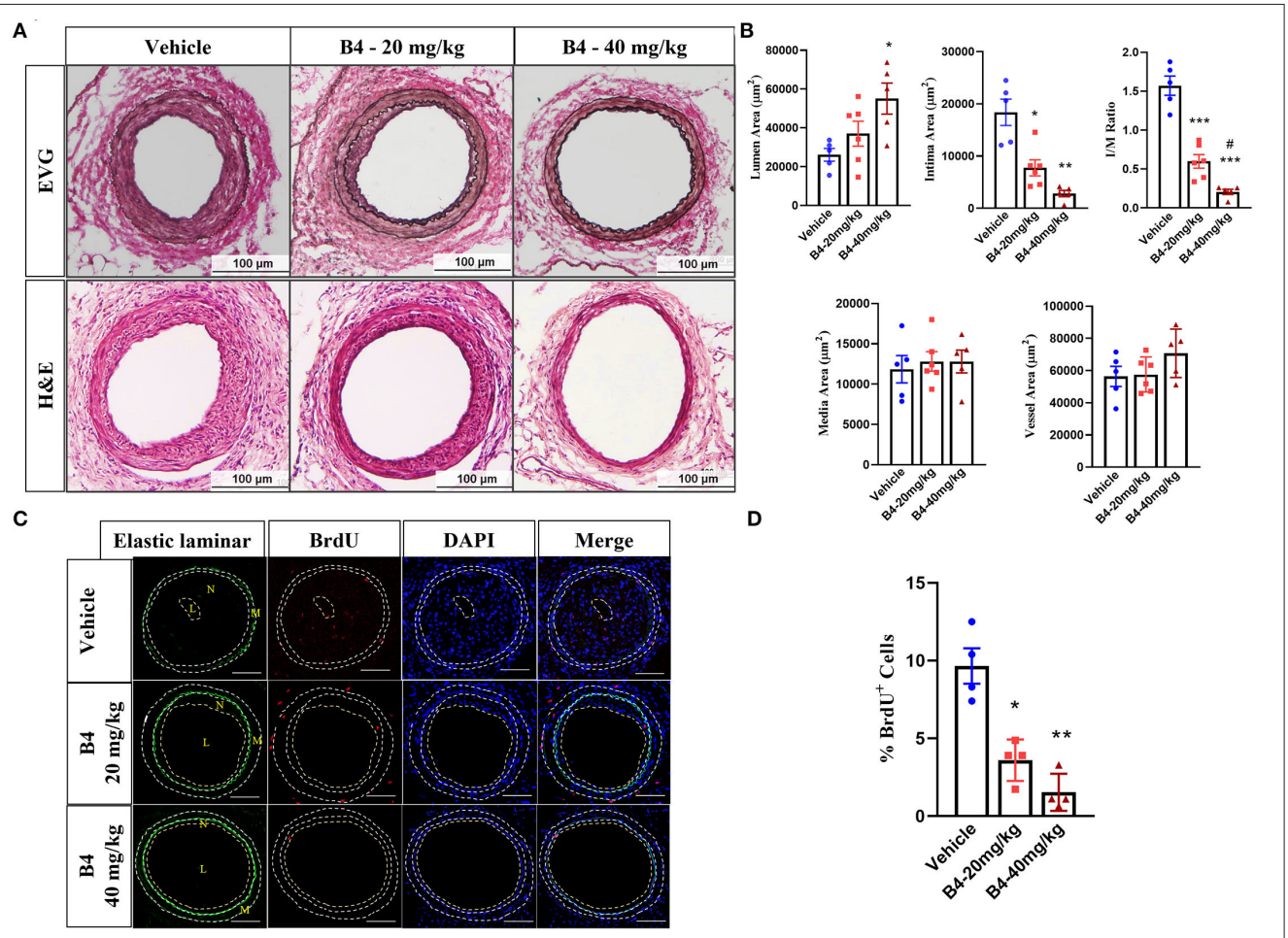

FIGURE 1 | B4 attenuates neointima formation in a murine femoral artery wire injury model. Six-week-old C57BL/6J male mice were intraperitoneally injected with B4 (20 mg/kg/d), (40 mg/kg/d), or saline (Vehicle) daily for 3 weeks. **(A)** Elastic van Gieson (EVG, upper panel) and H&E staining (lower panel) staining of injured femoral arteries (Vehicle) and B4 (20 mg/kg/d), (40 mg/kg/d). Scale bar, 100 μm. **(B)** Morphometric analysis of lumen area, neointima area, intima-to-media ratio, media area, and vessel area of injured femoral arteries from mice injected with vehicle or B4. **(C)** Representative BrdU immunofluorescence stained images of the sections from vehicle or B4. The dotted line represents the auto-fluorescent of elastic laminar. Scale bar, 100 μm. **(D)** The percentage of BrdU positive cell number was quantified in sections from sham-operated and injured femoral arteries from vehicle or B4 treated mice. Cells in the media and neointima layers (between the external elastic laminar and the lumen of each section) were included. Data shown are means ± SEM. $N = 5$ for control and $N = 6$ for B4 treatment. $^{*}P < 0.05$; $^{**}P < 0.01$; $^{***}P < 0.001$; compared with Vehicle group. $\#P < 0.05$; compared with B4-20mg/kg group.

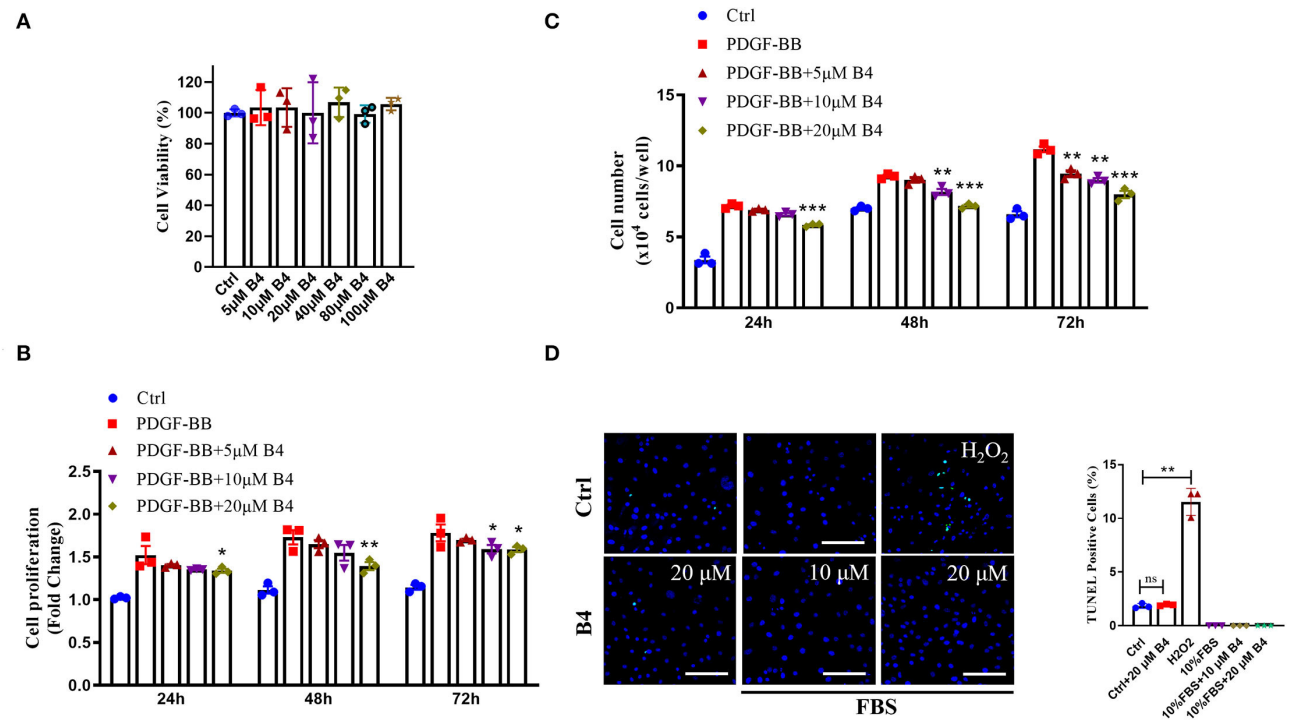

FIGURE 2 | B4 inhibits MVSMCs proliferation but not cell viability or apoptosis. **(A)** Cell viability was measured by MTT assays. PDGF-BB-deprived MVSMCs were pretreated with 5–100 μM of B4 for 24 h and incubated with/without PDGF-BB in the absence or presence of B4 for the indicated times. Cell proliferation was detected by **(B)** MTT assays. **(C)** Direct cell counting. **(D)** MVSMC apoptosis was measured by TUNEL staining. Data shown are means ± SEM. $N = 3$. $^{*}P < 0.05$; $^{**}P < 0.01$; $^{***}P < 0.001$; compared with PDGF-BB control group. Scale bar, 100 μm. All experiments were repeated at least for three times.

secondary antibody (anti-rat, 1:250) was used. Nuclei were stained with DAPI.

Cell Proliferation and Viability Assay

Mouse VSMCs proliferation was examined by MTT assay and cell counting. MTT assays were performed as described previously with minor modifications (30). Briefly, MVSMCs (7,000 cells/well) were cultured overnight in a 96-well plate in starvation media for 24 h and pretreated with varying concentrations of Anemoside B4. Cells were then stimulated with PDGF-BB (10 ng/ml) in the absence or presence of different concentrations of Anemoside B4 or/and LY294002, SB203580. MTT stock solution (20 μl, 5 mg/ml in PBS) was added to wells at various time points, incubated for 4 h at 37 °C, and 200 μl DMSO was added to the media to solubilize the crystal for 10 min. The absorbance of cells was measured at 570 nm using a microplate reader. MVSMCs incubated with the starvation medium were used as controls. To obtain direct cell counts, MVSMCs (3×10^4 cells/well) were cultured in 24-well and treated as described above, except for MTT addition. Cells were trypsinized and counted using a hemocytometer.

TUNEL Staining for Detection of Cell Apoptosis

Mouse VSMCs were cultured on the pre-coated coverslips overnight and treated with the conditions described in the cell proliferation assay. TUNEL and Fluor 488 Apoptosis detection assay (Roche) was performed following the manufacturer's protocol to detect VSMC apoptosis. DAPI was used as the nuclear DNA marker.

Wound Healing Assays

Mouse VSMCs were seeded into 12-well plates, cultured up to 85% confluency, and then starved (0.3% FBS) for 24 h. Cell monolayers were scratched using a 1 ml pipette tip (31). Cells were then treated with PDGF-BB (10 ng/ml) in the absence or presence of different concentrations of Anemoside B4, LY294002, SD98059, SB203580, SP600125, or combination for 12 or 24 h. Images were captured at 0, 12, and 24 h with inverted Olympus IX71microscopes and a digital camera. Quantification was made by using ImageJ.

Modified Boyden Chamber Assay

Three-dimensional cell migration was performed using the 8 μm pore size polycarbonate filters modified Boyden chamber (Costar, 3422) transwell assay. MVSMCs were plated at a density of 3×10^4 cells/well cultured in starvation media in the upper chamber pre-coated with 0.1% gelatin. PDGF-BB (10 ng/ml) and varying concentrations. Anemoside B4 was added to the lower chamber. Cells in starvation media or PDGF-BB served as controls. Twelve hours later, the migrated cells in the lower chamber were fixed with 2% PFA for 20 min and then stained with 0.1% crystal violet

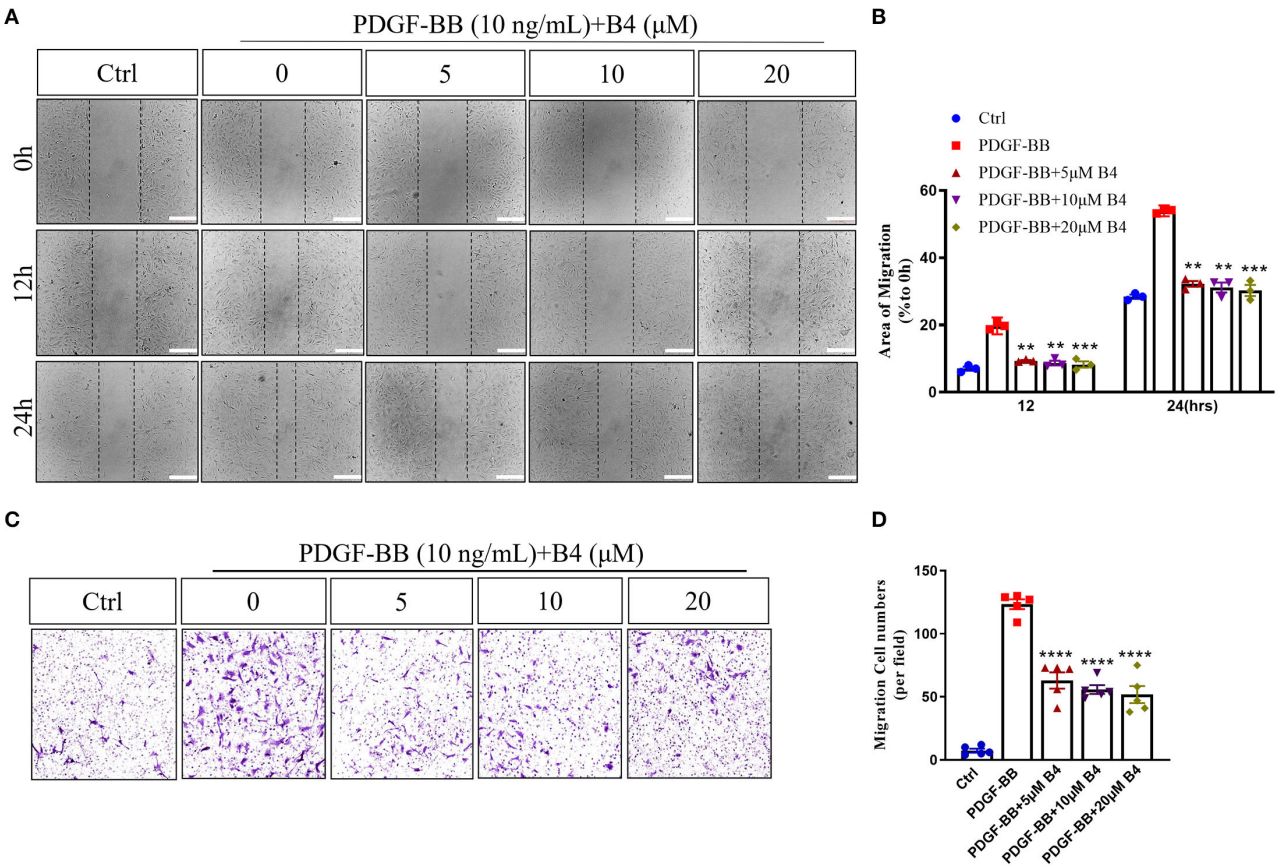

FIGURE 3 | B4 prevents MVSMCs migration. **(A)** Representative images of quiescent MVSMCs were pretreated with B4 for 24 h and stimulated with PDGF-BB for 24 h. Images were captured at 0, 12, 24 h. The percentage of area covered by migrated cells over time was calculated using ImageJ **(B)**. $N = 3$. Scale bar, 200 μm. **(C)** Representative images from transwell migration assay with different conditions. **(D)** Quantification for the number of migrated cells is shown in the bar graph. $N = 5$. All experiment was repeated at least three times. Data shown are means ± SEM. $^{**}P < 0.01$; $^{***}P < 0.001$; $^{****}P < 0.0001$ vs. PDGF-BB control group.

for another 20 min. The five views migrated cells from each well were captured and quantified using ImageJ (NIH).

Western Blotting

Cells were briefly washed with cold PBS and scraped in cold 1 × TBSN buffer supplemented with protease inhibitor and phosphatase inhibitors on ice. Cell lysates were centrifuged at 12,000 × g for 30 min at 4°C. Supernatants were mixed with loading buffer and denatured at 95°C for 5 min. Equal amounts of protein from each sample were separated on 10%SDS-PAGE gels, transferred onto nitrocellulose membranes and block with 5%BSA 1 h, and then immunoblotted with primary antibodies at 4°C overnight and secondary antibodies (IRDye) at Room temperature for 1 h. Digital images were taken with a Gel DocTM XR+ System using Image Lab software (BioRad). Densitometry of western blot bands was quantitated using ImageJ.

RNA Extraction and Quantitative Real-Time (RT)-PCR Analysis

According to the manufacturer's protocol, the MVSMCs were briefly washed with cold PBS, and total RNA was extracted using Trizol (Invitrogen, Camarillo, USA). One μg of total RNA was reverse transcribed to cDNA using the iScript reverse transcript synthesis kit (Bio-Rad). cDNA was then used for quantitative real-time RT-PCR analysis (Bio-Rad CFX96 Real-Time System) using SYBR Green supermix (Bio-Rad). The mRNA level was normalized to ribosomal RNA 18S as a housekeeping gene. Real-time RT-PCR was analyzed using the $2^{-\Delta\Delta CT}$ method (CT, comparative threshold cycle). CT values were normalized to the internal control 18s for MVSMCs samples. $\Delta\Delta CT$ = (CT experimental gene – CT housekeeping gene) – (CT control gene-housekeeping gene). All samples were run in triplicates.

Statistical Analysis

Values are presented as mean ± SEM from at least three independent Experiments. GraphPad Prism Software version 8.0 was used for statistical analysis. One-way ANOVA followed by Tamhane T2 test to correct for multiple comparisons was used to perform multiple groups comparisons. Two-tailed Student's-test was used to analyze the differences between the two groups. $P < 0.05$ were considered statistically significant.

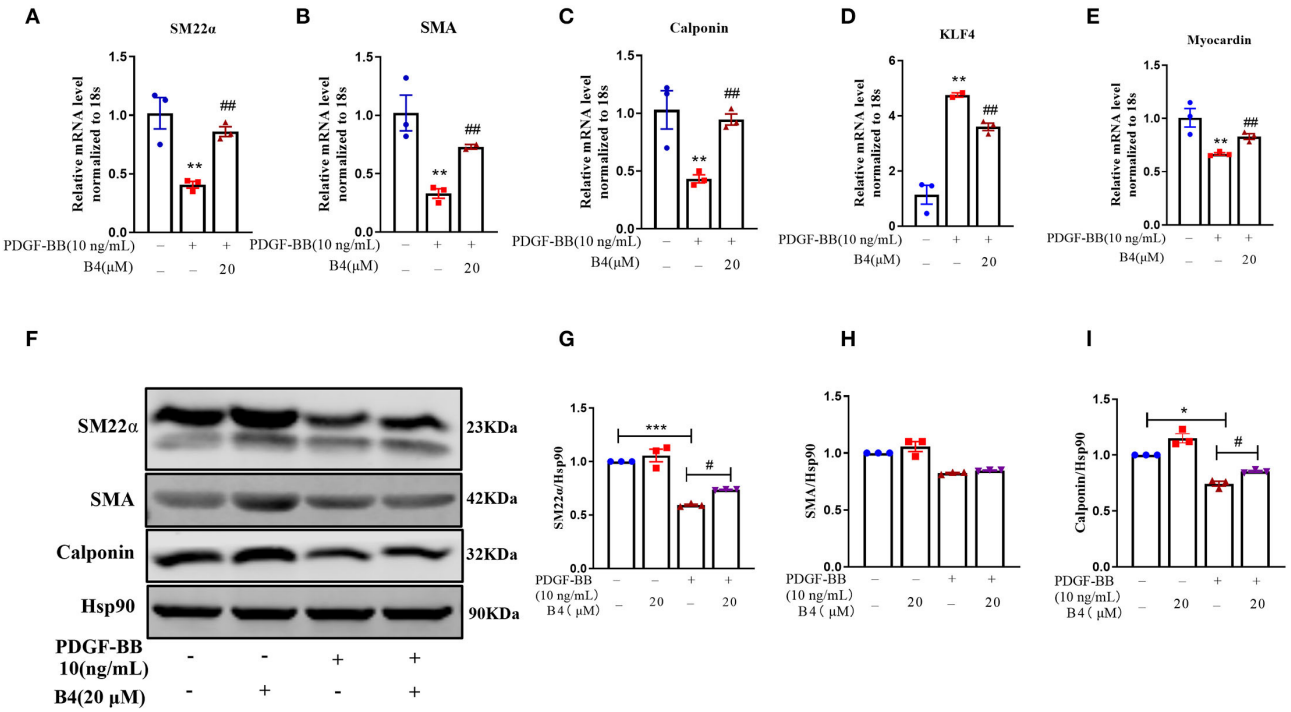

FIGURE 4 | B4 abrogates PDGF-BB-induced MVSMCs dedifferentiation. MVSMCs were pretreated with B4 (20 μM) for 24 h, followed by PDGF-BB (10 ng/ml) stimulation for 48 h. **(A–E)** Bar graph showing the relative mRNA level of SM22α, SMA, Calponin, KLF-4, and Myocardin. **(F)** Western blot was employed to quantitate the expression levels of contractile protein SM22α, SMA, Calponin. Hsp90 was used as a loading control. **(G–I)** Bar graph showing the relative protein level of SM22α, SMA, and Calponin. Values are mean ± SEM. $^{*}P < 0.05$; $^{**}P < 0.01$; $^{***}P < 0.001$ vs. Control, $^{\#}P < 0.05$; $^{\#\#}P < 0.01$ vs. PDGF-BB. $N = 3$ for each group.

RESULTS

Animoside B4 Attenuates Neointima Formation Induced by Femoral Artery Injury *in vivo*

To determine whether B4 (chemical structure shown in **Supplementary Figure 1**) affects neointima formation, we performed the mouse femoral artery wire injury model in C57BL/6J mice treated with vehicle or B4. In this model, the endothelial layer of the femoral artery is denuded by passaging an angioplasty guided wire three times, and extensive neointima is formed as a result of medial VSMC proliferation and migration (26, 27). No difference in the gross vessel morphology was observed in femoral arteries of mice given a systemic injection of vehicle or B4 (not shown). A robust neointima formation was observed in vehicle-treated mice 3 weeks following femoral arterial wire injury. The treatment of B4 exhibited a significant reduction in intimal thickness and intima to media ratio compared to the vehicle treatment (**Figures 1A,B**). The media area and vessel area determined by internal and external elastic laminar were not changed between groups (**Figures 1A,B**). Following injury, pathological vascular remodeling is attributed to increased VSMC proliferation (1, 32). We evaluated VSMC proliferation by BrdU incorporation *in vivo*. As shown in **Figure 1C**, we observed growing numbers of BrdU labeled VSMC in the injured vehicle-treated femoral arteries (**Figure 1C**, top panel). Notably, B4 treatment significantly reduced the number of BrdU-positive cells detected in the media and neointima layers of the injured vessels (**Figure 1C**, middle and bottom panels, and **Figure 1D**). Together, these results indicate that B4 treatment significantly reduced neointima formation by inhibiting VSMC proliferation *in vivo*.

B4 Inhibits PDGF-BB Induced VSMC Proliferation and Migration but Does Not Affect Cell Viability and Apoptosis

To examine the role of B4 on VSMC function *in vitro*, we first determined its toxicity. MTT assay showed that B4 did not affect MVSMC viability even at the highest concentration (100 μM) tested at 24, 48 h (**Supplementary Figure 2**), and 72 h (**Figure 2A**) after treatment. The abnormal proliferation and migration of VSMCs play a pivotal role in developing neointimal hyperplasia after vascular injury (27, 29). To investigate the possible mechanisms underlying B4's ability to attenuate neointima hyperplasia, MVSMCs were stimulated with or without PDGF-BB in varying concentrations (0, 5, 10, and 20 μM) of B4, and cell proliferation, migration, and apoptosis assays were performed. MVSMCs cultured without PDGF-BB proliferated at a standard rate, and B4 did not affect MVSMC proliferation under these basal conditions. Proliferation was significantly increased with the addition of PDGF-BB, and this response to PDGF-BB was attenuated by B4 treatment

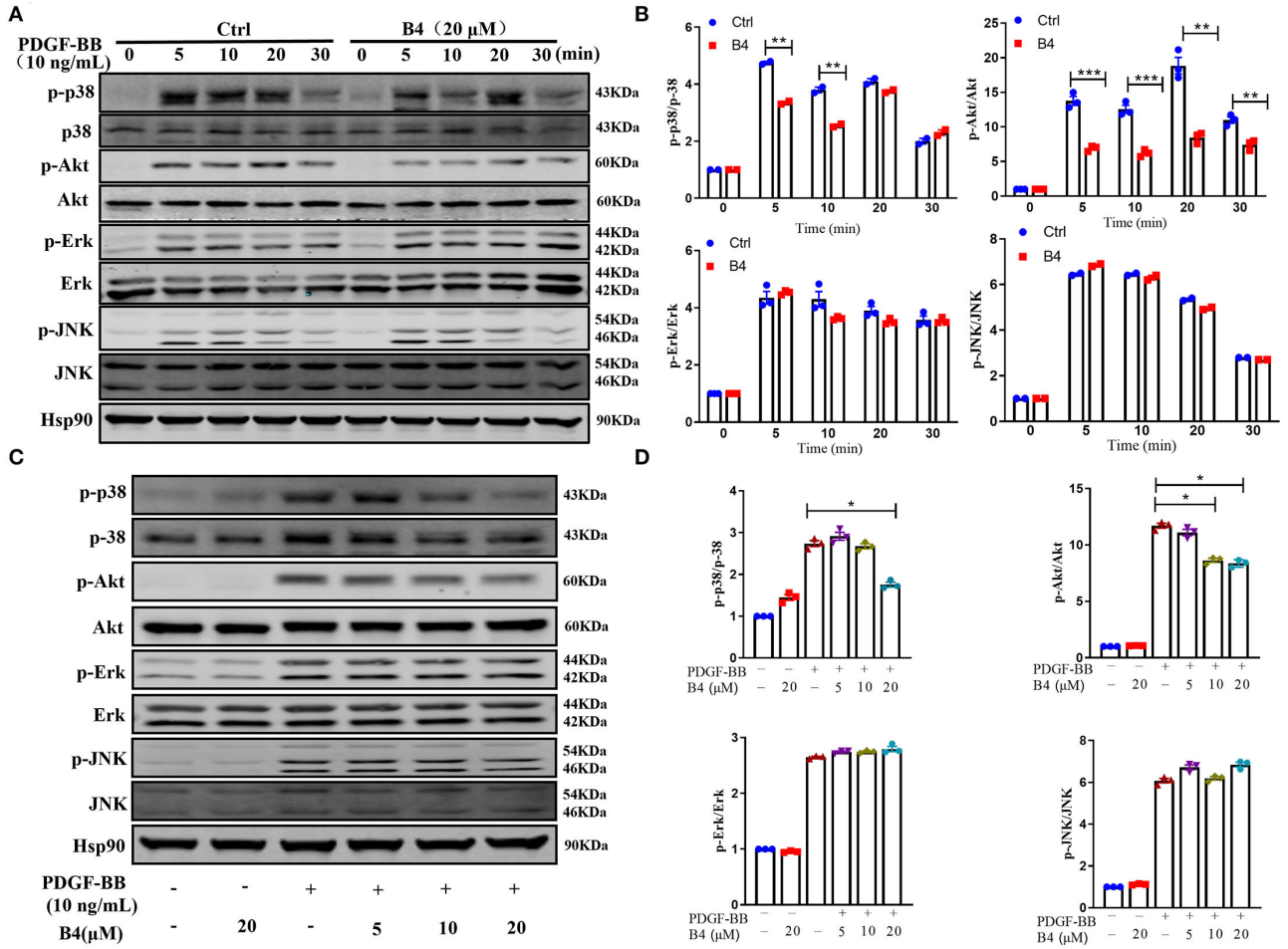

FIGURE 5 | B4 inhibits PDGF-BB-induced PI3K/Akt and p-38 MAPK signaling pathway. **(A)** Western blot analysis of p-Akt/Akt, p-p38/p38, p-ERK/ERK, p-JNK/JNK in MVSMCs treated with B4 for 24 h and stimulated with PDGF-BB for 0–30 min. Hsp90 was used as the loading control. **(B)** Densitometry analysis of the phosphorylation protein normalized to the total protein levels. **(C)** Western blot analysis of MVSMCs treated with different concentrations of B4 (0, 5, 10, 20 μM) for 24 h and stimulated with PDGF-BB 10 ng/ml for 15 min. The protein expression levels of p-p38/p38, p-Akt/Akt, p-ERK/ERK, and p-JNK/JNK were blotted. Hsp90 was used as a loading control. Representative western blots from three experiments are shown. **(D)** Densitometrical analysis of the western blots. Data shown are means ± SEM. $N = 3$. $^{*}P < 0.05$; $^{**}P < 0.01$; $^{***}P < 0.001$; compared to non-stimulated control group. All experiments were repeated at least for three times.

in a time- and dose-dependent manner (**Figures 2B,C**). To exclude the possibility that the anti-proliferation effect of B4 on MVSMC was due to increased apoptosis, we examined MVSMC apoptosis under both basal (0.3% FBS) and stimulated (20% FBS) conditions. TUNEL staining showed B4 did not increase MVSMCs apoptosis (**Figure 2D**). These results suggest that B4 inhibits PDGF-BB-induced VSMC proliferation but does not affect cell cytotoxicity or apoptosis.

In addition to proliferation, VSMC migration is another critical process in promoting neointimal hyperplasia (33). PDFG-BB is an effective growth factor that could increase VSMC migration (10). To determine the potential effect of B4 on MVSMC migration, we performed 2D wound healing and 3D transwell migration assays. **Figures 3A,B** shows that B4 dose-dependently inhibited PDGF-BB induced MVSMC migration and wound closure. The transwell assay further indicated the inhibitory effect where B4 dose-dependently inhibited the PDGF-BB-induced MVSMC transmigration (**Figures 3C,D**). These results suggest that B4 inhibits VSMC proliferation and migration but does not adversely affect cellular viability.

B4 Abrogates PDGF-BB-Induced VSMC Dedifferentiation

Vascular smooth muscle cells in mature, healthy blood vessels are highly specialized cells with a quiescent, differentiated, and contractile phenotype. They express high levels of contractile proteins such as SMA, SM22α, and calponin. In response to vascular injury, VSMCs switch to a dedifferentiated, proliferative, and migratory phenotype (synthetic phenotype), with decreased levels of contractile proteins (34, 35). To test whether B4 affects PDGF-BB-induced VSMC dedifferentiation, after starvation, MVSMCs were stimulated with PDGF-BB (10 ng/ml) and 20 μM B4, alone or in combination for 48 h. The results showed that PDGF-BB promoted the MVSMC phenotypic alteration from

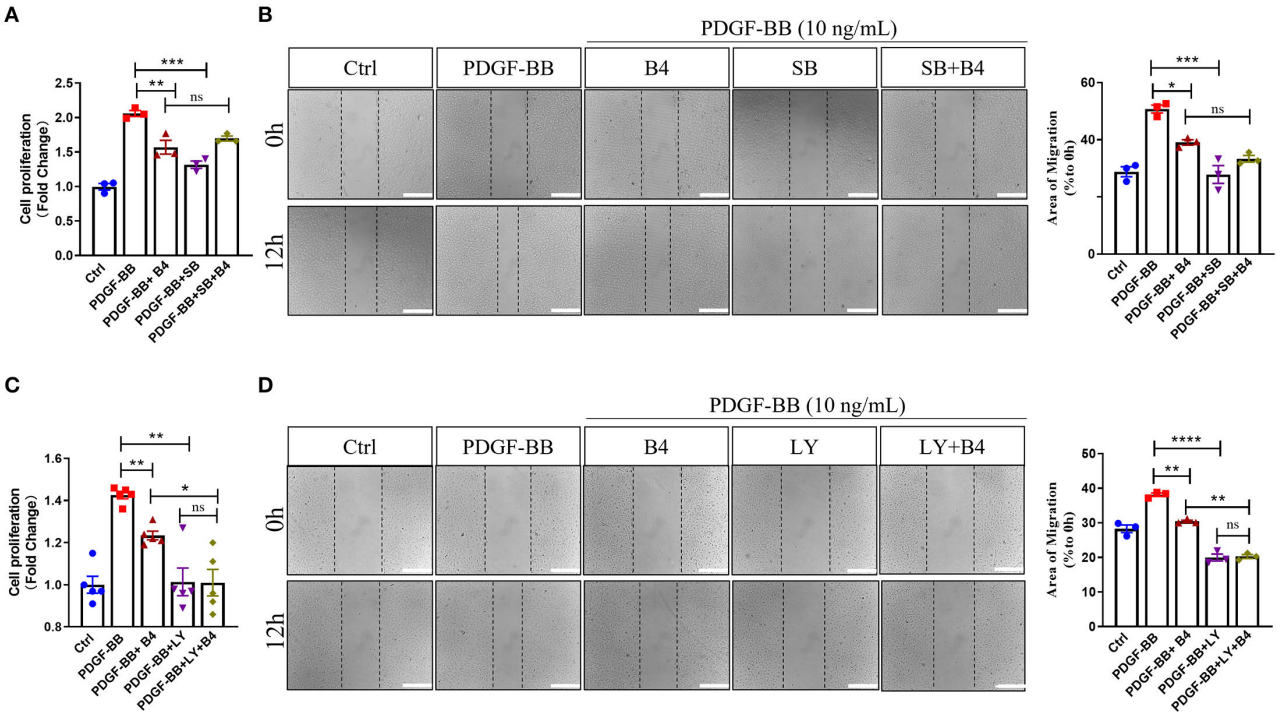

FIGURE 6 | B4 inhibits cell proliferation and migration by targeting the p38 MAPK and PI3K/Akt signaling pathways in VSMC. Quiescent MVSMCs were treated with B4 (20 μM) for 24 h and incubated with SB203580 (20 μM) or SB203580 and B4 in the presence or absence of PDGF-BB for 48 h. **(A)** Cell proliferation was quantified as a fold increase of control. **(B)** Cell migration was quantified as the percentage of the area of migrated cells covered area relative to time 0. Quiescent MVSMCs were treated with B4 (20 μM) for 24 h and incubated with LY294002 (10 μM) or LY294002 and B4 in the presence or absence of PDGF-BB for 48 h. **(C)** Cell proliferation was quantified as a fold increase of control. **(D)** Cell migration was quantified as the percentage of the area of migrated cells covered area relative to time 0. Data shown are means ± SEM. $^{*}P < 0.05$; $^{**}P < 0.01$; $^{***}P < 0.001$ compared with PDGF-BB control group. All experiments were repeated for at least three times.

a differentiated to a dedifferentiated status, as evidenced by decreased VSMC contractile genes SMA, calponin, and SM22α at mRNA (**Figures 4A–C**) and protein levels (**Figures 4F–I**). B4 treatment reversed PDGF-induced MVSMC contractile gene down-regulation. KLF4 and myocardin are master regulators of VSMC plasticity (36–38). We examined whether B4 regulates VSMC contractile genes through KLF4 and myocardin. As shown in **Figures 4D,E**, B4 reversed the effect of PDGF-BB in the upregulation of KLF4 and downregulation of myocardin. Our study suggests that B4 antagonizes VSMC dedifferentiation through the transcriptional regulation of KLF4 and myocardin.

B4 Inhibits PDGF-BB-Induced VSMC Proliferation and Migration Through p38 MAPK and PI3K/Akt Signaling Pathways

It is well known that phosphorylation and subsequent activation of MAPK and PI3K/Akt are the major signals involved in PDGF-BB stimulated VSMC proliferation and migration (39, 40). To determine the effect of B4 on these signaling pathways, the phosphorylation of Akt and MAPKs was examined in MVSMCs stimulated with PDGF-BB. We observed a rapid decrease in p38 MAPK and Akt phosphorylation, but not ERK1/2 or JNK activation, in MVSMCs following B4 treatment in a time- and dose-dependent manner (**Figure 5**). The total protein levels of Akt and MAPKs were unaffected by PDGF-BB or B4 treatment.

To further determine that B4 inhibits MVSMC proliferation and migration through p38 MAPK and PI3K/Akt signaling, we tested the effect of inhibiting p38 MAPK, PI3K/Akt, ERK, or JNK signaling in cultured MVSMC with their respective specific small molecule inhibitors SB203580, LY294002, PD98059, and SP600125. We compared VSMC proliferation, migration, MAPK, and Akt activity in MVSMC at baseline, with PDGF-BB stimulation in the presence of B4, treated with the pharmacological inhibitors, or both. MVSMC proliferation and migration were significantly reduced in the presence of B4 or p38 MAPK inhibitor SB203580 compared to PDGF-BB treated cells. Treatment of B4 with SB203580 showed no synergistic or additive effect on VSMC proliferation and migration (**Figures 6A,B**). Similarly, MVSMC proliferation and migration were significantly attenuated in the presence of B4 or Akt inhibitor LY294002 compared to PDGF-BB treated cells. Notably, co-treatment of MVSMC with LY294002 and B4 showed that B4 had no effect in further reducing cell proliferation compared to LY294002 alone (**Figure 6C**). The same observations were found for migration and Akt activity (**Figure 6D** and **Supplementary Figures 3A,B**). However, co-treatment of B4 with the ERK or JNK inhibitors showed a synergistic effect on VSMC proliferation and/or

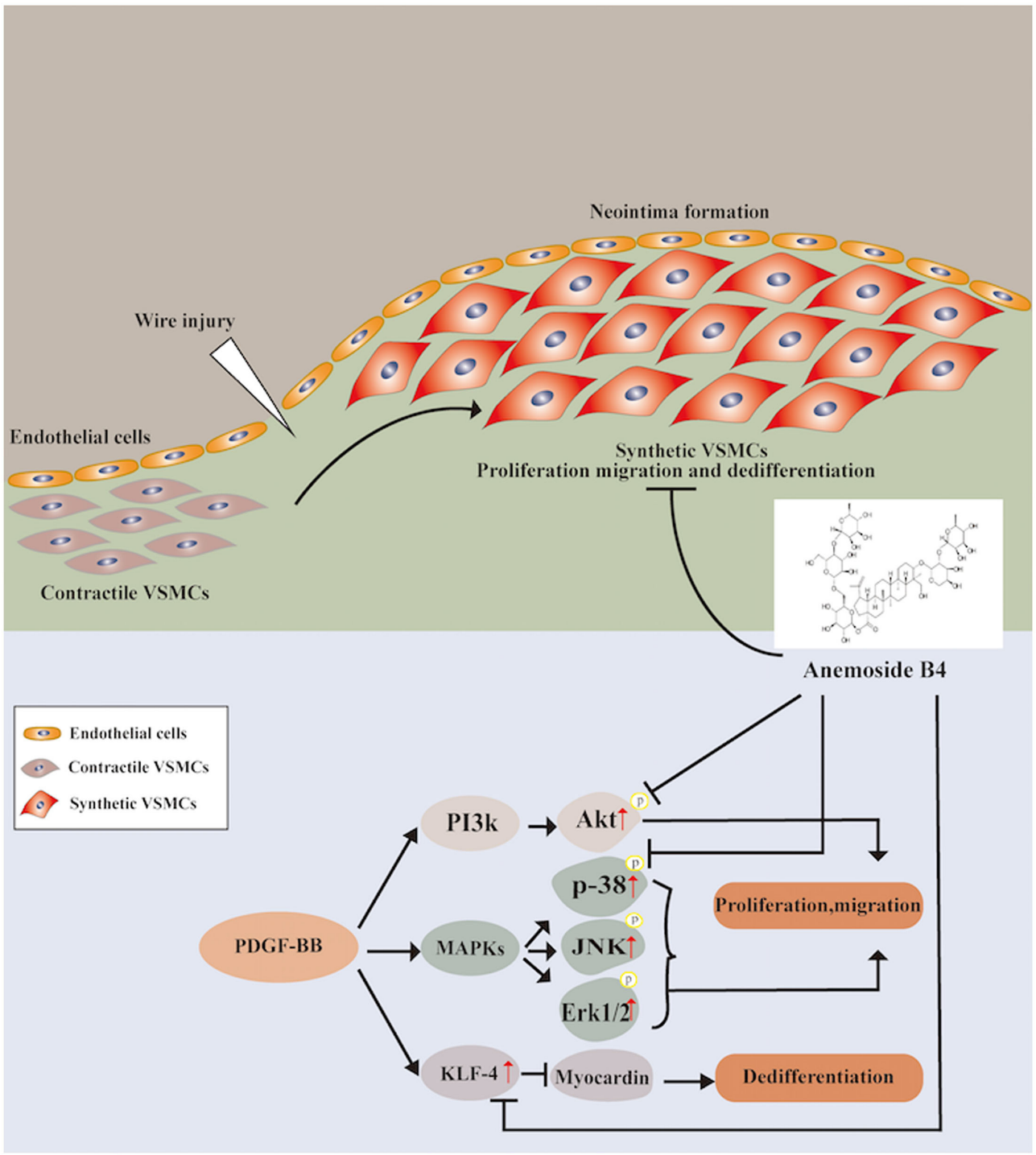

FIGURE 7 | Schematic diagram of the potential mechanisms of B4 in regulating PDGF-BB-induced VSMC proliferation, migration, and dedifferentiation.

migration (**Supplementary Figures 3C–G**). These data suggest that B4 inhibits VSMC proliferation and migration, at least in part, through p38 MAPK and PI3K/Akt but not ERK or JNK signaling pathways.

Our results indicate that B4 targets the p38 MAPK and PI3K/Akt signaling pathway and inhibits cell proliferation and migration in VSMC, contributing to the attenuation of neointima hyperplasia.

DISCUSSION

In the present study, we used a preclinical mouse model of endothelial denudation-induced vascular neointima hyperplasia to examine whether a novel saponin, Anemoside B4, has potential pharmacological effects on preventing neointima formation and vascular remodeling. B4 significantly attenuated neointima formation by inhibiting VSMC proliferation *in vivo*. We demonstrated that B4 inhibits VSMC proliferation and migration by inhibiting the p38 MAPK and PI3K/Akt signaling pathways and regulating the VSMC contractile gene expression. These results provided the molecular basis by which B4 exerted a protective role in VSMC biology.

It is well known that dysregulated VSMCs play a critical role in vascular restenosis, atherosclerosis and hypertension (41). Unlike skeletal or cardiac muscle cells, VSMCs are not terminally differentiated, and their phenotype can be modulated between contractile and synthetic states in response to environmental stimuli (42). The phenotypic switching of VSMCs is one of the major cellular events for the proliferation and migration of VSMCs. Increased VSMC proliferation and migration are essential to atherosclerosis, postangioplasty restenosis, and hypertension (43). Therefore, restenosis treatments after PTA have mainly focused on inhibiting VSMC proliferation and migration. Drugs such as Rapamycin (sirolimus) and Paclitaxel (Taxol), which inhibit VSMC proliferation and migration, have been widely used in drug-eluting stents to prevent in-stent restenosis (44, 45). Our current study indicated that B4 attenuated neointimal hyperplasia induced by endothelium denudation injury while maintaining the lumen diameter (**Figures 1A,B**). The therapeutic benefit of B4 lies in its ability to inhibit excessive VSMC proliferation, as demonstrated by decreased BrdU incorporation (**Figures 1C,D**, **2C,D**).

The healthy and mature VSMCs express high-level contractile proteins, including α-SMA, SM22α, and calponin, which significantly regulate vascular tone and blood pressure (43). VSMCs have remarkable plasticity without terminally differentiated properties (34). In response to the environmental stimuli, VSMCs undergo phenotypic switching from a differentiated and contractile state to a synthetic state (2). The phenotypic switch of VSMC is one of the major cellular events underlying many VSMC-related pathological conditions like restenosis (43). In the current study, we observed that B4 pretreatment prevented PDGF-BB induced VSMC differentiation, as reflected by increased VSMC contractile genes α-SMA, Calponin, and SM22α at both mRNA (**Figures 4A–C**) and protein levels (**Figures 4F–I**). KLF4 is a potent repressor of differentiation markers involving binding to the TGF-β control element within the promoter/enhancer regions of VSMC differentiation genes. KLF4 also interacts with serum response factor (SRF) and represses the expression of an SRF coactivator and VSMC differentiation master regulator, myocardin (36, 46, 47). B4 reduced KLF4 and elevated myocardin expression in mRNA levels (**Figures 4D,E**). These findings may represent a mechanism by which B4 inhibited VSMC dedifferentiation through the regulation of KLF4. However, further study is required to reveal its upstream mediators.

An abnormal increase in VSMC proliferation and migration is pivotal to neointima development in post-angioplasty restenosis. Inhibiting the VSMC migration and proliferation may be a plausible strategy for controlling the neointima hyperplasia in vascular remodeling-related disorders (48, 49). Our results indicate that the B4 inhibitory affects PDGF-BB-induced VSMC proliferation and migration (**Figures 3A–C**), protecting against neointimal hyperplasia *in vivo* (**Figure 1**). Our study provides the first direct evidence for the inhibitory effect of the B4 on PDGF-BB-induced VSMC migration, proliferation, and pathological vascular remodeling processes such as neointimal hyperplasia.

Numerous studies have indicated that the MAPK pathway, including p38 MAPK, ERK1/2, and JNK pathways, plays a crucial role in VSMC differentiation and proliferation (50). Inhibition of p38 MAPK decreased PDGF–BB–induced VSMC proliferation and neointimal formation after vascular injury (51). In the present study, we found that B4 blocked p38 MAPK activation induced by the stimulation of PDGF-BB (**Figure 5**). The p38 MAPK inhibition or B4 inhibited VSMC proliferation and migration. SB203580 had no additive effect when used with B4 treatment (**Figures 6A,B**), indicating B4 inhibits VSMC proliferation and migration, at least in part, through p38 MAPK inhibition.

PI3K/Akt pathway also plays a pivotal role in growth factors or cytokines (such as PDGF, interleukin-1, and TNF-α) induced VSMC proliferation and migration (15, 16, 40). The current study shows that B4 attenuated PDGF-BB-induced Akt phosphorylation but not ERK1/2, JNK activation (**Figure 5**). Furthermore, pharmacological inhibition of PI3K/Akt, but not antagonizing ERK or JNK, abolished the effect of B4 on VSMC proliferation and migration (**Figures 6C,D** and **Supplementary Figures 3C–G**). These results suggest B4 modulates VSMC function primarily through Akt signaling. Akt kinase is essential in many cellular processes, including proliferation, migration, cell growth, and metabolism. There are three known Akt isoforms, Akt1, Akt2, and Akt3, which play critical and diverse roles in the cardiovascular system (52). Akt1 is the major isoform expressed in VSMCs, endothelial cells, and macrophages, mediating cell survival and proliferation (53). Akt2 is required for rapamycin-induced VSMC differentiation (54), while Akt3 is mainly localized to the brain and testes (55, 56). The current study demonstrated that B4 inhibits VSMC proliferation and migration by inhibiting Akt activation. However, further studies are needed to determine whether the anti-proliferation and anti-migration effect of B4 is Akt isoform-specific.

In conclusion, for the first time, the present study provides evidence that B4 attenuates neointimal hyperplasia in response to arterial injury *in vivo*. B4 inhibits growth factor-induced VSMC proliferation, migration, and dedifferentiation. The dual regulatory effect on the p38 MAPK and PI3K/Akt pathways provides the first insight into the molecular mechanisms underlying the vascular remodeling effect of Anemoside B4 (**Figure 7**). Our findings shed light on the clinical use of B4 in managing vascular restenosis.

DATA AVAILABILITY STATEMENT

The original contributions presented in the study are included in the article/**Supplementary Material**, further inquiries can be directed to the corresponding author.

ETHICS STATEMENT

The animal study was reviewed and approved by IACUC Committee, Temple Univesity.

AUTHOR CONTRIBUTIONS

JY designed the study and coordinated all experimental work. DS, PQ, CZ, LH, GZ, YF, and JY carried out the experimental work. DS, PQ, QZ, GZ, WH, YF, SY, X-fY, and JY analyzed and interpreted the data. DS and JY wrote the manuscript with valuable input from all other authors. All authors have approved the submitted version of the manuscript.

FUNDING

This work was supported by an award from the American Heart Association (18EIA33900065) to JY. DS and CZ were supported by Jiangxi Key Laboratory of Traditional Chinese Medicine for Prevention and Treatment of Vascular Remodeling Related Diseases (No. 20202BCD42014).

SUPPLEMENTARY MATERIAL

The Supplementary Material for this article can be found online at: https://www.frontiersin.org/articles/10.3389/fcvm.2022.907490/full#supplementary-material

REFERENCES

1. Marx SO, Totary-Jain H, Marks AR. Vascular smooth muscle cell proliferation in restenosis. *Circ Cardiovasc Interv*. (2011) 4:104–11. doi: 10.1161/CIRCINTERVENTIONS.110.957332
2. Owens GK, Kumar MS, Wamhoff BR. Molecular regulation of vascular smooth muscle cell differentiation in development and disease. *Physiol Rev*. (2004) 84:767–801. doi: 10.1152/physrev.00041.2003
3. Osman I, He X, Liu J, Dong K, Wen T, Zhang F, et al. TEAD1 (TEA Domain Transcription Factor 1) promotes smooth muscle cell proliferation through upregulating SLC1A5 (Solute Carrier Family 1 Member 5)-mediated glutamine uptake. *Circ Res*. (2019) 124:1309–22. doi: 10.1161/CIRCRESAHA.118.314187
4. Mylonaki I, Allain E, Strano F, Allémann E, Corpataux JM, Meda P, et al. Saucy. Evaluating intimal hyperplasia under clinical conditions. *Interact Cardiovasc Thorac Surg*. (2018) 27:427–36. doi: 10.1093/icvts/ivy101
5. Bennett MR, Sinha S, Owens GK. Vascular smooth muscle cells in atherosclerosis. *Circ Res*. (2016) 118:692–702. doi: 10.1161/CIRCRESAHA.115.306361
6. Owens GK. Regulation of differentiation of vascular smooth muscle cells. *Physiol Rev*. (1995) 75:487–517. doi: 10.1152/physrev.1995.75.3.487
7. Owens GK, Wise G. Regulation of differentiation/maturation in vascular smooth muscle cells by hormones and growth factors. *Agents Actions Suppl*. (1997) 48:3–24. doi: 10.1007/978-3-0348-7352-9_1
8. Davies MG, Hagen PO. Pathobiology of intimal hyperplasia. *Br J Surg*. (1994) 81:1254–69. doi: 10.1002/bjs.1800810904
9. Schwartz SM. Smooth muscle migration in atherosclerosis and restenosis. *J Clin Invest*. (1997) 100(11 Suppl):S87–9.
10. Claesson-Welsh L. Mechanism of action of platelet-derived growth factor. *Int J Biochem Cell Biol*. (1996) 28:373–85. doi: 10.1016/1357-2725(95)00156-5
11. Wang C, Liu Y, He D. Diverse effects of platelet-derived growth factor-BB on cell signaling pathways. *Cytokine*. (2019) 113:13–20. doi: 10.1016/j.cyto.2018.10.019
12. Heldin CH, Westermark B. Mechanism of action and *in vivo* role of platelet-derived growth factor. *Physiol Rev*. (1999) 79:1283–316. doi: 10.1152/physrev.1999.79.4.1283
13. Roskoski R Jr. The role of small molecule platelet-derived growth factor receptor (PDGFR) inhibitors in the treatment of neoplastic disorders. *Pharmacol Res*. (2018) 129:65–83. doi: 10.1016/j.phrs.2018.01.021
14. Sun Y, Liu WZ, Liu T, Feng X, Yang N, Zhou HF. Signaling pathway of MAPK/ERK in cell proliferation, differentiation, migration, senescence and apoptosis. *J Recept Signal Transduct Res*. (2015) 35:600–4. doi: 10.3109/10799893.2015.1030412
15. Choi KH, Kim JE, Song NR, Son JE, Hwang MK, Byun S, et al. Phosphoinositide 3-kinase is a novel target of piceatannol for inhibiting PDGF-BB-induced proliferation and migration in human aortic smooth muscle cells. *Cardiovasc Res*. (2010) 85:836–44. doi: 10.1093/cvr/cvp359
16. Goncharova EA, Ammit AJ, Irani C, Carroll RG, Eszterhas AJ, Panettieri RA, et al. PI3K is required for proliferation and migration of human pulmonary vascular smooth muscle cells. *Am J Physiol Lung Cell Mol Physiol*. (2002) 283: L354–63. doi: 10.1152/ajplung.00010.2002
17. Blank RS, Owens GK. Platelet-derived growth factor regulates actin isoform expression and growth state in cultured rat aortic smooth muscle cells. *J Cell Physiol*. (1990). 142:635–42. doi: 10.1002/jcp.1041420325
18. Holycross BJ, Blank RS, Thompson MM, Peach MJ, Owens GK. Platelet-derived growth factor-bb-induced suppression of smooth muscle cell differentiation. *Circ Res*. (1992) 71:1525–32. doi: 10.1161/01.RES.71.6.1525
19. Lu QB, Wan MY, Wang PY, Zhang CX, Xu DY, Liao X, et al. Chicoric acid prevents PDGF-BB-induced VSMC dedifferentiation, proliferation and migration by suppressing ROS/NFkappaB/mTOR/P70S6K signaling cascade. *Redox Biol*. (2018) 14:656–68. doi: 10.1016/j.redox.2017.11.012
20. Guo X, Xie Y, Lian S, Li Z, Gao Y, Xu Z, et al. A sensitive HPLC-MS/MS method for the simultaneous determination of anemoside B4, anemoside A3 and 23-hydroxybetulinic acid: application to the pharmacokinetics and liver distribution of Pulsatilla chinensis saponins. *Biomed Chromatogr*. (2018) 32:e4124. doi: 10.1002/bmc.4124
21. Ma J, Yin G, Lu Z, Xie P, Zhou H, Liu J, Yu L. Casticin prevents DSS induced ulcerative colitis in mice through inhibitions of NF-κB pathway and ROS signaling. *Phytother Res*. (2018) 32:1770–83. doi: 10.1002/ptr.6108
22. Gong Q, He LL, Wang ML, Ouyang H, Gao HW, Feng YL, et al. Anemoside B4 protects rat kidney from adenine-induced injury by attenuating inflammation and fibrosis and enhancing podocin and nephrin expression. *Evid Based Complement Alternat Med*. (2019) 2019:8031039. doi: 10.1155/2019/8031039
23. Liu M, Zhao X, Xiao L, Liu G, Liu H, Wang X, et al. Cytotoxicity of the compounds isolated from Pulsatilla chinensis saponins and apoptosis induced by 23-hydroxybetulinic acid. *Pharm Biol*. (2015) 53:1–9. doi: 10.3109/13880209.2014.907323
24. Xue S, Zhou Y, Zhang J, Xiang Z, Liu Y, Miao T, et al. Anemoside B4 exerts anti-cancer effect by inducing apoptosis and autophagy through inhibiton of PI3K/ Akt/mTOR pathway in hepatocellular carcinoma. *Am J Transl Res*. (2019) 11:2580–9.
25. Ma H, Zhou M, Duan W, Chen L, Wang L, Liu P. Anemoside B4 prevents acute ulcerative colitis through inhibiting of TLR4/NF-κB/MAPK signaling pathway. *Int Immunopharmacol*. (2020) 87:106794: doi: 10.1016/j.intimp.2020.106794

26. Yu J, Rudic RD, Sessa WC. Nitric oxide-releasing aspirin decreases vascular injury by reducing inflammation and promoting apoptosis. *Lab Invest.* (2002) 82:825–32. doi: 10.1097/01.LAB.0000018828.61722.BD
27. Acevedo L, Yu J, Erdjument-Bromage H, Miao RQ, Kim JE, Fulton D, et al. A new role for Nogo as a regulator of vascular remodeling. *Nat Med.* (2004) 10:382–8. doi: 10.1038/nm1020
28. Xie Y, Ostriker AC, Jin Y, Hu H, Sizer AJ, Peng G, et al. LMO7 is a negative feedback regulator of transforming growth factor beta signaling and fibrosis. *Circulation.* (2019) 139:679–93. doi: 10.1161/CIRCULATIONAHA.118.034615
29. Fang H, Yang S, Luo Y, Zhang C, Rao Y, Liu R, Feng Yet al. Notoginsenoside R1 inhibits vascular smooth muscle cell proliferation, migration and neointimal hyperplasia through PI3K/Akt signaling. *Sci Rep.* (2018) 8:7595. doi: 10.1038/s41598-018-25874-y
30. Fan T, He J, Yin Y, Wen K, Kang Y, Zhao H, et al. Dioscin inhibits intimal hyperplasia in rat carotid artery balloon injury model through inhibition of the MAPK-FoxM1 pathway. *Eur J Pharmacol.* (2019) 854:213–23. doi: 10.1016/j.ejphar.2019.03.050
31. Shao W, Li X, Peng J, Fan S, Liang M, Huang K. Apatinib attenuates phenotypic switching of arterial smooth muscle cells in vascular remodelling by targeting the PDGF Receptor-β. *J Cell Mol Med.* (2020). 24:10128–39. doi: 10.1111/jcmm.15623
32. Shanahan CM, Weissberg PL. Smooth muscle cell heterogeneity patterns of gene expression in vascular smooth muscle cells *in vitro* and *in vivo*. *Arterioscler Thromb Vasc Biol.* (1998) 18:333–8: doi: 10.1161/01.ATV.18.3.333
33. Gerthoffer WT. Mechanisms of vascular smooth muscle cell migration. *Circ Res.* (2007) 100:607–21. doi: 10.1161/01.RES.0000258492.96097.47
34. Shi N, Chen SY. Mechanisms simultaneously regulate smooth muscle proliferation and differentiation. *J Biomed Res.* (2014) 28:40–6.
35. Rzucidlo EM, Martin KA, Powell RJ. Regulation of vascular smooth muscle cell differentiation. *J Vasc Surg.* (2007) 45(Suppl A):A25–32. doi: 10.1016/j.jvs.2007.03.001
36. Liu Y, Sinha S, McDonald OG, Shang Y, Hoofnagle MH, Owens GK. Kruppel-like factor 4 abrogates myocardin-induced activation of smooth muscle gene expression. *J Biol Chem.* (2005) 280:9719–27. doi: 10.1074/jbc.M412862200
37. Chen J, Kitchen CM, Streb JW, Miano JM. Myocardin: a component of a molecular switch for smooth muscle differentiation. *J Mol Cell Cardiol.* (2002) 34:1345–56. doi: 10.1006/jmcc.2002.2086
38. Du KL, Ip HS Li J, Chen M, Dandre F, Yu W, Lu MM, et al. Myocardin is a critical serum response factor cofactor in the transcriptional program regulating smooth muscle cell differentiation. *Mol Cell Biol.* (2003) 23:2425–37. doi: 10.1128/MCB.23.7.2425-2437.2003
39. Campbell M, Trimble ER. Modification of PI3K- and MAPK-dependent chemotaxis in aortic vascular smooth muscle cells by protein kinase CbetaII. *Circ Res.* (2005) 96:197–206. doi: 10.1161/01.RES.0000152966.88353.9d
40. Morello F, Perino A, Hirsch E. Phosphoinositide 3-kinase signalling in the vascular system. *Cardiovasc Res.* (2008) 82:261–71. doi: 10.1093/cvr/cvn325
41. Basatemur GL, Jørgensen HF, Clarke MCH, Bennett MR, Mallat Z. Vascular smooth muscle cells in atherosclerosis. *Nat Rev Cardiol.* (2019) 16:727–44. doi: 10.1038/s41569-019-0227-9
42. Shi N, Chen SY. Smooth muscle cell differentiation: model systems, regulatory mechanisms, vascular diseases. *J Cell Physiol.* (2016) 231:777–87. doi: 10.1002/jcp.25208
43. Gomez D, Owens GK. Smooth muscle cell phenotypic switching in atherosclerosis. *Cardiovasc Res.* (2012) 95:156–64. doi: 10.1093/cvr/cvs115
44. Jin R, Sun W, Bai Y, Huang LJ, Qu FJ. Inhibitory effect of rapamycin on proliferation of human umbilical arterial smooth muscle cells. *Immunopharmacol Immunotoxicol.* (2019) 41:485–9. doi: 10.1080/08923973.2019.1628045
45. Poon M, Marx SO, Gallo R, Badimon JJ, Taubman MB, Marks AR. Rapamycin inhibits vascular smooth muscle cell migration. *J Clin Invest.* (1996) 98:2277–83. doi: 10.1172/JCI119038
46. Liu Y, Sinha S, Owens G. A transforming growth factor-beta control element required for SM alpha-actin expression *in vivo* also partially mediates GKLF-dependent transcriptional repression. *J Biol Chem.* (2003) 278:48004–11. doi: 10.1074/jbc.M301902200
47. Pipes GC, Creemers EE, Olson EN. The myocardin family of transcriptional coactivators: versatile regulators of cell growth, migration, and myogenesis. *Genes Dev.* (2006) 20:1545–56. doi: 10.1101/gad.1428006
48. Won KJ, Lee KP, Baek S, Cui L, Kweon MH, Jung SH, et al. Desalted Salicornia europaea extract attenuated vascular neointima formation by inhibiting the MAPK pathway-mediated migration and proliferation in vascular smooth muscle cells. *Biomed Pharmacother.* (2017) 94:430–8. doi: 10.1016/j.biopha.2017.07.108
49. Wang D, Uhrin P, Mocan A, Waltenberger B, Breuss JM, Tewari D, et al. Vascular smooth muscle cell proliferation as a therapeutic target Part 1: molecular targets and pathways. *Biotechnol Adv.* (2018) 36:1586–607. doi: 10.1016/j.biotechadv.2018.04.006
50. Pearson G, Robinson F, Beers Gibson T, Xu BE, Karandikar M, Berman K, et al. Mitogen-activated protein (MAP) kinase pathways: regulation and physiological functions. *Endocr Rev.* (2001) 22:153–83. doi: 10.1210/edrv.22.2.0428
51. Proctor BM, Jin X, Lupu TS, Muglia LJ, Semenkovich CF, Muslin AJ. Requirement for p38 mitogen-activated protein kinase activity in neointima formation after vascular injury. *Circulation.* (2008) 118:658–66. doi: 10.1161/CIRCULATIONAHA.107.734848
52. Abeyrathna P, Su Y. The critical role of Akt in cardiovascular function. *Vascul Pharmacol.* (2015) 74:38–48. doi: 10.1016/j.vph.2015.05.008
53. Manning BD, Cantley LC. AKT/PKB signaling: navigating downstream. *Cell.* (2007) 129:1261–74. doi: 10.1016/j.cell.2007.06.009
54. Martin KA, Merenick BL, Ding M, Fetalvero KM, Rzucidlo EM, Kozul CD, et al. Rapamycin promotes vascular smooth muscle cell differentiation through insulin receptor substrate-1/phosphatidylinositol 3-kinase/Akt2 feedback signaling. *J Biol Chem.* (2007) 282:36112–20. doi: 10.1074/jbc.M703914200
55. Zhao J, Zhu L, Wijesekera N, Jones C. Specific Akt family members impair stress mediated transactivation of viral promoters and enhance neuronal differentiation: important functions for maintaining latency. *J Virol.* (2020) 94:e00901–20. doi: 10.1128/JVI.00901-20
56. Hers I, Vincent EE, Tavaré JM. Akt signalling in health and disease. *Cell Signal.* (2011) 23:1515–27. doi: 10.1016/j.cellsig.2011.05.004

Conflict of Interest: The authors declare that the research was conducted in the absence of any commercial or financial relationships that could be construed as a potential conflict of interest.

Publisher's Note: All claims expressed in this article are solely those of the authors and do not necessarily represent those of their affiliated organizations, or those of the publisher, the editors and the reviewers. Any product that may be evaluated in this article, or claim that may be made by its manufacturer, is not guaranteed or endorsed by the publisher.

frontiers | Frontiers in Cardiovascular Medicine

ORIGINAL RESEARCH
published: 31 May 2022
doi: 10.3389/fcvm.2022.901225

Burden of Aortic Aneurysm and Its Attributable Risk Factors from 1990 to 2019: An Analysis of the Global Burden of Disease Study 2019

Zhuo Wang[1,2†], Yayu You[1†], Zhehui Yin[1], Qinyi Bao[1], Shuxin Lei[1], Jiaye Yu[1], Cuiping Xie[1], Feiming Ye[1] and Xiaojie Xie[1]*

[1] Department of Cardiology, The Second Affiliated Hospital, Zhejiang University School of Medicine, Hangzhou, China,
[2] International Institutes of Medicine, The Fourth Affiliated Hospital, Zhejiang University School of Medicine, Yiwu, China

OPEN ACCESS

Edited by:
Ting Zhou,
University of Wisconsin-Madison,
United States

Reviewed by:
Xiaorong Yang,
Qilu Hospital, Shandong University, China
Seyed Aria Nejadghaderi,
Shahid Beheshti University of Medical Sciences, Iran

***Correspondence:**
Xiaojie Xie
xiexj@zju.edu.cn

[†] These authors have contributed equally to this work

Specialty section:
This article was submitted to Cardiovascular Therapeutics, a section of the journal Frontiers in Cardiovascular Medicine

Received: 21 March 2022
Accepted: 26 April 2022
Published: 31 May 2022

Citation:
Wang Z, You Y, Yin Z, Bao Q, Lei S, Yu J, Xie C, Ye F and Xie X (2022) Burden of Aortic Aneurysm and Its Attributable Risk Factors from 1990 to 2019: An Analysis of the Global Burden of Disease Study 2019. Front. Cardiovasc. Med. 9:901225. doi: 10.3389/fcvm.2022.901225

Background: Global and national estimates on the epidemiology of aortic aneurysms are prerequisites for disease management and policymaking. Based on the Global Burden of Disease (GBD) 2019, this study aimed to discern the global aortic aneurysm burden by systematically analyzing demographic data on mortality and exploring the attributable risks and relevant factors.

Methods: The data analyzed in this study were available in the Global Health Data Exchange (GHDx) online query tool. The population in our study comprised individuals from 204 countries and territories from 1990 to 2019. The estimated annual percentage changes (EAPCs) were performed to assess the temporal trends of aortic aneurysms and their attributable risks. Spearman correlation analysis was performed to explore the relationship between the burden of aortic aneurysm and covariates.

Results: Although aortic aneurysm-related deaths (82.1%) and disability-adjusted life years (DALYs) (67%) increased from 1990 to 2019, the global trend of age-standardized rate of death (ASRD) (EAPC: −1.34, 95% CI = −1.46 to −1.22, $P < 0.001$) and age-standardized rate of DALY (ASDALYR) (EAPC: −1.06, 95% CI = −1.17 to −0.95, $P < 0.001$) decreased, both of which presented age dependence and gender differences. Smoking and high systolic blood pressure (SBP) were the main attributable risks of disease burden and tend to decease globally (EAPC: −1.89, 95% CI = −2.03 to −1.89, $P < 0.001$; −1.31 95% CI = −1.43 to −1.19, $P < 0.001$, respectively). Alcohol abstinence (male: $R = -0.71$, $P < 0.001$; female: $R = -0.73$, $P < 0.001$), smoking age of initiation (male: $R = -0.32$, $P < 0.001$; female: $R = -0.50$, $P < 0.001$), physical activity (male: $R = -0.50$, $P < 0.001$; female: $R = -0.55$, $P < 0.001$), and mean temperature ($R = -0.62$, $P < 0.001$) had negative correlation with ASRD. However, cholesterol level (male: $R = 0.62$, $P < 0.001$; female: $R = 0.39$, $P < 0.001$), body mass index (BMI) (male: $R = 0.30$, $P < 0.001$; female $R = -0.01$, $P > 0.05$), and alcohol consumption (male: $R = 0.46$, $P < 0.001$; female: $R = 0.42$, $P < 0.001$) had a positive correlation with ASRM. Besides, standard of living and medical resources positively related to burden of aortic aneurysm.

Conclusion: In this study, a decreasing trend of aortic aneurysm burden was found globally, especially in advanced regions. Aged men who smoke and women who have hypertension should pay close attention to, particularly in deprived economic groups, and many approaches can be performed to reduce the burden of aortic aneurysms.

Keywords: aortic aneurysm, Global Burden of Diseases Study, systematic analysis, mortality, disability-adjusted life year (DALY)

INTRODUCTION

An aortic aneurysm is defined as a permanent localized dilatation of the aorta that is more than 50% of the predicted. It is usually developed in weak locations of the aorta and is classified by its location as a thoracic aortic aneurysm (TAA) and an abdominal aortic aneurysm (AAA). Most aortic aneurysms develop silently without any indications, causing sudden death due to aortic rupture with ∼20% chance of survival. Unfortunately, to date, there is no effective medication to prevent or reverse the progression of the disease. Therefore, it is essential to comprehend the epidemiological traits of the disease and take effective interventions.

Unlike some dominant cardiovascular diseases such as coronary heart disease and stroke, less attention has been paid to aortic aneurysms by social economists and government officials. Previous studies suggested prevalence rates of AAA ranged from 1.6 to 7.2% in the general population aged 60 years or older (1). However, aortic aneurysm-related mortality is estimated at 150,000–200,000 deaths per year worldwide, which is equivalent to various types of cancer, e.g., bladder cancer (2), representing a considerable public health burden. Some risk factors, such as being elderly, gender differences, hypertension, smoking, and genetic or metabolic abnormalities, might contribute to the development of aortic aneurysm (3, 4).

The epidemiology of aortic aneurysms based on the global population has been described in previous studies based on the Global Burden of Disease (GBD) study. They focused on the association between healthcare access and quality index (HAQ index) system with aortic aneurysm mortality and YLLs in different incomes and age groups (5). Associations between estimated average percentage change (EAPC) and burden of aortic aneurysm, human development index (HDI) were found respectively (6), and aortic aneurysm-related death and attributable risks in the next decade were projected (7). However, they did extensive efforts on the health epidemiology of aortic aneurysms, and much remains to be performed. Compared with GBD2017 studies, the GBD2019 study used new methods to better measure risk factors by integrating the data of globally multiple high-quality epidemiological studies (8).

This study performed EAPC to quantify the trends of aortic aneurysm death and disability-adjusted life years (DALYs) and its four attributable risk factors based on GBD 2019 data (9). Furthermore, population attributable fractions (PAFs) were calculated to assess the impact of attributable risk factors in populations (10). In addition, we analyzed the association between the burden of aortic aneurysm and various covariates including physical condition, environment, occupation, socio-demographic factors, individual lifestyle, nutrition, and disease states using the Spearman rank-order correlation.

METHODS

Study Data

All data analyzed, in this study, were available in the Global Health Data Exchange (GHDx) online query tool, which was conducted by the Institute for Health Metrics and Evaluation (IHME). The GBD 2019 is a comprehensive multinational epidemiological collaboration to provide an unbiased perspective estimation of population health over time and offers the opportunity to obtain estimates of incidence, prevalence, mortality, and health risk factors (8, 11). In brief, patients involved are identified from 86,249 sources including published studies, authoritative organization websites, and primary data sources of GBD collaborators (11). In the 2019 GBD database, aortic aneurysms, including both abdominal and thoracic aortic aneurysms, correspond to ICD-9 codes of 441–441.9 and ICD-10 codes of I71–I71.9 (11, 12). We presented data for five socio-demographic index (SDI) regions, four World Bank income (WBI) level groups, 21 GBD regions, and 204 countries and territories from 1990 to 2019, by age and sex. SDI is a comprehensive indicator including education, economics, and fertility rate. Based on SDI, the world was divided into 5 SDI regions, including low (0–0.454743), low-middle (0.4547430.45–0.607679), middle (0.607679–0.689504), high-middle (0.689504–0.805129), and high (0.805129–1) SDI regions (**Supplementary Table 1**) (13). Income is calculated using the World Bank Atlas method to convert local currency to gross national income (GNI) per capita, in dollars (14). Based on World Bank income (WBI) levels, the world was divided into 4 WBI regions including low (≤1,035 $), lower-middle (1,036–4,045$), upper-middle (4,046–12,535$), and high (> 12,535$) WBI region (**Supplementary Table 2**) (14, 15).

Mortality data of aortic aneurysms from multiple versions of the International Classification of Diseases and Injuries (ICD) were analyzed and matched to the GBD 2019 cause list (11). Cause of Death Ensemble model (CODEm) and DisMod-MR 2.1 were used to standardize data for global and regional estimates (11). In brief, CODem produces a wide range of submodels with different functional forms on the same data to best reflect all the available input data (16, 17). DisMod-MR 2.1 was a Bayesian meta-regression model used to pool epidemiological outcomes and assessed the age-sex-location-year-specific burden of aortic

aneurysms (18). More detail on CODem and DisMod-MR 2.1 could be seen in previous studies (11).

Disability-adjusted life years were the sum of the number of years of life lost (YLLs) and the number of years lived with disability (YLDs). In brief, YLLs are based on cause-specific prevalence and disability weight, which can be calculated by deaths being multiplied by standard life expectancy at each age. YLDs were calculated by disability weights for mutually exclusive sequela multiplying the prevalence of disease (11). The formulas of YLLs and YLDs are as follows:

$$\mathrm{YLL} = \mathrm{N} \times \mathrm{L1}$$
$$\mathrm{YLD} = \mathrm{I} \times \mathrm{DW} \times \mathrm{L2} = \mathrm{P} \times \mathrm{DW}$$

where N refers to the number of deaths; L1 for standard life expectancy at age of death in years; I for the number of incident cases; DW for disability weight; L2 for the average duration of disability years; and P for the number of prevalent cases.

Furthermore, the GBD 2019 study provided 87 risk factors at the global and regional levels using the comparative risk assessment framework (CRA). In brief, CRA can be divided into six key steps: (1) inclusion of risk-outcome pairs; (2) estimation of relative risk; (3) estimation of distributions and exposure; (4) determination of the counterfactual level of exposure and the theoretical minimum risk exposure level (TMREL); (5) computation of PAF and attributable burden; and (6) computation of the burden attributable to combinations of risks (8). Four attributable risks of aortic aneurysm burden were found including smoking, high systolic blood pressure (SBP), diet high in sodium, and lead exposure. PAF, also called the population attributable proportion or attributable proportion among the total population, is the estimated fraction of all cases that would not have occurred if there had been no exposure. Therefore, the computational formula of PAF is as follows:

$$\mathrm{PAF} = \frac{A}{O} \times 100\%$$

where O and A refer to the observed number of cases and the number of cases that can be attributed to exposure, respectively (8, 11, 19). EAPC of the four attributable risks was calculated as well.

In addition, various covariates were downloaded from GBD 2019 covariate dataset (https://cloud.ihme.washington.edu/s/b2tQnbsjAyWgeHm?path=%2FGBD%202019%20Covariates). The dataset contained information of every country and its province. The correlation between the burden of aortic aneurysm and covariates was further analyzed, and the correlation coefficient (R) was calculated at the level of groups.

Statistical Analysis

The age-standardized rates (ASRs), including the age-standardized rate of death (ASRD) and age-standardized DALYs rate (ASDALYR), were calculated to make valid comparisons between different groups. In brief, the sum of the products of age-specific rates (α_i) and the number of persons (or weight) (w_i) in the same age subgroup i of the standard population and then divide the sum of the standard population weights. The formula of ASR (per 100,000 populations) is as follows:

$$\mathrm{ASR} = \frac{\sum_{i=1}^{A} a_i w_i}{\sum_{i=1}^{A} a_i} \times 100,00$$

where i denotes the ith age class (11). The temporal trend of ASR of the aortic aneurysm was quantified using the estimated annual percentage change (EAPC), calculated using log-linear regression. It is assumed that the natural logarithm of ASR is linear along with time. Thus, $Y = \alpha + \beta X + \varepsilon$, where Y refers to ln(ASR), X represents the calendar year, and ε represents the error term. Based on this formula, β determines the positive or negative trends of ASR. The formula for calculating EAPC is as follows:

$$\mathrm{EAPC} = 100 \times (exp(\beta) - 1).$$

In addition, its 95% confidence interval (CI) was computed similarly. When the EAPC was positive, the ASR was deemed to be increasing, while the ASR was decreasing when EAPC was negative (20, 21). In addition, Spearman's correlation coefficient was calculated for the correlation between ASRD, ASDALYR, and covariates. Data analysis was performed using the open-source software R (version 4.1.0) with the package of "ggplot2," "ggpubr," "tidyverse," "data.table," and "Hmisc." A 2-tailed $P < 0.05$ was considered statistically significant.

RESULTS

Mortality of Aortic Aneurysm

Deaths of Aortic Aneurysm Globally

Aortic aneurysm led to 172,427 deaths (95% UI = 157,357–182,899) in 2019, which increased 82.1% from the 94,698 deaths (95% UI = 87,009–102,685) in 1990 (**Supplementary Table 3**). Aortic aneurysm-related deaths presented the slowest increase by 33.5% in the high SDI region from 1990 (892,344, 95% UI = 860,937–915,453) to 2019 (1,013,966, 95% UI = 930,098–1,063,166), whereas they nearly doubled in the other four SDI regions (**Supplementary Table 3**). Regionally, the fastest increase of deaths caused by aortic aneurysms was found in the United Arab Emirates (more than 8.3-folds), followed by Taiwan China (4.9-folds) and Qatar (4.87-folds), whereas the fastest decrease found in Niue (−28.17%) from 1990 to 2019. The maximal death numbers caused by an aortic aneurysm in 2019 were found in Japan (20,169, 95% UI = 16,270–22,321) (**Supplementary Table 4**).

ASRD of Aortic Aneurysm

Conversely, the global ASRD of aortic aneurysm decreased by 17.9% from 2.70/100,000 (95% UI = 2.47–2.91/100,000) in 1990 to 2.21/100,000 (95% UI = 2.00–2.35/100,000) in 2019 (**Supplementary Table 3**), with decreasing by 24.74% in men and 9.45% in women (**Figure 1A**; **Supplementary Table 3**). The ASRD of aortic aneurysm dramatically decreased by 44.34% in men in the high SDI region whereas the most increase was found in men in the low-middle SDI region

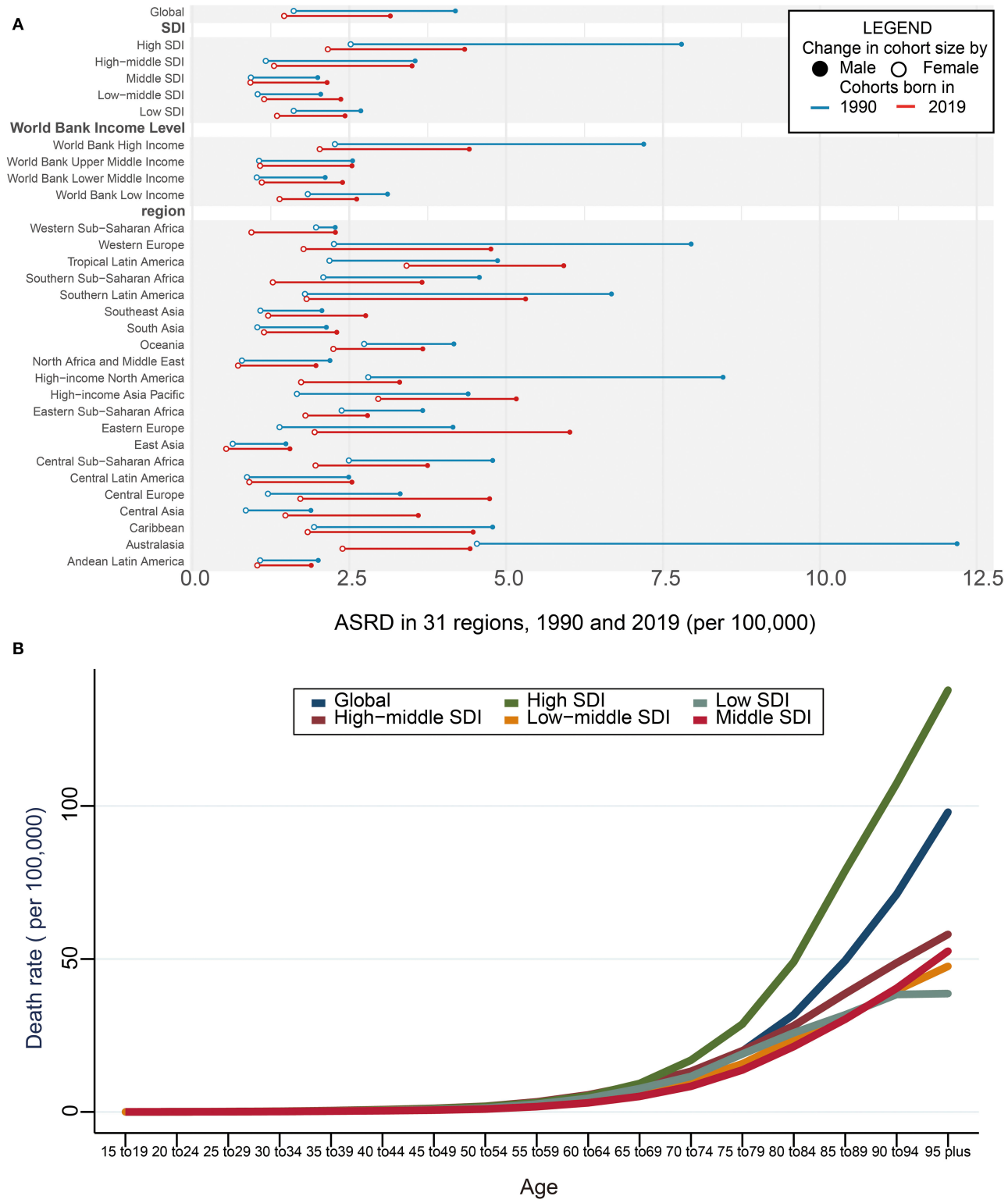

FIGURE 1 | Death and ASRD of aortic aneurysm. **(A)** Global ASRD with 31 regions from 1990 to 2019. The blue line represents differences in ASRD of men and women in 1990 and the red line represents 2019 year. The black solid circle indicates the male group and the hollow circle the female group. **(B)** Global ASRD stratified by age and SDI with 5 SDI regions in 2019. SDI, sociodemographic index; ASRD, age-standardized death rate.

TABLE 1 | The relevant factors of aortic aneurysm burden in 2019.

Item	ASDALYR			ASRD		
	Man	Female	Both	Man	Female	Both
Physical condition						
Population over age 65	0.59	0.49		0.62	0.53	
Cholesterol	0.60	0.40		0.62	0.39	
Bone mineral density	0.74	−0.46		0.78	−0.49	
BMI	0.30	−0.02*		0.30	−0.01*	
Obesity	0.21	−0.03*		0.24	−0.04*	
Diabetes fasting plasma glucose (mmol/L)	0.11	−0.05*		0.11	−0.04*	
Disease prevalance						
Alcoholic cirrhosis	0.67	0.54		0.70	0.57	
Diabetes	−0.55	−0.55		−0.60	−0.59	
HepA	−0.67	−0.59		−0.72	−0.63	
HepB	−0.40	−0.43		−0.45	−0.47	
Melanoma	0.64	0.63		0.68	0.69	
Severe anemia	−0.53	−0.33		−0.59	−0.40	
Tuberculosis	0.60	0.39		0.63	0.39	
Lifestyle						
Alcohol abstain	−0.68	−0.68		−0.71	−0.73	
Alcohol binge	0.74	0.69		0.76	0.72	
Alcohol g/day	0.45	0.39		0.46	0.42	
Cannabis dependence		0.54			0.61	
Age of smoking initiation	−0.28	−0.48		−0.32	−0.50	
Physical activity MET-min/week	−0.48	−0.54		−0.50	−0.55	
Agricultural activities	−0.64	−0.56		−0.70	−0.51	
Diet habit						
Energy kcal/p/day			0.22			0.24
Fruits g/p/d			−0.05*			−0.03*
Milk g/day			0.50			0.53
Poultry g/day			0.31			0.33
Pufa			0.32			0.33
Red meats			0.47			0.48
Sugar g/p/d			0.20			0.26
Vegetables g/day			0.27			0.30
Nutrient						
Calcium g/day			0.54			0.58
Iron mg/day			0.41			0.44
Vitamin A ug/day			0.36			0.41
Zinc			0.31			0.34
Environment and occupation						
Asbestos consumption			0.34			0.31
Coal production (per capita)			0.70			0.64
Latitude			0.63			0.68
Mean temperature			−0.57			−0.62
People living at 500–1,500 m elevation			−0.51			−0.55
People living at above 1,500 m elevation			−0.53			−0.55
Education and health support						
Education			0.53			0.58
GDP-PPP			0.30			0.35
Fraction of health expenditure			−0.40			−0.45
HAQI			0.58			0.65

(Continued)

TABLE 1 | Continued

Item	ASDALYR			ASRD		
	Man	Female	Both	Man	Female	Both
Health expenditure (per capita)			0.55			0.50
Health worker density			0.64			0.69
Hospital beds per 1,000			0.52			0.52
Health industry workers			0.71			0.76
Pharmacists per capita			0.53			0.58
Physicians per capita			0.48			0.52
Sanitation			0.53			0.56
UHC			0.59			0.65

*UHC, universal health coverage; BMI, body mass index; PUFA, polyunsaturated fatty acid; asbestos consumption, estimated as production plus imports minus exports (metric tons per year per capita); health industry workers, the proportion of the employed population aged 15–69 years working in health and social work; education, mean level of educational attainment. *$p > 0.05$.*

(15.68%) (**Figure 1A**; **Supplementary Table 3**). Consistent results were found in the ASRD of aortic aneurysm stratified by WBI Levels (**Figure 1A**; **Supplementary Table 3**). Regionally, the highest ASRD of the aortic aneurysm was found in tropical Latin America in 2019 (4.53/100,000, 95% UI = 4.14–4.84/100,000) and the lowest ASRD of the aortic aneurysm was found in East Asia (0.98/100,000, 95% UI = 0.84–1.12/100,000) (**Supplementary Table 3**). The highest decrease in the ASRD of the aortic aneurysm was found in Australasia (-56.9%), with −63.7% in men and −45.9% in women. However, men in central Asia had the largest increase in ASRD (90.63%) (**Figure 1A**; **Table 1**).

Age and ASRD of Aortic Aneurysm

It has been demonstrated that the ASRD of the aortic aneurysm was positively related to age, gradually increasing after the age of 65 years. Compared with the patients aged 65-69 years, the ASRD of aortic aneurysm had a 1.7-fold increase in those aged 75–79 years, a 5.7-fold increase in those aged 85–89 years, and a 12.3-fold increase in those aged more than 95 years. Among the 5 SDI regions, the fastest elevation of the ASRD of the aortic aneurysm was found in the high SDI region in the elderly patients (**Figure 1B**; **Supplementary Table 5**).

DALYs and Its ASR of Aortic Aneurysm

DALYs of Aortic Aneurysm

Global DALYs caused by aortic aneurysm increased 67.0% from 1990 (1,989,613.52, 95% UI = 1,819,554.20–2,192,796.33) to 2019 (3,322,343.13, 95% UI = 3,107,724.62–3,524,925.22) (**Supplementary Table 3**) especially in the low-middle SDI region. The high SDI region presented the slowest increase by 13.6% from 1990 to 2019 but the fastest was in the low-middle SDI region (150.55%) (**Supplementary Table 3**). Regionally, the highest DALYs in 2019 were observed in China, followed by India, Japan, the United States of America, and Brazil (**Supplementary Table 4**).

ASDALYR of Aortic Aneurysm

On the contrary, the ASDALYR caused by aortic aneurysm declined by 24.1% from 50.79/100,000 (95% UI = 46.50–55.66) in 1990 to 40.94/100,000 (95% UI: 38.20–43.43) in 2019 (**Supplementary Table 3**). A similar trend was noted in both genders, with a 24.3% decrease in men and 12.7% in women. The changes in different WBI levels were consistent with those of SDI regions (**Figure 2A**; **Supplementary Table 3**). Australasia showed the greatest decrease of ASDALYR in both genders during the past 30 years, presenting 53.49/100,000 (95% UI = 48.10-57.71/100,000) in 2019, which was almost one-third of that in 1990 (**Figure 2A**; **Supplementary Table 3**). Regionally, the highest ASDALYR was observed in Montenegro, followed by Armenia, Brunei Darussalam, Saint Lucia, and Fiji (**Supplementary Table 4**).

Age and ASDALYR of Aortic Aneurysm

In addition, the global ASDALYR increased with age in 2019, which slightly increased in patients aged below 55 years but grew dramatically among patients aged over 55 years. The other four SDI regions remained stable. Compared with the patients aged 65–69 years, the ASDALYR of aortic aneurysm had a 73% increase in those aged 75–79 years, a 1.5-fold increase in those aged 85–89 years, and a 1.9-fold increase in those aged over 95 years, respectively. In high SDI countries, patients aged below 65 years shared a similar increasing rate with those from the other four regions. However, patients aged over 65 years had the fastest elevation (**Figure 2B**; **Supplementary Table 5**).

EAPC of ASRD and ASDALYR

EAPC of ASRD

The global trend of ASRD from 1990 to 2019 decreased with EAPC being −1.34 (95% CI = −1.46 to −1.22, $P < 0.001$) in men and −0.61 (95% CI = −0.71 to −0.50, $P < 0.001$) in women (**Figure 3A**; **Supplementary Table 6**). The greatest decrease was found in high SDI region for both genders (male: −2.55, female: −0.9), while a rising tendency of ASRD was observed in low-middle SDI regions with EAPC being 0.4 (95% CI = 0.33–0.47, $P < 0.001$) in men and 0.2 (95% CI = −0.14 to

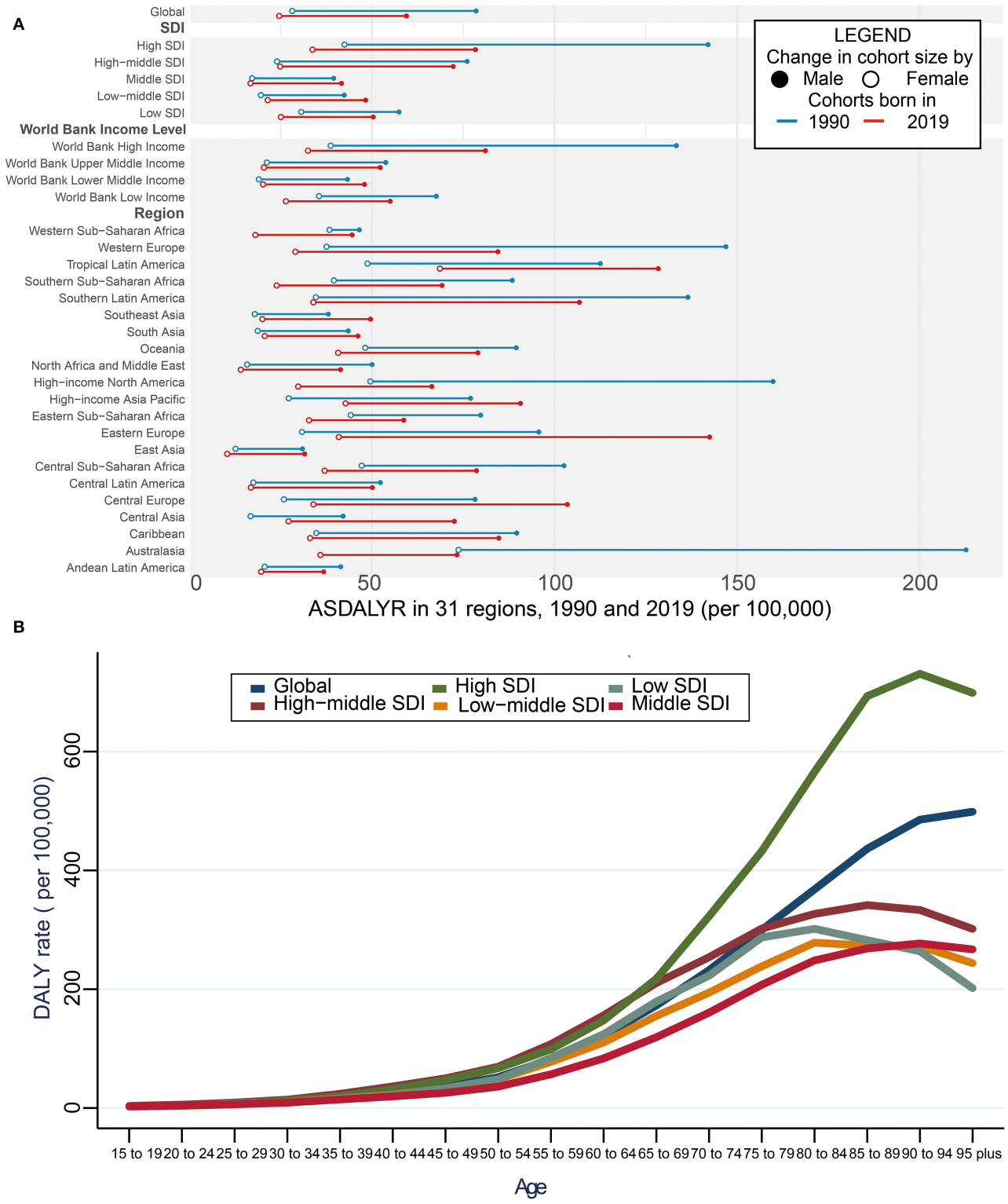

FIGURE 2 | DALYs of aortic aneurysm. **(A)** Global ASDALYR with 31 regions from 1990 to 2019. The blue line represents differences in ASDALYR of men and women in 1990 and the red line represents 2019 year. The black solid circle shows the male group and the hollow circle the female group. **(B)** Global ASDALYR stratified by age and SDI with 5 SDI regions in 2019. SDI, sociodemographic index; DALY, disability-adjusted life year rate; ASDALYR, age-standardized DALY rate.

0.27, $P < 0.001$) in women (**Figure 3A**; **Supplementary Table 6**). Regionally, the fastest decrease of ASRD was found in Australasia with EAPC being −4.3 (95% CI = −4.62 to −4.02, $P < 0.001$) in men and −2.92 (95% CI = −3.16 to −2.68, $P < 0.001$) in women (**Figure 3A**; **Supplementary Table 6**). The trends in male patients of high-income North America and female patients of Western and Southern Sub-Saharan Africa dramatically declined, in contrast to the moderate increase of trends in male patients of Central Asia and female patients of the high-income Asia Pacific and the high-income Asia Pacific and Tropical Latin America (**Figure 3A**).

The fastest decline of ASRD was found in the Northern Mariana Islands, followed by Guam, Australia, Canada, and the United States of America. In contrast, the top five positive EAPCs of ASRD were found in Georgia, Uzbekistan, Turkmenistan, Taiwan China, and Armenia (**Figure 3B**; **Supplementary Table 7**).

EAPC of ASDALYR

Consistent trends were discovered in the ASDALYR (EAPC: −1.06, 95% CI = −1.17 to −0.95, $P < 0.001$). The global EAPC of ASDALYR from 1990 to 2019 was −1.29 (95% CI = −1.40 to −1.18, $P < 0.001$) for men and 0.76 (95% CI = −0.86 to −0.65, $P < 0.001$) for women. The greatest decrease was found in the high SDI region for both genders, while a raising trend was found in low-middle SDI in both genders. The consistent trends were observed in the regions by WBI level stratification (**Figure 3C**; **Supplementary Table 6**). Regionally, the fastest decreasing of ASDALYR was found in Australasia, with EAPC being −4.47 (95% CI = −4.78 to −4.16, $P < 0.001$) in men and −3.23 (% CI = −3.48 to −2.98, $P < 0.001$) in women. The tendency of ASDALYR in male patients of high-income North America and female patients of Western and Southern Sub-Saharan Africa dramatically declined, in contrast to the moderate increase of ASDALYR in male patients of Central Asia and female patients of high-income Asia Pacific, high-income Asia Pacific, and Tropical Latin America (**Figure 3C**).

The fastest decline of ASDALYR was found in the Northern Mariana Islands, followed by Australia, Canada, Uzbekistan, Turkmenistan, Philippines, and Taiwan China (**Figure 3D**; **Supplementary Table 7**).

Attributable Risks of Aortic Aneurysm

Four attributable risks of aortic aneurysm were concluded in GBD 2019, including smoking, high SBP, diet high in sodium, and lead exposure.

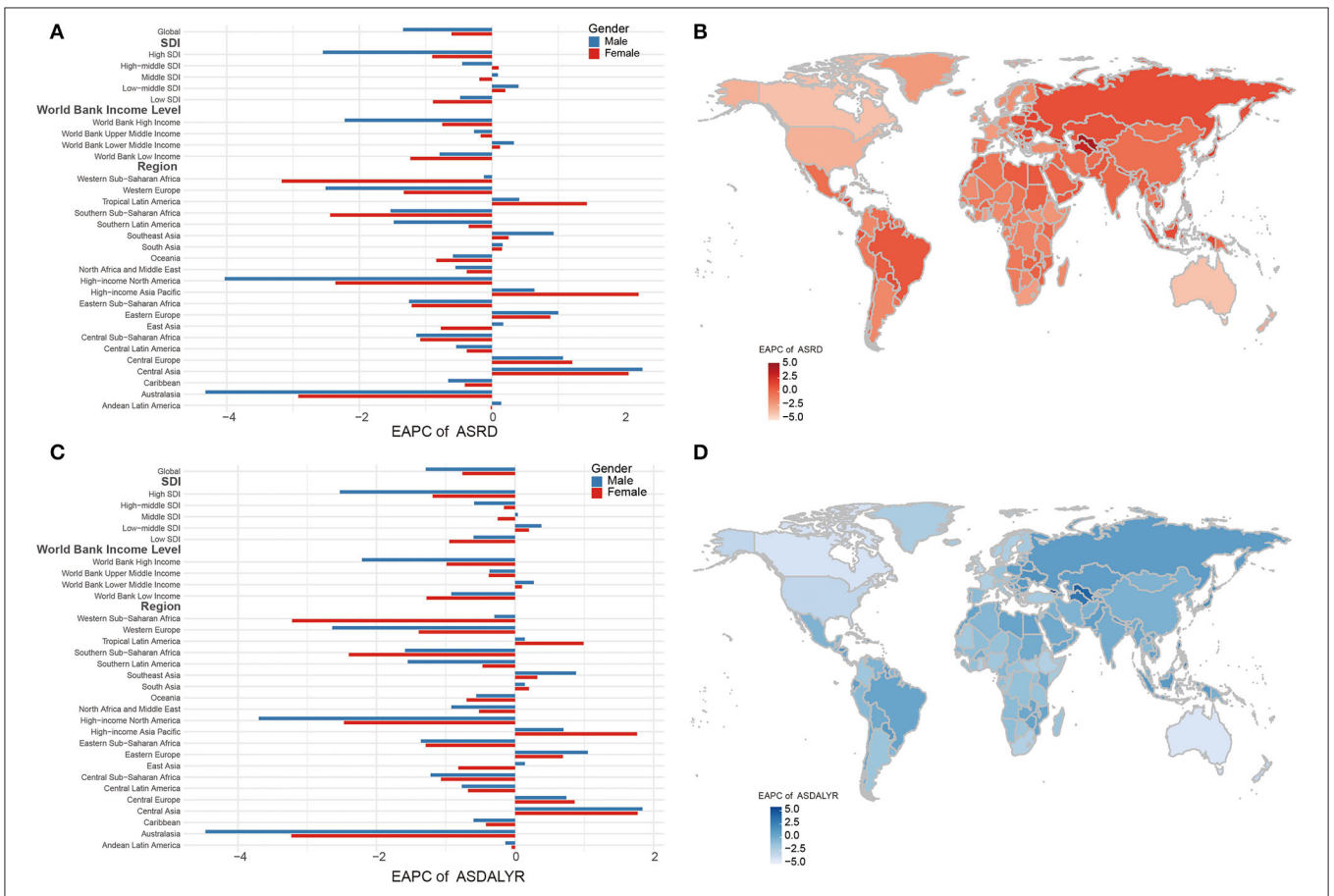

FIGURE 3 | EAPC in ASRD and ASDALYR. **(A)** Global EAPC of ASRD with 31 regions. **(B)** EAPC of ASRD in 204 countries and territories in 2019. **(C)** Global EAPC of ASDALYR in 30 regions. **(D)** EAPC of ASDALYR in 204 countries and territories in 2019. EAPC, estimated annual percentage change; ASRD, age-standardized death rate; ASDALYR, age-standardized DALY rate.

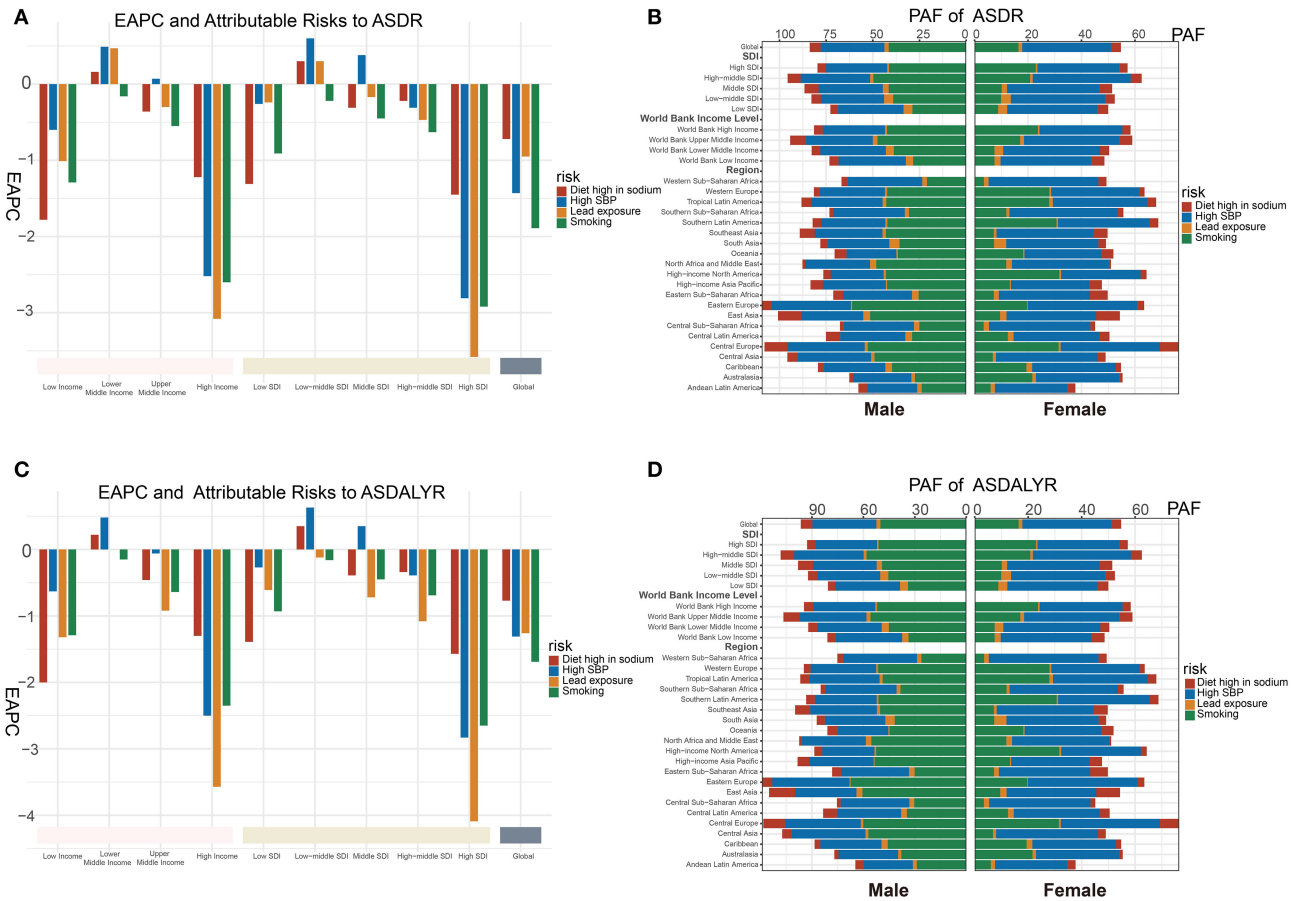

FIGURE 4 | Attributable risks of aortic aneurysm burden. **(A)** PAF of attributable risks of ASRD in 2019. **(B)** PAF of attributable risks of ASDALYR in 2019. **(C)** Global EAPC of attributable risks of ASRD with 30 regions. **(D)** Global EAPC of attributable risks of ASDALYR with 30 regions. PAF, population attributable fraction; ASRD, age-standardized death rate; ASDALYR, age-standardized DALY rate; EAPC, estimated annual percentage change.

The four attributable risks to ASRD showed dramatic decreasing in the world especially in the high SDI region or high WBI region (**Figure 4A**). Smoking, attributable to ASDR, had a reduced trend around the world (EAPC: −1.89 95% CI = −2.03 to −1.89, $P < 0.001$) (**Figure 4A**) especially in men in Australasia with EAPC being −5.8 (95% CI = −6.13 to −5.46, $P < 0.001$) but increased in central Asia (EAPC: 1.83 95% CI = 1.68 to 1.97, $P < 0.001$) and eastern Europe (EAPC: 1.88, 95% CI = 1.46 to 2.3, $P < 0.001$) (**Supplementary Table 8**). ASRD of aortic aneurysm from high SBP had a rising tendency in middle (EAPC: 0.38, 95% CI = 0.28 to 0.47, $P < 0.001$) and low-middle SDI regions (EAPC: 0.6, 95% CI = 0.55 to 0.66, $P < 0.001$) (**Figure 4A**; **Supplementary Table 8**). Regionally, ASRD of aortic aneurysm from high SBP had a biggest increase in men in central Asia with EAPC being 2.25 (95% CI = 2.11 to 2.38, $P < 0.001$) and a highest decrease in men in Australasia (EAPC: −5.21, 95% CI = −5.59 to −4.83, $P < 0.001$) (**Supplementary Table 8**). Diet high in sodium, another attributable risk, had a slight rising trend in low middle SDI region (EAPC: 0.3, 95% CI = 0.26 to 0.35, $P < 0.001$) and in lower middle WBI region (EAPC: 0.16, 95% CI = 0.12 to 0.20, $P < 0.001$) (**Figure 4A**; **Supplementary Table 8**). Lead exposure had a biggest drop in high SDI religion (EAPC: −3.58, 95% CI = −3.81 to −3.85, $P < 0.001$) (**Figure 4A**; **Supplementary Table 8**).

Smoking was globally considered the major contributor to ASRD of aortic aneurysms in male patients (PAF = 33.02%) while high SBP is the major contributor for female patients (PAF = 34.11%). Regionally, the highest PAF of smoking was found in male patients in Eastern Europe (61.1%), as well as female patients in high-income North America (31.7%). Meanwhile, the highest PAF of high SBP was found in female patients in Western Sub-Saharan Africa (41.05%), as well as male patients of Eastern Europe (42.2%) (**Figure 4BA**; **Supplementary Table 9**).

Similar tendency and PAF of the four attributable risks were seen in ASDALYR of aortic aneurysm. The highest PAF of smoking was found in the ASDALYR of male patients in Eastern Europe (67.4%), as well as female patients of Central Europe (41.6%). Meanwhile, the highest PAF of high SBP in the ASDALYR was found in both genders (male: 45.0%; female: 43.3%) of Eastern Europe (**Figures 4C,D**; **Supplementary Tables 8**, **9**).

Relevant Factors of ASRD and ASDALYR

To explore the promising intervention strategies for aortic aneurysms, the correlation of population exposure factors with ASRD and ASDALYR was analyzed, including physical condition, disease prevalence, lifestyle, diet habits, nutrient environment, education, economics, and health support.

Physical Condition and Burden of Aortic Aneurysm

Population aged over 65 years (male: $R = 0.62$, $P < 0.001$; female: $R = 0.53$, $P < 0.001$) and cholesterol level (male: $R = 0.62$, $P < 0.001$; female: $R = 0.39$, $P < 0.001$) had a positive moderate correlation with ASRD of aortic aneurysm in both genders. However, there are differences between men ($R = 0.78$, $P < 0.001$) and women ($R = -0.49$, $P < 0.001$) in correlation between bone mineral density and ASRD of aortic aneurysm. Body mass index (BMI), obesity, and fasting plasma glucose have a weak relationship with ASRD in men ($R = 0.30$, $P < 0.001$; $R = 0.24$, $P < 0.001$; $R = 0.11$, $P < 0.01$, respectively) but negligible in women ($R = -0.01$, $P > 0.05$; $R = -0.04$, $P > 0.05$, respectively). The relationship between physical condition and ASDALYR of aortic aneurysm was similar (**Table 1**), and other physical condition could be found in **Supplementary Tables 10**, **11**.

Disease Prevalence and Burden of Aortic Aneurysm

In terms of disease prevalence, age-standardized prevalence of diabetes (male: $R = -0.60$, $P < 0.001$; female: $R = -0.59$, $P < 0.001$), hepatitis A (male: $R = -0.72$, $P < 0.001$; female: $R = -0.63$, $P < 0.001$), hepatitis B (male: $R = -0.45$, $P < 0.001$; female: $R = -0.47$, $P < 0.001$), and severe anemia (male: $R = -0.59$, $P < 0.001$; female: $R = -0.40$, $P < 0.001$) was negatively correlated with ASRD. In contrast, age-standardized prevalence of alcoholic cirrhosis (male: $R = 0.70$, $P < 0.001$; female: $R = 0.57$, $P < 0.001$), melanoma (male: $R = 0.68$, $P < 0.001$; female: $R = 0.69$, $P < 0.001$), and tuberculosis (male: $R = 0.63$, $P < 0.001$; female: $R = 0.39$, $P < 0.001$) was positively correlated with ASRD and ASDALYR ($P < 0.001$). Consistent results were found in the relationship between ASDALYR and those diseases (**Table 1**). The relationship between the other disease and burden of aortic aneurysm is shown in **Supplementary Tables 10**, **11**.

Lifestyle and Burden of Aortic Aneurysm

As for the lifestyle, age-standardized proportions of alcohol abstinence were negatively correlated with ASRD using R being −0.71 in the male group and −0.73 in the female group. But alcohol binge (male: $R = 0.76$, $P < 0.001$; female: $R = 0.72$, $P < 0.001$) and alcohol consumption (male: $R = 0.46$, $P < 0.001$; female: $R = 0.42$, $P < 0.001$) had a positive relationship. Taking part in physical activity (male: $R = -0.50$, $P < 0.001$; female: $R = -0.55$, $P < 0.001$) and farm work (male: $R = -0.70$, $P < 0.001$; female: $R = -0.51$, $P < 0.001$) was negatively related to ASRD. Additionally, the later the smoking age, the lower the mortality rate (male: $R = -0.32$, $P < 0.001$; female: $R = -0.50$, $P < 0.001$). Age-standardized prevalence of cannabis dependence in women of reproductive-age was positively correlated with ASRD (female: $R = 0.61$, $P < 0.001$) (**Table 1**). The relationship between the other life style and burden of aortic aneurysm is shown in **Supplementary Tables 10**, **11**.

Diet Habit and Burden of Aortic Aneurysm

As for diet habits, positive correlation was found in daily intake of energy ($R = 0.24$, $P < 0.001$), milk ($R = 0.53$, $P < 0.001$), poultry ($R = 0.33$, $P < 0.001$), polyunsaturated fatty acids (PUFA) ($R = 0.33$, $P < 0.001$), red meats ($R = 0.48$, $P < 0.001$), sugar ($R = 0.26$, $P < 0.001$), and vegetables ($R = 0.30$, $P < 0.001$) with ASRD (**Table 1**). The relationship between the other diet habit and burden of aortic aneurysm is shown in **Supplementary Tables 10**, **11**.

Nutrient and Burden of Aortic Aneurysm

Daily intake of calcium ($R = 0.58$, $P < 0.001$), iron ($R = 0.44$, $P < 0.001$), vitamin A ($R = 0.41$, $P < 0.001$), and zinc ($R = 0.34$, $P < 0.001$) was positively related to ASDR of aortic aneurysm (**Table 1**). The relationship between the other nutrient and burden of aortic aneurysm is shown in **Supplementary Tables 10**, **11**.

Environment and Burden of Aortic Aneurysm

In the aspect of environment, population-weighted mean temperature ($R = -0.62$, $P < 0.001$) and proportion of the population living altitude 500–1,500 m ($R = -0.55$, $P < 0.001$) and 1,500 m plus ($R = -0.55$, $P < 0.001$) had negative correlation with ASRD, whereas social coal production ($R = 0.64$, $P < 0.001$) and proportion of the population living latitude ($R = 0.68$, $P < 0.001$) showed positive correlation with ASRD (**Table 1**). The relationship between the other environment factors and burden of aortic aneurysm is shown in **Supplementary Tables 10**, **11**.

Education, Economics, Health Support, and Burden of Aortic Aneurysm

Considering education, economics, and health support, positive correlation was found age-standardized level of educational attainment ($R = 0.58$, $P < 0.001$), GDP-purchase power parity (GDP-PPP) ($R = 0.35$, $P < 0.001$), healthcare access and quality index (HAQI) ($R = 0.65$, $P < 0.001$), health expenditure ($R = 0.50$, $P < 0.001$), health worker density ($R = 0.69$, $P < 0.001$), hospital beds per 1,000 ($R = 0.52$, $P < 0.001$), health industry workers ($R = 0.76$, $P < 0.001$), pharmacists per capita ($R = 0.58$, $P < 0.001$), physicians per capita ($R = 0.52$, $P < 0.001$), and Universal health coverage (UHC) ($R = 0.59$, $P < 0.001$) with ASRD (**Table 1**).

DISCUSSION

In this study, we comprehensively analyzed the current burden and trends in the deaths and DALY of aortic aneurysms at global and regional levels from 1990 to 2019 based on the GBD 2019 study.

Our results revealed that aortic aneurysms remained a public health concern, with progressive effects on deaths and DALYs but declining in ASRD and ASDALYR. The presence of heterogeneities was found in the level of gender, age, social economy, and geography. Smoking and high SBP, major attributable risks to aortic aneurysms in the male group and female group, respectively, were trending downward. Various covariates in the aspect of physical condition,

disease prevalence, lifestyle, diet habits, nutrients, environment, education, economics, and health support were found relative to the burden of aortic aneurysm. Our results might serve as an important extension to the previous knowledge and provide intervention targets for clinical scientists and prevention strategies for socio-economists.

Similar to previous global epidemiological reports of aortic aneurysms based on the GBD 2017 study, the decreasing tendency of ASRD and ASDALYR was observed particularly in high SDI and high WBI regions. Stefanos Tyrovolas and his colleagues suggested that a higher HAQI had a relationship with lower mortality and YLLs of aortic aneurysm in multi-level mixed modeling (5). Compared with YLLs, DALY may be more suitable to describe the burden of disease for not all aortic aneurysms being fatal (22). Additionally, the team of Linyan Wei described qualitatively attributable risk factors changes and found high SBP and smoking-caused aortic aneurysm decreased (6). Similar results were found in our study with quantitative analysis including EAPC and PAF. Based on GDB 2019 study, another research predicted a rebounding tendency in death of aortic, and high SBP would be the major risk factor (7). However, according to our result, a decreasing trend in ASRD, ASDALYR, and attributable risks was obtained, which means that the burden of aortic aneurysms would have a continuing decline globally. The difference could be explained that Huang et al. calculated the average annual percentage change every 3 years, not as a general tendency.

Our study generated some novel insights. Besides two attributable risk factors described in previous studies (smoking, high SBP), we calculated PAF and EAPC of two new attributable risks (diet high in sodium and lead exposure) of the aortic aneurysm to quantify the effect and trend. Additionally, we found that generally, smoking remains a major attributable risk factor to aortic aneurysms for men and high SBP for women. All attributable risk factors globally tend to decrease, but high SBP had poor management in underdeveloped areas. Moreover, we explored the relationship between various covariates and ASRD and ASDALYR of aortic aneurysms and found areas having rich medical resources and high-quality life tended to higher burden of aortic aneurysms. This tendency may be explained by the increase in human lifespan and the number of people aging, more advanced diagnosis and treatment techniques, and better health awareness in developed countries (12, 23). The latest deaths and DALY estimates of aortic aneurysms differed widely across regions. In the high SDI region, especially in Australasia and high-income North America, the trend of aortic aneurysm burden was the most rapid decline, whereas a slight upward trend was observed in less developed areas such as some Asia and Tropical Latin America regions. Inversely, the burden of aortic aneurysms is greater in developed regions than developing regions, just as the previous reports indicated (6, 24). This difference suggested that the burden of aortic aneurysms can be under control and under diagnosis of aortic aneurysms occurred in developing regions (24). Therefore, effective means can be performed to improve the level of diagnosis and treatment and ease the burden of aortic aneurysms.

Low-cost screening for aortic aneurysms was effective preventive care and performed more in advanced countries such as Australia and the UK (25–27). Population-wide screening projects in men aged 65 years had shown a prevalence of AAAs as low as 1.0–1.5% in Sweden (28) and the UK (29). A high-quality meta-analysis shows that screening for men 65 years or older could reduce AAA-related mortality by 35–45% but lead to higher rates of surgery (1). Compared with those with no population-based screening, such as Hungary, Austria, and Romania, the mortality rate of AAA in countries with population-based screening, such as the UK, Australia, and Sweden, constantly declines (30). Therefore, population-wide screening projects for aortic aneurysms were necessary for deprived economic groups. Since screening with conventional ultrasound for aortic aneurysms would make a considerable cost to the developing countries, handheld portable echo devices may be a better choice given their cost performance higher and easy availability (31).

Furthermore, it was necessary to improve education attainment and medical quality for aortic aneurysms. Within the past few years, some training programs for endovascular aneurysm repair have been organized by the Australian Vascular Surgery Community to elevate the surgery success and thus improve the prognosis for the patients (26). Additionally, minimally invasive surgery for AAA was a preferred method in the developed world since it lowered mortality and quicker recovery (32).

In addition, investing health system resources in the control of risk factors was important, especially smoking cessation and hypertension management. Our results suggested that attributable risk factors of aortic aneurysm had the most obvious downward trend in high SDI regions which is in accordance with the trend of aortic aneurysm burden. In most regions, smoking was the dominant contributor to aortic aneurysm burden in male patients and high SBP in female patients. The burden of aneurysms associated with smoking was decreasing but hypertension tended to increase in the middle and low SDI regions. Previous studies found that men aged $\geq$65 years have decreasing prevalence rates of AAA largely owning to smoking cessation in the developed region (33). As Laroche et al. (34) suggested, the reduction of AAA prevalence was parallel to a reduction in cigarettes and tobacco consumption. A significant measure of smoking cessation is that most low-income countries do not follow WHO recommendations for tobacco cessation, resulting in a slow reduction in tobacco consumption (35). Compared with that in high-income countries, hypertensive patients in low-income countries had lower proportions of awareness, treatment, and control (36). As a result, deprived economic groups had an increasing trend of aortic aneurysm burden with poor management of hypertension and slow reduction of tobacco consumption.

Some covariates related to the burden of aortic aneurysm also provided ideas of prevention and control. Our results suggested that temperature, alcohol abstain, age of smoking initiation, physical activity, and altitude had a negative relationship with the burden of aortic aneurysm, whereas aging, cholesterol, BMI, and obesity had a positive relationship. Supporting our results, Chen J and his team performed a time-stratified case-crossover study and found that a rising in AAD risk was associated with lower temperatures when the mean temperature was below 24°C (37).

Alcohol consumption and physical activity was found associated with aortic aneurysm with HR = 1.15(95% CI = 1.03 to 1.28) (38) and HR = 0.54 (95% CI = 0.34 to 0.93) (39). Moderate-intensity exercise was beneficial to older adults with AAA by improving vascular function (40). Lowering the cholesterol level was a beneficial method to control aortic aneurysms (41). However, an association between BMI or obesity and aortic aneurysm remains controversial. A Mendelian randomization study showed that BMI did not impact aortic aneurysms (42). But a prospective study showed that BMI was related to a rising risk of incident isolated AAA (43). High BMI or obesity would lead to atherosclerosis and hypertension, which were important incentives for aortic aneurysm (44, 45). Therefore, abstaining from tobacco and drinking, managing hypertension and weight, doing appropriate exercise, dieting in low fat, keeping warm, and living in moderately high altitude may be cost-effective approaches, especially for the aging population.

Some limitations had listed as follows. First, based on GBD 2019, the data about the prevalence, incidence, and subtype of aortic aneurysm were not provided, which partly limits the analysis of the results. Second, the predictions relied largely on the quality of the primitive population-based registry data. A sparsity of data on aortic aneurysms, particularly in low SDI regions, could affect the precision of estimates. However, GBD 2019 study utilized many powerful statistical tools to reduce that impact. Third, as a population epidemiological study, we could not get individual-level data, and our work was inevitably affected by confounding factors when calculating correlation coefficients. However, our results do provide clinical scientists and socio-economists with the latest big data and a more comprehensive analysis of the aortic aneurysm burden.

CONCLUSION

Based on GBD 2019, aortic aneurysm, as a public health challenge worldwide, has a decreased ASRD and ASDALYR. Aging men who smoke and women who have hypertension should pay close attention to, particularly in deprived economic groups. A lot of approaches could be performed to reduce the burden of aortic aneurysms. These findings provide valuable insights to formulate increasingly integrated interventions to meet global vascular health challenges.

DATA AVAILABILITY STATEMENT

The original contributions presented in the study are included in the article/**Supplementary Material**, further inquiries can be directed to the corresponding author/s.

AUTHOR CONTRIBUTIONS

ZW and YY conducted the study, analyzed the data, interpreted the results and drafted the manuscript. ZY, QB, SL, and JY assisted with data analysis. CX and FY critically read the manuscript. XX designed, guided, and revised the manuscript. All authors read and approved the final manuscript.

FUNDING

XX was supported by a grant from the National Health Commission, Key Program of Science and Technology of Medical and Health of Zhejiang Province (WKJ-ZJ-2028).

ACKNOWLEDGMENTS

We do appreciate the visionary global health leadership of the IHME and the contribution of all anonymous collaborators, without whom this report would not be possible.

SUPPLEMENTARY MATERIAL

The Supplementary Material for this article can be found online at: https://www.frontiersin.org/articles/10.3389/fcvm.2022.901225/full#supplementary-material

Supplementary Table 1 | Socio-demographic index value for GBD 2019 location. SDI, socio-demographic index; GBD, Global Burden of Disease.

Supplementary Table 2 | World bank income level in 2019.

Supplementary Table 3 | Global burden of aortic aneurysm in 31 GBD regions in 1990 and 2019. Changes mean increasing times from 1990 to 2019. DALY, disability-adjusted life year rate. SDI, socio-demographic index; GBD, Global Burden of Disease.

Supplementary Table 4 | Global burden of aortic aneurysm in 204 countries and territories in 1990 and 2019. Changes mean increasing times from 1990 to 2019. DALY, disability-adjusted life year rate.

Supplementary Table 5 | Global burden of aortic aneurysm in different age groups in 2019. DALY, disability-adjusted life year rate. SDI, socio-demographic index.

Supplementary Table 6 | Estimated annual percentage changes of aortic aneurism-related age-standardized deaths and DALYs in 31 GBD regions from 1990 to 2019. DALY, disability-adjusted life year rate. SDI, socio-demographic index; EAPC, estimated annual percentage changes; GBD, Global Burden of Disease.

Supplementary Table 7 | Estimated annual percentage changes of aortic aneurism-related age-standardized deaths and DALYs in 204 countries and territories from 1990 to 2019. DALY, disability-adjusted life year rate. SDI, socio-demographic index; EAPC, estimated annual percentage changes.

Supplementary Table 8 | Estimated annual percentage changes of aortic aneurism-related attributable risks in 31 GBD regions from 1990 to 2019. DALY, disability-adjusted life year rate. SDI, socio-demographic index; EAPC, estimated annual percentage changes; GBD, Global Burden of Disease.

Supplementary Table 9 | Population attributable fractions of aortic aneurism-related attributable risks in 31 GBD regions in 2019. DALY, disability-adjusted life year rate. SDI, socio-demographic index; PAF, population attributable fractions; GBD, Global Burden of Disease.

Supplementary Table 10 | Correlation analysis of aortic aneurism-related age-standardized deaths and DALYs in 2019, by gender. DALY, disability-adjusted life year rate.

Supplementary Table 11 | Correlation analysis of aortic aneurism-related age-standardized deaths and DALYs in 2019. DALY, disability-adjusted life year rate.

REFERENCES

1. Guirguis-Blake JM, Beil TL, Senger CA, Coppola EL. Primary care screening for abdominal aortic aneurysm: updated evidence report and systematic review for the US Preventive Services Task Force. *JAMA.* (2019) 322:2219–38. doi: 10.1001/jama.2019.17021
2. Collaborators GBDCoD. Global, regional, and national age-sex-specific mortality for 282 causes of death in 195 countries and territories, 1980–2017: a systematic analysis for the Global Burden of Disease Study 2017. *Lancet.* (2018) 392:1736–88. doi: 10.1016/S0140-6736(18)32203-7
3. Obel LM, Diederichsen AC, Steffensen FH, Frost L, Lambrechtsen J, Busk M, et al. Population-based risk factors for ascending, arch, descending, and abdominal aortic dilations for 60-74-year-old individuals. *J Am Coll Cardiol.* (2021) 78:201–11. doi: 10.1016/j.jacc.2021.04.094
4. Li W, Luo S, Luo J, Liu Y, Ning B, Huang W, et al. Predictors associated with increased prevalence of abdominal aortic aneurysm in Chinese patients with atherosclerotic risk factors. *Eur J Vasc Endovasc Surg.* (2017) 54:43–9. doi: 10.1016/j.ejvs.2017.04.004
5. Tyrovolas S, Tyrovola D, Gine-Vazquez I, Koyanagi A, Bernabe-Ortiz A, Rodriguez-Artalejo F, et al. Global, regional, and national burden of aortic aneurysm, 1990–2017: a systematic analysis of the Global Burden of Disease Study 2017. *Eur J Prev Cardiol.* (2021). doi: 10.1093/eurjpc/zwab015
6. Wei L, Bu X, Wang X, Liu J, Ma A, Wang T. Global burden of aortic aneurysm and attributable risk factors from 1990 to 2017. *Glob Heart.* (2021) 16:35. doi: 10.5334/gh.920
7. Huang X, Wang Z, Shen Z, Lei F, Liu YM, Chen Z, et al. Projection of global burden and risk factors for aortic aneurysm—timely warning for greater emphasis on managing blood pressure. *Ann Med.* (2022) 54:553–64. doi: 10.1080/07853890.2022.2034932
8. Collaborators GBDRF. Global burden of 87 risk factors in 204 countries and territories, 1990-2019: a systematic analysis for the Global Burden of Disease Study 2019. *Lancet.* (2020) 396:1223–49. doi: 10.1016/S0140-6736(20)30752-2
9. Li X, Cao X, Guo M, Xie M, Liu X. Trends and risk factors of mortality and disability adjusted life years for chronic respiratory diseases from 1990 to 2017: systematic analysis for the Global Burden of Disease Study 2017. *BMJ.* (2020) 368:m234. doi: 10.1136/bmj.m234
10. Kaneko H, Yano Y, Itoh H, Morita K, Kiriyama H, Kamon T, et al. Association of blood pressure classification using the 2017 American College of Cardiology/American Heart Association Blood Pressure Guideline With Risk of Heart Failure and Atrial Fibrillation. *Circulation.* (2021) 143:2244–53. doi: 10.1161/CIRCULATIONAHA.120.052624
11. Diseases GBD, Injuries C. Global burden of 369 diseases and injuries in 204 countries and territories, 1990–2019: a systematic analysis for the Global Burden of Disease Study 2019. *Lancet.* (2020) 396:1204–22. doi: 10.1016/S0140-6736(20)30925-9
12. Roth GA, Mensah GA, Johnson CO, Addolorato G, Ammirati E, Baddour LM, et al. Global burden of cardiovascular diseases and risk factors, 1990–2019: update from the GBD 2019 Study. *J Am Coll Cardiol.* (2020) 76:2982–3021. doi: 10.1016/j.jacc.2020.11.010
13. Collaborators GBDAM. Global, regional, and national mortality among young people aged 10-24 years, 1950-2019: a systematic analysis for the Global Burden of Disease Study 2019. *Lancet.* (2021) 398:1593–618. doi: 10.1016/S0140-6736(21)01546-4
14. Bank TW. *The World Bank Atlas Method—Detailed Methodology*. Available online at: https://datahelpdesk.worldbank.org/knowledgebase/articles/378832-what-is-the-world-bank-atlas-method (accessed April 15, 2022).
15. Bank W. *World Bank Country and Lending Groups.* Available online at: https://datahelpdesk.worldbank.org/knowledgebase/articles/906519-world-bank-country-and-lending-groups (accessed April 15, 2022).
16. Foreman KJ, Lozano R, Lopez AD, Murray CJ. Modeling causes of death: an integrated approach using CODEm. *Popul Health Metr.* (2012) 10:1. doi: 10.1186/1478-7954-10-1
17. Collaborators GBDN. Global, regional, and national burden of neurological disorders, 1990-2016: a systematic analysis for the Global Burden of Disease Study 2016. *Lancet Neurol.* (2019) 18:459–80. doi: 10.1016/S1474-4422(18)30499-X
18. Bhuia MR, Islam MA, Nwaru BI, Weir CJ, Sheikh A. Models for estimating and projecting global, regional and national prevalence and disease burden of asthma: a systematic review. *J Glob Health.* (2020) 10:020409. doi: 10.7189/jogh.10.020409
19. Siddiqi K, Husain S, Vidyasagaran A, Readshaw A, Mishu MP, Sheikh A. Global burden of disease due to smokeless tobacco consumption in adults: an updated analysis of data from 127 countries. *BMC Med.* (2020) 18:222. doi: 10.1186/s12916-020-01677-9
20. Yi M, Li A, Zhou L, Chu Q, Song Y, Wu K. The global burden and attributable risk factor analysis of acute myeloid leukemia in 195 countries and territories from 1990 to 2017: estimates based on the global burden of disease study 2017. *J Hematol Oncol.* (2020) 13:72. doi: 10.1186/s13045-020-00908-z
21. Fay MP, Tiwari RC, Feuer EJ, Zou Z. Estimating average annual percent change for disease rates without assuming constant change. *Biometrics.* (2006) 62:847–54. doi: 10.1111/j.1541-0420.2006.00528.x
22. Bossone E, Eagle KA. Epidemiology and management of aortic disease: aortic aneurysms and acute aortic syndromes. *Nat Rev Cardiol.* (2021) 18:331–48. doi: 10.1038/s41569-020-00472-6
23. Leong DP, Joseph PG, McKee M, Anand SS, Teo KK, Schwalm JD, et al. Reducing the global burden of cardiovascular disease, part 2: prevention and treatment of cardiovascular disease. *Circ Res.* (2017) 121:695–710. doi: 10.1161/CIRCRESAHA.117.311849
24. Sampson UK, Norman PE, Fowkes FG, Aboyans V, Song Y, Harrell FE, Jr., et al. Estimation of global and regional incidence and prevalence of abdominal aortic aneurysms 1990 to 2010. *Glob Heart.* (2014) 9:159–70. doi: 10.1016/j.gheart.2013.12.009
25. Thompson S, Kim L, Scott A. Screening for abdominal aortic aneurysm: screening reduces deaths related to aneurysm. *BMJ.* (2005) 330:601; author reply-2. doi: 10.1136/bmj.330.7491.601-a
26. Force USPST, Owens DK, Davidson KW, Krist AH, Barry MJ, Cabana M, et al. Screening for abdominal aortic aneurysm: US Preventive Services Task Force Recommendation Statement. *JAMA.* (2019) 322:2211–8. doi: 10.1001/jama.2019.18928
27. Altobelli E, Rapacchietta L, Profeta VF, Fagnano R. Risk factors for abdominal aortic aneurysm in population-based studies: a systematic review and meta-analysis. *Int J Environ Res Public Health.* (2018) 15:2805. doi: 10.3390/ijerph15122805
28. Wanhainen A, Hultgren R, Linne A, Holst J, Gottsater A, Langenskiold M, et al. Outcome of the Swedish Nationwide Abdominal Aortic Aneurysm Screening Program. *Circulation.* (2016) 134:1141–8. doi: 10.1161/CIRCULATIONAHA.116.022305
29. Jacomelli J. *AAA Screening Annual Data Published for 2017 to 2018: Public Health England.* (2019). Available online at: https://phescreening.blog.gov.uk/2019/01/31/aaa-screening-annual-data-published-for-2018-to-2018/ (accessed April 13, 2022).
30. Sidloff D, Stather P, Dattani N, Bown M, Thompson J, Sayers R, et al. Aneurysm global epidemiology study: public health measures can further reduce abdominal aortic aneurysm mortality. *Circulation.* (2014) 129:747–53. doi: 10.1161/CIRCULATIONAHA.113.005457
31. Munoz-Mendoza J, Pinto Miranda VA, Quevedo HC, Hebert K. Trends in abdominal aortic aneurysm prevalence and mortality in non-European countries. *Int J Cardiol.* (2013) 170:e38–40. doi: 10.1016/j.ijcard.2013.10.074
32. Powell JT, Sweeting MJ, Ulug P, Blankensteijn JD, Lederle FA, Becquemin JP, et al. Meta-analysis of individual-patient data from EVAR-1, DREAM, OVER and ACE trials comparing outcomes of endovascular or open repair for abdominal aortic aneurysm over 5 years. *Br J Surg.* (2017) 104:166–78. doi: 10.1002/bjs.10430
33. Oliver-Williams C, Sweeting MJ, Turton G, Parkin D, Cooper D, Rodd C, et al. Lessons learned about prevalence and growth rates of abdominal aortic aneurysms from a 25-year ultrasound population screening programme. *Br J Surg.* (2018) 105:68–74. doi: 10.1002/bjs.10715
34. Laroche JP, Becker F, Baud JM, Miserey G, Jaussent A, Picot MC, et al. Ultrasound screening of abdominal aortic aneurysm: lessons from Vesale 2013. *J Mal Vasc.* (2015) 40:340–9. doi: 10.1016/j.jmv.2015.07.104
35. World Health Organization. *WHO Report on the Global Tobacco Epidemic 2019: Offer Help to Quit Tobacco Use.* (2019). Available online at: https://www.who.int/teams/health-promotion/tobacco-control/who-report-on-the-global-tobacco-epidemic-2019 (accessed November 18, 2021).

36. Mills KT, Bundy JD, Kelly TN, Reed JE, Kearney PM, Reynolds K, et al. Global disparities of hypertension prevalence and control: a systematic analysis of population-based studies from 90 countries. *Circulation.* (2016) 134:441–50. doi: 10.1161/CIRCULATIONAHA.115.018912
37. Chen J, Gao Y, Jiang Y, Li H, Lv M, Duan W, et al. Low ambient temperature and temperature drop between neighbouring days and acute aortic dissection: a case-crossover study. *Eur Heart J.* (2022) 43:228–35. doi: 10.1093/eurheartj/ehab803
38. Wood AM, Kaptoge S, Butterworth AS, Willeit P, Warnakula S, Bolton T, et al. Risk thresholds for alcohol consumption: combined analysis of individual-participant data for 599 912 current drinkers in 83 prospective studies. *Lancet.* (2018) 391:1513–23. doi: 10.1016/S0140-6736(18)30134-X
39. Hamer M, O'Donovan G, Stamatakis E. Association between physical activity and sub-types of cardiovascular disease death causes in a general population cohort. *Eur J Epidemiol.* (2019) 34:483–7. doi: 10.1007/s10654-018-0460-2
40. Bailey TG, Perissiou M, Windsor MT, Schulze K, Nam M, Magee R, et al. Effects of acute exercise on endothelial function in patients with abdominal aortic aneurysm. *Am J Physiol Heart Circ Physiol.* (2018) 314:H19–30. doi: 10.1152/ajpheart.00344.2017
41. Nastasi DR, Norman R, Moxon JV, Quigley F, Velu R, Jenkins J, et al. The potential benefits and costs of an intensified approach to low density lipoprotein cholesterol lowering in people with abdominal aortic aneurysm. *Eur J Vasc Endovasc Surg.* (2021) 62:643–50. doi: 10.1016/j.ejvs.2021.06.031
42. Larsson SC, Back M, Rees JMB, Mason AM, Burgess S. Body mass index and body composition in relation to 14 cardiovascular conditions in UK Biobank: a Mendelian randomization study. *Eur Heart J.* (2020) 41:221–6. doi: 10.1093/eurheartj/ehz388
43. Acosta S, Fatemi S, Melander O, Engstrom G, Gottsater A. Prospective comparison of plasma biomarker and traditional risk factor profiles for incident isolated atherosclerotic disease and incident isolated abdominal aortic aneurysm. *Front Cardiovasc Med.* (2021) 8:818656. doi: 10.3389/fcvm.2021.818656
44. Hall JE, Mouton AJ, da Silva AA, Omoto ACM, Wang Z, Li X, et al. Obesity, kidney dysfunction, and inflammation: interactions in hypertension. *Cardiovasc Res.* (2021) 117:1859–76. doi: 10.1093/cvr/cvaa336
45. Commodore-Mensah Y, Lazo M, Tang O, Echouffo-Tcheugui JB, Ndumele CE, Nambi V, et al. High burden of subclinical and cardiovascular disease risk in adults with metabolically healthy obesity: the Atherosclerosis Risk in Communities (ARIC) Study. *Diabetes Care.* (2021) 44:1657–63. doi: 10.2337/dc20-2227

Conflict of Interest: The authors declare that the research was conducted in the absence of any commercial or financial relationships that could be construed as a potential conflict of interest.

Publisher's Note: All claims expressed in this article are solely those of the authors and do not necessarily represent those of their affiliated organizations, or those of the publisher, the editors and the reviewers. Any product that may be evaluated in this article, or claim that may be made by its manufacturer, is not guaranteed or endorsed by the publisher.

frontiers | Frontiers in Cardiovascular Medicine

ORIGINAL RESEARCH
published: 03 June 2022
doi: 10.3389/fcvm.2022.871546

Awareness and Feasibility of Women Chairing Cardiology Sessions in Scientific Meetings: A Nationwide Survey by the Japanese Circulation Society

Atsuko Nakayama[1,2], Chizuko A. Kamiya[3], Sachiko Kanki[4], Tomomi Ide[5], Yasuko K. Bando[6], Yukari Uemura[7] and Yayoi Tetsuou Tsukada[8]*

[1] Department of Cardiovascular Medicine, The University of Tokyo, Tokyo, Japan, [2] Department of Cardiovascular Medicine, Sakakibara Heart Institute, Fuchu, Japan, [3] Department of Obstetrics and Gynecology, National Cerebral and Cardiovascular Center, Osaka, Japan, [4] Department of Thoracic and Cardiovascular Surgery, Osaka Medical and Pharmaceutical University, Osaka, Japan, [5] Department of Cardiovascular Medicine, Graduate School of Medical Sciences Kyushu University, Fukuoka, Japan, [6] Department of Cardiology, Nagoya University Graduate School of Medicine, Nagoya, Japan, [7] Center for Clinical Sciences, National Center for Global Health and Medicine, Tokyo, Japan, [8] Department of General Medicine and Health Science, Nippon Medical School, Tokyo, Japan

OPEN ACCESS

Edited by:
Liya Yin,
Northeast Ohio Medical University, United States

Reviewed by:
Roberta A. Gottlieb,
Cedars Sinai Medical Center, United States
Anna Furniss,
University of Colorado, Denver, United States

****Correspondence:***
Atsuko Nakayama
atsukonakanaka@gmail.com

Specialty section:
This article was submitted to Cardiovascular Therapeutics, a section of the journal Frontiers in Cardiovascular Medicine

Received: *08 February 2022*
Accepted: *26 April 2022*
Published: *03 June 2022*

Citation:
Nakayama A, Kamiya CA, Kanki S, Ide T, Bando YK, Uemura Y and Tsukada YT (2022) Awareness and Feasibility of Women Chairing Cardiology Sessions in Scientific Meetings: A Nationwide Survey by the Japanese Circulation Society. Front. Cardiovasc. Med. 9:871546. doi: 10.3389/fcvm.2022.871546

Background: Diversity and inclusion remain a concern in the field of cardiology. Female cardiologists have less opportunity to chair sessions in scientific meetings than men. However, cardiologists' awareness and perspectives on feasibility of chairing sessions is poorly understood.

Methods and Results: A web-based survey on awareness regarding the commitment of chairing sessions was sent to 14,798 certificated cardiologists registered with the Japanese Circulation Society (JCS). A total of 3,412 valid responses were obtained, such as 523 women and 2,889 men. Female cardiologists exhibited less interest in serving as chairpersons in Japanese and English sessions (71% women vs. 82% men, $p < 0.001$, 30% women vs. 40% men, $p < 0.001$). Influencing factors of chair acceptance in Japanese sessions for female cardiologists were being a cardiologist for over 10 years [odds ratio (*OR*) 1.84, 95% confidence interval (*CI*) 1.02–3.33], experience studying abroad (OR 3.35, 95% *CI* 1.93–5.81) and chairing sessions (*OR* 8.39, 95% *CI* 5.48–12.9), having a Doctor of Philosophy (*OR* 2.82, 95% *CI* 1.09–7.31), presence of 4 or more female cardiovascular specialists in the hospital (*OR* 1.70, 95% *CI* 1.10–2.61) and of role models (*OR* 2.86, 95% *CI* 1.93–4.24), and awareness of the JCS chairperson's manual (*OR* 10.7, 95% *CI* 6.67–17.1). The receiver operating characteristic (ROC) curve revealed that the number of female cardiovascular specialists in a hospital was a more sensitive predictor of chair acceptance among male than female cardiologists.

Conclusions: Female cardiologists were less likely to accept chairing sessions compared with male cardiologists and the presence of female cardiovascular specialists positively influenced chair acceptance.

Keywords: women, sex, gender, diversity, cardiologist, session chair

INTRODUCTION

As society matures, the symbiosis of diversity becomes increasingly important. Diversity and inclusion (D/I) focuses not only on gender but also race, age, and other aspects of life to improve the world. Due to historical and cultural backgrounds, the acceptance of diversity in Japan has been hindered compared to other developed countries (1).

The Japanese Circulation Society (JCS) had 26,645 members as of June 2020 and annual host's large medical academic conferences in Japan, such as 18,600 participants in 2020 (2). However, there have been few female chairpersons, large restricted to senior physicians, and researchers. Since 2011, the JCS has implemented D/I action and independently used the D/I session chair ratio as an indicator of leadership allocation (3).

In addition, the JCS–Josei Junkanki Consortium (JCS–JJC) released a chairperson's manual (4). As the format of the academic conference recently changed due to the corona virus disease-19 (COVID-19) pandemic and information technology (IT) development, shifting to an online format, the feasibility of chairing sessions may be changing (5, 6). Although studies have examined female presenters in academic societies (7), research on feasibility of chairing sessions in academic meetings is lacking.

Keeping this in mind, this study aimed to examine the factors influencing session chair acceptance for Japanese and English sessions among cardiologists across gender.

MATERIALS AND METHODS

Study Design

A qualitative survey was conducted by our research team of the Committee for Diversity Promotion of the JCS to investigate cardiologists' perspectives on chairing sessions. The questionnaire was emailed to 14,798 medical doctors who were the JCS members also. Doctors belonged to the 1,408 non-duplicate hospitals which covered 92% of all active cardiovascular hospital in Japan (8) responded to this survey. Data were obtained from 3,412 doctors (23% response rate), with all personal information removed. Because we used the Google form for the questionnaire, all responses were valid responses which replied for all questions in this survey.

The process of how JCS decides who serves as chair in the JCS meetings was according to the recommendation by the councilors of JCS from a pool of expert lists. Subsequently, session chairs were selected after confirming the acceptance of the candidates who received the offering email from JCS office. For the annual meeting of JCS (2021), the Committee for Diversity Promotion of the JCS made the list of chair candidates who have cardiovascular specialist qualifications and accept a chair, for the councilors with recommendation of the positive invitation to female doctors to a chair.

This study was conducted in accordance with the ethical principles of the Declaration of Helsinki. Further, the study design was approved by the JCS Ethics Committee (ID: 14). Informed consent was obtained from all patients according to the protocol approved by the JCS Ethics Committee.

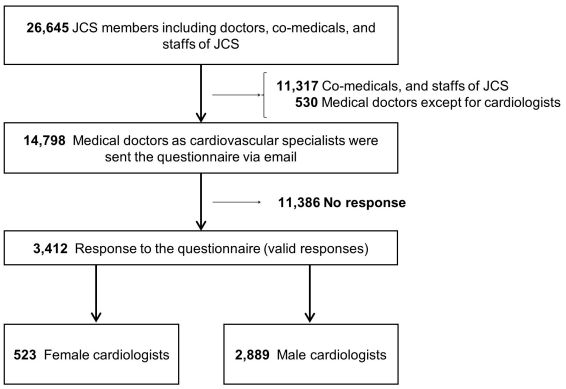

FIGURE 1 | Flowchart of response to the questionnaire. The JCS had 26,645 members such as doctors, co-medicals, and staffs of JCS. The 14,798 doctors in the cardiovascular field were registered until April 2021 in JCS (2021) and were sent the questionnaire *via* email at April 28, 2021. Data were obtained from 3,412 doctors. Of the 3,412 responses, 523 were from women and 2,889 from men.

Doctor's Degree

In Japan, students usually become physicians after graduating from high school and medical school continuously and then passing the national examinations of Doctor of Medicine (M.D.).Doctor of Philosophy (Ph.D.) is degree for a physician after completing a doctoral course in a medical graduate. Ph.D. is the higher degree of M.D. for a physician in Japan.

Outcomes

The main aim of investigating the acceptance rate of Japanese or English session chairs was to determine whether significant differences in chair acceptance were seen between male vs. female cardiologists.

Statistical Analysis

The cardiologist's characteristics were compared using the $\chi 2$-test for non-continuous variables, unpaired *t*-test for normative continuous data, using SPSS v22 (IBM Inc., Armonk, NY, United States). Logistic regression analysis was used to analyze the contribution of each factor to the chair's acceptance, while the analysis was carried out using interactive P was used to measure whether the strength of each factor within male vs. female group was heterogeneous. We performed a receiver operating characteristic (ROC) curve analysis to explore whether the number of female cardiovascular specialists belonging to each hospital could be a prospective marker for chair acceptance. The significance level was set at the alpha level of 0.05.

RESULTS

Background of Respondents

Of the 3,412 valid responses (**Figure 1**), 523 were from women and 2,889 from men (**Table 1**). A total of 3,406 respondents (99.8%) had cardiovascular specialist qualifications.

TABLE 1 | Respondent characteristics.

	Female cardiologists	Male cardiologists	*p*-value
Total number, *n* (%)	523	2889	
Age, years ± SD	47 ± 8	50 ± 9	<0.001
Years as a doctor, years ± SD	21 ± 8	25 ± 9	<0.001
Years as a cardiologist, years ± SD	18 ± 9	22 ± 11	<0.01
Qualified Ph.D., *n* (%)	386 (74%)	2292 (79%)	0.14
JCS fellow, *n* (%)	25 (5%)	259 (9%)	<0.01
Study abroad experience, *n* (%)	127 (24%)	1125 (39%)	<0.001
Experience as session chairperson, *n* (%)	359 (69%)	2470 (86%)	<0.001
Chair acceptance in Japanese sessions, *n* (%)	371 (71%)	2378 (82%)	<0.001
Chair acceptance in English sessions, *n* (%)	155 (30%)	1142 (40%)	<0.001
JCS session chairperson acquaintances, *n* (%)	446 (85%)	2419 (84%)	0.21
Presence of role models, *n* (%)	348 (67%)	2041 (71%)	0.03
Only female role models, *n* (%)	119 (23%)	11 (0%)	<0.001
Only malerole models, *n* (%)	60 (12%)	1714 (59%)	
Bothrole models, *n* (%)	163 (31%)	324 (11%)	
Childcare duties, *n* (%)	297 (57%)	1426 (49%)	0.001
Preschool child, *n* (%)	76 (15%)	289 (10%)	<0.001
Juvenile child, n (%)	59 (11%)	449 (16%)	
Preschool and juvenile children, *n* (%)	36 (7%)	238 (8%)	
Childcare support by the conference			
Need childcare support during the session, *n* (%)	210 (40%)	1329 (46%)	<0.001
Do not need childcare support during the session, *n* (%)	103 (20%)	330 (11%)	
Need not to ask for childcare support during the session, *n* (%)	93 (18%)	671 (23%)	
Social childcare service			
Social childcare service allows for chairperson duties, *n* (%)	76 (15%)	233 (8%)	<0.001
Social childcare service does not allow for chairperson duties, *n* (%)	52 (10%)	174 (6%)	
Need not to ask for social childcare service, *n* (%)	240 (46%)	1784 (62%)	
Awareness of the JCS–JJC chairperson's manual, *n* (%)	281 (54%)	1140 (40%)	<0.001
The JCS–JJC chairperson's manual was useful*, *n* (%)	257 (91%)	1034 (91%)	<0.001
The JCS–JJC chairperson's manual was helpful for chair acceptance, *n* (%)	429 (82%)	2168 (75%)	<0.01

**Rate was calculated among manual readers.*
JCS, Japanese circulation society; JJC, Josei Junkanki Consortium; Ph.D., Doctor of Philosophy.

Significant differences were observed between men and women in the cardiovascular specialty in all fields, except imaging and emergency medicine (**Figure 2A**). In the fields of preventive medicine, echocardiography, and congenital heart disease, the rate of female cardiologists was higher. However, the rate of female vs. male cardiologists was markedly lower in the field of coronary artery disease (7 vs. 24%, $p < 0.0001$).

Of the 1,408 non-duplicate hospitals in this survey, 1,193 (85%) had one or less female specialist, 161 (11%) had two to three, and only 56 (4%) had four or more (**Figure 3A**). Limited to the 205 academically inclined hospitals, 102 (50%) had one or less female specialist, 58 (28%) had two to three, and 45 (22%) had four or more.

Preference for Form of Scientific Meetings

A 2 × 2-group comparison by age (younger, <45 years; older, ≥45 years) and gender indicated that younger female cardiologists preferred to participate in online sessions and have a travel time to the meeting of less than 1 h (**Figures 2B,C**). Most respondents in all groups stated that the experience required to chair sessions was 11–20 years; however, older female cardiologists considered it inappropriate to select a chairperson based on experience, with the lowest proportion answering 21–30 years of experience in the four groups ($p < 0.001$; indicated with a red bar in **Figure 2D**).

Factors Influencing Chairperson Acceptance

Female cardiologists had a lower rate of experience studying abroad and chairing sessions compared with male cardiologists (24 vs. 39%, $p < 0.001$, 69 vs. 86%, $p < 0.001$, respectively) and a lower rate of acceptance for Japanese and English sessions (71 vs. 82%, $p <$ 0,001, 30 vs. 40%, $P < 0.001$, respectively; **Table 1**). Female cardiologists had fewer role models than male cardiologists (67 vs. 71%, $p = 0.03$), more childcare duties (57 vs. 49%, $p = 0.001$), and higher awareness of the JCS–JJC chairperson's manual (54 vs. 40%, $p < 0.001$). In addition, male cardiologists with male role models accounted for 70% (male 59% and both 11%), while

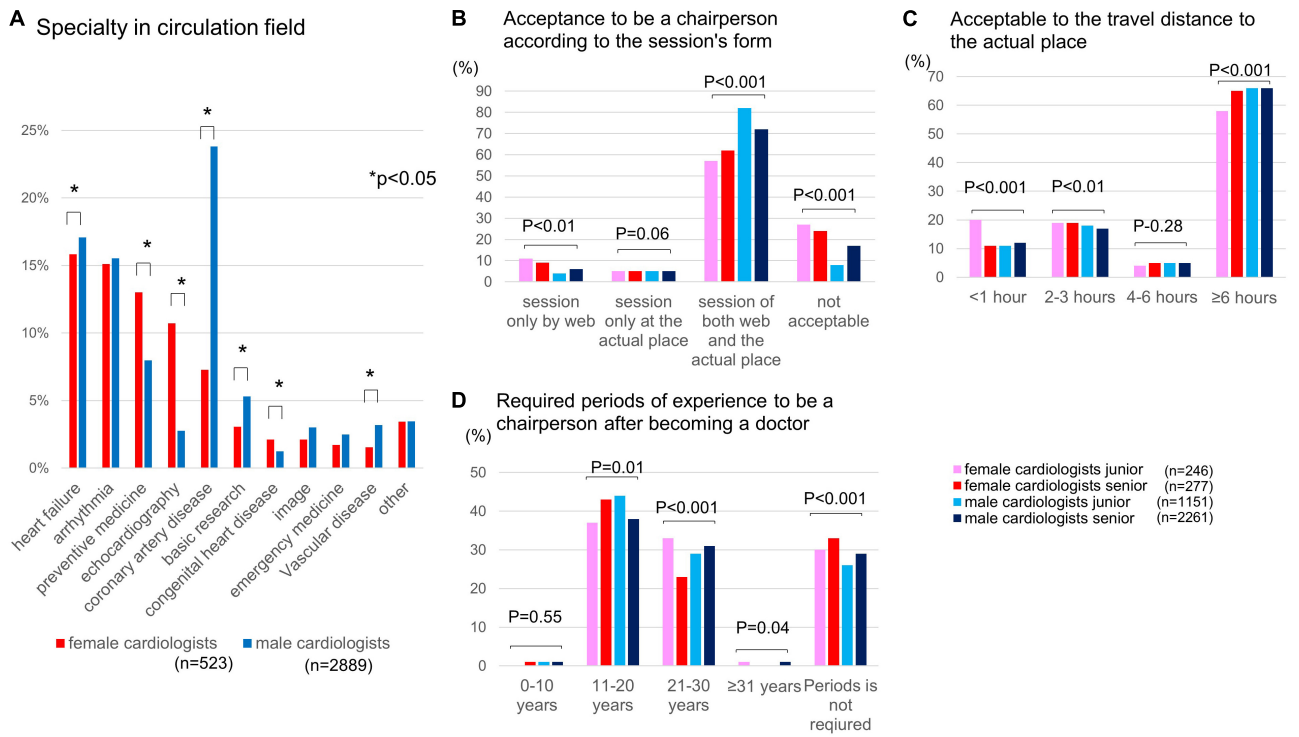

FIGURE 2 | Specialty of cardiologists in Japan, awareness of chair acceptance for scientific meetings, and changes in the rates of female cardiologists. **(A)** Background of cardiologist specialties in the cardiovascular field. **(B)** Chair acceptance for scientific meetings. **(C)** Chair acceptance based on travel distance to the meeting. **(D)** Experience required to be a chairperson (years). *$p < 0.01$.

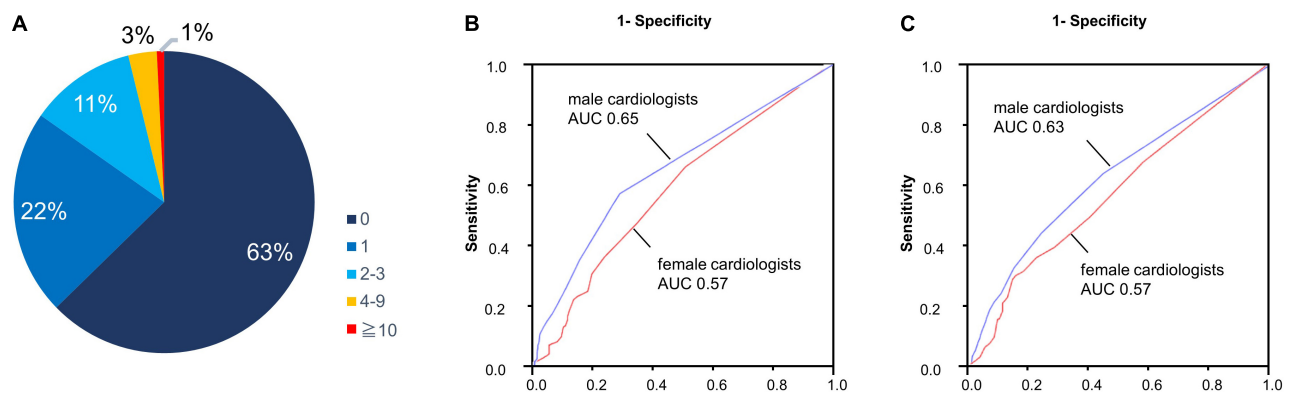

FIGURE 3 | Number of female cardiovascular specialists belonging to each hospital. **(A)** Number of female cardiovascular specialists belonging to each hospital in all registered hospitals (n = 1408). **(B)** Acceptance of chairperson by the number of female cardiovascular specialists belonging to each hospital: Japanese session. **(C)** Acceptance of chairperson by the number of female cardiovascular specialists belonging to each hospital: English session.

54% (female 23% and both 31%) of female cardiologists had female role models.

Subgroup Analysis of Chair Acceptance

A logistic regression analysis on answers regarding acceptance for chairing Japanese sessions revealed that male cardiologists who were younger [odds ratio (OR) 2.13, 95% confidence interval (CI) 1.69–2.70, $p < 0.001$], had 4 or more female cardiovascular specialists in the hospital (*OR* 3.05, 95% *CI* 2.12–4.39, $p < 0.0001$), and had role models (*OR* 3.86, 95% *CI* 3.17–4.71, $p < 0.001$) were significantly more often accepted as chair (**Figure 4**). Female cardiologists with 10 or more years of experience in cardiovascular treatment (*OR* 1.84, 95% *CI* 1.02–3.33, $p < 0.001$), who studied abroad (*OR* 3.35, 95% *CI* 1.93–5.81, $p < 0.0001$), who chaired sessions in the past (*OR* 8.39, 95% *CI* 5.48–12.9, $p < 0.0001$), and were aware of the JCS–JJC chairperson's manual (*OR* 10.7, 95% *CI* 6.62–17.1, $p < 0.0001$) had a higher rate of

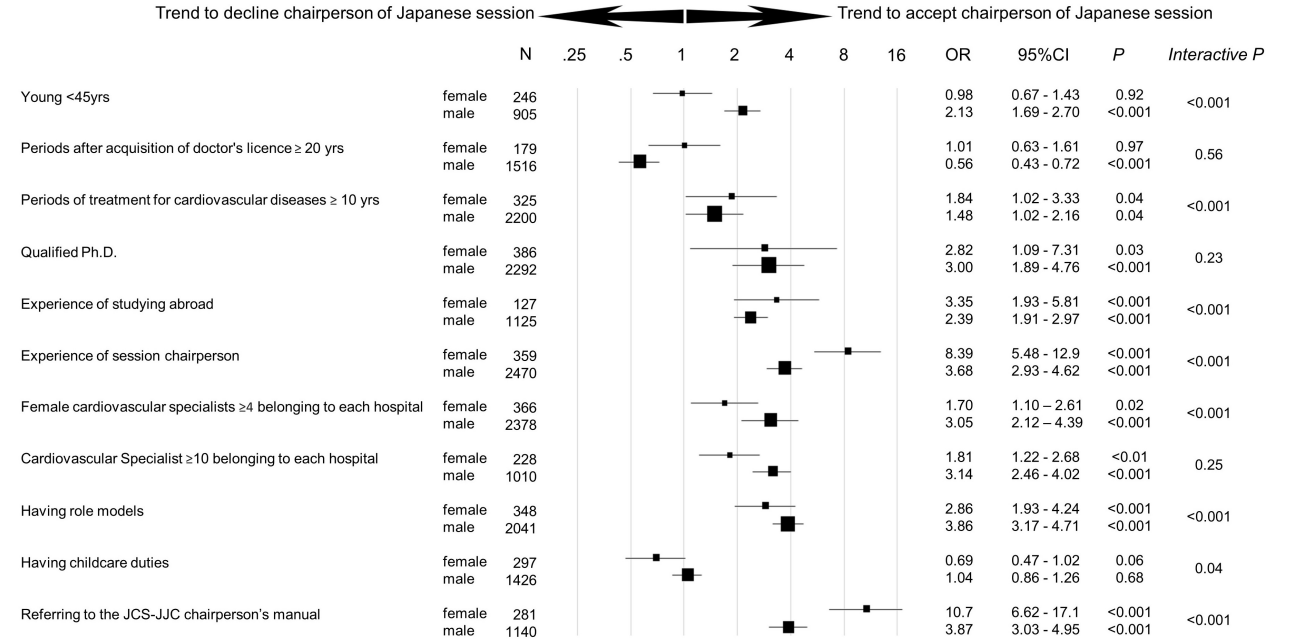

FIGURE 4 | Trend to accept chairperson of Japanese session by gender. Odds ratio [95% confidence interval (*CI*)] for the trend to accept the chairperson of the Japanese session by gender was analyzed in each subgroup. Interactive *p* was used as an index to measure the strength of each factor within male vs. female group. Ph.D., Doctor of Philosophy.

chair acceptance. Among respondents with childcare needs, female cardiologists tended to decline Japanese session chairs (*OR* 0.69, 95% *CI* 0.47–1.02, $p = 0.06$), whereas male cardiologists didn't decline (*OR* 1.04, 95% *CI* 0.86–1.26, $p = 0.68$).

The official language of the session was an important factor that positively affected the decision to accept the role of chairperson. For the English sessions, male cardiologists who were younger (*OR* 1.18, 95% *CI* 1.01–1.69, $p = 0.04$), had 4 or more female cardiovascular specialists in the hospital (*OR* 2.69, 95% *CI* 2.20–3.31, $p < 0.001$), and had role models (*OR* 1.62, 95% *CI* 1.37–1.92, $p < 0.001$) accepted chair (**Figure 5**). Female cardiologists who studied abroad (*OR* 9.94, 95% *CI* 6.32–15.7, $p < 0.001$), chaired sessions in the past (*OR* 4.34, 95% *CI* 2.59–7.26, $p < 0.001$), and were aware of the JCS–JJC chairperson's manual (*OR* 4.01, 95% *CI* 2.63–6.12, $p < 0.001$) accepted chairing English sessions more often. In the subgroup with childcare duties, there were no significant differences between male and female cardiologists in the English session chair acceptance rate.

The ROC curve analysis demonstrated that the number of female cardiovascular specialists in the hospital was a more sensitive predictor of chair acceptance among men than women for Japanese and English sessions [area under the curve (AUC) 0.65 vs. 0.57, AUC 0.63 vs. 0.57, respectively] (**Figures 3B,C**). Limited to the academically inclined hospitals, the number of female cardiovascular specialists was a still more sensitive predictor of chair acceptance among men than women for Japanese and English sessions (AUC 0.65 vs. 0.58, AUC 0.62 vs. 0.59, respectively).

DISCUSSION

A nationwide survey of cardiologists revealed that women had a lower chair acceptance than men. Acceptance for official language session was significantly higher among men than women for younger cardiologists (<45 years), hospitals with four or more female cardiovascular specialists, and those who had role models. Chair acceptance for English session was significantly higher among women than men for cardiologists with over 10 years of cardiovascular practice, who studied abroad, who chaired sessions in the past, and who were aware of the JCS–JJC chairperson's manual.

New Format of Scientific Meetings and Family Duties

During the COVID-19 pandemic, conventional on-site meetings were switched to an online format (5, 6), enabling participation without visiting the conference venue. Nursing and child care duty may disable young cardiologists from participating in onsite conference. The results of the present study indicated that young female cardiologists preferred an online format and were less likely to attend local conferences, perhaps due to parenting duties. Therefore, web-based venues should continue to be partially implemented in the future, even after the pandemic.

The working condition of the female is greatly changed by the existence of marriage, pregnancy, delivery, childcare, and caring for family members with illness or disability in Japan, where the traditional thinking of gender role beliefs strongly remains. Although housework hours are longer for women than men in

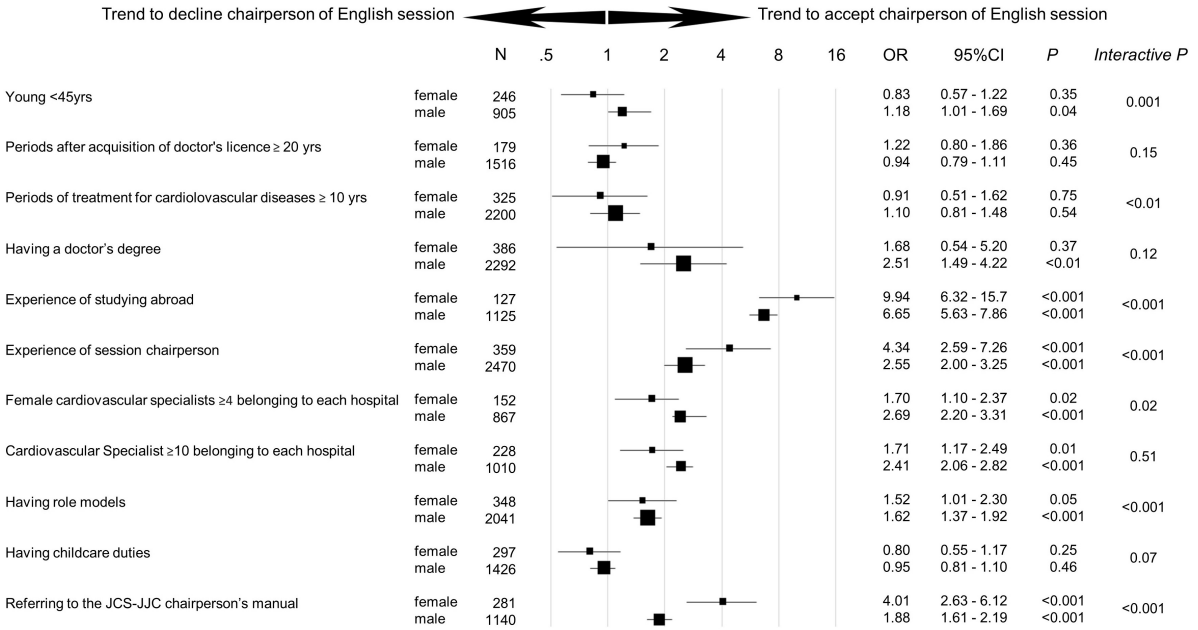

FIGURE 5 | Trend to accept chairperson of English session by gender. Odds ratio [95% confidence interval (*CI*)] for the trend to accept the chairperson of the English session by gender was analyzed in each subgroup. Interactive *P* was used as an index to measure the strength of each factor within male vs. female group. Ph.D., Doctor of Philosophy.

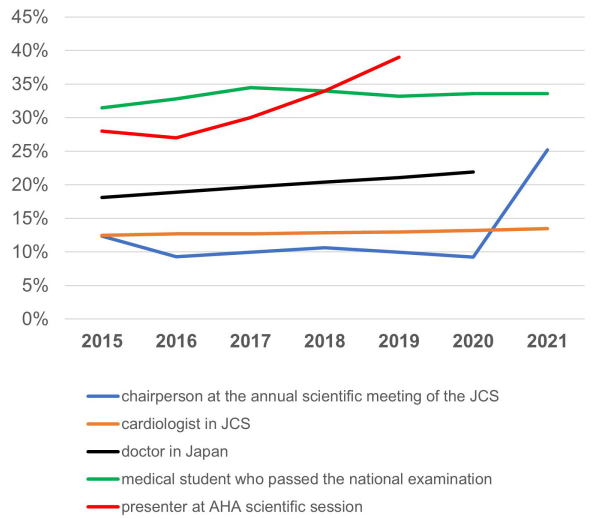

FIGURE 6 | Changes in rates of female cardiologists. The changes in female cardiologist rates of female chairpersons at the annual scientific meeting of the JCS, female cardiologists in JCS, female doctors in Japan, female medical students who passed the national examination for medical practitioners, and female presenters at the AHA scientific session. JCS, Japan Circulation Society; AHA, American Heart Association.

all countries, focusing on the male-to-female ratio (the ratio of women with men set as 1), Japan has the highest ratio (5.5-fold), followed by 4.4-fold in Korea, and 2.3-fold in Italy among the OECD countries (9).

This survey showed the trend of declining chairing a Japanese session among female than male cardiologists in the subgroup of having childcare duties. Childcare services rapidly developed in Japan (10) and the JCS provides the nursery service for the participants' pre-school children after the birth of 3 months at the scientific meetings. In Japan, high quality childcare services are provided by both public and private, and many female doctors also use the services. It is expected that even in the academic conference, a temporary childcare center is set up for the participants. In such a background, temporary childcare services would satisfy the participants who need the service; therefore, childcare might not a strong factor for rejecting chairing sessions in this survey.

Effects of Diversity Promotion

The number of female cardiology specialists in the hospital impacted chair acceptance, with a stronger positive influence on men than women. The acceptance rate to the chair in the hospital where female cardiovascular specialists ≥4 were belonging might be elevated by academically inclined hospitals. However, limited to the academically inclined university hospitals, the more cardiologists accepted chairing a session in the hospitals which more female specialists belonged to.

Numerous studies investigated the promotion of diversity to improve the overall workplace environment and quality of work (11). Gender diversity can improve the quality of healthcare, as it provides a flexible workplace environment for both men and women and healthcare services with diverse values (12). Moreover, gender differences in healthcare delivery allow for

more patient-centered communication (13), guideline adherence (14), and testing for patients by female doctors (15).

Importance of Role Models

More male than female cardiologists in this study had role models. Female cardiologists with a same-gender role model accounted only for 54% of the total, which may be due to a lower rate of female mentors (16), while male cardiologists accounted for 70%. Role models of the same gender are considered more appreciated for female cardiologists, as work situations for women are disproportionately influenced by marriage, childcare, and nursing. Otherwise, male role models also play an important role on female cardiologists because they can offer valuable guidance on many aspects of career development. To find role models of both genders, the construction of network systems, such as mentor–mentee matching on the national or worldwide scale is being awaited (17).

Initiatives of the Committee for Diversity Promotion Committee of the Japanese Circulation Society

To encourage female cardiologists, the JCS–JJC subcommittee was formed to increase proportion for chairing session in annual academic meetings (**Figure 6**). To meet the demands of a growing number of female doctors, future policies should improve the work environment of female cardiologists, provide support for research, increase the number of female doctors in instructive positions, allowing them to become role models, and strengthen communities with active communication using IT.

Limitations

This study had some limitations. People who answered the questionnaire may have been more interested in chairing sessions than those who did not respond, which may differ from the usual population within an academic society.

CONCLUSION

This study revealed that female cardiologists were less likely to accept chairing sessions compared with male cardiologists and that the presence of female cardiovascular specialists in the hospital positively influenced chair acceptance among both genders. Active and targeted promotion for this population would contribute to the revitalization of the field of cardiology through the empowerment of human resources.

DATA AVAILABILITY STATEMENT

The raw data supporting the conclusions of this article will be made available by the authors, without undue reservation.

ETHICS STATEMENT

The studies involving human participants were reviewed and approved by this study design was approved by the JCS Ethics Committee (ID: 14). Written informed consent for participation was not required for this study in accordance with the national legislation and the institutional requirements.

AUTHOR CONTRIBUTIONS

AN, CK, SK, TI, YB, and YT planned and conducted the study. AN wrote the manuscript. YU analyzed the data. All authors contributed to data collection, analysis, interpretation, and approved the final version of the manuscript.

ACKNOWLEDGMENTS

We would like to express our appreciation to the members of the JCS who participated in this survey, members of the Committee for Diversity Promotion of JCS, such as Tatsuoki Taniguchi, JCS–JJC Subcommittee, and the Executive Committee of the annual meeting of JCS (2021). We would like to express our heartfelt gratitude to the JCS office for the administrative work involved in conducting this survey. We are grateful to Yuka Otaki for helpful discussions.

REFERENCES

1. Guo J, Browne CV. Women's employment, work-life balance policies, and inequality across the life course: a comparative analysis of Japan, Sweden and the United States. *J Women Aging.* (2021) 34:294–308. doi: 10.1080/08952841.2021.1917242
2. The Number of Members, Japanese Circulation Society. *Data by the Japanese Circulation Society*. (2021). Available online at: http://www.j-circ.or.jp/english/about/riji.html (accessed August 4, 2021).
3. News by Japanese Circulation Society. *Data by the Japanese Circulation Society*. (2021). Available online at: https://www.j-circ.or.jp/cms/wp-content/uploads/2021/07/JCS_85th_Female_chairperson_ratio.pdf (accessed August 4, 2021).
4. The chairperson's manual by The JCS-Josei Junkanki Consortium. *Data by the Japanese Circulation Society*. (2021). Available online at: https://www.j-circ.or.jp/information/kyodo/pdf/zachou_tebiki.pdf (accessed August 4, 2021).
5. Schwarz M, Scherrer A, Hohmann C, Heiberg J, Brugger A, Nuñez-Jimenez A. COVID-19 and the academy: it is time for going digital. *Energy Res Soc Sci.* (2020) 68:101684. doi: 10.1016/j.erss.2020.101684
6. Shimbo M, Nakayama A. The vulnerable cardiologists of the COVID-19 era. *Int Heart J.* (2021) 62: 465–9.
7. Yong CM, Balasubramanian S, Douglas PS, Agarwal P, Birgersdotter-Green U, Gummidipundi S, et al. Temporal trends in the proportion of women physician speakers at major cardiovascular conferences. *Circulation.* (2021) 143:755–7. doi: 10.1161/CIRCULATIONAHA.120.052663
8. Japanese Registry Of All Cardiac and Vascular Diseases [JROAD]. *Data by the Japanese Registry Of All Cardiac and Vascular Diseases (JROAD).* (2021). Available online at: https://j-circ.or.jp/jittai_chosa/jittai_chosa2018web.pdf (accessed August 4, 2021).

9. OECD iLibrary. *Data by OECD Balancing Paid Work, Unpaid Work And Leisure*. (2020). Available online at: https://www.oecd-ilibrary.org/economics/how-s-life-2020_e6597da1-en (accessed March 26, 2022).
10. Fukai T. Childcare availability and fertility: evidence from municipalities in Japan. *J Japanese Int Econ.* (2017) 43:1–18. doi: 10.1016/j.jjie.2016.11.003
11. Astrid P, Daniela G, Marina K, Cornelia S, Karen DZ. Managing a culturally diverse workforce: diversity perspectives in organizations. *Int J Intercult Relat.* (2013) 37:159–75. doi: 10.1016/j.ijintrel.2012.09.001
12. Dwyer S, Richard O, Chadwick K. Gender diversity in management and firm performance: the influence of growth orientation and organizational culture. *J Bus Res.* (2003) 56:1009–19. doi: 10.1016/S0148-2963(01)00329-0
13. Nakayama A, Morita H, Fujiwara T, Komuro I. Effect of treatment by female cardiologists on short-term readmission rates of patients hospitalized with cardiovascular diseases. *Circ J.* (2019) 83:1937–43. doi: 10.1253/circj.CJ-19-0357
14. Baumhäkel M, Müller U, Böhm M. Influence of gender of physicians and patients on guideline-recommended treatment of chronic heart failure in a cross-sectional study. *Eur J Heart Fail.* (2009) 11:299–303. doi: 10.1093/eurjhf/hfn041
15. Sergeant A, Saha S, Shin S, Weinerman A, Kwan J, Lapointe-Shaw L, et al. Variations in processes of care and outcomes for hospitalized general medicine patients treated by female vs male physicians. *JAMA Health Forum.* (2021) 2:e211615. doi: 10.1001/jamahealthforum.2021.1615
16. Sakushima K, Mishina H, Fukuhara S, Sada K, Koizumi J, Sugioka T, et al. Mentoring the next generation of physician-scientists in Japan: a cross-sectional survey of mentees in 6 academic medical centers. *BMC Med Educ.* (2015) 15:54. doi: 10.1186/s12909-015-0333-2
17. Obara H, Saiki T, Imafuku R, Fujisaki K, Suzuki Y. Influence of national culture on mentoring relationship. *BMC Med Educ.* (2021) 21:300. doi: 10.1186/s12909-021-02744-2

Conflict of Interest: The authors declare that the research was conducted in the absence of any commercial or financial relationships that could be construed as a potential conflict of interest.

frontiers | Frontiers in Cardiovascular Medicine

CLINICAL TRIAL
published: 09 June 2022
doi: 10.3389/fcvm.2022.864837

Efficacy and Safety of Granulocyte-Colony Stimulating Factor Therapy in Chagas Cardiomyopathy: A Phase II Double-Blind, Randomized, Placebo-Controlled Clinical Trial

*Carolina T. Macedo[1,2,3†], Ticiana F. Larocca[2†], Márcia Noya-Rabelo[1,4], Roque Aras Jr.[5], Cristiano R. B. Macedo[5], Moisés I. Moreira[1], Alessandra C. Caldas[1], Jorge A. Torreão[1], Victor M. A. Monsão[6], Clarissa L. M. Souza[5], Juliana F. Vasconcelos[2,4], Milena R. Bezerra[3], Daniela P. Petri[7], Bruno S. F. Souza[2,7,8], Antônio G. F. Pacheco[9], André Daher[10], Ricardo Ribeiro-dos-Santos[2,3] and Milena B. P. Soares[2,3]**

[1] Department of Cardiology, Hospital São Rafael, Salvador, Brazil, [2] Gonçalo Moniz Institute, Oswaldo Cruz Foundation, Salvador, Brazil, [3] Senai Institute on Innovation in Advanced Health Systems, SENAI CIMATEC, Salvador, Brazil, [4] Escola Bahiana de Medicina e Saúde Pública, Salvador, Brazil, [5] University Hospital Professor Edgard Santos, Federal University of Bahia, Salvador, Brazil, [6] Hospital Geral Roberto Santos, Salvador, Brazil, [7] Center for Biotechnology and Cell Therapy, Hospital São Rafael, Salvador, Brazil, [8] D'Or Institute for Research and Education, Rio de Janeiro, Brazil, [9] Scientific Computing Program, Oswaldo Cruz Foundation, Rio de Janeiro, Brazil, [10] Vice-Presidency of Research and Reference Laboratories, Oswaldo Cruz Foundation, Rio de Janeiro, Brazil

Aim: Previous studies showed that granulocyte-colony stimulating factor (G-CSF) improved heart function in a mice model of Chronic Chagas Cardiomyopathy (CCC). Herein, we report the interim results of the safety and efficacy of G-CSF therapy vs. placebo in adults with Chagas cardiomyopathy.

Methods: Patients with CCC, New York Heart Association (NYHA) functional class II to IV and left ventricular ejection fraction (LVEF) 50% or below were included. A randomization list using blocks of 2 and 4 and an allocation rate of 1:1 was generated by R software which was stratified by functional class. Double blinding was done to both arms and assessors were masked to allocations. All patients received standard heart failure treatment for 2 months before 1:1 randomization to either the G-CSF (10 mcg/kg/day subcutaneously) or placebo group (1 mL of 0.9% saline subcutaneously). The primary endpoint was either maintenance or improvement of NYHA class from baseline to 6–12 months after treatment, and intention-to-treat analysis was used.

Results: We screened 535 patients with CCC in Salvador, Brazil, of whom 37 were randomized. Overall, baseline characteristics were well-balanced between groups. Most patients had NYHA class II heart failure (86.4%); low mean LVEF was 32 ± 7% in the G-CSF group and 33 ± 10% in the placebo group. Frequency of primary endpoint was 78% (95% CI 0.60–0.97) vs. 66% (95% CI 0.40–0.86), p = 0.47, at 6 months

OPEN ACCESS

Edited by:
Liya Yin,
Northeast Ohio Medical University,
United States

Reviewed by:
Reinaldo Bulgarelli Bestetti,
University of Ribeirão Preto, Brazil
Lyda Rojas,
Fundación Cardiovascular de Colombia, Colombia

***Correspondence:**
Milena B. P. Soares
milena.soares@fiocruz.br

† These authors have contributed equally to this work

Specialty section:
This article was submitted to Cardiovascular Therapeutics, a section of the journal Frontiers in Cardiovascular Medicine

Received: *28 January 2022*
Accepted: *26 April 2022*
Published: *09 June 2022*

Citation:
Macedo CT, Larocca TF, Noya-Rabelo M, Aras R Jr, Macedo CRB, Moreira MI, Caldas AC, Torreão JA, Monsão VMA, Souza CLM, Vasconcelos JF, Bezerra MR, Petri DP, Souza BSF, Pacheco AGF, Daher A, Ribeiro-dos-Santos R and Soares MBP (2022) Efficacy and Safety of Granulocyte-Colony Stimulating Factor Therapy in Chagas Cardiomyopathy: A Phase II Double-Blind, Randomized, Placebo-Controlled Clinical Trial. Front. Cardiovasc. Med. 9:864837. doi: 10.3389/fcvm.2022.864837

and 68% (95% CI 0.43–0.87) vs. 72% (95% CI 0.46–0.90), p = 0.80, at 12 months in placebo and G-CSF groups, respectively. G-CSF treatment was safe, without any related serious adverse events. There was no difference in mortality between both arms, with five deaths (18.5%) in treatment vs. four (12.5%) in the placebo arm. Exploratory analysis demonstrated that the maximum rate of oxygen consumption during exercise (VO_2 max) showed an improving trend in the G-CSF group.

Conclusion: G-CSF therapy was safe and well-tolerated in 12 months of follow-up. Although prevention of symptom progression could not be demonstrated in the present study, our results support further investigation of G-CSF therapy in Chagas cardiomyopathy patients.

Clinical Trial Registration: [www.ClinicalTrials.gov], identifier [NCT02154269].

Keywords: G-CSF therapy, safety study, cardiac functional analysis, NYHA functional class, Chagas cardiomyopathy

INTRODUCTION

Chronic Chagas cardiomyopathy (CCC) is a life-threatening clinical condition that is responsible for most of the morbidity and mortality caused by infection by the protozoan *Trypanosoma cruzi*. About 30% of asymptomatic infected patients, i.e., those who have the indeterminate form of Chagas disease, will develop cardiac manifestations at some point in their lives, although this might take up to 30 years to occur following the primary infection. The main clinical features include heart failure, sudden death, arrhythmias, stroke, and systemic embolism, with heart failure being the most common cause of death (1–3).

Chronic Chagas cardiomyopathy is the leading cause of non-ischemic heart failure in Latin America, with most of the 2 million cases and 12,500 deaths per year occurring in Brazil and Argentina (4, 5). Chagas disease prevalence is also increasing in Europe and in the United States. In the United States, it is currently estimated that 30,000 to 40,000 individuals may have CCC, and Chagas disease has already been listed by the Centers for Disease Control (CDC) as one of the five most neglected parasitic infections (6).

Although the first reports of Chagas disease date back more than 100 years, the pathogenesis of CCC is still not fully understood. Several studies have demonstrated that the persistence of *T. cruzi* causes permanent myocardial inflammation due to both direct parasite–target response and infection-trigged auto-reactivity, leading to interstitial edema, fibrosis, apoptosis, and chronic myocarditis (7).

Currently, nifurtimox and benznidazole are the only effective anti-trypanosomal therapies available for Chagas disease, but their use is not recommended in patients with chronic cardiomyopathy due to the lack of evidence that these drugs can potentially avert progression of the disease (8, 9). Despite its unique pathophysiological mechanism, standard therapy for CCC is the same as that used to treat any other heart failure syndrome, usually including beta blockers, diuretics, angiotensin-converting enzyme inhibitors (or angiotensin receptor blockers), and spironolactone. Management of late-phase chronic cardiac disease may also include implanted cardiac defibrillators and pacemakers. Although the outcome following heart transplantation in patients with end-stage Chagas cardiomyopathy is better than that observed in patients with non-Chagas disease (10), this procedure is not widely performed in Latin America due to its high costs, limited number of donors, and potential complications (5, 8). Therefore, new therapeutic approaches, mainly targeting specific features of the pathogenic mechanisms of CCC, are urgently needed.

Granulocyte colony-stimulating factor (G-CSF) is a pleotropic cytokine widely used in clinical practice essentially as an adjunctive drug to chemotherapy, due to its ability to induce granulopoiesis and mobilize bone marrow-derived stem cells to the peripheral blood for bone marrow transplantation. The G-CSF receptor is expressed in several cell types, including immune cells, and G-CSF treatment was shown to induce T cell tolerance in several immune-mediated disease models (9). Moreover, there is evidence that G-CSF induces cardiomyogenesis and plays an important role in heart development during embryogenesis (11–13). Therefore, this cytokine has been explored over the last few years as a potential adjuvant therapy for cardiac diseases (14).

In previous studies, it was shown that G-CSF administration improved exercise capacity; reduced inflammation, fibrosis, and tissue parasitism; and modulated the production of pro-inflammatory mediators in a mouse model of CCC (15, 16). These effects were attributed, at least partially, to the immunomodulatory activity of G-CSF (16). In addition, genetically modified mesenchymal stem cells overexpressing G-CSF have also demonstrated immunomodulatory effects by reducing inflammatory mediators, leukocyte infiltration, and myocardial fibrosis (17).

In an attempt to address the lack of effective therapy for CCC, we performed a double-blind, randomized, placebo-controlled

Abbreviations: CCC, chronic Chagas cardiomyopathy; G-CSF, granulocyte-colony stimulating factor; NYHA, class, New York Heart Association functional class; CDC, centers for disease control; LVEF, left ventricular ejection fraction; NT-proBNP, N-terminal brain natriuretic peptide; ECG, electrocardiogram; TNF-α, tumor necrosis alpha; AE, adverse events; MLHF, Minnesota Living with Heart Failure.

clinical trial to evaluate the efficacy and safety of G-CSF therapy with concomitant use of standard heart failure therapy in patients with CCC.

METHODS

Ethical Approval

The clinical study protocol and informed consent form were reviewed and approved by the Ethics Committee at HSR (Certificate of Presentation of Ethical Appreciation number 22133513.4.0000.0048), which was accredited by the Brazilian National Council on Ethics in Research (CONEP), Ministry of Health. The study was registered at https://www.clinicaltrials.gov on 06/03/2014 (unique identifier: NCT02154269) and was conducted in accordance with Good Clinical Practice Guidelines (GCP) and Brazilian National Health Council resolution 466/20121. During the study, monitoring visits were conducted carried out to ensure GCP adherence.

Written informed consent was obtained from every subject prior to enrollment. If the study subject was illiterate, an impartial third party witnessed the informed consent process. All subjects were informed of the nature and possible associated risks of the trial and that they were free to withdraw their consent to participate at any time. The investigators and study staff ensured the confidentiality of all records.

Study Design

This study was a double-blind, randomized, placebo-controlled, prospective, comparative superiority trial designed to evaluate the efficacy and safety of G-CSF therapy with concomitant use of standard heart failure therapy in patients with CCC, conducted at two tertiary hospitals in Salvador, northeast Brazil: Hospital São Rafael (HSR) and Hospital Edgard Santos. Double-blinding was limited to the G-CSF and placebo arms.

All patients received standard therapy for heart failure and were randomly assigned to additionally receive either: (a) 10 mcg/kg/day of G-CSF, or (b) 1 mL of 0.9% saline as placebo. Both groups received four cycles of subcutaneous injections for five consecutive days of either saline or G-CSF solution prepared for administration with indistinguishable 1 mL syringes. There were 9-day intervals (a weekend followed by a full week) between cycles. G-CSF was manufactured by the Aché laboratory. If G-CSF therapy effectiveness were demonstrated at the end of the study, patients in the placebo arm were offered G-CSF treatment.

Study Participants

Between September 24, 2015 and July 30, 2018, 535 patients with Chagas cardiomyopathy were screened in Salvador, Bahia, Brazil, of whom 37 were randomized. The inclusion criteria were previous diagnosis of heart failure as per the Framingham criteria; Chagas disease diagnosis confirmed by two serological tests using distinct methods; age between 20 and 75 years; New York Heart Association (NYHA) functional class II to IV heart failure; and echocardiogram showing left ventricular ejection fraction (LVEF) of 50% or below using the Simpson method. Exclusion criteria were: severe valvular heart disease (except for functional mitral or tricuspid regurgitation); myocardial infarction or history of confirmed coronary artery disease; viral myocarditis; alcohol or drug abuse; acute or chronic kidney disease or previous dialysis therapy; evidence of acute systemic infection; chronic obstructive pulmonary disease with continuous use of steroids or bronchodilators; liver, blood, and neoplastic diseases or hemostasis disorders; chronic inflammatory or infectious diseases; other diseases that could affect life expectancy; any other comorbidity affecting 2-year survival; pregnancy confirmed by human chorionic gonadotropin (β-hCG) testing; and breastfeeding.

Randomization and Masking

A randomization list using blocks of 2 and 4 and an allocation rate of 1:1 was generated by R software version 3.2. using the Mersenne–Twister method, which was stratified by functional class. The study coordinators provided sealed opaque envelopes. Subjects, clinical study staff, statisticians, and investigators were masked to treatment assignment. Two nurses, a medical investigator, and a hematologist were not blinded. The hematologist was responsible for checking the full blood count on a regular basis in order to monitor G-CSF safety. The blinded investigators did not have access to full blood count tests. The nurses were responsible for preparing and administering the treatments. All laboratory tests, clinical assessments, exams, and imaging were masked to group allocation.

Procedures

Before randomization, all patients received standard heart failure treatment for 2 months in order to optimize baseline drugs and doses for the follow-up visits. According to the current heart failure guidelines (16), when the study was started, the standard drug regimen for CCC was spironolactone (25 mg/day); furosemide and digoxin, in selected cases; captopril (37.5–150 mg/day); or hydralazine (75 mg/day) with isosorbide mononitrate (20 mg/day), in case of contraindication with angiotensin-converting enzyme inhibitors or angiotensin receptor blockers; carvedilol (6.25–50 mg/day); and amiodarone (200–400 mg/day), if appropriate.

After this 60 days period, all patients underwent clinical evaluation and were submitted to the following baseline tests: urinalysis, blood indices (including full blood count, renal function, electrolytes, liver function, troponin I, ultrasensitive PCR, N-terminal brain natriuretic peptide and cytokines), transthoracic echocardiogram, 6 min walk test, treadmill test, cardiac magnetic resonance, 24 h electrocardiogram (ECG) reading, 12-lead conventional electrocardiogram, urinary and serum β-hCG test (before every treatment cycle, if appropriate), and chest x-ray. The echocardiogram was performed according to current guidelines and the Simpson rule was used to calculate LVEF. Complete follow-up assessments were performed at 6 and 12 months after treatment. Although only two cardiologists followed up the patients clinically, each patient was assessed only once per visit. Regarding the echocardiogram measurements, three cardiologists performed the tests throughout the study, but also each measurement was taken only once per visit

as well. Hematologic assessments were done after every treatment cycle.

Outcomes

The primary outcome, NYHA functional class, was assessed at baseline and at 6, 9, and 12 months of follow-up by a blinded cardiologist. According to the protocol, improvement was defined as either regression or maintenance of baseline functional class within 12 months of follow-up for patients in NYHA class II or III and regression of functional class, or no more than one hospitalization due to acutely decompensated heart failure during follow-up for patients in NYHA class IV.

Secondary efficacy endpoints included LVEF (measured by echocardiogram and cardiac magnetic resonance), functional capacity (assessed by treadmill test and 6-min walking test), quality of life (Minnesota Living with Heart Failure Questionnaire), presence of tachyarrhythmia on 24 h ECG reading, prognostic biomarkers of heart failure (NT-proBNP), and cytokine profile [tumor necrosis alpha (TNF-α) concentration]. The study time chart is presented in **Figure 1**.

A safety analysis was conducted in the intention-to-treat population, describing frequency, causality, and severity of adverse events (AEs) in each arm. All AEs were subdivided into serious and non-serious events, and were also classified as not related, probably related, or highly likely related to the assigned treatment.

Patients were encouraged to seek immediate advice from the investigators if any AE was suspected. AEs were reported using the Medical Dictionary for Regulatory Activities (MedDra). All clinical or laboratory abnormalities were categorized as grade I to IV according to the Common Terminology Criteria for Adverse Events (CTCAE) of the National Cancer Institute. Any suspected serious AEs (by standard definitions) were reported to the sponsor and to the Ethical Review Committee.

A Data and Safety Monitoring Board (DSMB) was established by the study coordinators, composed of Chagas disease specialists, a cardiologist, a statistician, and another health professional. Meetings occurred periodically, and all changes in the study protocol had to be approved by an independent DSMB and the local ethical committee.

Statistical Analysis

Study data were collected and managed using Research Electronic Data Capture (REDCap) electronic data capture tools hosted at the Oswaldo Cruz Foundation (FIOCRUZ). REDCap is a secure, web-based software platform designed to support data capture, including double entry.

This study was powered to provide evidence of the superiority of G-CSF treatment over placebo. Based on the current literature, subjects with NYHA functional class II to IV heart failure treated only with standard therapy were expected to have a functional class improvement of 10% in the placebo group and 40% in the G-CSF group during the 12-month follow-up. Thus, for a 30% absolute difference in NYHA class to be detected with a 95% confidence level and 80% statistical power, a sample size of 29 subjects per treatment group was needed. Taking into account a 15% loss of follow-up in 12 months, the final sample size was 35 subjects per treatment group. An interim analysis with half the sample size was planned in the DSMB charter. Those interim results are presented here, using intention-to-treat analysis.

Primary endpoint analysis was done by intention-to-treat and for missing data, last observation carrying forward as replacement strategy was used, and death before the final assessment was considered as treatment failure.

Baseline characteristics and adverse events of the study population were summarized using descriptive statistics with frequencies and percentages for categorical variables. For numerical variables, mean and standard deviation (SD) values were used.

The proportions of categorical variables were compared using Pearson's chi-squared test with Yates's continuity correction at a significance level of 5%. Differences in continuous variables between groups were compared using the *t*-test or Mann–Whitney test. Two-sided p-values < 0.05 were considered statistically significant. Analyses were performed using IBM SPSS statistics software version 25.

RESULTS

A total of 535 subjects were assessed for eligibility at both trial sites (Hospital São Rafael and Hospital Edgard Santos) in

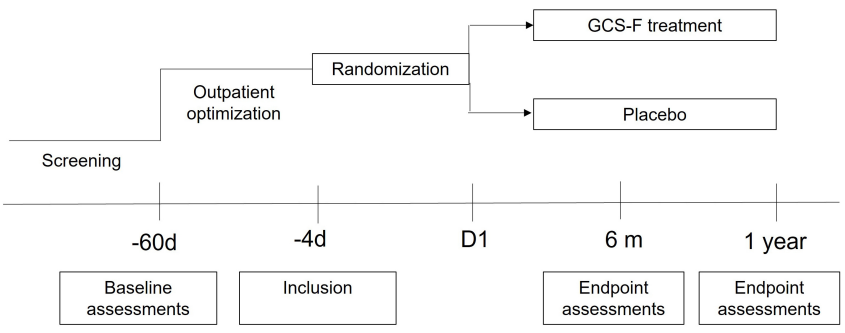

FIGURE 1 | Study time chart. Patients were screened for eligibility before optimization of pharmacological therapy for at least 8 weeks. Patients included in the study were randomized to receive granulocyte-colony stimulating factor (G-CSF) or placebo and were followed up for 12 months.

Salvador, Brazil, from September 2015 to October 2018. Thirty-seven subjects were randomized (1:1) to one of the treatment arms: (a) G-CSF (10 mcg/kg/day) with concomitant use of standard heart failure therapy, or (b) 0.9% saline plus standard heart failure therapy (placebo). Eighteen subjects were allocated to the treatment group and 19 to the placebo group. The main reason for not including most subjects was unavailability for follow-up, as the vast majority of patients lived in the countryside or remote areas. Nine patients died during follow-up (**Figure 2**).

The baseline characteristics of the subjects were similar between the treatment groups (**Table 1**). The primary outcome was measured by evaluating NYHA functional class improvement, comparing baseline with 6 and 12-month data. All 37 subjects were included in this intent-to-treat analysis. Death before end of follow-up was considered as deterioration. The overall frequency of either maintenance or improvement of clinical condition was primary endpoint was 78% (95% CI 0.60–0.97) vs. 66% (95% CI 0.40–0.86), $p = 0.47$, at 6 months and 68% (95% CI 0.43–0.87) vs. 72% (95% CI 0.46–0.90), $p = 0.80$, at 12 months in placebo and G-CSF groups, respectively (**Figure 3**). The distribution across the NYHA classes in both groups at inclusion ($T = 0$) and at 6 and 12 months after treatment is shown in **Figure 4**.

The secondary outcomes included improvement of LVEF (as measured by echocardiogram) at 6 and 12 months compared to baseline results (**Table 2**). The frequency of improvement in placebo and G-CSF arms was 23 vs. 26% ($p = 0.83$) at 6 months and 31 vs. 20% at 12 months, respectively ($p = 0.47$). The difference in percentage of myocardial fibrosis measured by cardiac magnetic resonance at baseline and 12 months between placebo (23.5%) and G-CSF (30.6%) groups was not significant ($p = 0.23$).

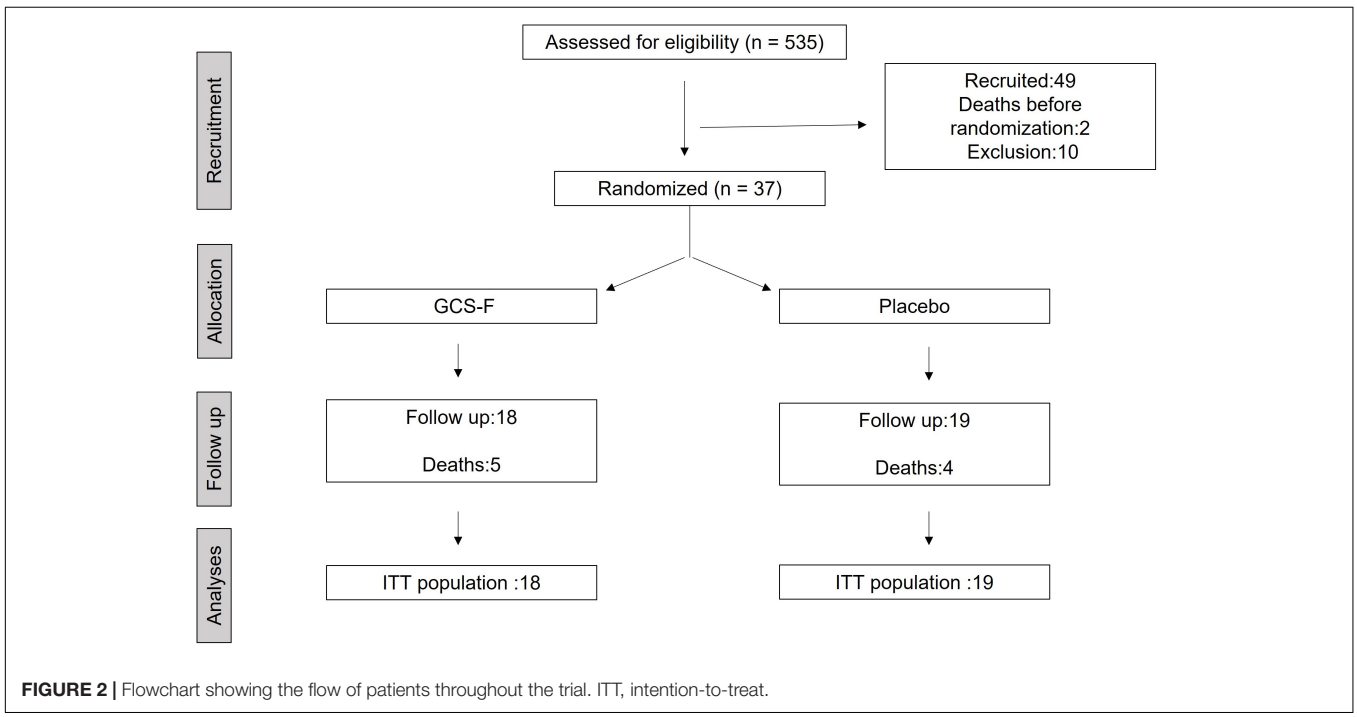

FIGURE 2 | Flowchart showing the flow of patients throughout the trial. ITT, intention-to-treat.

TABLE 1 | Baseline characteristics of subjects.

		Treatment groups	
		Placebo + SHFT (19 subjects)	**G-CSF + SHFT (18 subjects)**
Gender	Male	11 (57.8%)	10 (55.0%)
NYHA class	II	16 (43.2%)	16 (43.2%)
	III or IV	3 (8.1%)	2 (5.4%)
Hypertension	No	12 (63%)	14 (77%)
Dyslipidemia	No	12 (63%)	9 (50%)
Age (years)		59 (±8)	60 (±8)
BMI		24.38 (±7.14)	23.33 (±5.94)
LVEF (Simpson method)		33 (±10)	32 (±7)

Absolute number and percentage (%) were used to present categorical variables. Quantitative data presented using mean ± standard deviation (SD). SHFT, standard heart failure therapy; NYHA, New York Heart Association; BMI, body mass index; LVEF, left ventricular ejection fraction.

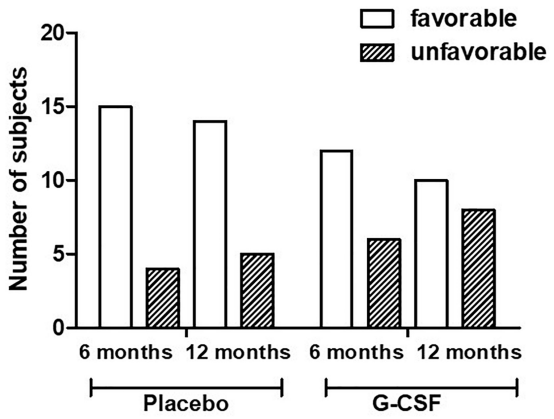

FIGURE 3 | Progression of NYHA functional class at 6 and 12 months (p = 0.47 and 0.80, respectively). Favorable: Improvement of NYHA class; Unfavorable: Worsening of NYHA class.

Twenty-two subjects performed a treadmill test at enrollment and the last follow-up visit. Nine subjects (41%) had 10% higher oxygen consumption than at baseline. Although not statistically significant, the maximum oxygen consumption at 12 months was better in the G-CSF group than in the placebo group, showing a tendency of improvement (p = 0.06). Quality of life was assessed using the Minnesota questionnaire at randomization and at 6 and 12 months. An independent samples median test of the total score showed no statistical difference between the groups at 6 or 12 months (p = 1.0 and 0.69).

Analysis of incidence of non-sustained ventricular tachycardia (NSVT) was performed by 24 h ECG monitoring. At 12 months, the median NSVT was maintained in the G-CSF group and increased in the placebo group compared to baseline, even though no statistical significance was found (p = 0.7).

N-terminal pro-BNP (NT-proBNP) concentration was measured at enrollment and at 12 months, and no statistical significance was detected between the groups at both time points (p = 0.47 and 0.86, respectively) (**Supplementary Table 1**). Finally, tumor necrosis factor-alpha (TNF-α) concentration was measured as an exploratory analysis. We found a significant increase in TNF-α concentration at days 5 and 47 during the G-CSF application period, followed by a decrease in concentration until the values were similar to those in the placebo group at 12 months (p = 0.69) (**Supplementary Table 2**).

There were 11 deaths during the study, two of which happened before randomization. Overall mortality was 24.3% and, out of the nine remaining deaths, five occurred in the treatment group and four in the placebo group. Fifty-nine serious adverse events (SAE) were reported, none of which were related to G-CSF treatment. The classification of SAEs and their frequency per treatment group is presented in **Table 3**.

A total of 283 adverse events were reported using MedDra. The AEs were aggregated using the system organ classes (SOC), and those with a frequency higher than 3% in either treatment arm are presented in **Table 4**.

DISCUSSION

Chronic Chagas cardiomyopathy is a life-threatening condition for which no specific and effective treatment has been found. Since drug repurposing is the quickest research and development strategy to deliver a new treatment, our group designed this trial in an attempt to repurpose G-CSF as a potential treatment for CCC, given its well-established safety profile and promising results in experimental models of this disease. The present study was the first randomized clinical trial assessing the effects of therapy with G-CSF in symptomatic patients with CCC. Although it was well-tolerated, no statistically significant clinical improvement was demonstrated in terms of efficacy.

The New York Heart Failure (NYHF) classification has been shown to be an independent predictor of mortality in patients with chronic heart failure, including Chagas cardiomyopathy (18). Additionally, it is easily applied, well-validated, and widely used for risk stratification in heart failure. In this study, for most of the subjects, their NYHA classification was either maintained or improved during the study follow-up. This may have been the result of standard heart failure treatment optimization before randomization and close monitoring throughout the follow-up, as the same trend was observed in both study arms. No parameters used to evaluate the influence of G-CSF treatment were statistically significant, including the primary outcome (NYHA); however, there was a trend showing that G-CSF treatment could potentially avert the natural progression of CCC, promoting some improvement in the clinical condition

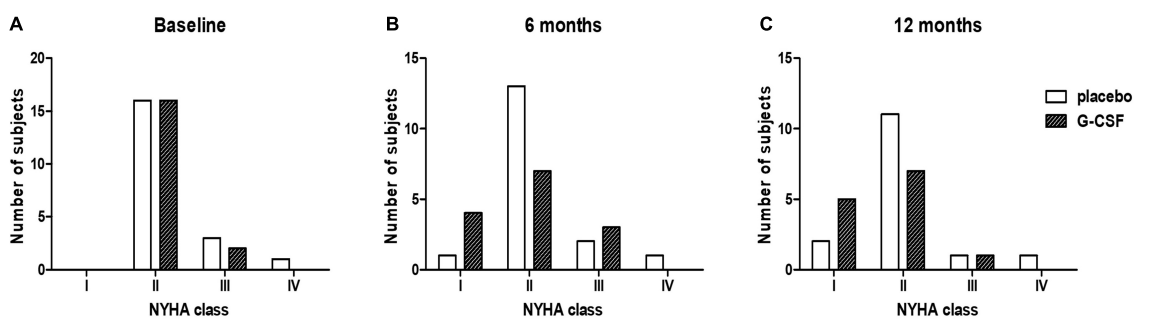

FIGURE 4 | NYHA class distributions at baseline (T = 0) **(A)**, at 6 months **(B)** and 12 months **(C)** after treatment (p = 0.20 and 0.38, respectively).

TABLE 2 | Secondary endpoints at baseline and 12 months after treatment.

	Group	Baseline	*p*-value	12 months	*p*-value
LVEF (%)	Placebo	33 (±10.7)	0.63	35 (±12)	0.24
	G-CSF	31 (±7.8)		31 (±6.7)	
VO_2 max	Placebo	22.7 (±10.7)	0.95	20 (±12)	0.064
	G-CSF	22.9 (±7.8)		26 (±6.7)	
Myocardial fibrosis (%)	Placebo	23.8 (±13.4)	0.75	23.5 (±13.7)	0.23
	G-CSF	25.5 (±14)		30.6 (±9.9)	
Six minutes walking test	Placebo	450 (390–480)	0.86	450 (348–502)	1.0
	G-CSF	456 (390–471)		429 (360–495)	
MLHLQ	Placebo	43.2 (±19.5)	0.43	35.1 (±17.3)	0.23
	G-CSF	38.4 (±16.7)		26 (±20.5)	

LVEF, left ventricular ejection fraction; VO_2 max, maximum oxygen consumption during exercise (mL/kg/min). Myocardial fibrosis evaluated by cardiac magnetic resonance. Six-minute walking test distance: median (first to third quartile). Scores for Minnesota Living with Heart Failure (MLHFQ) physical subscale range from 0 to 40, emotional subscale from 0 to 25, and total scale from 0 to 105, with higher scores indicating worse health status.

TABLE 3 | Classification and frequency of serious adverse events (SAEs) per treatment group.

SAE	Placebo (32 SAEs) *n* (%)	G-CSF (27 SAEs) *n* (%)
Death	4 (12.5%)	5 (18.5%)
Life-threatening	8 (25.0%)	7 (25.9%)
Inpatient hospitalization or prolonged existing hospitalization	20 (62.5%)	9 (33.3%)
Clinically significant	0 (0%)	6 (22.2%)

n: total number of events in each group, not number of patients who had events.

TABLE 4 | AEs with a frequency higher than 3.0% per treatment arm.

AE	Placebo (108 AEs) *n* (%)	G-CSF (148 AEs) *n* (%)
Cardiac disorders	7 (6.4%)	5 (3.3%)
Gastrointestinal disorders	28 (25.9%)	25 (16.8%)
General disorders and administration site conditions	16 (14.8%)	31 (20.9%)
Infections and infestations	5 (4.6%)	14 (9.4%)
Investigations (other clinical disorders investigated)*	4 (3.7%)	5 (3.3%)
Metabolic and nutrition disorders	6 (5.5%)	1 (0.6%)
Musculoskeletal and connective tissue disorders	13 (12.0%)	18 (12.1%)
Nervous system disorders	12 (11.1%)	16 (10.8%)
Reproductive system and breast disorders	1 (0.9%)	6 (4.0%)
Respiratory, thoracic, and mediastinal disorders	11 (10.1%)	19 (12.8%)
Skin and subcutaneous tissue disorders	1 (0.9%)	6 (4.0%)
Vascular disorders	4 (3.7%)	2 (1.3%)

**Total number of events in each group, not number of patients who had events.*

of patients 6 months after treatment. This may indicate that a different treatment regimen, with courses of G-CSF distributed over longer periods, might be more effective in inducing prolonged improvement in CCC.

Regarding cardiomyopathies with other etiologies and the use of G-CSF, the overall mortality in our study was higher (24.3%). A study recently published on ischemic cardiomyopathy showed an overall mortality of 15.8% with no statistical difference between G-CSF and placebo groups (19). However, we did not expect to have a similar mortality rate, as it is well-known that CCC carries a worse prognosis with a higher mortality rate compared to heart failure with other etiologies. In a recent study, mortality from cardiovascular and other causes was 40% higher in patients with CCC than in patients with ischemic heart disease (20). Our study might more accurately reflect this aspect, as we had a follow-up period of 12 months. Our mortality rate is in keeping with what was described by Shen and collaborators. Their overall mortality rate by CCC was 29.2% in a study with more than 2,000 patients comparing cardiovascular mortality and hospitalization between heart diseases with different etiologies, including Chagas (20, 21).

The relationship between myocardial fibrosis with ventricular dysfunction and cardiac arrhythmias in patients with CCC is well-established (22). In our study, assessment of fibrosis by

cardiac magnetic resonance showed a trend in regression of myocardial fibrosis in 18.8% of patients, without a significant difference between the groups. This reduction in the percentage of myocardial fibrosis, along with some improvement in the incidence of cardiac arrhythmias, was previously demonstrated by our group in an experimental model of CCC (15, 17). A possible explanation for the better therapeutic response in mice is the earlier time of intervention during the course of the disease, when the inflammatory response and fibrosis may be more effectively modulated by G-CSF.

The influence of the timing of G-CSF administration on its effects has been suggested in the literature. Several studies demonstrated that earlier application of G-CSF led to further improvement in parameters such as functional class, left ventricular function, and cardiac remodeling (19, 23–25). In our study, G-CSF therapy was carried out at an advanced stage of the disease, in patients with greatly reduced left ventricular function. It is reasonable to suppose that earlier administration of G-CSF could potentially promote better results. Additionally, the worst response to G-CSF in patients with Chagas disease, compared to other cardiomyopathies, might also be related to differences in their pathogenesis. In addition to the presence of the parasite, CCC has greater myocardial inflammatory infiltrates, as shown by an analysis of explanted hearts from patients with CCC compared to other etiologies of heart failure (26).

Other studies have also shown that G-CSF can improve left ventricular function and reduce cardiac remodeling and TNF-α levels (16, 19, 24). Here we found a transient increase in G-CSF-treated group, which decreased to levels similar to those of placebo group at the end of follow-up. We also measured the concentration of NT-proBNP, a biomarker that is strongly correlated with NYHA functional class, as previously described (27). No statistically significant differences in NT-proBNP concentration between the experimental groups were demonstrated.

Regarding exercise tolerance, the maximum rate of oxygen consumption during exercise (VO_2) is an index widely used to objectively assess exercise capacity and cardiovascular reserve. Szlachcic et al. demonstrated that the survival rate in individuals with VO_2 levels greater than 10 mL/kg/min was 80%, whereas it was 20% in those with lower VO_2 levels (28). Mady et al. demonstrated that the VO_2 level, along with LVEF, was an independent predictor of mortality during a 30-month follow-up of patients with CCC (29). In our study, there was a trend of improved VO_2 in the G-CSF group at 12 months, but it did not reach statistical significance.

For quality-of-life assessment, the Minnesota Living with Heart Failure (MLHF) questionnaire was used. Although not statistically significant, the difference between groups was greater in the final evaluation at 12 months, with a tendency toward lower scores (better quality of life) in the G-CSF group.

The follow-up duration may also have had an influence on the results. Although 12 months might have been adequate for assessing functional class and quality of life, this period is unlikely to be long enough to show differences in parameters with slower and more progressive changes, such as left ventricular function, myocardial fibrosis, and functional capacity on exercise testing. In fact, assessment of G-CSF treatment showed benefits when patients with ischemic cardiomyopathy were evaluated 10 years after treatment (19).

Potential Limitations

A low recruitment rate, possible measurement bias, and a lack of statistically significant results are the main limitations of our study and were considered relevant enough to halt the study following the interim analysis. Despite its underpower to both efficacy and safety outcomes, our study suggests that the treatment with G-CSF is safe in patients with chronic Chagas disease cardiomyopathy. G-CSF has been widely applied in clinical practice with few serious side effects (25, 30–33).

CONCLUSION

This study is the first randomized clinical trial to assess the effects of G-CSF in Chagas cardiomyopathy. Since its efficacy in preventing the clinical progression of the disease could not be demonstrated in the present study, G-CSF therapy shall not be advised as a standard treatment for this condition. Further investigations need to be carried out in order to confirm the safety and evaluate the possible efficacy of the G-CSF in Chagas cardiomyopathy, possibly testing the administration of G-CSF earlier in the course of the disease, and with a longer follow-up period.

DATA AVAILABILITY STATEMENT

The original contributions presented in the study are included in the article/**Supplementary Material**, further inquiries can be directed to the corresponding author/s.

ETHICS STATEMENT

The studies involving human participants were reviewed and approved by Ethics Committee at HSR (Certificate of Presentation of Ethical Appreciation number 22133513.4.0000.0048). The patients/participants provided their written informed consent to participate in this study.

AUTHOR CONTRIBUTIONS

AD, CaM, TL, MS, RR-d-S, and AP participated in the study concept and design. CaM and TL were the principal investigators. CaM, TL, MB, DP, BS, CS, MN-R, RA, and CrM conducted data collection and quality assurance. JV, VM, MM, AC, and JT performed imaging exams and laboratory analysis. AD, CaM, and AP performed data analysis. AD, CaM, TL, MS, and AP

participated in interpretation of the data and writing and critical revision of the manuscript. All authors have read and agreed to the published version of the manuscript.

FUNDING

The Fiocruz Programme of Excellence in Clinical Research, through the Brazilian National Council of Research (CNPq), a public organization, sponsored this study. It had a role in study design, monitoring, and data analysis, and no role in data collection, data interpretation, or writing of the report.

ACKNOWLEDGMENTS

The authors thank all subjects who participated in this study, Hospital São Rafael and Hospital Edgard Santos, and the VPPCB/FIOCRUZ teams.

SUPPLEMENTARY MATERIAL

The Supplementary Material for this article can be found online at: https://www.frontiersin.org/articles/10.3389/fcvm.2022.864837/full#supplementary-material

REFERENCES

1. Manzullo EC, Chuit R. Risk of death due to chronic chagasic cardiopathy. *Mem Inst Oswaldo Cruz.* (1999) 94(Suppl. 1):317–20. doi: 10.1590/S0074-02761999000700060
2. Gonçalves JG, Dias Silva VJ, Calzada Borges MC, Prata A, Correia D. Mortality indicators among chronic Chagas patients living in an endemic area. *Int J Cardiol.* (2010) 143:235–42. doi: 10.1016/j.ijcard.2009.02.011
3. Ayub-Ferreira SM, Mangini S, Issa VS, Cruz FD, Bacal F, Guimarães GV, et al. Mode of death on Chagas heart disease: comparison with other etiologies. A subanalysis of the REMADHE prospective trial. *PLoS Negl Trop Dis.* (2013) 7:e2176. doi: 10.1371/journal.pntd.0002176
4. Rassi A Jr., Rassi A, Marin-Neto JA. Chagas disease. *Lancet.* (2010) 375:1388–402. doi: 10.1016/S0140-6736(10)60061-X
5. Andrade JP, Marin Neto JA, Paola AA, Vilas-Boas F, Oliveira GM, Bacal F, et al. I Latin American guidelines for the diagnosis and treatment of Chagas' heart disease: executive sum-mary. *Arq Bras Cardiol.* (2011) 96:434–42. doi: 10.1590/s0066-782x2011000600002
6. Bern C, Montgomery SP. An estimate of the burden of Chagas disease in the United States. *Clin Infect Dis.* (2009) 49:e52–4. doi: 10.1016/S0140-6736(12)61728-0
7. Marin-Neto JA, Cunha-Neto E, Maciel BC, Simões MV. Pathogenesis of chronic Chagas heart disease. *Circulation.* (2007) 115:1109–23. doi: 10.1161/CIRCULATIONAHA.106.624296
8. Dias JC, Ramos AN Jr., Gontijo ED, Luquetti A, Shikanai-Yasuda MA, Coura JR, et al. II Consenso Brasileiro em doença de Chagas, 2015. *Epidemiol Serv Saúde.* (2016) 25:7–86. doi: 10.5123/S1679-49742016000500002
9. Rutella S, Zavala F, Danese S, Kared H, Leone G. Granulocyte colony-stimulating factor: a novel mediator of T cell tolerance. *J Immunol.* (2005) 175:7085–91. doi: 10.4049/jimmunol.175.11.7085
10. Bocchi EA, Fiorelli A. The paradox of survival results after heart transplantation for cardiomyo-pathy caused by *Trypanosoma cruzi*. First guidelines group for heart transplantation of the Brazilian society of cardiology. *Ann Thorac Surg.* (2001) 71:1833–8. doi: 10.1016/s0003-4975(01)02587-5
11. Hamamoto M, Tomita S, Nakatani T, Yutani C, Yamashiro S, Sueda T, et al. Granulocyte-colony stimulating factor directly enhances proliferation of human troponin I-positive cells derived from idiopathic dilated cardiomyopathy through specific receptors. *J Heart Lung Transplant.* (2004) 23:1430–7. doi: 10.1016/j.healun.2003.09.031
12. Shimoji K, Yuasa S, Onizuka T, Hattori F, Tanaka T, Hara M, et al. G-CSF promotes the prolif-eration of developing cardiomyocytes in vivo and in derivation from ESCs and iPSCs. *Cell Stem Cell.* (2010) 6:227–37. doi: 10.1016/j.stem.2010.01.002
13. Tsukamoto T, Sogo T, Ueyama T, Nakao S, Harada Y, Ihara D, et al. Chimeric G-CSF recep-tor-mediated STAT3 activation contributes to efficient induction of cardiomyocytes from mouse induced pluripotent stem cells. *Biotechnol J.* (2020) 15:e1900052. doi: 10.1002/biot.201900052
14. Pourtaji A, Jahani V, Moallem SMH, Karimani A, Mohammadpour AH. Application of G-CSF in congestive heart failure treatment. *Curr Cardiol Rev.* (2019) 15:83–90. doi: 10.2174/1573403X14666181031115118
15. Macambira SG, Vasconcelos JF, Costa CR, Klein W, Lima RS, Guimarães P, et al. Granulocyte colony stimulating factor treatment in chronic Chagas disease: preservation and improvement of cardiac structure and function. *FASEB J.* (2009) 23:3843–50. doi: 10.1096/fj.09-137869
16. Vasconcelos JF, Souza BS, Lins TF, Garcia LM, Kaneto CM, Sampaio GP, et al. Administration of granulocyte colony stimulating factor induces immunomodulation, recruitment of T regulatory cells, reduction of myocarditis and decrease of parasite load in a mouse model of chronic Chagas disease cardiomyopathy. *FASEB J.* (2013) 27:4691–702. doi: 10.1096/fj.13-229351
17. Silva DN, Souza BSF, Vasconcelos JF, Azevedo CM, Valim CXR, Paredes BD, et al. Granulo-cyte-colony stimulating factor-overexpressing mesenchymal stem cells exhibit enhanced im-munomodulatory actions through the recruitment of suppressor cells in experimental Chagas disease cardiomyopathy. *Front Immunol.* (2018) 9:1449. doi: 10.3389/fimmu.2018.01449
18. Scrutenid D, Lagioia R, Ricci A, Clemente M, Boni L, Rizzon P. Prediction of mortality in mild to moderately symptomatic patients with left ventricular dysfunction: the role of the New York Heart association classification, cardiopulmonary exercise testing, two-dimensional echocardiography and Holter Monitoring. *Eur Heart J.* (1994) 15:1089–95. doi: 10.1093/oxfordjournals.eurheartj.a060633
19. Leone AM, D'Amario D, Cannata F, Graziani F, Borovac JA, Leone G, et al. The effects of granulocyte colony-stimulating factor in patients with a large anterior wall acute myocardial infarction to prevent left ventricular remodeling: a 10-year follow-up of the RIGENERA study. *J Clin Med.* (2020) 9:1214. doi: 10.3390/jcm9041214
20. Rohde LEP, Montera MW, Bocchi EA, Clausell NO, Albuquerque DC, Rassi S, et al. Diretriz Brasileira de insuficiência cardíaca crônica e aguda. *Arq Bras Cardiol.* (2018) 111:436–539. doi: 10.5935/abc.20180190
21. Shen L, Ramires F, Martinez F, Bodanese LC, Echeverría LE, Gómez EA, et al. Contemporary characteristics and outcomes in Chagasic heart failure compared with other nonischemic and is-chemic cardiomyopathy. *Circ Heart Fail.* (2017) 10:e004361. doi: 10.1161/CIRCHEARTFAILURE.117.004361
22. Rochitte CE, Nacif MS, de Oliveira Júnior AC, Siqueira-Batista R, Marchiori E, Uellendahl M, et al. Cardiac magnetic resonance in Chagas' disease. *Artif Organs.* (2007) 31:259–67. doi: 10.1111/j.1525-1594.2007.00373.x
23. Leone AM, Galiuto L, Garramone B, Rutella S, Giannico MB, Brugaletta S, et al. Usefulness of granulocyte colony-stimulating factor in patients with a large anterior wall acute myocardial in-farction to prevent left ventricular remodeling (the RIGENERA study). *Am J Cardiol.* (2007) 100:397–403. doi: 10.1016/j.amjcard.2007.03.036
24. Achilli F, Malafronte C, Maggiolini S, Lenatti L, Squadroni L, Gibelli G, et al. G-CSF treatment for STEMI: final 3-year follow-up of the randomised placebo-controlled STEM-AMI trial. *Heart.* (2014) 100:574–81. doi: 10.1136/heartjnl-2013-304955
25. Achilli F, Pontone G, Bassetti B, Squadroni L, Campodonico J, Corrada E, et al. G-CSF for extensive STEMI. *Circ Res.* (2019) 125:295–306. doi: 10.1161/CIRCRESAHA.118.314617

26. Larocca TF, Souza BSF, Macedo CT, Azevedo CM, Vasconcelos JF, Silva DN, et al. Assessment of syndecan-4 expression in the hearts of *Trypanosoma cruzi*-infected mice and human subjects with chronic Chagas disease cardiomyopathy. *Surg Exp Pathol.* (2018) 1:5. doi: 10.1186/s42047-018-0012-9
27. Vilas-Boas F, Feitosa GS, Soares MB, Pinho-Filho JA, Nascimento T, Barojas MM, et al. Invasive and noninvasive correlations of B-type natriuretic peptide in patients with heart failure due to Chagas cardiomyopathy. *Congest Heart Fail.* (2008) 14:121–6. doi: 10.1111/j.1751-7133.2008.08166.x
28. Szlachcic J, Massie BM, Kramer BL, Topic N, Tubau J. Correlates and prognostic implication of exercise capacity in chronic congestive heart failure. *Am J Cardiol.* (1985) 55:1037–42. doi: 10.1016/0002-9149(85)90742-8
29. Mady C, Cardoso RH, Barretto AC, da Luz PL, Bellotti G, Pileggi F. Survival and predictors of survival in patients with congestive heart failure due to Chagas' cardiomyopathy. *Circulation.* (1994) 90:3098–102. doi: 10.1161/01.cir.90.6.3098
30. Miller AM. Hematopoietic growth factors in autologous bone marrow transplantation. *Semin Oncol.* (1993) (5 Suppl 6):88–95.
31. Abdel-Latif A, Bolli R, Zuba-Surma EK, Tleyjeh IM, Hornung CA, Dawn B. Granulocyte colo-ny-stimulating factor therapy for cardiac repair after acute myocardial infarction: a systematic review and meta-analysis of randomized controlled trials. *Am Heart J.* (2008) 156:216–26.e9. doi: 10.1016/j.ahj.2008.03.024
32. Tigue CC, McKoy JM, Evens AM, Trifilio SM, Tallman MS, Bennett CL. Granulocyte-colony stimulating factor administration to healthy individuals and persons with chronic neutropenia or cancer: an overview of safety considerations from the research on adverse drug events and reports project. *Bone Marrow Transplant.* (2007) 40:185–92. doi: 10.1038/sj.bmt.1705722
33. Ponikowski P, Voors AA, Anker SD, Bueno H, Cleland JG, Coats AJ, et al. 2016 ESC guidelines for the diagnosis and treatment of acute and chronic heart failure. *Rev Esp Cardiol.* (2016) 18:891–975. doi: 10.1002/ejhf.592

Conflict of Interest: The authors declare that the research was conducted in the absence of any commercial or financial relationships that could be construed as a potential conflict of interest.

Publisher's Note: All claims expressed in this article are solely those of the authors and do not necessarily represent those of their affiliated organizations, or those of the publisher, the editors and the reviewers. Any product that may be evaluated in this article, or claim that may be made by its manufacturer, is not guaranteed or endorsed by the publisher.

frontiers | Frontiers in Cardiovascular Medicine

BRIEF RESEARCH REPORT
published: 22 June 2022
doi: 10.3389/fcvm.2022.936142

Distinct Contribution of Global and Regional Angiotensin II Type 1a Receptor Inactivation to Amelioration of Aortopathy in *Tgfbr1*$^{M318R/+}$ Mice

Emily E. Bramel[1,2], *Rustam Bagirzadeh*[1], *Muzna Saqib*[1], *Tyler J. Creamer*[1], *Wendy A. Espinoza Camejo*[1,2], *LaToya Ann Roker*[3], *Jennifer Pardo Habashi*[4], *Harry C. Dietz*[1,5] *and Elena Gallo MacFarlane*[1,6]*

[1] McKusick-Nathans Department of Genetic Medicine, Johns Hopkins University School of Medicine, Baltimore, MD, United States, [2] Predoctoral Training in Human Genetics and Molecular Biology, Johns Hopkins University School of Medicine, Baltimore, MD, United States, [3] School of Medicine Microscope Facility, Johns Hopkins University School of Medicine, Baltimore, MD, United States, [4] Division of Pediatric Cardiology, Johns Hopkins Medicine, Baltimore, MD, United States, [5] Howard Hughes Medical Institute, Chevy Chase, MD, United States, [6] Department of Surgery, Johns Hopkins University School of Medicine, Baltimore, MD, United States

OPEN ACCESS

Edited by:
Hong S. Lu,
University of Kentucky, United States

Reviewed by:
Jeff Zheying Chen,
University of Texas Southwestern Medical Center, United States
Takayuki Morisaki,
The University of Tokyo, Japan

***Correspondence:**
Elena Gallo MacFarlane
egallo1@jhmi.edu

Specialty section:
This article was submitted to Cardiovascular Therapeutics, a section of the journal Frontiers in Cardiovascular Medicine

Received: *04 May 2022*
Accepted: *30 May 2022*
Published: *22 June 2022*

Citation:
Bramel EE, Bagirzadeh R, Saqib M, Creamer TJ, Espinoza Camejo WA, Roker LA, Pardo Habashi J, Dietz HC and Gallo MacFarlane E (2022) Distinct Contribution of Global and Regional Angiotensin II Type 1a Receptor Inactivation to Amelioration of Aortopathy in Tgfbr1$^{M318R/+}$ Mice. Front. Cardiovasc. Med. 9:936142. doi: 10.3389/fcvm.2022.936142

Angiotensin II (Ang II) type 1 receptor (AT1R) signaling controls both physiological and pathogenetic responses in the vasculature. In mouse models of Loeys-Dietz syndrome (LDS), a hereditary disorder characterized by aggressive aortic aneurysms, treatment with angiotensin receptor blockers (ARBs) prevents aortic root dilation and associated histological alterations. In this study we use germline and conditional genetic inactivation of *Agtr1a* (coding for the AT1a receptor) to assess the effect of systemic and localized AT1R signaling attenuation on aortic disease in a mouse model of LDS (*Tgfbr1*$^{M318R/+}$). Aortic diameters and histological features were examined in control and *Tgfbr1*$^{M318R/+}$ mice with either germline or *Mef2C*^{SHF}*-Cre* mediated genetic inactivation of *Agtr1a*, the latter resulting in deletion in second heart field (SHF)-derived lineages in the aortic root and proximal aorta. Both systemic and regional AT1R signaling attenuation resulted in reduction of diameters and improvement of tissue morphology in the aortic root of LDS mice; these outcomes were associated with reduced levels of Smad2/3 and ERK phosphorylation, signaling events previously linked to aortic disease in LDS. However, regional AT1a inactivation in SHF-derived lineages resulted in a more modest reduction in aortic diameters relative to the more complete effect of germline *Agtr1a* deletion, which was also associated with lower blood pressure. Our findings suggest that the therapeutic effects of AT1R antagonisms in preclinical models of aortic disease depend on both regional and systemic factors and suggest that combinatorial approaches targeting both processes may prove beneficial for aneurysm mitigation.

Keywords: Loeys-Dietz Syndrome, aortic aneurysm, ARBs, angiotensin II type 1 receptor, VSMC

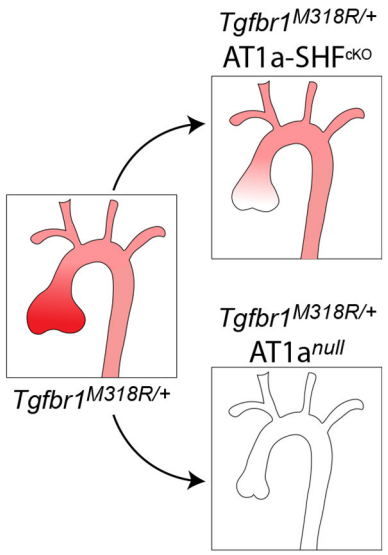

GRAPHICAL ABSTRACT | The aortic root, which is composed primarily of SHF-derived cells, is a site of increased susceptibility to dilation in both patients and mouse models of Loeys-Dietz Syndrome (*Tgfbr1*$^{M318R/+}$). This increased risk associates with regionally increased expression of AT1a (shown in red). Both SHF-specific (AT1a-SHF^{cKO}) and germline (AT1a^{null}) deletion of AT1a reduce aortic root dilation and associated histopathological alterations in *Tgfbr1*$^{M318R/+}$ mice, with the latter, however, having a more pronounced effect.

INTRODUCTION

Aneurysms of the thoracic aorta are characterized by progressive weakening of the aortic wall resulting first in dilation and, ultimately, life-threatening dissection and rupture (1, 2). Aortic pathology is primarily linked to maladaptive changes in vascular smooth muscle cells (VSMC) and defective remodeling of the extracellular matrix; however, systemic factors, such as elevated blood pressure, can further promote disease (3). Angiotensin II (Ang II) signaling *via* the Ang II type 1 receptor (AT1R) activates several signaling pathways that can influence aneurysm pathogenesis both systemically, through regulation of vasoconstriction and fluid homeostasis, and locally, through regulation of VSMC phenotype, matrix deposition and inflammation (4–6). Although rodents have two types of AT1R, AT1a and AT1b, signaling *via* the AT1a receptor (encoded by the *Agtr1a* gene) plays the primary role in promotion of aneurysm pathogenesis (7, 8). Binding of Ang II to AT1R directly activates specific signaling cascades, including those mediated by mitogen-activated protein kinases (MAPK) (6); engagement of AT1R can also lead to transactivation of growth factor receptors and increased expression of components of other signaling pathways, including those activated by Transforming Growth Factor-β (TGF-β), Platelet-derived growth factor (PDGF), and reactive oxygen species (ROS) (5, 9–11).

Loeys-Dietz Syndrome (LDS) is a hereditary aneurysm disorder caused by heterozygous inactivating mutations in positive effectors of the TGF-β signaling pathway; these mutations result in an initial impairment of signaling output, which is followed by compensatory upregulation at sites of disease (12–19). Although these mutations occur in genes expressed ubiquitously in the aorta, the aortic root is a site of increased susceptibility to dilation (18, 19). As observed in other mouse models of aortic aneurysm, aortic root dilation in LDS mouse models is prevented by treatment with angiotensin receptor blockers (ARB), in association with lowered blood pressure and attenuated AT1R-dependent signaling in the aortic wall (5, 18–20).

Second heart field (SHF) progenitors, identified in mice by conditional genetic reporters and the *Mef2C*^{SHF}*-Cre* transgene (21), give rise to vascular smooth muscle cells (VSMCs), aortic fibroblasts and endothelial cells, all of which contribute to morphogenesis of the aortic wall (22). Whereas SHF-derived cells predominate in the root and proximal aorta, the contribution of VSMCs derived from the cardiac-neural crest (CNC) increases progressively along the proximal-to-distal axis (23, 24). Our previous work and that of others have shown that SHF-derived VSMCs are intrinsically more sensitive to the effects of LDS-causing mutations (18, 25, 26), express higher levels of *Agtr1a*, and show increased responsiveness to Ang II in culture (18), suggesting that AT1R signaling in these cells is a contributor to pathogenesis. In this study, we test the systemic and SHF-specific contribution of AT1a receptor signaling to aortic dilation in the *Tgfbr1*$^{M318R/+}$ LDS mouse model by examining the aortic phenotype in mice with either germline or *Mef2C*^{SHF}*-Cre* mediated *Agtr1a* deletion.

METHODS

Animals

All animal experiments were conducted following protocols approved by the Animal Care and Use Committee at Johns Hopkins University School of Medicine. Mice were housed in the animal facility with unlimited access to standard chow and water with a light/dark cycle of 10/14 h. All mice were backcrossed to 129S6/SvEv mice (Taconic, 129SVE) for at least five generations; all experiments used littermates and cohort-mates as controls. *Tgfbr1*$^{+/+}$and *Tgfbr1*$^{M318R/+}$(19) were bred to *Agtr1a*$^{flox/flox}$ (The Jackson Laboratory, strain #016211) (27) mice, some bearing the *Mef2c*^{SHF}-Cre transgene (gifted by the K.R. Chien lab at the Cardiovascular Research Center, Massachusetts General Hospital, Boston, Massachusetts, USA), to generate mice with second heart field-specific deletion of *Agtr1a*. These mice are referred to as AT1a^{SHFcKO}. *Tgfbr1*$^{+/+}$and *Tgfbr1*$^{M318R/+}$ were also bred to mice with a global deletion of *Agtr1a*$^{D/D}$, which were generated by deletion of the *Agtr1a*^{flox} allele *via* a germline recombination event. These mice are referred to as AT1a^{null}. Mice were genotyped twice, once at the beginning and then at the end of the study, using protocols described in Chen et al. (8) for the *Agtr1a* locus and Gallo et al. (19) for the *Tgfbr1* locus.

Echocardiography and Blood Pressure Measurements

Aortic dimensions were monitored by serial echocardiography using the Visual Sonics Vivo 2100 machine and a 30

mHz probe using a parasternal long-axis view, as previously described (18). Three independent measurements of the maximal internal diameters at the sinus of Valsalva were averaged for aortic root measurements; for ascending aorta measurements, measurements were taken at the maximal diameter. All measurements were taken during systole, with on open aortic valve. Operators blinded to genotype were responsible for imaging and measurements. Tail cuff blood pressure measurements were taken for mice using the Visitech BP-2000 Non-Invasive tail cuff device, also as previously described (19).

RNA Extraction and qPCR

RNA was extracted according to previously described protocols (28). In brief, dissected aortic root tissue was placed in TRIzol (ThermoFisher, 15596018) and lysed using an MP Biomedicals FastPrep-24 5G automatic bead homogenizer. A Direct-zol RNA MiniPrep kit (Zymo Research, R2052) was used to extract and purify RNA according to the manufacturer's instructions. The High-Capacity cDNA Reverse Transcription kit (Applied Biosystems, 4368813) was used according to the manufacturer's protocol and qPCR was performed using TaqMan reagents and probes (Applied Biosystems, 4369016; *Agtr1a* Mm01166161_m1, *Hprt* Mm00446968_m1) and run on the QuantStuido7 Flex.

Aortic Tissue Preparation and Histology

After euthanasia by halothane inhalation (Millipore Sigma, H0150000) at a standard concentration (4%, 0.2 ml/L of container volume), the heart and thoracic aorta were dissected *en bloc*. Samples were then fixed overnight at 4°C in 4% paraformaldehyde in PBS (Electron Microscopy Sciences, 15710). The following day, samples were transferred to six well plates containing 70% ethanol and left overnight at 4°C. The entire sample was embedded in 2% agarose prior to paraffin embedding. Paraffin blocks were then cut into 5-μm radial sections (resulting in a longitudinal view of the vessel) that were either stained with Verhoeff-van Gieson (VVG; StatLab, STVGI) or used for immunofluorescence as described below. Slides stained with VVG were imaged using an Eclipse E400 microscope (Nikon Inc.) at 40× magnification.

Quantification of Elastic Fiber Content

Elastic fiber content per area unit was quantified by a staff member of the Johns Hopkins School of Medicine Microscope Facility, who was blinded to the genotype of the VVG-stained sections. Color-decon2 (29) was used for unbiased automated selection of the two regions of interest (ROIs), elastic fibers and the cellular area in-between, and separation of corresponding vectors to individual channels. High intensity results, which identified blood cells, and very low intensity results, which identified non-vascular areas, were excluded from further analysis. Individual channels for each ROI were then converted to "binary" to measure the corresponding gray value (30), and this value was then converted to area to obtain the relative ratio of "elastic fiber" to "cells" content.

Immunofluorescence

The following protocol was adapted from Cell Signaling Technology's Immunofluorescence Protocol with Formaldehyde Fixation. Paraffin-embedded sections were baked at 60°C for 15 min. Slides were deparaffinized in xylene and rehydrated by immersing in a graded alcohol series: 100% ethanol, 95% ethanol, 70% ethanol and 1× PBS for 3 min each. Slides were then incubated in an antigen retrieval solution (10 mM sodium citrate buffer, 0.05% tween, pH 6.0) for 15 min at 90°C in a water bath. After cooling to room temperature, slides were incubated in fresh sodium borohydride solution (10 mg/ml PBS; Sigma-Aldrich, 452882) for 20 min. Slides were permeabilized with 1× TBS (Quality Biological, 351086101) + 0.1% Triton X-100 (Sigma-Aldrich, T9284) + 0.1 M glycine (Sigma-Aldrich, G8898) for 20 min, then incubated with Fc Receptor Blocker (Innovex, NB309) for 20 min at room temperature, and then Background Buster (Innovex, NB306) for another 20 min. Slides were rinsed with 1× TBS + Triton X-100 (TBT) and then incubated with either P-Smad3 (Abcam, ab52903) at 1:50 or P-ERK (Cell Signaling Technology, 4370) at 1:200 overnight at 4°C in a humid chamber. Slides were rinsed twice with TBT for 5 min in Donkey Anti-Rabbit Alexa Fluor 555 (ThermoFisher, A32794) at 1:100 for 45 min. Slides were again washed two times with TBT and once with TBS prior to mounting with Hard Set Mounting Media with DAPI (VECTASHIELD, H-1500). Images were acquired on a Zeiss LSM880 Airyscan FAST confocal microscope at 20× magnification and are presented as maximal intensity projection. Image adjustments to enhance visualization of information present in the original were applied equally across samples.

Statistics

All statistical analyses were performed using GraphPad Prism 9. A $Q = 5\%$ in ROUT test was selected *a priori* as an exclusion criterion for outliers. If present, outliers are shown in figures as gray circles, but not included in tests for assessment of normality, which were performed using the Shapiro-Wilk test. Data that passed normality test upon exclusion of outliers was considered normally distributed and analyzed using Brown-Forsythe and Welch ANOVA test, with no assumptions as to equal variance among groups. The two-stage linear step-up procedure of Benjamini, Krieger and Yekutieli was used for multiple comparison correction. Dataset that failed the normality test were analyzed using Kruskal–Wallis test, also followed by the two-stage linear step-up procedure of Benjamini, Krieger and Yekutieli for multiple comparison correction.

For individual time points, data are presented as a box-and-whiskers plot, with whiskers indicating minimum to maximum points, with all points shown. Growth curves over time were compared using a linear regression model, with least-square regression and no weighting; comparison between slopes was performed using the extra-sum-of-squares F-test, with $P = 0.05$. Error bars in growth curve plots refer to the 95% confidence interval (CI). Survival tables were analyzed using Fisher's exact test.

RESULTS

Tgfbr1$^{M318R/+}$ mice (also referred to as LDS mice in this text), recapitulate many of the features observed in LDS patients, including dilation of the aortic root (18, 19). To determine if global or SHF-specific attenuation of AT1R signaling mitigated aortic dilation in LDS mice, we crossed these and control mice to either mice homozygous for the *Agtr1a*^{D} allele (*Agtr1a*$^{D/D}$, referred to as AT1a^{null}) or to *Agtr1a*$^{flox/flox}$ mice also expressing the *Mef2c*^{SHF}*-Cre* (21) transgene. Serial echocardiography was performed from 8 to 24 weeks of age, and aortic tissue collected and processed for histological analysis at the 24-week timepoint as previously described (18, 19). Blood pressure was also measured prior to sacrifice. Analysis of an initial experimental cohort showed that there were no significant differences in aortic measurements or rate of aortic enlargement between male and female *Tgfbr1*$^{M318R/+}$ mice (**Supplementary Figures 1A–C**) however, control male mice were significantly larger than their female counterparts, and the difference in aortic diameters between female and male *Tgfbr1*$^{M318R/+}$ mice at the 24-week time point approached significance ($P = 0.06$; **Supplementary Figure 1B**). For these reasons, male and female mice were analyzed separately according to current guidelines.

We found that the presence of the *Mef2c*^{SHF}*-Cre* transgene in mice also carrying a *Agtr1a*^{flox}allele resulted in relatively frequent recombination in the germline, leading to generation of both *Agtr1a*$^{flox/D}$*; Mef2c*^{SHF}*-Cre* and *Agtr1a*$^{flox/flox}$*; Mef2c*^{SHF}*-Cre* litters when breeding *Agtr1a*$^{flox/+}$; *Mef2c*^{SHF}*-Cre* or *Agtr1a*$^{flox/flox}$ *Mef2c*^{SHF}*-Cre* mice. Germline recombination occurred in both male and female breeders whenever the *Agtr1a*^{flox}allele was present in mice also carrying the *Mef2c*^{SHF}*-Cre* transgene. However, the presence of the *Agtr1a*^{D} null allele in heterozygosity did not significantly affect blood pressure, *Agtr1a* expression in the aorta, nor aortic size in either *Tgfbr1*$^{+/+}$or *Tgfbr1*$^{M318R/+}$ mice (**Supplementary Figures 2**, **3**). Therefore, *Agtr1a*$^{flox/D}$ and *Agtr1a*$^{flox/flox}$are collectively referred to as controls (AT1a^{Ctrl}) in the absence of the *Cre* recombinase, and as AT1a SHF-deficient mice (AT1a^{SHFcKO}) if also expressing the *Mef2c*^{SHF}*-Cre* recombinase. All ultrasound measurements and genotypes are provided in **Supplementary Table 1**.

Homozygous deletion of *Agtr1a* in SHF-derived lineages resulted in reduced aortic root dimeters in both female and male *Tgfbr1*$^{M318R/+}$ mice relative to AT1a^{Ctrl} controls at the 16-week time-point; however, this effect remained significant only in female mice by 24 weeks of age (**Figures 1A–G**). Female AT1a^{SHFcKO} *Tgfbr1*$^{M318R/+}$ mice but not male mice also showed a reduced rate of growth from 8 to 24 weeks relative to AT1a^{Ctrl} *Tgfbr1*$^{M318R/+}$ mice (**Figures 1D,G**). Blood pressure was not significantly affected by deletion of *Agtr1a* in SHF-derived lineages (**Figures 1H,I**).

Homozygous germline *Agtr1a* deletion resulted in reduction of aortic root diameters and rate of growth in both male and female LDS mice up to 24 weeks of age (**Figures 1A–G**), and also associated with a reduction in blood pressure, consistent with previous analyses of AT1a^{null} mice (31) (**Figures 1H,I**). No significant differences were observed in the diameter of the ascending aorta (**Supplementary Figure 4A**). Although our study was not designed nor powered to detect differences in survival, a significant decrease in survival between male *Tgfbr1*$^{M318R/+}$ relative to control *Tgfbr1*$^{+/+}$ mice was noted (**Supplementary Figure 4B**).

Histological sections of aortas were stained to visualize tissue architecture and elastic fibers, and the relative content of elastic fiber to cellular area was quantified using an ImageJ macro. Both AT1a^{null} and AT1a^{SHFcKO} *Tgfbr1*$^{M318R/+}$ mice, of either sex, showed improved elastic fiber content relative to AT1a^{Ctrl} *Tgfbr1*$^{M318R/+}$ mice (**Figure 2** and **Supplementary Figure 5**). This improvement correlated with reduced levels of phosphorylation of both Smad2 and Smad3 (p-Smad2/3) and extracellular signal-regulated kinase 1 and 2 (p-ERK1/2), two signaling events previously shown to correlate with severity of aortic disease in mouse models of LDS and related conditions (5) (**Figures 3A,B** and **Supplementary Figure 6**). No specific localization relative to inner or outer media was noted for either p-Smad2/3 or p-ERK1/2 signal, possibly in consequence of the advanced stage of aortic disease and media disruption at the time point examined. However, whereas p-ERK1/2 signal was detectable in the endothelial and adventitial layer regardless of genotype or disease status, both systemic and SHF-specific AT1a deletion resulted in reduced p-ERK1/2 levels across the media compared *Tgfbr1*$^{M318R/+}$ mice, which is consistent with previous observations (19).

DISCUSSION

Administration of ARBs such as losartan has been shown to ameliorate aortic pathology in several mouse models of aneurysm, including LDS (5, 8, 18–20, 32). However, experiments based on pharmacological antagonism cannot disentangle the potential benefits of local antagonism from those accrued thanks to systemic effects. In addition, the existence of potential off-targets for drugs such as losartan has led to the hypothesis that some benefits of ARB administration may result from AT1R-independent effects (33).

In this study, we show that genetic deletion of AT1a in SHF-derived cells, which include VSMC residing primarily in the aortic root but also fibroblasts and subsets of endothelial cells (22), mitigates aortic dilation and improves aortic tissue architecture in LDS mice. However, this intervention fails to recapitulate the more robust reduction in aortic diameters observed after germline AT1a inactivation, particularly at later time points in male mice. We hypothesize that the additional benefit of systemic AT1a inactivation on aortic diameters may be due to both ablation in AT1a receptor signaling in non-SHF-derived cells and, possibly, lessening of mechanical stresses on the weakened wall secondary to reduction in blood pressure. Although our previous work showed that only SHF-derived VSMCs had higher expression of *Agtr1a* and increased responsiveness to Ang II (18), it is possible that AT1a receptor signaling in non-SHF-derived cells, including endothelial cells, may also play a role in LDS aortic dilation, similarly to what has been observed in other mouse models (27, 34).

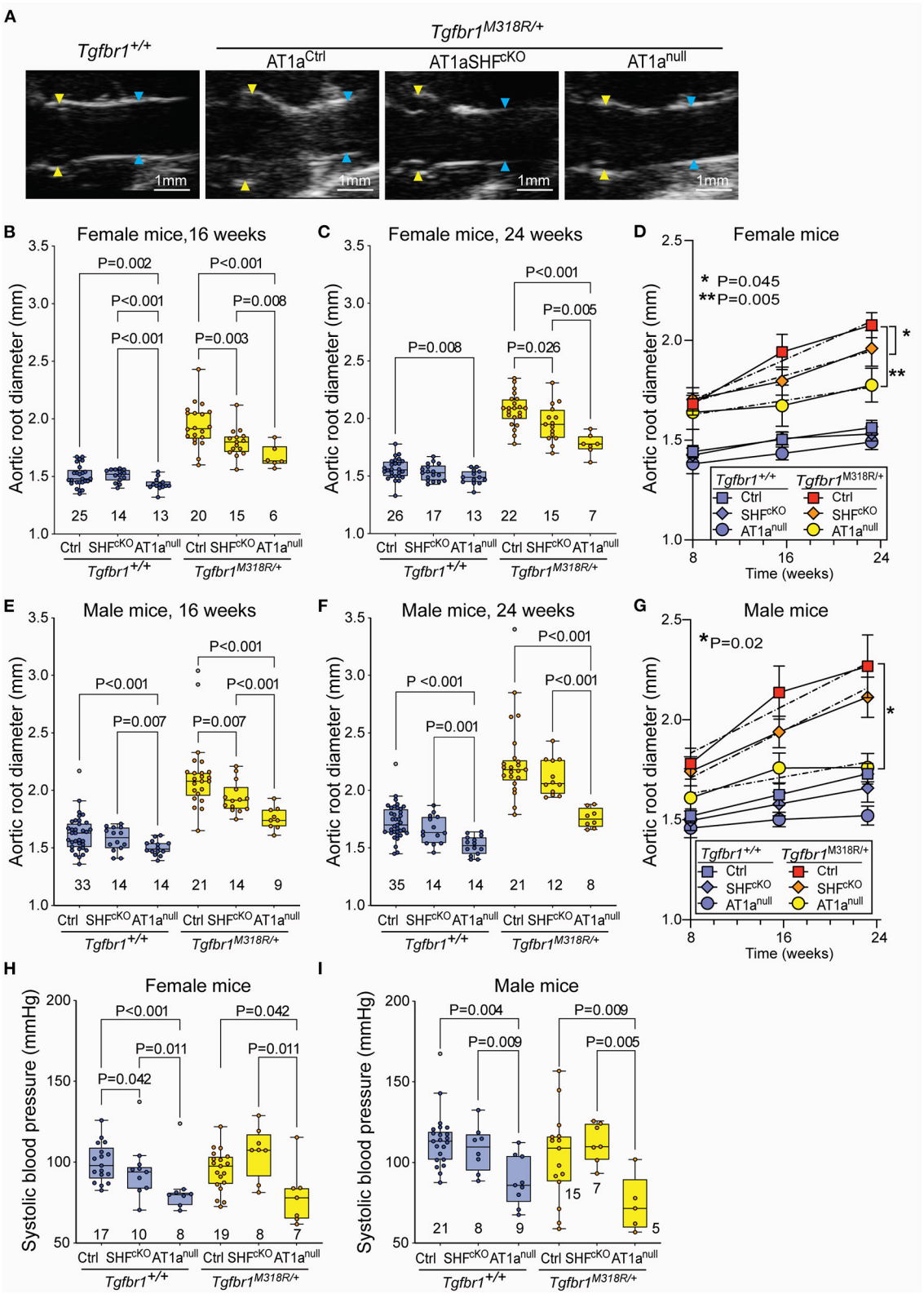

FIGURE 1 | Global and SHF-specific deletion of *Agtr1a* result in reduction of aortic root dilation in LDS mice. **(A)** Representative echocardiograms of *Tgfbr1*$^{+/+}$ and *Tgfbr1*$^{M318R/+}$mice with and without conditional (AT1a^{SHFcKO}) or global (AT1a^{null}) deletion of *Agtr1a*, the aortic root is indicated by yellow arrows while the ascending aorta is indicated by blue arrows. Aortic root diameter as measured by echocardiography in both females **(B–D)** and males **(E–G)** at indicated time points. *Tgfbr1*$^{+/+}$

(Continued)

FIGURE 1 | mice are shown in blue and *Tgfbr1*$^{M318R/+}$ are shown in yellow. The number of animals per group is indicated. *P*-values refer to Brown-Forsythe ANOVA, followed by *post-hoc* test with multiple comparison FDR correction. In panel **(C,E)**, the error bars represent the 95% Confidence Interval (CI), the dashed line indicates a simple linear-regression of serial echocardiographic measurements of aortic root diameter from 8 to 24 weeks of age; *P*-value refers to comparison between slopes using the extra-sum-of-squares *F*-test in GraphPad. **(H,I)** Systolic blood pressure as measured at 24 weeks of age. *P*-values refer to Brown-Forsythe ANOVA, followed by *post-hoc* test with multiple comparison FDR correction.

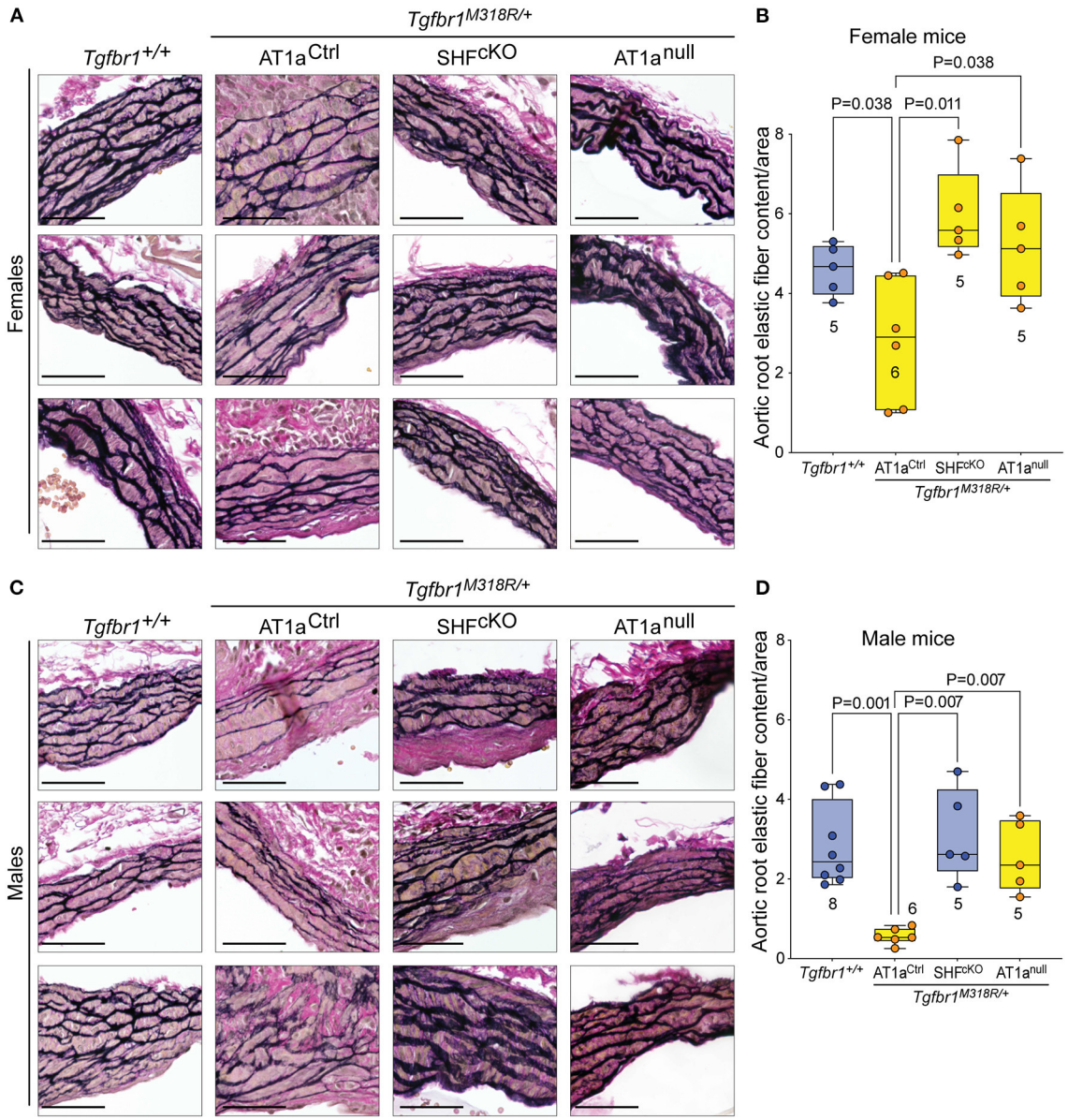

FIGURE 2 | Global and SHF-specific deletion of *Agtr1a* result in improved histopathology. Representative sections of VVG-stained aortic roots and quantification of elastic fiber content relative to cellular area for female **(A,B)** and male **(C,D)** samples of indicated genotypes. Three representative images are shown per genotype for each sex. Images are shown at 20× magnification. Scale bar is 50 μm. Quantification of elastic fiber content relative to cellular area is shown in **(C)** for female samples, and in **(D)** for male samples, with higher value indicating a greater content of elastic fiber per area unit. The number of mice scored per group is indicated. *P*-values refer to Brown-Forsythe ANOVA, followed by *post-hoc* test with multiple comparison FDR correction.

Although we did not observe significant sexual dimorphism in the absence of additional genetic perturbations, there was a trend for larger aortic root diameters in male *Tgfbr1*$^{M318R/+}$ mice relative to their female counterparts, especially at later time points. This was accompanied by a significant reduction of aortic root diameters in female but not male *Tgfbr1*$^{M318R/+}$ mice

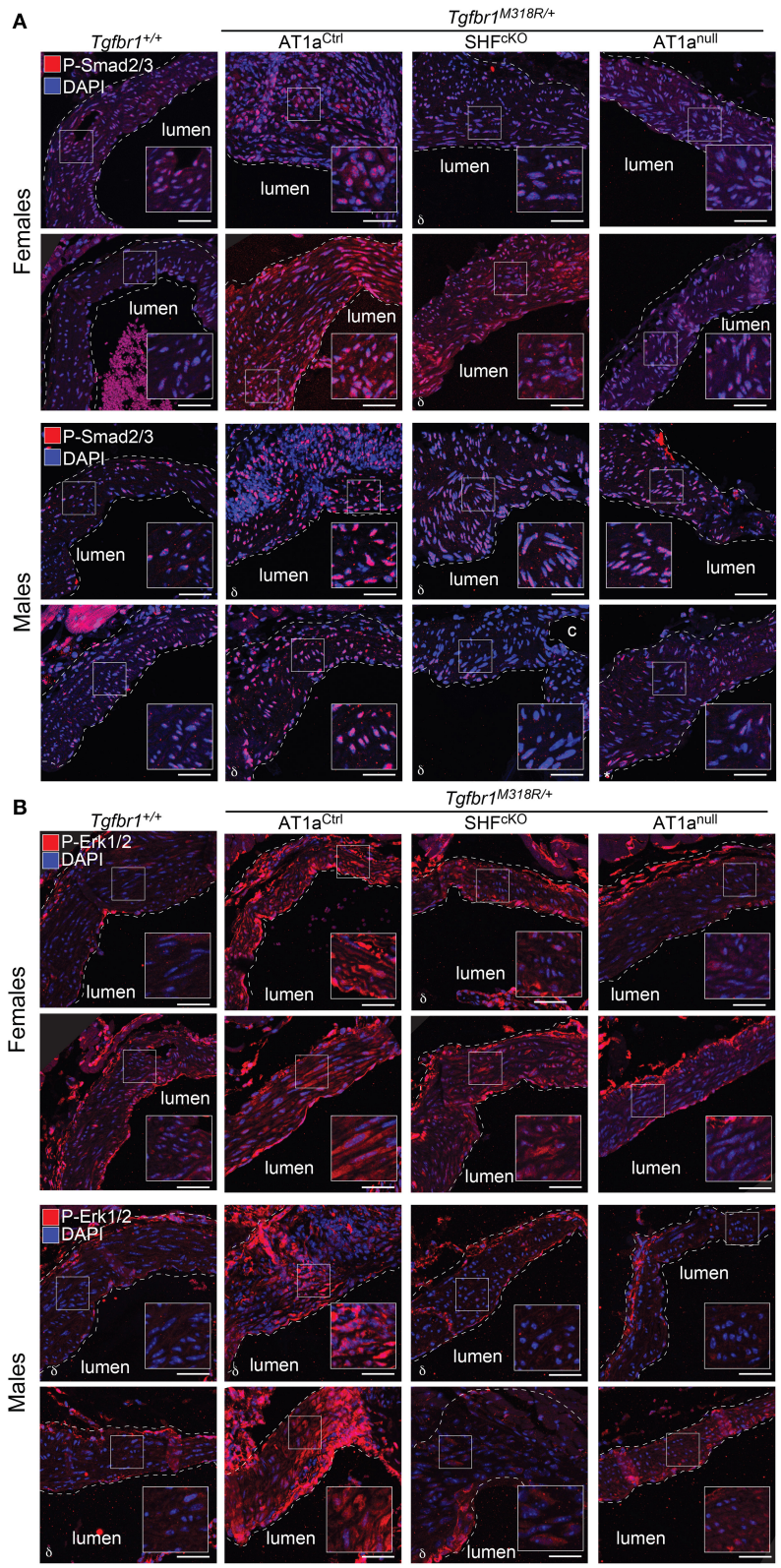

FIGURE 3 | Global and SHF-specific deletion of *Agtr1a* result in reduced p-Smad2/3 and p-ERK1/2 signaling. Representative images of immunofluorescence for **(A)** p-Smad2/3 and **(B)** p-ERK1/2 at 24 weeks of age. Four independent biological replicates are shown per genotype, two from male animals and two from female animals. Insets identify locations shown at higher magnification. Images were acquired at 20× magnification. Scale bar is 50 μm. δ symbol in the left-hand corner of a given image indicates the section is from an animal heterozygous for the *Agtr1a*^{D} null allele.

with homozygous *Agtr1a* deletion in SHF-derived cells relative to controls. The presence of sexual dimorphism in LDS mouse models under specific circumstances is consistent with reports showing similar patterns in other hereditary connective tissue disorders, including both patients and mouse models of Marfan and Ehlers-Danlos syndrome (35–38). Although the mechanisms remain unclear, angiotensin II-driven aortic pathogenesis has been consistently shown to be accentuated in males relatively to females (39). We hypothesize that the severity of aortic disease in LDS mouse models generally masks the subtle effect of sexually dimorphic hormonal or chromosomal contributions, and that these effects may become more apparent in specific contexts that result in moderate amelioration of pathogenesis.

Despite its well-documented efficacy in preclinical animal models, randomized trials using the ARB losartan at doses sufficient to successfully reduced blood pressure have shown more modest and sometimes mixed results in the treatment of aneurysm in Marfan syndrome (MFS) (5, 40–42). Our study suggests that regional AT1R inhibition may be important for amelioration of aortic tissue architecture, and that better outcomes may be possible using strategies able to suppress both local and systemic AT1R signaling. Although this study explored the effects of AT1R inhibition only in the proximal thoracic aorta, the multiplicity of roles played by this signaling pathway in both physiological and pathological processes suggests that its inhibition may influence other LDS-associated phenotypes (12–19). An exploration of the effects of AT1 inhibition on both vascular and non-vascular LDS connective tissue anomalies would provide stronger evidence of therapeutic benefit.

Notably, a recent study by Chen et al. (8) has shown that administration of antisense oligonucleotides results in stable and durable reduction in levels of angiotensinogen, the precursor to Ang II, resulting in protection from aortic disease in the *Fbn1*$^{C1041G/+}$ MFS mouse model. We speculate strategies that better mimic the early, robust, and continuous suppression of AT1R signaling achieved in animal models by germline deletion of *Agtr1a* (or by early ARB administration in drinking water and/or osmotic pump) may prove more efficacious for medical therapy in LDS and related conditions.

DATA AVAILABILITY STATEMENT

The original contributions presented in the study are included in the article/**Supplementary Material**, further inquiries can be directed to the corresponding author.

ETHICS STATEMENT

The animal study was reviewed and approved by the Johns Hopkins University Animal Care and Use Committee.

AUTHOR CONTRIBUTIONS

EG and HD are responsible for the conception and design of this study. RB initiated much of the experimental work, including animal breeding and echocardiography. JP acquired and analyzed echocardiographic images. EB and TC assisted with echocardiography and animal breeding. MS assisted in genotyping and performed the histological staining. EB and WE performed the immunofluorescence. LR developed a macro in Image J to quantify the elastic fiber content relative to cellular area in aortic sections. EB assisted EG in writing and preparing figures for the manuscript. All authors contributed to manuscript revision, read, and approved the submitted version.

FUNDING

Research reported in this publication was supported by the National Heart, Lung, and Blood Institute of the National Institutes of Health under award number R01HL147947 and by a generous gift from the Loeys-Dietz Foundation. EM was also supported by funding provided to Johns Hopkins by the Broccoli family. Image acquisition was also supported by NIH award number S10OD023548 to the School of Medicine Microscope Facility.

ACKNOWLEDGMENTS

We thank Djahida Bedja for assistance in the acquisition of ultrasound images, and the Dietz laboratory for sharing resources, protocols, and helpful advice for this work.

SUPPLEMENTARY MATERIAL

The Supplementary Material for this article can be found online at: https://www.frontiersin.org/articles/10.3389/fcvm.2022.936142/full#supplementary-material

REFERENCES

1. Shen YH, LeMaire SA, Webb NR, Cassis LA, Daugherty A, Lu HS. Aortic aneurysms and dissections series. *Arterioscler Thromb Vasc Biol.* (2020) 40:e37–46. doi: 10.1161/ATVBAHA.120.313991
2. Shen YH, LeMaire SA, Webb NR, Cassis LA, Daugherty A, Lu HS. Aortic aneurysms and dissections series: part II: dynamic signaling responses in aortic aneurysms and dissections. *Arterioscler Thromb Vasc Biol.* (2020) 40:e78–86. doi: 10.1161/ATVBAHA.120.313804
3. Boczar KE, Boodhwani M, Beauchesne L, Dennie C, Chan KL, Wells GA, et al. Aortic stiffness, central blood pressure, and pulsatile arterial load predict future thoracic aortic aneurysm expansion. *Hypertension.* (2021) 77:126–34. doi: 10.1161/HYPERTENSIONAHA.120.16249
4. Kawai T, Forrester SJ, O'Brien S, Baggett A, Rizzo V, Eguchi S. AT1 receptor signaling pathways in the cardiovascular system. *Pharmacol Res.* (2017) 125(Pt A):4–13. doi: 10.1016/j.phrs.2017.05.008
5. van Dorst DCH, de Wagenaar NP, van der Pluijm I, Roos-Hesselink JW, Essers J, Danser AHJ. Transforming growth factor-beta and the renin-angiotensin system in syndromic thoracic aortic aneurysms:

implications for treatment. *Cardiovasc Drugs Ther.* (2020) 41:1233–52. doi: 10.1007/s10557-020-07116-4
6. Forrester SJ, Booz GW, Sigmund CD, Coffman TM, Kawai T, Rizzo V, et al. Angiotensin II signal transduction: an update on mechanisms of physiology and pathophysiology. *Physiol Rev.* (2018) 98:1627–738. doi: 10.1152/physrev.00038.2017
7. Poduri A, Owens AP. 3rd, Howatt DA, Moorleghen JJ, Balakrishnan A, Cassis LA, et al. Regional variation in aortic AT1b receptor mRNA abundance is associated with contractility but unrelated to atherosclerosis and aortic aneurysms. *PLoS ONE.* (2012) 7:e48462. doi: 10.1371/journal.pone.0048462
8. Chen JZ, Sawada H, Ye D, Katsumata Y, Kukida M, Ohno-Urabe S, et al. Deletion of AT1a (Angiotensin II Type 1a) receptor or inhibition of angiotensinogen synthesis attenuates thoracic aortopathies in Fibrillin1$^{c1041g/+}$ mice. *Arterioscler Thromb Vasc Biol.* (2021) 41:2538–50. doi: 10.1161/ATVBAHA.121.315715
9. Gibbons GH, Pratt RE, Dzau VJ. Vascular smooth muscle cell hypertrophy vs. hyperplasia autocrine transforming growth factor-beta 1 expression determines growth response to angiotensin II. *J Clin Invest.* (1992) 90:456–61. doi: 10.1172/JCI115881
10. Marchesi C, Paradis P, Schiffrin EL. Role of the renin-angiotensin system in vascular inflammation. *Trends Pharmacol Sci.* (2008) 29:367–74. doi: 10.1016/j.tips.2008.05.003
11. Sanchez-Guerrero E, Midgley VC, Khachigian LM. Angiotensin II induction of PDGF-C expression is mediated by AT1 receptor-dependent Egr-1 transactivation. *Nucleic Acids Res.* (2008) 36:1941–51. doi: 10.1093/nar/gkm923
12. Loeys BL, Chen J, Neptune ER, Judge DP, Podowski M, Holm T, et al. A syndrome of altered cardiovascular, craniofacial, neurocognitive and skeletal development caused by mutations in TGFBR1 or TGFBR2. *Nat Genet.* (2005) 37:275–81. doi: 10.1038/ng1511
13. van de Laar IM, Oldenburg RA, Pals G, Roos-Hesselink JW, de Graaf BM, Verhagen JM, et al. Mutations in *SMAD3* cause a syndromic form of aortic aneurysms and dissections with early-onset osteoarthritis. *Nat Genet.* (2011) 43:121–6. doi: 10.1038/ng.744
14. Lindsay ME, Schepers D, Bolar NA, Doyle JJ, Gallo E, Fert-Bober J, et al. Loss-of-function mutations in *TGFB2* cause a syndromic presentation of thoracic aortic aneurysm. *Nat Genet.* (2012) 44:922–7. doi: 10.1038/ng.2349
15. Wischmeijer A, Van Laer L, Tortora G, Bolar NA, Van Camp G, Fransen E, et al. Thoracic aortic aneurysm in infancy in aneurysms-osteoarthritis syndrome due to a novel *SMAD3* mutation: further delineation of the phenotype. *Am J Med Genet A*. (2013) 161A:1028–35. doi: 10.1002/ajmg.a.35852
16. MacCarrick G, Black JH 3rd, Bowdin S, El-Hamamsy I, Frischmeyer-Guerrerio PA, Guerrerio AL, et al. Loeys-Dietz Syndrome: a primer for diagnosis and management. *Genet Med.* (2014) 16:576–87. doi: 10.1038/gim.2014.11
17. Bertoli-Avella AM, Gillis E, Morisaki H, Verhagen JM, de Graaf BM, van de Beek G, et al. Mutations in a TGF-beta ligand, *TGFB3*, cause syndromic aortic aneurysms and dissections. *J Am Coll Cardiol.* (2015) 65:1324–36.
18. MacFarlane EG, Parker SJ, Shin JY, Kang BE, Ziegler SG, Creamer TJ, et al. Lineage-specific events underlie aortic root aneurysm pathogenesis in Loeys-Dietz syndrome. *J Clin Invest.* (2019) 129:659–75. doi: 10.1172/JCI123547
19. Gallo EM, Loch DC, Habashi JP, Calderon JF, Chen Y, Bedja D, et al. Angiotensin II-dependent TGF-beta signaling contributes to Loeys-Dietz Syndrome vascular pathogenesis. *J Clin Invest.* (2014) 124:448–60. doi: 10.1172/JCI69666
20. Cook JR, Clayton NP, Carta L, Galatioto J, Chiu E, Smaldone S, et al. Dimorphic effects of transforming growth factor-beta signaling during aortic aneurysm progression in mice suggest a combinatorial therapy for Marfan syndrome. *Arterioscler Thromb Vasc Biol.* (2015) 35:911–7. doi: 10.1161/ATVBAHA.114.305150
21. Verzi MP, McCulley DJ, De Val S, Dodou E, Black BL. The right ventricle, outflow tract, and ventricular septum comprise a restricted expression domain within the secondary/anterior heart field. *Dev Biol.* (2005) 287:134–45. doi: 10.1016/j.ydbio.2005.08.041
22. Sawada H, Katsumata Y, Higashi H, Zhang C, Li Y, Morgan S, et al. Second heart field-derived cells contribute to angiotensin II-mediated ascending aortopathies. *Circulation.* (2022) 145:987–1001. doi: 10.1161/CIRCULATIONAHA.121.058173
23. Buckingham M, Meilhac S, Zaffran S. Building the mammalian heart from two sources of myocardial cells. *Nat Rev Genet.* (2005) 6:826–35. doi: 10.1038/nrg1710
24. Sawada H, Rateri DL, Moorleghen JJ, Majesky MW, Daugherty A. Smooth muscle cells derived from second heart field and cardiac neural crest reside in spatially distinct domains in the media of the ascending aorta-brief report. *Arterioscler Thromb Vasc Biol.* (2017) 37:1722–6. doi: 10.1161/ATVBAHA.117.309599
25. Gong J, Zhou D, Jiang L, Qiu P, Milewicz DM, Chen YE, et al. *In vitro* lineage-specific differentiation of vascular smooth muscle cells in response to Smad3 deficiency: implications for Smad3-related thoracic aortic aneurysm. *Arterioscler Thromb Vasc Biol.* (2020) 40:1651–63. doi: 10.1161/ATVBAHA.120.313033
26. Zhou D, Feng H, Yang Y, Huang T, Qiu P, Zhang C, et al. hiPSC modeling of lineage-specific smooth muscle cell defects caused by Tgfbr1(A230T) variant, and its therapeutic implications for Loeys-Dietz Syndrome. *Circulation.* (2021) 144:1145–59. doi: 10.1161/CIRCULATIONAHA.121.054744
27. Rateri DL, Moorleghen JJ, Balakrishnan A, Owens AP 3rd, Howatt DA, Subramanian V, et al. Endothelial cell-specific deficiency of Ang II type 1a receptors attenuates Ang II-induced ascending aortic aneurysms in Ldl receptor-/- mice. *Circ Res.* (2011) 108:574–81. doi: 10.1161/CIRCRESAHA.110.222844
28. Bramel EE, Creamer TJ, Saqib M, Camejo Nunez WA, Bagirzadeh R, Roker LA, et al. Postnatal *Smad3* inactivation in murine smooth muscle cells elicits a temporally and regionally distinct transcriptional response. *Front Cardiovasc Med.* (2022) 9:826495. doi: 10.3389/fcvm.2022.826495
29. Landini G, Martinelli G, Piccinini F. Colour deconvolution: stain unmixing in histological imaging. *Bioinformatics.* (2021) 37:1485–7. doi: 10.1093/bioinformatics/btaa847
30. Schindelin J, Arganda-Carreras I, Frise E, Kaynig V, Longair M, Pietzsch T, et al. Fiji: an open-source platform for biological-image analysis. *Nat Methods.* (2012) 9:676–82. doi: 10.1038/nmeth.2019
31. Chen D, La Greca L, Head GA, Walther T, Mayorov DN. Blood pressure reactivity to emotional stress is reduced in AT1a-receptor knockout mice on normal, but not high salt intake. *Hypertens Res.* (2009) 32:559–64. doi: 10.1038/hr.2009.59
32. Lu H, Rateri DL, Bruemmer D, Cassis LA, Daugherty A. Involvement of the renin-angiotensin system in abdominal and thoracic aortic aneurysms. *Clin Sci.* (2012) 123:531–43. doi: 10.1042/CS20120097
33. Sellers SL, Milad N, Chan R, Mielnik M, Jermilova U, Huang PL, et al. Inhibition of Marfan syndrome aortic root dilation by Losartan: role of angiotensin II receptor type 1-independent activation of endothelial function. *Am J Pathol.* (2018) 188:574–85. doi: 10.1016/j.ajpath.2017.11.006
34. Galatioto J, Caescu CI, Hansen J, Cook JR, Miramontes I, Iyengar R, et al. Cell type-specific contributions of the angiotensin II type 1a receptor to aorta homeostasis and aneurysmal disease-brief report. *Arterioscler Thromb Vasc Biol.* (2018) 38:588–91. doi: 10.1161/ATVBAHA.117.310609
35. Roman MJ, Devereux RB, Preiss LR, Asch FM, Eagle KA, Holmes KW, et al. Associations of age and sex with Marfan phenotype: the National Heart, Lung, and Blood Institute Gentac (Genetically Triggered Thoracic Aortic Aneurysms and Cardiovascular Conditions) registry. *Circ Cardiovasc Genet*. (2017) 10:e001647. doi: 10.1161/CIRCGENETICS.116.001647
36. Tashima Y, He H, Cui JZ, Pedroza AJ, Nakamura K, Yokoyama N, et al. Androgens accentuate TGF-beta dependent ERK/Smad activation during thoracic aortic aneurysm formation in Marfan syndrome male mice. *J Am Heart Assoc.* (2020) 9:e015773. doi: 10.1161/JAHA.119.015773
37. Bowen CJ, Calderon Giadrosic JF, Burger Z, Rykiel G, Davis EC, Helmers MR, et al. Targetable cellular signaling events mediate vascular pathology in vascular Ehlers-Danlos syndrome. *J Clin Invest.* (2020) 130:686–98. doi: 10.1172/JCI130730
38. Renard M, Muino-Mosquera L, Manalo EC, Tufa S, Carlson EJ, Keene DR, et al. Sex, pregnancy and aortic disease in Marfan syndrome. *PLoS ONE.* (2017) 12:e0181166. doi: 10.1371/journal.pone.0181166

39. Sawada H, Lu HS, Cassis LA, Daugherty A. Twenty years of studying Ang II (Angiotensin II)-induced abdominal aortic pathologies in mice: continuing questions and challenges to provide insight into the human disease. *Arterioscler Thromb Vasc Biol.* (2022) 42:277–88. doi: 10.1161/ATVBAHA.121.317058
40. Al-Abcha A, Saleh Y, Mujer M, Boumegouas M, Herzallah K, Charles L, et al. Meta-analysis examining the usefulness of angiotensin receptor blockers for the prevention of aortic root dilation in patients with the Marfan syndrome. *Am J Cardiol.* (2020) 128:101–6. doi: 10.1016/j.amjcard.2020.04.034
41. van Andel MM, Indrakusuma R, Jalalzadeh H, Balm R, Timmermans J, Scholte AJ, et al. Long-term clinical outcomes of losartan in patients with Marfan syndrome: follow-up of the multicentre randomized controlled compare trial. *Eur Heart J.* (2020) 35:4181–7. doi: 10.1093/eurheartj/ehaa377
42. Muino-Mosquera L, De Backer J. Angiotensin-II receptor blockade in Marfan syndrome. *Lancet.* (2019) 394:2206–7. doi: 10.1016/S0140-6736(19)32536-X

Conflict of Interest: The authors declare that the research was conducted in the absence of any commercial or financial relationships that could be construed as a potential conflict of interest.

Publisher's Note: All claims expressed in this article are solely those of the authors and do not necessarily represent those of their affiliated organizations, or those of the publisher, the editors and the reviewers. Any product that may be evaluated in this article, or claim that may be made by its manufacturer, is not guaranteed or endorsed by the publisher.

frontiers | Frontiers in Cardiovascular Medicine

TYPE Original Research
PUBLISHED 04 August 2022
DOI 10.3389/fcvm.2022.922534

OPEN ACCESS

EDITED BY
Xiaochun Long,
Augusta University, United States

REVIEWED BY
Yuxiang Dai,
Fudan University, China
Xiaofeng Chen,
Wenzhou Medical University, China

*CORRESPONDENCE
Xiaojie Xie
xiexj@zju.edu.cn
Jian'an Wang
wangjianan111@zju.edu.cn

SPECIALTY SECTION
This article was submitted to Cardiovascular Therapeutics, a section of the journal Frontiers in Cardiovascular Medicine

RECEIVED 18 April 2022
ACCEPTED 11 July 2022
PUBLISHED 04 August 2022

CITATION
Huang Y, Zhang N, Xie C, You Y, Guo L, Ye F, Xie X and Wang J (2022) Lipocalin-2 in neutrophils induces ferroptosis in septic cardiac dysfunction *via* increasing labile iron pool of cardiomyocytes. *Front. Cardiovasc. Med.* 9:922534. doi: 10.3389/fcvm.2022.922534

Lipocalin-2 in neutrophils induces ferroptosis in septic cardiac dysfunction *via* increasing labile iron pool of cardiomyocytes

Yuxue Huang, Ning Zhang, Cuiping Xie, Yayu You, Lei Guo, Feiming Ye, Xiaojie Xie* and Jian'an Wang*

Department of Cardiology, Cardiovascular Key Laboratory of Zhejiang Province, Second Affiliated Hospital, Zhejiang University School of Medicine, Hangzhou, China

Cardiac dysfunction is a common complication of sepsis with high mortality. The present study was designed to identify the effect of neutrophil-derived lipocalin-2 (LCN2) in septic cardiac dysfunction (SCD) and its potential mechanism. Wild-type (WT) and LCN2-knockout (LCN2 KO) mice were peritoneally injected with lipopolysaccharide (LPS) to induce SCD. The cardiac function was assessed 12 h after LPS injection by echocardiography. Cardiac tissue was harvested for the evaluation of malonaldehyde (MDA) and prostaglandin E synthase 2 (PTGS2) mRNA levels. LPS induced ferroptosis and SCD in mice. LCN2 deficiency attenuated cardiac injury post-LPS administration. *In vitro*, LCN2 expression in neutrophils increased in response to LPS. Ferroptosis of cardiomyocytes induced by conditioned medium (CM) from LPS-induced neutrophils of WT mice could be attenuated in CM from LPS-induced neutrophils of LCN2 KO mice. Exogenous LCN2 induced H9C2 cell ferroptosis *via* increasing labile iron pool (LIP). In conclusion, our results showed that LCN2 deficiency prevented heart dysfunction and ferroptosis in SCD mice and suggested that neutrophil-derived LCN2 might be a promising therapeutic target for SCD.

KEYWORDS

lipocalin-2, ferroptosis, labile iron pool, septic cardiac dysfunction, neutrophil, neutrophil gelatinase-associated lipocalin

Introduction

Sepsis is identified as a systemic dysregulated immune response to infection or injury, causing life-threatening multiple organ dysfunction. Cardiac dysfunction is present in 10–70% of septic patients and may lead to high mortality as 70–90% in subjects with sepsis (1, 2). Neutrophils, as the most abundant innate immune cells,

can immigrate to infected tissues, and exert anti-infection roles, including phagocytosis, degranulation, and formation of neutrophil extracellular traps (NETs) (3). It has been demonstrated that neutrophil recruitment is important for lipopolysaccharide (LPS)-induced septic mouse models (4).

Lipocalin-2 (LCN2), also known as neutrophil gelatinase-associated lipocalin (NGAL), siderocalin, or 24p3, belongs to the lipocalin superfamily. It is a β-barrel-secreted protein that binds to siderophore-complexed ferric iron with high affinity, which involves various inflammatory processes (5, 6). LCN2 was reported as a biomarker of kidney injury (7) and increased in the neutrophils of patients with alcoholic steatohepatitis (8). High plasma LCN2 also predicted high mortality and cardiac dysfunction in severe sepsis and septic shock patients (9). In the GALLANT trial, plasma LCN2, along with B-type natriuretic peptide, is deemed as a biomarker for patients with acutely decompensated heart failure (10). As for patients with chronic heart failure, plasma LCN2 serves as a predictor for clinical outcomes, including mortality and prognosis (11, 12). The divergent biological roles of LCN2 can be mediated by three receptors on cell membranes, namely, 24p3R, LRP2, and MC4R. 24p3R is the major receptor widely expressed in various cell types of humans and mouse models (6). The binding complex of LCN2/24p3R can carry iron and be internalized into the cytoplasm and subsequently increase intracellular iron (13). It is still unknown whether LCN2 is involved in LPS-induced septic cardiac dysfunction (SCD).

Ferroptosis is a newly identified form of regulated cell death discovered by Dixon et al. with a distinctive feature of iron-dependent lipid peroxidation (14–16). The fact that iron is a key factor in ferroptosis is supported by various experimental studies on the ability of iron chelators to attenuate ferroptosis (14, 15, 17, 18). Cellular labile iron pool (LIP), a transitory pool of chelatable and redox-active iron, serves as the crossroad of cell iron metabolism (19). Growing evidence has shown that ferroptosis is critical for many cardiovascular diseases, such as doxorubicin-induced cardiomyopathy and ischemia/reperfusion injury (20, 21). There are some reports of LPS in triggering myocardial pyroptosis, apoptosis (22), autophagy (23), necroptosis (24), and ferroptosis (25).

In this study, we established an LPS-induced SCD mouse model and found that LCN2 expression significantly increased in cardiac tissue, which was dominantly derived from neutrophils. Exogenous LCN2 led to myocardial ferroptosis by increasing free iron of LIP *in vitro*. *In vivo*, LCN2 deficiency improved the cardiac function of mice in response to LPS. Our results suggested that neutrophil-derived LCN2 might be a promising therapeutic target for SCD.

Abbreviations: LCN2, lipocalin-2; LIP, labile iron pool; MDA, malonaldehyde; PTGS2, prostaglandin E synthase 2; rmLCN2, recombinant LCN2; GPx4, glutathione peroxidase 4; FSP1, ferroptosis suppressor protein 1; ACSL4, acyl-CoA synthetase long-chain family member 4; ALOX12, 12-lipoxygenases; ALOX15, 15-lipoxygenases; Fer-1, ferrostatin-1; DFO, deferoxamine; SCD, septic cardiac dysfunction.

Materials and methods

Mice

Wild-type (WT) and LCN2 knockout (LCN2 KO) mice with a C57BL/6J background were purchased from SLAC Laboratory (Shanghai, China) and GemPharmatech (Jiangsu, China), respectively. The mice were bred in-house under specific pathogen-free conditions with free access to a normal chow diet and water, at a constant temperature (22 ± 2°C) and humidity (60–65%) with a 12-h dark/light cycle. All studies were performed in compliance with guidelines of the Institutional Animal Care and Use Committee at Second Affiliated Hospital, Zhejiang University School of Medicine.

In vivo drug administration

The genotypes were verified by PCR using primer sets for LCN2 KO and WT. In the study, 6–8-week-old male mice were used. Lipopolysaccharide (LPS) was purchased from Sigma-Aldrich (25 mg/kg, Escherichia coli 0111: B4) and dissolved in sterile phosphate-buffered saline (PBS), as described previously (26). Either LPS or PBS was injected intraperitoneally for 12 h.

To investigate the role of ferroptosis in the LPS-induced mice, WT male mice were intraperitoneally injected with Fer-1 (HY-100579/CS-0019733, MCE, United States) at a dose of 1 mg/kg per mouse or vehicle 24 and 2 h prior to LPS administration (21). Fer-1 was dissolved in DMSO and then diluted 1:9 in corn oil. The mice were inspected every 4 h for 3 days.

At termination, the right atrium was cut open, and PBS was perfused through the left ventricle to remove blood in the aorta. Subsequently, serum and cardiac tissue were collected and stored at −80°C for protein and RNA analyses.

Echocardiography and hemodynamics

Echocardiography was performed using a Vevo 2100 system (VisualSonics, Toronto, Canada). Two-dimensional and M-mode echocardiographic images at the papillary muscle level were obtained by two investigators independently. Left ventricle internal diameters at end-diastole and end-systole (LVIDd and LVIDs, respectively) were measured. The LV ejection fraction (EF), fractional shortening (FS), left ventricular end-diastolic volume (LVEDV), and left ventricular end-systolic volume (LVESV) were analyzed independently by

three investigators who were blinded to the experimental design (27).

The closed-chest approach was used to obtain the LV hemodynamics in anesthetized mice using a Millar MPVS-300 system equipped with a Millar SPR-839 catheter, according to described previously (28). Briefly, the anterior thorax and the neck of the mouse were shaved upon complete anesthesia. The neck of the mouse was then opened with a sagittal incision to expose the trachea. The conductance micromanometer was inserted into the right common carotid, and the catheter was placed in the left ventricle under the guidance of online pressure signal. The following indicators were used for the continuous monitoring of hemodynamics, left ventricular end-systolic pressure (LVSP), left ventricular end-diastolic pressure (LVEDP), and maximal left ventricular pressure rising and decreasing rates (LV ± dp/dt max). Data were analyzed using Lab Chart Pro software (AD Instruments).

In vitro cell culture

H9C2 cell line and RAW 264.7 cell line were purchased from the Cell Bank of Shanghai Institutes for Biological Sciences, Chinese Academy of Sciences. The H9C2 cells were cultured in Dulbecco's modified Eagle medium (DMEM, high glucose, Gibco) supplemented with 10% fetal bovine serum (FBS, Hyclone), as described previously (29). Cardiomyocytes and cardiac fibroblasts were isolated from the ventricles of neonatal mice by using the Neonatal Cardiomyocyte Isolation Kit (Cat#130100825, Miltenyi BioTec, Teterow, Germany) according to manufacturer's instructions and cultured in DMEM supplemented with 10% FBS, as described previously (30). Neutrophils were isolated from peripheral blood by using a Mouse Neutrophil Isolation kit (Cat#LZS1100, TBD, China) according to the manufacturer's instructions. RAW 264.7 cells and neutrophils were cultured in RPMI-1640 medium (Gibco) supplemented with 10% FBS, as described previously (31, 32).

The H9C2 cells were incubated with recombinant murine LCN2 (rmLCN2, Cat#CM17; Novoprotein, Shanghai, China) for 24 h at a final concentration of 1 μg/ml. Pre-incubation with either ferrostatin-1 (Fer-1, 10 μM) or deferoxamine (DFO, 25 μM) was carried out in H9C2 cells for 2 h prior to incubation with rmLCN2 at a final concentration of 1 μg/ml, and the cells were collected for next experiments.

Neutrophils and RAW 264.7 cells were incubated with either RPMI-1640 or LPS for 12 h at a final concentration of 100 ng/ml or vehicle. Neonatal cardiomyocytes and cardiac fibroblasts were incubated with either LPS for 24 h at a final concentration of 1 ug/ml or vehicle. The conditioned medium (CM) of neutrophils was harvested to incubate neonatal cardiomyocytes for another 24 h, and the cells were collected for next experiments.

Cell transfections

The H9C2 cells were transfected with 100 nM of 24p3R siRNA and its non-specific siRNA negative control (RiboBio, Guangzhou, China), using Lipofectamine 3000 (Cat#13778030, Invitrogen). Quantitative PCR was used to determine 24p3R expression in the transfected cells after 48 h.

Flow-cytometric analysis

Single cell suspension was prepared and stained at 4°C in PBS with antibodies against CD45 (CAT561869, BioLegend, Beijing, China), CD11b (CAT101212, BioLegend, Beijing, China), Ly6G (CAT127605, BioLegend, Beijing, China), and F4/80 (CAT123109, BioLegend, Beijing, China) for 30 min. Flow cytometric assay was performed using a CytoFLEX FACS machine (Beckman Coulter, Brea, CA), and data were analyzed by FlowJo (FLOWJO, LLC, Ashland, OR).

Enzyme-linked immunosorbent assay and western blotting

LCN2 levels of serum and tissue lysates were measured using enzyme-linked immunosorbent assay (ELISA) kits (Cat# DY1857-05, DY008, R&D, United States) according to manufacturer's recommendation.

Protein lysate samples were prepared from cells or snap-frozen tissues in RIPA solution (Cat# P0013B; Beyotime) supplemented with protease inhibitor (Cat# 05892791001; Roche). Denatured protein lysates were resolved by 10 and 12% (wt/vol) SDS-PAGE gels. After transfer, membranes were incubated with primary antibodies against GPx4 (1:1000,Cat# ET1706-45, HUABIO, Hangzhou, China), FSP1 (1:1000,Cat# ER62655, HUABIO, Hangzhou, China), and β-actin (1:3,000,Cat# KC-5A08, Kangcheng, Sichuan, China), LCN2 (1:1,000,Cat# ab216462, abcam, United States) overnight at 4°C and subsequently incubated with horseradish peroxidase (HRP)-conjugated secondary antibodies, which were detected by enhanced chemiluminescence (Cat# WBKLS0500; Millipore). Immunoblots were analyzed using Image Lab software (Bio-Rad).

Quantitative real-time PCR

Total RNA was isolated from cells or snap-frozen tissues using TRIzol (Takara), and RNA concentration and purity were measured by spectrophotometry. RNA was reverse-transcribed using the PrimeScript RT reagent Kit (Takara) in accordance with the manufacturer's instructions. Quantitative

PCR was performed using a CFX96 Real-Time System (Bio-Rad) and SYBR Green Supermix (Bio-Rad) in accordance with the manufacturer's instructions. The fold difference in gene expression was calculated using the $2^{-\Delta\Delta Ct}$ method and is presented relative to *actin* mRNA. All reactions were performed in triplicate, and specificity was monitored using melting curve analysis. See **Table 1** for the PCR primers used.

Lipid peroxidation assay

Lipid peroxidation was measured by malondialdehyde (MDA) and live cell analysis reagent BODIPY 581/591 C11 (redox-sensitive dye). The MDA level (Cat#A003-1-2, Jiancheng, Jiangsu, China) was measured according to the manufacturer's protocol. Briefly, lipid peroxide reacted with chromogenic reagents under the condition of 98°C for 40 min and produced a stable chromophore with a maximum absorption peak at 532 nm. For BODIPY 581/591 C11 (Cat#D3861, Invitrogen, United States) staining, the cells were incubated in the dark with the reagent at a working concentration of 2.5 μM at 37°C for 30 min, and then the cells were stained with Hoechst nuclear stain (Beyotime,C1017,China) for 10 min. Subsequently, the cells were washed with PBS. Images were acquired under an IX83 fluorescence microscope (Olympus, Tokyo, Japan). Analysis of BODIPY 581/591 C11 was performed by measuring the intensity of fluorescence. Images were from at least six randomly selected regions of interest across three independent experiments. The fluorescence intensity was measured by ImageJ (National Institutes of Health).

TABLE 1 Primers for qPCR (sequence: 5′- > 3′).

PTGS2 forward primer	TTCAACACACTCTATCACTGGC
PTGS2 reverse primer	AGAAGCGTTTGCGGTACTCAT
LCN2 forward primer	TGGCCCTGAGTGTCATGTG
LCN2 reverse primer	CTCTTGTAGCTCATAGATGGTGC
SLC7a11 forward primer	GGCACCGTCATCGGATCAG
SLC7a11 reverse primer	CTCCACAGGCAGACCAGAAAA
ACSL4 forward primer	CTCACCATTATATTGCTGCCTGT
ACSL4 reverse primer	TCTCTTTGCCATAGCGTTTTTCT
ALOX12 forward primer	TCCCTCAACCTAGTGCGTTTG
ALOX12 reverse primer	GTTGCAGCTCCAGTTTCGC
ALOX15 forward primer	GGCTCCAACAACGAGGTCTAC
ALOX15 reverse primer	AGGTATTCTGACACATCCACCTT
IL-1 β forward primer	GTGCTACTGGGGCTCATTTGT
IL-1 β reverse primer	GGAGTAAGAGGACACTTGCGAAT
TNF α forward primer	CCCTCACACTCAGATCATCTTCT
TNF α reverse primer	GCTACGACGTGGGCTACAG
IL-6 forward primer	TAGTCCTTCCTACCCCAATTTCC
IL-6 reverse primer	TTGGTCCTTAGCCACTCCTTC
Actin forward primer	GGCTGTATTCCCCTCCATCG
Actin reverse primer	CCAGTTGGTAACAATGCCATGT

Labile iron pool measurements

Labile iron pool was measured by calcein AM, as reported previously (33). Cells at a density of 2×10^5 per well were incubated with calcein AM (Cat#C2012, Beyotime, Shanghai, China) at a finial concentration of 0.05 μM for 30 min prior to incubation with DMEM for another 30 min and rinsing with PBS. Flow cytometric assay was performed using a CytoFLEX FACS machine (Beckman Coulter, Brea, CA) at a 488-nm laser on an FL1 detector.

Statistical analysis

GraphPad Prism version 7.0 (GraphPad Software) was used for statistical analyses. To compare continuous response variables between two groups, an unpaired two-tailed Student's *t*-test was applied for normally distributed variables that passed the equal variance test, and the Mann–Whitney *U*-test was used for variables not passing either the normality or equal variance test. To compare more than two groups, one-way ANOVA was performed for normally distributed variables that passed the equal variance test and Kruskal–Wallis one-way ANOVA on ranks using the Dunn method for variables failed to pass the normality or equal variance test, respectively. $P < 0.05$ was considered statistically significant. Data that passed the equal variance test were represented as mean ± SEM. Data that did not pass either the normality or equal variance test were shown as median with 95% CI.

Results

Neutrophil-derived lipocalin-2 was increased in lipopolysaccharide-induced septic cardiac dysfunction mice

To investigate the involvement of LCN2 on SCD, 6 to 8-week-old male C57Bl/6 mice were injected with either LPS (25 mg/kg) or PBS intraperitoneally for 12 h. Compared to the PBS group, EF and FS were significantly decreased (**Figures 1A,B**), indicating SCD establishment. We also found LVESV was increased in SCD mice, while LVEDV was not changed (**Figures 1A,B**). qPCR demonstrated that LCN2 mRNA was significantly upregulated in many organs, including the heart, liver, lung, and the kidney, but not spleen (**Supplementary Figure 1A**). Furthermore, compared to the PBS group, Western blot indicated that LCN2 expression in the

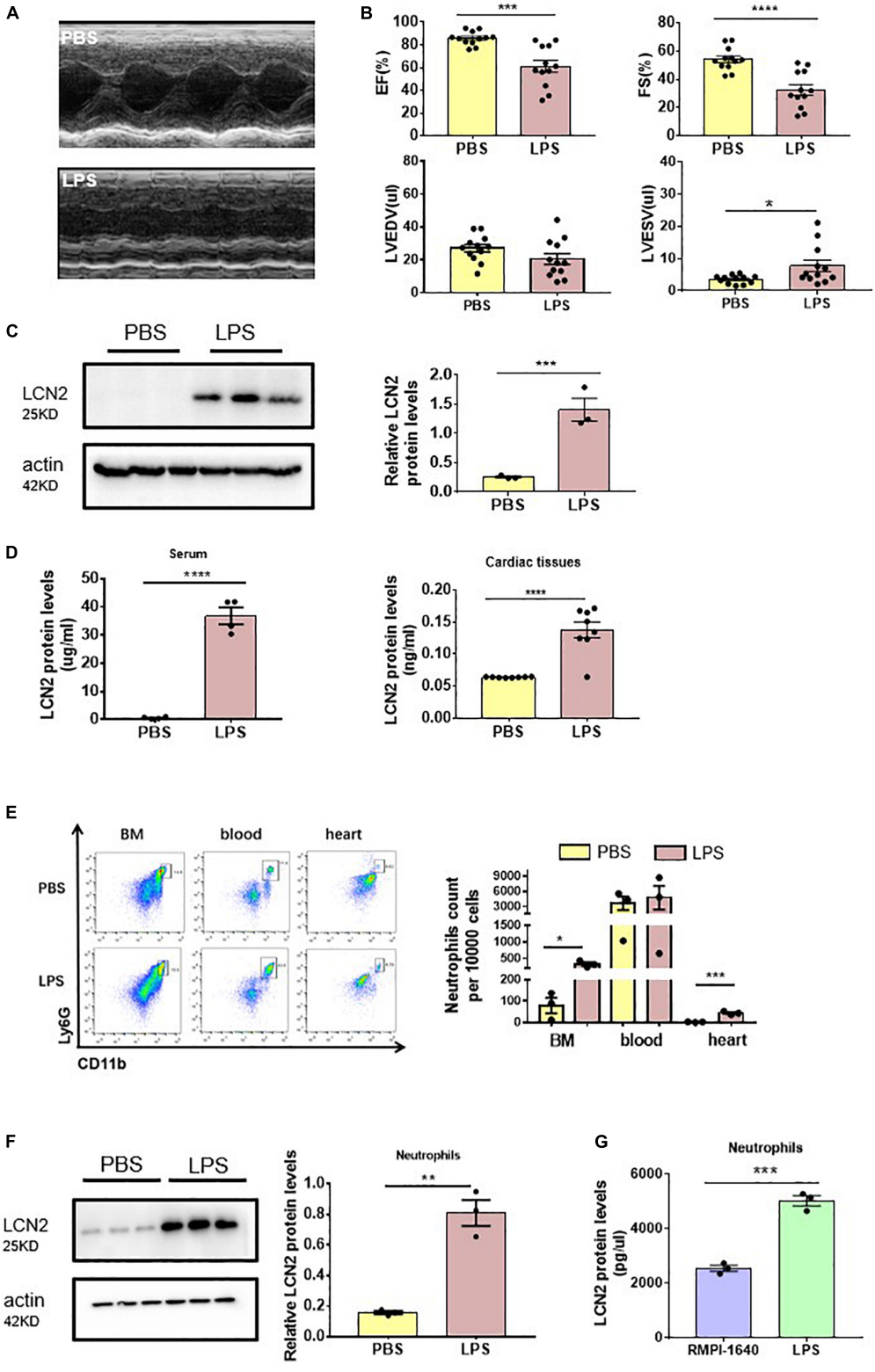

FIGURE 1
Neutrophil-derived LCN2 was increased in LPS-induced SCD mice. **(A,B)** Echocardiography was performed 12 h after intraperitoneal injection of either PBS or LPS (25 mg/kg) in WT mice and their representative images (n = 12 in each group). **(C)** Western blot was used to analyze LCN2 expressions in heart tissues 12 h after intraperitoneal injection with either PBS or LPS (n = 3 in each group). **(D)** ELISA was performed to detect serum (n = 4 in each group) and cardiac LCN2 protein levels (n = 8 in each group) 12 h after intraperitoneal injection with either PBS or LPS in
(Continued)

FIGURE 1
WT mice. **(E)** Flow cytometric analysis was performed to determine the number of CD45+CD11b+Ly6G+ cells in the bone marrow (BM), blood, and heart 12 h after intraperitoneal injection with either PBS (n = 3) or LPS (25 mg/kg, n = 3) in WT mice. **(F)** Western blot was used to analyze the LCN2 expressions in neutrophils isolated from peripheral blood 12 h post-intraperitoneal injection of PBS or LPS (25 mg/kg, n = 6 in each group) in WT mice. **(G)** ELISA was performed to detect the LCN2 protein levels in neutrophils after 12-h incubation with either RMPI-1640 or LPS (100 ng/ml, n = 3 in each group). Measurement data are presented as mean ± SEM. *$p < 0.05$, **$p < 0.01$, ***$p < 0.001$, ****$p < 0.0001$.

myocardial tissues of LPS-induced SCD mice was significantly increased (Figure 1C). ELISA was performed to show that LCN2 protein concentrations elevated in the serum and myocardial lysates in LPS-induced SCD mice, compared to the PBS group (Figure 1D).

According to the previous studies that LCN2 was dominantly from neutrophils, we screened mononuclear cell suspension in myocardial lysates, peripheral blood, and bone marrow for LCN2 expression. As a result, neutrophils (as CD45 + CD11b + Ly6G + cells by flow cytometry) were obviously increased in response to LPS in both the bone marrow and cardiac tissues, and in peripheral blood, there was a tendency of increasing neutrophils (Figure 1E). LCN2 protein expression by Western blot was dramatically upregulated in neutrophils isolated from the peripheral blood of LPS-induced SCD mice, compared to the PBS group (Figure 1F).

To further verify the cell origin of LCN2, neutrophils, RAW 264.7 cells, neonatal cardiomyocytes, and cardiac fibroblasts were cultured *in vitro* and incubated with or without LPS for 12 h. ELISA detection indicated that LCN2 secreted by neutrophils was much more than that secreted by RAW 264.7 cells (Figure 1G and Supplementary Figure 2A). However, Western blot indicated that LCN2 expression was not upregulated in neonatal cardiomyocytes or cardiac fibroblasts in response to LPS (Supplementary Figure 2B). Taken together, these data suggested that LCN2 was involved in the pathogenesis of LPS-induced SCD, which was mainly derived from neutrophils.

Lipocalin-2 deficiency improved cardiac function in lipopolysaccharide-induced mice

In order to investigate the roles of LCN2 in SCD, we purchased LCN2-knockout (LCN2 KO) mice from GemPharmatech. The expression of LCN2 protein was significantly declined in cardiac tissues in LCN2 KO mice (Supplementary Figure 3A).

There was no difference of EF, FS, LVEDV, or LVESV at the baseline of LCN2 KO mice and their littermates (Figures 2A,B). But compared to their WT littermates, EF and FS were significantly increased, LVESV was decreased in LCN2 KO mice in response to LPS (Figures 2A,B). Compared to their WT littermates after LPS administration, although there was no significant difference, an increasing tendency of LV-dp/dt max was observed in the LCN2 KO group (P = 0.053) (Figure 2C). Taken together, LCN2 deficiency led to the improvement of the cardiac function in LPS-induced mice.

Lipocalin-2 initiated ferroptosis in cardiomyocytes

To explore the potential mechanisms of LCN2 on SCD, lipid peroxidation was measured by the MDA level and BODIPY 581/591 C11 to indicate ferroptosis in cardiomyocytes. CMs of the neutrophils from either WT littermates without LPS preconditioning (CM^{WT-CTL}) or with LPS preconditioning (CM^{WT-LPS}), and from LCN2 KO mice without LPS-preconditioning ($CM^{LCN2-CTL}$) or with LPS-preconditioning ($CM^{LCN2-LPS}$) were harvested individually and incubated with neonatal cardiomyocytes. CM^{WT-LPS} significantly elevated MDA levels in neonatal cardiomyocytes, which was abrogated by $CM^{LCN2-LPS}$ (Figure 3A). Consistent results were observed in neonatal cardiomyocytes with CM^{WT-LPS} by Fer-1, a specific ferroptosis inhibitor (Figure 3B).

Next, exogenous recombinant LCN2 (rmLCN2) was adopted to incubate with H9C2 cells for 24 h. BODIPY 581/591 C11 staining and mean fluorescence intensity demonstrated that exogenous rmLCN2 enhanced lipid peroxidation in H9C2 cells (Figure 3C). Furthermore, exogenous rmLCN2 incubation significantly promoted prostaglandin E synthase 2 (PTGS2) mRNA expression (Figure 3D) and LIP levels (Figure 3E), which were diminished by Fer-1 (Figures 3C–E). However, exogenous rmLCN2 incubation did not alter glutathione peroxidase 4 (GPx4) protein levels by Western blot (Supplementary Figure 4A). Collectively, our findings suggested that LCN2 triggered ferroptosis in cardiomyocytes, independent of GPx4.

Lipocalin-2 induced ferroptosis *via* increasing labile iron pool in H9C2

To interpret the intracellular modulation of iron dynamic equilibrium by LCN2, H9C2 cells were incubated with or without deferoxamine (DFO), an iron chelator, while adapted with exogenous rmLCN2. DFO incubation obviously attenuated fluorescence staining and mean fluorescence intensity by

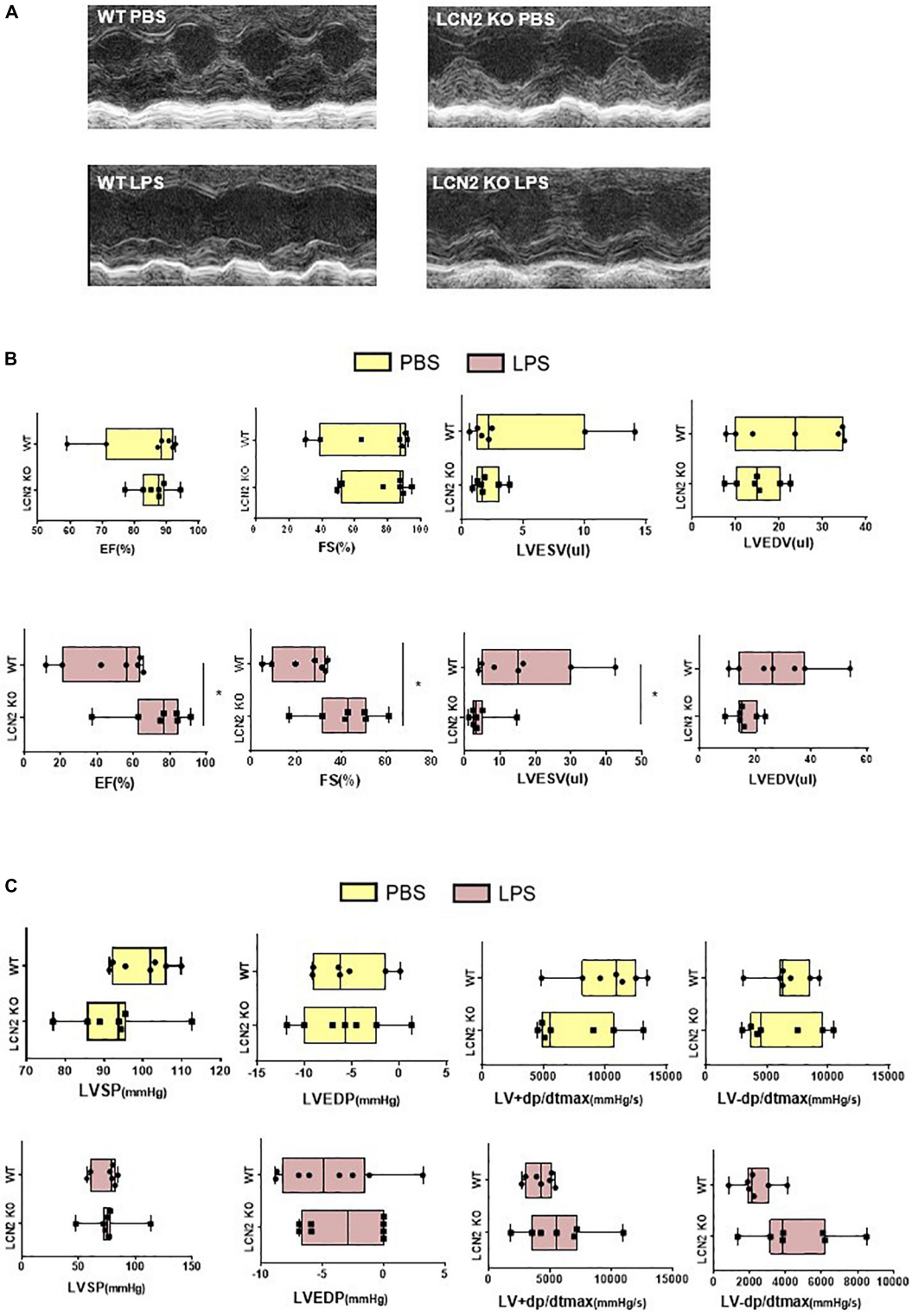

FIGURE 2
LCN2 deficiency improved cardiac function in LPS-induced SCD mice. **(A,B)** Echocardiography was performed 12 h after intraperitoneal injection of either PBS or LPS (25 mg/kg) to evaluate EF, FS, LVEDV, and LVESV in LCN2 KO mice and their WT littermates (n = 7 in each group). **(C)** Invasive hemodynamics was monitored 12 h after intraperitoneal injection with either PBS or LPS (25 mg/kg) in LCN2 KO mice and their WT littermates (n = 7 in each group). Measurement data are presented as median with 95% CI. *$p < 0.05$.

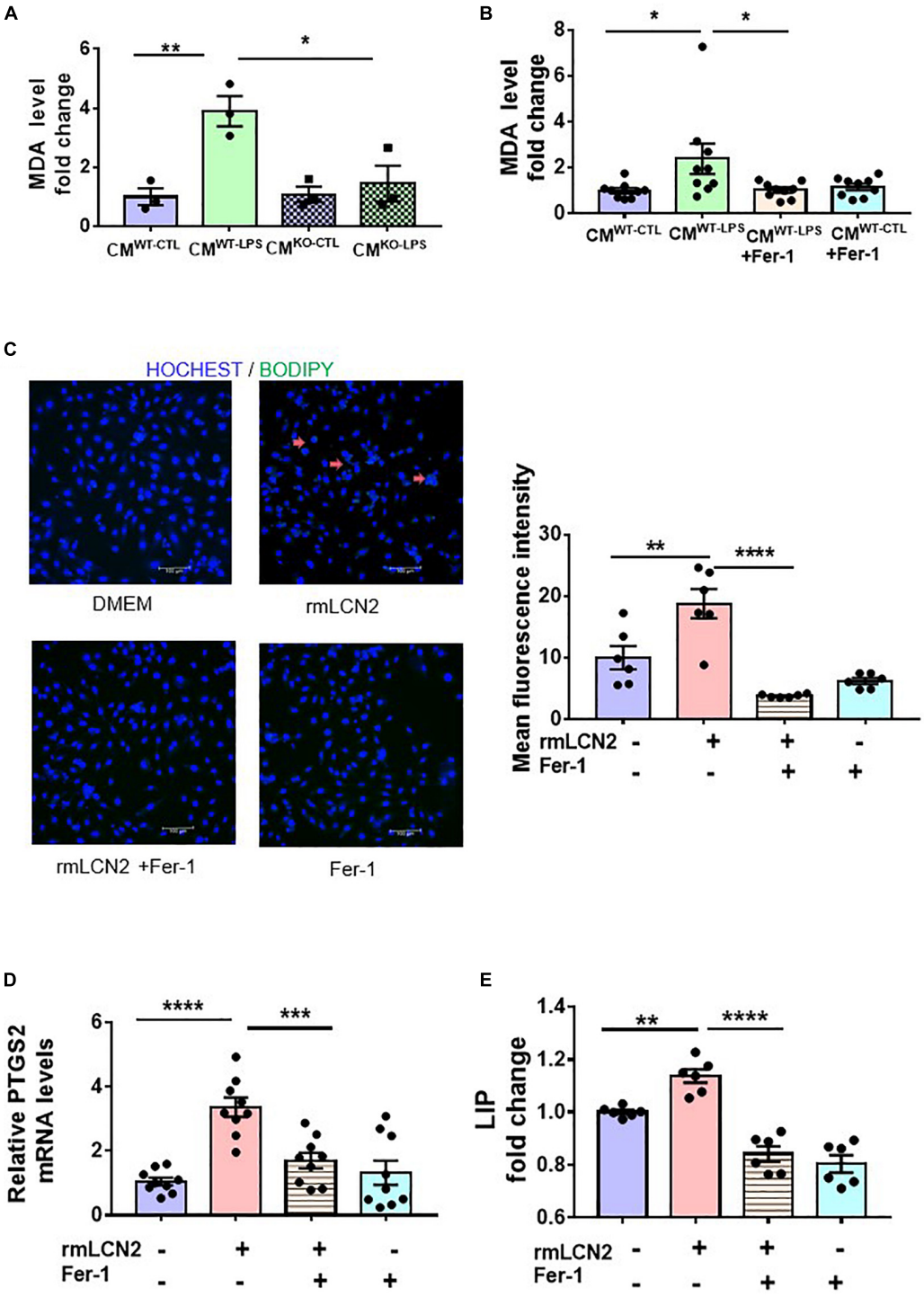

FIGURE 3
LCN2 initiated ferroptosis in cardiomyocytes. **(A)** Neonatal cardiomyocytes were incubated for 24 h with CMs of the neutrophils from either WT littermates without LPS-preconditioning (CM^{WT-CTL}) or with LPS-preconditioning (CM^{WT-LPS}), and from LCN2 KO mice without LPS-preconditioning ($CM^{LCN2-CTL}$) or with LPS-preconditioning ($CM^{LCN2-LPS}$) to detect MDA levels (n = 3 in each group). **(B)** Neonatal cardiomyocytes were pre-incubated for 2 h with or without Fer-1 (10 μM) prior to incubation with CMs for 24 h to detect MDA levels (n = 9 in each group). **(C)** Representative images and fluorescence intensity analysis of H9C2 cells pre-incubated with or without Fer-1 (10 μM) for 2 h prior to incubation with rmLCN2 (1 μg/ml) for 24 h by 581/591C11-BODIPY staining (red arrows indicate the fluorescence staining, n = 3 in each group). **(D)** PTGS2 mRNA expressions by qPCR in H9C2 cells pre-incubated with or without Fer-1 (10 μM) for 2 h prior to incubation with rmLCN2 (1 μg/ml) for 24 h (n = 9 in each group). **(E)** Labile iron pool (LIP) changes in H9C2 cells pre-incubated with or without Fer-1 (10 μM) for 2 h prior to incubation with rmLCN2 (1 μg/ml) for 24 h (n = 6 in each group). Measurement data are presented as mean ± SEM. *$p < 0.05$, **$p < 0.01$, ***$p < 0.001$, ****$p < 0.0001$.

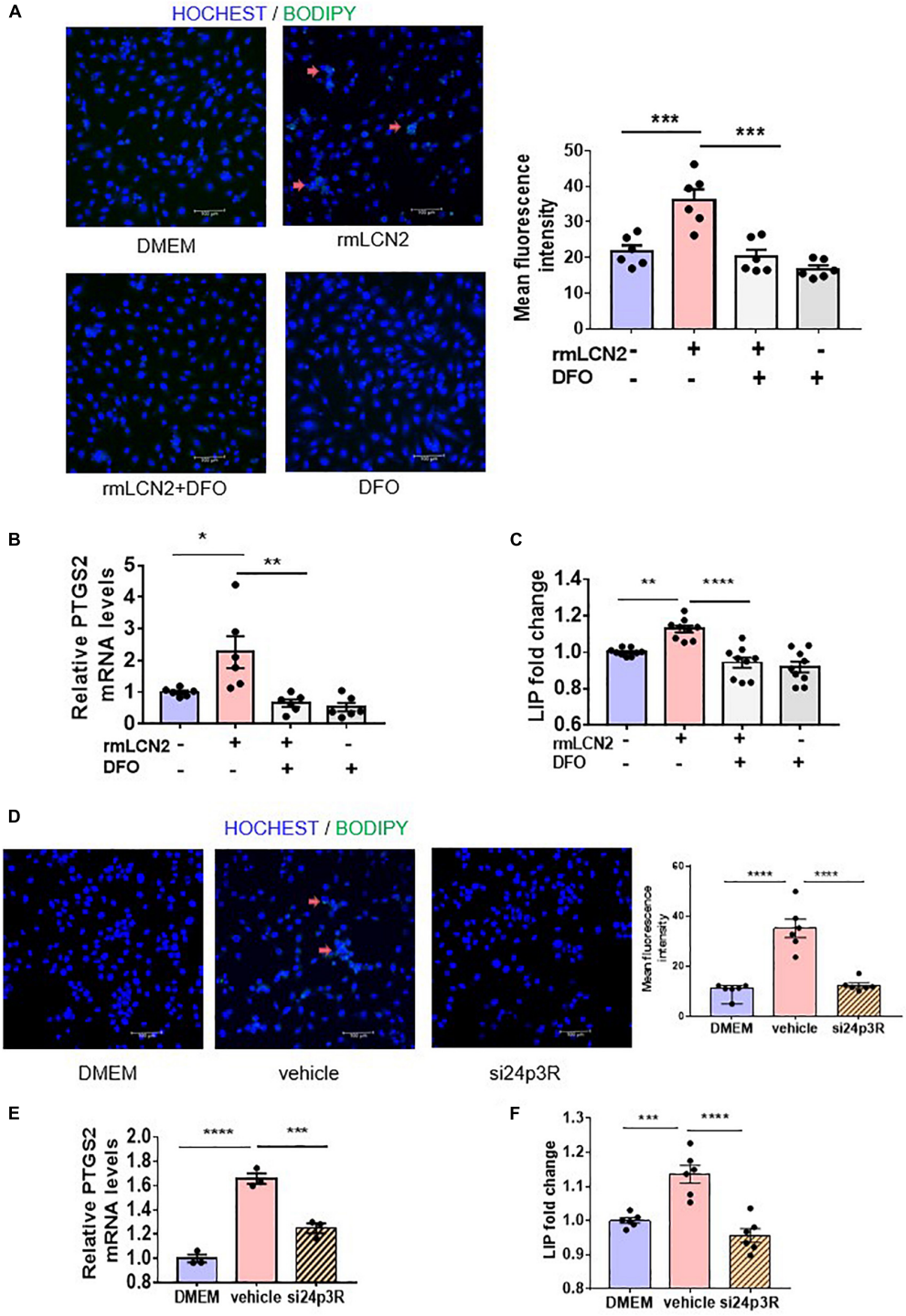

FIGURE 4
LCN2 induced ferroptosis *via* increasing LIP in H9C2 cells. **(A)** Representative images and fluorescence intensity analysis of H9C2 cells pre-incubated with or without DFO (25 μM) for 2 h prior to incubation with rmLCN2 (1 μg/ml) for 24 h by 581/591C11-BODIPY staining (red arrows indicate the fluorescence staining, $n = 3$ in each group). **(B)** PTGS2 mRNA expressions by qPCR in H9C2 cells pre-incubated with or without DFO (25 μM) for 2 h prior to incubation with rmLCN2 (1 μg/ml) for 24 h ($n = 6$ in each group). **(C)** LIP changes in H9C2 cells pre-incubated with or without DFO (25 μM) for 2 h prior to incubation with rmLCN2 (1 μg/ml) for 24 h ($n = 9$ in each group). **(D)** Representative images and fluorescence intensity analysis of H9C2 cells pre-incubated with or without 24p3R siRNA for 48 h prior to incubation with rmLCN2 (1 μg/ml) for 24 h by 581/591C11-BODIPY staining (red arrows indicate fluorescence staining, $n = 3$ in each group). **(E)** PTGS2 mRNA expressions by qPCR in H9C2 cells pre-incubated with or without 24p3R siRNA for 48 h prior to incubation with rmLCN2 (1 μg/ml) for 24 h $n = 3$ in each group). **(F)** LIP changes in H9C2 cells pre-incubated with or without 24p3R siRNA for 48 h prior to incubation with rmLCN2 (1 μg/ml) for 24 h ($n = 6$ in each group). *$p < 0.05$, **$p < 0.01$, ***$p < 0.001$, ****$p < 0.0001$.

BODIPY 581/591 C11 in H9C2 cells (**Figure 4A**), as well as PTGS2 mRNA expression and LIP levels (**Figures 4B,C**).

The membrane receptor, 24p3R, was expressed in H9C2 cells (34). Compared to the non-specific siRNA negative control (vehicle), 24p3R-siRNA (si24p3R) incubation markedly attenuated fluorescence staining and mean fluorescence intensity by BODIPY 581/591 C11 in H9C2 cells (**Figure 4D**), as well as PTGS2 mRNA expression and LIP levels (**Figures 4E,F**). These results indicated that rmLCN2 induced H9C2 ferroptosis by increasing LIP *via* 24p3R.

Septic cardiac dysfunction mice have increased ferroptosis

To evaluate the effect of ferroptosis inhibition on LPS-induced SCD, 6 to 8-week-old male C57Bl/6 mice were intraperitoneally injected with or without Fer-1 (1 mg/kg) 24 and 2 h prior to LPS administration. At termination, 60% mice eventually survived in the LPS-induced group, whereas no death occurred in the Fer-1 pre-treatment group (**Figure 5A**). Compared to the LPS group, EF and FS were significantly increased, and LVESV was significantly decreased in mice administrated with Fer-1 assessed by echocardiography (**Figures 5B,C**). The Fer-1-pretreated mice displayed an increase in LVSP, and a tendency of increased LV-dp/dt max was also been observed, although there was no significant difference ($P = 0.0651$) (**Figure 5D**) compared to SCD mice.

LPS induced elevations of cardiac MDA levels and PTGS2 mRNA levels in the WT mice, which were abrogated by Fer-1 administration (**Figures 5E,F**). The LCN2 protein level was upregulated in LPS-induced SCD mice, which was not affected by Fer-1 administration (**Supplementary Figure 5A**). Furthermore, cardiac MDA levels were declined in LCN2 KO mice compared to their WT littermates in response to LPS (**Figure 5G**).

We also measured other biomarkers of ferroptosis in heart tissues of SCD mice. However, no changes had been observed in ferroptosis suppressor protein 1 (FSP1) and GPx4 protein levels (**Supplementary Figure 6A**) and mRNA levels of acyl-CoA synthetase long-chain family member 4 (ACSL4), 12-lipoxygenases (ALOX12), and 15-lipoxygenases (ALOX15) (**Supplementary Figure 6B**). qPCR demonstrated that mRNA levels of SLC7A11 were significantly increased in heart tissues of SCD mice, which was not abrogated by Fer-1 administration (**Supplementary Figure 6C**). Thus, ferroptosis is involved in LPS-induced SCD, and it can be inhibited by Fer-1.

We further analyzed neutrophil infiltration in the WT and LCN2 KO mice. Inconsistent to the previous studies (35, 36), no difference of neutrophil infiltration (as CD45 + F4/80-Ly6G + cells by flow cytometry) was observed in the BM, blood, and heart tissue after intraperitoneal injection with either PBS or LPS (**Supplementary Figures 7A,B**). In addition, the mRNA expressions of IL-6, IL-1β, and TNFα in heart tissues by qPCR were not significant different between the WT mice and LCN2 KO mice (**Supplementary Figure 7C**). These data suggested that cardiac dysfunction and ferroptosis could be attenuated by LCN2 deficiency, independent of neutrophil recruitment.

Discussion

In the present study, we established an LPS-induced SCD murine model and generated LCN2 KO mice to investigate the role and the mechanisms of LCN2 in the development of SCD. Herein, LCN2 was highly expressed in cardiac tissue and accounted for heart failure in LPS-induced SCD mice, which dominantly originated from peripheral neutrophils. *In vitro* experiments showed that LCN2 was involved in myocardial ferroptosis by increasing intracellular LIP *via* 24p3R. LCN2 deficiency attenuated cardiac ferroptosis and improved cardiac function in SCD mice, which might be a potential therapeutic target for SCD patients.

LCN2, a member of neutrophil granule markers, is stored in the specific granules and can be carried to the local infection area (37). Regarded as a biomarker of infected diseases, LCN2 offers protection against *E. coli*-induced septicemia (38), pneumonia (39), and urinary tract infection (40). According to a previous study (3), we explored the LCN2 expression in cardiomyocytes, cardiac fibroblasts, neutrophils, and macrophages in response to LPS. Cell experiments showed that LCN2 was much more expressed in neutrophils than in other cells. Accordingly, based on the findings that neutrophils were dramatically infiltrated in cardiac tissue and LCN2 expression was upregulated in peripheral neutrophils of the LPS-induced SCD mice, we found that LCN2 was mainly derived from peripheral neutrophils.

LCN2 is widely reported to be involved in acute kidney injury (41, 42) and chronic kidney disease (43) and is a biomarker of hepatic ischemia reperfusion injury severity stages (44). As reported previously, LCN2 was widely distributed in the liver, lung, kidney, and other organs as an acute inflammatory protein in sepsis mice (45). Here, we reported that LCN2 was accumulated in LPS-induced cardiac tissue and contributed to heart failure, whereas LCN2 deficiency improved cardiac function. Future studies need to be designed to evaluate the function of LCN2 in other types of heart failure.

Ferroptosis is defined in 2012 as an iron-dependent regulated form of cell death, caused by intracellular accumulation of lipid-based reactive oxygen species (ROS) (46, 47). Relevant conditions underlying cardiac redox imbalance include iron overload associated with ROS production *via* the Fenton reaction and the magnitude of the LIP achieved (48, 49). For instance, it has demonstrated that free iron released on heme degradation is necessary and sufficient to induce cardiac injury, both in doxorubicin-induced cardiomyopathy and ischemia/reperfusion (I/R) injury (21, 50). Consistent with the previous result (16, 25), our study indicated that ferroptosis played a critical role in LPS-induced cardiac injury.

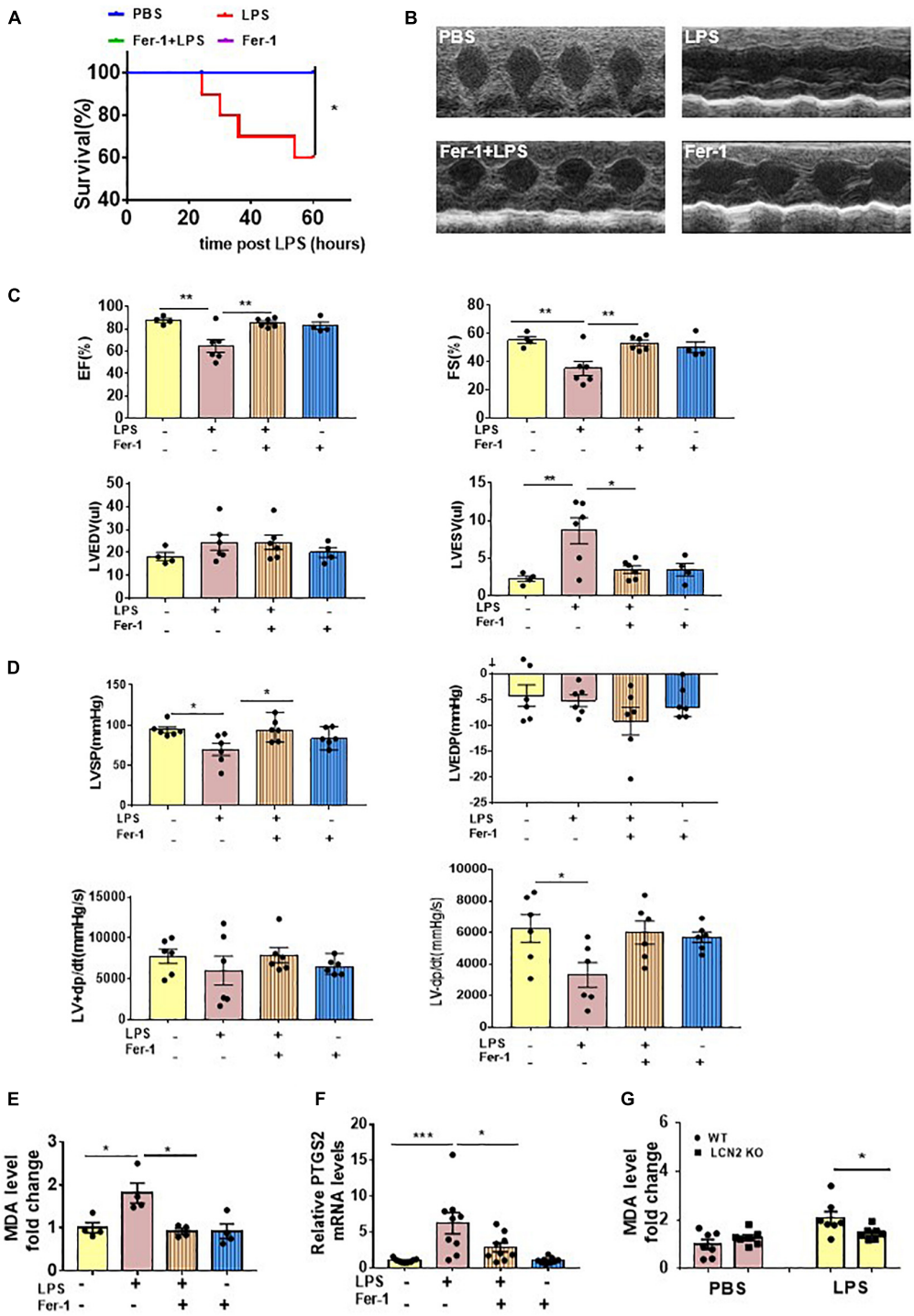

FIGURE 5
Ferroptosis presented in LPS-induced SCD mice. **(A)** Survival curve of WT mice intraperitoneally injected with either PBS or Fer-1 (1 mg/kg) at 24 h, 2 h before LPS (25 mg/kg, n = 10 in each group) administration. **(B,C)** Echocardiography was performed in WT mice intraperitoneally injected with either PBS or Fer-1 (1 mg/kg) at 24 h, 2 h followed by LPS (25 mg/kg) or PBS administration for 12 h (n = 4, 6, 6, 4, respectively). **(D)** Invasive hemodynamics was monitored in WT mice intraperitoneally injected with either PBS or Fer-1 (1 mg/kg) at 24 h, 2 h followed by LPS (25 mg/kg) or PBS administration for 12 h (n = 6 in each group). **(E)** Cardiac MDA levels were detected in WT mice intraperitoneally injected with either PBS or Fer-1 (1 mg/kg) at 24 h, 2 h followed by LPS (25 mg/kg) or PBS administration for 12 h (n = 4 in each group). **(F)** Cardiac PTGS2 mRNA expressions were determined by qPCR in WT mice intraperitoneally injected with either PBS or Fer-1 (1 mg/kg) at 24 h, 2 h followed by LPS (25 mg/kg) or PBS administration for 12 h (n = 9 in each group). **(G)** Cardiac MDA levels were detected in LCN2 KO mice and their WT littermates 12 h after intraperitoneal injection of either PBS or LPS (25 mg/kg) (n = 7 in each group). *$p < 0.05$, **$p < 0.01$, ***$p < 0.001$.

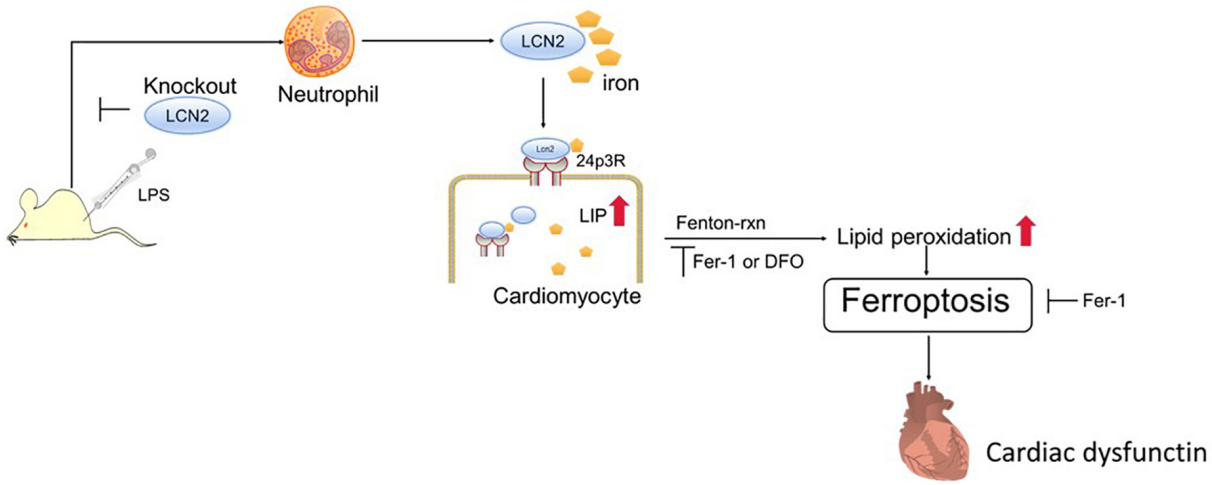

FIGURE 6
LCN2 and its potential mechanism on SCD. Neutrophil-derived LCN2 initiates intracellular LIP elevation *via* 24p3R, triggers ferroptosis, and eventually contributes to cardiac dysfunction.

In previous experimental studies, LCN2 deficiency improved the cardiac function by attenuating cardiac hypertrophy in human hypertrophic cardiomyopathy (51). Otherwise, LCN2 can exacerbate cardiac dysfunction by suppressing the beneficial cardiac autophagic response and accelerate cardiac apoptosis in myocardial infarction (52). As an iron transporter, LCN2 can deliver siderophore-bound iron into cells and increase cytoplasm LIP (53), which is supported by our study that exogenous rmLCN2 increased intracellular LIP in H9C2 cells and led to ferroptosis. Also, LCN2 deficiency decreased ferroptosis in LPS-induced mice.

To verify ferroptosis in LPS-induced SCD, ferroptosis-specific inhibitor (Fer-1) and iron chelator (DFO) were adopted in this study. As expected, both agents attenuated exogenous LCN2-induced ferroptosis in H9C2 cells. 24p3R, a dominant membrane receptor, was expressed in H9C2 cells. The blockade of 24p3R resulted in ferroptosis alleviation in H9C2 cells. The potential mechanism of LCN2 on SCD may be explained as the follows (**Figure 6**). LPS induced recruitment of peripheral neutrophils to cardiac tissues, followed by the release of LCN2. Neutrophil-derived LCN2 carried iron into cardiomyocytes *via* 24p3R and initiated intracellular LIP elevation, thereby leading to ferroptosis independent of GPx4, which could be reversed by both Fer-1 and DFO. It is indicated that targeted inhibition of LCN2 may act as a promising approach for the treatment of septic cardiomyopathy.

In summary, our study elucidates that neutrophil-derived LCN2 initiates intracellular LIP elevation *via* 24p3R and triggers ferroptosis in cardiomyocytes. SCD and ferroptosis could be attenuated by LCN2 deficiency, which implicated that LCN2 may act as a promising target for the treatment of septic cardiomyopathy.

Data availability statement

The original contributions presented in this study are included in the article/**Supplementary material**, further inquiries can be directed to the corresponding author/s.

Ethics statement

The animal study was reviewed and approved by Second Affiliated Hospital, Zhejiang University School of Medicine.

Author contributions

YH conducted the experiments, analyzed the results, and wrote the manuscript draft. CX, NZ, and YY participated in specific experiments and analyzed the results. YH and FY provided conceptual advice and revised the draft. XX and JW designed the study and modified the manuscript draft. All authors read and approved the final manuscript.

Funding

This research was supported by the National Key R&D Program of China (2019YFA0110400) and the National Health Commission, Key Program of Science and Technology of Medical and Health of Zhejiang Province (WKJ-ZJ-2028).

Conflict of interest

The authors declare that the research was conducted in the absence of any commercial or financial relationships that could be construed as a potential conflict of interest.

Publisher's note

All claims expressed in this article are solely those of the authors and do not necessarily represent those of their affiliated organizations, or those of the publisher, the editors and the reviewers. Any product that may be evaluated in this article, or claim that may be made by its manufacturer, is not guaranteed or endorsed by the publisher.

Supplementary material

The Supplementary Material for this article can be found online at: https://www.frontiersin.org/articles/10.3389/fcvm.2022.922534/full#supplementary-material

References

1. Merx MW, Weber C. Sepsis and the heart. *Circulation.* (2007) 116:793–802. doi: 10.1161/CIRCULATIONAHA.106.678359

2. Beesley SJ, Weber G, Sarge T, Nikravan S, Grissom CK, Lanspa MJ, et al. Septic cardiomyopathy. *Crit Care Med.* (2018) 46:625–34. doi: 10.1097/CCM.0000000000002851

3. Li H, Feng D, Cai Y, Liu Y, Xu M, Xiang X, et al. Hepatocytes and neutrophils cooperatively suppress bacterial infection by differentially regulating lipocalin-2 and neutrophil extracellular traps. *Hepatology.* (2018) 68:1604–20. doi: 10.1002/hep.29919

4. Sakuma M, Khan MAS, Yasuhara S, Martyn JA, Palaniyar N. Mechanism of pulmonary immunosuppression: extrapulmonary burn injury suppresses bacterial endotoxin-induced pulmonary neutrophil recruitment and neutrophil extracellular trap (NET) formation. *FASEB J.* (2019) 33:13602–16. doi: 10.1096/fj.201901098R

5. Kjeldsen L, Cowland JB, Borregaard N. Human neutrophil gelatinase-associated lipocalin and homologous proteins in rat and mouse. *Biochim Biophys Acta.* (2000) 1482:272–83. doi: 10.1016/s0167-4838(00)00152-7

6. Chi Y, Remsik J, Kiseliovas V, Derderian C, Sener U, Alghader M, et al. Cancer cells deploy lipocalin-2 to collect limiting iron in leptomeningeal metastasis. *Science.* (2020) 369:276–82. doi: 10.1126/science.aaz2193

7. Kim H, Hur M, Lee S, Marino R, Magrini L, Cardelli P, et al. Proenkephalin, neutrophil gelatinase-associated lipocalin, and estimated glomerular filtration rates in patients with sepsis. *Ann Lab Med.* (2017) 37:388–97. doi: 10.3343/alm.2017.37.5.388

8. Wieser V, Tymoszuk P, Adolph TE, Grander C, Grabherr F, Enrich B, et al. Lipocalin 2 drives neutrophilic inflammation in alcoholic liver disease. *J Hepatol.* (2016) 64:872–80. doi: 10.1016/j.jhep.2015.11.037

9. Wang B, Chen G, Li J, Zeng Y, Wu Y, Yan X. Neutrophil gelatinase-associated lipocalin predicts myocardial dysfunction and mortality in severe sepsis and septic shock. *Int J Cardiol.* (2017) 227:589–94. doi: 10.1016/j.ijcard.2016.10.096

10. Maisel AS, Mueller C, Fitzgerald R, Brikhan R, Hiestand BC, Iqbal N, et al. Prognostic utility of plasma neutrophil gelatinase-associated lipocalin in patients with acute heart failure: the NGAL EvaLuation Along with B-type NaTriuretic Peptide in acutely decompensated heart failure (GALLANT) trial. *Eur J Heart Fail.* (2011) 13:846–51. doi: 10.1093/eurjhf/hfr087

11. Bolignano D, Basile G, Parisi P, Coppolino G, Nicocia G, Buemi M. Increased plasma neutrophil gelatinase-associated lipocalin levels predict mortality in elderly patients with chronic heart failure. *Rejuvenation Res.* (2009) 12:7–14. doi: 10.1089/rej.2008.0803

12. van Deursen VM, Damman K, Voors AA, van der Wal MH, Jaarsma T, van Veldhuisen DJ, et al. Prognostic value of plasma neutrophil gelatinase-associated lipocalin for mortality in patients with heart failure. *Circ Heart Fail.* (2014) 7:35–42. doi: 10.1161/CIRCHEARTFAILURE.113.000242

13. Devireddy LR, Gazin C, Zhu X, Green MR. A cell-surface receptor for lipocalin 24p3 selectively mediates apoptosis and iron uptake. *Cell.* (2005) 123:1293–305. doi: 10.1016/j.cell.2005.10.027

14. Dixon SJ, Lemberg KM, Lamprecht MR, Skouta R, Zaitsev EM, Gleason CE, et al. Ferroptosis: an iron-dependent form of non-apoptotic cell death. *Cell.* (2012) 149:1060–72. doi: 10.1016/j.cell.2012.03.042

15. Lei P, Bai T, Sun Y. Mechanisms of ferroptosis and relations with regulated cell death: A review. *Front Physiol.* (2019) 10:139. doi: 10.3389/fphys.2019.00139

16. Li N, Wang W, Zhou H, Wu Q, Duan M, Liu C, et al. Ferritinophagy-mediated ferroptosis is involved in sepsis-induced cardiac injury. *Free Radic Biol Med.* (2020) 160:303–18. doi: 10.1016/j.freeradbiomed.2020.08.009

17. Friedmann Angeli JP, Schneider M, Proneth B, Tyurin VA, Hammond VJ, Herbach N, et al. Inactivation of the ferroptosis regulator Gpx4 triggers acute renal failure in mice. *Nat Cell Biol.* (2014) 16:1180–91. doi: 10.1038/ncb3064

18. Angeli JPF, Shah R, Pratt DA, Conrad M. Ferroptosis inhibition: mechanisms and opportunities. *Trends Pharmacol Sci.* (2017) 38:489–98. doi: 10.1016/j.tips.2017.02.005

19. Kakhlon O, Cabantchik ZI. The labile iron pool: Characterization, measurement, and participation in cellular processes(1). *Free Radic Biol Med.* (2002) 33:1037–46. doi: 10.1016/s0891-5849(02)01006-7

20. Fang X, Cai Z, Wang H, Han D, Cheng Q, Zhang P, et al. Loss of cardiac ferritin H facilitates cardiomyopathy *via* Slc7a11-mediated ferroptosis. *Circ Res.* (2020) 127:486–501. doi: 10.1161/CIRCRESAHA.120.316509

21. Fang X, Wang H, Han D, Xie E, Yang X, Wei J, et al. Ferroptosis as a target for protection against cardiomyopathy. *Proc Natl Acad Sci USA.* (2019) 116:2672–80. doi: 10.1073/pnas.1821022116

22. Li N, Zhou H, Wu H, Wu Q, Duan M, Deng W, et al. STING-IRF3 contributes to lipopolysaccharide-induced cardiac dysfunction, inflammation, apoptosis and pyroptosis by activating NLRP3. *Redox Biol.* (2019) 24:101215. doi: 10.1016/j.redox.2019.101215

23. Zhao H, Zhang M, Zhou F, Cao W, Bi L, Xie Y, et al. Cinnamaldehyde ameliorates LPS-induced cardiac dysfunction *via* TLR4-NOX4 pathway: The regulation of autophagy and ROS production. *J Mol Cell Cardiol.* (2016) 101:11–24. doi: 10.1016/j.yjmcc.2016.10.017

24. Fu G, Wang B, He B, Feng M, Yu Y. LPS induces cardiomyocyte necroptosis through the Ripk3/Pgam5 signaling pathway. *J Recept Signal Transduct Res.* (2021) 41:32–7. doi: 10.1080/10799893.2020.1783682

25. Kong C, Ni X, Wang Y, Zhang A, Zhang Y, Lin F, et al. ICA69 aggravates ferroptosis causing septic cardiac dysfunction *via* STING trafficking. *Cell Death Discov.* (2022) 8:187. doi: 10.1038/s41420-022-00957-y

26. Knuefermann P, Nemoto S, Misra A, Nozaki N, Defreitas G, Goyert SM, et al. CD14-deficient mice are protected against lipopolysaccharide-induced cardiac inflammation and left ventricular dysfunction. *Circulation.* (2002) 106:2608–15. doi: 10.1161/01.cir.0000038110.69369.4c

27. Zhang N, Ye F, Zhou Y, Zhu W, Xie C, Zheng H, et al. Cardiac ankyrin repeat protein contributes to dilated cardiomyopathy and heart failure. *FASEB J.* (2021) 35:e21488. doi: 10.1096/fj.201902802RR

28. Lips DJ, van der Nagel T, Steendijk P, Palmen M, Janssen BJ, van Dantzig JM, et al. Left ventricular pressure-volume measurements in mice: Comparison of closed-chest versus open-chest approach. *Basic Res Cardiol.* (2004) 99:351–9. doi: 10.1007/s00395-004-0476-5

29. Li Y, Ren S, Xia J, Wei Y, Xi Y. EIF4A3-induced circ-BNIP3 aggravated hypoxia-induced injury of H9c2 cells by targeting miR-27a-3p/BNIP3. *Mol Ther Nucleic Acids.* (2020) 19:533–45. doi: 10.1016/j.omtn.2019.11.017

30. Ieda M, Fu JD, Delgado-Olguin P, Vedantham V, Hayashi Y, Bruneau BG, et al. Direct reprogramming of fibroblasts into functional cardiomyocytes by defined factors. *Cell.* (2010) 142:375–86. doi: 10.1016/j.cell.2010.07.002

31. Zhao BS, Huo HR, Ma YY, Liu HB, Li LF, Sui F, et al. Effects of 3-phenyl-propenal on the expression of toll-like receptors and downstream signaling components on raw264.7 murine macrophages. *Am J Chin Med.* (2008) 36:159–69. doi: 10.1142/S0192415X08005679

32. Trevani AS, Andonegui G, Giordano M, López DH, Gamberale R, Minucci F, et al. Extracellular acidification induces human neutrophil activation. *J Immunol.* (1999) 162:4849–57.

33. Zughaier SM, Stauffer BB, McCarty NA. Inflammation and ER stress downregulate BDH2 expression and dysregulate intracellular iron in macrophages. *J Immunol Res.* (2014) 2014:140728. doi: 10.1155/2014/140728

34. Cabedo Martinez AI, Weinhaupl K, Lee WK, Wolff NA, Storch B, Żerko S, et al. Biochemical and structural characterization of the interaction between the siderocalin NGAL/LCN2 (neutrophil gelatinase-associated lipocalin/lipocalin 2) and the N-terminal domain of its endocytic receptor SLC22A17. *J Biol Chem.* (2016) 291:2917–30. doi: 10.1074/jbc.M115.685644

35. Ye D, Yang K, Zang S, Lin Z, Chau HT, Wang Y, et al. Lipocalin-2 mediates non-alcoholic steatohepatitis by promoting neutrophil-macrophage crosstalk *via* the induction of CXCR2. *J Hepatol.* (2016) 65:988–97. doi: 10.1016/j.jhep.2016.05.041

36. Tarin C, Fernandez-Garcia CE, Burillo E, Pastor-Vargas C, Llamas-Granda P, Castejón B, et al. Lipocalin-2 deficiency or blockade protects against aortic abdominal aneurysm development in mice. *Cardiovasc Res.* (2016) 111:262–73. doi: 10.1093/cvr/cvw112

37. Borregaard N, Sorensen OE, Theilgaard-Monch K. Neutrophil granules: A library of innate immunity proteins. *Trends Immunol.* (2007) 28:340–5. doi: 10.1016/j.it.2007.06.002

38. Berger T, Togawa A, Duncan GS, Elia AJ, You-Ten A, Wakeham A, et al. Lipocalin 2-deficient mice exhibit increased sensitivity to *Escherichia coli* infection but not to ischemia-reperfusion injury. *Proc Natl Acad Sci USA.* (2006) 103:1834–9. doi: 10.1073/pnas.0510847103

39. Gupta N, Krasnodembskaya A, Kapetanaki M, Mouded M, Tan X, Serikov V, et al. Mesenchymal stem cells enhance survival and bacterial clearance in murine *Escherichia coli* pneumonia. *Thorax.* (2012) 67:533–9. doi: 10.1136/thoraxjnl-2011-201176

40. Steigedal M, Marstad A, Haug M, Damås JK, Strong RK, Roberts PL, et al. Lipocalin 2 imparts selective pressure on bacterial growth in the bladder and is elevated in women with urinary tract infection. *J Immunol.* (2014) 193:6081–9. doi: 10.4049/jimmunol.1401528

41. Choi EK, Jung H, Kwak KH, Yi SJ, Lim JA, Park SH, et al. Inhibition of oxidative stress in renal ischemia-reperfusion injury. *Anesth Analg.* (2017) 124:204–13. doi: 10.1213/ANE.0000000000001565

42. Skrypnyk NI, Gist KM, Okamura K, Montford JR, You Z, Yang H, et al. IL-6-mediated hepatocyte production is the primary source of plasma and urine neutrophil gelatinase-associated lipocalin during acute kidney injury. *Kidney Int.* (2020) 97:966–79. doi: 10.1016/j.kint.2019.11.013

43. Wasung ME, Chawla LS, Madero M. Biomarkers of renal function, which and when? *Clin Chim Acta.* (2015) 438:350–7. doi: 10.1016/j.cca.2014.08.039

44. Cannistra M, Ruggiero M, Zullo A, Gallelli G, Serafini S, Maria M, et al. Hepatic ischemia reperfusion injury: A systematic review of literature and the role of current drugs and biomarkers. *Int J Surg.* (2016) 33:S57–70. doi: 10.1016/j.ijsu.2016.05.050

45. Vazquez DE, Nino DF, De Maio A, Cauvi DM. Sustained expression of lipocalin-2 during polymicrobial sepsis. *Innate Immun.* (2015) 21:477–89. doi: 10.1177/1753425914548491

46. Hirschhorn T, Stockwell BR. The development of the concept of ferroptosis. *Free Radic Biol Med.* (2019) 133:130–43. doi: 10.1016/j.freeradbiomed.2018.09.043

47. Gao M, Monian P, Pan Q, Zhang W, Xiang J, Jiang X. Ferroptosis is an autophagic cell death process. *Cell Res.* (2016) 26:1021–32. doi: 10.1038/cr.2016.95

48. Sun Y, Chen P, Zhai B, Zhang M, Xiang Y, Fang J, et al. The emerging role of ferroptosis in inflammation. *Biomed Pharmacother.* (2020) 127:110108. doi: 10.1016/j.biopha.2020.110108

49. Kajarabille N, Latunde-Dada GO. Programmed cell-death by ferroptosis: antioxidants as mitigators. *Int J Mol Sci.* (2019) 20:4968. doi: 10.3390/ijms20194968

50. Li W, Li W, Leng Y, Xiong Y, Xia Z. Ferroptosis is involved in diabetes myocardial ischemia/reperfusion injury through endoplasmic reticulum stress. *DNA Cell Biol.* (2020) 39:210–25. doi: 10.1089/dna.2019.5097

51. Marques FZ, Prestes PR, Byars SG, Ritchie SC, Würtz P, Patel SK, et al. Experimental and human evidence for lipocalin-2 (neutrophil gelatinase-associated lipocalin [NGAL]) in the development of cardiac hypertrophy and heart failure. *J Am Heart Assoc.* (2017) 6:e005971. doi: 10.1161/JAHA.117.005971

52. Sung HK, Chan YK, Han M, Jahng JWS, Song E, Danielson E, et al. Lipocalin-2 (NGAL) attenuates autophagy to exacerbate cardiac apoptosis induced by myocardial ischemia. *J Cell Physiol.* (2017) 232:2125–34. doi: 10.1002/jcp.25672

53. Bao G, Clifton M, Hoette TM, Mori K, Deng SX, Qiu A, et al. Iron traffics in circulation bound to a siderocalin (Ngal)-catechol complex. *Nat Chem Biol.* (2010) 6:602–9. doi: 10.1038/nchembio.402

frontiers | Frontiers in Cardiovascular Medicine

TYPE Original Research
PUBLISHED 06 September 2022
DOI 10.3389/fcvm.2022.971321

OPEN ACCESS

EDITED BY
Jun Yu,
Temple University, United States

REVIEWED BY
Monica Y. Lee,
University of Illinois Chicago, United States
Jing-Song Ou,
The First Affiliated Hospital of Sun Yat-sen University, China

*CORRESPONDENCE
Feng Dong
fdong@neomed.edu
Liya Yin
lyin@neomed.edu

SPECIALTY SECTION
This article was submitted to Cardiovascular Therapeutics, a section of the journal Frontiers in Cardiovascular Medicine

RECEIVED 16 June 2022
ACCEPTED 15 August 2022
PUBLISHED 06 September 2022

CITATION
Winnicki A, Gadd J, Ohanyan V, Hernandez G, Wang Y, Enrick M, McKillen H, Kiedrowski M, Kundu D, Kegecik K, Penn M, Chilian WM, Yin L and Dong F (2022) Role of endothelial CXCR4 in the development of aortic valve stenosis.
Front. Cardiovasc. Med. 9:971321.
doi: 10.3389/fcvm.2022.971321

Role of endothelial CXCR4 in the development of aortic valve stenosis

Anna Winnicki[1], James Gadd[1], Vahagn Ohanyan[1], Gilbert Hernandez[1], Yang Wang[1], Molly Enrick[1], Hannah McKillen[1], Matthew Kiedrowski[1], Dipan Kundu[1], Karlina Kegecik[1], Marc Penn[1,2], William M. Chilian[1], Liya Yin[1]* and Feng Dong[1]*

[1]Department of Integrative Medical Sciences, Northeast Ohio Medical University, Rootstown Township, OH, United States, [2]Summa Cardiovascular Institute, Summa Health, Akron, OH, United States

Background: CXCL12/CXCR4 signaling is essential in cardiac development and repair, however, its contribution to aortic valve stenosis (AVS) remains unclear. In this study, we tested the role of endothelial CXCR4 on the development of AVS.

Materials and methods: We generated CXCR4 endothelial cell-specific knockout mice (EC CXCR4 KO) by crossing $CXCR4^{fl/fl}$ mice with Tie2-Cre mice to study the role of endothelial cell CXCR4 in AVS. $CXCR4^{fl/fl}$ mice were used as controls. Echocardiography was used to assess the aortic valve and cardiac function. Heart samples containing the aortic valve were stained using Alizarin Red for detection of calcification. Masson's trichrome staining was used for the detection of fibrosis. The apex of the heart samples was stained with wheat germ agglutinin (WGA) to visualize ventricular hypertrophy.

Results: Compared with the control group, the deletion of CXCR4 in endothelial cells led to significantly increased aortic valve peak velocity and aortic valve peak pressure gradient, with decreased aortic valve area and ejection fraction. EC CXCR4 KO mice also developed cardiac hypertrophy as evidenced by increased diastolic and systolic left ventricle posterior wall thickness (LVPW), cardiac myocyte size, and heart weight (HW) to body weight (BW) ratio. Our data also confirmed increased microcalcifications, interstitial fibrosis, and thickened valvular leaflets of the EC CXCR4 KO mice.

Conclusion: The data collected throughout this study suggest the deletion of CXCR4 in endothelial cells is linked to the development of aortic valve stenosis and left ventricular hypertrophy. The statistically significant parameters measured indicate that endothelial cell CXCR4 plays an important role in aortic valve development and function. We have compiled compelling evidence that EC CXCR4 KO mice can be used as a novel model for AVS.

KEYWORDS

CXCR4, aortic stenosis, aortic valve stenosis, cardiac hypertrophy, endothelium

Introduction

Aortic valve stenosis (AVS), also known as aortic stenosis (AS), is the narrowing of the left ventricular outflow tract. It is among the most common valvular heart diseases and affects around 2–4% of the human population 65 years and older (1–3). As the human population rapidly ages, there is a marked increase in AVS worldwide (4). Patients with AVS are often asymptomatic for years before developing what is known as irreversible late-stage calcification, or calcific aortic disease (CAVD) (1). This advanced stage of valvular thickening and calcification can cause symptoms such as angina, syncope, dyspnea, and heart failure, being a significant cause of morbidity and mortality among the elderly population (2, 3). The morbidity rate of severe, symptomatic AVS is around 50% within 2 years of diagnosis (2). Risk factors such as bicuspid aortic valves (BAV), diabetes, mechanical injury, hypertension, maleness, smoking, and hypercholesterolemia all contribute to the development and progression of this disease (2, 3, 5, 6). It is important to note that AVS accounts for 3–6% of congenital heart defects in neonates and infants, often developing during the first trimester and evolving throughout gestation (7). With the only successful treatment option for AVS being surgical valve replacement, there is an urgent need to develop new target therapies (3).

CXCL12, also known as stromal cell-derived factor-1 (SDF-1), is a homeostatic chemokine expressed in many cell types throughout the body, especially in the presence of tissue damage (1, 8–10). Its receptor, CXCR4, is a G-protein coupled receptor expressed on the surface of cell types such as endothelial cells, platelets, neurons, and stem cells (9, 11, 12). Evidence has linked CXCR4 to biological processes such as stem cell recruitment, tissue regeneration, angiogenesis, tumor metastasis, cancer development and progression, CNS disease, and cardiovascular diseases (9, 11, 13). CXCR4 is upregulated under conditions of hypoxia, stress injury, and in damaged vascular tissues (10). Our previous studies have demonstrated the importance of the CXCL12/CXCR4 axis in myocardial repair (14, 15). The CXCL12/CXCR4 axis plays an important role in tissue repair (16) and inflammation (1, 17–19). However, the role of endothelial CXCR4 on the development of AVS remains unclear. In the current study, we provide evidence that the endothelial knockout of CXCR4 leads to the early onset of AVS.

Materials and methods

Animals

The animal work in this study was approved by the Institutional Animal Care and Use Committee (IACUC) of Northeast Ohio Medical University. Tie2-Cre mice (# 008863) were purchased from Jackson Laboratories. $CXCR4^{fl/fl}$ mice were reported before (16). Endothelial specific CXCR4 knockout mice (Tie2-Cre/$CXCR4^{fl/fl}$ mice) were generated by crossing the $CXCR4^{fl/fl}$ mice with Tie2-Cre mice. The deletion of CXCR4 in endothelial cells was confirmed by western blot. Animals were housed in temperature-controlled conditions allowing food and water *ad libitum* in an American Association for Accreditation of Laboratory Animal Care–approved animal facility. All animal experiments performed complied with the NIH guidelines (Guide for the Care and Use of Laboratory Animals). For this study, the control group, referenced throughout as "Control," are $CXCR4^{fl/fl}$ mice. The experimental group, referenced throughout as "EC CXCR4 KO," consisted of Tie2-Cre/$CXCR4^{fl/fl}$ mice. Equal numbers of both males and females were used throughout the study.

TABLE 1 PCR primers used.

Protocol # 28368		**CXCR4-Fl primers**
C-F	(5′-3′)	CAC TAC GCA TGA CTC GAA ATG
WT-lox C-F	(5′-3′)	GTG TGC GGT GGT ATC CAG C
Protocol # 41502		**Tie2-Cre primers**
WT forward	(5′-3′)	CTG TGA CCT GAG TGC CCA GT
Common	(5′-3′)	CCA CAC ACG TGC ACA TAT AGA
Mutant forward	(5′-3′)	GCG TTT AAG TAA TGG GAT GGT C

Genotyping

DNA samples used for genotyping were extracted from tissue samples using standard procedures. Briefly, tissue samples were collected from pups, aged 10 days. Ear clippings or tail clippings were placed in a 1.5 ml microcentrifuge tube and kept at −20°C until processed. Tissue was thawed and then digested overnight at 55°C in 675 μl DNA Extraction Buffer mixed with 25 μl proteinase K (Amresco, #97062-242). Samples were purified using 700 μl 25:24:1 Phenol/Chloroform/Isoamyl Alcohol (Fisher, # BP1752I-400), centrifuged at 14,000 rpm for 10 min, then the supernatant was saved. Further purification using Chloroform (B & J, #24263) was performed, following the previously listed steps. DNA was precipitated using equal volume of isopropanol (Fisher, #A451SK-4) and centrifuged (20 min at 14,000 rpm). DNA pellets were washed with 70% ethanol and resuspended in 1× TE Buffer (65–70 μl). PCR was set up using TAKARA polymerase kit (TAKARA, #RR0062) and Jackson Laboratories protocols (**Table 1**). Genotyping primer pairs are detailed in **Table 1**. PCR products were analyzed using gel electrophoresis on 3% agarose gels (MidSci, #BE-GCA-500, Fenton, MO, United States).

Tissue harvest and fixation

Mice were euthanized and hearts were thoroughly perfused using cold 1× PBS (Sigma, #P4417, Burlington, MA, United States). The heart was removed, washed in 1× PBS, weighed, and sectioned into thirds using a heart matrice (Braintree, #BS-SS-H

5005, Chicago, IL, United States), to ensure the valves were not damaged. The apex and base were fixed in 10% Neutral Buffered Formalin (Fisher, #22-110-683) overnight at room temperature. The midsection of the heart was snap frozen and stored at −80°C for later use. Tissue samples were then fixed, processed, and 5 μm sections were prepared using a Leica microtome.

Histology

All samples were stained using Hematoxylin and Eosin (H&E) for general morphology. Base samples containing the aortic valve were stained using Alizarin Red (Sigma, #A5533, Burlington, MA, United States) for detection of calcification. Masson's trichrome (Scytek, #TRM-1, Logan, UT, United States) staining was used for the detection of fibrosis and excess collagen deposition. Images were obtained using the slide scanner (Olympus BX61VS, Webster, TX, United States) at 40× magnification. Quantification and calculations for calcification, collagen deposition, and leaflet thickness were performed using ImageJ software (NIH website).

Immunohistochemical staining

Apex sample sections were stained with rhodamine-conjugated wheat germ agglutinin (WGA, Vector Laboratories, #RL1022), which labels myocyte membranes to visualize ventricular hypertrophy, as previously described (16). Images were acquired using a confocal microscope. All quantitative evaluations were performed with ImageJ software (NIH website).

Echocardiography

Echocardiography was performed on mice aged 3–40 weeks under 1.5–2% isoflurane using the VEVO 770 machine. Left ventricular wall thickness, ejection fraction, and fractional shortening were calculated with VEVO LAB 3.0 software. Aortic velocity and pressure were measured *via* the echocardiogram and the aortic valve area was measured using the continuity equation.

Endothelial cell isolation and culture

Mouse cardiac endothelial cells (ECs) were isolated as previously described (20). Briefly, mouse hearts were dissected and minced into small pieces. After the digestion of the heart using Collagenase I (Worthington, Lakewood, NJ, United States), cells were washed and incubated with Dynabeads conjugated with anti-CD31 antibody (Thermo Fisher Scientific, Oakwood, OH, United States). The beads with endothelial cells were washed several times and cultured in a mouse endothelial culture medium (Cell Biologics, Chicago, IL, United States). When confluent, cells were purified with Dynabeads conjugated with anti-Mouse CD102 (ICAM2) antibody.

Western blot

Protein was isolated from endothelial cells with a RIPA Kit (Sigma Aldrich, R0278, Burlington, MA, United States) supplemented with protease and phosphatase inhibitors. Protein concentration was determined *via* BCA protein assay (Thermo Fisher Scientific, 23227, Oakwood, OH, United States) per manufacturer's instructions. Protein lysates (40 μg/lane) were loaded for probing CXCR4 (1:500 dilution; Abcam, Ab181020, Waltham, MA, United States). Following primary antibody incubation (overnight at 4°C), blots were incubated (1 h at room temperature) with a mouse anti-rabbit IgG-HRP (1:3,000 dilution; Santa Cruz, SC-2357, Dallas, TX, United States). Immunoreactive bands were detected using a western blot imaging system (Cytiva, Amersham ImageQuant 800, Marlborough, MA, United States). GAPDH was used as a loading control (1:400 dilution; Millipore Sigma, MAB374, Burlington, MA, United States).

Statistical analysis

Data are represented as mean ± SD. Statistical significance between the two groups was determined using a 2-tailed Student *t*-test. One- or two-way ANOVA was used for multiple comparisons where appropriate. A probability value of $P \leq 0.05$ was used to establish statistical significance.

Results

Role of endothelial cell CXCR4 on the development of aortic valve stenosis

To evaluate if endothelial cell CXCR4 deletion affects the function of aortic valves, echocardiography was performed on EC CXCR4 KO and control mice, spanning an age range of 3–40 weeks old. AV pressure gradient and velocities between the EC CXCR4 KO group and the control group were significantly different in different aged mice (**Figures 1A,B**). We observed that 50% of 3-week-old EC CXCR4 KO mice ($n = 11$) presented with significant increase in aortic valve peak velocity and aortic valve peak pressure gradient (**Figures 1A,B,F**). By 6 weeks old, 90% of EC CXCR4 KO mice ($n = 11$) presented with AVS of varying severity (**Figures 1A,B**). Forty-five percentage of 6-week-old EC CXCR4 KO mice developed severe AVS (aortic valve pressure gradient ≥ 40 mmHg, peak aortic velocity ≥ 4 m/s). Interestingly, our data also show significant difference in the aortic peak pressure gradients and velocities between the male and female EC CXCR4 KO mice at 3 weeks

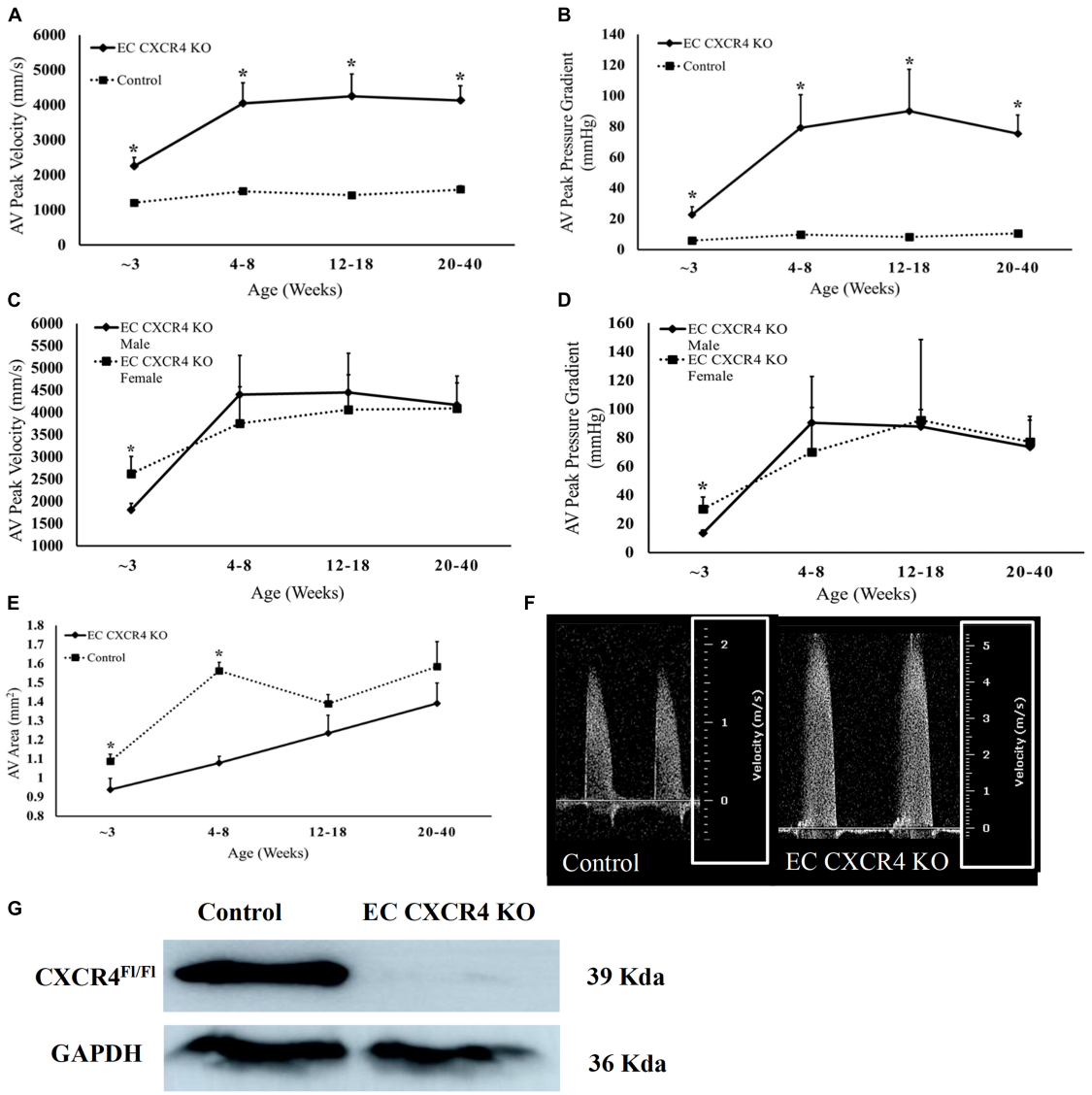

FIGURE 1
(A–F) Deletion of CXCR4 in endothelial cells led to Aortic Stenosis. **(A)** Aortic Valve Peak Velocity and **(B)** aortic peak pressure gradient (n = 10–13). **(C)** Aortic valve peak velocity and **(D)** aortic valve peak pressure gradient (n = 5–6), males and females are represented separately to show the difference in disease onset for EC CXCR4 KO mice. **(E)** Aortic valve area (n = 10–13) calculated using continuity equation. **(F)** Representative pulsed wave (PW) Doppler images of aortic flow for the control and EC CXCR4 KO groups, with images being from mice of the same sex and age. Note the different scales outlined in the white box. **(G)** Western Blot analysis of the CXCR4 knockout on endothelial cells. We observed a significant decrease in endothelial CXCR4 expression in EC CXCR4 KO mice compared with control mice. Data shows the average for mice aged 3–40 weeks. Calculated using Echocardiogram measurements on a VEVO 770 system. *Indicates a p-value $\leq$ 0.05 vs. control group.

old (Figures 1C,D). However, such a sex significance was lost by 6 weeks old (Figures 1C,D). Moreover, the aortic valve area (AVA) of the EC CXCR4 KO mice was notably smaller than the control mice at 3–8 weeks old measurements yielded ($p < 0.05$, Figure 1E). The efficiency of knockdown of CXCR4 in endothelial cells was confirmed by western blot. A significant decrease in endothelial CXCR4 expression was observed in the EC CXCR4 KO mice compared with the control mice (Figure 1G).

Role of endothelial cell CXCR4 on cardiac function and cardiac hypertrophy

The EC CXCR4 KO mice have a significantly decreased ejection fraction (EF) compared to the control mice at the age of 20–40 weeks (Figure 2A). There was no statistically significant difference between the EC CXCR4 KO and control mice in the left ventricular mass (Figure 2B) or the left ventricle posterior

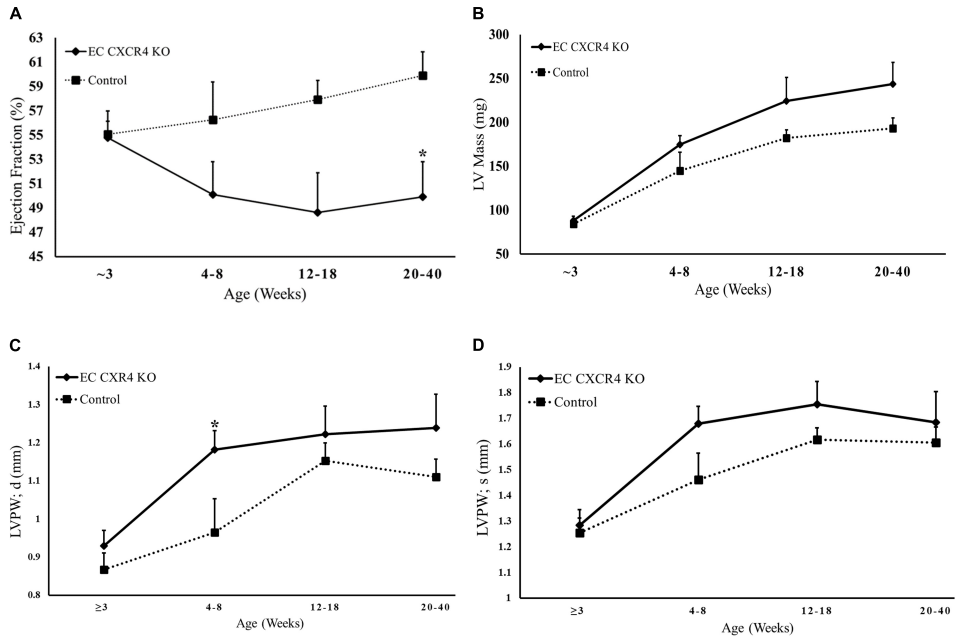

FIGURE 2
(A–D) Echocardiogram results indicate decreased Ejection Fraction and ventricular hypertrophy in EC CXCR4 KO mice. **(A)** Endocardial ejection fraction (B-mode) **(B)** Left ventricle mass **(C)** LVPWd, diastolic thicknesses of the LV posterior wall **(D)** LVPWs, systolic thicknesses of the LV posterior wall. Data shows the average for mice aged 3–40 weeks (n = 10–13). Calculated using echocardiogram measurements on a VEVO 770 system. *Indicates a p-value $\leq$ 0.05 vs. control group.

wall systolic (LVPWs) although there was a trend (Figure 2D). Interestingly, the left ventricle posterior wall diastolic (LVPWd) between the EC CXCR4 KO and control mice was significantly different at the age of 4–8 weeks (Figure 2C). There was no significant difference in heart rate between the groups (data not shown).

We also evaluated the effects of endothelial cell CXCR4 KO on cardiac myocyte size with WGA immunostaining. Our results showed a significant increase in cross-sectional area of cardiomyocytes from EC CXCR4 KO mice compared to control mice (Figures 3A,B). We also found that the EC CXCR4 KO mice had a significantly larger heart weight (HW) to body weight (BW) ratio compared to the control group (Figure 3C), indicating enlarged heart, which is consistent with the immunofluorescence staining and the echocardiogram findings for LV hypertrophy.

Endothelial cell CXCR4 KO led to increased microcalcifications, interstitial fibrosis, and thickened valvular leaflets

The H&E staining and Masson's trichrome staining show that valvular leaflets were thicker in the EC CXCR4 KO mice compared to the control mice (Figures 4A,C). Alizarin Red staining shows the deposition of calcium on the aortic valves of the EC CXCR4 KO mice (Figures 4B,D). Masson's trichrome staining shows significant increase in interstitial fibrosis in the EC CXCR4 KO mice compared to the control groups (Figures 4E,F).

Discussion

Deletion of CXCR4 in endothelial cells linked to the development of aortic valve stenosis

In this study, we report the effect of endothelial CXCR4 expression on the development of AVS for the first time using our EC CXCR4 null mice. In human AVS, the aortic valve leaflets stiffen and are unable to fully open, causing significant increases in AV peak velocity and pressure gradient. This leads the heart to have to work harder to pump blood out to the rest of the body as the AV opening is narrowed. Therefore, as AVS develops and progresses, the pressure overload within the left ventricle increases, leading to an increase in left ventricle mass and eventual left ventricular hypertrophy. We showed a spontaneous murine model of AVS with significant increases in AV peak velocity and pressure gradient, decreases in AVA (Figure 1), and significant increases in valvular microcalcifications (Figure 4). Such a mouse model recaptures the pathology of AVS

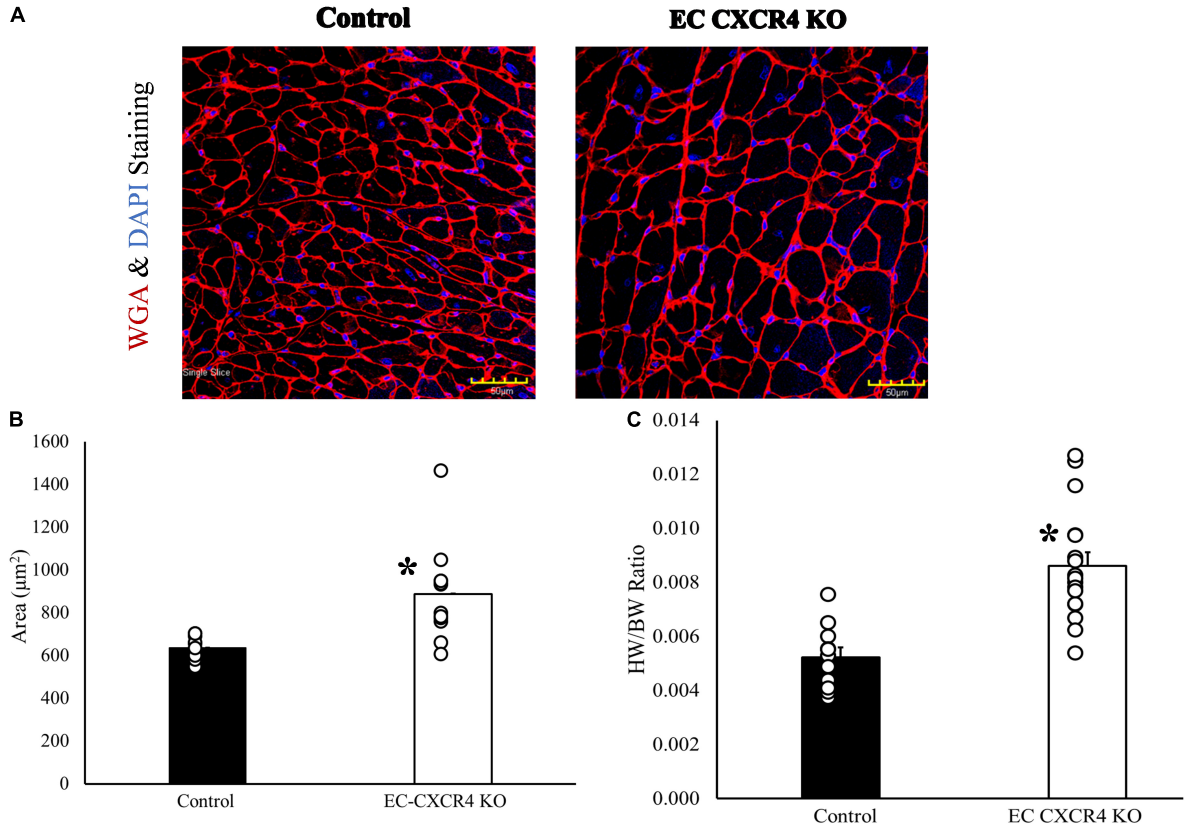

FIGURE 3
(A–C) Role of endothelial cell CXCR4 on cardiomyocyte hypertrophy. **(A)** Confocal image of representative immunofluorescent staining with WGA and DAPI to label myocyte membranes. **(B)** The average area of one cardiomyocyte was determined using WGA and DAPI staining (n = 10–12). **(C)** Heart weight/body weight ratio (n = 11–17). Our results showed a significantly increased cross-sectional area in cardiomyocytes and HW/BW ratio from EC CXCR4 KO mice compared to control mice. *Indicates a p-value $\leq$ 0.05 vs. control group.

documented in humans, linking the absence of CXCR4 on endothelial cells to the development of hemodynamically stable AVS. Our EC CXCR4 KO mice show increased left ventricle posterior wall thickness in diastolic, enlarged cardiac myocyte size, and heart weight (HW) to body weight (BW) ratio, all of which indicate cardiomyocyte hypertrophy. Progression of the AVS and hypertrophy combined will cause restricted coronary flow, possibly leading to myocardial ischemia and fibrosis (3, 7).

Over the past few years, disruption of the CXCL12/CXCR4 pathway has been studied during embryonic development, using genetic models to knock out each respective piece of the axis to examine their effects on cardiac development and more specifically, valvular development (10, 21–23). Knockouts involving the CXCL12/CXCR4 axis are known to cause ventricular septal defects (VSDs), and developmental disruption of aortic arch, pulmonary artery, and coronary artery in animal models (10, 19, 21, 22, 24). CXCL12 null mice also present with malformations and decreased cardiac function (21). Hyperplasia within the semilunar valve (SLV) has been observed in CXCR4 knockout models, indicating the important role this receptor plays during the endothelial-mesenchymal transition and beyond (24). However, there has been very little done to analyze the AV function of adult KO mouse models (10, 21). To the best of our knowledge, this is the first study that links the deletion of CXCR4 in endothelial cells to the development of hemodynamically stable AVS in a murine model.

EC CXCR4 KO mouse presents a new model for studying the development of aortic valve stenosis

Our Tie2-Cre driven, endothelial CXCR4 knockout mice show hemodynamically stable aortic valve stenosis, with calcification and ventricular hypertrophy. This genetic KO model develops AVS as early as 3 weeks in females and 6 weeks in males, maintaining increased AV peak velocities and pressures throughout their lifetime. Our mouse model of spontaneous AVS presents as a new avenue for AVS research, with a shorter development time compared to other

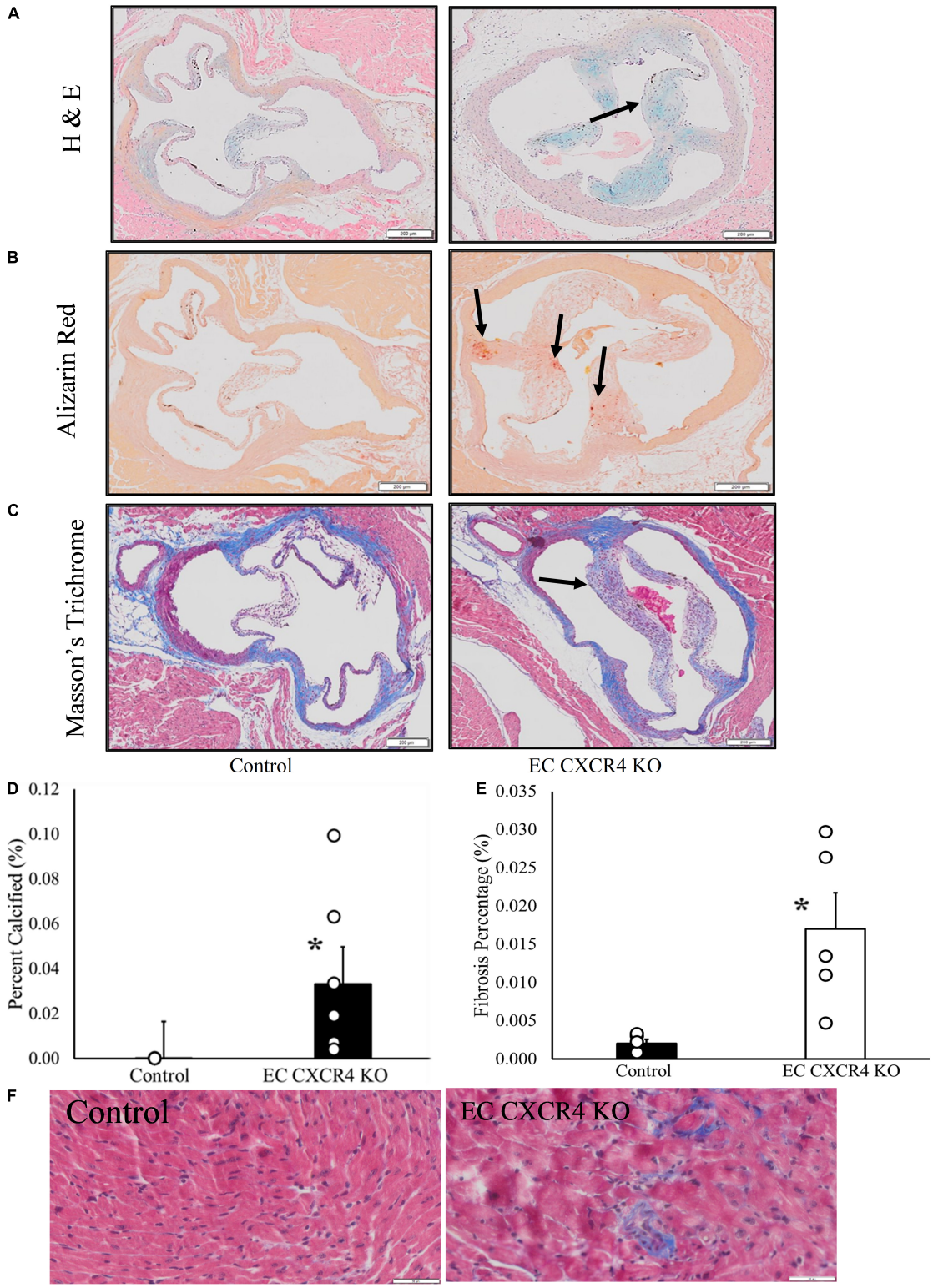

FIGURE 4
(A–F) Endothelial cell CXCR4 KO led to increased microcalcifications, interstitial fibrosis, and thickened valvular leaflets. **(A)** Modified Hematoxylin & Eosin staining. Arrows point to valve leaflet thickening. **(B)** Alizarin red staining. Arrows point to the positive stain results indicating the presence of microcalcifications. **(C)** Masson's trichrome staining results. Arrow indicates the presence of leaflet thickening on aortic valves of the EC CXCR4 KO group. **(D)** Alizarin red staining quantification (n = 3–5). **(E)** Interstitial fibrosis quantification (n = 5). **(F)** Representative Masson's trichrome staining images of interstitial fibrosis (scale bars = 50 μm). *Indicates a p-value $\leq$ 0.05 vs. control group.

AVS mouse models which normally take > 20 weeks to develop hemodynamically stable AVS (25, 26). Also, our AVS model does not need to feed the animals a special diet or induce a mechanical injury (25, 27). Even though about six varieties of dietary modification were used to develop AVS, they do not consistently develop hemodynamically significant AVS (25). Mechanical injury induced AVS models come with the risks associated with surgery (26). Our EC CXCR4 KO mice develop AVS early, presenting as a time frame friendly option to AVS without any forms of intervention.

Male and female difference in disease progression

Human AVS has shown to progress differently in males and females. For example, males have a higher risk for the disease while females often present with more severe symptoms (28). Female patients often develop severe AVS with more fibrosis, but less calcification compared to male patients (4). It has been reported that estrogen may play a protective role against AVS, leading human females to develop the disease post-menopause (29). Also, there are sex differences observed in the development of AVS-related LV hypertrophy. Human males tend to develop eccentric hypertrophy while females often develop concentric hypertrophy (30). Therefore, understanding the relationship between AVS development and sex differences is important and to address this, we decided to include equal number of males and females in our initial study. Knowing these differences could cause some variation in both groups, we looked specifically at the male vs. female numbers at each time point. Interestingly, female EC CXCR4 KO mice show the signs of AVS as early as 3 weeks of age while the males did not present until after 5 weeks of age. Although the underlying mechanism is unclear, this may indicate that developmental hormones could play a role in the disease development. Further study such as the relationship between the CXCL12/CXCR4 axis and the different sex hormones is needed to address it.

Possible mechanism and future directions

The goal of this study was to invest the role of endothelial CXCR4 on the development of AVS and establish the timeline for disease development. The mechanism to explain why AVS is occurring in the presence of an EC CXCR4 KO has not yet been determined. Previous research shows that CXCR4 is elevated in various organs at different stages in the developmental process, with CXCR4 KO mice presenting with defects in hematopoiesis, cardiogenesis, and fetal lethality *in utero* (31). CXCR4 is present on the endothelial cells that line both major vessels and the microvasculature throughout the body (32). This indicates that CXCL12/CXCR4 plays a key role in mediating cell migration and angiogenesis throughout development. Our findings that the endothelial-specific CXCR4 deficiency spontaneously developed AVS confirmed the critical role of CXCR4 in aortic valve development. It is possible that AVS developed in CXCR4 KO mice was due to congenital malformations.

Aortic valve stenosis may be brought on by multiple mechanisms, including mechanical injury and immune system activation (2, 3). CXCR4 signaling in blood vessels near calcified valves is speculated to be the cause of neovascularization and the promotion of inflammatory cell recruitment (13). Chemokines and their receptors are known for organizing and distributing immune responses throughout the body, so it is not surprising that the disruption of the CXCL12/CXCR4 pathway in any cell would lead to the development of diseases (9, 19, 32). AVS occurring in the EC CXCR4 KO mice may also be due to the role of CXCR4 in the recruitment of progenitor cells and immune-factor regulation as research has shown CXCR4 to impact endothelial progenitor cell migration and homing processes.

One limitation of our study pertains is the use of a Tie2-Cre for endothelial cell specific knockout. Although Tie2/Tek promoter are widely used in animal models that target endothelial cells, Tie2 may also express in hematopoietic cells (33), therefore, Tie2-Cre KO mice may affect the expression of CXCR4 in the hematopoietic cells. An inducible EC CXCR4 KO animal model will address the embryo developmental or postnatal contribution of CXCR4 to the AVS.

Conclusion

We demonstrated that mice with deletion of CXCR4 in endothelial cells develop hemodynamically significant aortic valve stenosis and left ventricular hypertrophy. This indicates that CXCR4 plays an important role in aortic valve development and function. It was also observed that female mice in this line developed AVS earlier than males. Our results indicate that Tie2-Cre/CXCR4 $^{fl/fl}$ mice can be used as a novel model for AVS study.

Data availability statement

The raw data supporting the conclusions of this article will be made available by the authors, without undue reservation.

Ethics statement

The animal study was reviewed and approved by the Institutional Animal Care and Use Committee (IACUC) of Northeast Ohio Medical University.

Author contributions

FD, MP, LY, and WC contributed to the conception and design of the study. AW, JG, VO, KK, and FD contributed to the echocardiography and data analysis. AW, FD, GH, MK, and HM contributed to the staining and data analysis. DK contributed to the EC cell culture and Western. LY, YW, AW, and ME contributed to the animal model breeding. AW organized the database and performed the statistical analysis. AW, LY, and FD wrote the manuscript. ME, VO, MK, DK, and HM contributed to the manuscript revision. All authors read and approved the submitted version.

Funding

This study was supported by the NEOMED research grant (FD) and R01 HL137008-01A1 (LY).

Conflict of interest

The authors declare that the research was conducted in the absence of any commercial or financial relationships that could be construed as a potential conflict of interest.

Publisher's note

All claims expressed in this article are solely those of the authors and do not necessarily represent those of their affiliated organizations, or those of the publisher, the editors and the reviewers. Any product that may be evaluated in this article, or claim that may be made by its manufacturer, is not guaranteed or endorsed by the publisher.

References

1. Di Vito A, Donato A, Presta I, Mancuso T, Brunetti FS, Mastroroberto P, et al. Extracellular matrix in calcific aortic valve disease: architecture, dynamic and perspectives. *Int J Mol Sci.* (2021) 22:913. doi: 10.3390/ijms22020913

2. Goody PR, Hosen MR, Christmann D, Niepmann ST, Zietzer A, Adam M, et al. Aortic valve stenosis: from basic mechanisms to novel therapeutic targets. *Arterioscler Thromb Vasc Biol.* (2020) 40:885–900. doi: 10.1161/ATVBAHA.119.313067

3. Miller JD, Weiss RM, Heistad DD. Calcific aortic valve stenosis: methods, models, and mechanisms. *Circ Res.* (2011) 108:1392–412. doi: 10.1161/CIRCRESAHA.110.234138

4. Nitsche C, Koschutnik M, Kammerlander A, Hengstenberg C, Mascherbauer J. Gender-specific differences in valvular heart disease. *Wien Klin Wochenschr.* (2020) 132:61–8. doi: 10.1007/s00508-019-01603-x

5. Fernández B, Soto-Navarrete MT, López-García A, López-Unzu MÁ, Durán AC. Bicuspid aortic valve in 2 model species and review of the literature. *Vet Pathol.* (2020) 57:321–31. doi: 10.1177/0300985819900018

6. Mosch J, Gleissner CA, Body S, Aikawa E. Histopathological assessment of calcification and inflammation of calcific aortic valves from patients with and without diabetes mellitus. *Histol Histopathol.* (2017) 32:293–306. doi: 10.14670/HH-11-797

7. Singh GK. Congenital aortic valve stenosis. *Children.* (2019) 6:69. doi: 10.3390/children6050069

8. Döring Y, Noels H, van der Vorst EPC, Neideck C, Egea V, Drechsler M. Vascular CXCR4 limits atherosclerosis by maintaining arterial integrity: evidence from mouse and human studies. *Circulation.* (2017) 136:388–403. doi: 10.1161/CIRCULATIONAHA.117.027646

9. Noels H, Weber C, Koenen RR. Chemokines as therapeutic targets in cardiovascular disease. *Arterioscler Thromb Vasc Biol.* (2019) 39:583–92. doi: 10.1161/ATVBAHA.118.312037

10. Ridge LA, Kewbank D, Schütz D, Stumm R, Scambler PJ, Ivins S. Dual role for CXCL12 signaling in semilunar valve development. *Cell Rep.* (2021) 36:109610. doi: 10.1016/j.celrep.2021.109610

11. Bianchi ME, Mezzapelle R. The chemokine receptor CXCR4 in cell proliferation and tissue regeneration. *Front Immunol.* (2020) 11:2109. doi: 10.3389/fimmu.2020.02109

12. Blancas AA, Balaoing LR, Acosta FM, Grande-Allen KJ. Identifying behavioral phenotypes and heterogeneity in heart valve surface endothelium. *Cells Tissues Organs.* (2016) 201:268–76. doi: 10.1159/000444446

13. Dorfmüller P, Bazin D, Aubert S, Weil R, Brisset F, Daudon M, et al. Crystalline ultrastructures, inflammatory elements, and neoangiogenesis are present in inconspicuous aortic valve tissue. *Cardiol Res Pract.* (2010) 2010:685926. doi: 10.4061/2010/685926

14. Mayorga M, Kiedrowski M, Shamhart P, Forudi F, Weber K, Chilian WM, et al. Early upregulation of myocardial CXCR4 expression is critical for dimethyloxalylglycine-induced cardiac improvement in acute myocardial infarction. *Am J Physiol Heart Circ Physiol.* (2016) 310:H20–8. doi: 10.1152/ajpheart.00449.2015

15. Mayorga ME, Kiedrowski M, McCallinhart P, Forudi F, Ockunzzi J, Weber K, et al. Role of SDF-1:CXCR4 in impaired post-myocardial infarction cardiac repair in diabetes. *Stem Cells Transl Med.* (2018) 7:115–24. doi: 10.1002/sctm.17-0172

16. Dong F, Harvey J, Finan A, Weber K, Agarwal U, Penn MS. Myocardial CXCR4 expression is required for mesenchymal stem cell mediated repair following acute myocardial infarction. *Circulation.* (2012) 126:314–24. doi: 10.1161/CIRCULATIONAHA.111.082453

17. Mousavi A. CXCL12/CXCR4 signal transduction in diseases and its molecular approaches in targeted-therapy. *Immunol Lett.* (2020) 217:91–115. doi: 10.1016/j.imlet.2019.11.007

18. Murad HAS, Alqurashi TMA, Hussien MA. Interactions of selected cardiovascular active natural compounds with CXCR4 and CXCR7 receptors: a molecular docking, molecular dynamics, and pharmacokinetic/toxicity prediction study. *BMC Complement Med Ther.* (2022) 22:35. doi: 10.1186/s12906-021-03488-8

19. Yu S, Crawford D, Tsuchihashi T, Behrens TW, Srivastava D. The chemokine receptor CXCR7 functions to regulate cardiac valve remodeling. *Dev Dyn.* (2011) 240:384–93. doi: 10.1002/dvdy.22549

20. Juguilon C, Wang Z, Wang Y, Enrick M, Jamaiyar A, Xu Y, et al. Mechanism of the switch from NO to H2O2 in endothelium-dependent vasodilation in diabetes. *Basic Res Cardiol.* (2022) 117:2. doi: 10.1007/s00395-022-00910-1

21. Ivins S, Chappell J, Vernay B, Suntharalingham J, Martineau A, Mohun TJ, et al. The CXCL12/CXCR4 axis plays a critical role in coronary artery development. *Dev Cell.* (2015) 33:455–68. doi: 10.1016/j.devcel.2015.03.026

22. Kim BG, Kim YH, Stanley EL, Garrido-Martin EM, Lee YJ, Oh SP. CXCL12-CXCR4 signalling plays an essential role in proper patterning of aortic arch and pulmonary arteries. *Cardiovasc Res.* (2017) 113:1677–87. doi: 10.1093/cvr/cvx188

23. LaRocca TJ, Altman P, Jarrah AA, Gordon R, Wang E, Hadri L, et al. .CXCR4 cardiac specific knockout mice develop a progressive cardiomyopathy. *Int J Mol Sci.* (2019) 20:2267. doi: 10.3390/ijms20092267

24. Gerrits H, van Ingen Schenau DS, Bakker NE, van Disseldorp AJ, Strik A, Hermens LS. Early postnatal lethality and cardiovascular defects in CXCR7-deficient mice. *Genesis.* (2008) 46:235–45. doi: 10.1002/dvg.20387

25. Herrmann J, Gummi MR, Xia M, van der Giet M, Tölle M, Schuchardt M. Vascular calcification in rodent models-keeping track with an extented method assortment. *Biology.* (2021) 10:459. doi: 10.3390/biology10060459

26. Honda S, Miyamoto T, Watanabe T, Narumi T, Kadowaki S, Honda Y, et al. A novel mouse model of aortic valve stenosis induced by direct wire injury. *Arterioscler Thromb Vasc Biol.* (2014) 34:270–8. doi: 10.1161/ATVBAHA.113.302610

27. Woodward HJ, Zhu D, Hadoke PWF, MacRae VE. Regulatory role of sex hormones in cardiovascular calcification. *Int J Mol Sci.* (2021) 22:4620. doi: 10.3390/ijms22094620

28. Tribouilloy C, Bohbot Y, Rusinaru D, Belkhir K, Diouf M, Altes A, et al. Excess mortality and undertreatment of women with severe aortic stenosis. *J Am Heart Assoc.* (2021) 10:e018816. doi: 10.1161/JAHA.120.018816

29. Osako MK, Nakagami H, Koibuchi N, Shimizu H, Nakagami F, Koriyama H. Estrogen inhibits vascular calcification via vascular RANKL system: common mechanism of osteoporosis and vascular calcification. *Circ Res.* (2010) 107:466–75. doi: 10.1161/CIRCRESAHA.110.216846

30. Dobson LE, Fairbairn TA, Plein S, Greenwood JP. Sex differences in aortic stenosis and outcome following surgical and transcatheter aortic valve replacement. *J Womens Health.* (2015) 24:986–95. doi: 10.1089/jwh.2014.5158

31. Britton C, Poznansky MC, Reeves P. Polyfunctionality of the CXCR4/CXCL12 axis in health and disease: implications for therapeutic interventions in cancer and immune-mediated diseases. *FASEB J.* (2021) 35:e21260. doi: 10.1096/fj.202001273R

32. Murdoch C. CXCR4: chemokine receptor extraordinaire. *Immunol Rev.* (2000) 177:175–84. doi: 10.1034/j.1600-065x.2000.17715.x

33. Tang Y, Harrington A, Yang X, Friesel RE, Liaw L. The contribution of the Tie2+ lineage to primitive and definitive hematopoietic cells. *Genesis.* (2010) 48:563–7. doi: 10.1002/dvg.20654

frontiers | Frontiers in Cardiovascular Medicine

TYPE Mini Review
PUBLISHED 30 September 2022
DOI 10.3389/fcvm.2022.1031293

OPEN ACCESS

EDITED BY
Liya Yin,
Northeast Ohio Medical University,
United States

REVIEWED BY
Jinjiang Pang,
University of Rochester, United States
Rongxue Wu,
The University of Chicago,
United States

*CORRESPONDENCE
Hong Chen
hong.chen@childrens.harvard.edu

SPECIALTY SECTION
This article was submitted to Cardiovascular Therapeutics, a section of the journal Frontiers in Cardiovascular Medicine

RECEIVED 29 August 2022
ACCEPTED 13 September 2022
PUBLISHED 30 September 2022

CITATION
Singh B, Li K, Cui K, Peng Q, Cowan DB, Wang D-Z, Chen K and Chen H (2022) Defective efferocytosis of vascular cells in heart disease. *Front. Cardiovasc. Med.* 9:1031293. doi: 10.3389/fcvm.2022.1031293

Defective efferocytosis of vascular cells in heart disease

Bandana Singh[1], Kathryn Li[1], Kui Cui[1], Qianman Peng[1], Douglas B. Cowan[1], Da-Zhi Wang[2], Kaifu Chen[3] and Hong Chen[1]*

[1]Vascular Biology Program, Department of Surgery, Harvard Medical School, Boston Children's Hospital, Boston, MA, United States, [2]Center for Regenerative Medicine, University of South Florida Health Heart Institute, Morsani College of Medicine, University of South Florida, Tampa, FL, United States, [3]Basic and Translational Research Division, Department of Cardiology, Boston Children's Hospital, Boston, MA, United States

The efficient phagocytic clearance of dying cells and apoptotic cells is one of the processes that is essential for the maintenance of physiologic tissue function and homeostasis, which is termed "efferocytosis." Under normal conditions, "find me" and "eat me" signals are released by apoptotic cells to stimulate the engulfment and efferocytosis of apoptotic cells. In contrast, abnormal efferocytosis is related to chronic and non-resolving inflammatory diseases such as atherosclerosis. In the initial steps of atherosclerotic lesion development, monocyte-derived macrophages display efficient efferocytosis that restricts plaque progression; however, this capacity is reduced in more advanced lesions. Macrophage reprogramming as a result of the accumulation of apoptotic cells and augmented inflammation accounts for this diminishment of efferocytosis. Furthermore, defective efferocytosis plays an important role in necrotic core formation, which triggers plaque rupture and acute thrombotic cardiovascular events. Recent publications have focused on the essential role of macrophage efferocytosis in cardiac pathophysiology and have pointed toward new therapeutic strategies to modulate macrophage efferocytosis for cardiac tissue repair. In this review, we discuss the molecular and cellular mechanisms that regulate efferocytosis in vascular cells, including macrophages and other phagocytic cells and detail how efferocytosis-related molecules contribute to the maintenance of vascular hemostasis and how defective efferocytosis leads to the formation and progression of atherosclerotic plaques.

KEYWORDS

atherosclerotic cardiovascular disease, efferocytosis, myocardial infarction, macrophage—cell, atheroma, atherosclerotic plaque (AP)

Introduction

Efferocytosis or programmed cell death (PrCR) is an immunological non-inflammatory and evolutionarily-conserved program required for maintaining normal physiological function, development and tissue homeostasis by removing aged, damaged, and senescent cells (1, 2). The Greek-derived term "efferocytosis" refers to a tightly regulated process mainly involving the "eat me" and "don't eat me" molecules

and related signaling pathways that drive phagocytic engulfment of apoptotic cells, but not off-target, healthy cells (3–5). The phagocytosis of apoptotic cells is maintained by both professional phagocytes such as macrophages, immature dendritic cells, and non-professional phagocytic cells (e.g., neighboring smooth muscle cells and endothelial cells). Macrophages, the main phagocytic cell type, play an important role in identifying dying cells for subsequent phagocytosis and clearance that would otherwise become intolerant of self-antigens and induce secondary necrosis. Moreover, the importance of efferocytosis in tissue hemostasis in physiological conditions is widely appreciated. Defective efferocytosis is believed to be an important feature of various autoimmune and chronic inflammatory diseases such as rheumatoid arthritis, atherosclerosis and systemic lupus erythematous (6). The treatment of efferocytosis-related disease has not yet been rectified. In this review, we summarize the underlying regulatory pathways of defective efferocytosis in the progression of cardiovascular disease and focus on future translational studies. Exploring the signaling molecules and regulatory molecular mechanisms associated with impaired efferocytosis in advanced atherosclerosis should enhance our knowledge for developing anti-atherosclerotic therapies focusing on improving efferocytosis.

Basic steps of efferocytosis

Efferocytosis is described as a highly-conserved, programmed cell removal process involving synergistic regulation of the engulfment and removal of apoptotic cells *via* phagocytes. Effective efferocytosis requires the accurate recognition, phagocytosis, and removal of apoptotic cells. Efferocytosis is regulated through several signaling molecules: (a) "find-me" signals: different chemokines, nucleotides, other proteins, lipid and lipid products released from apoptotic cells that recruit phagocytes to the area of cell death; (b) "bridging molecules" signals: opsonin like molecules that connect phagocytes to their targeting apoptotic cells; (c) "eat me" signals: cell surface ligand molecules that recognize and bind to the engulfment receptor on the phagocytes through bridging molecules and that initiate efferocytosis; (d) "don't eat me" signals: molecules such as CD47, which is ubiquitously expressed on viable cells that separate them from apoptotic cells and inhibit phagocytosis. These signal molecules regulate the efferocytotic processes and determine whether a cell is denoted for engulfment and removal from the body or ignored by phagocytic cells (7, 8).

"Find-me" signals in efferocytosis

Studies show that in the region of cell death, apoptotic cells release various molecules carrying "find-me" signals including nucleotides ATP, UTP (9), lysophosphatidylcholine (LPC) (10), sphingosine 1- phosphate (11), and CX_3C-chemokine ligand 1(CX_3CL1) (12). Some "find me" molecules express different signaling peptides that are required for preparing the microenvironment for cell clearance (13). Macrophages are guided by "find me" signals and rapidly migrate to the area of cell death for removing apoptotic corpses (7). Then, macrophages bind either directly or indirectly to the "eat- me" signal expressed on the surface of the apoptotic cells through "bridging molecules" (14).

"Eat-me" signals in efferocytosis

While several "eat-me" signals have been identified, mainly phosphatidylserine (PtdSer), intercellular adhesion molecules 3 (ICAM3), and calreticulin (Calr), these are required for the phagocytosis of apoptotic cells (15, 16). Among of them, PtdSer is the main "eat-me" signal. Under physiological conditions, PtdSer is located on the inner surface of the plasma membrane, but PtdSer in dying cells is reverted to the outer surface of the plasma membrane where it binds to the receptor of the phagocyte (17).

"Bridging-molecules" in efferocytosis

Upon arrival of the macrophage to the area of cell death, the macrophage directly binds to extracellular membrane-bound PtdSer through stabilin 1, stabilin 2, T cell immunoglobulin mucin receptors TIM1, TIM3, TIM4, or through GPCR brain angiogenesis inhibitor 1 (BAI1) (18–21). In some cases, macrophages bind to several bridging molecules, such as Gas6 and protein S, that bind to the tyrosine kinase receptor (TAM), to facilitate the interaction with PtdSer. In other cases, thrombospondin or MFG-E8 binds both PtdSer and integrins αVβ3 and αVβ5 or CD36. In addition, PtdSer-related receptors have different characteristics; some of the receptors (MerTK, BAI1 and integrins) play a role in the signaling process and others (e.g., Tyrosine kinase receptor and CD36) play a role in tethering and adhesion.

Phagocytosis of dying cells

The PtdSer on apoptotic cells binds to the PtdSer receptor on macrophages that form a phagocytic cup through actin cytoskeleton remodeling and the formation of filamentous (F)-actin around the apoptotic cell, promoting internalization of apoptotic cells into the phagosome and mechanical retraction of the phagosome into cells (22–24). The activated small GTPase family members (i.e., Rac1, Cdc42, and RhoA) are involved in the formation of the phagocytic cup and the

internalization of the phagosome (25). The effector of Rac1 activation also regulates the internalization of apoptotic cells through the association of adaptor proteins with the Rac GEF DOCK180 to activate Rac1 and initiate phagocytic cup formation, and leads to phagocytosis (26). Membrane trafficking is also important for efferocytosis, like the cytoskeleton remodeling that underlies Drp1-dependent mitochondrial fission. Mitochondrial fission increases cytosolic calcium by releasing endoplasmic reticulum calcium into the cytosol that drives vesicular trafficking.

After internalization of apoptotic cells, an autophagy-related protein LC3 binds to phagosomal membrane lipids through LC3-associated phagocytosis (LAP) and promotes lysosome degradation of apoptotic cell constituents (27). After phagolysosomal degradation of apoptotic cells, these macromolecular constituents are loaded into macrophages, then macrophages can either use or efflux these constituents through specific mechanisms. As a result, cholesterol released from degraded apoptotic cell induces the expression of ABCA1 and ABCG1 through activating peroxisome proliferate-activate receptor (PPAR) and liver X receptor (LXR) and leading to cholesterol efflux from the cells (28). Macrophage lysosome contains DNase II that degrades chromosomal DNA derived from degraded apoptotic cells. It has been reported that mice lacking DNase II induce an autoimmune disease, polyarthritis, similar to rheumatoid arthritis in humans (29).

Defective efferocytosis in heart disease

Coronary heart disease stems from atherogenesis and plaque vulnerability has been associated with the accumulation of apoptotic and necrotic debris (30–33). A necrotic core contributes to plaque expansion that disrupts luminal flow and, in turn, reduces coronary perfusion, leading to detrimental heart diseases such as ischemic myocardial infarction. Many studies report that impaired efferocytosis induces some changes in blood flow, which is directly related to plaque vulnerability and atherogenesis (34). In mammalian cells,

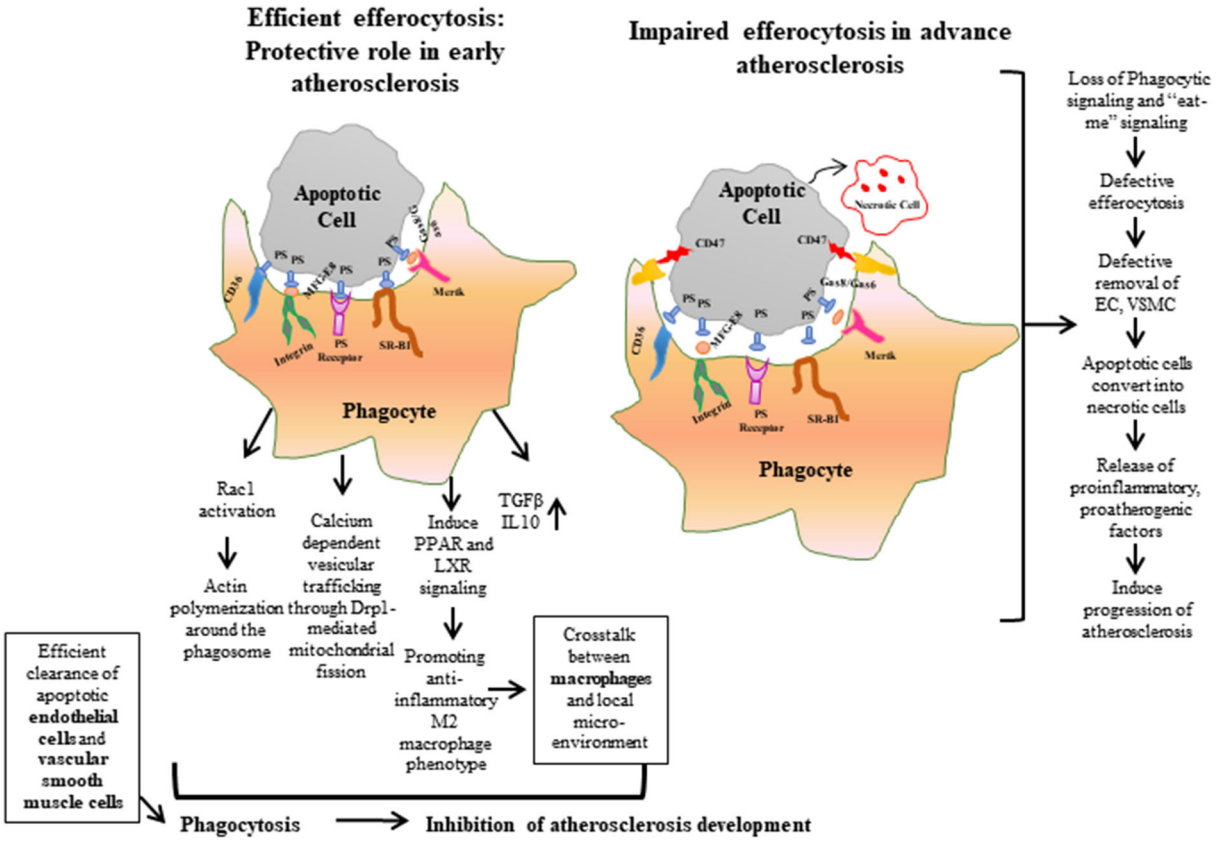

FIGURE 1
Efferocytosis is the phagocytic process required for maintaining normal vascular hemostasis. Efficient efferocytosis plays an important role in protecting against atherosclerosis by inducing phagocytic signals or "eat-me" signals and clearing apoptotic debris. Conversely, in defective efferocytosis, the phagocytic signals are reduced and the phagocytic ability of apoptotic cells is decreased. As a result, apoptotic cells are converted to necrotic cells, and accumulation of these uncleared cells form a necrotic core, which leads to the release of proatherogenic factors and progression of atherosclerosis plaque. ECs, Endothelial cells; VSMCs, Vascular Smooth Muscle Cells.

efferocytosis avoids intracellular accumulation of membrane-derived lipids by initiating the reverse cholesterol transport (RCT) machinery. In normal situations, apoptotic cells express externalized phosphatidylserine (PS) that upregulates ABCA1 in macrophages, which, in turn, induces the efflux of cholesterol to ApoA1 (35, 36). The necrotic core also expresses PS, but it fails to show similar responses for efflux of cholesterol to ApoA1 (35). Furthermore, in defective efferocytosis conditions, the signals that initiate the reverse cholesterol transport pathway in vascular cells are suppressed, leading to the formation of foam cells and the initiation of atherosclerosis.

In normal physiological conditions, efferocytosis suppresses inflammation by preventing accumulation of toxic cellular contents. Macrophages release interleukin (IL)-10 and transforming growth factor (TGF)-β to help clear dying cells and induce anti-inflammatory signaling (37–39). But, when efferocytosis fails to remove apoptotic debris, phagocytic cells convert to inflammatory cells, which leads to non-resolving vascular inflammation (36, 40, 41). Impaired efferocytosis leads to rapid degradation of apoptotic cell membranes, and, consequently, secretion of intracellular content to the interstitium (Figure 1). These intracellular materials contain cytokines and proteases that destabilize the plaque and promote angiogenesis of the vascular cells in the plaque, respectively, as well as the release of thrombogenic factors that play a role in atherogenesis and promote plaque vulnerability (32, 42). Thus, impaired efferocytosis can be viewed as a defective waste management program that plays a key role in the vascular biology of atherogenesis. Taken together, defective efferocytosis stimulates release of cytokines that promote plaque inflammation, and impairs reverse cholesterol transport that promotes foam cell accumulation and also induces plaque vulnerability through atherothrombotic modification in the extracellular matrix, which leads to pathogenesis and progression of atherosclerosis.

Mechanisms behind impaired efferocytosis in atherosclerosis

Reduced apoptosis

The accumulation of apoptotic cells and expansion of the necrotic core associated with atherogenesis, in turn, restricts luminal flow and reduces coronary perfusion (30–33). Studies have shown that impaired efferocytosis induces other maladaptive factors that directly cause atherogenesis and plaque vulnerability (34). Defective efferocytosis involved in lipid accumulation and secondary necrosis causes inflammatory responses and autoimmune responses. Studies have demonstrated that when high capacity efferocytosis occurs in early lesions (i.e., efferocytosis works properly), there is no accumulation of apoptotic cells (43, 44). It has been reported that reduction of the absolute number of phagocytes leads to weakened phagocytic ability of phagocytes.

During the progression of atherosclerosis, endothelial dysfunction and ER stress leads to macrophage and VSMC apoptosis and reduced phagocytic capacity (45). A reduced M2 macrophage population, increases macrophage polarization toward pro-inflammatory M1 phenotype, and lessens the phagocytic ability of smooth muscle cells in atherosclerosis (46, 47). Studies also show that reductions of phagocytic receptors on macrophages (i.e., CD36, Mertk and LRP1) resulted in a loss of their ability to phagocytically clear apoptotic debris. Increased expression of metalloproteinase, disintegrin and ADAM17 were also found in atherosclerotic plaques that cause reduced expression of Mertk and LRP1 on macrophages (48, 49). The inhibition of protein kinase B activation leading to decreased expression of LRP1 on macrophages causes plaque growth during atherosclerotic lesion progression (50). LRP1 receptor deficiency induces the secretion of pro-inflammatory cytokines such as TNF-α, monocyte chemoattractant protein-1 (MCP-1), and MMP-9 which causes reduced efferocytosis. Notably, it has recently been reported that the endocytic adaptor proteins known as epsins target ubiquitin-dependent internalization and downregulation of LRP1 in macrophages in hyperlipidemic conditions, hindering effective efferocytosis in macrophages and propelling atherosclerosis progression (51–53). Interestingly, it has been shown that deletion of LRP1 induces CCR7 expression in M1 macrophages and promotes atherosclerosis regression (54).

Endothelial dysfunction and macrophages in the pathophysiology of atherosclerosis

Atherosclerosis is a chronic inflammatory disease and common cause of cardiovascular disease (CVD), characterized by the thickening of the intima of large and medium-sized arteries (55). Abnormal immune responses, resulting from defective lipid metabolism leads to the accumulation of modified lipoproteins beneath the endothelium, inducing the formation of lipid rich plaques or "atheromas." The accumulation of apoptotic cells plays an important role in atherosclerotic progression and plaque stability (56–58). Although, how high cholesterol concentrations leads to the development of atherosclerosis remains unclear, it is believed that higher blood cholesterol levels is a common cause for the pathogenesis of atherosclerosis (57).

Excessive LDL-C forms reactive oxygen species in the intima and promotes the formation of foam cells by binding the LRP receptor on vascular phagocytes. As atherosclerosis disease progresses, foam cells fail to modify the lipoprotein and fail to distinguish the destructive lipoprotein, which leads to apoptosis

by inducing endoplasmic reticulum stress and ROS production (45). In addition, the areas of disturbed laminar flow in the arterial tree are more prone to lipoprotein accumulation as well as plaque formation. Over time, the rupture of foam cells leads to thrombus formation overlying the plaque and the occlusion of coronary vessels in the heart, leading to episodes like myocardial infarction and stroke (56).

The healthy endothelium plays a protective role against plaque formation through increased nitric oxide bioavailability, decreased adhesion molecule expression, and increased anti-inflammatory signaling process (59). Endothelial dysfunction (i.e., damaged endothelium) upregulates the expression of cell surface adhesion molecules which promote infiltration of macrophages and T lymphocytes into the atherosclerotic plaque (60, 61). Additionally, endothelial cells take part in cholesterol transcytosis through increasing expression of scavenger receptors that bind to the modified lipoproteins and transport them across the endothelium into arterial intima (62, 63). Accumulation of lipoproteins in the intima leads to endothelial activation, which induces sterile inflammation and further modification of retained lipoproteins in the plaque (56, 63).

However, many risk factors take part in inflammatory activation and a great deal of research has demonstrated that macrophages play key roles in the pathogenesis of atherosclerosis by sustaining a continuous inflammatory state and through the secretion of inflammatory mediators such as cytokines and chemokines. Macrophages also take part in the efferocytotic process. In the early stage of atherosclerosis, macrophages play a role in the efferocytotic clearance of apoptotic debris, which differs from lipid-laden foam cells. In the late stages of atherogenesis, macrophages produce pro-inflammatory mediators (60, 64, 65). For example, macrophages release major pathological proinflammatory cytokines (e.g., IL-6, IL-β, and TNFα) that play important roles in atherosclerotic plaque progression (58). Moreover, M2 macrophage populations elicit greater efferocytosis ability than M1 macrophage populations (66).

In murine models of atherosclerosis, higher levels of circulating monocytes have been found, supporting the idea that atherosclerosis not only affects vasculature, but also has a systemic impact on hematopoiesis (67, 68). Activated endothelial cells express some cell surface adhesion molecules, such as P- and E- selectin, that bind with their respective receptors expressed on the cell surface of monocytes, and stimulate monocyte rolling (69, 70). The tethering and transmigration of monocytes to the intima is followed by monocyte differentiation into macrophages in intima through binding of monocyte integrin very late antigen-4 (VLA-4) and lymphocyte function associated antigen (LFA-1) with their respective ligands—vascular adhesion molecule-1 (VCAM-1) and intracellular adhesion molecule-1 (ICAM-1) on the activated endothelium (37, 60).

In the initial stage of atherosclerosis, macrophages limit the expansion of early atheroma through efferocytotic clearance of apoptotic cells and debris (44, 71). In advance stages of atherosclerosis, macrophages play a role in development of necrotic cores and the thinning of fibrous caps (72). Macrophages contribute to fibrous cap thinning through two different mechanisms. One way is by inducing vascular smooth muscle cell apoptosis through involving Fas death receptor and production of pro-inflammatory, apoptotic cytokines (i.e., TNF-α) (73). Macrophages can also produce matrix metalloproteinases (MMP) that lead to the degradation of collagen which in turn destabilizes the cap (72). Specifically, MMP2 and MMP9 are involved in macrophage mediated fibrous cap thinning (74). Macrophages are also involved in the destabilization of atherosclerotic plaques which leads to the generation of necrotic cores (75, 76). The apoptosis of residential macrophages in the intima, along with the impaired efferocytosis of apoptotic cells from surrounding macrophages, induces the generation of a necrotic core and leads to the pathogenesis of atherosclerotic plaque progression (75, 76).

Upregulation of "don't eat-me" signals

It has been shown that the increased levels of proinflammatory molecule TNF-α in atherosclerotic tissues upregulates CD47, an important "don't eat me" molecule in the atherosclerosis plaque. Additionally, studies have shown that atherosclerotic mouse models treated with CD47 blocking antibodies improved atherosclerosis by enhancing clearance of dead vascular tissue and reversing impaired efferocytosis (77). It has been reported that a conserved mammalian lncRNA, myocardial infraction–associated transcript (MIAT), upregulates the expression of CD47 by sponging miR-149-5p and shows higher expression in atherosclerosis patients (78). High mobility group box1 protein (HMGB1), a pro-inflammatory molecule, inhibits phagocytosis by binding to PS expressed on the surface of apoptotic neutrophils. Consequently, pretreatment of macrophages with HMGB1 blocked efferocytosis as a result of the diminished activity of MFG-E8 factor, which bridges PS and integrin on the surface of phagocytes (79).

ER stress and ROS production

During the progression of atherosclerosis, ER stress leads to ROS production and oxidation of LDL. It has been reported that high density lipoprotein (HDL) upregulates the expression of SR-BI receptors on phagocytes which inhibit the ox-LDL induced free cholesterol accumulation and ER stress that impairs

efferocytosis (80). Ox-LDL upregulates the expression of toll-like receptor-4 (TLR-4) reduces the expression of SR-BI and LRP1. This reduced expression ultimately leads to an increase in the secretion of pro-inflammatory cytokines TNF-α and IL-1β, which in turn inhibit the activation of liver X receptor and reduce apoptotic clearance (81).

Studies have shown that defective efferocytosis is related to impaired macrophage phagocytosis. Transcription factor interferon regulatory factors (IRF5) play important roles in modulation of myeloid functions and programming. IRF5 also regulates efferocytosis and necrotic core formation in the atherosclerotic lesion. It has been reported that transcriptional regulator interferon regulatory factor 5 (IRF5) modulates the expression of proinflammatory CD11c+ macrophage phenotype within the atherosclerotic lesion and impairs efferocytosis by suppressing the expression of integrin receptor MFGE8 and Itgb3 (82). Furthermore, studies have shown that loss of IRF5 reduced the expression of $CD11c^{+}$ inflammatory macrophage phenotype within the atherosclerotic lesion. Deficiency of IRF5 increases the efferocytosis by $CD11c^{-}$ macrophages through increased expression of integrin β-3 (Itgb3) and milk fat globule-epidermal growth factor 8 (Mfge8) proteins (82). The inhibition of recognition of apoptotic cells by phagocytes in the atherosclerotic plaque is one of the reasons why atherosclerotic plaques exhibit defective efferocytosis.

Epigenetic modification

It has been also shown that dysfunctional microRNAs (miRs), a type of non-coding RNA, are associated with post-transcriptional modifications of gene expression that causes defective efferocytosis. Studies have shown that in early lesions, miR-155 plays an important role in impaired efferocytosis and macrophage proliferation through the targeting of colony-stimulating factor-1 receptor. In advanced stages of atherosclerosis, miR-155 suppresses the expression of B-cell leukemia/lymphoma 6 (Bcl6) and accelerates foam cell accumulation in the atherosclerotic lesion (83). Bcl6, a potent transcriptional inhibitor, decreases RhoA activity, modulates cytoskeletal remodeling of macrophages and impairs efferocytosis (84).

Lastly, a genome-wide association study of coronary atherosclerosis patients reveals that the 9p21.3 allele variant was related to atherosclerosis lesion burden and impaired efferocytosis. A GWAS study has also shown that the 9p21.3 locus is associated with a reduced expression of cyclin-dependent kinase inhibitor 2B (CDKN2B) and "eat me" ligand calreticulin (Calr). This leads to defect efferocytosis which is unable to remove large numbers of apoptotic vascular smooth muscle cells and causes the expansion of the atherosclerotic plaque (36, 85).

Conclusions

Under normal conditions, the phagocytic capacity of macrophages is sufficient to remove apoptotic cells completely. The reduction of phagocytic capacity and factors that inhibit the clearance of diseased vascular cells, such as genetics and inflammation, play an imperative role in the pathophysiology of atherosclerotic efferocytosis—a role that is worthy of future translational research.

Myriad research studies have been conducted in an effort to better understand the underlying causes of atherosclerosis. Emerging evidence suggests that the impairment of efferocytosis is a root cause of atherosclerosis and plaque vulnerability over the time. Thus, therapies targeting efferocytosis will provide a new platform for the treatment and prevention of cardiovascular disease through the limiting the necrotic core. Encouragingly, it has been shown that these therapeutic agents are safe and specific in ongoing clinical trials.

Author contributions

BS, KL, and HC wrote the manuscript. BS created figures. All authors performed the literature search and approved the final version of the manuscript.

Funding

This work was supported in part by NIH grants R01HL093242, R01HL146134, R01HL137229, R01HL156362, R01HL16236, and R01HL158097 to HC, R01HL130845 and R01HL141853 to D-ZW, and American Heart Association Transformative Program Award to HC.

Conflict of interest

The authors declare that the research was conducted in the absence of any commercial or financial relationships that could be construed as a potential conflict of interest.

Publisher's note

References

1. Kinchen JM, Ravichandran KS. Phagocytic signaling: you can touch, but you can't eat. *Curr Biol.* (2008) 18:R521–4. doi: 10.1016/j.cub.2008.04.058

2. Thorp EB. Mechanisms of failed apoptotic cell clearance by phagocyte subsets in cardiovascular disease. *Apoptosis.* (2010) 15:1124–36. doi: 10.1007/s10495-010-0516-6

3. Ravichandran KS, Lorenz U. Engulfment of apoptotic cells: signals for a good meal. *Nat Rev Immunol.* (2007) 7:964–74. doi: 10.1038/nri2214

4. Thorp E, Tabas I. Mechanisms and consequences of efferocytosis in advanced atherosclerosis. *J Leukoc Biol.* (2009) 86:1089–95. doi: 10.1189/jlb.0209115

5. de Cathelineau AM, Henson PM. The final step in programmed cell death: phagocytes carry apoptotic cells to the grave. *Essays Biochem.* (2003) 39:105–17. doi: 10.1042/bse0390105

6. Evans AL, Blackburn JWD, Taruc K, Kipp A, Dirk BS, Hunt NR, et al. Antagonistic coevolution of MER tyrosine kinase expression and function. *Mol Biol Evol.* (2017) 34:1613–28. doi: 10.1093/molbev/msx102

7. Hochreiter-Hufford A, Ravichandran KS. Clearing the dead: apoptotic cell sensing, recognition, engulfment, and digestion. *Cold Spring Harb Perspect Biol.* (2013) 5:a008748. doi: 10.1101/cshperspect.a008748

8. Gardai SJ, McPhillips KA, Frasch SC, Janssen WJ, Starefeldt A, Murphy-Ullrich JE, et al. Cell-surface calreticulin initiates clearance of viable or apoptotic cells through trans-activation of LRP on the phagocyte. *Cell1.* (2005) 23:321–34. doi: 10.1016/j.cell.2005.08.032

9. Elliott MR, Chekeni FB, Trampont PC, Lazarowski ER, Kadl A, Walk SF, et al. Nucleotides released by apoptotic cells act as a find-me signal to promote phagocytic clearance. *Nature.* (2009) 461:282–6. doi: 10.1038/nature08296

10. Mueller RB, Sheriff A, Gaipl US, Wesselborg S, Lauber K. Attraction of phagocytes by apoptotic cells is mediated by lysophosphatidylcholine. *Autoimmunity.* (2007) 40:342–4. doi: 10.1080/08916930701356911

11. Gude DR, Alvarez SE, Paugh SW, Mitra P, Yu J, Griffiths R, et al. Apoptosis induces expression of sphingosine kinase 1 to release sphingosine-1-phosphate as a "come-and-get-me" signal. *FASEB J.* (2008) 22:2629–38. doi: 10.1096/fj.08-107169

12. Truman LA, Ford CA, Pasikowska M, Pound JD, Wilkinson SJ, Dumitriu IE, et al. CX3CL1/fractalkine is released from apoptotic lymphocytes to stimulate macrophage chemotaxis. *Blood.* (2008) 112:5026–36. doi: 10.1182/blood-2008-06-162404

13. Medina CB, Ravichandran KS. Do not let death do us part: 'find-me' signals in communication between dying cells and the phagocytes. *Cell Death Different.* (2016) 23:979–89. doi: 10.1038/cdd.2016.13

14. Li W. Eat-me signals: keys to molecular phagocyte biology and "appetite" control. *J Cell Physiol.* (2012) 227:1291–7. doi: 10.1002/jcp.22815

15. Fadok VA, Voelker DR, Campbell PA, Cohen JJ, Bratton DL, Henson PM, et al. Exposure of phosphatidylserine on the surface of apoptotic lymphocytes triggers specific recognition and removal by macrophages. *J Immunol.* (1992) 148:2207–16.

16. Fadok VA, de Cathelineau A, Daleke DL, Henson PM, Bratton DL. Loss of phospholipid asymmetry and surface exposure of phosphatidylserine is required for phagocytosis of apoptotic cells by macrophages and fibrblasts. *J Biol Chem.* (2001) 276:1071–7. doi: 10.1074/jbc.M003649200

17. Kobayashi N, Karisola P, Pena-Cruz V, Dorfman DM, Jinushi M, Umetsu SE, et al. TIM-1 and TIM-4 glycoproteins bind phosphatidylserine and mediate uptake of apoptotic cells. *Immunity.* (2007) 27:927–40. doi: 10.1016/j.immuni.2007.11.011

18. Park D, Tosello-Trampont AC, Elliott MR, Lu M, Haney LB, Ma Z, et al. BAI1 is an engulfment receptor for apoptotic cells upstream of the ELMO/Dock180 / Rac module. *Nature.* (2007) 450:430–4. doi: 10.1038/nature06329

19. Park SY, Jung MY, Kim HJ, Lee SJ, Kim SY, Lee BH, et al. Rapid cell corpse clearance by stabilin-2, a membrane phosphatidylserine receptor. *Cell Death Differ.* (2008) 15:192–201. doi: 10.1038/sj.cdd.4402242

20. Park SY, Jung MY, Lee SJ, Kang KB, Gratchev A, Riabov V, et al. Stabilin-1 mediates phosphatidylserine-dependent clearance of cell corpses in alternatively activated macrophages. *J Cell Sci.* (2009) 122(Pt 18):3365–73. doi: 10.1242/jcs.049569

21. Freeman GJ, Casasnovas JM, Umetsu DT, DeKruyff RHTIM. genes: a family of cell surface phosphatidylserine receptors that regulate innate and adaptive immunity. *Immunol Rev.* (2010) 235:172–89. doi: 10.1111/j.0105-2896.2010.00903.x

22. Segawa K, Suzuki J, Nagata S. Constitutive exposure of phosphatidylserine on viable cells. *Proc Natl Acad Sci USA.* (2011) 108:19246–51. doi: 10.1073/pnas.1114799108

23. Hoffmann PR, de Cathelineau AM, Ogden CA, Leverrier Y, Bratton DL, Daleke DL, et al. Phosphatidylserine (PS) induces PS receptor-mediated macropinocytosis and promotes clearance of apoptotic cells. *J Cell Bio.* (2001) 155:649–59. doi: 10.1083/jcb.200108080

24. Castellano F, Montcourrier P, Chavrier P. Membrane recruitment of Rac1 triggers phagocytosis. *J Cell Sci.* (2000) 113(Pt 17):2955–61. doi: 10.1242/jcs.113.17.2955fcvm-09-1031293

25. Nakaya M, Kitano M, Matsuda M, Nagata S. Spatiotemporal activation of Rac1 for engulfment of apoptotic cells. *Proc Natl Acad Sci USA.* (2008) 105:9198–203. doi: 10.1073/pnas.0803677105

26. Albert ML, Kim JI, Birge RB. alphavbeta5 integrin recruits the CrkII-Dock180-rac1 complex for phagocytosis of apoptotic cells. *Nat Cell Biol.* (2000) 2:899–905. doi: 10.1038/35046549

27. Martinez J, Malireddi RK, Lu Q, Cunha LD, Pelletier S, Gingras S, et al. Molecular characterization of LC3-associated phagocytosis reveals distinct roles for Rubicon, NOX2 and autophagy proteins. *Nat Cell Biol.* (2015) 17:893–906. doi: 10.1038/ncb3192

28. Kidani Y, Bensinger SJ. Liver X receptor and peroxisome proliferator-activated receptor as integrators of lipid homeostasis and immunity. *Immunol Rev.* (2012) 249:72–83. doi: 10.1111/j.1600-065X.2012.01153.x

29. Kawane K, Ohtani M, Miwa K, Kizawa T, Kanbara Y, Yoshioka Y, et al. Chronic polyarthritis caused by mammalian DNA that escapes from degradation in macrophages. *Nature.* (2006) 443:998–1002. doi: 10.1038/nature05245

30. Finn AV, Nakano M, Narula J, Kolodgie FD, Virmani R. Concept of vulnerable/unstable plaque. *Arterioscler Thromb Vasc Biol.* (2010) 30:1282–92. doi: 10.1161/ATVBAHA.108.179739

31. Kolodgie FD, Narula J, Burke AP, Haider N, Farb A, Hui-Liang Y, et al. Localization of apoptotic macrophages at the site of plaque rupture in sudden coronary death. *Am J Pathol.* (2000) 157:1259–68. doi: 10.1016/S0002-9440(10)64641-X

32. Martinet W, Schrijvers DM, De Meyer GR. Necrotic cell death in atherosclerosis. *Basic Res Cardiol.* (2011) 106:749–60. doi: 10.1007/s00395-011-0192-x

33. Tabas I. Pulling down the plug on atherosclerosis: finding the culprit in your heart. *Nat Med.* (2011) 17:791–3. doi: 10.1038/nm0711-791

34. Schrijvers DM, De Meyer GR, Kockx MM, Herman AG, Martinet W. Phagocytosis of apoptotic cells by macrophages is impaired in atherosclerosis. *Arterioscler Thromb Vasc Biol.* (2005) 25:1256–61. doi: 10.1161/01.ATV.0000166517.18801.a7

35. Kiss RS, Elliott MR, Ma Z, Marcel YL, Ravichandran KS. Apoptotic cells induce a phosphatidylserine-dependent homeostatic response from phagocytes. *Curr Biol.* (2006) 16:2252–8. doi: 10.1016/j.cub.2006.09.043

36. Kojima Y, Downing K, Kundu R, Miller C, Dewey F, Lancero H, et al. Cyclin-dependent kinase inhibitor 2B regulates efferocytosis and atherosclerosis. *J Clin Invest.* (2014) 124:1083–97. doi: 10.1172/JCI70391

37. Moore KJ, Tabas I. Macrophages in the pathogenesis of atherosclerosis. *Cell.* (2011) 145:341–55. doi: 10.1016/j.cell.2011.04.005

38. Cui D, Thorp E, Li Y, Wang N, Yvan-Charvet L, Tall AR, et al. Pivotal advance: macrophages become resistant to cholesterol-induced death after phagocytosis of apoptotic cells. *J Leukoc Biol.* (2007) 82:1040–50. doi: 10.1189/jlb.0307192

39. Fadok VA, Bratton DL, Konowal A, Freed PW, Westcott JY, Henson PM, et al. Macrophages that have ingested apoptotic cells in vitro inhibit proinflammatory cytokine production through autocrine/paracrine mechanisms involving TGF-beta, PGE2, and PAF. *J Clin Invest.* (1998) 101:890– 8. doi: 10.1172/JCI1112

40. Schrijvers DM, De Meyer GR, Herman AG, Martinet W. Phagocytosis in atherosclerosis: Molecular mechanisms and implications for plaque progression and stability. *Cardiovasc Res.* (2007) 73:470–80. doi: 10.1016/j.cardiores.2006.09.005

41. Ravichandran KS. Beginnings of a good apoptotic meal: the find-me and eat-me signaling pathways. *Immunity.* (2011) 35:445–55. doi: 10.1016/j.immuni.2011.09.004

42. Mallat Z, Hugel B, Ohan J, Lesèche G, Freyssinet JM, Tedgui A, et al. Shed membrane microparticles with procoagulant potential in human atherosclerotic plaques: a role for apoptosis in plaque thrombogenicity. *Circulation.* (1999) 99:348–53. doi: 10.1161/01.CIR.99.3.348

43. Liu J, Thewke DP, Su YR, Linton MF, Fazio S, Sinensky MS, et al. Reduced macrophage apoptosis is associated with accelerated atherosclerosis in low-density

lipoprotein receptor-null mice. *ArterioscIerThromb Vasc Biol.* (2005) 25:174–9. doi: 10.1161/01.ATV.0000148548.47755.22

44. Gautier EL, Huby T, Witztum JL, Ouzilleau B, Miller ER, Saint-Charles F, et al. Macrophage apoptosis exerts divergent effects on atherogenesis as a function of lesion stage. *Circulation.* (2009) 119:1795–804. doi: 10.1161/CIRCULATIONAHA.108.806158

45. Chistiakov DA, Bobryshev YV, Orekhov AN. Macrophage-mediated cholesterol handling in atherosclerosis. *J Cell Mol Med.* (2016) 20:17–28. doi: 10.1111/jcmm.12689

46. Yamamoto S, Yancey PG, Zuo YQ, Ma LJ, Kaseda R, Fogo AB, et al. Macrophage polarization by angiotensin ii-type 1 receptor aggravates renal injury-acceleration of atherosclerosis. *Arterioscler Thromb Vasc Biol.* (2011) 31:2856–64. doi: 10.1161/ATVBAHA.111.237198

47. Vengrenyuk Y, Nishi H, Long XC, Ouimet M, Savji N, Martinez FO, et al. Cholesterol Loading reprograms the microRNA-143/145-myocardin axis to convert aortic smooth muscle cells to a dysfunctional macrophage-like phenotype. *Arterioscler Thromb Vasc Biol.* (2015) 35:535–46. doi: 10.1161/ATVBAHA.114.304029

48. Gorovoy M, Gaultier A, Campana WM, Firestein GS, Gonias SL. Inflammatory mediators promote production of shed LRP1/CD91, which regulates cell signaling and cytokine expression by macrophages. *J Leukocyte Biol.* (2010) 88:769–78. doi: 10.1189/jlb.0410220

49. Thorp E, Vaisar T, Subramanian M, Mautner L, Blobel C, Tabas I, et al. Shedding of the mer tyrosine kinase receptor is mediated by ADAM17 protein through a pathway involving reactive oxygen species, protein kinase C delta, and p38 mitogen-activated protein kinase (MAPK). *J Biol Chem.* (2011) 286:33335–44. doi: 10.1074/jbc.M111.263020

50. Yancey PG, Blakemore J, Ding L, Fan DP, Overton CD, Zhang YM, et al. Macrophage LRP-1 controls plaque cellularity by regulating efferocytosis and Akt activation. *Arterioscler Thromb Vasc Biol.* (2010) 30:787–95. doi: 10.1161/ATVBAHA.109.202051

51. Brophy ML, Dong YZ, Tao H, Yancey PG, Song K, Zhang K, et al. Myeloid-specific deletion of epsins 1 and 2 reduces atherosclerosis by preventing LRP-1 Downregulation. *Circ Res.* (2019) 124:e6–19. doi: 10.1161/CIRCRESAHA.118.313028

52. Bhattacharjee S, Lee Y, Zhu B, Wu H. Chen Y, Chen H, et al. Epsins in vascular development, function and disease. *Cell Mol Life Sci.* (2021) 78:833–42. doi: 10.1007/s00018-020-03642-4

53. Cui K, Dong Y, Wang B, Cowan DB, Chan SL, Shyy J, et al. Endocytic adaptors in cardiovascular disease. *Front Cell Dev Biol.* (2020) 8:624159. doi: 10.3389/fcell.2020.624159

54. Mueller PA, Zhu L, Tavori H, Huynh K, Giunzioni I, Stafford JM, et al. Deletion of macrophage low-density lipoprotein receptor-related protein 1 (LRP1) accelerates atherosclerosis regression and increases C-C chemokine receptor type 7 (CCR7) expression in plaque macrophages. *Circulation.* (2018) 138:185063. doi: 10.1161/CIRCULATIONAHA.117.031702

55. Falk E. Pathogenesis of atherosclerosis. *J Am Coll Cardiol.* (2006) 47:C7–12. doi: 10.1016/j.jacc.2005.09.068

56. Hansson GK, Libby P, Tabas I. Inflammation and plaque vulnerability. *J Internal Med.* (2015) 278:483–93. doi: 10.1111/joim.12406

57. Solanki A, Bhatt LK, Johnston TP. Evolving targets for the treatment of atherosclerosis. *Pharmacol Ther.* (2018) 187:1–12. doi: 10.1016/j.pharmthera.2018.02.002

58. Tabas I. Molecular-cellular mechanisms in the progression of atherosclerosis. Russell ross memorial lecture in vascular biology. *Arterioscler Thromb Vasc Biol.* (2017) 37:183–9. doi: 10.1161/ATVBAHA.116.308036

59. Messner B, Bernhard D. Smoking and cardiovascular disease: mechanisms of endothelial dysfunction and early atherogenesis. *Arterioscler Thromb Vasc Biol.* (2014) 34:509–15. doi: 10.1161/ATVBAHA.113.300156

60. Moore KJ, Sheedy FJ, Fisher E. Macrophages in atherosclerosis: a dynamic balance. *Nat Rev Immunol.* (2013) 13:709–21. doi: 10.1038/nri3520

61. Tse K, Tse H, Sidney J, Sette A, Ley K. T Cells in atherosclerosis. *Int Immunol.* (2013) 25:615–22. doi: 10.1093/intimm/dxt043

62. Armstrong SM, Sugiyama MG, Fung KYY, et al. A novel assay uncovers an unexpected role for SR-BI in LDL transcytosis. *Cardiovasc Res.* (2015) 108:268–77. doi: 10.1093/cvr/cvv218

63. Moore KJ, Freeman MW. Scavenger receptors in atherosclerosis: beyond lipid uptake. *Arterioscler Thromb Vasc Biol.* (2006) 26:1702–11. doi: 10.1161/01.ATV.0000229218.97976.43

64. Tabas I, Bornfeldt KE. Macrophage phenotype and function in different stages of atherosclerosis. *Circ Res.* (2016) 118:653–67. doi: 10.1161/CIRCRESAHA.115.306256

65. Mills CD, Lenz LL, Ley K. Macrophages at the fork in the road to health or disease. *Front Immunol.* (2015) 6:59. doi: 10.3389/fimmu.2015.00059

66. Chang HY, Lee HN, Kim W, Surh YJ. Docosahexaenoic acid induces M2 macrophage polarization through peroxisome proliferator-activated receptor gamma activation. *Life Sci.* (2015) 120:39–47. doi: 10.1016/j.lfs.2014.10.014

67. Landsman L, Liat BO, Zernecke A, et al. CX3CR1 is required for monocytehomeostasis and atherogenesis by promoting cell survival. *Blood.* (2009) 113:963–72. doi: 10.1182/blood-2008-07-170787

68. Rahman K, Vengrenyuk Y, Ramsey SA, et al. Inflammatory Ly6Chimonocytes and their conversion to M2 macrophages drive atherosclerosis regression. *J Clin Invest.* (2017) 127:2904–15. doi: 10.1172/JCI75005

69. VanderLaan P, Reardon C, Getz GS. Site specificity of atherosclerosis: site-selective responses to atherosclerotic modulators. *Arterioscler Thromb Vasc Biol.* (2004) 24:12–22. doi: 10.1161/01.ATV.0000105054.43931.f0

70. Bunting M, Harris ES, McIntyre TM, Prescott SM, Zimmerman GA. Leukocyte adhesion deficiency syndromes: adhesion and tethering defects involving β 2 integrins and selectin ligands. *Curr Opin Hematol.* (2002) 9:30–5. doi: 10.1097/00062752-200201000-00006

71. Linton MF, Babaev VR, Huang J, Linton EF, Tao H, Yancey PG, et al. Macrophage apoptosis and efferocytosis in the pathogenesis of atherosclerosis. *Circ J.* (2016) 80:2259–68. doi: 10.1253/circj.CJ-16-0924

72. Tabas I. Macrophage death and defective inflammation resolution in atherosclerosis Nat Rev Immunol. *Nat Rev Immunol.* (2010) 10:36–46. doi: 10.1038/nri2675

73. Clarke M, Bennett M. The emerging role of vascular smooth muscle cell apoptosis in atherosclerosis and plaque stability. *Am J Nephrol.* (2006) 26:531–5. doi: 10.1159/000097815

74. Dick W, Zhu C, Björkegren J, Skogsberg J, Eriksson P. MMP-2 and MMP-9 are prominent matrix metalloproteinases during atherosclerosis development in the Ldlr -/- Apob 100/100 mouse. *Int J Mol Med.* (2011) 28:247–53. doi: 10.3892/ijmm.2011.693

75. Tabas I. Apoptosis and plaque destabilization in atherosclerosis: the role of macrophage apoptosis induced by cholesterol. *Cell Death Differ.* (2004)11 Suppl 1:S12–6. doi: 10.1038/sj.cdd.4401444

76. Gonzalez L, Trigatti BL. Macrophage apoptosis and necrotic core development in atherosclerosis: a rapidly advancing field with clinical relevance to imaging and therapy. *Can J Cardiol.* (2017) 33:303–12. doi: 10.1016/j.cjca.2016.12.010

77. Kojima Y, Volkmer JP, McKenna K, Civelek M, Lusis AJ, Miller CL, et al. CD47-blocking antibodies restore phagocytosis and prevent atherosclerosis. *Nature.* (2016) 536:86–90. doi: 10.1038/nature18935

78. Ye ZM, Yang S, Xia YP, Hu RT, Chen SC, Li BW, et al. LncRNA MIAT sponges miR-149-5p to inhibit efferocytosis in advanced atherosclerosis through CD47 upregulation. *Cell Death Dis.* (2019) 10:138. doi: 10.1038/s41419-019-1409-4

79. Friggeri A, Yang Y, Banerjee S, Park, Y.-J., Liu G, Abraham E. HMGB1 inhibits macrophage activity in efferocytosis through binding to the alphavbeta3-integrin. *Am J Physiol Cell Physiol.* (2010) 299:C1267– 76. doi: 10.1152/ajpcell.00152.2010

80. Song G, Wu X, Zhang P, Yu Y, Yang M, Jiao P, et al. High-density lipoprotein inhibits ox-LDL-induced adipokine secretion by upregulating SR-BI expression and suppressing ER Stress pathway. *Sci Rep.* (2016) 6:30889. doi: 10.1038/srep30889

81. A-Gonzalez N, Bensinger SJ, Hong C, Beceiro S, Bradley MN, Zelcer N, et al. Apoptotic cells promote their own clearance and immune tolerance through activation of the nuclear receptor LXR. *Immunity.* (2009) 31:245–58. doi: 10.1016/j.immuni.2009.06.018

82. Seneviratne AN, Edsfeldt A, Cole JE, Kassiteridi C, Swart M, Park I, et al. Interferon regulatory factor 5 controls necrotic core formation in atherosclerotic lesions by impairing efferocytosis. *Circulation.* (2017) 136:1140–54. doi: 10.1161/CIRCULATIONAHA.117.027844

83. Wei YY, Zhu MY, Corbalan-Campos J, Heyll K, Weber C, Schober A, et al. Regulation of Csf1r and Bcl6 in macrophages mediates the stage-specific effects of microRNA-155 on atherosclerosis. *Arterioscler Thromb Vasc Biol.* (2015) 35:796–803. doi: 10.1161/ATVBAHA.114.304723

84. Pixley FJ, Xiong Y, Yu RYL, Sahai EA, Stanley ER, Ye BH, et al. BCL6 suppresses RhoA activity to alter macrophage morphology and motility. *J Cell Sci.* (2005) 118:1873–83. doi: 10.1242/jcs.02314

85. Leeper NJ, Raiesdana A, Kojima Y, Kundu RK, Cheng H, Maegdefessel L, et al. Loss of CDKN2B promotes p53-dependent smooth muscle cell apoptosis and aneurysm formation. *Arterioscler Thromb Vasc Biol.* (2013) 33:e1–10. doi: 10.1161/ATVBAHA.112.300399

frontiers | Frontiers in Cardiovascular Medicine

TYPE Mini Review
PUBLISHED 18 October 2022
DOI 10.3389/fcvm.2022.1011192

OPEN ACCESS

EDITED BY
Liya Yin,
Northeast Ohio Medical University,
United States

REVIEWED BY
Wuqiang Zhu,
Mayo Clinic Arizona, United States
Vahagn Ohanyan,
Northeast Ohio Medical University,
United States

*CORRESPONDENCE
Paul C. Tang
tangpaul@med.umich.edu

SPECIALTY SECTION
This article was submitted to Cardiovascular Therapeutics, a section of the journal Frontiers in Cardiovascular Medicine

RECEIVED 03 August 2022
ACCEPTED 13 September 2022
PUBLISHED 18 October 2022

CITATION
Jones-Ungerleider KC, Rose A, Knott K, Comstock S, Haft JW, Pagani FD and Tang PC (2022) Sex-based considerations for implementation of ventricular assist device therapy.
Front. Cardiovasc. Med. 9:1011192.
doi: 10.3389/fcvm.2022.1011192

Sex-based considerations for implementation of ventricular assist device therapy

K. Candis Jones-Ungerleider[1], Angela Rose[1], Kevin Knott[1], Sarah Comstock[1], Jonathan W. Haft[1], Francis D. Pagani[1] and Paul C. Tang[1,2]*

[1]Department of Cardiac Surgery, School of Medicine, University of Michigan, Ann Arbor, MI, United States, [2]Department of Cardiac Surgery, University of Michigan, Ann Arbor, MI, United States

Women with advanced heart failure receive advanced surgical therapies such as durable left ventricular assist device (LVAD) implantation or heart transplantation at a rate much lower compared to males. Reasons for this discrepancy remain largely unknown. Much of what is understood reflects outcomes of those patients who ultimately receive device implant or heart transplantation. Females have been shown to have a higher mortality following LVAD implantation and experience higher rates of bleeding and clotting phenomena and right ventricular failure. Beyond outcomes, the literature is limited in the identification of pre-operative factors that drive lower than expected LVAD implant rates in this population. More focused research is needed to define the disparities in advance heart failure therapy delivery in women and other underserved populations.

KEYWORDS

LVAD, sex, female, heart failure, right heart failure (RHF)

Introduction

Women represent ∼30–50% of patients with stage D heart failure (1, 2), but account for only 21% of the patients receiving durable left ventricular assist device (LVAD) implants (3). Approximately 3,000 durable LVAD implants occur annually and the relatively low proportion of female recipients has remained relatively constant across eras (2010–2014 vs. 2015–2019). This disparity in women receiving durable LVAD therapy can be explained by a myriad of factors such as sex-based differences in disease biology, patient size considerations, comorbidities, pre-implant considerations and post-implant outcomes. Perhaps more difficult to delineate objectively are the less explicit contributions of system and provider bias that may result in fewer women ultimately receiving a device.

Etiology of heart failure

The epidemiology of heart failure in women varies significantly from that of men and, therefore, disparities in the treatment of advanced heart failure are frequently attributed

to distinct biologies. While the lifetime risk of heart failure is similar in males and females (4), heart failure with preserved ejection fraction disproportionally affects women and heart failure with reduced ejection fraction disproportionately affects men (5). Females account for ∼30–40% of all systolic heart failure (6), with non-ischemic disease being the most common etiology. In contrast, ischemic cardiomyopathy is much more prevalent in males. Additionally, females are uniquely susceptible to other forms of heart failure such as peri-partem cardiomyopathy, chemotherapy (e.g., breast cancer therapy) induced cardiomyopathies, takotsubo cardiomyopathy, and autoimmune mediated disease.

Demographic and comorbidity profile

There have been two large analyses of Interagency Registry for Mechanically Assisted Circulatory Support (INTERMACS) data that specifically address sex differences in utilization of LVAD therapy (7, 8). Both these studies report specific trends in the continuous flow device era where women who receive LVADs tend to be younger than their male counterparts. While the age of females receiving LVADs has been relatively stable across eras, men receiving devices in the continuous flow era tend to be older relative to the previous era of pulsatile devices. Females receiving durable LVADs are more frequently African Americans when compared to the male population. Further, female LVAD recipients are more likely to suffer from obesity, thyroid disorders, rheumatoid arthritis, collagen vascular disease, chronic blood loss anemia and depression, whereas men are more likely to experience diabetes, hypertension, coronary artery disease, prior coronary artery bypass grafting, chronic renal failure, and greater alcohol use. The primary payer is more likely Medicaid for females and the overall median household income is shifted toward the lower percentiles for female LVAD recipients in the continuous flow device era.

Pre-implant considerations: From diagnosis to device delivery

Ventricular assist devices improve survival, functional status and quality of life. Although women in the greater heart failure community tend to have better survival, women report worse quality of life compared to age and ejection fraction matched male counterparts (9). While it is apparent that females have much to gain from advanced heart failure therapies, improving patient access to advanced surgical heart failure therapies is complex. Connecting female patients with advanced heart failure to advanced surgical heart failure therapies requires navigation of the greater healthcare system, medical decision making by many levels of providers, and the willingness of the patient to commit to the treatment plan.

There is a paucity of data to help assess potential sex differences in decision making at the clinician or system level. It is known that females are less likely to receive temporary mechanical circulatory support in the setting of cardiogenic shock (OR = 0.76); this is also true of black patients and those insured by Medicare and Medicaid (10). An additional challenge in understanding durable device delivery is the interplay of decision making with that of heart transplantation. There are unique barriers to heart transplantation in females including increased rates of obesity and allosensitization. In a study from Emory University assessing eligibility for advanced heart failure therapies, females were less likely to be eligible for heart transplant (21 vs. 47% of patients evaluated) and more likely to be recommended a VAD as destination therapy (24 vs. 9.7%) (11). Furthermore, a separate study demonstrated that females who underwent LVAD implantation were less likely to undergo subsequent transplantation and had higher transplant waitlist mortality (12).

Sex specific patient related treatment preferences may also contribute to differences in delivery of advanced heart failure therapies. Females have been shown to be less willing to undergo heart transplantation due to self refusal (13). Additionally, in a multi-institutional study of socioeconomic factors and patient preferences for LVADs, lower income and lesser education were associated with an increased willingness to undergo VAD implantation (14). While there was no discernable relationship between patient acceptance of a device and sex or marital status, only 25% of respondents were female.

Outcomes with VAD

Outcomes following durable LVAD implantation have improved over time with trends following device innovation and market approvals. LVAD therapy outcomes are frequently stratified by device era, with distinction between the early pulsatile flow devices (pre 2008) and more modern continuous flow devices (post 2008) corresponding to regulatory approval of the Heartmate II for destination therapy. A further distinction of the continuous flow era can be made between continuous flow design including axial devices (i.e., Heartmate II, Abbott Labs, Chicago, IL) and centrifugal devices (i.e., Heartware HVAD, Medtronic Inc., Minneapolis, MN; Heartmate 3, Abbott Labs, Chicago, IL), with the regulatory approval of the Heartware HVAD for BTT in November 2012. This is particularly pertinent given a demonstrated era effect in improved survival when stratifying implants prior to and post 2013, which favors the more recent era (15). Lastly, in 2019 the MOMENTUM3 trial published 2 year data on the latest LVAD technology, the Heartmate III device, which was engineered for improved hemocompatibility. Use of these new, innovative pumps was

associated with superior outcomes relative to predecessor devices, including most notably a dramatic reduction in rate of stroke (16).

Historically, broad utilization of pulsatile devices was often precluded in females due to smaller body habitus, as pulsatile LVADs were bulky and not suitable for patients with body surface areas <1.5 m^2. With FDA approval of the Heartmate II, an era of smaller and lighter continuous flow devices (17) became newly available to populations—in large part females—who were underserved by prior generations of mechanical support.

Mortality

Sex related disparities in outcomes following VAD implantation are most pronounced in the pulsatile flow era, with more modern data of continuous flow devices being more nuanced. In an analysis of National Inpatient Sample data reflecting over 6,000 patients undergoing implants from 2004 to 2016, inpatient mortality in women during the pulsatile flow era was higher than that of men (47 vs. 31%); however, there was no discernable difference in the continuous flow era (13 and 12%, respectively) (18). An INTERMACS study reflecting nearly 2,000 patients, 400 females, spanning 2006 to 2010 showed no difference in mortality between females and males (16 and 17%) at average of 7 months of follow-up, irrespective of device type (8). In contrast, the eighth annual INTERMACS report published in 2017 suggests that among patients with continuous flow devices there is a higher risk of early (3 month) mortality in women (HR 1.47), potentially attributable to right ventricular failure and major bleeding events (15). Similarly, in a study of International Society for Heart and Lung Transplantation (ISHLT) Mechanically Assisted Circulatory Support (IMACS) data limited to the centrifugal era (post 2013), women had an increased risk of mortality (HR 1.36) attributable to an early hazard of death (HR 1.74 in the first 4 months) (19). Nearly a quarter of this increased mortality risk was mediated by pre-operative echo findings of smaller left ventricular volumes and increased tricuspid regurgitation (both surrogates for patient size and right ventricular function). Most recently, sub-analyses of Heartmate III clinical trial data suggests no difference in morbidity and mortality profile for this new generation device with no apparent difference in the composite outcome of survival out to 2 years free of stroke or reoperation for malfunctioning device across sex (16).

Morbidity

There is a differential morbidity profile following VAD implantation in females largely attributable to bleeding, thromboembolic phenomena and right ventricular failure. The origins of dysregulated coagulation in females have been explored through a broad range of investigations, including estrogen effects on clotting factors, sex differences in pharmacokinetics and dynamics of anticoagulants, as well as lower pump speeds, particularly in the era of the Heartmate II.

Neurological events (stroke)

Females who undergo LVAD implantation are at higher risk of neurologic events than their male counterparts. Early data with the Heartmate II highlighted an increased risk of hemorrhagic, but not ischemic stroke in females (20) (incidence 12 vs. 3%, 0.1 vs. 0.04 events per patient year). This risk of increased hemorrhagic stroke in women remained a trend even after matching for body surface area (BSA). In an analysis of 900 Heartmate II recipients (23% female) and risk factors for stroke, female sex was associated with a hazard ratio of 1.92 for hemorrhagic and 1.84 for ischemic stroke (21). More recent INTERMACS data support that women may have an intrinsically increased risk of stroke, even after adjusting for common risk factors. Females were found to have a shorter time to first neurologic event in the pulsatile flow era and a trend toward the same in the continuous flow era. This difference occurred even while the overall rate of neurologic events declined significantly with continuous flow devices (8). Heartmate III data suggests an overall decrease in stroke risk with this contemporary device; outcomes by sex however are limited to the primary composite end point, which incorporates neurologic morbidity, for which there was no discernable difference.

Bleeding

A number of studies indicate that women are at higher risk of bleeding events both in the immediate post-operative period and more chronically while on anticoagulation therapy. A review of European Registry for Patients with Mechanical Circulatory Support (EuroMACS) data of 966 patients receiving a durable VAD (151 women) revealed that females were twice as likely as males to have a major bleeding event as defined by INTERMACs adverse event definitions. This applied for the first 30 days of post-implant period and also identified twice as many bleeding events per patient year compared to males (22). A single center study of 375 recipients (84 females) receiving continuous flow devices observed that, although mediastinal bleeding was similar between men and women in the immediate post-operative period, women had a 60% higher hazard of overall bleeding complications. This was largely driven by clinically significant mucosal (gynecologic and oronasal pharyngeal) bleeding occurring after the first 30 days post implant but prior to the 1st year (23). Ten percent of all females in this study experienced gynecological bleeding with a

need for transfusion or surgical intervention. A separate study noted that freedom from gynecological bleeding was 84% at 1 year and 73% at 2 years for females on long term LVAD support. Gynecological-bleeding after LVAD implantation in this study was defined as needing emergency outpatient visits, hospitalization, blood transfusions, hormonal therapy, and/or surgery (24). In larger datasets, females do not appear to be at higher risk for gastrointestinal bleeding, although there are limited reports which suggest that gastrointestinal bleeding risk is lower in males (25).

Right ventricular failure

Right ventricular failure is more common in women potentially due to a greater occurrence of non-ischemic cardiomyopathy, later presentation of disease, and higher incidence of arrhythmias (26). In a systematic review with meta-analysis of sex specific differences in outcomes for patients receiving continuous flow LVADs, females were 2.12 times more likely to develop right heart failure necessitating right ventricular assist implantation (27). Similarly, a study of EuroMACS data from 2011 to 2014 revealed that right ventricular failure, defined as requiring additional temporary right ventricular assist device (RVAD) support, occurred at a rate of 0.11 events per patient year in females and 0.04 events per patient year in males (22). Women who underwent RVAD implantation had a higher probability of death compared to isolated LVAD, but mortality following RVAD implantation was not significantly different across sex distributions.

Discussion

Women reflect a minority proportion of patients receiving advanced surgical heart failure therapies. There is a discrepancy between the high burden of heart failure in females and the number of females who ultimately receive LVAD therapy. Females who present for advanced heart failure therapies have a disparate preoperative profile compared to male counterparts, including the very nature of the underlying heart disease and associated comorbidities. Additionally, sex differences in pre-implant factors such as candidacy for transplantation and decision making at the patient, physician, and systems level may impact presentation for surgical evaluation and patient willingness to accept a device when offered. Much of what is

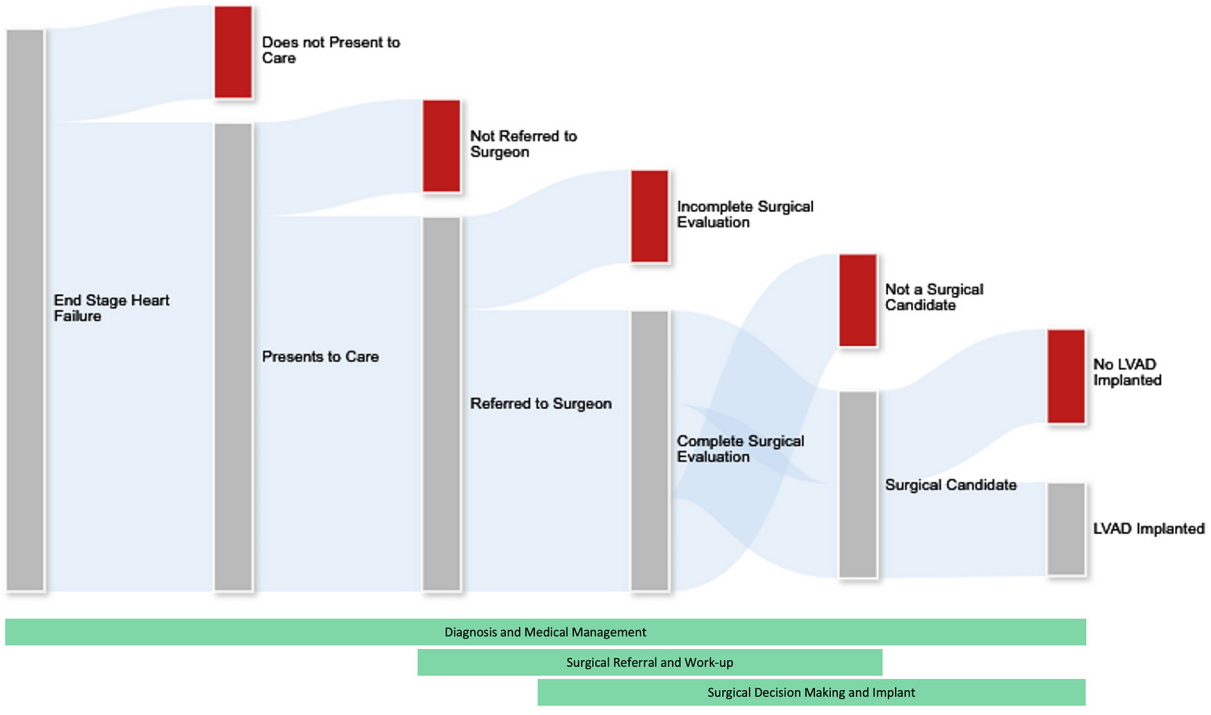

FIGURE 1
The process of patient attrition in the ability to deliver advanced heart failure therapies. Not all patients with end stage heart failure will undergo advanced heart failure therapies. We must understand the processes of diagnosis, medical management, referral for surgery, and surgical decision making to better address disparities in care. This is challenging as attrition of would-be surgical candidates occurs throughout the healthcare system and across medical and surgical specialties. Future research efforts should focus on medical and socioeconomic aspects of this attrition including but certainly not limited to physician bias, system factors, and patient preferences and limitations.

known about LVADs in females with advanced heart failure is derived from the endpoint of device delivery, particularly at the clinical trial level; female sex has been associated with a historically higher rate of mortality and higher incidences of stroke, bleeding, and right ventricular failure following implant. While the representation of females within VAD study cohorts has increased with advances in technology, heart failure therapy and device trials overall continue to underrepresent females, with participation by females far lagging prevalence of the disease by 0.55:1.0 (28). Newer data reflecting outcomes with the Heartmate III is encouraging however sub-analysis by sex is limited and interpretation should be measured given females overall still represent a small proportion of the study cohort. Outcome measures across large datasets such as INTERMACS, EuroMACS, National Inpatient Sample (NIS), and single institutional study cohorts support sex related gaps demonstrating less favorable morbidity and mortality in females. Although sex-based data often were obtained from powerful databases with large populations, there is insufficient granularity to provide specific insight into the likely multifactorial reasons for these observations. Smaller, more comprehensive datasets are limited by power, regional differences in patient populations, and institutional practices and physician preferences that may not be universal. In the absence of datasets specifically built to address disparities, it is often inferred that the origins of sex related discrepancies following LVAD implantation are attributable to differences in biology and physiology such as heart failure etiology and comorbidity profile.

The treatment algorithm connecting a woman in the community with heart failure with successful LVAD implantation is complex. Patients with heart failure should be appropriately identified, medically managed, referred for surgical evaluation and ultimately undergo treatment. There is a critical knowledge gap in understanding the true number of females who could be eligible for or benefit from advanced heart failure therapies out in the community. Our current understanding of advanced heart failure care in females mainly reflects the outcomes of those patients who were able to obtain mechanical support or heart transplantation. To address disparities in access to care, we should understand the processes of advanced heart failure diagnosis, medical management, referral for surgery, and surgical decision making, as well as how each of these processes may be uniquely influenced by sex (Figure 1). Developing appropriately specific tools to collect data illuminating disparities across LVAD therapy delivery stands to benefit women and other underserved populations within the advanced heart failure community.

Author contributions

KJ-U, AR, KK, SC, JH, FP, and PT contributed to conception and design of the review. KJ-U wrote the first draft of the manuscript. KJ-U, FP, and PT wrote sections of the manuscript. All authors contributed to manuscript revision, read, and approved the submitted version.

Funding

This study was partially supported by the National Institutes of Health grant HL164416 awarded to PT.

Conflict of interest

The authors declare that the research was conducted in the absence of any commercial or financial relationships that could be construed as a potential conflict of interest.

Publisher's note

All claims expressed in this article are solely those of the authors and do not necessarily represent those of their affiliated organizations, or those of the publisher, the editors and the reviewers. Any product that may be evaluated in this article, or claim that may be made by its manufacturer, is not guaranteed or endorsed by the publisher.

References

1. Costanzo MR, Mills RM, Wynne J. Characteristics of "Stage D" heart failure: insights from the acute decompensated heart failure national registry longitudinal module (ADHERE LM). *Am Heart J.* (2008) 155:339–47. doi: 10.1016/j.ahj.2007.10.020

2. Ammar KA, Jacobsen SJ, Mahoney DW, Kors JA, Redfield MM, Burnett JC Jr, et al. Prevalence and prognostic significance of heart failure stages: application of the American college of cardiology/American heart association heart failure staging criteria in the community. *Circulation.* (2007) 115:1563–70. doi: 10.1161/CIRCULATIONAHA.106.666818

3. Molina EJ, Shah P, Kiernan MS, Cornwell WK III, Copeland H, Takeda K, et al. The society of thoracic surgeons intermacs 2020 annual report. *Ann Thorac Surg.* (2021) 111:778–92. doi: 10.1016/j.athoracsur.2020.12.038

4. Lloyd-Jones DM, Larson MG, Leip EP, Beiser A, D'Agostino RB, Kannel WB, et al. Lifetime risk for developing congestive heart failure: the Framingham

heart study. *Circulation.* (2002) 106:3068–72. doi: 10.1161/01.CIR.0000039105.49749.6F

5. Benjamin EJ, Blaha MJ, Chiuve SE, Cushman M, Das SR, Deo R, et al. Heart disease and stroke statistics-2017 update: a report from the american heart association. *Circulation.* (2017) 135:e146–603. doi: 10.1161/CIR.0000000000000485

6. Hernandez AF, Fonarow GC, Liang L, Al-Khatib SM, Curtis LH, LaBresh KA, et al. Sex and racial differences in the use of implantable cardioverter-defibrillators among patients hospitalized with heart failure. *JAMA.* (2007) 298:1525–32. doi: 10.1001/jama.298.13.1525

7. Ahmed A, Adegbala O, Akintoye E, Inampudi C, Ajam M, Yassin AS, et al. Gender differences in outcomes after implantation of left ventricular assist devices. *Ann Thorac Surg.* (2020) 109:780–6. doi: 10.1016/j.athoracsur.2019.07.032

8. Hsich EM, Naftel DC, Myers SL, Gorodeski EZ, Grady KL, Schmuhl D, et al. Should women receive left ventricular assist device support? : findings from INTERMACS. *Circ Heart Fail.* (2012) 5:234–40. doi: 10.1161/CIRCHEARTFAILURE.111.963272

9. Riedinger MS, Dracup KA, Brecht ML, Padilla G, Sarna L, Ganz PA. Quality of life in patients with heart failure: do gender differences exist? *Heart Lung.* (2001) 30:105–16. doi: 10.1067/mhl.2001.114140

10. Thangam M, Luke AA, Johnson DY, Amin AP, Lasala J, Huang K, et al. Sociodemographic differences in utilization and outcomes for temporary cardiovascular mechanical support in the setting of cardiogenic shock. *Am Heart J.* (2021) 236:87–96. doi: 10.1016/j.ahj.2020.12.014

11. Steinberg RS, Nayak A, O'Connell C, Burford S, Pekarek A, Chesnut N, et al. Sex differences in eligibility for advanced heart failure therapies. *Clin Transplant.* (2020) 34:e13839. doi: 10.1111/ctr.13839

12. DeFilippis EM, Truby LK, Garan AR, Givens RC, Takeda K, Takayama H, et al. Sex-related differences in use and outcomes of left ventricular assist devices as bridge to transplantation. *JACC Heart Fail.* (2019) 7:250–7. doi: 10.1016/j.jchf.2019.01.008

13. Aaronson KD, Schwartz JS, Goin JE, Mancini DM. Sex differences in patient acceptance of cardiac transplant candidacy. *Circulation.* (1995) 91:2753–61. doi: 10.1161/01.CIR.91.11.2753

14. Tchoukina I, Shah KB, Thibodeau JT, Estep JD, Lala A, Lanfear DE, et al. Impact of socioeconomic factors on patient desire for early LVAD therapy prior to inotrope dependence. *J Card Fail.* (2020) 26:316–23. doi: 10.1016/j.cardfail.2019.11.026

15. Kirklin JK, Pagani FD, Kormos RL, Stevenson LW, Blume ED, Myers SL, et al. Eighth annual INTERMACS report: special focus on framing the impact of adverse events. *J Heart Lung Transplant.* (2017) 36:1080–6. doi: 10.1016/j.healun.2017.07.005

16. Mehra MR, Uriel N, Naka Y, Cleveland JC Jr, Yuzefpolskaya M, Salerno CT, et al. A fully magnetically levitated left ventricular assist device - final report. *N Engl J Med.* (2019) 380:1618–27. doi: 10.1056/NEJMoa1900486

17. Englert JA III, Davis JA, Krim SR. Mechanical circulatory support for the failing heart: continuous-flow left ventricular assist devices. *Ochsner J.* (2016) 16:263–9.

18. Joshi AA, Lerman JB, Sajja AP, Dahiya G, Gokhale AV, Dey AK, et al. Sex-based differences in left ventricular assist device utilization: insights from the nationwide inpatient sample 2004 to 2016. *Circ Heart Fail.* (2019) 12:e006082. doi: 10.1161/CIRCHEARTFAILURE.119.006082

19. Nayak A, Hu Y, Ko YA, Mehta A, Liu C, Pennington J, et al. Gender differences in mortality after left ventricular assist device implant: a causal mediation analysis approach. *ASAIO J.* (2021) 67:614–21. doi: 10.1097/MAT.0000000000001288

20. Bogaev RC, Pamboukian SV, Moore SA, Chen L, John R, Boyle AJ, et al. Comparison of outcomes in women versus men using a continuous-flow left ventricular assist device as a bridge to transplantation. *J Heart Lung Transplant.* (2011) 30:515–22. doi: 10.1016/j.healun.2010.12.009

21. Boyle AJ, Jorde UP, Sun B, Park SJ, Milano CA, Frazier OH, et al. Pre-operative risk factors of bleeding and stroke during left ventricular assist device support: an analysis of more than 900 HeartMate II outpatients. *J Am Coll Cardiol.* (2014) 63:880–8. doi: 10.1016/j.jacc.2013.08.1656

22. Magnussen C, Bernhardt AM, Ojeda FM, Wagner FM, Gummert J, de By T, et al. Gender differences and outcomes in left ventricular assist device support: the European registry for patients with mechanical circulatory support. *J Heart Lung Transplant.* (2018) 37:61–70. doi: 10.1016/j.healun.2017.06.016

23. Yavar Z, Cowger JA, Moainie SL, Salerno CT, Ravichandran AK. Bleeding complication rates are higher in females after continuous-flow left ventricular assist device implantation. *ASAIO J.* (2018) 64:748–53. doi: 10.1097/MAT.0000000000000734

24. Tominaga Y, Yoshioka D, Toda K, Saito T, Kawamura T, Kashiyama N, et al. Risk factors of gynecological bleeding in female patients with left-ventricular assist device. *J Artif Organs.* (2022) 25:110–6. doi: 10.1007/s10047-021-01292-2

25. Taylor C, Bittner K, Bartell N, Aranez J, Alexis JD, Carlson B, et al. Outcomes of gastrointestinal bleeding in patients with left ventricular assist devices: a tertiary care experience. *Endosc Int Open.* (2020) 8:E301–E9. doi: 10.18574/nyu/9780814783320.001.0001

26. Sherazi S, Kutyifa V, McNitt S, Papernov A, Hallinan W, Chen L, et al. Effect of gender on the risk of neurologic events and subsequent outcomes in patients with left ventricular assist devices. *Am J Cardiol.* (2017) 119:297–301. doi: 10.1016/j.amjcard.2016.09.032

27. Blumer V, Mendirichaga R, Hernandez GA, Zablah G, Chaparro SV. Sex-specific outcome disparities in patients receiving continuous-flow left ventricular assist devices: a systematic review and meta-analysis. *ASAIO J.* (2018) 64:440–9. doi: 10.1097/MAT.0000000000000695

28. Preventza O, Critsinelis A, Simpson K, Olive JK, LeMaire SA, Cornwell LD, et al. Sex, racial, and ethnic disparities in US cardiovascular trials in more than 230,000 patients. *Ann Thorac Surg.* (2021) 112:726–35. doi: 10.1016/j.athoracsur.2020.08.075

frontiers | Frontiers in Cardiovascular Medicine

TYPE Original Research
PUBLISHED 23 November 2022
DOI 10.3389/fcvm.2022.1020006

OPEN ACCESS

EDITED BY
Ting Zhou,
University of Wisconsin-Madison,
United States

REVIEWED BY
Takuro Miyazaki,
Showa University, Japan
Chieko Mineo,
University of Texas Southwestern
Medical Center, United States

*CORRESPONDENCE
Priya Raman
praman@neomed.edu

SPECIALTY SECTION
This article was submitted to
Cardiovascular Therapeutics,
a section of the journal
Frontiers in Cardiovascular Medicine

RECEIVED 15 August 2022
ACCEPTED 04 November 2022
PUBLISHED 23 November 2022

CITATION
Gupta S, Khanal S, Bhavnani N,
Mathias A, Lallo J, Kiriakou A, Ferrell J
and Raman P (2022) Sex-specific
differences in atherosclerosis,
thrombospondin-1, and smooth
muscle cell differentiation
in metabolic syndrome versus
non-metabolic syndrome mice.
Front. Cardiovasc. Med. 9:1020006.
doi: 10.3389/fcvm.2022.1020006

Sex-specific differences in atherosclerosis, thrombospondin-1, and smooth muscle cell differentiation in metabolic syndrome versus non-metabolic syndrome mice

Shreya Gupta[1,2], Saugat Khanal[1,2], Neha Bhavnani[1,2], Amy Mathias[1], Jason Lallo[1], Ariana Kiriakou[3], Jessica Ferrell[1,2] and Priya Raman[1,2]*

[1]Department of Integrative Medical Sciences, Northeast Ohio Medical University, Rootstown, OH, United States, [2]School of Biomedical Sciences, Kent State University, Kent, OH, United States, [3]Department of Biological Sciences, Kent State University, Kent, OH, United States

Introduction: Metabolic syndrome (MetS) amplifies the risks of atherosclerosis. Despite well-known sexual dimorphism in atherosclerosis, underlying mechanisms are poorly understood. Our previous findings highlight a proatherogenic protein, thrombospondin-1 (TSP-1), in hyperglycemia- or hyperleptinemia (mimicking obesity)-induced atherosclerosis. However, the role of TSP-1 in the development of atherosclerosis prompted by co-existing hyperglycemia and obesity, characteristic of MetS, is unknown. The goal of this study was to examine sex-specific differences in lesion progression in a model of combined MetS and atherosclerosis (KKAyApoE) and interrogate how these differences relate to TSP-1 expression.

Methods: Male and female KKAy$^{+/-}$ApoE$^{-/-}$ (with ectopic agouti gene expression) and age-matched non-agouti KKAy$^{-/-}$ApoE$^{-/-}$ littermates were placed on a standard laboratory diet from 4 to 24 weeks age followed by blood and tissue harvests for biochemical, molecular, and aortic root morphometric studies.

Results: Metabolic profiling confirmed MetS phenotype of KKAy$^{+/-}$ApoE$^{-/-}$; however, only male genotypes were glucose intolerant with elevated VLDL-cholesterol and VLDL-triglyceride levels. Aortic root morphometry demonstrated profound lipid-filled lesions, increased plaque area, and augmented inflammatory and SMC abundance in MetS vs non-MetS males. This increase in lesion burden was accompanied with elevated TSP-1 and attenuated LMOD-1 (SM contractile marker) and SRF (transcriptional activator of SM differentiation) expression in male MetS aortic vessels. In contrast, while lipid burden, plaque area, and TSP-1 expression increased in MetS and

non-MetS female mice, there was no significant difference between these genotypes. Increased collagen content was noted in MetS and non-MetS genotypes, specific to female mice. Measurement of plasma testosterone revealed a link between the atherogenic phenotype and abnormally high or low testosterone levels. To interrogate whether TSP-1 plays a direct role in SMC de-differentiation in MetS, we generated KKAy$^{+/-}$ mice with and without global TSP-1 deletion. Immunoblotting showed increased SM contractile markers in male KKAy$^{+/-}$TSP-1$^{-/-}$ aortic vessels vs male KKAy$^{+/-}$TSP-1$^{+/+}$. In contrast, TSP-1 deletion had no effect on SM contractile marker expression in female genotypes.

Conclusion: Together, the current study implicates a role of plasma testosterone in sex-specific differences in atherosclerosis and TSP-1 expression in MetS vs non-MetS mice. Our data suggest a sex-dependent differential role of TSP-1 on SMC de-differentiation in MetS. Collectively, these findings underscore a fundamental link between TSP-1 and VSMC phenotypic transformation in MetS.

KEYWORDS

TSP-1, metabolic syndrome, SMC differentiation, atherosclerosis, KKAy mice, sex-specific differences

Introduction

Cardiovascular disease is the leading cause of morbidity and mortality world-wide accounting for nearly 19 million deaths in 2020, and this number is expected to escalate by 2030 (1). Atherosclerosis is a major player in the development of several cardiovascular complications including myocardial infarction, heart failure and stroke (1). Current lipid-lowering therapies, including the gold-standard statins, have provided limited benefit against major macrovascular events and cardiovascular mortality (2); moreover, many of these agents have reported significant toxicity and side-effects associated with their use (3, 4). Metabolic disorders such as hyperglycemia, obesity and dyslipidemia have a devastating impact on vascular function. Numerous clinical studies and trials including animal data highlight hyperglycemia, a hallmark of diabetes, and obesity as independent risk-factors for atherosclerosis (5–13). Risk of atherosclerotic complications is amplified two-to-four-fold (14) in individuals with metabolic syndrome (MetS), a cluster of metabolic anomalies characterized by hyperglycemia and obesity. Despite extensive work, mechanisms responsible for accelerated atherosclerotic complications in MetS remain incompletely understood.

Earlier work from our laboratory demonstrates that high glucose, mimicking diabetes, and high leptin, mimicking obesity, upregulate the expression of a potent proatherogenic protein, thrombospondin-1 (TSP-1), in human and mouse aortic smooth muscle cells (SMC) (15, 16). TSP-1 is a multifunctional extracellular matrix protein that has been linked to metabolic disease and related cardiovascular complications (17). Growing literature indicates that TSP-1 expression is significantly increased in the plasma, visceral adipose tissue, heart, blood vessels and kidneys of patients with diabetes and obesity and related murine models (18–22). Earlier studies have also shown that TSP-1 expression is significantly enhanced in the injured vascular wall (23, 24) and atherosclerotic lesions (25). Additionally, multiple cell types within the vascular wall including endothelial cells, SMC, fibroblasts and macrophages produce TSP-1 in response to numerous proatherogenic stimuli (15, 16, 20). Recent studies from our laboratory have documented that global TSP-1 deletion *in vivo* reduces atherosclerotic lesion burden in ApoE$^{-/-}$ mice in response to both STZ-induced hyperglycemia (26) and exogenous leptin administration (27), mimicking obesity. However, the role of TSP-1 in the development of atherosclerotic lesions under pathological conditions prompted by co-existing hyperglycemia and obesity, characteristic of MetS, remains elusive.

The pathophysiology of human atherosclerosis in MetS is highly complex, triggered by a combination of metabolic risk factors. Therefore, an understanding of the underlying molecular mechanisms that drive the disease requires animal models that most closely mimic the human state. While there are several genetically-modified murine models of diabetes and obesity such as db/db, and ob/ob mice, most of these existing mouse models do not fully represent the polygenic form of the disease and in turn, fail to recapitulate the complex spectrum of the human disease.

Moreover, a plethora of growing literature emphasizes sex-specific differences in the incidence, clinical manifestations and etiology of atherosclerosis, including differential response to major cardiovascular risk factors (28–30). Despite the widely-accepted sexual dimorphism in atherosclerosis, mechanisms underlying sex as a biological variable in atherosclerosis are poorly understood. Such limitations have been largely attributed to the lack of well-powered, preclinical animal studies that encompass both male and female progenies.

Therefore, the objective of the current study was to examine sex-specific differences in the development of atherosclerosis between a murine model of MetS versus non-MetS developed on an atherosclerotic background, and to interrogate how these differences relate to TSP-1 expression in the vasculature. Our data suggest a putative link between plasma testosterone levels, atherogenic phenotype and TSP-1 expression in MetS vs non-MetS mice. These findings implicate a sex-specific differential role of TSP-1 on atherosclerotic lesion progression and SMC de-differentiation in MetS.

Materials and methods

Mouse models

All animal experiments and euthanasia procedures utilized in this study were conducted in accordance with animal protocols annually approved by Northeast Ohio Medical University Institutional Animal Care and Use Committee (NEOMED IACUC). ApoE$^{-/-}$ (stock no. 002052) and TSP-1$^{-/-}$ (stock no. 006141) mice on C57BL/6J background, and agouti KKAy$^{+/-}$ (stock no. 002468) mice were purchased from The Jackson Laboratory (Bar Harbor, ME, USA) and further expanded in our animal facility. Generation of KKAy$^{+/-}$ mice are known to involve transfer of the yellow agouti gene (Ay^{+}) into the KK spontaneously diabetic mice by repeated crossing of the yellow obese mice with KK mice (black fur at weaning). Unlike the KK mice that carry only the diabetes gene, the KKAy$^{+/-}$ mice have an ectopic expression of the agouti gene which blocks the melanocortin type 4 receptor signaling in the hypothalamus resulting in hyperphagic mice with a stronger expression of obesity than in the original KK mice (31). Male KKAy$^{+/-}$ mice were crossbred with either female ApoE$^{-/-}$ or female TSP-1$^{-/-}$ mice. The resulting agouti KKAy$^{+/-}$ApoE$^{-/-}$ and non-agouti KKAy$^{-/-}$ApoE$^{-/-}$ as well as KKAy$^{+/-}$/TSP-1$^{-/-}$ and KKAy$^{+/-}$TSP-1$^{+/+}$ mice produced in F2 generation were utilized in this study. ApoE$^{-/-}$ and TSP-1$^{-/-}$ genotypes were confirmed by polymerase chain reaction based on established protocols, per The Jackson Laboratories. KKAy$^{+/-}$ and KKAy$^{-/-}$ genotypes were identified based on coat color, with yellow indicative of agouti Ay$^{+/-}$ and black depicting non-agouti Ay$^{-/-}$ allele transmission. Mice were housed in a pathogen-free environment and kept on a 12-hour:12-hour light/dark cycle.

Study design

Male and female KKAy$^{+/-}$ApoE$^{-/-}$ and age-matched KKAy$^{-/-}$ApoE$^{-/-}$ littermate mice were weaned at 4 weeks of age and maintained on standard laboratory diet (Purina LabDiet 5008) *ad libitum* until 24 weeks of age (study end point). Body weight and non-fasted blood glucose levels were monitored in all animals on a monthly-basis. For agouti KKAy$^{+/-}$ mice, animals with body weight <40 g and non-fasted blood glucose <200 mg/dl at 8-weeks-age were excluded from the study. Similarly, non-agouti KKAy$^{-/-}$ genotypes with body weight >40 g and non-fasted blood glucose >200 mg/dl at 8 weeks of age were also excluded from the study. At 22 weeks of age, subsets of mice were subjected to either intraperitoneal glucose tolerance test (IPGTT) or insulin tolerance test (ITT) followed by Treadmill Exercise Test conducted at 23 weeks of age. After overnight fasting, animals were harvested at 24 weeks of age following euthanasia with Fatal Plus, per institutionally approved methods. Blood and tissue samples were collected and utilized for experiments as described below. In a parallel study, male and female KKAy$^{+/-}$ TSP-1$^{+/+}$ and age-matched KKAy$^{+/-}$TSP-1$^{-/-}$ littermates, weaned at 4-weeks-age, were maintained on standard laboratory diet (Purina LabDiet 5008) *ad libitum* until 18 weeks of age (study end point). Body weight and non-fasted blood glucose levels were monitored in all animals on a monthly basis. At 17 weeks of age, KKAy$^{+/-}$TSP-1$^{+/+}$ and KKAy$^{+/-}$TSP-1$^{-/-}$ mice were subjected to IPGTT; after overnight fasting, animals were harvested at 18 weeks of age for blood and tissue collection following euthanasia using Fatal Plus.

Intraperitoneal glucose tolerance test and insulin tolerance test

After overnight fasting, an initial blood sample was collected from each mouse via lateral tail incision. This was followed by intraperitoneal injection of either sterile glucose solution (2 g/kg body weight) or sterile insulin (0.75 U/kg body weight) for glucose tolerance test (GTT) or insulin tolerance test (ITT), respectively. Thereafter, blood samples were collected at 15-, 30-, 60-, 90-, and 120-min post-glucose or insulin injections. All blood glucose measurements were made using a hand-held glucometer.

Plasma lipid analyses

After an overnight fast, blood was collected from each animal via cardiac puncture; plasma was separated, aliquoted

and stored at −80°C for future analyses. Total cholesterol and total triglyceride levels were measured in the plasma samples collected from each mouse using Infinity Reagents (Thermo Fisher Scientific, Waltham, MA, USA). Distribution of cholesterol and triglyceride among plasma lipoproteins was measured using fast-performance liquid chromatography (FPLC), as described earlier (27).

Plasma testosterone assay

Total testosterone levels were measured in plasma samples collected from each mouse using the testosterone parameter assay kit (R&D Systems, Minneapolis, MN, USA), per manufacturer's instructions.

Treadmill exercise test

This test involves measurement of maximal oxygen consumption (VO_{2max}) during exercise and was performed as reported earlier (32). One day prior to the experiment, mice were trained and acclimated to using the treadmill at walking speeds for 10–15 min. The next day, mice were allowed to run to exhaustion at incrementally increasing speeds ranging from 10 to 48 m/min at a constant incline of 5°. Briefly, mice were kept in sealed clear Plexiglass cages fitted with an automated conveyer belt used as a treadmill and shocker grid to stimulate running. Fresh room air was provided at 0.5 L/min for the duration of the acclimation and recording periods. On the day of the experimentation, initial baseline readings of oxygen consumption and carbon dioxide production were followed by measurement of gas exchange, maximum speed and maximum runtime until the animals reached exhaustion. Once the mice were exhausted and exposed to the shocker, they were removed from the apparatus and returned to their home cages. Care was taken to ensure that each mouse was not exposed to the shocker more than five times within a 1-min span; failure of the mouse to continue running determined termination of measurements for that mouse. Maximum oxygen consumption (VO_{2max}), carbon dioxide production at the time of VO_{2max} (VCO_{2max}), maximum running speed at which VO_{2max} was achieved, maximum run time until exhaustion and respiratory exchange ratio (RER [V_{CO2}/V_{O2}], an estimate of fuel usage) were calculated based on the readings and analyzed using Graph Pad.

Aortic root morphometry

At the study endpoint, hearts were removed from each mouse following PBS perfusion. After a brief PBS wash, individual mouse hearts were embedded in OCT and stored at −80°C until further use. About 8–10-micron serial sections of the aortic root were obtained by cutting the OCT-embedded hearts, as described earlier (27). Care was taken to ensure that only serial sections collected from aortic root regions representing about 100–150 microns following the valve leaflet were utilized in all morphometric experiments. Additional care was exercised to ensure that staining was performed on sections within similar regions of the aortic root across all treatment groups for quantification and comparison. Aortic root sections were concurrently stained with 0.5% w/v Oil red O (ORO) and hematoxylin and eosin (H&E) to assess the lipid burden and plaque area, respectively. Additional sections were utilized for the detection of collagen content within aortic root lesions using Masson's Trichrome stain kit (Polysciences). For ORO-stained and MT-stained sections, hematoxylin counterstaining was utilized. All sections were mounted with DPX mounting media, observed using Olympus BX61VS microscope and images were captured using 10× magnification. For quantitative morphometry, eight animals per genotype for each sex with at least 30 sections within each group were analyzed.

Immunohistochemistry

Serial root sections acquired from each animal as described above were subjected to immunohistochemistry using CD68, CD45, and α-SMA (Abcam) antibodies, as described earlier (27). Briefly, tissue sections were incubated in ice-cold acetone (5–10 min) and blocked with 5% donkey or goat serum (60–90 min) at room temperature. Following an overnight incubation with primary antibodies (anti-CD68-1:800; anti-CD45-1:200; anti-α-SMA-1: 400) at 4°C, sections were incubated with donkey Alexa Flour 594 anti-rabbit IgG secondary antibodies (1:200) and mounted on DAPI-containing mounting media (Vectashield, Vector Laboratories, Newark, CA, USA). To control for non-specific staining, identical tissue sections were incubated with species-specific IgG control antibody in the absence of the corresponding primary antibodies or no primary antibody, wherein no background staining was noted. Sections were observed using Olympus fluorescence IX71 microscope (10× magnification) and images were digitally captured using a set of identical parameters across all sections, specific for each antibody. For all image quantifications, at least five mice per genotype for each sex with an average of 20 tissue sections within each group were utilized.

Immunoblotting

Lysates from aortae of harvested animals were prepared in RIPA lysis buffer. Protein content was measured using the BCA protein assay (Thermo Fisher Scientific, Waltham, MA, USA). Equal concentrations of protein (25 μg of aortic lysates) were resolved on 8% SDS-PAGE followed by wet transfer to PVDF membranes. Immunoblotting was performed using anti-TSP-1 (1:200, Invitrogen, Waltham, MA, USA), anti-LMOD-1

(1:1000, ProteinTech, Rosemont, IL, USA), anti-SRF (1:1000, Cell Signaling, Danvers, MA, USA) and anti-Calponin (1.5:1000, Cell Signaling, Danvers, MA, USA). Equal protein loading of samples was confirmed by staining the membranes with Ponceau S. All immunoblot images were captured using Protein Simple and densitometric analyses was performed using Image J software. For representative immunoblots, lane images depict proteins loaded and detected on a single immunoblot; however, lanes were re-arranged to improve the clarity of presentation.

Image quantification

For morphometry and immunohistochemistry studies, lesion area defined by the internal elastic lamina to luminal edge of the lesion was selected using the polygon selection tool in Image J; this region was cropped, saved as a new image file and subsequently used for analyses using Image J software. Briefly, the color thresholding option was utilized to measure the total lesion area and stained area for each image. For immunohistochemistry, specific positive staining was expressed as a percentage of the total lesion area. For measurement of plaque area in H&E-stained images, within each aortic root image, line tracings were drawn to mark the area enclosed by the internal elastic lamina (total aortic root area) and the area enclosed by the luminal edge of the lesions (aortic root luminal area). Plaque area was then determined by subtracting the aortic root luminal area from the total aortic root area for each H&E-stained image. All image quantifications were performed by team members blinded to the identity of all sections. For ORO and MT images, area was measured in μm^2; for H&E images, area was measured in mm^2; for CD45, CD68, and α-SMA images, area was measured in sq. pixels.

Statistical analyses

All results are expressed as mean ± SEM. Statistical analyses was performed using GraphPad Prism 9.3.1 and Excel's Real Statistics Resource pack. Prior to statistical analyses, each data set was tested for normality (Shapiro–Wilks; D'Agostino–Pearson; Kolmogorov–Smirnov; Cramer–von Mises; Ryan–Joiner) and variance on the original scale or after square root data transformation. Parametric methods were applied if assumption of normality was met, while non-parametric methods were used if the assumption was violated. For data following normal gaussian distribution with similar variance, ordinary one-way ANOVA followed by Tukey's multiple correction *post-hoc* test was used for 4-group comparison. For normally distributed data with unequal variance, Welch correction was applied followed by Dunnett's *post-hoc* test. Unpaired Student's *t*-test was used for 2-group comparisons of normally-distributed data. Mann–Whitney and Kruskal–Wallis were applied as the non-parametric counterparts of Student's *t*-test and one-way ANOVA, respectively; further, Kruskal–Wallis was followed by Dunn *post-hoc* test. Statistical significance was set at $p \leq 0.05$.

Results

Metabolic profile of agouti KKAy$^{+/-}$ApoE$^{-/-}$ and non-agouti KKAy$^{-/-}$ApoE$^{-/-}$ mice

Yellow agouti KKAy$^{+/-}$ApoE$^{-/-}$ and age-matched black non-agouti KKAy$^{-/-}$ApoE$^{-/-}$ mice were monitored for body weight and non-fasted blood glucose levels once-a-month until harvest. Regardless of sex, body weight and non-fasted blood glucose levels were significantly elevated in 16-week-old agouti KKAy$^{+/-}$ApoE$^{-/-}$ mice compared with age-matched non-agouti KKAy$^{-/-}$ApoE$^{-/-}$ littermates (**Figures 1A,B**). Specifically, body weight was increased by 21 and 39% in male and female KKAy$^{+/-}$ApoE$^{-/-}$ vs. age- and sex-matched KKAy$^{-/-}$ApoE$^{-/-}$ littermate mice, respectively. Moreover, in non-agouti KKAy$^{-/-}$ApoE$^{-/-}$ genotypes, body weight was reduced by 15% in female vs male mice. Both male and female 16-week-old agouti KKAy$^{+/-}$ApoE$^{-/-}$ mice revealed non-fasted blood glucose levels >250 mg/dl, reflective of diabetes, with greater than 2-fold increase in glucose levels noted in these animals compared to age- and sex-matched non-agouti KKAy$^{-/-}$ApoE$^{-/-}$. In addition, a sex-specific difference in non-fasted blood glucose levels was observed in both agouti and non-agouti genotypes. Specifically, blood glucose was reduced by 25% in female non-agouti KKAy$^{-/-}$ApoE$^{-/-}$ mice compared to males, and in female agouti KKAy$^{+/-}$ApoE$^{-/-}$ mice it was reduced even further by 37% vs. male mice. Interestingly, GTT revealed a significant impairment in glucose tolerance in only male agouti KKAy$^{+/-}$ApoE$^{-/-}$ genotypes, while there was no difference in insulin sensitivity between the genotypes in either sex, shown via ITT (**Figures 1C,D**). We next measured plasma lipid levels in these animals. Regardless of sex, total cholesterol levels were significantly increased in both male and female agouti KKAy$^{+/-}$ApoE$^{-/-}$ mice as compared with age-matched KKAy$^{-/-}$ApoE$^{-/-}$ (**Figure 1E**). Specifically, there were 1.5- and 2.2-fold increases in plasma total cholesterol levels in male and female agouti KKAy$^{+/-}$ApoE$^{-/-}$ mice vs. corresponding non-agouti KKAy$^{-/-}$ApoE$^{-/-}$ genotypes, respectively. However, in non-agouti KKAy$^{-/-}$ApoE$^{-/-}$ mice, while plasma total cholesterol was 78% higher in male mice vs. age-matched females, no sex-specific difference was noted in the yellow agouti KKAy$^{+/-}$ApoE$^{-/-}$ genotype. Concomitant to total cholesterol levels, a significant increase in plasma total triglyceride was also noted in 16-week-old male agouti KKAy$^{+/-}$ApoE$^{-/-}$ mice (66% vs non-agouti KKAy$^{-/-}$ApoE$^{-/-}$ mice, $p < 0.05$; **Figure 1F**). However, there was no difference in plasma total triglycerides between the agouti and non-agouti genotypes in female mice. Likewise, no

10.3389/fcvm.2022.1020006

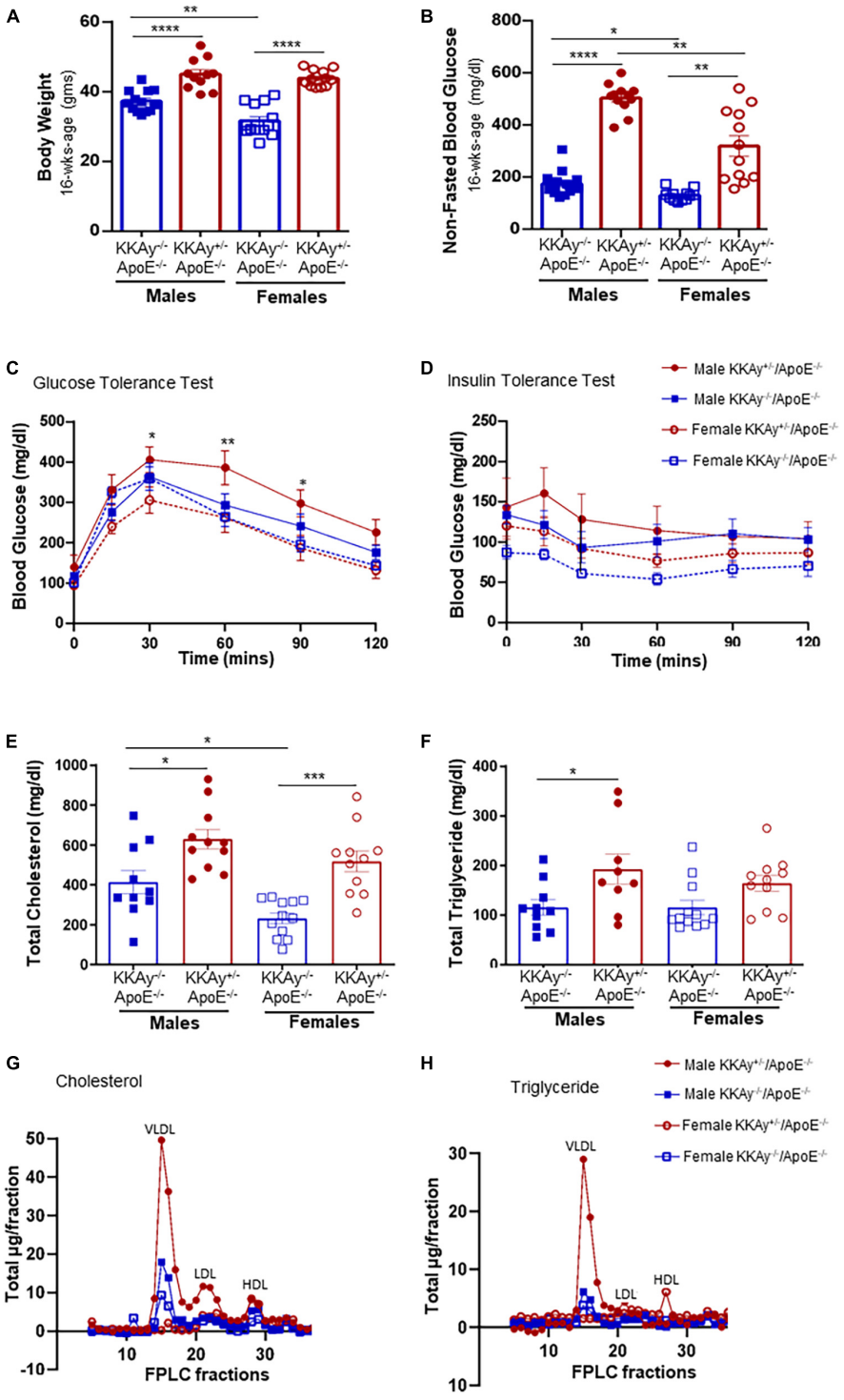

FIGURE 1
Sex-based differences in metabolic profile of agouti KKAy$^{+/-}$ApoE$^{-/-}$ and non-agouti KKAy$^{-/-}$ApoE$^{-/-}$ mice. Male and female age-matched KKAy$^{+/-}$ApoE$^{-/-}$ and KKAy$^{-/-}$ApoE$^{-/-}$ littermate mice were maintained on standard laboratory diet from 4 to 24 weeks of age. At 22 weeks of age, subsets of mice were subjected to either intraperitoneal glucose tolerance test (GTT) or insulin tolerance test (ITT) followed by mice harvest at 24 weeks age for blood and tissue collection. Shown are **(A)** body weight at 16 weeks age; **(B)** non-fasted blood glucose at 16 weeks age; **(C)** glucose tolerance test (GTT) *$p < 0.05$ and **$p < 0.01$ for male KKAy$^{+/-}$ApoE$^{-/-}$ vs. female KKAy$^{+/-}$ApoE$^{-/-}$; **(D)** insulin tolerance test (ITT); **(E)** plasma total cholesterol; **(F)** plasma total triglyceride; **(G)** cholesterol lipoprotein distribution via FPLC fractionation; **(H)** triglyceride lipoprotein distribution via FPLC fractionation. Results are expressed as mean ± SEM. For panels **(A,B,E,F)** ****$p < 0.0001$, ***$p < 0.0005$, **$p < 0.005$, *$p < 0.05$. n = 11–14/genotype/sex.

sex-specific difference in total triglyceride levels was observed in either the agouti or non-agouti genotypes. To further interrogate differences in plasma lipoprotein distribution, we next performed fast-performance liquid chromatography plasma fractionation. As shown in **Figures 1G,H**, only male agouti KKAy$^{+/-}$ApoE$^{-/-}$ mice revealed a significant increase in both VLDL-cholesterol and VLDL-triglyceride levels as compared to the other animal cohorts. Together, these results directly confirm the metabolic syndrome phenotype of yellow agouti KKAy$^{+/-}$ApoE$^{-/-}$ mice, characterized by increased body weight, blood glucose and total cholesterol levels. Moreover, our data demonstrate sex-specific differences in the metabolic profiles of agouti and non-agouti mice on an atherosclerotic background.

Cardiometabolic fitness of agouti KKAy$^{+/-}$ApoE$^{-/-}$ and non-agouti KKAy$^{-/-}$ApoE$^{-/-}$ mice

To examine the cardiometabolic fitness of MetS and non-MetS atherosclerotic mice, a subset of male and female 23-week-old KKAy$^{+/-}$ApoE$^{-/-}$ and KKAy$^{-/-}$ApoE$^{-/-}$ mice were subjected to treadmill exercise test. Although a downward trend in maximum oxygen consumption (VO_{2max}) was noted in MetS KKAy$^{+/-}$ApoE$^{-/-}$ mice during exercise as compared with non-MetS KKAy$^{-/-}$ApoE$^{-/-}$ genotypes of both sexes, this difference was not statistically significant (**Figure 2A**). Notably, while there was 2.1-fold decrease in VO_{2max} in female vs male mice among non-MetS KKAy$^{-/-}$ApoE$^{-/-}$ genotypes ($p < 0.005$), this sex-related difference was not observed in the MetS KKAy$^{+/-}$ApoE$^{-/-}$ mice. In addition, while we observed a sex-specific difference in VCO_{2max} in both MetS and non-MetS genotypes, there was no difference in VCO_{2max} between MetS and non-MetS animals (**Figure 2B**). Further, maximum run speed corresponding to maximal oxygen uptake and maximum runtime until exhaustion in MetS KKAy$^{+/-}$ApoE$^{-/-}$ mice were reduced by 24 and 20% respectively, vs non-MetS KKAy$^{-/-}$ApoE$^{-/-}$ genotypes, and this difference was noted in both sexes ($p < 0.005$; **Figures 2C,D**). RER, the ratio of carbon dioxide produced to oxygen consumed which can be used as an estimate of metabolic fuel usage, was consistently elevated in both male and female MetS KKAy$^{+/-}$ApoE$^{-/-}$ mice (**Figures 2E,F**). Together, these results suggest an impaired metabolic fitness in MetS KKAy$^{+/-}$ApoE$^{-/-}$ genotypes.

Differences in lipid burden, plaque area and collagen content between MetS KKAy$^{+/-}$ApoE$^{-/-}$ and non-MetS KKAy$^{-/-}$ApoE$^{-/-}$ genotypes

Using aortic root morphometry, we next examined atherosclerotic lesion formation in 24-week-old MetS KKAy$^{+/-}$ApoE$^{-/-}$ and age-matched non-MetS KKAy$^{-/-}$ApoE$^{-/-}$ genotypes. Oil red O (ORO) staining of aortic root sections revealed robust lipid-filled lesions in MetS KKAy$^{+/-}$ApoE$^{-/-}$ mice of both sexes and in female non-MetS KKAy$^{-/-}$ApoE$^{-/-}$ mice (**Figures 3A,B**). Specifically, in male mice, aortic root lipid burden was increased by 5.7-fold in KKAy$^{+/-}$ApoE$^{-/-}$ as compared with non-MetS KKAy$^{-/-}$ApoE$^{-/-}$ mice ($p < 0.0001$). In contrast, no statistically significant difference in lipid burden was noted between MetS and non-MetS genotypes in the female mice. Of note, ORO-positive staining area, reflective of lipid burden, was significantly higher in the female non-agouti KKAy$^{-/-}$ApoE$^{-/-}$ mice (6-fold vs. male KKAy$^{-/-}$ApoE$^{-/-}$; $p < 0.0001$). Next, we assessed the plaque area using H&E staining of aortic root sections. Consistent with the enhanced ORO-positive lipid burden, we found a significant increase in plaque area in MetS KKAy$^{+/-}$ApoE$^{-/-}$ aortic root sections compared with those derived from non-MetS KKAy$^{-/-}$ApoE$^{-/-}$ mice. Moreover, this difference in plaque area was specific to only male mice (**Figures 3C,D**, $p < 0.0001$), with no statistically significant difference between the female genotypes. Of note, elevated lipid burden in root sections of female black KKAy$^{-/-}$ApoE$^{-/-}$ mice was accompanied with increased plaque area in these animals. Interestingly, Masson's Trichrome (MT) staining of aortic root sections did not reveal a statistically significant difference in lesion collagen content between MetS KKAy$^{+/-}$ApoE$^{-/-}$ and non-MetS KKAy$^{-/-}$ApoE$^{-/-}$ genotypes, regardless of sex. However, both agouti and non-agouti female mice revealed a much higher collagen content in aortic root lesions as compared to the corresponding male genotypes. Specifically, MT-positive collagen content was profoundly augmented in female vs. male mice in both genotypes (**Figures 3E,F**, KKAy$^{-/-}$ApoE$^{-/-}$: 3-fold; KKAy$^{+/-}$ApoE$^{-/-}$: 1.8-fold). Together, these results clearly demonstrate sex-specific differences in atherogenic phenotype between agouti MetS and non-agouti non-MetS mice on an atherosclerotic background.

Sex-specific differences in inflammatory and SMC lesion burden between MetS KKAy$^{+/-}$ApoE$^{-/-}$ and non-MetS KKAy$^{-/-}$ApoE$^{-/-}$ mice

Immunohistochemistry demonstrated enhanced CD45 expression, reflective of leukocyte infiltration, in aortic root lesions of MetS KKAy$^{+/-}$ApoE$^{-/-}$ vs. age-matched non-MetS KKAy$^{-/-}$ApoE$^{-/-}$ genotypes in male mice. In contrast, CD45 expression was significantly lower in aortic root lesions of MetS agouti vs. non-MetS non-agouti female mice (**Figure 4A**). Specifically, while male KKAy$^{+/-}$ApoE$^{-/-}$ demonstrated 2.5-fold increase in CD45 expression ($p < 0.05$

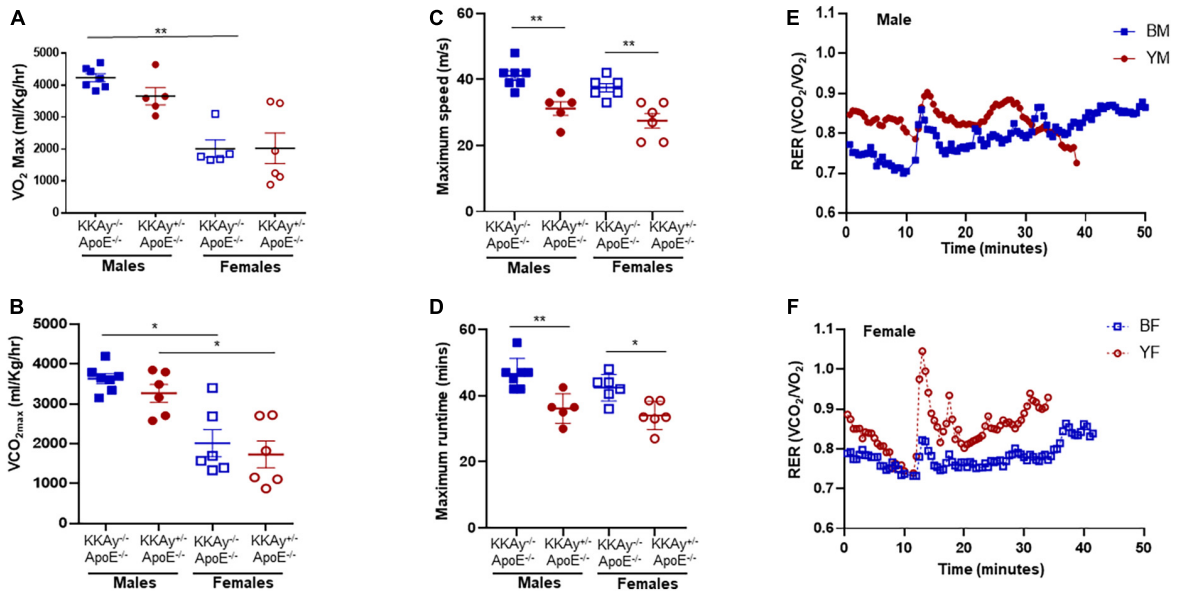

FIGURE 2
Sex-specific differences in cardiometabolic fitness of MetS KKAy$^{+/-}$ApoE$^{-/-}$ and non-MetS KKAy$^{-/-}$ApoE$^{-/-}$ mice using Treadmill Exercise Test. Mice were trained on the treadmill on day 1 and tested using a treadmill exercise test on day 2 with gradial increase in speed at constant incline. Shown are **(A)** maximum oxygen consumption (VO_{2max}), **(B)** carbon dioxide produced relevant to maximal oxygen uptake (VCO_{2max}), **(C)** maximum running speed, **(D)** maximum runtime until exhaustion. Line graphs depicting average RER for **(E)** representative male MetS KKAy$^{+/-}$ApoE$^{-/-}$ (YM) and non-MetS KKAy$^{-/-}$ApoE$^{-/-}$ (BM) mice and **(F)** representative female MetS KKAy$^{+/-}$ApoE$^{-/-}$ (YF) and non-MetS KKAy$^{-/-}$ApoE$^{-/-}$ (BF) mice. For panels **(A–D)**, data are mean ± SEM. For all the panels n = 5–7 mice per genotype. *$p < 0.05$, **$p < 0.005$.

vs. male KKAy$^{-/-}$ApoE$^{-/-}$), CD45-stained positive area was reduced by 79% in MetS KKAy$^{+/-}$ApoE$^{-/-}$ vs. non-MetS KKAy$^{-/-}$ApoE$^{-/-}$ genotypes in female mice (**Figure 4B**, $p < 0.0001$). Interestingly, the highest leukocyte burden was detected in aortic root lesions of non-MetS KKAy$^{-/-}$ApoE$^{-/-}$ females; specifically, CD45 expression increased by 6-fold ($p < 0.0001$) in these animals compared to the male genotypes. We next assessed the macrophage content of lesions in these animals via CD68 immunostaining. As shown in **Figures 4C,D**, the difference in CD68 expression depicting macrophage infiltration in aortic root lesion of KKAy$^{+/-}$ApoE$^{-/-}$ vs. KKAy$^{-/-}$ApoE$^{-/-}$ failed to reach statistical significance, and this effect was consistent in both male and female mice. These data suggest a lack of sex-specific difference in macrophage infiltration between MetS and non-MetS genotypes. To define SMC distribution in lesions, we next performed α-SMA immunostaining of aortic root sections. As shown in **Figure 4E**, there was a significant increase in α-SMA expression, illustrating augmented lesion SMC content in agouti KKAy$^{+/-}$ApoE$^{-/-}$ vs. age-matched non-agouti KKAy$^{-/-}$ApoE$^{-/-}$ mice. Moreover, this increase in SMC abundance in the lesions was noted in both male and female mice, with > 5-fold increase in MetS vs. non-MetS genotypes (**Figure 4F**, $p < 0.005$ in males; $p < 0.05$ in females). Together, these results clearly demonstrate sex-specific differences in lesion inflammatory and SMC content between MetS and non-MetS mice on an atherosclerotic background.

Increased TSP-1 expression associates with reduced LMOD-1 and SRF expression specific to male mice

Concomitant to increased atherosclerotic lesion burden in male MetS KKAy$^{+/-}$ApoE$^{-/-}$ mice, immunoblotting of aortic tissue lysates revealed augmented TSP-1 expression in these animals. Specifically, TSP-1 protein expression increased by 3-fold in aortic vessels of agouti KKAy$^{+/-}$ApoE$^{-/-}$ male mice ($p = 0.0056$ vs. non-agouti KKAy$^{-/-}$ApoE$^{-/-}$ males). This increase in TSP-1 expression was accompanied with reduced LMOD-1 and SRF expression in male KKAy$^{+/-}$ApoE$^{-/-}$ genotypes (50 and 55%, respectively, vs. KKAy$^{-/-}$ApoE$^{-/-}$ male mice, $p < 0.005$; **Figures 5A,C–E**). On the contrary, there was no statistically significant difference in TSP-1, LMOD-1, and SRF expression between MetS and non-MetS genotypes in female mice (**Figures 5B,C–E**). These data clearly demonstrate a correlation between augmented TSP-1 expression and reduced LMOD-1 and SRF expression in MetS KKAy$^{+/-}$ApoE$^{-/-}$ genotypes, that is specific to only male mice.

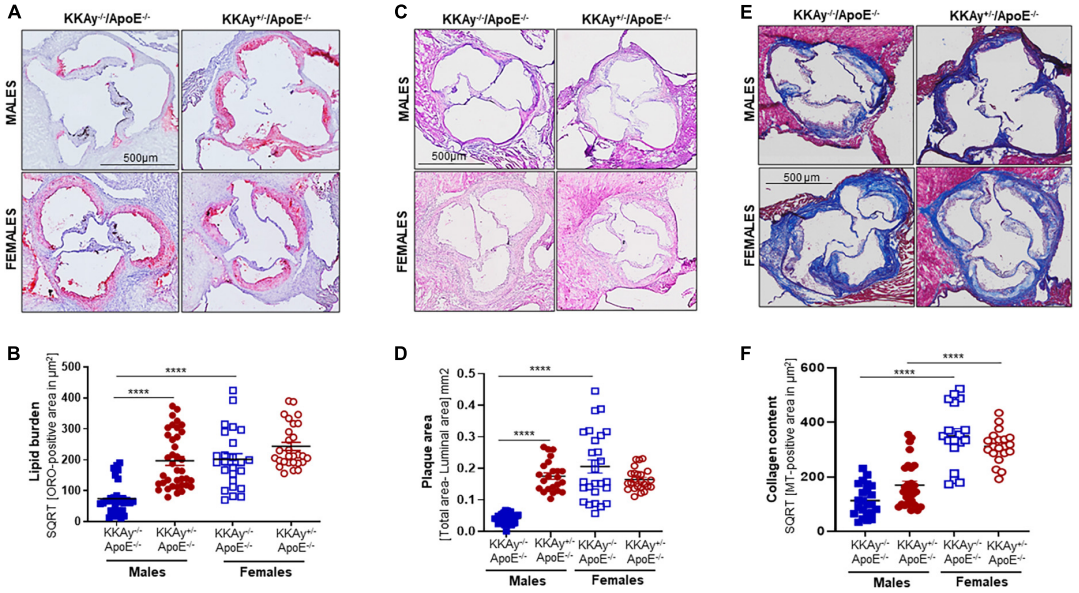

FIGURE 3
Sex-specific differences in lesion lipid burden, plaque area and collagen content in MetS KKAy$^{+/-}$ApoE$^{-/-}$ and non-MetS KKAy$^{-/-}$ApoE$^{-/-}$ mice. Serial sections of equivalent regions of the aortic root were stained with 0.5% Oil red O (ORO) followed by hematoxylin counterstaining. ORO-positive area (measured in μm^2) was quantified using Image J. Shown are **(A)** representative ORO-stained aortic root sections, **(B)** summary data for ORO-positive area. n = 7–9 mice per genotype per sex (2–5 sections per mouse). Aortic root serial sections were stained with hematoxylin and eosin (H&E). Aortic root luminal area and total aortic root area (i.e., area enclosed by the internal elastic lamina in mm^2) were measured using Image J; difference between total root area and luminal area denotes plaque area. Shown are **(C)** representative images for H&E-staining, **(D)** summary data for plaque area. n = 5–8 mice per genotype per sex (4–5 sections per mouse). Identical aortic root sections were stained with Masson's Trichrome (MT) followed by hematoxylin counterstaining. MT-positive area (measured in μm^2) depicting collagen content was quantified in Image J. Shown are **(E)** representative images for MT staining and **(F)** summary data for collagen content, $n > 12$ individual sections for each genotype per sex. All images were captured at 10× magnification. ****$p < 0.0001$.

Lack of TSP-1 upregulates SM contractile marker expression specific to male mice

To interrogate whether TSP-1 plays a direct role in SMC de-differentiation in MetS, we generated MetS KKAy$^{+/-}$ mice with and without global TSP-1 deletion. Metabolic profiling of these animals revealed sex-specific differences in blood glucose and glucose tolerance between agouti KKAy$^{+/-}$TSP-1$^{+/+}$ and KKAy$^{+/-}$TSP-1$^{-/-}$ mice, without significant changes in body weight (**Figure 6**). Specifically, in mice with intact TSP-1, non-fasted blood glucose was lower in the female genotypes at 8 weeks of age ($p < 0.005$); however, this sex-specific difference in blood glucose level was obviated at later time points. Lack of TSP-1 significantly reduced non-fasted blood glucose levels in female agouti KKAy$^{+/-}$ vs. male agouti KKAy$^{+/-}$ genotypes as early as 8 week of age, and this effect was sustained until 16 weeks age ($p < 0.005$). Moreover, KKAy$^{+/-}$TSP-1$^{-/-}$ mice exhibited a significant decrease in non-fasted blood glucose vs. KKAy$^{+/-}$TSP-1$^{+/+}$ only in the female genotypes. In contrast, TSP-1 deletion had no effect on blood glucose levels in male agouti genotypes (**Figure 6B**). GTT further revealed that in the presence of intact TSP-1, male KKAy$^{+/-}$ were significantly glucose intolerant compared with female genotypes at both 90- and 120-min after glucose injection. In addition, KKAy$^{+/-}$ mice lacking TSP-1 manifested impaired glucose tolerance 120-min following glucose injection vs. KKAy$^{+/-}$ with intact TSP-1 in male mice; however, this difference in glucose tolerance was not observed in female agouti genotypes with and without TSP-1 (**Figures 6C,D**). Immunoblotting of aortic lysates demonstrated that TSP-1 deletion augmented LMOD-1 expression (SM contractile marker) in aortic vessels of male MetS KKAy$^{+/-}$ mice (**Figures 7A,C,E**). Specifically, there was >1.7-fold increase in LMOD-1 expression (**Figures 7A,E**; $p < 0.05$) in male KKAy$^{+/-}$TSP-1$^{-/-}$ aortic vessels vs. age-matched KKAy$^{+/-}$TSP1$^{+/+}$ mice (with intact TSP-1). While an upward trend was also noted in calponin expression in aortic vessels derived from male agouti KKAy$^{+/-}$ mice lacking TSP-1, this increase was not statistically significant (**Figures 7A,D**). On the contrary, TSP-1 loss had no effect on SM contractile marker expression in aortic vessels derived from MetS KKAy$^{+/-}$TSP1$^{-/-}$ vs. agouti genotypes with intact TSP-1 in female mice (**Figures 7B,D,E**). Moreover, while Calponin expression significantly differed between male and female KKAy$^{+/-}$ aortic vessels with intact TSP-1, sex-specific difference noted among the TSP-1 knockouts failed to reach

10.3389/fcvm.2022.1020006

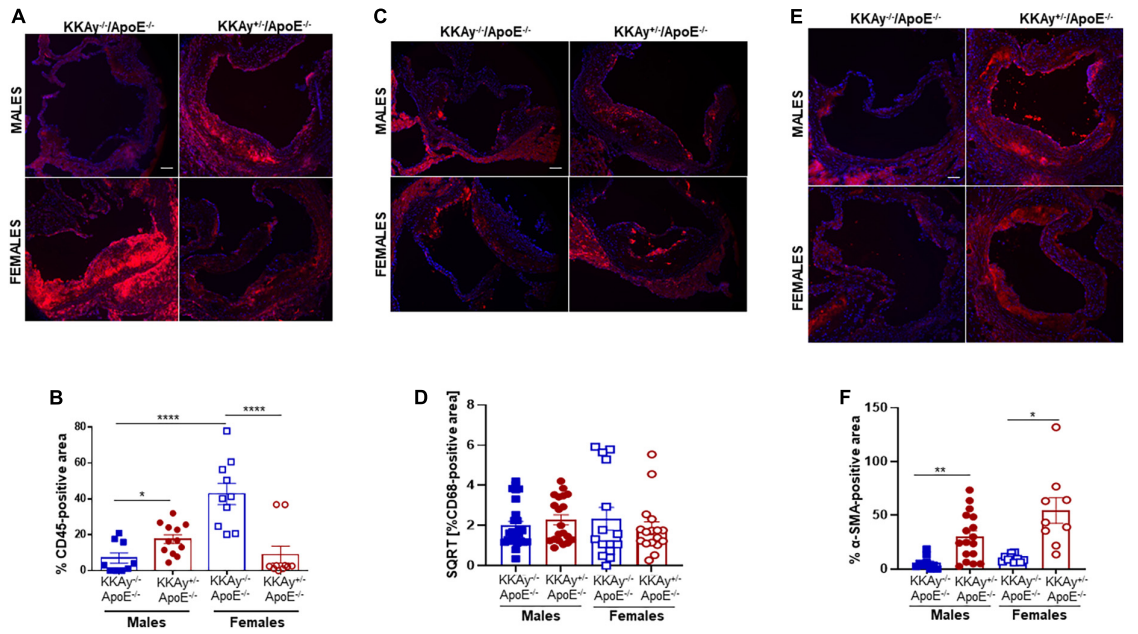

FIGURE 4

Leukocyte and macrophage infiltration and SMC content in aortic root lesions of MetS KKAy$^{+/-}$ApoE$^{-/-}$ and non-MetS KKAy$^{-/-}$ApoE$^{-/-}$ mice. Aortic root sections were subjected to immunohistochemistry using CD45, CD68, and α-SMA antibodies. Images were taken at 10x magnification. Total lesion area and positive staining area of lesions (in sq. pixels) were quantified in each section using Image J. Shown are **(A)** representative images for CD45 staining (leukocyte content), **(B)** summary graph for %CD45-positive area, **(C)** representative images for CD68 staining (macrophage content), **(D)** summary graph for %CD68-positive area, **(E)** representative images for α-SMA staining (SMC content), and **(F)** summary graph for %SMA-positive area (n = 5–6 mice per genotype per sex (2–4 sections per mouse). All values are expressed as mean ± SEM; *$p < 0.05$, **$p < 0.005$, ****$p < 0.0001$, scale bar = 115 μm.

statistical significance. Together, these data suggest a regulatory role of TSP-1 on SMC de-differentiation, characterized by reduced SM contractile marker expression, in MetS specific to male genotypes.

Sex-specific differences in plasma testosterone levels in MetS KKAy$^{+/-}$ApoE$^{-/-}$ and non-MetS KKAy$^{-/-}$ApoE$^{-/-}$ mice

To interrogate the link between sex hormones and atherogenic phenotype observed in MetS vs non-MetS mice, we measured plasma testosterone levels in a subset of our animals. As shown in **Figure 8A**, testosterone levels were significantly elevated in both MetS and non-MetS genotypes in female mice as compared to the corresponding male genotypes. Specifically, there was 20% increase in testosterone concentration in female non-agouti KKAy$^{-/-}$ApoE$^{-/-}$ vs. age-matched male non-agouti genotypes. In case of MetS KKAy$^{+/-}$ApoE$^{-/-}$ mice, testosterone levels increased >2-fold in female vs male mice. Interestingly, both agouti and non-agouti female mice displayed remarkably higher testosterone concentrations compared to levels typically reported in healthy females (33). In contrast, testosterone levels were found to be considerably lower in male agouti KKAy$^{+/-}$ApoE$^{-/-}$ mice compared to normal values reported in healthy males (33). Furthermore, while in female mice, testosterone levels were augmented in MetS KKAy$^{+/-}$ApoE$^{-/-}$ (76% vs. non-MetS KKAy$^{-/-}$ApoE$^{-/-}$; $p < 0.0001$), male MetS genotypes revealed attenuated testosterone levels vs. non-MetS mice. Collectively, these data clearly demonstrate sex-related differences in plasma testosterone levels in MetS and non-MetS genotypes.

Conclusion

In the current study, we provide novel evidence for sex-specific differences in atherosclerotic lesion burden, expression of SM contractile markers and a proatherogenic protein TSP-1 expression between MetS and non-MetS mice. Our results suggest a link between accelerated atherosclerosis and TSP-1 expression in the vessel wall, specific to male MetS mice. Notably, our data implies a sex-specific causal role of TSP-1 on SMC de-differentiation in MetS. It is a generally accepted dogma that men and women present significant differences in the incidence and progression of atherosclerosis and related cardiovascular complications. Yet, the molecular basis of such sexual dimorphism has remained inconclusive, to a large

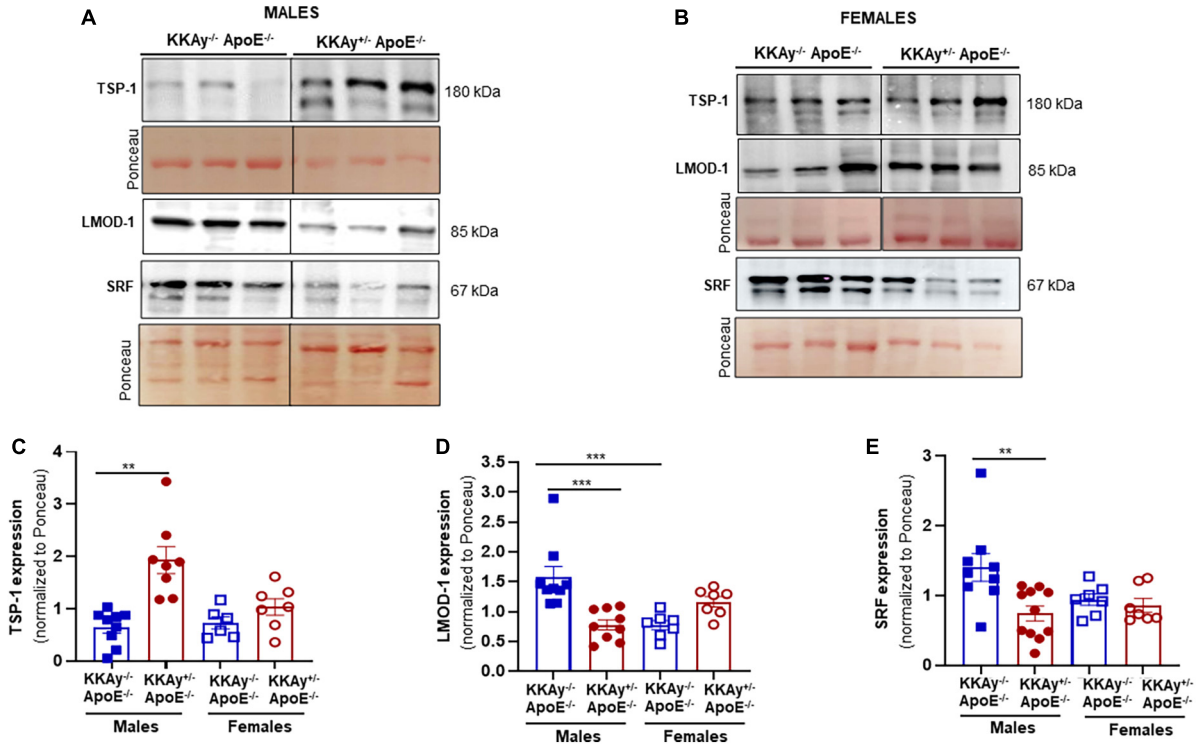

FIGURE 5
Increased TSP-1 expression is accompanied with reduced LMOD-1 and SRF expression in MetS KKAy$^{+/-}$ApoE$^{-/-}$ mice. Shown are **(A)** representative western blots for TSP-1, LMOD-1, and SRF expression in aortic lysates from male MetS KKAy$^{+/-}$ApoE$^{-/-}$ and non-MetS KKAy$^{-/-}$ApoE$^{-/-}$ mice; **(B)** representative western blots for TSP-1, LMOD-1, and SRF expression in aortic lysates from female MetS KKAy$^{+/-}$ApoE$^{-/-}$ and non-MetS KKAy$^{-/-}$ApoE$^{-/-}$ mice. Shown are summary graphs depicting densitometric quantification of western blots for panels **(C)** TSP-1; **(D)** LMOD-1, and **(E)** SRF expression (n = 6–11 animals per genotype per sex). Loading control = Ponceau S. Data shown illustrates protein expression normalized to Ponceau S. Results are expressed as mean ± SEM. $^{**}p < 0.005$; $^{***}p < 0.0005$. For each representative immunoblot, lane images depict proteins loaded and detected on a single immunoblot (full blots shown in Supplementary Figures 1, 2); however, lanes were re-arranged to improve the clarity of presentation.

extent, due to the lack of robust preclinical animal studies employing both sexes.

The KKAy$^{+/-}$ mouse is a classical murine model of MetS characterized by hyperglycemia, insulin resistance, glucose intolerance and severe hyperinsulinemia by approximately 8 weeks of age. Previous studies have reported (31) that KKAy$^{+/-}$ mice develop polygenic forms of metabolic anomalies, analogous to humans. Accordingly, in the present work, we chose the KKAy$^{+/-}$ mice backcrossed for six generations with ApoE$^{-/-}$ to generate a mouse model of combined MetS and atherosclerosis. In line with earlier findings (34), our data confirm the MetS phenotype of agouti KKAy$^{+/-}$ApoE$^{-/-}$ mice, characterized by hyperglycemia, obesity, and dyslipidemia, as compared with non-agouti KKAy$^{-/-}$ApoE$^{-/-}$ littermates. Of note, only male agouti KKAy$^{+/-}$ApoE$^{-/-}$ were observed to be glucose intolerant and hypertriglyceridemic versus age-matched non-agouti KKAy$^{-/-}$ApoE$^{-/-}$ males. Interestingly, a remarkable sex-specific difference in plasma total cholesterol was noted only in the non-agouti genotypes, with male KKAy$^{-/-}$ApoE$^{-/-}$ revealing elevated total cholesterol levels vs. age-matched female genotypes. The observed differences between the agouti and non-agouti mice in the current study emphasize the need for using age-matched littermate mice for such studies. Moreover, our data suggest that knockout of ApoE in female non-agouti KKAy$^{-/-}$ genotypes may trigger a state of hypertriglyceridemia in these animals. Consistent with earlier reports (34), lack of ApoE in agouti KKAy$^{+/-}$ mice led to significant aberrations in the lipoprotein distribution patterns in these animals, with elevated VLDL-cholesterol and VLDL-triglyceride levels. However, this difference was specific to only male genotypes implicating sex-related differences in this murine model of combined MetS and atherosclerosis. Owing to limited plasma sample volume availability, we were unable to measure plasma insulin levels in our animals. However, based on earlier published literature (35, 36), we expect the agouti KKAy$^{+/-}$ApoE$^{-/-}$ mice to have elevated insulin levels compared to non-agouti genotypes. Indeed, previous studies have reported increased pancreatic beta cell degranulation and islet cell hypertrophy triggering increased insulin production

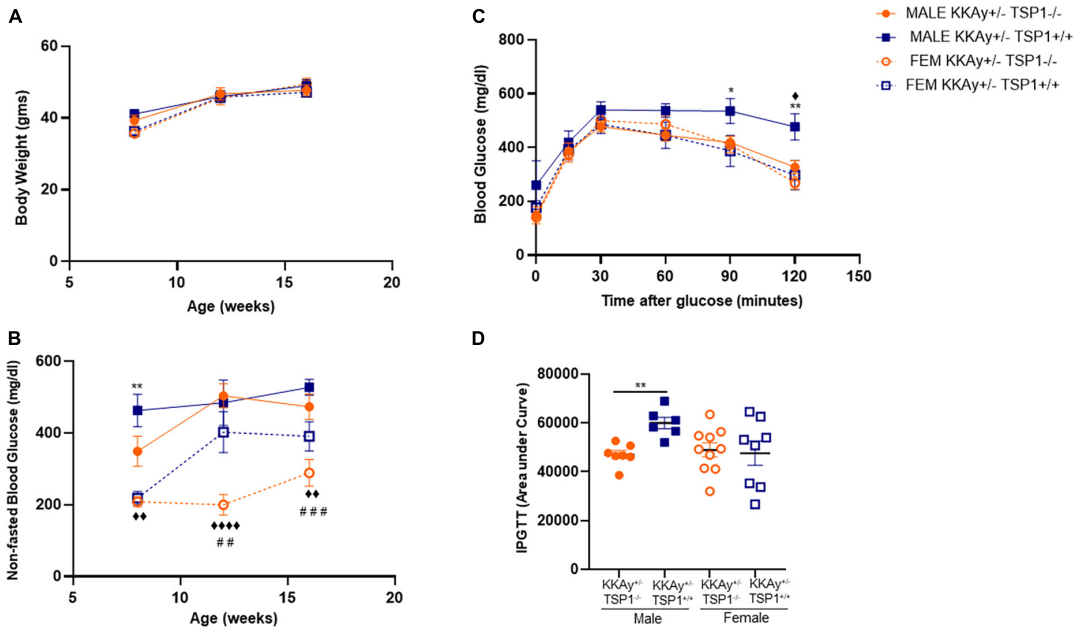

FIGURE 6
Effect of global TSP-1 deletion on metabolic profile of MetS KKAy$^{+/-}$ mice. Male and female age-matched agouti KKAy$^{+/-}$TSP-1$^{+/+}$ and KKAy$^{+/-}$TSP-1$^{-/-}$ littermate mice were maintained on standard lab diet from 4 to 18 weeks of age. Shown are **(A)** body weight and **(B)** non-fasted blood glucose levels measured in subsets of mice genotypes of each sex at 8-, 12- and 16-weeks-age. ♦$p < 0.005$, ♦♦♦♦$p < 0.0001$ denotes male KKAy$^{+/-}$TSP-1$^{-/-}$ vs. female KKAy$^{+/-}$TSP-1$^{-/-}$; **$p < 0.005$ denotes male KKAy$^{+/-}$TSP-1$^{+/+}$ vs. female KKAy$^{+/-}$TSP-1$^{+/+}$; ##$p < 0.005$, ###$p < 0.0005$ denotes female KKAy$^{+/-}$TSP-1$^{+/+}$ vs. female KKAy$^{+/-}$TSP-1$^{-/-}$. **(C)** glucose tolerance test (GTT) done at 17 weeks age. *$p < 0.05$, **$p < 0.005$ denotes male KKAy$^{+/-}$TSP-1$^{+/+}$ vs. female KKAy$^{+/-}$TSP-1$^{+/+}$, ♦$p < 0.05$ denotes male KKAy$^{+/-}$TSP-1$^{+/+}$ vs. male KKAy$^{+/-}$TSP-1$^{-/-}$. **(D)** Area under curve for GTT. n = 7–10 per genotype per sex for panels **(B,C)**; n = 5–10 per genotype per sex for panels **(D,E)**. All results are expressed as mean ± SEM.

in KKAy$^{+/-}$ mice, and such observations were noted as early as 5-weeks of age.

Metabolic profiling of MetS agouti KKAy$^{+/-}$ApoE$^{-/-}$ mice revealed sex-specific differences in response to forced activity. Maximal oxygen consumption was reduced in female non-MetS KKAy$^{-/-}$ApoE$^{-/-}$ mice compared to male mice, and this sex-specific phenotype was lost in MetS KKAy$^{+/-}$ApoE$^{-/-}$ genotypes. In both male and female mice, run time until exhaustion was significantly lower in the MetS genotypes, suggesting lower exercise performance in these animals, compared with non-MetS genotypes; these observations are consistent with what is expected in obese mice. RER, which can be used to estimate metabolic fuel oxidation, was elevated in both male and female MetS KKAy$^{+/-}$ApoE$^{-/-}$ mice, indicating potentially increased glucose oxidation over fat (37) in these mice.

Among the currently available mouse models of diabetes and obesity, ob/ob and db/db mice are the most extensively utilized murine models in cardiovascular research. Despite relative similarities in the metabolic phenotype of ob/ob and db/db mice (38), previous studies have reported considerable variability in the extent of atherosclerotic lesions that develop in these mice on an ApoE$^{-/-}$ background. For instance, obese hyperglycemic leptin-deficient ob/ob;ApoE$^{-/-}$ mice have been reported to develop relatively smaller lesions, with marked suppression in lesion progression from fatty streaks to fibrous plaques as compared to ApoE$^{-/-}$ mice (39). On the other hand, leptin receptor-deficient db/db;ApoE$^{-/-}$ have demonstrated accelerated atherosclerosis accompanying hyperglycemia, obesity, hyperinsulinemia and dyslipidemia vs. age-matched ApoE$^{-/-}$ mice (40). It should be noted that while metabolic anomalies in ob/ob and db/db mice are consistent with that observed in humans, leptin-deficiency or leptin receptor mutation are rare or absent in individuals with MetS. To this end, the agouti KKAy$^{+/-}$ApoE$^{-/-}$ mice developed in this study more closely mimics the clinical features associated with MetS.

While both male and female MetS KKAy$^{+/-}$ApoE$^{-/-}$ mice developed profound lipid-filled lesions accompanying increased plaque area, there was a significant difference in the progression of atherosclerotic lesions between MetS and non-MetS genotypes that was specific to only male mice. While these results are in line with a previous report (34), the current work has provided the first evidence of sex-specific variations in lesion development in this murine model of MetS. Moreover, atherosclerotic lesion formation correlated with augmented TSP-1 expression in the vascular

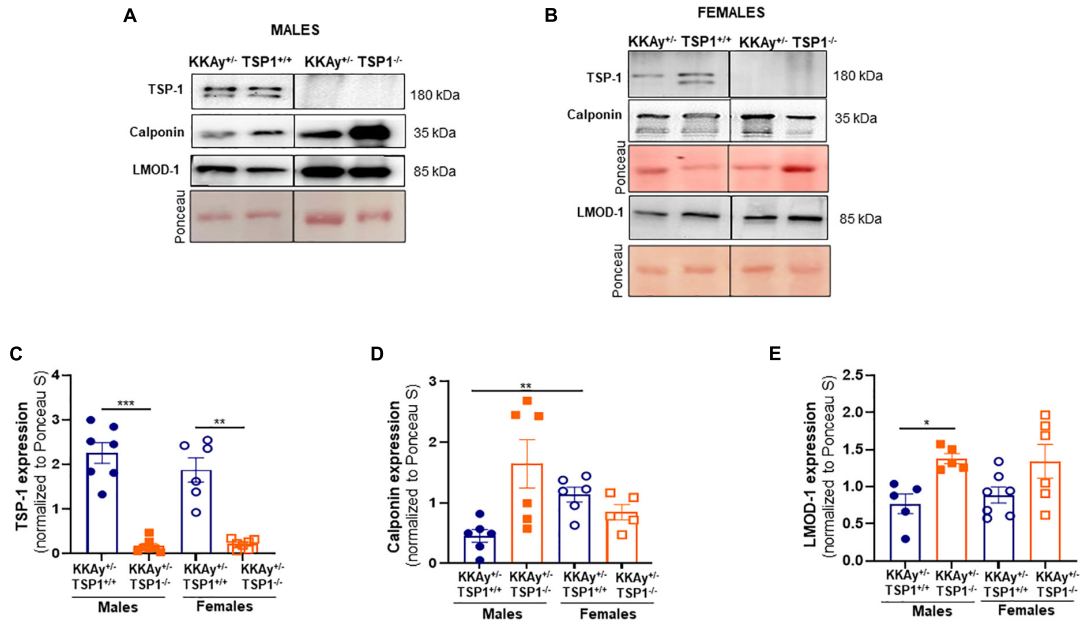

FIGURE 7
TSP-1 deletion increases LMOD-1 and calponin expression in aortic vessels of male MetS KKAy$^{+/-}$ mice. Shown are representative western blots for TSP-1, LMOD-1 and calponin expression in aortic lysates derived from **(A)** male KKAy$^{+/-}$TSP-1$^{+/+}$ and KKAy$^{+/-}$TSP-1$^{-/-}$ mice and **(B)** female KKAy$^{+/-}$TSP-1$^{+/+}$ and KKAy$^{+/-}$TSP-1$^{-/-}$ mice. Shown are summary graphs for densitometric quantification of immunoblots for **(C)** TSP-1, **(D)** Calponin, and **(E)** LMOD-1 expression. n = 5–7 animals per genotype per sex. All results are expressed as mean ± SEM. *$p < 0.05$, ***$p < 0.0005$. Loading control = Ponceau S. Data shown illustrates protein expression normalized to Ponceau S. For representative immunoblots, lane images depict proteins loaded and detected on a single immunoblot (full blots shown in **Supplementary Figures 3, 4**); however, lanes were re-arranged to improve the clarity of presentation.

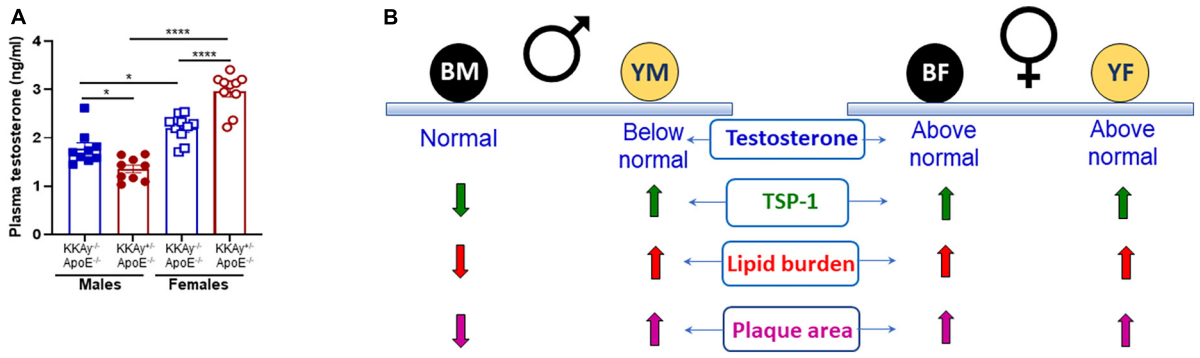

FIGURE 8
Sex-specific differences in plasma testosterone levels in MetS KKAy$^{+/-}$ApoE$^{-/-}$ and non-MetS KKAy$^{-/-}$ApoE$^{-/-}$ mice. **(A)** Shown are summary graphs for plasma testosterone levels in 24-weeks-old male and female MetS KKAy$^{+/-}$ApoE$^{-/-}$ and non-MetS KKAy$^{-/-}$ApoE$^{-/-}$ mice. *$p < 0.05$; ****$p < 0.0001$ (n = 9–10 mice per genotype per sex). **(B)** Overview of findings. BM, black male KKAy$^{-/-}$ApoE$^{-/-}$; YM, yellow male KKAy$^{+/-}$ApoE$^{-/-}$; BF, black female KKAy$^{-/-}$ApoE$^{-/-}$; YF, yellow female KKAy$^{+/-}$ApoE$^{-/-}$.

wall. TSP-1 is a multifunctional protein with cell- and tissue-specific effects, attributed to its differential interaction with and regulation of several cell-surface receptors and matrix-binding partners, in turn modulating cell-cell and cell-matrix interactions (41). Accumulating literature indicates that TSP-1 signaling via differential receptor activation (CD36, CD47) regulates the function of different vascular cell types, triggering inflammatory cell adhesion and transmigration through the vascular endothelium, LDL pinocytosis by macrophages and foam cell formation, endothelial cell (EC) dysfunction and EC senescence (17, 42, 43). In a healthy vessel, TSP-1 expression is typically low; however, in response to proatherogenic insults such as hyperglycemia and obesity, TSP-1 expression is significantly augmented. Previous studies have shown increased

TSP-1 expression in injured vessels and atherosclerotic lesions (23, 25). *In vitro* findings from our laboratory demonstrate that both high glucose and high leptin, at concentrations reflective of diabetes and obesity respectively, stimulate TSP-1 expression in human aortic SMC primary cultures (15, 16). We previously reported that global TSP-1 loss attenuates lesion burden and proliferative VSMC content in STZ-induced hyperglycemic ApoE$^{-/-}$ mice (26). In a follow-up study, we further showed that global TSP-1 deletion abrogates lipid-filled lesion burden and VSMC abundance in ApoE$^{-/-}$ mice treated with recombinant leptin, at concentrations mimicking obesity (27). In the context of the present study, our findings that augmented TSP-1 expression in the vessel wall associates with robust atherosclerotic lesions displaying increased SMC content in MetS KKAy$^{+/-}$ApoE$^{-/-}$ mice underscore a TSP-1-dependent mechanism underlying MetS-induced atherosclerosis.

Clinical and animal studies have highlighted a role of TSP-1 in the pathophysiology of metabolic disorders including diabetes and obesity (17). For instance, Li et al. (44) reported improved glucose tolerance and increased insulin sensitivity in obese TSP-1 knockout mice vs. obese wild-type mice in response to high fat feeding. Such improvement in metabolic profile was attributed to reduced systemic and adipose tissue inflammation in association with reduced macrophage accumulation in the adipose tissue of these animals. Likewise, a subsequent study demonstrated that myeloid-specific TSP-1 deletion protects long term diet-induced obese mice against inflammation and insulin resistance (45). In line with these earlier reports, we have shown that TSP-1 deletion in MetS agouti KKAy$^{+/-}$ mice significantly improved glucose tolerance in these animals compared with MetS genotypes with intact TSP-1. Of particular note, the improved metabolic profile in these animals was found to be specific to only male genotypes. These data suggest a sex-related differential role of TSP-1 on glucose metabolism and support a therapeutic potential of TSP-1 in metabolic disease.

In murine models of vascular injury, TSP-1 has been reported to facilitate arterial SMC activation (46, 47), attributing to its proatherogenic properties. Earlier findings from our laboratory indicate that under high glucose- or high leptin-stimulated conditions, augmented TSP-1 expression associates with increased VSMC proliferation (15, 16, 48). Conversely, we have shown that loss of TSP-1 attenuated VSMC proliferative response to high glucose or high leptin *in vitro* (15, 16). In line with these findings, we further reported that global TSP-1 deficiency blocks proliferative SMC lesion abundance in both STZ-induced hyperglycemic and leptin-treated ApoE$^{-/-}$ mice (26, 27). In view of this literature, our data raises the possibility that TSP-1 drives SMC de-differentiation in MetS in a sex-specific manner. Future studies are currently underway in our laboratory to interrogate whether TSP-1 directly modulates VSMC fate changes to a diseased phenotype in MetS, and to delineate underlying molecular mechanisms. Additionally, our findings suggest a sex-specific interaction of TSP-1 with lesion inflammatory burden in MetS KKAy$^{+/-}$ApoE$^{-/-}$ mice. Specifically, while lesion leukocyte infiltration was increased in male agouti KKAy$^{+/-}$ApoE$^{-/-}$ concomitant to enhanced TSP-1 expression in the vascular wall, inflammatory cell content was markedly attenuated in MetS KKAy$^{+/-}$ApoE$^{-/-}$ vs. non-MetS genotypes in female mice. These data illuminate sex-specific differences in lesion inflammatory status driven by MetS, highlighting the need for sex-based precision medicine to combat MetS-induced vascular dysfunction.

Accumulating epidemiological studies have suggested that men have a higher propensity for atherosclerotic disease than women, particularly at a younger age. However, as opposed to clinical data, animal studies on sex differences in plaque size and plaque burden have yielded conflicting results. For example, while some reports (49, 50) have suggested an atheroprotective effect of higher estrogen levels in female mice, others, summarized in (28) have shown either enhanced or similar plaque area in female ApoE$^{-/-}$ vs. age-matched male mice. In agreement with these earlier reports, we show augmented atherogenic phenotypes in both male and female MetS mice on ApoE$^{-/-}$ background. It would be remiss not to mention that in the current study, female non-agouti KKAy$^{-/-}$ApoE$^{-/-}$ mice developed large lipid-filled lesions resulting in enhanced plaque area within aortic roots similar to lesion progression in age-matched female agouti KKAy$^{+/-}$ApoE$^{-/-}$ mice; moreover, increased plaque area and lipid burden was associated with elevated TSP-1 expression in both genotypes in the female mice. Emerging literature support the idea that sex hormones (testosterone and estrogen) and sex chromosomes as well as their interactive pathways may contribute to sex-specific differential effects in various pathological conditions. Testosterone and estrogen are known to affect atherosclerosis in both sexes and multiple mechanisms have been postulated to play an underlying role (50). While testosterone was previously reported to improve insulin sensitivity, lower visceral adiposity and exert vasodilatory effects (51), clinical and animal research on the role of testosterone in atherosclerosis and related cardiovascular health remains inconclusive and rather contradictory (52, 53). For instance, multiple epidemiological studies suggest that testosterone deficiency may attribute to an increased incidence of adverse cardiovascular events (54–56). Congruently, animal studies using atherosclerotic murine models have shown that testosterone can retard atherogenesis (57, 58), possibly via its conversion to cardioprotective estradiol in the vessel wall. Few other studies have reported a beneficial effect of short- or long-term testosterone administration on arterial stiffness and vasomotor function (52). In the current work, we found significant differences in plasma testosterone levels between MetS and non-MetS genotypes, and this difference was observed in both male and female mice. Of note, while testosterone levels in both MetS and non-MetS female mice were found to be considerably above the typical range reported

for healthy females (33, 59), only male MetS genotypes revealed plasma testosterone relatively below values typically reported for healthy males (33, 60, 61). Intriguingly, in the current study we found that mice with either above normal or below normal testosterone concentrations developed robust lipid-filled lesions. Accordingly, we speculate that supraphysiological testosterone levels may contribute to worsened atherosclerosis in MetS and non-MetS female genotypes compared to male KKAy$^{-/-}$ mice. Paradoxically, it is likely that testosterone deficiency in male agouti KKAy$^{+/-}$ApoE$^{-/-}$ may be responsible for accelerated atherosclerosis vs. non-agouti genotypes. These data lend additional support to the concept that testosterone concentrations both above, and below physiologic range may increase risks of atherosclerotic disease. In terms of the relationship between testosterone and TSP-1, our data prompt us to speculate that low testosterone concentrations as noted in male MetS genotypes may induce TSP-1 expression in the vessel wall, thereby blocking SMC differentiation. Additional studies to delineate the underlying molecular mechanism are warranted.

The current study has a few limitations. A limitation of our study design is that ApoE$^{-/-}$ mice lacking the diabetic KK background was not utilized. We postulate that the diabetic background is necessary to facilitate atherosclerosis such that in the absence of the KK background, animals may fail to show detectable lesions at the timepoint studied. Thus, while the KK background alone may result in a pre-diabetic phenotype manifesting sex-specific differences in lesion burden and proatherogenic status, an ectopic expression of the agouti gene on the KK background (KKAy$^{+/-}$) is more likely to augment TSP-1 expression accelerating atherosclerosis, and this effect occurs independent of differences in sex. It should be further noted that while our study suggests a causal role of TSP-1 in atherosclerosis driven by metabolic aberrations, whether TSP-1 plays a direct role in MetS-induced atherosclerosis is yet to be determined and would require generation of atherosclerotic KKAy$^{+/-}$ApoE$^{-/-}$ mice lacking TSP-1. While such studies are beyond the scope of this manuscript, future work in our laboratory will interrogate the contribution of VSMC-derived TSP-1 to atherosclerotic lesion progression and VSMC phenotypic transformation prompted by MetS, using VSMC-specific TSP-1 knockout mice expressing VSMC-specific reporter gene to enable lineage tracing. Finally, although we did not measure plasma estradiol in the current study due to limited sample availability, we do acknowledge its role in vascular pathology. Future studies are warranted to determine the relative contribution of testosterone vs. estradiol to MetS-induced atherosclerosis and delineate underlying molecular mechanisms.

In conclusion, the present study provides the first demonstration of sex-specific differences in the development of atherosclerosis and TSP-1 expression in MetS vs non-MetS mice. Our data suggest a sex-specific differential role of TSP-1 on lesion progression and SMC differentiation in MetS. These findings underscore a fundamental link between TSP-1 and VSMC phenotypic switching in MetS. Importantly, the current work provides evidence for a role of testosterone prompting sex-related differences in lesion severity and complexity (**Figure 8B**), independent of MetS.

Data availability statement

The original contributions presented in this study are included in the article/**Supplementary material**, further inquiries can be directed to the corresponding author.

Ethics statement

The animal study was reviewed and approved by Northeast Ohio Medical University IACUC.

Author contributions

SG designed and performed the experiments, analyzed the data, and wrote the first draft of the manuscript. SK and NB performed the experiments and analyzed the data. AM and JL performed the mice genotyping, measured body weight and blood glucose, and sectioned aortic root samples. AK performed the imaging data analyses. JF assisted with treadmill exercise test and reviewed and revised the manuscript. PR conceived the project, designed the experiments, analyzed the data, and revised and edited the manuscript. All authors contributed to the article and approved the submitted version.

Funding

This work was supported by the National Institute of Health 1R15HL147245-01, R56HL141409-01, and NEOMED research funds to PR.

Acknowledgments

We thank Yanqiao Zhang and Yingdong Zhu (Northeast Ohio Medical University) for technical assistance and advice with fast-performance liquid chromatography (FPLC) studies.

Conflict of interest

The authors declare that the research was conducted in the absence of any commercial or financial relationships that could be construed as a potential conflict of interest.

Publisher's note

All claims expressed in this article are solely those of the authors and do not necessarily represent those of their affiliated organizations, or those of the publisher, the editors and the reviewers. Any product that may be evaluated in this article, or claim that may be made by its manufacturer, is not guaranteed or endorsed by the publisher.

Supplementary material

The Supplementary Material for this article can be found online at: https://www.frontiersin.org/articles/10.3389/fcvm.2022.1020006/full#supplementary-material

References

1. Tsao CW, Aday AW, Almarzooq ZI, Alonso A, Beaton AZ, Bittencourt MS, et al. Heart disease and stroke statistics-2022 update: a report from the American heart association. *Circulation.* (2022) 145:e153–639.

2. Alla VM, Agrawal V, DeNazareth A, Mohiuddin S, Ravilla S, Rendell M. A reappraisal of the risks and benefits of treating to target with cholesterol lowering drugs. *Drugs.* (2013) 73:1025–54. doi: 10.1007/s40265-013-0072-9

3. Wilkinson MJ, Laffin LJ, Davidson MH. Overcoming toxicity and side-effects of lipid-lowering therapies. *Best Pract Res Clin Endocrinol Metab.* (2014) 28:439–52. doi: 10.1016/j.beem.2014.01.006

4. Jones M, Tett S, Peeters GM, Mishra GD, Dobson A. New-onset diabetes after statin exposure in elderly women: the Australian longitudinal study on women's health. *Drugs Aging.* (2017) 34:203–9. doi: 10.1007/s40266-017-0435-0

5. Chait A, Bornfeldt KE. Diabetes and atherosclerosis: is there a role for hyperglycemia? *J Lipid Res.* (2009) 50:S335–9. doi: 10.1194/jlr.R800059-JLR200

6. Bornfeldt KE. Does elevated glucose promote atherosclerosis? Pros cons. *Circ Res.* (2016) 119:190–3. doi: 10.1161/CIRCRESAHA.116.308873

7. Malmberg K. Prospective randomised study of intensive insulin treatment on long term survival after acute myocardial infarction in patients with diabetes mellitus. DIGAMI (diabetes mellitus, insulin glucose infusion in acute myocardial infarction) study group. *BMJ.* (1997) 314:1512–5. doi: 10.1136/bmj.314.7093.1512

8. Nagareddy PR, Murphy AJ, Stirzaker RA, Hu Y, Yu S, Miller RG, et al. Hyperglycemia promotes myelopoiesis and impairs the resolution of atherosclerosis. *Cell Metab.* (2013) 17:695–708. doi: 10.1016/j.cmet.2013.04.001

9. Kanter JE, Johansson F, LeBoeuf RC, Bornfeldt KE. Do glucose and lipids exert independent effects on atherosclerotic lesion initiation or progression to advanced plaques? *Circ Res.* (2007) 100:769–81. doi: 10.1161/01.RES.0000259589.34348.74

10. Selvin E, Coresh J, Golden SH, Brancati FL, Folsom AR, Steffes MW. Glycemic control and coronary heart disease risk in persons with and without diabetes: the atherosclerosis risk in communities study. *Arch Intern Med.* (2005) 165:1910–6. doi: 10.1001/archinte.165.16.1910

11. Kim S, Kyung C, Park JS, Lee SP, Kim HK, Ahn CW, et al. Normal-weight obesity is associated with increased risk of subclinical atherosclerosis. *Cardiovasc Diabetol.* (2015) 14:58. doi: 10.1186/s12933-015-0220-5

12. Grundy SM. Obesity, metabolic syndrome, and coronary atherosclerosis. *Circulation.* (2002) 105:2696–8. doi: 10.1161/01.CIR.0000020650.86137.84

13. Reardon CA, Lingaraju A, Schoenfelt KQ, Zhou G, Cui C, Jacobs-El H, et al. Obesity and insulin resistance promote atherosclerosis through an IFNgamma-regulated macrophage protein network. *Cell Rep.* (2018) 23:3021–30. doi: 10.1016/j.celrep.2018.05.010

14. Aboonabi A, Meyer RR, Singh I. The association between metabolic syndrome components and the development of atherosclerosis. *J Hum Hypertens.* (2019) 33:844–55. doi: 10.1038/s41371-019-0273-0

15. Chavez RJ, Haney RM, Cuadra RH, Ganguly R, Adapala RK, Thodeti CK, et al. Upregulation of thrombospondin-1 expression by leptin in vascular smooth muscle cells via JAK2- and MAPK-dependent pathways. *Am J Physiol Cell Physiol.* (2012) 303:C179–91. doi: 10.1152/ajpcell.00008.2012

16. Raman P, Krukovets I, Marinic TE, Bornstein P, Stenina OI. Glycosylation mediates up-regulation of a potent antiangiogenic and proatherogenic protein, thrombospondin-1, by glucose in vascular smooth muscle cells. *J Biol Chem.* (2007) 282:5704–14. doi: 10.1074/jbc.M610965200

17. Gutierrez LS, Gutierrez J. Thrombospondin 1 in metabolic diseases. *Front Endocrinol.* (2021) 12:638536. doi: 10.3389/fendo.2021.638536

18. Matsuo Y, Tanaka M, Yamakage H, Sasaki Y, Muranaka K, Hata H, et al. Thrombospondin 1 as a novel biological marker of obesity and metabolic syndrome. *Metabolism.* (2015) 64:1490–9. doi: 10.1016/j.metabol.2015.07.016

19. Gonzalez-Quesada C, Cavalera M, Biernacka A, Kong P, Lee DW, Saxena A, et al. Thrombospondin-1 induction in the diabetic myocardium stabilizes the cardiac matrix in addition to promoting vascular rarefaction through angiopoietin-2 upregulation. *Circ Res.* (2013) 113:1331–44. doi: 10.1161/CIRCRESAHA.113.302593

20. Stenina OI, Krukovets I, Wang K, Zhou Z, Forudi F, Penn MS, et al. Increased expression of thrombospondin-1 in vessel wall of diabetic zucker rat. *Circulation.* (2003) 107:3209–15. doi: 10.1161/01.CIR.0000074223.56882.97

21. Kong P, Cavalera M, Frangogiannis NG. The role of thrombospondin (TSP)-1 in obesity and diabetes. *Adipocyte.* (2014) 3:81–4. doi: 10.4161/adip.26990

22. Varma V, Yao-Borengasser A, Bodles AM, Rasouli N, Phanavanh B, Nolen GT, et al. Thrombospondin-1 is an adipokine associated with obesity, adipose inflammation, and insulin resistance. *Diabetes.* (2008) 57:432–9. doi: 10.2337/db07-0840

23. Raugi GJ, Mullen JS, Bark DH, Okada T, Mayberg MR. Thrombospondin deposition in rat carotid artery injury. *Am J Pathol.* (1990) 137:179–85.

24. Sajid M, Hu Z, Guo H, Li H, Stouffer GA. Vascular expression of integrin-associated protein and thrombospondin increase after mechanical injury. *J Investig Med.* (2001) 49:398–406. doi: 10.2310/6650.2001.33784

25. Riessen R, Kearney M, Lawler J, Isner JM. Immunolocalization of thrombospondin-1 in human atherosclerotic and restenotic arteries. *Am Heart J.* (1998) 135:357–64. doi: 10.1016/s0002-8703(98)70105-x

26. Ganguly R, Sahu S, Ohanyan V, Haney R, Chavez RJ, Shah S, et al. Oral chromium picolinate impedes hyperglycemia-induced atherosclerosis and inhibits proatherogenic protein TSP-1 expression in STZ-induced type 1 diabetic ApoE-/- mice. *Sci Rep.* (2017) 7:45279. doi: 10.1038/srep45279

27. Ganguly, R, Khanal S, Mathias A, Gupta S, Lallo J, Sahu S, et al. TSP-1 (thrombospondin-1) deficiency protects ApoE(-/-) mice against leptin-induced atherosclerosis. *Arterioscler Thromb Vasc Biol.* (2020) 41:e112–27. doi: 10.1161/ATVBAHA.120.314962

28. Man JJ, Beckman JA, Jaffe IZ. Sex as a biological variable in atherosclerosis. *Circ Res.* (2020) 126:1297–319.

29. Taylor LE, Sullivan JC. Sex differences in obesity-induced hypertension and vascular dysfunction: a protective role for estrogen in adipose tissue inflammation? *Am J Physiol Regul Integr Comp Physiol.* (2016) 311:R714–20. doi: 10.1152/ajpregu.00202.2016

30. Vakhtangadze T, Singh Tak R, Singh U, Baig MS, Bezsonov E. Gender differences in atherosclerotic vascular disease: from lipids to clinical outcomes. *Front Cardiovasc Med.* (2021) 8:707889. doi: 10.3389/fcvm.2021.707889

31. Suto J, Matsuura S, Imamura K, Yamanaka H, Sekikawa K. Genetics of obesity in KK mouse and effects of A(y) allele on quantitative regulation. *Mamm Genome.* (1998) 9:506–10. doi: 10.1007/s003359900809

32. Petrosino JM, Heiss VJ, Maurya SK, Kalyanasundaram A, Periasamy M, LaFountain RA, et al. Graded maximal exercise testing to assess mouse cardio-metabolic phenotypes. *PLoS One.* (2016) 11:e0148010. doi: 10.1371/journal.pone.0148010

33. Kemp CJ, Drinkwater NR. Genetic variation in liver tumor susceptibility, plasma testosterone levels, and androgen receptor binding in six inbred strains of mice. *Cancer Res.* (1989) 49:5044–7.

34. Martinez HG, Quinones MP, Jimenez F, Estrada CA, Clark K, Muscogiuri G, et al. Critical role of chemokine (C-C motif) receptor 2 (CCR2) in the KKAy + Apoe -/- mouse model of the metabolic syndrome. *Diabetologia.* (2011) 54:2660–8. doi: 10.1007/s00125-011-2248-8

35. Diani AR, Sawada GA, Hannah BA, Jodelis KS, Connell MA, Connell CL, et al. Analysis of pancreatic islet cells and hormone content in the spontaneously diabetic KKAy mouse by morphometry, immunocytochemistry and radioimmunoassay. *Virchows Arch A Pathol Anat Histopathol.*(1987) 412:53–61. doi: 10.1007/BF00750731

36. Moroki T, Yoshikawa Y, Yoshizawa K, Tsubura A, Yasui H. Morphological characterization of systemic changes in KK-A(y) mice as an animal model of type 2 diabetes. *In Vivo.* (2013) 27:465–72.

37. Peronnet F, Massicotte D. Table of nonprotein respiratory quotient: an update. *Can J Sport Sci.* (1991) 16:23–9.

38. Suriano F, Vieira-Silva S, Falony G, Roumain M, Paquot A, Pelicaen R, et al. Novel insights into the genetically obese (ob/ob) and diabetic (db/db) mice: two sides of the same coin. *Microbiome.* (2021) 9:147. doi: 10.1186/s40168-021-01097-8

39. Chiba T, Shinozaki S, Nakazawa T, Kawakami A, Ai M, Kaneko E, et al. Leptin deficiency suppresses progression of atherosclerosis in apoE-deficient mice. *Atherosclerosis.* (2008) 196:68–75. doi: 10.1016/j.atherosclerosis.2007.01.040

40. Wu KK, Wu TJ, Chin J, Mitnaul LJ, Hernandez M, Cai TQ, et al. Increased hypercholesterolemia and atherosclerosis in mice lacking both apoE and leptin receptor. *Atherosclerosis.* (2005) 181:251–9. doi: 10.1016/j.atherosclerosis.2005.01.029

41. Adams JC. Thrombospondins: multifunctional regulators of cell interactions. *Annu Rev Cell Dev Biol.* (2001) 17:25–51.

42. Morandi V, Petrik J, Lawler J. Endothelial cell behavior is determined by receptor clustering induced by thrombospondin-1. *Front Cell Dev Biol.* (2021) 9:664696. doi: 10.3389/fcell.2021.664696

43. Meijles DN, Sahoo S, Al Ghouleh I, Amaral JH, Bienes-Martinez R, Knupp HE, et al. The matricellular protein TSP1 promotes human and mouse endothelial cell senescence through CD47 and Nox1. *Sci Signal.* (2017) 10:eaaj1784. doi: 10.1126/scisignal.aaj1784

44. Li Y, Tong X, Rumala C, Clemons K, Wang S. Thrombospondin1 deficiency reduces obesity-associated inflammation and improves insulin sensitivity in a diet-induced obese mouse model. *PLoS One.* (2011) 6:e26656. doi: 10.1371/journal.pone.0026656

45. Memetimin H, Li D, Tan K, Zhou C, Liang Y, Wu Y, et al. Myeloid-specific deletion of thrombospondin 1 protects against inflammation and insulin resistance in long-term diet-induced obese male mice. *Am J Physiol Endocrinol Metab.* (2018) 315:E1194–203. doi: 10.1152/ajpendo.00273.2018

46. Gupta N, Li W, Willard B, Silverstein RL, McIntyre TM. Proteasome proteolysis supports stimulated platelet function and thrombosis. *Arterioscler Thromb Vasc Biol.* (2014) 34:160–8. doi: 10.1161/ATVBAHA.113.302116

47. Moura R, Tjwa M, Vandervoort P, Cludts K, Hoylaerts MF. Thrombospondin-1 activates medial smooth muscle cells and triggers neointima formation upon mouse carotid artery ligation. *Arterioscler Thromb Vasc Biol.* (2007) 27:2163–9. doi: 10.1161/ATVBAHA.107.151282

48. Ganguly R, Sahu S, Chavez RJ, Raman P. Trivalent chromium inhibits TSP-1 expression, proliferation and o-glcnac signaling in vascular smooth muscle cells in response to high glucose *in vitro*. *Am J Physiol Cell Physiol.* (2014) 308:ajcell.00256.2014. doi: 10.1152/ajpcell.00256.2014

49. Zhang G, Li C, Zhu N, Chen Y, Yu Q, Liu E, et al. Sex differences in the formation of atherosclerosis lesion in apoE(-/-)mice and the effect of 17β-estrodiol on protein S-nitrosylation. *Biomed Pharmacother.* (2018) 99:1014–21. doi: 10.1016/j.biopha.2018.01.145

50. Arnold AP, Cassis LA, Eghbali M, Reue K, Sandberg K. Sex hormones and sex chromosomes cause sex differences in the development of cardiovascular diseases. *Arterioscler Thromb Vasc Biol.* (2017) 37:746–56.

51. Mw C, Collins P. Role of testosterone in the treatment of cardiovascular disease. *Eur Cardiol.* (2017) 12:83–7.

52. Kaur H, Werstuck GH. The effect of testosterone on cardiovascular disease and cardiovascular risk factors in men: a review of clinical and preclinical data. *CJC Open.* (2021) 3:1238–48. doi: 10.1016/j.cjco.2021.05.007

53. Rexrode K. Sex differences in sex hormones, carotid atherosclerosis, and stroke. *Circ Res.* (2018) 122:17–9.

54. Kelly DM, Jones TH. Testosterone and cardiovascular risk in men. *Front Horm Res.* (2014) 43:1–20. doi: 10.1159/000360553

55. Shores MM, Walsh TJ, Korpak A, Krakauer C, Forsberg CW, Fox AE, et al. Association between testosterone treatment and risk of incident cardiovascular events among US male veterans with low testosterone levels and multiple medical comorbidities. *J Am Heart Assoc.* (2021) 10:e020562. doi: 10.1161/JAHA.120.020562

56. Heinze-Milne S, Banga S, Howlett SE. Low testosterone concentrations and risk of ischaemic cardiovascular disease in ageing: not just a problem for older men. *Lancet Healthy Longev.* (2022) 3:e83–4. doi: 10.1016/S2666-7568(22)00008-3

57. Nettleship JE, Jones TH, Channer KS, Jones RD. Physiological testosterone replacement therapy attenuates fatty streak formation and improves high-density lipoprotein cholesterol in the Tfm mouse: an effect that is independent of the classic androgen receptor. *Circulation.* (2007) 116:2427–34. doi: 10.1161/CIRCULATIONAHA.107.708768

58. Wilhelmson AS, Lantero Rodriguez M, Svedlund Eriksson E, Johansson I, Fogelstrand P, Stubelius A, et al. Testosterone protects against atherosclerosis in male mice by targeting thymic epithelial cells-brief report. *Arterioscler Thromb Vasc Biol.* (2018) 38:1519–27. doi: 10.1161/ATVBAHA.118.311252

59. Brouillette J, Rivard K, Lizotte E, Fiset C. Sex and strain differences in adult mouse cardiac repolarization: importance of androgens. *Cardiovasc Res.* (2005) 65:148–57. doi: 10.1016/j.cardiores.2004.09.012

60. Machida T, Yonezawa Y, Noumura T. Age-associated changes in plasma testosterone levels in male mice and their relation to social dominance or subordinance. *Horm Behav.* (1981) 15:238–45.

61. Nelson JF, Latham KR, Finch CE. Plasma testosterone levels in C57BL/6J male mice: effects of age and disease. *Acta Endocrinol.* (1975) 80:744–52.

frontiers | Frontiers in Cardiovascular Medicine

TYPE Original Research
PUBLISHED 16 December 2022
DOI 10.3389/fcvm.2022.995216

OPEN ACCESS

EDITED BY
Ting Zhou,
University of Wisconsin-Madison,
United States

REVIEWED BY
Jianing Gao,
Health Science Centre, Peking University, China
Dirk J. Duncker,
Erasmus University Medical Center, Netherlands

*CORRESPONDENCE
Jingang Zheng
✉ mdjingangzheng@yeah.net
Yanxiang Gao
✉ gaoyanxiang@zryhyy.com.cn

SPECIALTY SECTION
This article was submitted to Cardiovascular Therapeutics, a section of the journal Frontiers in Cardiovascular Medicine

RECEIVED 15 July 2022
ACCEPTED 02 December 2022
PUBLISHED 16 December 2022

CITATION
Tu Y, Li Q, Zhou Y, Ye Z, Wu C, Xie E, Li Y, Li P, Wu Y, Guo Z, Yu C, Zheng J and Gao Y (2022) Empagliflozin inhibits coronary microvascular dysfunction and reduces cardiac pericyte loss in db/db mice. *Front. Cardiovasc. Med.* 9:995216. doi: 10.3389/fcvm.2022.995216

Empagliflozin inhibits coronary microvascular dysfunction and reduces cardiac pericyte loss in db/db mice

Yimin Tu[1], Qing Li[2], Yuanchen Zhou[2], Zixiang Ye[2], Chao Wu[2], Enmin Xie[1], Yike Li[1], Peizhao Li[2], Yaxin Wu[2], Ziyu Guo[2], Changan Yu[3], Jingang Zheng[1,3]* and Yanxiang Gao[1,3]*

[1]Department of Cardiology, China-Japan Friendship School of Clinical Medicine, Graduate School of Peking Union Medical College, Chinese Academy of Medical Sciences, Beijing, China, [2]Department of Cardiology, Peking University China-Japan Friendship School of Clinical Medicine, Beijing, China, [3]Department of Cardiology, China-Japan Friendship Hospital, Beijing, China

Background: Coronary microvascular dysfunction (CMD) is a pathophysiological feature of diabetic heart disease. However, whether sodium-glucose cotransporter 2 (SGLT2) inhibitors protect the cardiovascular system by alleviating CMD is not known.

Objective: We observed the protective effects of empagliflozin (EMPA) on diabetic CMD.

Materials and methods: The mice were randomly divided into a db/db group and a db/db + EMPA group, and db/m mice served as controls. At 8 weeks of age, the db/db + EMPA group was given empagliflozin 10 mg/(kg·d) by gavage for 8 weeks. Body weight, fasting blood glucose and blood pressure were dynamically observed. Cardiac systolic and diastolic function and coronary flow reserve (CFR) were detected using echocardiography. The coronary microvascular structure and distribution of cardiac pericytes were observed using immunofluorescence staining. Picrosirius red staining was performed to evaluate cardiac fibrosis.

Results: Empagliflozin lowered the increased fasting blood glucose levels of the db/db group. The left ventricular ejection fraction, left ventricular fractional shortening, E/A ratio and E/e' ratio were not significantly different between the three groups. CFR was decreased in the db/db group, but EMPA significantly improved CFR. In contrast to the sparse and abnormal expansion of coronary microvessels observed in the db/db group, the number of coronary microvessels was increased, and the capillary diameter was decreased in the db/db + EMPA group. The number and microvascular coverage of cardiac pericytes were reduced in the db/db mice but were

improved by EMPA. The cardiac fibrosis was increased in db/db group and may alleviate by EMPA.

Conclusion: Empagliflozin inhibited CMD and reduced cardiac pericyte loss in diabetic mice.

KEYWORDS

diabetes, coronary microvascular dysfunction, pericytes, sodium-glucose cotransporter 2 inhibitors, empagliflozin

1 Introduction

Coronary microvascular dysfunction (CMD) refers to abnormalities in the structure and function of the coronary microcirculation that lead to impaired coronary blood flow and a mismatch between myocardial blood supply and oxygen consumption (1, 2). CMD is the pathophysiological basis of various cardiovascular diseases, including diabetic heart disease (3), in which the microvasculature of the diabetic heart shows microaneurysm, sparse capillaries, and basement membrane thickening (4, 5). Recent research revealed that coronary microcirculation disorder caused a fourfold increase in cardiovascular mortality and a fivefold increase in major adverse cardiovascular events (6). There are no effective drugs for the treatment of CMD. Therefore, elucidating the pathological characteristics and mechanisms of CMD is of great significance for preventing and treating cardiovascular diseases.

Pericytes, also known as Rouget cells, are parietal cells distributed on the basement membrane side of endothelial cells in the microvascular system (7) that characteristically express neural glial antigen 2 (NG2), platelet-derived growth factor receptor beta (PDGFRβ) and α-smooth muscle actin (α-SMA) (8). Pericytes play an important role in maintaining vascular stability (9). Under pathological conditions, pericyte injury and apoptosis are associated with breakdown of the vascular wall barrier, activation of the inflammatory response and fibrosis, and promoting the occurrence and development of vascular diseases (10). One of the earliest manifestations of diabetic microvascular complications, such as diabetic retinopathy and diabetic nephropathy, is the loss of pericytes (11). Pericytes are the second most abundant cells in the ventricle and account for 20% of all cells in the heart (8). Pericytes play an important role in regulating myocardial blood flow (12, 13). However, the role of pericytes in diabetic CMD is not clear.

Sodium-glucose cotransporter-2 (SGLT2) inhibitors are a new type of hypoglycemic drug that reduce the reabsorption of glucose by the kidney to exert hypoglycemic effects (14, 15). Several studies revealed that SGLT2 inhibitors reduced blood glucose in diabetic patients and decreased the risk of cardiovascular events (16). Potential mechanisms underlying the cardioprotective effects of SGLT2 inhibitors include improving myocardial energy metabolism (16), alleviating myocardial oxidative stress and fibrosis (17) and reducing myocardial sodium/hydrogen exchange (18). However, whether SGLT2 inhibitors inhibit CMD and its underlying mechanism have not been elucidated.

The present study investigated the features of coronary microcirculation function and structure in type 2 diabetes and pericyte changes in CMD using the db/db mouse model. We treated the diabetic mice with the SGLT2 inhibitor empagliflozin (EMPA) to observe its effects on CMD. The results of this research provide new insights into the prevention and treatment of CMD.

2 Materials and methods

2.1 Experimental animals

Seven-week-old male db/db mice and littermate db/m mice were purchased from GemPharmatech Co., Ltd. (Nanjing, China). All experimental mice were housed in a 12-h/12-h light/dark cycle room with controlled humidity (50–60%) and temperature (22 ± 2°C) at the Animal Platform of China-Japan Friendship Hospital and provided free access to standard rodent food and water. After adaptive feeding for 1 week, db/db mice were randomly assigned to the db/db group or the db/db + EMPA group. Mice in the db/db + EMPA group were given 10 mg/kg/day EMPA (Boehringer-Ingelheimat, Ingelheim am Rhein, Germany) dissolved in saline intragastrically for 8 weeks, and the mice in the db/m and db/db groups were gavaged with equal amounts of saline. The Institutional Animal Care and Use Committee of China-Japan Friendship Hospital approved all of the animal experiments, which were performed in accordance with all relevant ethical regulations.

2.2 Measurement of fasting blood glucose

Mouse fasting blood glucose levels were measured using the hand-held glucometer Accu-Chek Performa (Roche Diabetes

Care GmbH) at the following five time points: baseline and 10, 12, 14, and 16 weeks of age. The fasting blood glucose levels in mice were determined from tail snip blood using blood glucose test strips after fasting for 12 h.

2.3 Measurement of systolic blood pressure

Systolic blood pressure was measured in conscious mice using a non-invasive tail-cuff device (BP2000 VisiTech International, Sunderland, UK) at 8, 10, 12, 14, and 16 weeks of age. During the procedure, conscious mice were placed in a retainer tube on a warming chamber maintained at 37°C. Mice were acclimatized to the instrument for at least 1 week before baseline measurements were taken. All measurements were performed between 8 and 10 a.m. to avoid variations in blood pressure due to the time of day. Individual mice received 10 initial pressure readings to acclimatize them to the procedure, and 10 additional cycles were measured to obtain the mean systolic pressure. The criteria for data inclusion were the acquisition of at least 10 of 20 measurements and an SD of < 30 mmHg per session.

2.4 Urine collection

Mice were placed in metabolic cages for 24 h urine collection within 48 h of the end of treatment.

2.5 Echocardiographic evaluation

Echocardiographic measurements were performed in all mice, including coronary microvascular function and cardiac systolic and diastolic function at 8, 10, 12, 14, and 16 weeks of age. We used a high-frequency ultrasound imaging system (Vevo 1100 VisualSonics, Inc., Toronto, ON, Canada) equipped with a 40-MHz central frequency transducer. A single investigator who was blinded to the experimental groups performed all measurements. All parameters were measured at least 3 times, and the means are presented. First, coronary microvascular function assessment was performed. The concentration and duration of isoflurane was referred to the previous study (19). Mice were anesthetized with isoflurane (R510-22-10 RWD Life Science) in a closed chamber with 1% isoflurane in 1 L/min oxygen for 2–5 min until immobile. Each mouse was placed supine on a heated procedure board with isoflurane at 1% supplied by a nose cone connected to the anesthesia machine. Chest hair was removed with chemical cream (Veet, Reckitt Benckiser, London, UK), and ultrasound gel was applied to the chest. The velocity profile in the left coronary artery was monitored for 3 min to ensure that a stable basal signal was achieved, then signals were collected and stored. The isoflurane level was increased to 3% to induce hyperemia, and the velocity profile was monitored for up to 10 min, ensuring the hyperemic CFV becoming maximum and stable. The time signals during this time were stored for analysis of the maximum hyperemic response. Coronary flow reserve was determined as the ratio of hyperemic coronary flow velocity to basal coronary flow velocity.

Cardiac systolic and diastolic function were assessed. The isoflurane concentration was adjusted to approximately 2% to maintain the heart rate of the mice at approximately 400 beats per minute. Diastolic function was obtained using pulsed-wave Doppler from the apical four-chamber view. The isoflurane concentration was reduced to maintain the heart rate at approximately 450–500 beats per minute. Indices of systolic function were obtained from short-axis M-mode scans at the midventricular level, as indicated by the presence of papillary muscles. The following main variables were assessed: left ventricular ejection fraction (LVEF), LV fractional shortening (LVFS), mitral valve (peak E) and maximal peak blood flow levels during mitral atrial systole (peak A) ratio (E/A). The results of E/e′ values were finally measured in 16 weeks of age, which was performed in the Institute of Laboratory Animal Science, CAMS, and PUMC.

2.6 Immunostaining

The mice were anesthetized at the conclusion of the experiment. Heparin solution (10 mL/kg, 1000 U/mL) was injected intraperitoneally into the mice. Mice were injected with 10% KCl through the apex until the heart stopped beating, and the right atrial appendage was incised to allow the blood to drain out. The heart and vessels were perfused with a cold heparin-saline solution (10 U/mL) under a constant pressure of 70 mmHg and a 5 mL/min perfusion velocity. When clear fluid flowed out from the right atrial appendage, the heart was perfused with cold 4% paraformaldehyde (PFA) solution for fixation. The hearts were excised from the mice and fixed *via* immersion in 4% PFA solution for 24 h. The hearts were cut transversely into 8 μm (thin) and 150 μm (thick) sections for immunofluorescence staining.

The thick heart slices were sufficiently washed with PBS (2 h * 3) and immersed in 200 μL staining buffer (0.1% w/v sodium azide, 10% Triton X-100, and 0.5% w/v bovine serum albumin in ddH_2O) with anti-neuroglial cell 2 chondroitin sulfate proteoglycan (NG2) antibody (AB5320, Merck Millipore, Darmstadt, Germany, 1:200) for 3 days at 37°C with gentle shaking. After washing with PBS (2 h * 3), the heart tissues were incubated in 200 μL staining buffer with secondary antibody conjugated to Alexa Fluor 647 (AB32733, Invitrogen, Carlsbad, CA, United States, 1:200) and isolectin B4 conjugated to FITC (L2895, Merck Millipore, Darmstadt, Germany, 1:20)

for 3 days at 37°C with gentle shaking. After final washing (PBS, 2 h * 3), the heart slices were attached to glass slides and mounted using antifade reagents with 4′,6-diamidino-2-phenylindole (DAPI) (S36938, Invitrogen, Carlsbad, CA, United States) or a 50% glycerol solution (49767, Sigma, St. Louis, MO, United States).

2.7 Laser scanning confocal microscope imaging

Stained sections were imaged using confocal microscopy (Zeiss LSM 800, Leica TCS SP8 DIVE), and 40× objectives (NA = 0.95) were used to visualize cardiac microvessels and pericytes. All images were generated with a 1024 × 1024 pixel frame resolution, and the confocal pinhole was set to 1 AU. For z-stack imaging, the z-step size was set to 1.0 μm to avoid undersampling. At least 6 different fields per sample section were randomly chosen for analysis. The laser power, gain and offset settings were maintained when the same molecule was evaluated in different samples. Images were quantified using ImageJ software. The number of capillaries was counted manually using ImageJ. Ten-micron maximum projection z-stacks were reconstructed for the analysis of capillary diameter, pericyte number and pericyte coverage. The capillary diameter was measured using the Fiji ImageJ "Plot Profile" plug-in analysis tool. The number of NG2-positive perivascular cell bodies that colocalized with DAPI (4′,6-diamidino-2-phenylindole)-positive nuclei was counted using the Fiji ImageJ "ImageJ Cell Counter" plug-in analysis tool to quantify pericytes. The NG2-positive and IB4-positive areas were analyzed using the area analysis module, and pericyte coverage was quantified as the ratio of the NG2 immunostained area to the IB4 immunostained area.

2.8 Picrosirius red staining

Picrosirius red staining (PSR) was performed to evaluate cardiac fibrosis. The rehydrated cardiac tissues were stained with Picrosirius red solution (G1018, Servicebio, Wuhan, China) for 8 min. The samples were quickly washed three times with absolute alcohol for 1 min, followed by clearing in xylene. Finally, the specimens were mounted with neutral gum. The picrosirius red–stained sections were scanned with a Pannoramic MIDI slide scanner (3DHISTECH, Budapest, Hungary). The sections were imaged by means of birefringence using polarized light on a microscope (Nikon Eclipse ci, Tokyo, Japan) at ×200 and ×400 magnification. The results of polarized images were red to yellow color for thick fibers and green color for thin fibers. In addition, some part show no polarized effect and appear as black. The percentage of fibrotic area was calculated with the Fiji image J software (20).

2.9 Statistical analysis

The results are presented as the means ± SEM. The Shapiro–Wilk test was used to examine the normal distribution of all data. Comparisons between two groups were performed using Student's t-test for unpaired groups. Comparisons between three groups were performed using one-way or two-way analysis of variance (ANOVA). For multiple comparisons, p-values were corrected using the Holm–Bonferroni method. $P < 0.05$ was considered significant. Data analyses were performed using the GraphPad Prism program 8.2.1 version (La Jolla, CA, USA).

3 Results

3.1 Effects of EMPA on body weight, fasting blood glucose, systolic blood pressure and 24-h urine volume in mice

From 8 to 16 weeks of age, db/db mice were consistently heavier than db/m mice (**Figure 1A**). Body weights were initially similar in db/db mice and db/db + EMPA mice. However, mice in the db/db + EMPA group were significantly heavier than db/db mice at 6 and 8 weeks of administration (**Figure 1A**). At 8 weeks of age, there was no significant difference in fasting blood glucose between the 3 groups (db/m vs. db/db vs. db/db + EMPA: 6.2 ± 0.3 vs. 8.1 ± 0.9 vs. 8.3 ± 1.0 mmol/L, $p = 0.307$) (**Figure 1B**). However, the fasting blood glucose of db/db mice was significantly higher than db/m mice at 10–16 weeks of age (**Figure 1B**). From 10 to 16 weeks of age, the fasting blood glucose of the db/db + EMPA group was significantly lower than the db/db mice and similar to the db/m mice (**Figure 1B**). No significant difference in systolic blood pressure was observed between the 3 groups during the experiment (**Figure 1C**). At 16 weeks of age, the 24-h urine volume of db/db mice was significantly higher than the db/m mice (3.3 ± 0.4 vs. 1.8 ± 0.2 mL, $p = 0.035$) (**Figure 1D**), and there was no significant difference between the db/db group and the db/db + EMPA group (4.0 ± 0.4 vs. 3.3 ± 0.4 mL, $p = 0.352$) (**Figure 1D**).

3.2 Effects of EMPA on cardiac function of mice

Left ventricular systolic parameters, including the LVEF and LVFS (**Figure 2A**), increased in the db/db group compared to the db/m group from 12 to 16 weeks of age, but no significant difference was found between the db/db and db/db + EMPA groups

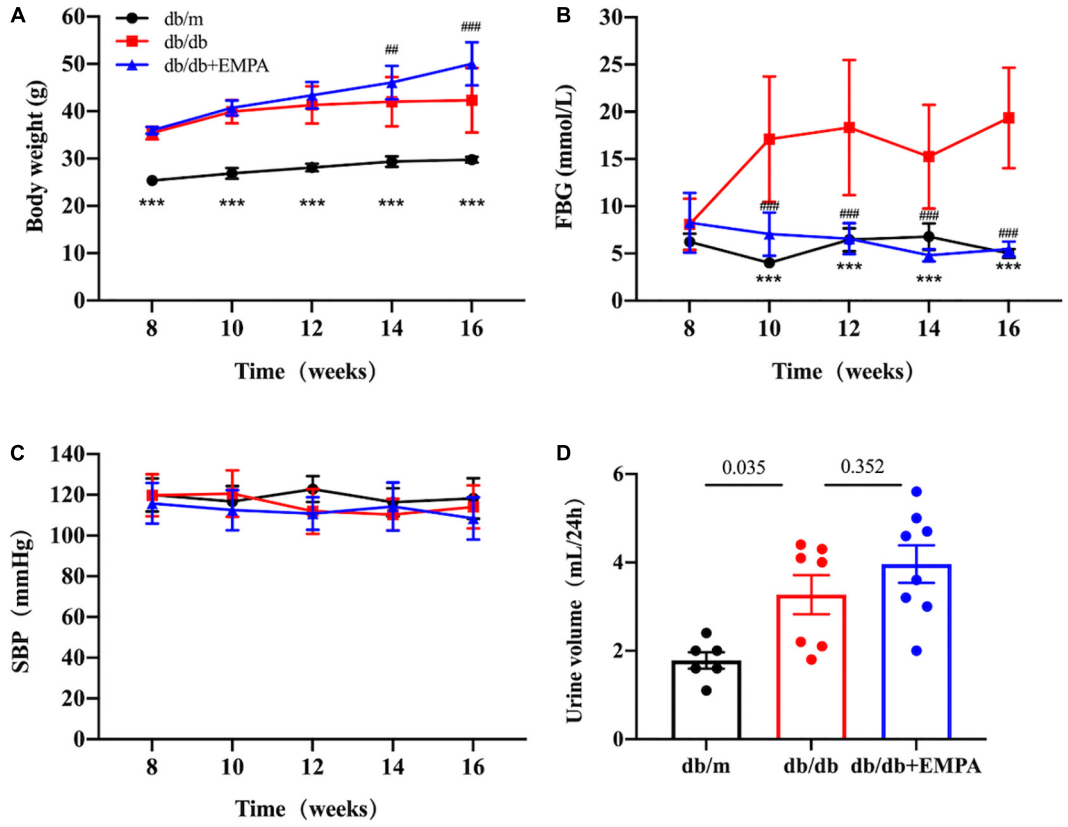

FIGURE 1
Effects of empagliflozin treatment on basic parameters in different groups. Body weight, fasting blood glucose, urine volume, and systolic blood pressure of mice after different treatments from 8 to 16 weeks of age. Data are presented as the means ± SEM, **(A–C)** the db/m group vs. the db/db group vs. the db/db + EMPA group = 6 vs. 10 vs. 11. **(D)** The db/m group vs. the db/db group vs. the db/db + EMPA group = 6 vs. 7 vs. 8. ***$p < 0.001$, and the db/m group vs. the db/db group; $^{\#\#}p < 0.01$ and $^{\#\#\#}p < 0.001$, the db/db + EMPA group vs. the db/db group. FBG, fasting blood glucose; SBP, systolic blood pressure.

(Figures 2B,C). There was no significant difference in E/A and E/e′ between the three groups during treatment (Figures 2D,E).

3.3 Empagliflozin inhibited coronary microvascular dysfunction in diabetic mice

There was no significant difference in baseline coronary flow velocity (CFV) or hyperemic CFV between the three groups of mice from 8 to 14 weeks of age. At 16 weeks of age, the baseline CFV of db/db mice was significantly higher than the db/m mice (412 ± 2 vs. 321 ± 30 mm/s, $p = 0.006$), and the baseline CFV of the db/db + EMPA group was significantly lower than the db/db group (340 ± 16 vs. 412 ± 2 mm/s, $p = 0.008$). In contrast, the hyperemic CFV of mice in the db/db group was significantly lower than the control group (805 ± 18 vs. 1024 ± 75 mm/s, $p = 0.012$), and the hyperemic CFV in the db/db + EMPA group was higher than the db/db group (952 ± 51 vs. 805 ± 18 mm/s, $p = 0.048$). However, the CFR showed a significant difference between the 3 groups from 12 weeks of age. At 16 weeks of age, the CFR of the db/db group was significantly lower than the control group (1.9 ± 0.1 vs. 3.3 ± 0.2, $p < 0.001$), and the CFR of the db/db + EMPA group was higher than the db/db group (2.8 ± 0.1 vs. 1.9 ± 0.1, $p < 0.001$) (Figure 3).

3.4 Empagliflozin ameliorated abnormal microvascular structure in the hearts of diabetic mice

Microvessels were labeled with IB4, and higher magnification images of thick heart slices were acquired to assess the coronary microvascular structure of the mice (Figures 4A,C) and calculated per high power field (HPF). The number of cardiac capillaries was significantly reduced in db/db mice compared to controls (73 ± 2/HPF vs. 107 ± 4/HPF, $p < 0.001$), and the cardiac capillary

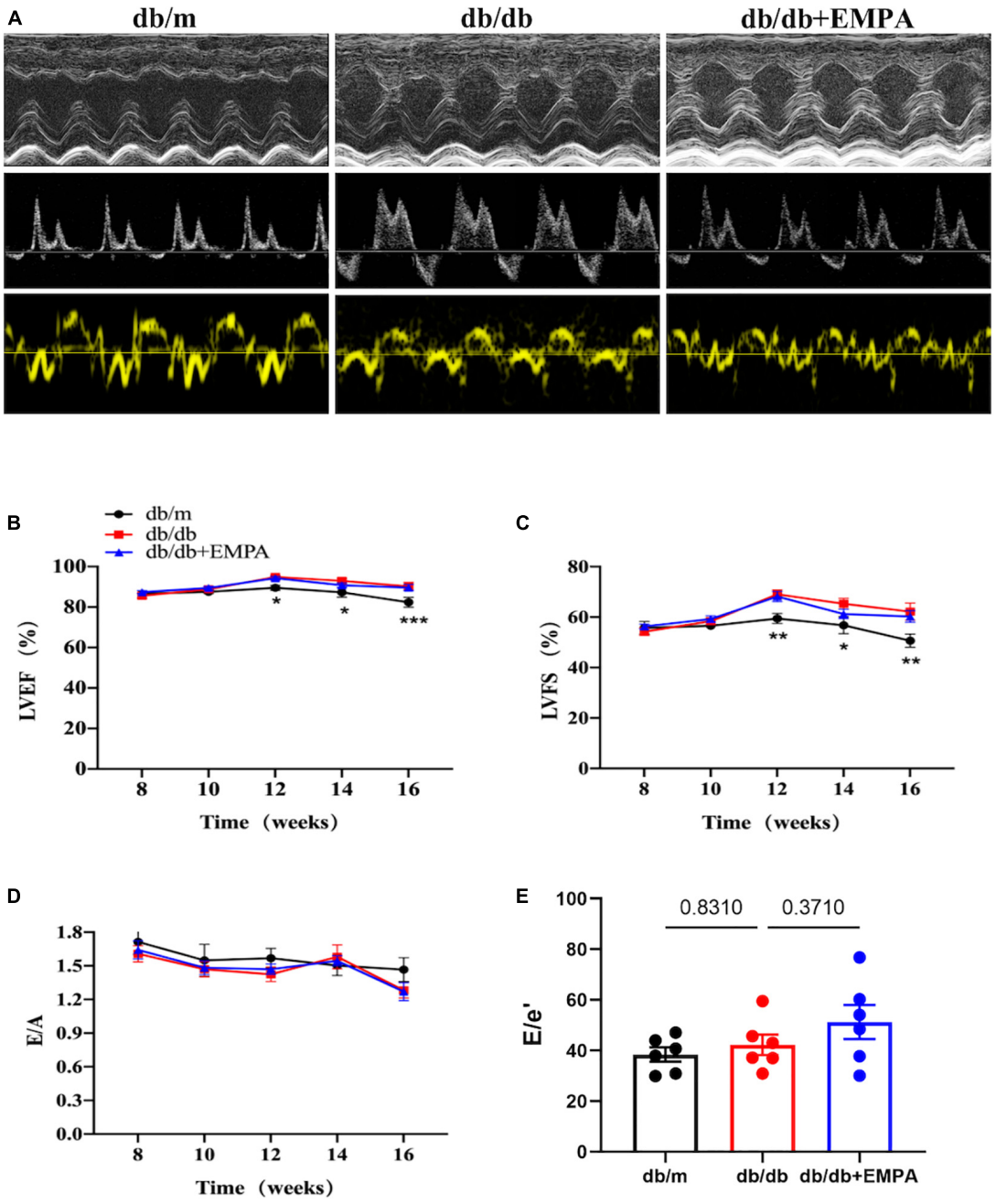

FIGURE 2
Effects of empagliflozin treatment on cardiac function in db/db mice. **(A)** Representative M-mode (top), pulse-wave Doppler (middle) and Tissue Doppler (bottom) tracings from different experimental groups. **(B)** Left ventricular ejection fraction (LVEF) of different experimental groups over time. **(C)** Left ventricular fractional shortening (LVFS) of different experimental groups over time. **(B,C)** The db/m group vs. the db/db group vs. the db/db + EMPA group = 6 vs. 10 vs. 11. **(D)** E/A ratio of different experimental groups over time, $n = 6$ per group. **(E)** E/e' ratio of different experimental groups of 16 weeks of age, $n = 6$ per group. Data are represented as the means ± SEM, $^{*}p < 0.05$, $^{**}p < 0.01$ and $^{***}p < 0.001$ the db/m group vs. the db/db group.

density of db/db + EMPA mice was higher than the db/db mice (82 ± 2/HPF vs. 73 ± 2/HPF, $p = 0.015$) (Figure 4B). The diameter of cardiac capillaries was significantly increased in db/db mice compared to controls (12.5 ± 0.2 vs. 9.7 ± 0.1 μm, $p < 0.001$), and the capillary diameter was decreased in db/db + EMPA mice compared to db/db mice (11.3 ± 0.2 vs. 12.5 ± 0.2 μm, $p < 0.001$) (Figure 4D). In summary, EMPA ameliorated the abnormal dilation and sparseness of cardiac capillaries in db/db mice.

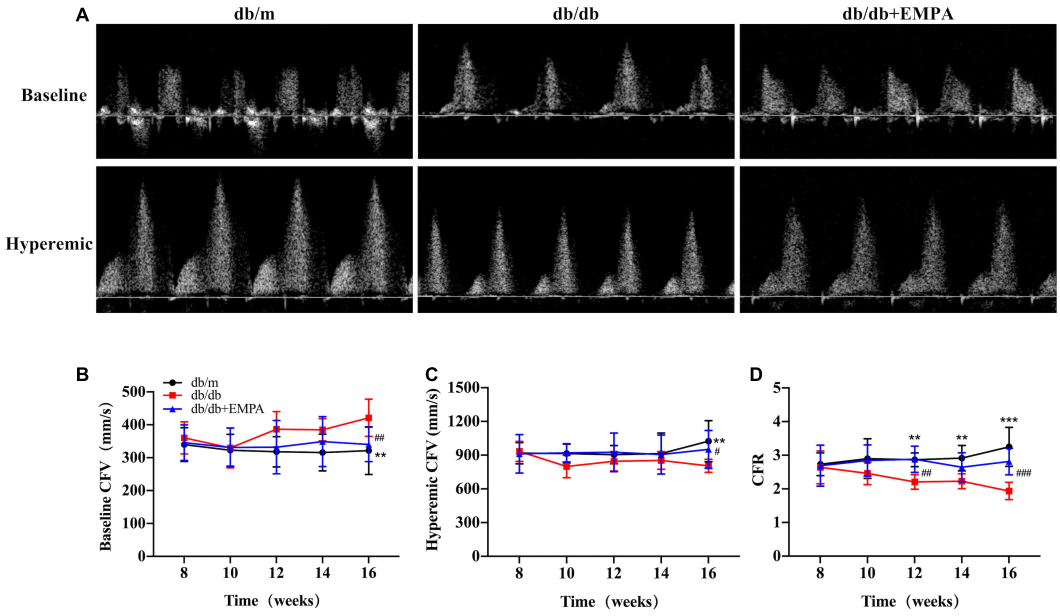

FIGURE 3
Empagliflozin inhibited coronary microvascular dysfunction in db/db mice. **(A)** Representative images of coronary flow velocity (CFV) recording in the mouse coronary artery. **(B)** Quantitative analyses of baseline CFV of different groups over time. **(C)** Quantitative analyses of hyperemic CFV of different groups over time. **(D)** Quantitative analyses of coronary flow reserve (CFR) of different groups over time. CFR was calculated as the ratio of hyperemic and basal coronary flow velocities. Data are presented as the means ± SEM, the db/m group vs. the db/db group vs. the db/db + EMPA group = 6 vs. 9 vs. 11. $^{**}p < 0.01$ and $^{***}p < 0.001$ the db/m group vs. the db/db group; $^{\#}p < 0.05$, $^{\#\#}p < 0.01$ and $^{\#\#\#}p < 0.001$ the db/db group vs. the db/db + EMPA group.

3.5 Empagliflozin inhibited pericyte loss in the hearts of diabetic mice

Pericytes were labeled with an anti-NG2 antibody, and higher magnification images of thick heart slices were acquired to assess the role of pericytes in the coronary microcirculation. The number of pericytes was significantly reduced in db/db mice compared to the controls (7.6 ± 0.3/HPF vs. 12.6 ± 0.6/HPF, $p < 0.001$), and that of db/db + EMPA mice was higher than db/db mice (9.4 ± 0.7/HPF vs. 7.6 ± 0.3/HPF, $p = 0.035$). Pericyte coverage, represented as the ratio of the NG2-positive area to the IB4-positive area (**Figure 5A**), was significantly decreased in the hearts of the db/db group (53 ± 1% vs. 66 ± 1%, $p < 0.001$). Cardiac pericyte coverage was higher in db/db + EMPA mice than db/db mice (61 ± 2% vs. 53 ± 1%, $p < 0.001$) (**Figures 5B,C**). Overall, EMPA inhibited cardiac pericyte loss and increased the pericyte coverage of the coronary microvasculature in diabetic mice.

3.6 Empagliflozin improved cardiac fibrosis in the hearts of diabetic mice

Picrosirius red staining and polarized light microscopy were used to determine the cardiac fibrosis between 3 groups. Representative images of PSR staining illustrating different collagen levels were shown in **Supplementary Figure 1A**. Subsequent image processing enabled measuring the percentage of positive area per image for PSR. This suggested the collagen in myocardium increased in db/db mice compared with db/m mice (0.35 ± 0.14 vs. 0.98 ± 0.39%, $p = 0.009$), and was improved in db/db + EMPA mice (0.98 ± 0.39% vs. 0.59 ± 0.19%, $p = 0.0191$) (**Supplementary Figure 1B**). In db/db group, the myocardial fibrosis was severer than the other groups, which might lead to the cardiac stiffness and be improved by EMPA.

4 Discussion

The present study observed the functional and structural characteristics of the coronary microcirculation in db/db mice and the effects of EMPA on the coronary microcirculation in db/db mice using echocardiography, immunofluorescence staining and confocal laser. The results showed that coronary blood flow reserve decreased in db/db mice, the number of cardiac capillaries was reduced, and cardiac capillaries were abnormally dilated. The number and coverage of cardiac pericytes also decreased. The results of PSR revealed EMPA might decrease the cardiac collagen caused by diabetes. Empagliflozin ameliorated the functional and structural abnormalities of the coronary microcirculation and inhibited

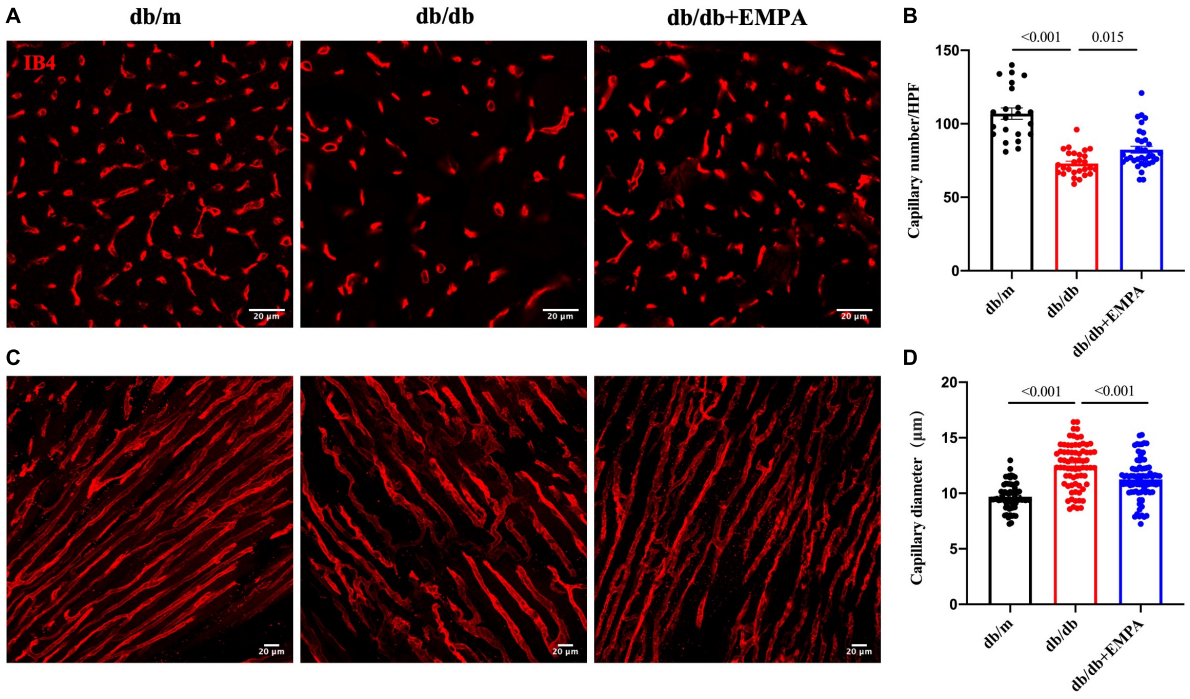

FIGURE 4
Effects of empagliflozin treatment on the cardiac microvasculature of db/db mice. **(A)** Representative transverse images of myocardial vasculature showing capillaries (IB4+, red). **(B)** Statistical analysis of the density of capillaries in the transverse sections of myocardial tissue between the db/m group, db/db group, and db/db + EMPA group. **(C)** Representative longitudinal images of myocardial vasculature showing capillaries (IB4+, red). **(D)** Statistical analysis of the diameter of capillaries in the longitudinal sections of myocardial tissue between the db/m group, db/db group, and db/db + EMPA group. Data are presented as the means ± SEM. *P*-values are corrected for multiple comparisons. IB4, isolectin B4; HPF, high power field.

the decrease in cardiac pericyte number and coverage in db/db mice. These results indicated that cardiac pericyte loss was related to CMD, and EMPA ameliorated cardiac pericyte loss and alleviated CMD in type 2 diabetes.

Our study showed that db/db mice had mildly increased cardiac systolic function from 12 to 16 weeks of age without any significant change in diastolic function. However, the coronary microvascular function index CFR decreased significantly at 12 weeks of age in db/db mice, and the coronary microvessels were sparse and dilated at 16 weeks of age. These results suggest that coronary microvascular function and structural disturbances in db/db mice appear before cardiac systolic and diastolic dysfunction. Therefore, CMD is one of the early pathological manifestations of diabetic heart disease. Guimbal et al. (21) observed the structure and function of cardiac microvessels in 12-week-old female db/db mice and found that cardiac microvessel density was reduced. In a prospective cohort study, impaired CFR was independently associated with diastolic dysfunction and adverse events, especially HFpEF hospitalization in symptomatic patients without overt coronary artery disease (22). Microvascular rarefaction might precede disease development, as HFpEF-associated comorbidities, type 2 diabetes mellitus, aging, hypertension, and obesity, show microvascular rarefaction (23). For example, microvascular rarefaction is suggested to impede insulin delivery to muscles and adipose tissue, contributing to poor insulin uptake (24). Furthermore, increased subepicardial and pericoronary adipose tissue, as observed in obese, T2DM, and elderly patients, correlated with an impaired CFR, microvasculature, and coronary function, leading to deteriorated diastolic function (25–27). Our observations corroborate and extend these findings by suggesting that CMD plays an important role in the development of diabetic heart disease.

Single-cell sequencing results revealed that there were many pericytes in the human heart (8). Increasing evidence indicates that pericytes perform diverse functions, such as promoting angiogenesis, maintaining vascular stability, regulating blood flow, forming the blood-brain barrier/blood-retina barrier, and regulating neuroinflammation (9). Previous studies showed that pericyte abnormalities played an important role in microvascular diseases (28). For example, after coronary ischemia-reperfusion in rats, the reduction in cardiac capillary perfusion in the ischemic region was associated with pericyte contraction (29). Pericyte loss is a well-established hallmark of diabetic retinopathy (30) and diabetic heart disease in patients (31). Our study found that the number and coverage of

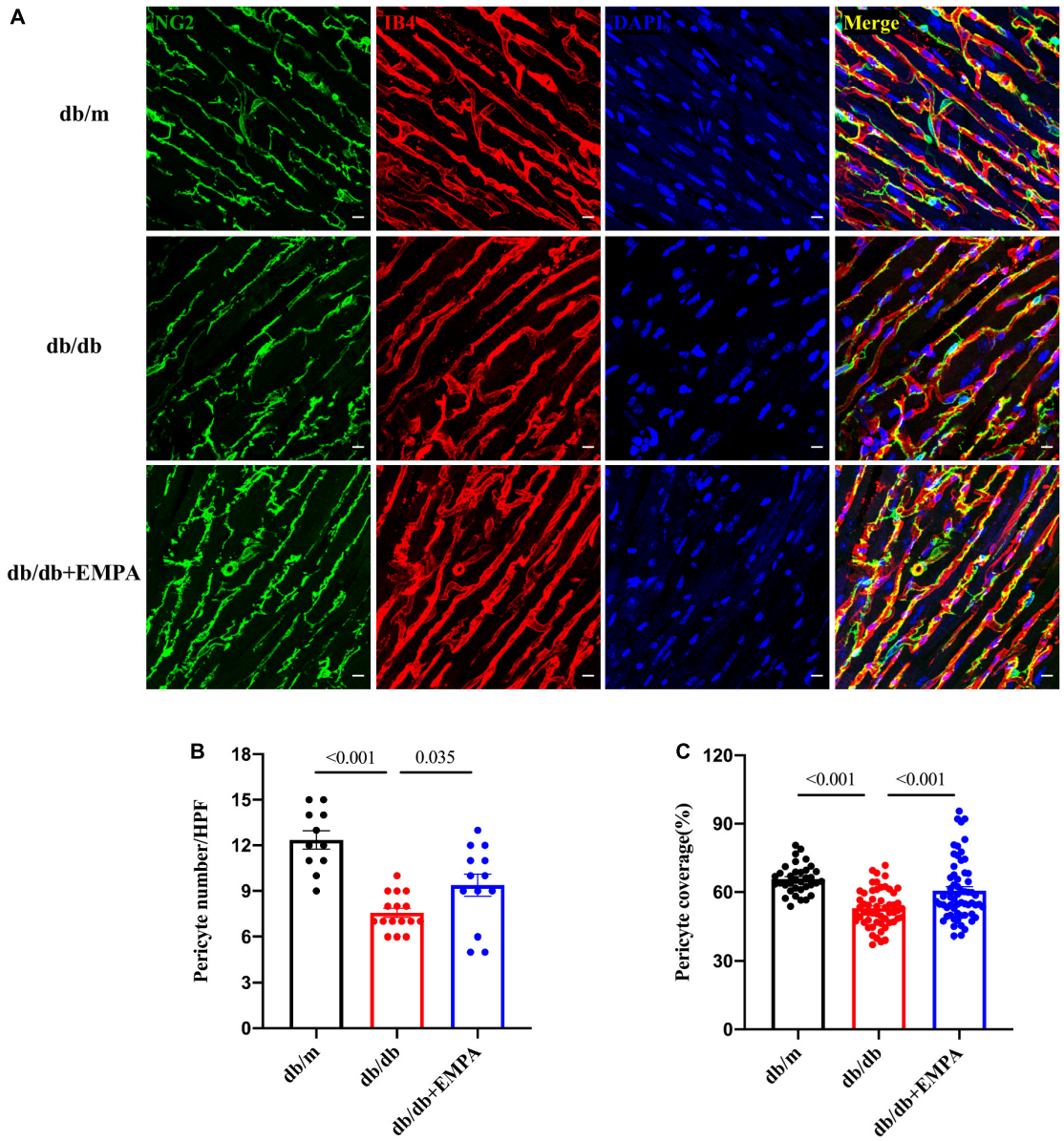

FIGURE 5
Effects of empagliflozin treatment on pericytes in the hearts of db/db mice. **(A)** Representative myocardial sections showing pericytes (NG2+, green), capillaries (IB4+, red) and nuclei (DAPI+, blue). **(B)** Statistical analysis of pericyte number/HPF between the three groups. **(C)** Statistical analysis of pericyte coverage between the three groups, pericyte coverage = (NG2 + area/IB4 + area)/HPF*100%. Data are presented as the means ± SEM. *P*-values are corrected for multiple comparisons. NG2, neuroglial cell 2 chondroitin sulfate proteoglycan; IB4, isolectin B4; DAPI, 4′,6-diamidino-2-phenylindole; HPF, high power field.

pericytes in the hearts of db/db mice were significantly reduced and coexisted with functional and structural abnormalities of coronary microcirculation in diabetic mice. Therefore, pericyte loss may be an important factor in the development of diabetic CMD.

Although evidence from large clinical trials is lacking, EMPA improved coronary microvascular function in diabetic mice in preclinical studies (32). Another study showed that empagliflozin prevented coronary microangiopathy in mice with type 2 diabetes by acting on sGC-cGMP-PKG (33). The effect of empagliflozin on cardiac microvascular endothelial cell-mediated preservation of cardiomyocyte function suggests that empagliflozin could be used to treat the cardiac mechanical implications of microvascular dysfunction in HFpEF (34). Kidney and retinal pericytes express SGLT2, and SGLT2 inhibitors inhibit high glucose-induced pericyte swelling (35). A recent study showed that a low-dose SGLT2 inhibitor ameliorated ischemic brain injury in mice *via*

pericyte protection without glucose-lowering effects (36). Our study found that EMPA inhibited cardiac pericyte loss and ameliorated CMD in type 2 diabetic mice. The protective effects of EMPA on pericytes may play an important role in the treatment of coronary microvascular diseases, such as diabetic CMD.

In diabetic subjects, fibrotic expansion of the cardiac interstitium assessed through MRI is also associated with adverse outcome (37). HFpEF patients exhibit prominent interstitial myocardial fibrosis, associated with coronary microvascular rarefaction (38). Pericyte loss or dysfunction is commonly observed in diverse fibrotic diseases, such as cardiac fibrosis (39), diabetic retinopathy, and neurodegenerative diseases (40). Several cell types, including pericytes, were implicated in fibrotic remodeling of the heart, either by secreting fibrogenic mediators and matricellular proteins, or in some cases, by undergoing conversion to activated myofibroblasts. It is interesting to investigate the association and mechanism between pericytes loss and cardiac fibrosis. The analysis of the picrosirius red staining pictures in our study revealed that cardiac fibrosis might be improved by EMPA. This result was consistent with the previous study (17).

The current study has some limitations that should be addressed in future research. First, the contribution of SGLT2 inhibitors in alleviating pericyte loss and CMD must be further explored. Previous studies showed that a high glucose state induced pericyte apoptosis, migration, or differentiation into other types of cells. It is necessary to investigate the expression of SGLT2 in the heart and examine whether SGLT2 inhibitors directly act on the cells that constitute the coronary microcirculation, such as pericytes and endothelial cells, or indirectly protect the coronary microcirculation by lowering blood glucose. CMD, in the absence of appreciable atherosclerosis, was severe enough to produce perturbations in myocardial oxygen balance (41), which might affect the pericytes loss. *In vivo* data of diabetic retinopathy showed that the early disappearance of pericytes was quickly followed by the loss of ECs and capillary network collapse, leading to reduced blood flow in the retina (42). Therefore, these speculations of cardiac pericyte loss are promising research directions. Second, 16-week-old male db/db mice showed no abnormal cardiac systolic or diastolic function in our study, and EMPA had no significant effect on cardiac function. An extended experiment may clarify the relationship between diabetic CMD and abnormal cardiac function and whether EMPA improved cardiac systolic or diastolic function by protecting the coronary microcirculation. Third, the use of CFR based on flow velocity rather than volumetric flow per gram of myocardial tissue. CFR measurement is now recommended by international guidelines (43) as a diagnostic method for the identification of patients with microvascular angina who could benefit from targeted therapy (44). In INOCA patients with functional CMD (45), in patients with residual CMD after undergoing percutaneous coronary intervention for obstructive CAD (46), and in patients with diabetes mellitus (47), an increase in basal coronary blood flow per gram of myocardium (45) or increases in basal coronary flow velocity (46, 47), as compared to healthy individuals, appears primarily responsible for the reduction in CFR. Forth, the lack of measurement of arterial blood pressure at the time of CFR measurements, preventing the assessment of coronary vascular conductance/resistance. In our laboratory, it's difficult for us to measure blood pressure and CFR at the same time. Because the non-invasive tail-cuff device and echocardiographic device were separate. However, before CFR was measured per 2 weeks, arterial blood pressure was measured. Blood pressure was not significantly different in the 3 groups from 8 to 16 weeks of age. Therefore, the CFR should not be influenced by blood pressure. We will examine these issues in future studies.

5 Conclusion

Abnormal coronary microvascular structure and function occur in the early stage of diabetic heart disease. The decreased number and coverage of cardiac pericytes may be involved in the progression of CMD. Empagliflozin attenuated coronary microvascular function and structural abnormalities and protected cardiac pericytes in diabetic mice. Therefore, EMPA may be an effective drug for the treatment of diabetic CMD.

Data availability statement

The original contributions presented in this study are included in the article/**Supplementary material**, further inquiries can be directed to the corresponding author/s.

Ethics statement

The animal study was reviewed and approved by Institutional Animal Care and Use Committee of China-Japan Friendship Hospital.

Author contributions

YT: validation, methodology, visualization, writing—original draft, and writing—review and editing. QL: methodology, visualization, and data curation. YZ: data curation, software, and writing—review and editing. ZY: visualization, software, data curation, and writing—review and editing. CW and EX: data analysis and writing—review and editing. YL, PL, and YW: methodology and writing–review and editing. ZG and

CY: visualization, software, and writing–review and editing. JZ: conceptualization, methodology, investigation, resources, data curation, visualization, supervision, funding acquisition, and writing—review and editing. YG: conceptualization, investigation, resources, data curation, supervision, project administration, visualization, and writing—review and editing. All authors contributed to the article and approved the submitted version.

Funding

This work was supported by the National Natural Science Foundation of China (Grant no. 82270352), National Natural Science Foundation of China (Grant no. 91639110), Capital's Founds for Health Improvement and Research (Grant no. 2022-1-4062), National High Level Hospital Clinical Research Funding (Grant no. 2022-NHLHCRF-YSPY-01), and National Key Clinical Specialty Construction Project (Grant no. 2020-QTL-009).

Acknowledgments

We thank Weiliang Sun and Jing Guo for professional instruction on histological staining.

Conflict of interest

The authors declare that the research was conducted in the absence of any commercial or financial relationships that could be construed as a potential conflict of interest.

The reviewer JG declared a shared affiliation with the authors at the time of review.

Publisher's note

Supplementary material

The Supplementary Material for this article can be found online at: https://www.frontiersin.org/articles/10.3389/fcvm.2022.995216/full#supplementary-material

References

1. Kaski J, Crea F, Gersh B, Camici P. Reappraisal of ischemic heart disease. *Circulation.* (2018) 138:1463–80. doi: 10.1161/CIRCULATIONAHA.118.031373

2. Camici P, Crea F. Coronary microvascular dysfunction. *N Engl J Med.* (2007) 356:830–40. doi: 10.1056/NEJMra061889

3. Crea F, Camici P, Bairey Merz C. Coronary microvascular dysfunction: an update. *Eur Heart J.* (2014) 35:1101–11. doi: 10.1093/eurheartj/eht513

4. Quercioli A, Pataky Z, Montecucco F, Carballo S, Thomas A, Staub C, et al. Coronary vasomotor control in obesity and morbid obesity: contrasting flow responses with endocannabinoids, leptin, and inflammation. *JACC Cardiovasc Imaging.* (2012) 5:805–15. doi: 10.1016/j.jcmg.2012.01.020

5. Hayashi T, Sohmiya K, Ukimura A, Endoh S, Mori T, Shimomura H, et al. Angiotensin II receptor blockade prevents microangiopathy and preserves diastolic function in the diabetic rat heart. *Heart.* (2003) 89:1236–42. doi: 10.1136/heart.89.10.1236

6. Gdowski M, Murthy V, Doering M, Monroy-Gonzalez A, Slart R, Brown D. Association of isolated coronary microvascular dysfunction with mortality and major adverse cardiac events: a systematic review and meta-analysis of aggregate data. *J Am Heart Assoc.* (2020) 9:e014954. doi: 10.1161/JAHA.119.014954

7. Birbrair A. Pericyte biology: development, homeostasis, and disease. *Adv Exp Med Biol.* (2018) 1109:1–3. doi: 10.1007/978-3-030-02601-1_1

8. Litvinukova M, Talavera-Lopez C, Maatz H, Reichart D, Worth C, Lindberg E, et al. Cells of the adult human heart. *Nature.* (2020) 588:466–72. doi: 10.1038/s41586-020-2797-4

9. Trost A, Lange S, Schroedl F, Bruckner D, Motloch K, Bogner B, et al. Brain and retinal pericytes: origin, function and role. *Front Cell Neurosci.* (2016) 10:20. doi: 10.3389/fncel.2016.00020

10. Ferland-McCollough D, Slater S, Richard J, Reni C, Mangialardi G. Pericytes, an overlooked player in vascular pathobiology. *Pharmacol Ther.* (2017) 171:30–42. doi: 10.1016/j.pharmthera.2016.11.008

11. Barber A, Gardner T, Abcouwer S. The significance of vascular and neural apoptosis to the pathology of diabetic retinopathy. *Invest Ophthalmol Vis Sci.* (2011) 52:1156–63. doi: 10.1167/iovs.10-6293

12. Nees S, Juchem G, Eberhorn N, Thallmair M, Forch S, Knott M, et al. Wall structures of myocardial precapillary arterioles and postcapillary venules reexamined and reconstructed *in vitro* for studies on barrier functions. *Am J Physiol Heart Circ Physiol.* (2012) 302:H51–68. doi: 10.1152/ajpheart.00358.2011

13. Ostergaard L, Kristiansen S, Angleys H, Frokiaer J, Michael Hasenkam J, Jespersen S, et al. The role of capillary transit time heterogeneity in myocardial oxygenation and ischemic heart disease. *Basic Res Cardiol.* (2014) 109:409. doi: 10.1007/s00395-014-0409-x

14. Cai L, Kang Y. Cell death and diabetic cardiomyopathy. *Cardiovasc Toxicol.* (2003) 3:219–28. doi: 10.1385/ct:3:3:219

15. Tate M, Grieve D, Ritchie R. Are targeted therapies for diabetic cardiomyopathy on the horizon? *Clin Sci.* (2017) 131:897–915. doi: 10.1042/CS20160491

16. Hu X, Bai T, Xu Z, Liu Q, Zheng Y, Cai L. Pathophysiological fundamentals of diabetic cardiomyopathy. *Compr Physiol.* (2017) 7:693–711. doi: 10.1002/cphy.c160021

17. Li C, Zhang J, Xue M, Li X, Han F, Liu X, et al. SGLT2 inhibition with empagliflozin attenuates myocardial oxidative stress and fibrosis in diabetic mice heart. *Cardiovasc Diabetol.* (2019) 18:15. doi: 10.1186/s12933-019-0816-2

18. Baartscheer A, Schumacher C, Wust R, Fiolet J, Stienen G, Coronel R, et al. Empagliflozin decreases myocardial cytoplasmic Na(+) through inhibition of the cardiac Na(+)/H(+) exchanger in rats and rabbits. *Diabetologia.* (2017) 60:568–73. doi: 10.1007/s00125-016-4134-x

19. Lenzarini F, Di Lascio N, Stea F, Kusmic C, Faita F. Time course of isoflurane-induced vasodilation: a doppler ultrasound study of the left coronary artery in mice. *Ultrasound Med Biol.* (2016) 42:999–1009. doi: 10.1016/j.ultrasmedbio.2015.11.026

20. Alcaraz J, Carrasco J, Millares L, Luis I, Fernandez-Porras F, Martinez-Romero A, et al. Stromal markers of activated tumor associated fibroblasts predict poor survival and are associated with necrosis in non-small cell lung cancer. *Lung Cancer.* (2019) 135:151–60. doi: 10.1016/j.lungcan.2019.07.020

21. Guimbal S, Cornuault L, Rouault P, Hollier P, Chapouly C, Bats M, et al. Mast cells are the trigger of small vessel disease and diastolic dysfunction in diabetic obese mice. *Arterioscler Thromb Vasc Biol.* (2021) 41:e193–207. doi: 10.1161/ATVBAHA.121.315900

22. Taqueti V, Solomon S, Shah A, Desai A, Groarke J, Osborne M, et al. Coronary microvascular dysfunction and future risk of heart failure with preserved ejection fraction. *Eur Heart J.* (2018) 39:840–9. doi: 10.1093/eurheartj/ehx721

23. Cuijpers I, Simmonds S, van Bilsen M, Czarnowska E, Gonzalez Miqueo A, Heymans S, et al. Microvascular and lymphatic dysfunction in HFpEF and its associated comorbidities. *Basic Res Cardiol.* (2020) 115:39. doi: 10.1007/s00395-020-0798-y

24. Baron A, Tarshoby M, Hook G, Lazaridis E, Cronin J, Johnson A, et al. Interaction between insulin sensitivity and muscle perfusion on glucose uptake in human skeletal muscle: evidence for capillary recruitment. *Diabetes.* (2000) 49:768–74. doi: 10.2337/diabetes.49.5.768

25. Nakanishi K, Fukuda S, Tanaka A, Otsuka K, Taguchi H, Shimada K. Relationships between periventricular epicardial adipose tissue accumulation, coronary microcirculation, and left ventricular diastolic dysfunction. *Can J Cardiol.* (2017) 33:1489–97. doi: 10.1016/j.cjca.2017.08.001

26. Sorop O, Heinonen I, van Kranenburg M, van de Wouw J, de Beer V, Nguyen I, et al. Multiple common comorbidities produce left ventricular diastolic dysfunction associated with coronary microvascular dysfunction, oxidative stress, and myocardial stiffening. *Cardiovasc Res.* (2018) 114:954–64. doi: 10.1093/cvr/cvy038

27. van Dijk C, Oosterhuis N, Xu Y, Brandt M, Paulus W, van Heerebeek L, et al. Distinct endothelial cell responses in the heart and kidney microvasculature characterize the progression of heart failure with preserved ejection fraction in the obese ZSF1 rat with cardiorenal metabolic syndrome. *Circ Heart Fail.* (2016) 9:e002760. doi: 10.1161/CIRCHEARTFAILURE.115.002760

28. Lindahl P, Johansson B, Leveen P, Betsholtz C. Pericyte Loss and Microaneurysm Formation in PDGF-B-deficient mice. *Science.* (1997) 277:242–5. doi: 10.1126/science.277.5323.242

29. O'Farrell F, Mastitskaya S, Hammond-Haley M, Freitas F, Wah W, Attwell D. Capillary pericytes mediate coronary no-reflow after myocardial ischaemia. *eLife.* (2017) 6:e29280. doi: 10.7554/eLife.29280

30. Cogan D, Toussaint D, Kuwabara T. Retinal vascular patterns. IV. Diabetic retinopathy. *Arch Ophthalmol.* (1961) 66:366–78. doi: 10.1001/archopht.1961.00960010368014

31. Hinkel R, Howe A, Renner S, Ng J, Lee S, Klett K, et al. Diabetes mellitus-induced microvascular destabilization in the myocardium. *J Am Coll Cardiol.* (2017) 69:131–43. doi: 10.1016/j.jacc.2016.10.058

32. Adingupu D, Gopel S, Gronros J, Behrendt M, Sotak M, Miliotis T, et al. SGLT2 inhibition with empagliflozin improves coronary microvascular function and cardiac contractility in prediabetic Ob/Ob(−/−) mice. *Cardiovasc Diabetol.* (2019) 18:16. doi: 10.1186/s12933-019-0820-6

33. Xue M, Li T, Wang Y, Chang Y, Cheng Y, Lu Y, et al. Empagliflozin prevents cardiomyopathy Via sGC-cGMP-PKG pathway in type 2 diabetes mice. *Clin Sci.* (2019) 133:1705–20. doi: 10.1042/CS20190585

34. Juni R, Kuster D, Goebel M, Helmes M, Musters R, van der Velden J, et al. Cardiac microvascular endothelial enhancement of cardiomyocyte function is impaired by inflammation and restored by empagliflozin. *JACC Basic Transl Sci.* (2019) 4:575–91. doi: 10.1016/j.jacbts.2019.04.003

35. Wakisaka M, Nagao T, Yoshinari M. Sodium glucose cotransporter 2 (SGLT2) plays as a physiological glucose sensor and regulates cellular contractility in rat mesangial cells. *PLoS One.* (2016) 11:e0151585. doi: 10.1371/journal.pone.0151585

36. Takashima M, Nakamura K, Kiyohara T, Wakisaka Y, Hidaka M, Takaki H, et al. Low-dose sodium-glucose cotransporter 2 inhibitor ameliorates ischemic brain injury in mice through pericyte protection without glucose-lowering effects. *Commun Biol.* (2022) 5:653. doi: 10.1038/s42003-022-03605-4

37. Wong T, Piehler K, Kang I, Kadakkal A, Kellman P, Schwartzman D, et al. Myocardial extracellular volume fraction quantified by cardiovascular magnetic resonance is increased in diabetes and associated with mortality and incident heart failure admission. *Eur Heart J.* (2014) 35:657–64. doi: 10.1093/eurheartj/eht193

38. Mohammed S, Hussain S, Mirzoyev S, Edwards W, Maleszewski J, Redfield M. Coronary microvascular rarefaction and myocardial fibrosis in heart failure with preserved ejection fraction. *Circulation.* (2015) 131:550–9. doi: 10.1161/CIRCULATIONAHA.114.009625

39. Frangogiannis N. Cardiac fibrosis: cell biological mechanisms, molecular pathways and therapeutic opportunities. *Mol Aspects Med.* (2019) 65:70–99. doi: 10.1016/j.mam.2018.07.001

40. Di Carlo S, Peduto L. The perivascular origin of pathological fibroblasts. *J Clin Invest.* (2018) 128:54–63. doi: 10.1172/JCI93558

41. van de Wouw J, Sorop O, van Drie R, van Duin R, Nguyen I, Joles J, et al. Perturbations in myocardial perfusion and oxygen balance in swine with multiple risk factors: a novel model of ischemia and no obstructive coronary artery disease. *Basic Res Cardiol.* (2020) 115:21. doi: 10.1007/s00395-020-0778-2

42. van Dijk C, Nieuweboer F, Pei J, Xu Y, Burgisser P, van Mulligen E, et al. The complex mural cell: pericyte function in health and disease. *Int J Cardiol.* (2015) 190:75–89. doi: 10.1016/j.ijcard.2015.03.258

43. Knuuti J, Wijns W, Saraste A, Capodanno D, Barbato E, Funck-Brentano C, et al. 2019 ESC guidelines for the diagnosis and management of chronic coronary syndromes. *Eur Heart J.* (2020) 41:407–77. doi: 10.1093/eurheartj/ehz425

44. Kelshiker M, Seligman H, Howard J, Rahman H, Foley M, Nowbar A, et al. Coronary flow reserve and cardiovascular outcomes: a systematic review and meta-analysis. *Eur Heart J.* (2022) 43:1582–93. doi: 10.1093/eurheartj/ehab775

45. Rahman H, Ryan M, Lumley M, Modi B, McConkey H, Ellis H, et al. Coronary microvascular dysfunction is associated with myocardial ischemia and abnormal coronary perfusion during exercise. *Circulation.* (2019) 140:1805–16. doi: 10.1161/CIRCULATIONAHA.119.041595

46. Herrmann J, Haude M, Lerman A, Schulz R, Volbracht L, Ge J, et al. Abnormal coronary flow velocity reserve after coronary intervention is associated with cardiac marker elevation. *Circulation.* (2001) 103:2339–45. doi: 10.1161/01.cir.103.19.2339

47. Picchi A, Limbruno U, Focardi M, Cortese B, Micheli A, Boschi L, et al. Increased basal coronary blood flow as a cause of reduced coronary flow reserve in diabetic patients. *Am J Physiol Heart Circ Physiol.* (2011) 301:H2279–84. doi: 10.1152/ajpheart.00615.2011

frontiers | Frontiers in Cardiovascular Medicine

TYPE Brief Research Report
PUBLISHED 28 February 2023
DOI 10.3389/fcvm.2023.1103784

OPEN ACCESS

EDITED BY
Ting Zhou,
University of Wisconsin-Madison, United States

REVIEWED BY
Anis Hanna,
Albert Einstein College of Medicine, United States
Jianing Gao,
Brigham and Women's Hospital and Harvard Medical School, United States

*CORRESPONDENCE
Mary B. Sheppard
✉ mary.sheppard@uky.edu
Jakub K. Famulski
✉ jakub.famulski@uky.edu

SPECIALTY SECTION
This article was submitted to Clinical and Translational Cardiovascular Medicine, a section of the journal Frontiers in Cardiovascular Medicine

RECEIVED 21 November 2022
ACCEPTED 31 January 2023
PUBLISHED 28 February 2023

CITATION
Sheppard MB, Smith JD, Bergmann LL and Famulski JK (2023) Novel *SMAD3* variant identified in a patient with familial aortopathy modeled using a zebrafish embryo assay. *Front. Cardiovasc. Med.* 10:1103784. doi: 10.3389/fcvm.2023.1103784

Novel *SMAD3* variant identified in a patient with familial aortopathy modeled using a zebrafish embryo assay

Mary B. Sheppard[1,2,3,4,5]*, Jeffrey D. Smith[1,2], Lisa L. Bergmann[6] and Jakub K. Famulski[7]*

[1]Saha Aortic Center, University of Kentucky, Lexington, KY, United States, [2]Saha Cardiovascular Research Center, University of Kentucky, Lexington, KY, United States, [3]Department of Family Medicine, University of Kentucky, Lexington, KY, United States, [4]Department of Surgery, University of Kentucky, Lexington, KY, United States, [5]Department of Physiology, University of Kentucky, Lexington, KY, United States, [6]Department Radiology, University of Kentucky, Lexington, KY, United States, [7]Department of Biology, University of Kentucky, Lexington, KY, United States

In human, pathogenic variants in smad3 are one cause of familial aortopathy. We describe a novel *SMAD3* variant of unknown significance (VUS), V244F, in a patient who presented with aortic root dilation, right coronary artery ectasia, abdominal aortic aneurysm, right vertebral artery atresia, and cavernoma. Determination of variant pathogenicity impacted multiple aspects of the patient's care, including the most appropriate surgical threshold for which to recommend a valve-sparing aortic root replacement. To determine whether the newly identified *SMAD3* variant, and whether *SMAD3* induced aortopathy in general, can be assayed in a zebrafish embryo model, we injected *smad3a* mRNA into Tg[*kdrl*:mCherry] zebrafish embryos. By measuring the size of the dorsal aorta at 48hpf we found a correlation between pathogenic *SMAD3* variants and increased dorsal aortic diameter. The newly identified V244F variant increased dorsal aortic diameter ($p < 0.0001$) similar to that of the pathogenic control variant T261I ($p < 0.0084$). In addition, we examined several previously identified variants of uncertain significance and found P124T ($p < 0.0467$), L296P ($p < 0.0025$) and A349P ($p < 0.0056$) to behave like T261I. These results demonstrate that the zebrafish embryo assay was successful in validating known pathogenic variants, classifying our newly identified variant V244F as likely pathogenic, and classifying previously identified variants P124T, L296P, and A349P as likely pathogenic. Overall, our findings identify a novel *SMAD3* variant that is likely pathogenic as well as offer a new mechanism to model *SMAD3* VUSs *in vivo*.

KEYWORDS

zebrafish, aorta, familial aortopathy, *SMAD3*, pathogenic variant

Introduction

Aortic aneurysms are permanent dilations that increase an individual's risk for aortic rupture or dissection, a tear that occurs between layers of the aortic wall. Ruptured aortic aneurysms and dissections are estimated to cause more than 17,000 deaths in the United States each year (1, 2). Aneurysms in the proximal regions of the thoracic aorta have been associated with several

genetic mutations. These mutations can cause syndromes (such as Marfan syndrome) or isolated dilation of the thoracic aorta (called Familial Thoracic Aortic Aneurysm and Dissection or FTAAD). FTAAD is believed to account for at least 20 percent of thoracic aortic aneurysms and dissections (3). Gene panels are now available to determine the presence of a FTAAD mutation. However, many mutations in these genes have never been functionally verified and are given the assignment of variants of uncertain significance (VUS). These VUSs could be disease-causing or normal variants that occur in the population. Additional work is needed to determine whether (1) the mutation causes aortic dilation and (2) current pharmacological approaches for aortic aneurysm benefit patients harboring the specific mutation.

Mutations in *SMAD3* cause 2% of heritable aortopathy (4). Mutations in other genes, such as *FBN1* (5), *TGFBR1* (6), *TGFBR2* (7, 8), *MYH11* (9), *ACTA2* (10), *MYLK* (11), *PRKG1* (12) have been identified as a cause of up to another 25% of familial aortopathy (13). These genes encode proteins that are necessary for either the contraction of smooth muscle cells or transduction of transforming growth factor-beta (TGF-β) signaling. SMAD3, specifically, is an essential protein in TGF-beta signaling. TGF-β ligand binding of the type II TGF-β receptor phosphorylates type I receptors in order to activate intracellular SMAD-dependent and SMAD-independent cascades. In SMAD-dependent signaling, SMAD2/SMAD3 become phosphorylated, bind the transcription factor SMAD4, and enter the nucleus to interact with a SBE (Smad Binding Element), modulating the expression of target genes downstream. *SMAD3* has been well characterized to play a functional role in familial aortopathy (14, 15). Although the molecular mechanism by which genetic mutations in SMAD3 and other TGF-beta signaling molecules lead to TAA is unknown (16), Gong et al. found that SMAD3 deficiency could impair differentiation of vascular smooth muscle cells from cardiovascular progenitor cells (CPC-VSMC) in human-induced pluripotent stem cells. Furthermore, $SMAD3^{-/-}$ CPC-VSMC contractility was significantly decreased compared to wild type CPC-VSMC (16). Loss of SMAD3 function also increased collagen fiber deposition and enhanced stiffness in CPC-VSMC tissue rings, consistent with the clinical phenotype seen in people with loss of function mutations in *SMAD3* (16). Currently, over 65 mutations have been discovered in people with FTAAD, however, many of these mutations, up to 35, are classified as variants of uncertain significance (VUS) (14). Additional work needs to determine whether these 35 mutations cause FTAAD in these patients or if they are benign variants.

In addition to aortic aneurysms, *SMAD3* mutations can cause a number of additional vascular manifestations, including intracranial aneurysm, abdominal aortic aneurysm, iliac artery aneurysm, and arterial tortuosity (4). Cardiac manifestations include mitral valve prolapse, myxomatous valve disease, and atrial fibrillation. Extravascular manifestations include early onset osteoarthritis as well as degenerative disk disease (4). Although inheritance occurs in an autosomal dominant fashion, reduced penetrance and phenotypic variability exists within families (4).

In our current study, we identify a novel VUS in *SMAD3*, V244F, in a patient presenting with aortic root aneurysm, right coronary artery ectasia, abdominal aortic aneurysm, right vertebral artery atresia, and cavernoma. Definitive classification of the variant had many implications for patient care. First, if pathogenic, the patient is an immediate candidate for a valve-sparing aortic root replacement. This is because surgery would generally be offered to a person at an aortic root diameter of 50-55 mm. However, in the setting of a pathogenic *SMAD3* variant, the threshold to consider surgical repair is 4.5 cm (17). Second, classification can affect pharmacologic management, such as the initiation of an angiotensin-receptor blocker (17). Finally, a pathogenic classification helps direct screening and surveillance strategies for the patient's three children. To validate the pathogenicity of this mutation, and therefore offer potential therapeutic options to the patient, we designed a zebrafish embryo based *in vivo* assay. Using a transgenic line Tg[*kdrl*:mCherry] to visualize vasculature, we tested known pathogenic variants of *SMAD3* as well as our newly identified VUS. Results from this novel assay indicate that $SMAD3^{V244F}$ acts like a pathogenic variant of *SMAD3* and that zebrafish modeling of FTAAD associated *SMAD3* variants may be possible.

Results

A 55 year-old male with a past medical history of paroxysmal atrial fibrillation, hypertension, and thoracic aortic aneurysm presented for evaluation of heritable aortopathy. Past history included eosinophilic esophagitis as well as atraumatic herniated disc at the age of 49. Family history was notable for fatal aortic dissection in a maternal grandmother in the eighth decade of life, abdominal aortic aneurysm in a paternal grandfather in the eighth decade of life, as well as atrial fibrillation in his father, paternal grandmother, paternal aunt, and paternal cousin (**Figure 1A**). Patient was a non-smoker. Aortopathy panel testing was performed by Invitae, which included sequencing of the following genes: *ACTA2, CBS, COL3A1, COL5A2, EFEMP2, FBN1, FBN2, FLNA, MAT2A, MED12, MYH11, MYLK, NOTCH1, PLOD1, PRKG1, SKI, SCL2A10, SMAD3, SMAD4, SMAD6, TGFB2, TGFB3, TGFBR1, and TGFBR2*. No pathogenic variants were identified. One variant of uncertain significance was identified in *SMAD3*, c.730G > T (p.Val244Phe). Segregation analysis in the patient's parents and brother was recommended, but family members were not willing to undergo testing at the time. Given the young age of the patient's three children, segregation analysis in progeny was deferred pending variant reclassification. At the time of initial evaluation, computed tomographic angiography (CTA) of the chest demonstrated an aortic root aneurysm of 45 mm (**Figure 1B**). The right coronary artery was found to be focally ectatic (>6.0 mm) (**Figure 1C**). Computed tomography (CT) of the abdomen and pelvis did not reveal aneurysmal disease. Screening of head and neck vasculature was deferred by the patient. Three years later, surveillance CTA of the chest revealed a stable aortic root diameter. However, CTA of the abdomen and pelvis revealed interval development of an infrarenal aortic aneurysm with mural atherosclerotic plaque, which had increased in size from a diameter of 25 mm x 25 mm to 32 mm x 37 mm (**Figure 1D**). Due to onset of intermittent chest discomfort with exertion, cardiac CT was performed. Cardiac CT revealed severe coronary calcification (**Figure 1E**) with an Agatston score of 383 using the AJ-130 method, which represents the 91st percentile when matched for age, gender, and ethnicity. In the AJ-130 method, coronary artery calcific densities of at least 130 Hounsfield units (HU) with an area of at least 1 mm^2 are scored 1 to 4, and each score is multiplied by the area. Based on these results, vascular age was calculated to be 82 years. The proximal to mid left anterior descending coronary artery (LAD) and proximal right coronary artery (RCA)

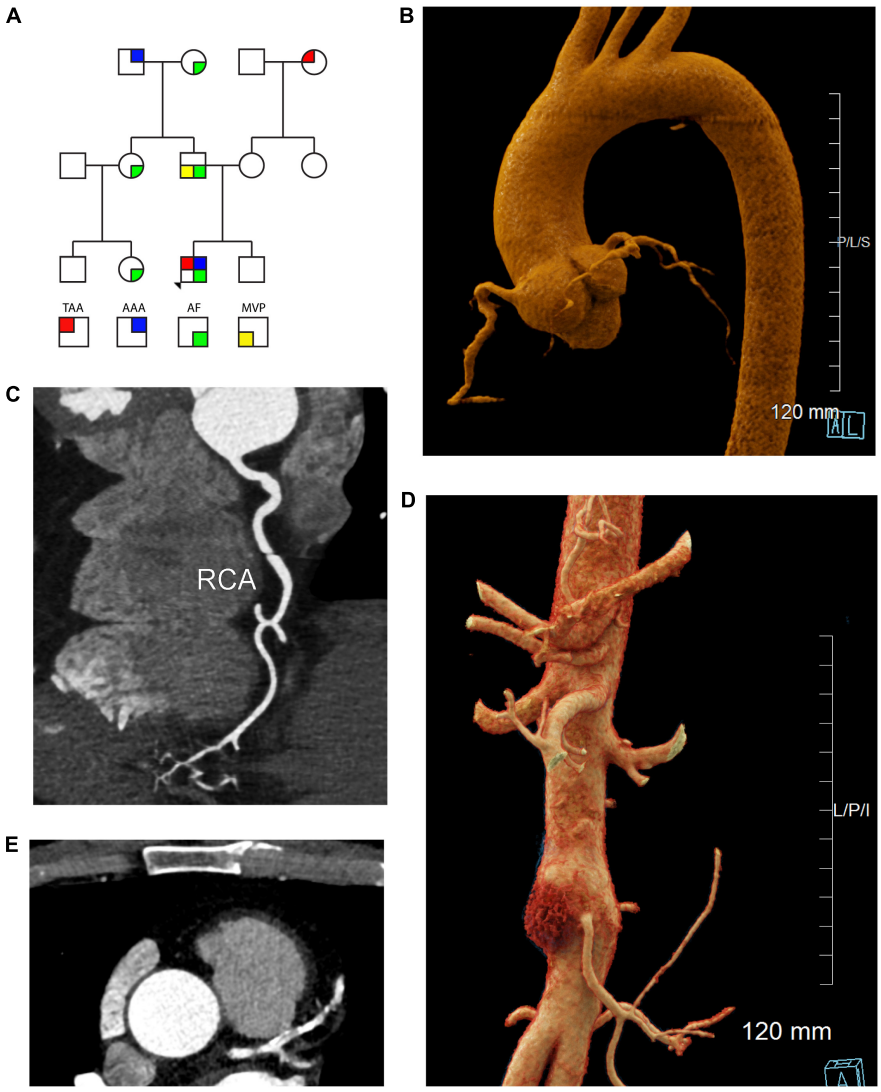

FIGURE 1
Cardiac, aortic, and coronary artery findings in a 55 year old male with the *SMAD3* V244F variant. **(A)** Pedigree demonstrating sex and phenotype. Squares and circles represent males and females, respectively. TAA is red upper left quadrant. AAA is blue upper right quadrant. AF is green lower right quadrant. MVP is yellow lower left quadrant. **(B)** Aortic root aneurysm and Focal bilobed fusiform ectasia of the proximal RCA. Linear reformat of coronary CTA was created using TeraRecon (Durham, North Carolina). **(C)** Axial CTA demonstrating tortuosity and ectasia of the right coronary artery (RCA). **(D)** Infrarenal abdominal aortic aneurysm, 37 mm in maximum diameter. Mural hematoma in the right lateral aspect of the aneurysm is displayed in red. Cinematic 3D reformatted images of CTA abdomen and pelvis. Cinematic 3D were created using *syngo*.via (Siemens, Erlangen). **(E)** Calcification of the left coronary artery and its branches with 25-49% stenosis in the LAD. TAA is thoracic aorta aneurysm, AAA is abdominal aortic aneurysm, AF is atrial fibrillation, MVP is mitral valve prolapse 3D is 3-dimensional, CTA is computed tomographic angiography, RCA is right coronary artery, LAD is left anterior descending artery.

contained mixed plaque causing mild stenosis. Cardiovascular risk factors were optimized, including initiation of high-intensity statin. Regular echocardiography monitoring revealed an absence of mitral valve prolapse or significant valvular regurgitation. After six months, aortoiliac duplex demonstrated stable size of the infrarenal abdominal aortic aneurysm (AAA).

Screening CTA of the head and neck revealed atresia of the right vertebral artery (**Figure 2A**), but no evidence of intracranial aneurysm. Six months later, the patient underwent magnetic resonance angiography (MRA) of the head, neck, chest, abdomen, and pelvis, which revealed stability of both the thoracic aorta aneurysm (TAA) and AAA as well as mild tortuosity of the external iliac arteries. Incidental findings included a 1.7 cm cavernous malformation in the left cingulate gyrus (**Figures 2C, D**), which remained stable over the course of six months and continues to be monitored.

Sequencing revealed a change in the sequence of exon 6 in *SMAD3* resulting in a change of valine with phenylalanine at codon 244. The valine residue is highly conserved and there is a small physicochemical difference between valine and phenylalanine. The variant was not present in population databases and *in silico* analyses did not agree on the potential impact of the missense change (SIFT: "Deleterious"; PolyPhen-2: "Probably Damaging"; Align-GVGD: "Class C0"). However, classification of the variant as pathogenic would alter the patient's medical care in multiple ways. First, patients with pathogenic mutations in *SMAD3* are recommended to have aortic root replacement at smaller diameters compared to the general population (17, 18). Given that segregation analysis in the extended family was not an option at the time, a

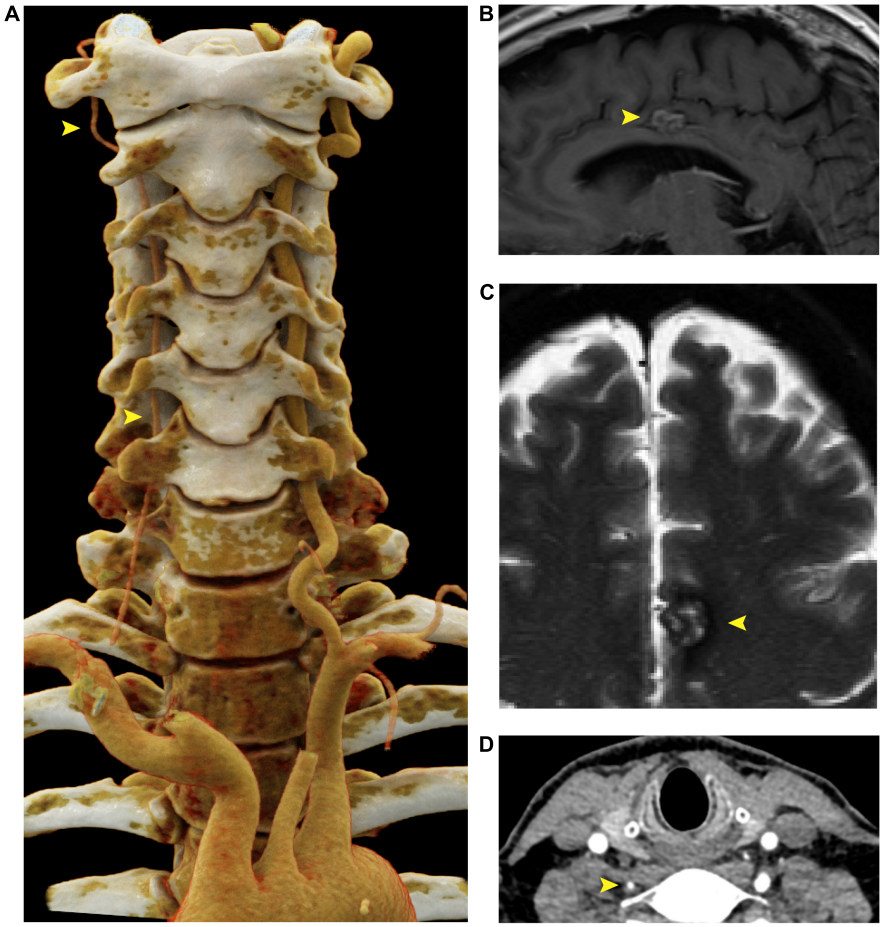

FIGURE 2
Right vertebral artery atresia and cavernoma in a 55 year old male harboring a *SMAD3* V244F variant. **(A)** Cinematic 3D reformatted images of the atretic < 2mm right vertebral artery. The origin of the right vertebral artery was sufficiently narrow in caliber that volume averaging resulted in below-threshold density required for visualization in the reformat. For best visualization of the vertebral arteries, the carotid arteries were digitally removed using *syngo*.via (Siemens, Erlangen). The dominant left vertebral artery measures 5 mm in diameter throughout most of its length, which is the upper limit of normal. **(B)** Sagittal T1-weighted FLAIR MRI of the brain at the midline shows a cavernous malformation in the left mid cingulate gyrus, just superior to the body of the corpus callosum. **(C)** Axial T2-weighted MRI with fat saturation demonstrates characteristic signal intensity of cavernous malformation with central hyperintensity, peripheral hypointensity, and susceptibility artifact. **(D)** Axial CTA demonstrating atretic < 2mm right vertebral artery. FLAIR is fluid-attenuated inversion recovery, MRI is magnetic resonance imaging.

project to investigate the feasibility of modeling *SMAD3* mutations in zebrafish was undertaken.

To model and assess potential pathogenicity of the SMAD3^{V244F} variant we employed the zebrafish embryo system. Zebrafish embryos are readily accessible for manipulation, including mRNA injections. To that end we sought to determine if overexpression of SMAD3 pathogenic variants, possibly including SMAD3^{V244F} would have functional consequences on developing vasculature. Alterations in vasculature integrity or assembly would be considered as validations variant dysfunction when compared to wildtype. As such, we employed a transgenic line of zebrafish which labels the developing vasculature, Tg[*kdrl*:mCherry]. Human and zebrafish smad3a share 97% identify and total conservation of V244 (**Figure 3A**). First, we generated the T261I variant of smad3a which has been shown to be pathogenic (15) as our positive control. Zebrafish smad3a cDNA was cloned into the pCS2 vector and subsequent site directed mutagenesis was performed to generate the zebrafish T261I and V244F variants. Using an *in vitro* transcription system, we next generated mRNA for WT, T261I and V244F *smad3a*. 1 cell stage embryos were injected with 50pg of WT, V244F or T261I mRNA and allowed to develop up to 48hpf. At this stage of development, the dorsal vein and aorta are lined with endothelial cells expressing the mCherry fluorescent protein. Using 3D confocal microscopy, we captured images of the vasculature at the termination of the yolk extension and subsequently compared the diameters between treatments (**Figure 3B**). In doing so, we observed that injection of WT ($n = 8$) smad3a mRNA had no significant effect when compared to un-injected controls ($n = 14$). When we injected our smad3a pathogenic positive control mRNA, T261I, we saw an increase in the diameter (6.3%, $p < 0.0068$, $n = 9$), suggesting our assay can correlate pathogenic smad3 variants with an abnormal vasculature phenotype. Importantly, when we injected V244F mRNA we again saw an increase in diameter measurements of 21% ($p < 0.0001$, $n = 10$) (**Figure 3C**). One-way ANOVA analysis of the variants, WT and controls resulted in p value of 0.001. Taken together we concluded that our zebrafish embryo assay can correlate SMAD3 pathogenicity to alterations of vasculature at early developmental time points and thus classify V244F as likely pathogenic. Considering the results, we sought to further expand our assay by examining several other SMAD3 variants previously classified as VUS or likely pathogenic.

These include P124T (19), R287W (15, 20), L296P (20) and A349P (21). All four are conserved between human and zebrafish smad3a. Overall, the variants chosen span the MH1 and MH2 domains of Smad3 (**Figure 4A**). Upon injection of corresponding mRNAs we again collected measurements and observed an increase in diameter for P124T (10%, $p < 0.0467$, $n = 6$), L296P (15.5%, $p < 0.0025$, $n = 17$) and A349P (18.3%, $p < 0.0056$, $n = 6$) (**Figures 4B, C**). One-way ANOVA analysis of the variants, WT and controls, resulted in p value of 0.001. Thus, these VUSs are also classified pathogenic according to our assay. R278W did not differ from controls ($n = 9$) and therefore is either not pathogenic or remains a likely pathogenic (LP) VUS (**Figure 4D**). Taken together, our zebrafish embryo assay was successful in validating known pathogenic variants and classifying our newly identified variant V244F as well as previously identified variants P124T, L296P, and A349P as likely pathogenic.

Materials and methods

Zebrafish care

Zebrafish were maintained using husbandry procedures approved by University of Kentucky IACUC committee (protocol #2021-3781). Embryos were kept at 28.5°C in E3 embryo media. Tg[*kdrl*:mCherry] transgenic line was used to visualize vasculature (22).

mRNA synthesis and injections

Coding sequence for zebrafish *smad3a* (zfsmad3) was amplified using 24hpf cDNA and cloned into pCS2 using BamH1 and *Xho*I. For variant synthesis, overlapping primers with corresponding sequence changes were used to amplify pCS2-zfsmad3 with Fusion taq polymerase. Primer sequences can be found in **Supplementary Figure 1**. Template plasmid was removed via Dpn1 digest and mutagenized product transformed into DH5a cells (NEB). Sanger sequencing (Eurofins genomics) was used to confirm the mutations using ClustalW alignment with wildtype *smad3a* coding sequence using MacVector software (**Supplementary Figure 1**). WT or variant *smad3a* mRNA was synthesized using the message Machine SP6 kit (Ambion) and purified using Sigma Spin clean up columns. Injections were done using 1 cell stage embryos, 50 pg of mRNA was injected into the cell using a pressure microinjector along with dextran green as a marker for injection control. At minimum 25 embryos were injected for each mRNA construct. At 24 hpf the embryos were screened for green fluorescence using a stereo microscope. Positive embryos were subsequently grown to 48hpf and fixed in 4% PFA.

Confocal imaging and measurements

Whole zebrafish embryos were mounted in low melting point agarose (sigma) on glass cover slip bottom Fluorodishes (WPI). Images were collected using a Nikon C2 + confocal microscope using a 20 × 0.95 NA objective. 3D stacks were collected using 3 µm steps and analyzed using Nikon Elements software. Diameter measurements were done using Nikon Elements software. Statistical significance was calculated using one-way ANOVA with Bonferroni's multiple comparisons test for individual comparisons using Prism software.

Discussion

This study advances current knowledge in multiple ways. First, we identified a novel variant in *SMAD3*, c.730G > T (p. Val244Phe) and provided clinical and laboratory data to support its classification as likely pathogenic. This discovery can have immediate clinical relevance for patients. For the patient described in this paper, he would be considered a candidate for valve-sparing aortic root surgery as his aortic root was above the 4.5 cm threshold. Furthermore, we initiated an angiotensin receptor-blocker, which generally would not have been considered in the absence of hypertension if the patient was not suspected to have SMAD3-associated aortopathy. In addition to advancing knowledge to inform this specific patient's care, we also demonstrated the feasibility of modeling *SMAD3* variants using a zebrafish embryo system. In fact, we were able to take previously-identified variants of uncertain significance in *SMAD3* (P124T, L296P, and A349P) and provide data from a functional assay to assist in their reclassification as likely pathogenic. In our interpretation, the R287W variant remains suspicious due to the large range in diameter measurements. We suspect that increasing the number of embryos testing for R287W pathogenicity may result in reclassification of this variant as well.

Limitations of the study include a lack of regionally-specific anatomic correlation between the zebrafish dorsal aorta and the regions known as the ascending thoracic aorta, descending thoracic aorta, and abdominal aorta in human. It is important to note that at the time aortic diameter measurements were made in the zebrafish, the primordial heart had not yet formed. Our measurements were taken at the end of the yolk extension, in the region of the intersegmental vessels, downstream from the area where the lateral dorsal aortas have joined together to form a single blood vessel. A portion of the dorsal aorta develops into the zebrafish heart (23, 24). Therefore, it is very difficult to say exactly which portion of the primordial zebrafish aorta is the most similar to the human ascending aorta. We feel that this is less of a concern when discussing modeling *SMAD3* variants in a zebrafish embryo system because, per the patient case described above, *SMAD3*-dependent aortic pathology is not limited to only the ascending thoracic aorta in humans. The patient in whom this *SMAD3* variant was first identified has developed both a thoracic aortic aneurysm as well as an abdominal aortic aneurysm. To this extent, we believed that it was most critical that we measured aortic diameter in the exact same location for all the zebrafish in our study. Whether or not that region can be exactly correlated with the ascending aorta in humans was thought to be less critical.

An additional limitation of the study includes the inability to determine how variants impact vascular formation in later stages of development. Given that mRNAs are injected at the single cell embryonic stage, we limited aortic diameter measurements prior to the timeframe in which we would have expected the mRNA to remain active. 48-72 hpf are the expected maximum timelines for durability of injected mRNAs. Future mutagenesis of the germline, such as those that can be done more easily with the widespread availability of CRISPR-Cas9-mediated homologous recombination techniques, will

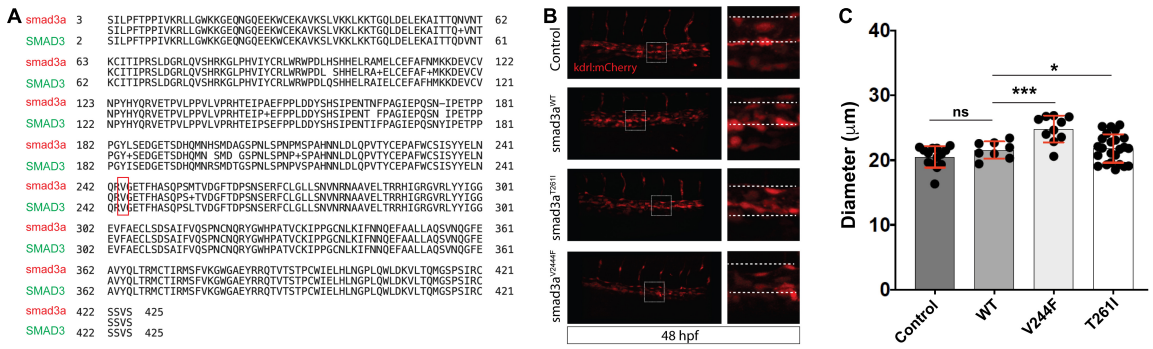

FIGURE 3
Zebrafish embryo-based assay for *SMAD3* variant pathogenesis. **(A)** Degree of conservation in amino acid sequence between Smad3a in zebrafish and human SMAD3. Overall, similarity is at ~97% indicating a very high level of conservation between the species. Residue V244 is highlighted to emphasize total conservation between zebrafish and human Smad3. **(B)** Confocal images of the tail aorta/vein labeled in Tg[kdrl:mCherry] in 48hpf embryos. White dashed boxes indicate the enlargement regions used to highlight differences in diameter (white dashed lines). Embryos imaged were either control, injected with smad3a^{WT} mRNA or smad3a^{T261I} or smad3a^{V244F}. **(C)** Quantification of diameter counts. Each point represents an individual embryo measured. Standard deviation is depicted in red. *$p < 0.05$, ***$p < 0.001$.

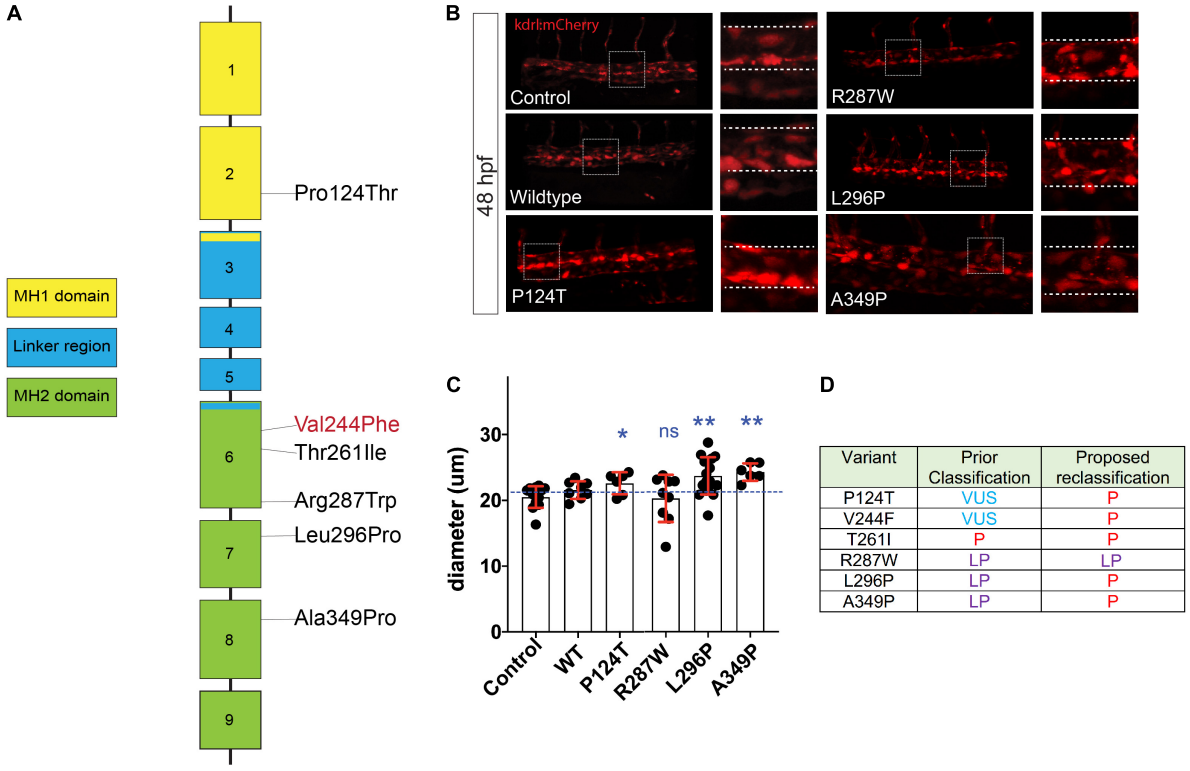

FIGURE 4
Assessment of *SMAD3* VUS pathogenicity using a zebrafish embryonic assay. **(A)** Diagram of the spatial distribution of specific VUS mutations examined. **(B)** Confocal images of the tail aorta/vein labeled in Tg[kdrl:mCherry] in 48hpf embryos. White dashed boxes indicate the enlargement regions used to highlight differences in diameter (white dashed lines). Embryos imaged were either control, injected with smad3a^{WT} mRNA or smad3a^{P124T}, smad3a^{R287W}, smad3a^{L296P} or smad3a^{A349P}. **(C)** Quantification of diameter counts. Each point represents an individual embryo measured. Standard deviation is depicted in red. Variants were compared to WT: *$p < 0.05$, **$p < 0.01$. **(D)** Summary of VUS classification changes based on the zebrafish embryonic assay results. P, pathogenic, LP, likely pathogenic.

enable observation of variant impacts at later stages of development. Another limitation of the use of mRNA injection includes the inability to model all types of variants identified, especially those that result in frameshift and nonsense mutations as these are most likely not dominant. We therefore recognize that certain *SMAD3* variants are not amenable to a mRNA injection approach.

One of the most compelling reason to pursue the embryonic zebrafish system for modeling of *SMAD3* variants is the potential for high-throughput as well as modeling of pharmacologic efficacy. The amount of time and money to conduct this study is minimal compared to the time and money that would be required to model this variant in mouse. Even when money is available, patient care can require more immediate decision-making.

Secondly, an advantage of this model is that zebrafish can absorb pharmacotherapeutics dissolved in their ambient water while they swim (25). This can be an efficient and inexpensive way to model pharmacologic impacts compared to other alternatives that enable readouts at the system level of physiology. Furthermore, zebrafish skin is translucent, enabling detection of changes in vascular phenotype over time without requiring echocardiology or computed tomography/magnetic resonance imaging. Additional studies could provide data to demonstrate the promise of certain pharmacologic interventions in humans, both with *SMAD3*-induced aortopathy as well as those with mutations in additional genes that cause familial aortic aneurysms.

Data availability statement

The original contributions presented in this study are included in this article/**Supplementary material**, further inquiries can be directed to the corresponding authors.

Ethics statement

The animal study was reviewed and approved by the University of Kentucky Institutional Animal Care and Use Committee.

Author contributions

MS: study conception and design, data interpretation, writing and editing the manuscript. JS and LB: figure preparation, reviewing and editing the manuscript. JF: study conception and design, zebrafish manipulation, microscopy, data analysis and interpretation, and writing and editing. All authors contributed to the article and approved the submitted version.

Funding

Funding for the work was provided by Igniting Research Collaborations (IRC) from the University of Kentucky, National Heart Lung and Blood Institute (K01-HL149984), and National Center for Advancing Translational Sciences (UL1-TR001998).

Acknowledgments

The authors would like to acknowledge the patient who generously agreed to have his anonymized clinical history included in this manuscript. The authors would also like to acknowledge J.R. Wallace, RT (R,CT), an Advanced Imaging Technologist in the Multidisciplinary 3D Imaging Lab of the Department of Radiology, University of Kentucky HealthCare for his assistance acquiring and preparing the radiographic images depicted in **Figures 1**, **2**.

Conflict of interest

The authors declare that the research was conducted in the absence of any commercial or financial relationships that could be construed as a potential conflict of interest.

Publisher's note

Supplementary material

The Supplementary Material for this article can be found online at: https://www.frontiersin.org/articles/10.3389/fcvm.2023.1103784/full#supplementary-material

References

1. Go A, Mozaffarian D, Roger V, Benjamin E, Berry J, Blaha M, et al. Heart disease and stroke statistics–2014 update: a report from the American Heart Association. *Circulation.* (2014) 129:e28–292.

2. Go A, Mozaffarian D, Roger V, Benjamin E, Berry J, Borden W, et al. Heart disease and stroke statistics–2013 update: a report from the American Heart Association. *Circulation.* (2013) 127:e6–245.

3. Biddinger A, Rocklin M, Coselli J, Milewicz D. Familial thoracic aortic dilatations and dissections: a case control study. *J Vasc Surg.* (1997) 25:506–11.

4. Regalado E, Guo D, Villamizar C, Avidan N, Gilchrist D, McGillivray B, et al. Exome sequencing identifies SMAD3 mutations as a cause of familial thoracic aortic aneurysm and dissection with intracranial and other arterial aneurysms. *Circ Res.* (2011) 109:680–6. doi: 10.1161/CIRCRESAHA.111.248161

5. Dietz H, Cutting C, Pyeritz R, Maslen C, Sakai L, Corson G, et al. Marfan syndrome caused by a recurrent de novo missense mutation in the fibrillin gene. *Nature.* (1991) 352:337–9. doi: 10.1038/352337a0

6. Loeys B, Chen J, Neptune E, Judge D, Podowski M, Holm T, et al. A syndrome of altered cardiovascular, craniofacial, neurocognitive and skeletal development caused by mutations in TGFBR1 or TGFBR2. *Nat Genet.* (2005) 37:275–81.

7. Mizuguchi T, Collod-Beroud G, Akiyama T, Abifadel M, Harada N, Morisaki T, et al. Heterozygous TGFBR2 mutations in Marfan syndrome. *Nat Genet.* (2004) 36:855–60.

8. Pannu H, Fadulu V, Chang J, Lafont A, Hasham S, Sparks E, et al. Mutations in transforming growth factor-beta receptor type II cause familial thoracic aortic aneurysms and dissections. *Circulation.* (2005) 112:513–20.

9. Zhu L, Vranckx R, Khau Van Kien P, Lalande A, Boisset N, Mathieu F, et al. Mutations in myosin heavy chain 11 cause a syndrome associating thoracic aortic aneurysm/aortic dissection and patent ductus arteriosus. *Nat Genet.* (2006) 38:343–9. doi: 10.1038/ng1721

10. Guo D, Pannu H, Tran-Fadulu V, Papke C, Yu R, Avidan N, et al. Mutations in smooth muscle alpha-actin (ACTA2) lead to thoracic aortic aneurysms and dissections. *Nat Genet.* (2007) 39:1488–93.

11. Wang L, Guo DC, Cao J, Gong L, Kamm K, Regalado E, et al. Mutations in myosin light chain kinase cause familial aortic dissections. *Am J Hum Genet.* (2010) 87:701–7.

12. Guo DC, Regalado E, Casteel D, Santos-Cortez R, Gong L, Kim J, et al. Recurrent gain-of-function mutation in PRKG1 causes thoracic aortic aneurysms and acute aortic dissections. *Am J Hum Genet.* (2013) 93:398–404. doi: 10.1016/j.ajhg.2013.06.019

13. Guo DC, Gong L, Regalado E, Santos-Cortez R, Zhao R, Cai B, et al. MAT2A mutations predispose individuals to thoracic aortic aneurysms. *Am J Hum Genet.* (2015) 96:170–7. doi: 10.1016/j.ajhg.2014.11.015

14. Schepers D, Tortora G, Morisaki H, MacCarrick G, Lindsay M, Liang D, et al. A mutation update on the LDS-associated genes TGFB2/3 and SMAD2/3. *Hum Mutat.* (2018) 39:621–34. doi: 10.1002/humu.23407

15. van de Laar I, Oldenburg R, Pals G, Roos-Hesselink J, de Graaf B, Verhagen J, et al. Mutations in SMAD3 cause a syndromic form of aortic aneurysms and dissections with early-onset osteoarthritis. *Nat Genet.* (2011) 43:121–6. doi: 10.1038/ng.744

16. Gong J, Zhou D, Jiang L, Qiu P, Milewicz D, Chen Y, et al. In vitro lineage-specific differentiation of vascular smooth muscle cells in response to SMAD3 deficiency: implications for SMAD3-related thoracic aortic aneurysm. *Arterioscler Thromb Vasc Biol.* (2020) 40:1651–63. doi: 10.1161/ATVBAHA.120.313033

17. Isselbacher E, Preventza O, Black J, Augoustides J, Beck A, Bolen M, et al. 2022 ACC/AHA guideline for the diagnosis and management of aortic disease: a report of the American heart association/American college of cardiology joint committee on clinical practice guidelines. *Circulation.* (2022) 146:e334–482. doi: 10.1161/CIR.0000000000001106

18. Norton E, Yang B. The impact of genetic factors and testing on operative indications and extent of surgery for aortopathy. *JTCVS Open.* (2021) 6:15–23. doi: 10.1016/j.xjon.2021.01.013

19. Garcia-Bermúdez M, Moustafa A, Barrós-Membrilla A, Tizón-Marcos H. Repeated loss of consciousness in a young woman: a suspicious SMAD3 mutation underlying spontaneous coronary artery dissection. *Can J Cardiol.* (2017) 33:292.e1–3. doi: 10.1016/j.cjca.2016.09.004

20. Campens L, Callewaert B, Muiño Mosquera L, Renard M, Symoens S, De Paepe A, et al. Gene panel sequencing in heritable thoracic aortic disorders and related entities – results of comprehensive testing in a cohort of 264 patients. *Orphanet J Rare Dis.* (2015) 10:9. doi: 10.1186/s13023-014-0221-6

21. Van de Laar I, van der Linde D, Oei E, Bos P, Bessems J, Bierma-Zeinstra S, et al. Phenotypic spectrum of the SMAD3-related aneurysms–osteoarthritis syndrome. *J Med Genet.* (2012) 49:47–57. doi: 10.1136/jmedgenet-2011-100382

22. Wang Y, Kaiser M, Larson J, Nasevicius A, Clark K, Wadman S, et al. Moesin1 and Ve-cadherin are required in endothelial cells during in vivo tubulogenesis. *Dev Camb Engl.* (2010) 137:3119–28. doi: 10.1242/dev.048785

23. Lawson N, Weinstein B. Arteries and veins: making a difference with zebrafish. *Nat Rev Genet.* (2002) 3:674–82. doi: 10.1038/nrg888

24. Asnani A, Peterson R. The zebrafish as a tool to identify novel therapies for human cardiovascular disease. *Dis Model Mech.* (2014) 7:763–7.

25. Kithcart A, MacRae C. Using zebrafish for high-throughput screening of novel cardiovascular drugs. *JACC Basic Transl Sci.* (2017) 2:1–12.

Frontiers in
Cardiovascular Medicine

Innovations and improvements in cardiovascular treatment and practice

Focuses on research that challenges the status quo of cardiovascular care, or facilitates the translation of advances into new therapies and diagnostic tools.

Discover the latest Research Topics

See more →

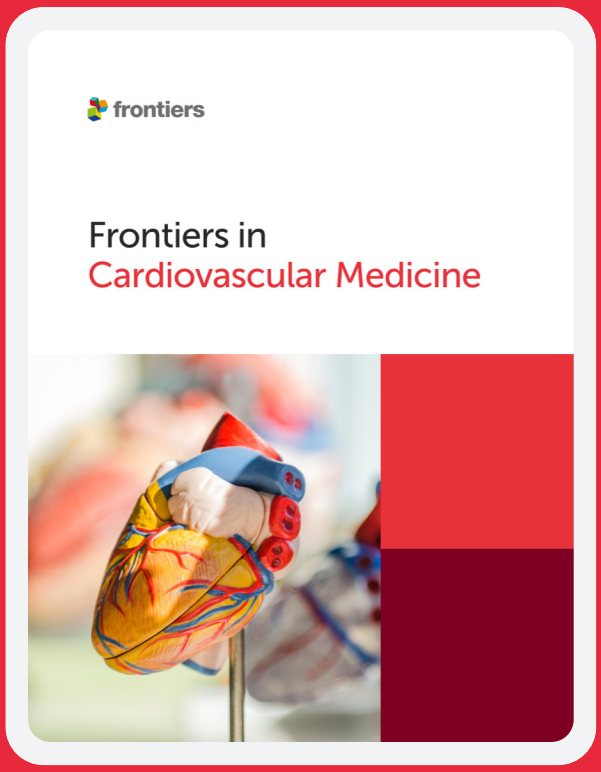

Frontiers

Avenue du Tribunal-Fédéral 34
1005 Lausanne, Switzerland
frontiersin.org

Contact us

+41 (0)21 510 17 00
frontiersin.org/about/contact